

# **Effect of LWR Coolant Environments on the Fatigue Life of Reactor Materials**

Draft Report for Comment

## AVAILABILITY OF REFERENCE MATERIALS IN NRC PUBLICATIONS

### NRC Reference Material

As of November 1999, you may electronically access NUREG-series publications and other NRC records at NRC's Public Electronic Reading Room at <http://www.nrc.gov/reading-rm.html>. Publicly released records include, to name a few, NUREG-series publications; *Federal Register* notices; applicant, licensee, and vendor documents and correspondence; NRC correspondence and internal memoranda; bulletins and information notices; inspection and investigative reports; licensee event reports; and Commission papers and their attachments.

NRC publications in the NUREG series, NRC regulations, and Title 10, "Energy," in the *Code of Federal Regulations* may also be purchased from one of these two sources.

1. The Superintendent of Documents  
U.S. Government Printing Office Mail Stop SSOP  
Washington, DC 20402-0001  
Internet: [bookstore.gpo.gov](http://bookstore.gpo.gov)  
Telephone: 202-512-1800  
Fax: 202-512-2250
2. The National Technical Information Service  
Springfield, VA 22161-0002  
[www.ntis.gov](http://www.ntis.gov)  
1-800-553-6847 or, locally, 703-605-6000

A single copy of each NRC draft report for comment is available free, to the extent of supply, upon written request as follows:

Address: U.S. Nuclear Regulatory Commission  
Office of Administration  
Publications Branch  
Washington, DC 20555-0001

E-mail: [DISTRIBUTION.RESOURCE@NRC.GOV](mailto:DISTRIBUTION.RESOURCE@NRC.GOV)  
Facsimile: 301-415-2289

Some publications in the NUREG series that are posted at NRC's Web site address <http://www.nrc.gov/reading-rm/doc-collections/nuregs> are updated periodically and may differ from the last printed version. Although references to material found on a Web site bear the date the material was accessed, the material available on the date cited may subsequently be removed from the site.

### Non-NRC Reference Material

Documents available from public and special technical libraries include all open literature items, such as books, journal articles, transactions, *Federal Register* notices, Federal and State legislation, and congressional reports. Such documents as theses, dissertations, foreign reports and translations, and non-NRC conference proceedings may be purchased from their sponsoring organization.

Copies of industry codes and standards used in a substantive manner in the NRC regulatory process are maintained at—

The NRC Technical Library  
Two White Flint North  
11545 Rockville Pike  
Rockville, MD 20852-2738

These standards are available in the library for reference use by the public. Codes and standards are usually copyrighted and may be purchased from the originating organization or, if they are American National Standards, from—

American National Standards Institute  
11 West 42<sup>nd</sup> Street  
New York, NY 10036-8002  
[www.ansi.org](http://www.ansi.org)  
212-642-4900

Legally binding regulatory requirements are stated only in laws; NRC regulations; licenses, including technical specifications; or orders, not in NUREG-series publications. The views expressed in contractor-prepared publications in this series are not necessarily those of the NRC.

The NUREG series comprises (1) technical and administrative reports and books prepared by the staff (NUREG-XXXX) or agency contractors (NUREG/CR-XXXX), (2) proceedings of conferences (NUREG/CP-XXXX), (3) reports resulting from international agreements (NUREG/IA-XXXX), (4) brochures (NUREG/BR-XXXX), and (5) compilations of legal decisions and orders of the Commission and Atomic and Safety Licensing Boards and of Directors' decisions under Section 2.206 of NRC's regulations (NUREG-0750).

**DISCLAIMER:** This report was prepared as an account of work sponsored by an agency of the U.S. Government. Neither the U.S. Government nor any agency thereof, nor any employee, makes any warranty, expressed or implied, or assumes any legal liability or responsibility for any third party's use, or the results of such use, of any information, apparatus, product, or process disclosed in this publication, or represents that its use by such third party would not infringe privately owned rights.

# **Effect of LWR Coolant Environments on the Fatigue Life of Reactor Materials**

## **Draft Report for Comment**

Manuscript Completed: March 2014  
Date Published: March 2014

Prepared by:  
Omesh Chopra<sup>1</sup> and Gary L. Stevens<sup>2</sup>

<sup>1</sup>Argonne National Laboratory  
9700 South Cass Avenue  
Argonne, IL 60439

<sup>2</sup>U.S. Nuclear Regulatory Commission

G. Stevens, NRC Project Manager

NRC Job Codes V6069 & V6269

Office of Nuclear Regulatory Research

## COMMENTS ON DRAFT REPORT

Any interested party may submit comments on this report for consideration by the NRC staff. Comments may be accompanied by additional relevant information or supporting data. Please specify the report number **NUREG/CR-6909 Rev. 1** in your comments, and send them by the end of the comment period specified in the *Federal Register* notice announcing the availability of this report.

**Addresses:** You may submit comments by any one of the following methods. Please include Docket ID **NRC-2014-0023** in the subject line of your comments. Comments submitted in writing or in electronic form will be posted on the NRC website and on the Federal rulemaking website <http://www.regulations.gov>.

**Federal Rulemaking Website:** Go to <http://www.regulations.gov> and search for documents filed under Docket ID **NRC-2014-0023**. Address questions about NRC dockets to Carol Gallagher at 301-287-3422 or by e-mail at [Carol.Gallagher@nrc.gov](mailto:Carol.Gallagher@nrc.gov).

**Mail comments to:** Cindy Bladey, Chief, Rules, Announcements, and Directives Branch (RADB), Division of Administrative Services, Office of Administration, Mail Stop: 3WFN-06-A44MP, U.S. Nuclear Regulatory Commission, Washington, DC 20555-0001. Faxes may be sent to RADB at 301-287-9368.

For any questions about the material in this report, please contact: Gary L. Stevens, Senior Materials Engineer at (301) 251-7569 or by e-mail at [Gary.Stevens@nrc.gov](mailto:Gary.Stevens@nrc.gov).

Please be aware that any comments that you submit to the NRC will be considered a public record and entered into the Agencywide Documents Access and Management System (ADAMS). Do not provide information you would not want to be publicly available.



## Abstract

The ASME Boiler and Pressure Vessel Code provides rules for the design of Class 1 components of nuclear power plants. Figures I–9.1 through I–9.6 of Appendix I to Section III of the Code specify fatigue design curves for applicable structural materials. However, the effects of light water reactor (LWR) coolant environments are not explicitly addressed by the Code design curves. The existing fatigue strain–vs.–life ( $\epsilon$ – $N$ ) data illustrate potentially significant effects of LWR coolant environments on the fatigue resistance of pressure vessel and piping steels. Under certain environmental and loading conditions, fatigue lives in water relative to those in air can be a factor of approximately 12 lower for austenitic stainless steels, approximately 3 lower for Ni-Cr-Fe alloys, and approximately 17 lower for carbon and low-alloy steels. In 2007, the original version of NUREG/CR-6909, which is the technical basis document for NRC Regulatory Guide 1.207, summarized the work performed at Argonne National Laboratory on the fatigue of piping and pressure vessel steels in LWR environments. In that document, the existing fatigue  $\epsilon$ – $N$  data were evaluated to identify the various material, environmental, and loading parameters that influence fatigue crack initiation, and to establish the effects of key parameters on the fatigue lives of these steels. The report presented fatigue life models for estimating fatigue lives as a function of material, loading, and environmental conditions, and described the environmental fatigue correction factor,  $F_{en}$ , for incorporating the effects of LWR environments into ASME Section III fatigue evaluations. The report also presented a critical review of the ASME Code Section III fatigue adjustment factors of 2 on stress (or strain) and 20 on life and assessed the possible conservatism in the choice of these adjustment factors.

This report provides updates and improvements to the environmental fatigue correction factor approach based on an extensive update to the fatigue  $\epsilon$ – $N$  data from testing and results available over the past decade since this report was first published. The updated expressions also address concerns from interested stakeholders related to: (a) the constants in the  $F_{en}$  expressions that result in  $F_{en}$  values of approximately 2 even when the strain rate is very high or the temperature is very low, (b) the temperature dependence of  $F_{en}$  for carbon and low-alloy steels, and (c) the dependence of  $F_{en}$  on water chemistry for austenitic SSs. The  $F_{en}$  methodology was validated by comparing the results of five different experimental data sets obtained from fatigue tests that simulate actual plant conditions with estimates of fatigue usage adjusted for environmental effects using the updated  $F_{en}$  expressions. The potential effects of dynamic strain aging on cyclic deformation and environmental effects are also discussed.



## FOREWORD

---

This report summarizes, reviews, and quantifies the effects of the light-water reactor (LWR) environments on the fatigue lives of reactor materials, including carbon steels, low-alloy steels, nickel-chromium-iron (Ni-Cr-Fe) alloys, and austenitic stainless steels. The primary purpose of this report is to provide the background and technical bases to support Regulatory Guide 1.207, “Guidelines for Evaluating Fatigue Analyses Incorporating the Life Reduction of Metal Components Due to the Effects of the Light-Water Reactor Environment for New Reactors.”

The initial revision of this report included a review of the fatigue  $\epsilon$ -N data available at that time for carbon steels, low-alloy steels, Ni-Cr-Fe alloys, and austenitic stainless steels to define the potential effects of key material, loading, and environmental parameters on the fatigue lives of the steels. By drawing upon a larger database than was used in earlier published reports, the U.S. Nuclear Regulatory Commission (NRC) updated the Argonne National Laboratory (ANL) fatigue life models used to estimate the fatigue curves as a function of those parameters, and presented a procedure for incorporating environmental effects into fatigue evaluations. In this revision, additional fatigue  $\epsilon$ -N data available since the original publication of this report, most particularly from Japan, was incorporated into the database and the fatigue life models were updated. In addition, feedback from interested stakeholders obtained since the original publication of this report were evaluated and incorporated, where appropriate.

The database described in this report reinforces the position espoused by the NRC that the previously published guideline for incorporating the LWR environmental effects in fatigue life evaluations should be revised. Toward that end, this report maintains the previously established methods for establishing reference air fatigue curves, and defines updated environmental correction factors for use in evaluating the fatigue lives of reactor components exposed to LWR coolants and operational experience.

The data described in this updated review were used to verify the previously developed fatigue design curves in air that are consistent with the available fatigue data. The published data indicate that the existing ASME Code Section III curves are appropriate for austenitic stainless steels (e.g., Types 304, 316, and 316NG), and are conservative for carbon and low-alloy steels. Regulatory Guide 1.207 endorses the fatigue design curves presented herein for incorporation in fatigue analyses for new and operating reactors.

Brian W. Sheron, Director  
Office of Nuclear Regulatory Research  
U.S. Nuclear Regulatory Commission



## CONTENTS

---

Abstract .....	iii
Foreword .....	v
Contents .....	vii
Figures .....	xiii
Tables .....	xxi
Executive Summary .....	xxiii
Abbreviations .....	xxvii
Acknowledgments .....	xxxix
1. Introduction .....	1
1.1 Definition of Fatigue Life .....	1
1.2 Air Fatigue Design Curves in Section III of the ASME Code .....	3
1.3 Subfactors Included in ASME Section III Air Fatigue Design Curves .....	5
1.3.1 Effects of Reactor Coolant Environment on Fatigue Lives .....	6
1.3.2 Effects of Neutron Irradiation .....	9
1.4 Modeling of Environmental Effects .....	13
2. Mechanism of Fatigue .....	17
2.1 Formation of an Engineering Crack in Air .....	17
2.2 Fatigue Cracking in LWR Environments .....	21
2.2.1 Carbon and Low-Alloy Steels .....	21
2.2.1.1 Effects of Surface Micropits .....	21
2.2.1.2 Mechanisms of Corrosion Fatigue .....	22
2.2.1.3 Effects of Dynamic Strain Aging (DSA) .....	26
2.2.1.4 Crack Growth Rates in Smooth Fatigue Specimens .....	28
2.2.2 Austenitic Stainless Steels .....	29
2.2.2.1 Effects of Surface Micropits .....	31
2.2.2.2 Mechanisms of Corrosion Fatigue .....	31
2.2.2.3 Effects of Dynamic Strain Aging (DSA) .....	34
2.2.2.4 Crack Growth Rates in Smooth Fatigue Specimens .....	34

3.	Fatigue Strain vs. Life ( $\epsilon$ -N) Behavior in Air .....	39
3.1	Carbon and Low-Alloy Steels and Weld Metals .....	39
3.1.1	Experimental Data .....	39
3.1.2	Temperature .....	42
3.1.3	Strain Rate.....	42
3.1.4	Sulfide Morphology .....	43
3.1.5	Cyclic Strain Hardening Behavior .....	43
3.1.6	Fatigue Life Model .....	44
3.1.7	Heat-to-Heat Variability.....	47
3.1.8	Fatigue $\epsilon$ -N Behavior of Weld Metals .....	50
3.1.9	Surface Finish.....	50
3.1.10	Extension of the Best-Fit Mean Curve from $10^6$ to $10^{11}$ Cycles .....	51
3.1.11	Fatigue Design Curves .....	53
3.2	Wrought and Cast Austenitic Stainless Steels and Weld Metals .....	56
3.2.1	Experimental Data .....	56
3.2.2	Specimen Geometry and Type of Loading .....	60
3.2.3	Strain Rate.....	61
3.2.4	Temperature .....	61
3.2.5	Cyclic Strain Hardening Behavior .....	62
3.2.6	Fatigue Life Model .....	63
3.2.7	Heat-to-Heat Variability.....	65
3.2.8	Fatigue $\epsilon$ -N Behavior of Cast Austenitic Stainless Steels .....	66
3.2.9	Fatigue $\epsilon$ -N Behavior of Weld Metals .....	67
3.2.10	Surface Finish.....	68
3.2.11	Fatigue Design Curve .....	69
3.3	Ni-Cr-Fe Alloys and Weld Metals .....	71
3.3.1	Experimental Data .....	72

	3.3.2	Fatigue Life Model .....	74
4.		Fatigue $\epsilon$ -N Behavior in LWR Environments.....	77
4.1		Carbon and Low-Alloy Steels.....	77
	4.1.1	Experimental Data .....	79
	4.1.2	Strain Rate.....	82
	4.1.3	Strain Amplitude .....	84
	4.1.4	Temperature .....	88
	4.1.5	Dissolved Oxygen.....	91
	4.1.6	Water Conductivity.....	92
	4.1.7	Sulfur Content in Steel .....	92
	4.1.8	Hold Periods .....	93
	4.1.9	Flow Rate .....	96
	4.1.10	Fatigue Life Model .....	97
	4.1.11	Environmental Fatigue Correction Factor.....	98
	4.1.12	Surface Finish.....	104
	4.1.13	Heat-to-Heat Variability.....	106
	4.1.14	Modified Rate Approach .....	107
4.2		Wrought and Cast Austenitic Stainless Steels .....	110
	4.2.1	Experimental Data .....	111
	4.2.2	Strain Rate.....	115
	4.2.3	Strain Amplitude .....	116
	4.2.4	Temperature .....	118
	4.2.5	Dissolved Oxygen.....	119
	4.2.6	Water Conductivity.....	120
	4.2.7	Material Heat Treatment .....	121
	4.2.8	Cast Austenitic Stainless Steels.....	121
	4.2.9	Stainless Steel Weld Metals.....	124

4.2.10	Hold Periods .....	125
4.2.11	Flow Rate .....	126
4.2.12	Fatigue Life Model .....	127
4.2.13	Environmental Correction Factor .....	128
4.2.14	Surface Finish.....	135
4.2.15	Heat-to-Heat Variability .....	136
4.3	Ni-Cr-Fe Alloys .....	138
4.3.1	Experimental Data .....	138
4.3.2	Effects of Key Parameters .....	140
4.3.3	Environmental Correction Factor .....	141
5	Adjustment Factors in ASME Code Fatigue Design Curves .....	147
5.1	Material Variability and Data Scatter .....	149
5.2	Size and Geometry .....	150
5.3	Surface Finish.....	151
5.4	Loading Sequence.....	151
5.5	Air Fatigue Design Curve Adjustment Factors Summarized.....	152
6.	Validation of $F_{en}$ Expressions.....	157
6.1	Spectrum Straining .....	158
6.2	Complex Loading – Safety Injection Transient .....	162
6.3	U-Bend Tests in Inert and PWR Water Environments .....	166
6.4	Simulation of Actual Plant Conditions .....	170
7.	Summary .....	173
8.	References .....	177
APPENDIX A: Incorporating Environmental Effects into Fatigue Evaluations .....		A-1
A1	Scope .....	A-1
A2	Environmental Correction Factor ( $F_{en}$ ).....	A-1
A3	Fatigue Evaluation Procedure.....	A-3
APPENDIX B: MATERIAL INFORMATION .....		B-1



B1	Carbon and Low-Alloy Steels Included in the Fatigue Database .....	B-1
B2	Wrought and Cast Austenitic Stainless Steels and Welds.....	B-4
B3	Ni-Cr-Fe Alloys and Welds.....	B-7
APPENDIX C: SAMPLE PROBLEM.....		C-1
C1	Background .....	C-1
C2	Problem Description .....	C-1
C3	Evaluation.....	C-8
C4	Results .....	C-11
C5	References .....	C-73



## FIGURES

---

Figure 1.	Fatigue $\epsilon$ -N data for low-alloy steels and austenitic stainless steels in water compared to ASME Air Design Curve; RT = room temperature. ....	6
Figure 2.	The effects of neutron irradiation on fatigue lives of Type 347 SSs at room temperature: (a) the fatigue $\epsilon$ -N behavior, and (b) variations in plastic strain amplitude as a function of fatigue cycles (Ref. 109). ....	10
Figure 3.	Strain amplitude vs. fatigue life data in 325°C air or simulated PWR primary water environments for CW Type 316 SS irradiated to (a) less than $10^{22}$ , (b) $2-6 \times 10^{25}$ , and (c) greater than $3 \times 10^{26}$ n/m <sup>2</sup> ( $E > 1.0$ MeV) (Ref. 110). ....	12
Figure 4.	Strain amplitude vs. fatigue life data in 325°C air and simulated PWR primary water environments for Type 304 SS irradiated to $5 \times 10^{25}$ – $10^{26}$ n/m <sup>2</sup> ( $E > 0.1$ MeV) (Ref. 110). ....	12
Figure 5.	Two stages of fatigue crack growth in smooth test specimens. ....	17
Figure 6.	Schematic illustration of the plastic blunting process of fatigue crack growth in Stage II: (a) zero load; (b) small tensile load; (c) maximum tensile load, widening of slip bands; (d) crack closure, and formation of “ears” at crack tip; (e) maximum compressive load; (f) small tensile load in the subsequent cycle. ....	18
Figure 7.	Crack depth plotted as a function of fractional life for carbon and low-alloy steels tested in air (Refs. 11, 165-167). ....	19
Figure 8.	Schematic illustration of (a) growth of short cracks in smooth specimens as a function of fatigue life fraction, and (b) crack velocity as a function of crack depth. ....	20
Figure 9.	Fatigue life of carbon and low-alloy steel specimens in high-DO water at 288°C compared with the fatigue life of specimens preoxidized in high-DO water and tested in either air or low-DO water at 288°C (Refs. 40, 41, 176). ....	22
Figure 10.	Schematic illustration of slip oxidation/dissolution process. ....	23
Figure 11.	Schematic illustration of hydrogen-induced cracking of low-alloy steel. ....	25
Figure 12.	Fatigue cracks on gauge surfaces of A106-Gr. B carbon steel tested in (a) air and (b) high-DO water at 288°C (Ref. 10). ....	26
Figure 13.	Fatigue cracks along longitudinal sections of A106-Gr. B carbon steel tested in (a) air and (b) high-DO water at 288°C (Ref. 10). ....	26
Figure 14.	(a) Fatigue crack initiation and (b) crack growth in DSA susceptible low-alloy steel exposed to high-temperature water environment (Ref. 147). ....	27
Figure 15.	Depth of largest crack plotted as a function of (a) fatigue cycles and (b) fraction of fatigue life for A533-Gr B low-alloy steel in air and water environments (Ref. 11). ....	28
Figure 16.	(a) Morphology and length of surface crack after various numbers of cycles for A533-Gr. B steel in air at room temperature, and (b) fracture surface and probable crack front for surface cracks shown in (a) (Ref. 11). ....	28
Figure 17.	Crack growth rates plotted as a function of crack depth for A533-Gr B low-alloy steel tested in air and water environments (Ref. 11). ....	29

Figure 18.	Photomicrographs of oxide films that formed on Type 316NG stainless steel in (a) simulated PWR water and (b) high-DO water (Ref. 13).	30
Figure 19.	Schematic of the corrosion oxide film formed on austenitic stainless steels in LWR environments.	30
Figure 20.	Effects of environment on formation of fatigue cracks in Type 316NG SS in air and low-DO water at 288°C. Preoxidized specimens were exposed for 10 days at 288°C in water that contained either less than 5 ppb DO and approximately 23 cm <sup>3</sup> /kg dissolved H <sub>2</sub> or approximately 500 ppb DO and no dissolved H <sub>2</sub> (Ref. 13).	31
Figure 21.	Photomicrographs of the fatigue crack morphology of Type 304 SS in (a) air, (b) high-DO BWR water, and (c) low-DO PWR water at 289°C (Ref. 47).	32
Figure 22.	Photomicrographs showing sites of fatigue crack initiation on fracture surfaces of Type 304 SS tested at 289°C in (a) air, (b) high-DO BWR water, and (c) low-DO PWR water (Ref. 47).	33
Figure 23.	Photomicrographs showing fatigue striations on fracture surfaces of Type 304 SS tested at 289°C in (a) air, (b) high-DO BWR water, and (c) low-DO PWR water (Ref. 47).	33
Figure 24.	Depth of largest crack plotted as a function of fatigue cycles for austenitic stainless steels in air and water (Refs. 13,207).	35
Figure 25.	Crack growth rates plotted as a function of crack length for austenitic stainless steels in (a) water and (b) air environments (Refs. 13,44,207).	35
Figure 26.	Crack growth rate data for Type 304 SS in high temperature water determined from (a) fracture mechanics CT specimens and (b) smooth cylindrical fatigue specimens (Ref. 208).	36
Figure 27.	Fatigue strain vs. life data for carbon and low-alloy steels in air at room temperature (JNUFAD database and Refs. 10,18,19,48).	41
Figure 28.	The change in fatigue lives of carbon and low-alloy steels in air as a function of temperature.	42
Figure 29.	Effect of strain rate and temperature on cyclic stress of carbon and low-alloy steels.	44
Figure 30.	Schematic diagram of the best-fit of the experimental data by minimizing the distance between the data point and the S-N curve.	45
Figure 31.	Experimental and predicted fatigue lives of (a, b) carbon steels and (c, d) low-alloy steels in air.	46
Figure 32.	Estimated cumulative distribution of constant A in the ANL models for fatigue life data in the original revision of NUREG/CR-6909 (a, c) and this report (b, d); (a, b) for heats of carbon steels and (c, d) low-alloy steels in air.	48
Figure 33.	Fatigue $\epsilon$ -N behavior for carbon and low-alloy steel weld metals in air at room temperature and 289°C (Ref. 136).	50
Figure 34.	Effect of surface finish on the fatigue life of A106-Gr B carbon steel in air at 289°C (Ref. 46).	51
Figure 35.	Fatigue design curves based on the ANL model for (a) carbon steels and (b) low-alloy steels in air.	54

Figure 36.	Fatigue design curve for carbon steels in air. The curve developed from the ANL model is based on factors of 12 on life and 2 on stress.....	55
Figure 37.	Fatigue design curve for low-alloy steels in air. The curve developed from the ANL model is based on factors of 12 on life and 2 on stress. ....	55
Figure 38.	Fatigue $\epsilon$ -N behavior for Types 304, 304L, 316, and 316NG SS austenitic stainless steels in air at various temperatures up to 400°C (Refs. 13,42-47, 61,136). ....	58
Figure 39.	Influence of specimen geometry on fatigue lives of Types 304 and 316 stainless steels (JNUFAD data). ....	60
Figure 40.	Influence of bending loading on fatigue lives of Types 304 and 316 stainless steels (JNUFAD data). ....	60
Figure 41.	Influence of temperature on fatigue lives of austenitic stainless steels in air (Ref. 61-63). ....	61
Figure 42.	Effects of strain amplitude, temperature, and strain rate on cyclic strain-hardening behavior of Types 304 and 316NG SSs in air at 288°C and room temperature. ....	62
Figure 43.	Cyclic stress-strain curves for Types 316, 304 and 316NG SSs in air at room temperature and 288°C. ....	63
Figure 44.	Experimental and predicted fatigue lives (using the ANL model) for austenitic SSs in air. ....	64
Figure 45.	Estimated cumulative distribution of constant A in the ANL model for fatigue lives for heats of austenitic SSs in air included in (a) the initial revision of NUREG/CR-6909 and (b) those included in this report. ....	65
Figure 46.	Fatigue $\epsilon$ -N behavior for several heats of CF-8M cast austenitic SSs in air at various temperatures. ....	67
Figure 47.	Fatigue $\epsilon$ -N behavior for austenitic SS weld metals in air at room temperature. ....	68
Figure 48.	Effects of surface roughness on fatigue lives of (a) Type 316NG and (b) Type 304 SSs in air (Ref. 46). ....	68
Figure 49.	Fatigue design curves for austenitic SSs in air. ....	70
Figure 50.	Fatigue $\epsilon$ -N behavior for Alloys 600, 690 and 800 in air at temperatures between room temperature and 315°C (Refs. JNUFAD data, 61,66-75). ....	73
Figure 51.	Fatigue $\epsilon$ -N behavior for Alloys 62, 82, 132, 152, and 182 welds in air at various temperatures (Refs. JNUFAD data,61,66-75). ....	73
Figure 52.	Fatigue $\epsilon$ -N behavior for Inconel 718 in air at room temperature and 427°C (Refs. 61,72,73,136,210). ....	73
Figure 53.	Fatigue $\epsilon$ -N behavior for carbon and low-alloy steels in air at room temperature and high-purity water at temperatures below 150°C (Ref. 137). ....	79
Figure 54.	Strain amplitude vs. fatigue life data for (a) A533-Gr B and (b) A106-Gr B steels in air and high-dissolved-oxygen water at 288°C (Ref. 10). ....	81
Figure 55.	Dependence of fatigue lives of carbon and low-alloy steels on strain rate (Refs. 10,23). ....	83

Figure 56.	Fatigue life of A533–Gr. B low-alloy steel as a function of strain rate in high purity water with 0.1 or 2.0 ppm dissolved oxygen (Refs. 141,143).....	84
Figure 57.	Fatigue strain-life behavior of A533–Gr. B and A508–Gr. 3 low-alloy steels at 288°C in air and high-purity water with 0.1 ppm dissolved oxygen (Ref. 151). ....	84
Figure 58.	Fatigue life of A106–Gr B carbon steel at 288°C and 0.75% strain range in air and water environments under different loading waveforms (Ref. 10).....	85
Figure 59.	Fatigue lives of carbon and low–alloy steels tested with loading waveforms where slow strain rate was applied during a fraction of the tensile loading cycle (Refs. 10,24).....	86
Figure 60.	Experimental values of fatigue life and those predicted from the modified rate approach (a) without and (b) with consideration of a threshold strain (Ref. 136). ....	87
Figure 61.	Change in fatigue life of A333–Gr. 6 carbon steel and A508–Gr. 3 low-alloy steel with temperature and DO (Ref. 136).....	89
Figure 62.	Waveforms for changes in temperatures and strains during exploratory fatigue tests (Ref. 21). ....	90
Figure 63.	Fatigue lives of A333–Gr. 6 carbon steel tube specimens under varying temperature conditions, as indicated by horizontal bars (Ref. 21). ....	90
Figure 64.	Dependence on DO of the fatigue lives of carbon and low alloy steels in high-purity water (Ref. 18, 19, 22).....	91
Figure 65.	Effect of strain rate on fatigue life of low–alloy steels with different sulfur contents (Refs. 10, 136).....	92
Figure 66.	Effect of strain rate on the fatigue lives of A333–Gr. 6 carbon steels with different sulfur contents (Ref. 10).....	93
Figure 67.	Fatigue lives of A106–Gr B steel in air and water environments at 288°C, 0.78% strain range, and hold periods at peak tensile strain (Ref. 10). Hysteresis loops are for tests in air. ....	94
Figure 68.	Effect of hold periods on the fatigue lives of A333–Gr. 6 carbon steel at 289°C in water with 1 ppm DO (Ref. 24). ....	95
Figure 69.	Effects of water flow rate on fatigue lives of A333–Gr. 6 and A508–Gr. 1 carbon steels and A533–Gr. B low-alloy steel at 289°C and 0.3 or 0.6% strain amplitudes and various strain rates (Ref. 25,26). ....	96
Figure 70.	Effect of flow rate on low–cycle fatigue of carbon steel tube bends in high–purity water at 240°C (Ref. 55). RT = room temperature.....	97
Figure 71.	Experimental fatigue lives of carbon steels in LWR environments vs. fatigue lives predicted from the (a) new expression, (b) JNES expression, and (c) the previous NUREG/CR-6909 expression. ....	99
Figure 72.	Experimental fatigue lives of low-alloy steels in LWR environments vs. fatigue lives predicted from the (a) new expression, (b) JNES expression, and (c) the previous NUREG/CR-6909 expression. ....	100
Figure 73.	Comparison of the fatigue lives of carbon and low-alloy steels predicted from the new $F_{en}$ expression and the JNES $F_{en}$ expression. ....	101

Figure 74.	Residuals for predicted fatigue lives of carbon steels as a function of (a) Material ID, (b) water dissolved oxygen content, (c) strain rate, (d) temperature, (e) steel sulfur content, and (f) strain amplitude. ....	102
Figure 75.	Residuals for predicted fatigue lives of low-alloy steels as a function of (a) Material ID, (b) water dissolved oxygen content, (c) strain rate, (d) temperature, (e) steel sulfur content, and (f) strain amplitude. ....	103
Figure 76.	Residuals for predicted fatigue lives in air of carbon and low-alloy steels as a function of Material ID. ....	104
Figure 77.	Effect of surface finish on the fatigue lives of (a) A106–Gr B carbon steel and (b) A533 low–alloy steel in air and high–purity water at 289°C (Ref. 46). ...	105
Figure 78.	Relationship between surface finish and fatigue life reduction fraction for A533–Gr. B low-alloy steel in water at 288°C (Ref. 144). ....	105
Figure 79.	Estimated cumulative distribution of parameter A in the ANL model for fatigue lives for heats of carbon and low–alloy steels in LWR environments. ....	107
Figure 80.	Application of the modified rate approach to determine the environmental fatigue correction factor $F_{en}$ during the increasing strain portion of a transient. ....	108
Figure 81.	Example showing $F_{en}$ values computed using average temperatures compared to the $F_{en}$ computed using an integrated (modified rate) approach. ...	109
Figure 82.	Strain amplitude vs. fatigue life data for (a) Type 304 and (b) Type 316NG SSs in water at 288°C (JNUFAD and Refs. 13,45). ....	113
Figure 83.	Fatigue stress - life data from load-controlled tests on Type 304L SSs, with and without mean stress, in air and PWR water (Ref. 60). ....	114
Figure 84.	Fatigue strain - life data from load-controlled tests on Type 304L SSs, with and without mean stress, in air (a, c) and PWR water (b, d) (Refs. 58,60). ....	115
Figure 85.	Dependence of fatigue lives of austenitic stainless steels on strain rate in low–DO water (Refs. 13,45,47,60). ....	116
Figure 86.	Dependence of fatigue lives of Types (a) 304 and (b) 316NG SSs on strain rate in high– and low–DO water at 288°C (Ref. 13,45,47). ....	116
Figure 87.	Results of strain rate change tests on Type 316 SSs in low–DO water at 325°C. Low strain rate was applied during only a fraction of the tensile loading cycle. Fatigue life is plotted as a function of fraction of strain at high strain rate (Refs. 30,35). ....	117
Figure 88.	Change in fatigue lives of austenitic stainless steels in low–DO water with temperature (Refs. 13,29–31,34,45–47). ....	118
Figure 89.	Fatigue lives of Type 316 SSs under constant and varying test temperatures (Ref. 29,30). ....	119
Figure 90.	Effects of water conductivity and soaking period on fatigue lives of Type 304 SSs in high–DO water (Ref. 13,45). ....	120
Figure 91.	The effects of material heat treatment on fatigue lives of Type 304 SSs in air, BWR and PWR environments at 289°C, approximately 0.38% strain amplitude, sawtooth waveform loading, and 0.004%/s tensile strain rate (Ref. 47). ....	121

Figure 92.	Fatigue lives of cast austenitic SSs in high-purity water at 289°C and 0.3% and 0.6% strain amplitude plotted as a function of DO content (Ref. 136). .....	122
Figure 93.	Strain amplitude vs. fatigue life data for cast austenitic SSs at 325°C and various strain rates in water with 0.005 ppm DO content (Ref. 29,34).....	122
Figure 94.	Dependence of fatigue lives of CF–8M cast SSs on strain rate in low–DO water at various strain amplitudes (Refs. 136,43,45). .....	123
Figure 95.	Change in fatigue lives of cast austenitic SSs in low–DO water with temperature (Ref. 136). .....	124
Figure 96.	Strain amplitude vs. fatigue lives for Types 308 and 316TP SS weld metals at 325°C and various strain rates in water with 0.005 ppm DO content (Ref. 136). .....	124
Figure 97.	Change in fatigue lives of SS weld metals in LWR environments with strain rate and temperature (Ref. 136).....	125
Figure 98.	Fatigue lives of Type 304 SSs tested in high–DO water at 260–288°C with trapezoidal or triangular waveform loadings (Refs. 14,31). .....	125
Figure 99.	Effect of hold periods on the fatigue lives of Types 316NG and 316 SSs in LWR environments at various strain rates (Ref. 136).....	126
Figure 100.	Effects of water flow rate on the fatigue lives of Types 304, 304L, 316NG and CF-8M cast SSs in high-purity water at 289°C (Ref. 136). .....	127
Figure 101.	Effects of water flow rates on the fatigue lives of Type 304 and 316 austenitic SSs in PWR primary water at 325°C (Ref. 136). .....	127
Figure 102.	Experimental fatigue lives of wrought and cast austenitic SSs in LWR environments vs. fatigue lives predicted from (a) the updated ANL expression, (b) the JNES expression, (c) the previous NUREG/CR-6909 expression, and (d) fatigue lives of SS weld metals predicted from the updated ANL expression.....	130
Figure 103.	Fatigue lives of wrought and cast austenitic SSs in LWR environments estimated from the new $F_{en}$ expressions vs. those estimated from the JNES expression. ....	131
Figure 104.	Experimental fatigue lives of Types 304L and 316N austenitic SSs in LWR environments vs. fatigue lives predicted from (a) the updated ANL expression and (b) the JNES expression. ....	132
Figure 105.	Experimental fatigue lives of wrought and cast austenitic SSs in water containing greater than 0.1 ppm DO vs. fatigue lives predicted from (a) the updated ANL expression and (b) the JNES expression.....	132
Figure 106.	Residuals for predicted fatigue lives of wrought and cast austenitic SSs as a function of (a) ANL Material ID, (b) water DO content, (c) strain rate, (d) temperature, and (e) strain amplitude.....	134
Figure 107.	Residuals for predicted fatigue lives of wrought and cast austenitic SSs in air as a function of ANL Material ID. ....	135
Figure 108.	Effect of surface finish on fatigue life of (a) Type 316NG and (b) Type 304 stainless steels in air and high–purity water at 289°C. ....	136



Figure 109.	Effects of surface finish on the fatigue lives of Type 304L SSs in air and PWR primary water environments at 300°C (Refs. 155,157). .....	136
Figure 110.	Estimated cumulative distribution of constant A in the ANL model for fatigue lives of heats of austenitic SSs in LWR environments.....	137
Figure 111.	Fatigue $\epsilon$ -N behavior for Alloy 600 and its weld alloys in simulated BWR water at approximately 289°C (Refs. 136, 39).....	139
Figure 112.	Fatigue $\epsilon$ -N behavior for Alloys 600 and 690 and associated weld metals in simulated PWR water at 325°C (Refs. 136, 75). .....	139
Figure 113.	Dependence of fatigue lives of Alloys 690 and 600 and associated weld metals on strain rate in PWR and BWR environments (Refs. 39, 75, 136).....	140
Figure 114.	Dependence of fatigue lives of Alloy 600 on temperature in a PWR environment (Refs. 39, 75, 136).....	141
Figure 115.	Experimental fatigue lives vs. fatigue lives predicted from the updated $F_{en}$ expression for Ni-Cr-Fe alloys and weld metals in simulated (a) BWR and (b) PWR environments. ....	142
Figure 116.	Experimental fatigue lives vs. fatigue lives predicted from the $F_{en}$ expression in the original revision of NUREG/CR-6909 for Ni-Cr-Fe alloys and weld metals in simulated (a) BWR and (b) PWR environments. ....	143
Figure 117.	Experimental fatigue lives vs. fatigue lives predicted from the JNES $F_{en}$ expression for Ni-Cr-Fe alloys and associated weld metals in simulated (a) BWR and (b) PWR environments. ....	143
Figure 118.	Residuals for predicted fatigue lives of Ni-Cr-Fe alloys and associated weld metals as a function of (a) material ID, (b) water DO content, (c) strain rate, (d) temperature, and (e) strain amplitude.....	145
Figure 119.	Residuals for predicted fatigue lives of Ni-Cr-Fe alloys and associated weld metals in air as a function of ANL Material ID. ....	146
Figure 120.	Fatigue data for (a) carbon and low-alloy steel and (b) Type 304 stainless steel components (Refs. 237,238). ....	148
Figure 121.	Estimated cumulative distribution of parameter A in the ANL models that represent the fatigue lives of test specimens and actual components in air. ....	155
Figure 122.	Schematic of the repeated sequence of randomized block of 50 strain cycles (Ref. 158). ....	159
Figure 123.	Fatigue strain-life data for Type 316NG SS in PWR water at 320°C and for Ti-stabilized 316 SS in VVER water at 293°C (Refs. 158,159).....	161
Figure 124.	Experimental and estimated fatigue lives for Type 316NG and Ti-stabilized 316 SS tested with constant and spectrum strain loading (Refs. 158,159).....	162
Figure 125.	Typical strain cycle of cold and hot thermal shocks corresponding to a PWR safety injection transient (Ref. 155).....	163
Figure 126.	Fatigue strain-life data for Type 304L SS in air and PWR environments at 300°C (Refs. 155-157).....	164

Figure 127.	The experimental and estimated fatigue lives for Type 304L SS tested at 300°C in air and a PWR environment using triangular and complex loading that simulated a PWR safety injection transient (Refs. 155-157).....	165
Figure 128.	U-bend test specimen and nomenclature (Ref. 97). ....	166
Figure 129.	Overview of the extent and location of fatigue cracking in U-bend tests at strain amplitude of 0.6% (Ref. 97).....	168
Figure 130.	Overview of the extent and location of fatigue cracking in U-bend tests at strain amplitude of 0.4% (Ref. 97).....	169
Figure 131.	The experimental and predicted fatigue lives for Type 304L SS U-bend specimens at 240°C in inert and PWR environments (Refs. 97-99). ....	170
Figure 132.	Loading waveforms for Fatigue Test Nos. 1 and 7 (Ref. 154). ....	171
Figure 133.	The experimental and predicted fatigue lives of Type 316 SS tested in PWR primary water using two blocks of fatigue cycles of different strain amplitudes and varying temperature and strain rate (Ref. 154).....	172
Figure A.1.	Fatigue design curves for carbon steels in air. The curve developed from the ANL model is based on factors of 12 on life and 2 on stress. ....	A-4
Figure A.2.	Fatigue design curves for low-alloy steels in air. The curve developed from the ANL model is based on factors of 12 on life and 2 on stress. ....	A-4
Figure A.3	Fatigue design curve for austenitic stainless steels in air. The curve developed from the ANL model is based on factors of 12 on life and 2 on stress.....	A-5
Figure C.1.	Sample Problem Geometry.....	C-2
Figure C.2.	Sample Problem Transient Time Histories .....	C-4
Figure C.3.	Sample Problem Transient Membrane Plus Bending Stress Histories for SCL 2 .....	C-5
Figure C.4.	Sample Problem Transient Total Stress Histories for SCL 2 .....	C-6
Figure C.5.	Sample Problem Combined Transient Stress History for SCL 2.....	C-7
Figure C.6.	Principal Stress Intensity Histories and Peaks and Valleys Used in Limiting CUF Calculation for Sample Problem for SCL 2 .....	C-13

## TABLES

---

Table 1.	Sources of the fatigue $\epsilon$ -N data on carbon and low-alloy steels in air environment.....	40
Table 2.	Values of constant A in the ANL fatigue life model for carbon steels in air and the factors on life as a function of confidence level and percentage of population bounded. ....	49
Table 3.	Values of constant A in the ANL fatigue life model for low-alloy steels in air and the factors on life as a function of confidence level and percentage of population bounded. ....	50
Table 4.	Fatigue design curves for carbon and low-alloy steels including proposed updated extension to $10^{11}$ cycles.....	54
Table 5.	Fatigue design curves for carbon and low-alloy steels and the extension to $10^{11}$ cycles proposed in the initial revision to NUREG/CR-6909. ....	55
Table 6.	Sources of the fatigue $\epsilon$ -N data on wrought and cast austenitic stainless steels in an air environment. ....	56
Table 7.	Values of constant A in the ANL fatigue life model for austenitic SSs and the factors on fatigue lives for austenitic SSs in air as a function of confidence level and percentage of population bounded.....	66
Table 8.	The ASME Code fatigue design curves for austenitic SSs in air. ....	69
Table 9.	Sources of the fatigue $\epsilon$ -N data on Ni-Cr-Fe alloys and their weld metals in an air environment. ....	71
Table 10.	Sources of the fatigue $\epsilon$ -N data for carbon and low-alloy steels in LWR environments. ....	80
Table 11.	Sources of the fatigue $\epsilon$ -N data for cast and austenitic stainless steels in LWR environments. ....	112
Table 12.	Sources of the fatigue $\epsilon$ -N data for Ni-Cr-Fe alloys and their weld metals in LWR environments. ....	138
Table 13.	Statistical information for the constant A used to evaluate material variability and data scatter. ....	150
Table 14.	Factors on life applied to the mean fatigue $\epsilon$ -N air curve to account for the effects of various material, loading, and environmental parameters. ....	153
Table 15.	Factor applied to the mean values of fatigue life to bound 95% of the data population. ....	154
Table 16.	Chemical composition and tensile strength of test materials for the constant and spectrum strain amplitude fatigue tests. ....	158
Table 17.	Environmental conditions for the constant and spectrum strain amplitude fatigue tests. ....	159
Table 18.	The conditions and results of fatigue tests on austenitic SSs obtained under constant and spectrum strain amplitude loading. ....	160
Table 19.	Chemical composition and tensile strength of Type 304L SS.....	163

Table 20.	Environmental conditions for fatigue tests in simulated PWR environment. ....	163
Table 21.	The conditions and results of fatigue tests on Type 304L austenitic SS at 300°C in air and PWR environments using a triangular or complex strain cycle. ....	165
Table 22.	Summary of the key conditions and results of the U-bend tests at 240°C. ....	168
Table 23.	Chemical composition and tensile strength of Type 316 SS material. ....	170
Table 24.	Test matrix for the two blocks fatigue damage tests. ....	172
Table 25.	Results of the two blocks fatigue damage tests. ....	172
Table A.1.	Fatigue design curves for carbon and low-alloy steels in air. ....	A-5
Table A.2.	Fatigue design curves for austenitic stainless steels in air. ....	A-5
Table C.1.	Sample Problem Transient Definitions. ....	C-3
Table C.2.	Limiting CUF Results for Sample Problem for SCL 2. ....	C-12
Table C.3.	CUF <sub>en</sub> Results Based for Sample Problem for SCL 2 (Average Strain Rate Approach). ....	C-14
Table C.4.	CUF <sub>en</sub> Results Based for Sample Problem for SCL 2 (Modified Strain Rate Approach). ....	C-15
Table C.5.	Principal Stress Intensity Histories Used in Limiting CUF Calculation for Sample Problem for SCL 2. ....	C-16

## EXECUTIVE SUMMARY

---

Cyclic loadings on a reactor pressure boundary component occur because of changes in mechanical and thermal loadings as the system goes from one load set (e.g., pressure, temperature, moment, and force loading) to another. The American Society of Mechanical Engineers (ASME) Boiler and Pressure Vessel Code Section III, Subsection NB contains rules for the design of Class 1 components of nuclear power plants and recognizes fatigue as a possible mode of failure in pressure vessel steels and piping materials. ASME Code Section III fatigue analysis procedures consider all fatigue cycles based on the anticipated number of thermal and pressure transients, and for each load-cycle or load set pair, an individual fatigue usage factor is determined by the ratio of the number of cycles anticipated during the design lifetime of the component, as specified by the Owner, to the number of allowable cycles. Figures I-9.1 through I-9.6 of Mandatory Appendix I to Section III of the ASME Code specify fatigue design curves that define the allowable number of cycles as a function of applied stress amplitude. Those fatigue design curves have evolved significantly since the initial publication of Section III in 1963. However, Paragraph NB-3121 of the 2011 Addenda to Section III of the Code continues to state that the effects of coolant environments on the fatigue resistance of materials were not addressed in the fatigue design curves. Therefore, the effects of water environments on the fatigue resistance of materials used in operating pressurized water reactor (PWR) and boiling water reactor (BWR) plants, whose components were designed in accordance with the ASME Code Section III, may not adequately address long-term environmental effects on fatigue based on the data available at the time the fatigue design curves were derived.

The current Section III design fatigue curves in air contained in Section III of the ASME Code were based primarily on strain-controlled fatigue tests of small polished specimens at room temperature in laboratory air environments. Best-fit curves to the experimental test data were first adjusted to account for the effects of mean stress and then lowered by a factor of 2 on stress and 20 on cycles (whichever was more conservative) to obtain the design fatigue air curves. These factors were not intended as “safety margins,” but rather they were intended as “adjustment factors” that were applied to the experimental laboratory data to obtain estimates of the fatigue lives of actual reactor components. Recent fatigue-strain-vs.-life ( $\epsilon$ -N) data obtained primarily in the U.S. and Japan demonstrate that light water reactor (LWR) environments have potentially significant effects on the fatigue resistance of materials. Specimen lives obtained from laboratory tests in simulated LWR environments were much shorter than those obtained from corresponding tests in an air environment.

In the original version of NUREG/CR-6909, the existing fatigue  $\epsilon$ -N data for carbon and low-alloy steels, wrought and cast austenitic stainless steels (SSs), and nickel-chromium-iron (Ni-Cr-Fe) alloys in air and LWR environments were evaluated to identify the various material, environmental, and loading parameters that influence fatigue crack initiation. The results of those evaluations were used to establish the effects of key parameters on the fatigue lives of steels. The fatigue lives of materials were decreased in LWR environments; the magnitude of the reduction depended on the temperature, strain rate, dissolved oxygen (DO) level in the water, and, for carbon and low-alloy steels, the sulfur (S) content of the steels. For all steels, environmental effects on fatigue lives were significant only when critical parameters (temperature, strain rate, DO level, and strain amplitude) met certain threshold values. Environmental effects were moderate, e.g., less than a factor of 2 decrease in fatigue lives, when any one of the threshold conditions was not satisfied. The threshold values of the critical parameters and the effects of other parameters (such as water conductivity, water flow rate, and material heat treatment) on the fatigue lives of the steels were also discussed.

In this report, the comprehensive review of the fatigue  $\epsilon$ -N data for nuclear power plant piping and pressure vessel steels presented in the original version of NUREG/CR-6909 was reevaluated using a much larger database. The results were updated to include this reevaluation, as well as to address concerns from interested stakeholders regarding the  $F_{en}$  methodology for incorporating environmental effects into ASME Code Section III fatigue cumulative usage factor (CUF) evaluations. The resulting effects of various material, loading, and environmental parameters on the fatigue lives of steels are summarized in this report.

The results indicated that the ASME Code Section III mean air curve for low-alloy steels is in good agreement with the available experimental data, and the ASME Code Section III mean air curve for carbon steels is conservative. In addition, the best-fit mean air data used to develop the fatigue design air curve for austenitic SSs in ASME Code Section III editions prior to 2009b Addenda is not consistent with the experimental data at strain amplitudes less than 0.5%; fatigue lives predicted by the ASME Code Section III mean air curve were longer than those obtained from experiments. Therefore, in the initial version of NUREG/CR-6909, new fatigue design air curves were developed for carbon and low-alloy steels and austenitic SSs that were based on the ANL fatigue life models and were consistent with the fatigue  $\epsilon$ -N data available at that time. The air design curves were extended up to  $10^{11}$  cycles using available high-cycle fatigue data. In 2009, the ANL design air curve for austenitic SSs was adopted into Mandatory Appendix I of Section III of the ASME Code. The reevaluation of the fatigue  $\epsilon$ -N behavior of austenitic SS materials using a much larger database indicated that the air fatigue design curves previously developed by ANL are consistent with the available fatigue data, and do not warrant any modifications. However, in the present report, the extension of the air fatigue design curves for carbon and low-alloy steels up to  $10^{11}$  cycles was modified to be consistent with the extension of the current ASME Code Section III fatigue design curve beyond  $10^6$  cycles.

The reevaluation results also indicated that the fatigue data for Ni-Cr-Fe alloys were not consistent with the current ASME Code mean air curve for austenitic SSs. The rather limited fatigue  $\epsilon$ -N data for Ni-Cr-Fe alloys, such as Alloys 600, 690, and 800 and their welds, were consistent with the best-fit mean air curve for austenitic SSs at fatigue lives less than  $10^4$  cycles, and showed longer fatigue lives than the predicted values for fatigue lives greater than  $10^4$  cycles. However, a separate air fatigue design curve was not developed for Ni-Cr-Fe alloys, and the current ASME Code fatigue air design curve for austenitic SSs, which is based on the ANL model, was used to represent the fatigue  $\epsilon$ -N behavior of Ni-Cr-Fe alloys and associated weld metals. The data also indicated that the fatigue resistance of Inconel 718 is superior to that of the other Ni-Cr-Fe alloys. The slope of the Inconel 718 fatigue  $\epsilon$ -N curve is flatter and the fatigue limit is higher than those for austenitic SSs.

The fatigue lives of carbon and low-alloy steels, austenitic SSs, and Ni-Cr-Fe alloys were decreased in LWR environments. The reduction depended on some key material, loading, and environmental parameters. The fatigue  $\epsilon$ -N data were consistent with the much larger database on enhancement of crack growth rates in these materials in LWR environments. The key parameters that influenced fatigue lives in these environments, e.g., temperature, DO level in the water, strain rate, strain (or stress) amplitude, and, for carbon and low-alloy steels, S content of the steel, were identified. In addition, the functional form of the dependence of fatigue lives on these parameters and the range of the values of these parameters within which environmental effects were significant was defined. If these critical loading and environmental conditions exist during reactor operation, then environmental effects may be significant and should be included in any relevant ASME Code Section III fatigue evaluations.

In the initial version of NUREG/CR-6909 (published in 2007), fatigue life models were developed to predict the fatigue lives of small smooth specimens of carbon and low-alloy steels, wrought and cast austenitic SSs, and Ni-Cr-Fe alloys as a function of material, loading, and environmental parameters using the existing fatigue  $\epsilon$ -N database. The functional form and bounding values of these parameters were based on experimental observations and data trends. An approach was presented that incorporated the effects of LWR coolant environments into the ASME Code Section III fatigue evaluations based on the environmental fatigue correction factor,  $F_{en}$ . The fatigue usage for a specific stress cycle or load set pair derived using the ASME Code Section III fatigue design air curves was multiplied by the  $F_{en}$  to account for environmental effects.

In the present report, the  $F_{en}$  expressions were updated using a much larger fatigue  $\epsilon$ -N database, primarily derived from extensive additional data provided from Japan. The updated expressions also address comments provided by interested stakeholders related to: (a) the constants in the  $F_{en}$  expressions that results in a  $F_{en}$  value of approximately 2 even when the strain rate is very high or temperature is very low, (b) the temperature dependence of  $F_{en}$  for carbon and low-alloy steels, and (c) the dependence of  $F_{en}$  on water chemistry for austenitic SSs.

This report also presents a brief description of the mechanisms for fatigue cracking in air and LWR coolant environments. Fatigue life is conventionally divided into two stages: initiation and propagation. In LWR environments, the initiation stage involves the growth of microstructurally small cracks characterized by decelerating crack growth. The propagation stage involves the growth of mechanically small cracks characterized by accelerating crack growth. The available fatigue  $\epsilon$ -N data indicated that LWR environments affect both the initiation and propagation of fatigue cracks. Two mechanisms are described in this report that potentially enhance both fatigue crack initiation and fatigue crack growth rates in LWR environments - slip oxidation/dissolution and hydrogen-induced cracking. The potential effects of dynamic strain aging on cyclic deformation and environmental effects are also discussed.

This report also presents a critical review of the ASME Code Section III fatigue adjustment factors of 2 on stress and 20 on life and assesses the possible conservatism in the choice of adjustment factors. Although these factors were intended to be conservative, they were not considered safety margins in the work presented in this report. Instead, these factors cover the effects of variables that influence fatigue lives but were not investigated in the experiments that were used to obtain the air fatigue design curves. Data available in the literature were reviewed to evaluate the factors on cycles that are needed to account for such differences and uncertainties. Monte Carlo simulations were performed to determine the factor on cycles needed to obtain a fatigue design curve in air that provided a conservative estimate of the number of cycles required to initiate a fatigue crack in reactor components. The results presented in the initial version of NUREG/CR-6909 indicated that, for carbon and low-alloy steels and austenitic SSs, the current ASME Code Section III requirements for a factor of 20 on cycles to account for the effects of material variability and data scatter, as well as size, surface finish, and loading history, may be decreased by at least a factor of 1.7. Thus, to reduce conservatism, fatigue design curves were developed based on the ANL fatigue life models and those curve were then adjusted for mean stress effects and by a factor of 2 on stress and 12 on cycles. These adjustments were made to account for the effects of four parameters - material variability and data scatter, size, surface finish, and loading sequence. In this report, the range of the these four parameters were modified and Monte Carlo simulations were repeated to determine the factor on cycles needed to obtain fatigue design curves in air. The results indicated that for carbon and low-alloy steels and austenitic SSs, a factor of 2 on stress and 10 on cycles are adequate to develop air fatigue design curves from the best-fit mean air curves.

However, until these results are further validated with applicable fatigue data  $\epsilon$ -N data, the air fatigue design curves presented in this report are based on factors of 2 on stress and 12 on life.

The  $F_{en}$  methodology was also validated by comparing the results of several experimental data sets obtained from fatigue tests that simulated actual plant conditions with estimated fatigue usage using the updated  $F_{en}$  expressions. The data sets represented fatigue tests with changing strain rate and/or temperature, complex loading that simulated a PWR safety injection transient, spectrum loading (i.e., random strain amplitudes), and pipe U-bend tests. In all cases, the results indicated that the predicted fatigue lives were in good agreement with the experimental values; the differences between the experimental and predicted fatigue lives were within a factor of two, which is within the experimental data scatter. The predicted fatigue lives for the tests with the complex strain loading cycle were lower than the experimental values by a factor of about 2. The reason for this deviation was not clear but may be unique to the specific test loading cycle. Nonetheless, although the predicted lives were all lower, the estimated values were within the range of data scatter.

Finally, the detailed procedure for incorporating environmental effects into ASME Code Section III fatigue evaluations is presented.

Revision 1 of this report represents a comprehensive and detailed expansion of the Revision 0 manuscript that incorporates significant additional background, test data, and test data descriptions. In addition, the content layout of the report was revised for clarity. As a result, the revisions made to the Revision 0 manuscript are not specifically identified throughout the text of this revision.



## ABBREVIATIONS

---

ANL	Argonne National Laboratory
ANN	Artificial Neural Network
ASME	American Society of Mechanical Engineers
ASTM	American Society for Testing and Materials
ATR	Advanced Test Reactor
BTP	Branch Technical Position
BNCS	Board on Nuclear Codes and Standards
BWR	Boiling Water Reactor
CGR	Crack Growth Rate
CLEE	Cyclic Life Environmental Effects
CT	Compact Tension
CUF	Cumulative Usage Factor
CVCS	Chemical and Volume Control System
CW	Cold Worked
da/dN	Fatigue Crack Growth Rate (expressed as the change in crack depth, da, divided by the number of applied cycles, dN)
DO	Dissolved Oxygen
DSA	Dynamic Strain Aging
E	Energy
EAC	Environmentally Assisted Cracking
EBR II	Experimental Breeder Reactor II
ECP	electrochemical Potential
EFD	Environmental Fatigue Data
EFT	Environmental Fatigue Testing
EPR	Electrochemical Potentiodynamic Reactivation
EPRI	Electric Power Research Institute
ETR	Experimental Test Reactor
FAP	Fatigue Action Plan
GE	General Electric Company
GSI	Generic Safety Issue
H	Hydrogen
HAZ	Heat Affected Zone
He	Helium
HWC	Hydrogen Water Chemistry
ID	Internal Diameter
IG	Intergranular

## ABBREVIATIONS (continued)

---

IHI	Ishikawajima-Harima Heavy Industries
INEL	Idaho National Engineering Laboratory
JAPEIC	Japan Power Engineering and Inspection Corporation
JNES	Japan Nuclear Energy Safety Organization
JNUFAD	Revised and Renamed Fatigue Database “FADAL” from Japan
KWU	Kraftwerk Union Laboratories
LEFM	Linear Elastic Fracture Mechanics
LWR	Light Water Reactor
MA	Mill Annealed
MEA	Materials Engineering Associates
MHI	Mitsubishi Heavy Industries
mm	Millimeters
MnS	Manganese Sulfide
MOU	Memorandum of Understanding
MPa	Megapascals
MPA	Materialprüfungsanstalt
MSC	Microstructurally Small Crack
N	Number of Cycles
$N_{\text{air}}$	Number of Cycles in Air
$N_{\text{water}}$	Number of Cycles in LWR Environment
Ni-Cr-Fe	Nickel-Chrome-Iron
NPS	Nominal Pipe Size
NRC	Nuclear Regulatory Commission
NWC	Normal Water Chemistry
OD	Outer Diameter
ORNL	Oak Ridge National Laboratory
ppb	Parts Per Billion
ppm	Parts Per Million
PSB	Persistent Slip Band
PVRC	Pressure Vessel Research Council
PWR	Pressurized Water Reactor
RCS	Reactor Coolant System
RG	Regulatory Guide
RHR	Residual Heat Removal
RMS	Root Mean Square
RT	Room Temperature
S	Sulfur

## **ABBREVIATIONS (concluded)**

---

SICC	Strain Induced Corrosion Cracking
SS	Stainless Steel
T	Temperature
TENPES	Thermal and Nuclear Power Engineering Society
TG	Transgranular
TMI	Three Mile Island
UTS	Ultimate Tensile Strength
VTT	Valtion Teknillinen Tutkimuskeskus (Finnish: Technical Research Center of Finland)
VVER	Voda-Vodyanoi Energetichesky Reaktor (Russian pressurized water reactor)
WRC	Welding Research Council
YS	Yield Strength



## **ACKNOWLEDGMENTS**

---

The authors are indebted to the Japan Nuclear Energy Safety Organization (JNES) for sharing their enormous fatigue ( $\epsilon$ -N) database for use in the evaluations documented in this report. The authors are also grateful to Bill Shack for his invaluable input and guidance in preparing this report. The authors acknowledge Yogen Garud for his contributions and helpful comments. This work was co-sponsored by the Office of Nuclear Regulatory Research, U.S. Nuclear Regulatory Commission; Project Manager: Gary L. Stevens and the Electric Power Research Institute (EPRI) as Cooperative Nuclear Safety Research under the Environmentally Assisted Fatigue Effects Addendum to the NRC/EPRI Memorandum of Understanding (MOU), under NRC Job Codes V6069 and V6269.



# 1. INTRODUCTION

---

The structural integrity of a metal component may gradually degrade when it is subjected to cyclic loading, even at magnitudes less than the design static loads, due to a well-known degradation mechanism called fatigue. The mechanism of fatigue damage can occur in flaw-free components by developing cracks during service. The American Society of Mechanical Engineers (ASME) Boiler and Pressure Vessel Code Section III, Subsection NB, which contains rules for the design of Class 1 components for nuclear power plants, recognizes fatigue as a possible mode of failure in pressure vessel steels and piping materials. Fatigue is a major consideration in the design of rotating machinery and aircraft, where the components are subjected to a very large number of cycles, i.e., high-cycle fatigue. In these situations, the primary concern is the endurance limit, which is the stress level below which an infinite number of cycles can be applied without fatigue failure. However, cyclic loadings on a reactor pressure boundary component occur because of changes in mechanical and thermal loadings as the system goes from one load state to another. The number of cycles applied during the design life of the component seldom exceeds 100,000 and is typically less than a few thousand (e.g., low-cycle fatigue). The main difference between high-cycle and low-cycle fatigue is that the former involves little or no plastic strain, whereas the latter involves strains in excess of the yield strain. Therefore, design curves for low-cycle fatigue are based on tests in which strain rather than stress is the controlled variable.

The ASME Code fatigue evaluation procedures are described in NB-3200, "Design by Analysis," and NB-3600, "Piping Design." The ASME Code fatigue analysis considers all transient loads based on the anticipated number of thermal and pressure transients, and for each load-cycle or load set pair, an individual fatigue usage factor is determined by the ratio of the number of cycles anticipated during the lifetime of the component to the allowable cycles. Figures I-9.1 through I-9.6 of Mandatory Appendix I to Section III of the ASME Boiler and Pressure Vessel Code specify fatigue design curves for various materials that define the allowable number of cycles as a function of applied stress amplitude. The cumulative usage factor (CUF) is the sum of the individual usage factors for all load set pairs, and ASME Code Section III requires that at each location the CUF, calculated based on Miner's rule, must not exceed unity for acceptable fatigue design.

Although the ASME Code Section III rules apply to Class 1 components, those fatigue design rules are sometimes applied to other classes of components to provide a robust fatigue design in situations where known fatigue issues exist or fatigue duty is high [e.g., Class 2 pressurized water reactor (PWR) feedwater nozzles]. As such, the methods described in this report are intended to apply to all components exposed to an LWR environment that utilize the fatigue calculation procedures from ASME Code Section III.

Revision 1 of this report represents a comprehensive and detailed expansion of the Revision 0 manuscript that incorporates significant additional background, test data, and test data descriptions. In addition, the content layout of the report was revised for clarity. As a result, the revisions made to the Revision 0 manuscript are not specifically identified throughout the text of this revision.

## 1.1 Definition of Fatigue Life

Before discussing the fatigue design curves used in the ASME Code Section III fatigue CUF analysis, it is important to first define "fatigue life" in terms of its use in this report. In the American Society for Testing and Materials (ASTM) Designation E 1823-09a<sup>1</sup> "Standard Terminology Relating to Fatigue and Fracture Testing," fatigue life is defined as "the number of

cycles of a specified character that a given specimen sustains before failure of a specified nature occurs. Fatigue life, or the logarithm of fatigue life, is a dependent variable.” Accordingly, the ASME Code fatigue design curves [i.e., stress amplitude ( $S_a$ ) vs. number of cycles ( $N$ ) curves] are generally considered to represent allowable number of cycles to failure. However, note that ASTM E1823 states that fatigue life is “failure of a specified nature.” Furthermore, Section 8.9 of ASTM Standard E 606-04<sup>2</sup> “Standard Practice for Strain-Controlled Fatigue Testing,” states that the definition of failure may vary with the ultimate use of the fatigue life information, and provides the following acceptable alternatives for determination of failure:

- (i) *Separation*: Total separation or fracture of the specimen into two parts at (1) some location within the uniform section of the uniform-gage specimen, or (2) the vicinity of the minimum diameter in the hourglass specimen.
- (ii) *Modulus Method*: For any specified number of cycles,  $N$ , during a fatigue test, the modulus for unloading following a peak tensile stress is defined as  $E_{NT}$  and the modulus for loading following a peak compressive stress is  $E_{NC}$ . Failure is defined as the number of cycles where the ratio  $E_{NT}/E_{NC}$  reaches one-half the value for the first cycle (i.e., is reduced by 50%). However, if total separation occurs first, as in item (i) above, fatigue life is defined by the number of cycles to separation.
- (iii) *Microcracking*: The existence of surface microcracks (e.g., as observed optically or by replicas) that are larger than some preselected size consistent with the test objective.
- (iv) *Force (Stress) Drop*: Failure is defined as the ability of a test specimen to sustain a tensile force (or stress). Failure is often defined as the point at which the maximum force (stress) or elastic modulus (as measured when unloading from a peak tensile stress) decreases by approximately 50% because of the presence of cracks. The exact method and the percentage drop should be documented.

In the fatigue  $\epsilon$ – $N$  data used to develop the original ASME Code best-fit or mean-data curves, failure was primarily defined as total separation or fracture of the specimen into two parts. However, in the fatigue tests performed during the last four decades, failure was defined according to the force (stress) drop method. In most of these tests, fatigue life was defined in terms of the number of cycles for the tensile stress to decrease 25% from its peak or steady-state value (i.e., 25% load drop). For the typical cylindrical specimens used in these studies, this corresponded to the number of cycles needed to produce approximately 3-mm-deep cracks in test specimens. Thus, the fatigue life of a material was described in terms of three parameters, viz., strain or stress, cycles, and crack depth. The best-fit curve to the existing fatigue  $\epsilon$ – $N$  data describes, for a given strain or stress amplitude, the number of cycles needed to develop a 3-mm deep crack. Note that, for consistency, all data used in this report were adjusted to be on an equivalent 25% load drop basis as discussed at the beginning of Chapter 3.

Based on the foregoing and the results of the majority of the test data evaluated, fatigue life is described in this report as the number of cycles of a specified strain amplitude that a specimen can sustain before the formation of a 3-mm-deep crack (i.e., an “engineering crack”). This equates to a 25% load drop in test specimens, and is assumed to equate to crack initiation in an actual component. Using this definition, a calculated fatigue CUF less than unity provides reasonable assurance that a fatigue crack has not formed in a component, and indicates that the probability of forming a crack in the component is low.



## 1.2 Air Fatigue Design Curves in Section III of the ASME Code

The ASME Code fatigue design curves, as given in Mandatory Appendix I of Section III, are based on strain-controlled tests of small polished specimens at room temperature in air. The data are typically obtained from fatigue tests conducted in accordance with ASTM Designation E 606-04 “Standard Practice for Strain-Controlled Fatigue Testing.” This practice covers the determination of fatigue properties of nominally homogeneous materials by the use of uniform gage section specimens subjected to axial strain-controlled, fully reversed (strain ratio,  $R$ , equal to -1) cycling. The practice is also applicable to hourglass specimens. The practice may be adapted to guide more general testing where strain or temperature may be varied according to application specific histories. The presentation and analysis of data are performed in accordance with ASTM Standard E 468, “Standard Practice for Presentation of Constant Amplitude Fatigue Test Results for Metallic Materials”<sup>3</sup> and ASTM Standard E 739, “Standard Practice for Statistical Analysis of Linear or Linearized Stress-Life ( $S$ - $N$ ) and Strain-Life ( $\epsilon$ - $N$ ) Fatigue Data.”<sup>4</sup> The guidance in Metals Handbook, Volume 8, “Fatigue Data Analysis”<sup>5</sup> can also be used. The definitions of terms related to fatigue testing are described in ASTM Standard E 1823, “Standard Terminology Relating to Fatigue and Fracture Testing.”<sup>6</sup>

The design curves were developed from the best-fit curves to the experimental fatigue-strain-vs.-life ( $\epsilon$ - $N$ ) data, which are expressed in terms of the Langer equation<sup>7</sup> of the form

$$\epsilon_a = A1(N)^{-n1} + A2, \quad (1)$$

where  $\epsilon_a$  is the applied strain amplitude,  $N$  is the fatigue life, and  $A1$ ,  $A2$ , and  $n1$  are coefficients of the model. Equation 1 may be written in terms of stress amplitude  $S_a$  instead of  $\epsilon_a$ . The stress amplitude is the product of  $\epsilon_a$  and elastic modulus  $E$ , i.e.,  $S_a = E \cdot \epsilon_a$  (stress amplitude is one-half the applied stress range). The current ASME Code best-fit or mean curve described in the Section III criteria document<sup>8</sup> for various steels is given by

$$S_a = \frac{E}{4\sqrt{N_f}} \ln \left( \frac{100}{100 - A_f} \right) + B_f, \quad (2)$$

where  $E$  is the elastic modulus (MPa),  $N_f$  is the number of cycles to failure, and  $A_f$  and  $B_f$  are constants related to reduction in area in a tensile test (percent) and endurance limit of the material at  $10^7$  cycles (MPa), respectively.<sup>7</sup> The current Code mean curves were obtained from Eq. 2 and  $A_f$  and  $B_f$  values of 68.5% and 149.2 MPa, 61.4% and 265.4 MPa, and 72.6% and 299.9 MPa, respectively, for carbon steels, low-alloy steels, and austenitic stainless steels (SSs).<sup>8</sup> Thus, using an elastic modulus of 206,843 MPa for carbon and low-alloy steels and 179,264 MPa for austenitic SSs, the mean curves are expressed for carbon steels, as

$$S_a = 59,734 (N_f)^{-0.5} + 149.2, \quad (3)$$

for low-alloy steel, as

$$S_a = 49,222 (N_f)^{-0.5} + 265.4, \quad (4)$$

and for austenitic SSs, as

$$S_a = 58,020 (N_f)^{-0.5} + 299.9. \quad (5)$$

The fatigue  $\varepsilon$ -N data are typically expressed by rewriting Eq. 1 as

$$\ln(N) = A - B \ln(\varepsilon_a - C), \quad (6)$$

where A, B, and C are constants; C represents the fatigue limit of the material; and B is the slope of the log-log plot of fatigue  $\varepsilon$ -N data. The ASME Code mean-data curves (i.e., Eqs. 3-5) may be expressed in terms of Eq. 6 as follows. The fatigue life of carbon steels is given by

$$\ln(N) = 6.726 - 2.0 \ln(\varepsilon_a - 0.072), \quad (7)$$

for low-alloy steels, by

$$\ln(N) = 6.339 - 2.0 \ln(\varepsilon_a - 0.128), \quad (8)$$

and, for austenitic SSs, the fatigue life corresponding to the fatigue design curve originally published in Section III of the ASME Code prior to the 2009b Addenda is given by

$$\ln(N) = 6.954 - 2.0 \ln(\varepsilon_a - 0.167), \quad (9)$$

and, as derived in Section 3.2.6, the fatigue life corresponding to the fatigue design curves in 2009b Addenda and later editions of the ASME Code, by

$$\ln(N) = 6.891 - 1.920 \ln(\varepsilon_a - 0.112), \quad (10)$$

where strain amplitude  $\varepsilon_a$  is in percent. The  $\varepsilon$ -N curve for austenitic SSs is also used for nickel-chromium-iron (Ni-Cr-Fe) alloys (e.g., Alloy 600).

The best-fit or mean-data curves (e.g., Eqs. 7-10) provide an estimate of the fatigue life that would lead to failure in 50% of the population under a given loading. However, as discussed later in this report, the ASME Code fatigue design curves are now defined to estimate acceptable fatigue life for at least 95% of the population under a given loading.

Another term that is often used in ASME Section III fatigue evaluations is fatigue limit (or endurance limit), which is defined as<sup>1</sup> “the limiting value of the median fatigue strength as the fatigue life,  $N_f$ , becomes very large.” However, certain materials (e.g., carbon and low-alloy steels and austenitic SSs) and environments preclude the attainment of a fatigue limit. Therefore, in the literature, fatigue limit is typically defined as a value of stress,  $S_N$ , for failure at a specified number of cycles, N (e.g., at  $10^6$  or  $10^{11}$  cycles).

The above  $\varepsilon$ -N curves describe the formation of engineering fatigue cracks in small, smooth test specimens in an air environment. To use the small-specimen data for actual reactor components, the best-fit  $\varepsilon$ -N curves for specimen data must be adjusted to account for the effects of variables that are known to affect fatigue life but were not accounted for in the small-specimen data. Such variables include mean stress, surface finish, size, and loading history. Furthermore, the best-fit curve represents the average behavior of the material. To obtain a curve that assures a low probability for formation of fatigue cracks, the small specimen curve must also be adjusted to account for data scatter and material variability.

The procedure used to develop the ASME Code fatigue design curves from the best-fit (or mean-data) curves for small specimens is as follows. First, the best-fit curves are adjusted to account for the effects of mean stress. This is necessary to account for mean stress effects not

considered during specimen testing, such as weld residual stress. Mean stress was accounted for using the modified Goodman relationship given by

$$S'_a = S_a \left( \frac{\sigma_u - \sigma_y}{\sigma_u - S_a} \right) \quad \text{for } S_a < \sigma_y, \quad (11)$$

and

$$S'_a = S_a \quad \text{for } S_a > \sigma_y, \quad (12)$$

where  $S'_a$  is the adjusted value of stress amplitude, and  $\sigma_y$  and  $\sigma_u$  are yield and ultimate strengths of the material, respectively. Equations 11 and 12 assume the maximum possible mean stress and typically give a conservative adjustment for mean stress. The original ASME Code Section III fatigue design curves were obtained by reducing the fatigue life at each point on the adjusted best-fit curve by a factor of 2 on strain (or stress) or 20 on cycles, whichever was more conservative.

As described in the Section III criteria document,<sup>8</sup> the factors of 2 and 20 are not safety margins, but rather adjustment factors that were applied to the small-specimen data to account for the effects of variables that are known to affect fatigue life but were not accounted for in the small-specimen data. These factors include (a) data scatter and material variability, (b) the differences in surface condition and size between the test specimens and actual reactor components, and (c) random load cycles as compared to constant strain cycles used to obtain the fatigue  $\epsilon$ -N data.

### 1.3 Subfactors Included in ASME Section III Air Fatigue Design Curves

In comments about the initial scope and intent of the ASME Code Section III fatigue design procedures, Cooper<sup>9</sup> states that the factor of 20 on life was regarded as the product of three subfactors:

Scatter of data (minimum to mean)	2.0
Size effect	2.5
Surface finish, atmosphere, etc.	4.0

Although the ASME Code Section III criteria document<sup>8</sup> states that these factors were intended to cover such effects as environment, Cooper<sup>9</sup> further states that the term “atmosphere” was intended to reflect the effects of an industrial atmosphere in comparison with an air-conditioned laboratory, which are different than the effects of a specific coolant environment. In addition, surface finish represented surface roughness of industrial-grade component surface compared to that of a polished test specimen. Subsubarticle NB-2160 (or Subsubarticle NG-2160 for core support structures) of Section III of the ASME Code states, “It is the responsibility of the Owner to select material suitable for the conditions stated in the Design Specifications (NCA-3250), with specific attention being given to the effects of service conditions upon the properties of the material.” The minimum contents of the Design Specifications are specified in Paragraph NCA-3252 of Section III of the ASME Code. Paragraph NCA-3252(a)(3) states that the Design Specifications shall include “the environmental conditions, including radiation.” The environmental conditions that are likely to influence the properties of materials used in nuclear

power plant structures and components include temperature, reactor coolant environment, and neutron irradiation.

Furthermore, Paragraph NB-3121 of Section III of the ASME Code (or Paragraph NG-3121 for core support structures) states, “It should be noted that the tests on which the fatigue design curves (Figs. I-9.0) are based did not include tests in the presence of corrosive environments which might accelerate fatigue failure.” Paragraph B-2131 in Nonmandatory Appendix B to Section III, “Owner’s Design Specifications,” states that the Owner’s Design Specification should provide information about, “any reduction to design stress intensity values, allowable stress, or fatigue design curves that is necessitated by environmental conditions.”

### 1.3.1 Effects of Reactor Coolant Environment on Fatigue Lives

Existing fatigue  $\epsilon$ -N data (Fig. 1) illustrate potentially significant effects of light water reactor (LWR) coolant environments on the fatigue resistance of carbon and low-alloy steels, wrought and cast austenitic SSs, and Ni-Cr-Fe alloys.<sup>10-75</sup> Small-scale laboratory fatigue test data indicate that under certain reactor operating conditions, fatigue lives of carbon and low-alloy steels can be a factor of 17 lower in the coolant environment than in air. Therefore, the factors in the ASME Code may be less conservative than originally intended.

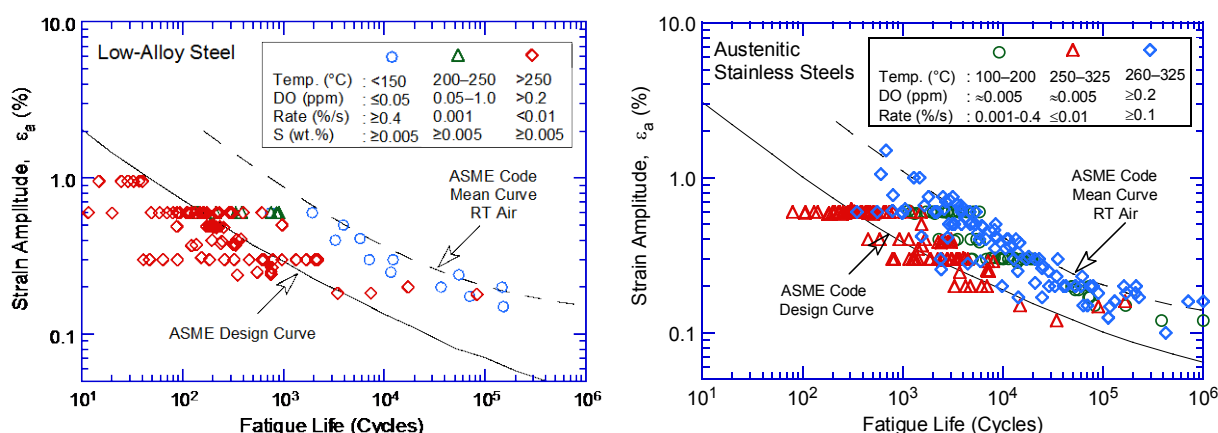


**Figure 1. Fatigue  $\epsilon$ -N data for low-alloy steels and austenitic stainless steels in water compared to ASME Air Design Curve; RT = room temperature.**

The fatigue  $\epsilon$ -N data are consistent with the much larger database on enhancement of crack growth rates (CGRs) in these materials in simulated LWR environments. The key parameters that influence fatigue life in these environments are temperature, the dissolved-oxygen (DO) level in the water, strain rate, strain (or stress) amplitude, and, for carbon and low-alloy steels, the sulfur content of the steel. The range of the values for these parameters within which environmental effects are significant has also been defined. If these critical loading and environmental conditions exist during reactor operation, then environmental effects may be significant and should be included in any associated ASME Code fatigue evaluations. Experience with nuclear power plants worldwide indicates that the critical range of loading and environmental conditions that leads to environmental effects on formation of fatigue cracks can and do occur during plant operation.<sup>56,76-92</sup> It therefore is important that component design include consideration of environmental effects to prevent premature fatigue failures.

Experience with operating nuclear power plants worldwide reveals that many failures of reactor components were attributed to fatigue; examples include piping, nozzles, valves, and pumps.<sup>76-83</sup> In most cases, these failures were associated with thermal loading due to thermal

stratification and striping, or mechanical loading due to vibratory loading. In piping components, several failures were associated with thermal loading due to thermal stratification and striping. Thermal stratification was typically caused by the injection of low-flow, relatively cold feedwater during plant startup, hot standby, and variations below 20% of full power, whereas thermal striping was caused by rapid, localized fluctuations of the interface between hot and cold feedwater.

Thermal loading due to flow stratification or striping was not typically included in the original design basis analyses for most U.S. nuclear power plants. Regulatory evaluation indicated that high-cycle thermal-stratification loading can occur in PWR surge lines as a result of in-surge and out-surge during heatup/cooldown transients.<sup>93</sup> During heatup or cooldown, when, the pressurizer water is heated to approximately 227°C (440°F), the hotter water can flow at a very low rate from the pressurizer through the surge line to the hot-leg piping over the cooler water layer in the piping. The thermal gradients between the upper and lower parts of the pipe can be as high as 149°C (300°F). As a result, all U.S. PWRs performed revised fatigue analyses to address thermal stratification effects in surge lines. Furthermore, the effect of these loadings may also be aggravated by corrosion effects due to a high-temperature aqueous environment. The increased fatigue duty caused by such thermal loading increases the importance of evaluating environmental effects.

The mechanism of cracking in feedwater nozzles and piping was attributed to corrosion fatigue or strain-induced corrosion cracking (SICC).<sup>84-86</sup> Case histories and identification of conditions that lead to SICC of low-alloy steels in LWR systems were summarized by Hickling and Blind. A review of significant occurrences of corrosion fatigue damage and failures in various nuclear power plant systems was presented in an Electric Power Research Institute (EPRI) report.<sup>56</sup> An assessment of the U.S. experience related to PWR primary system leaks observed during the period 1985 through 1996 was presented by Shah et al.<sup>88</sup>

Hirschberg et al. summarized the operating experience regarding thermal fatigue of non-isolable piping connected to PWR reactor coolant system (RCS).<sup>87</sup> Significant cracking occurred in non-isolable sections of the safety injection system and residual heat removal (RHR) system piping connected to the PWR coolant system.<sup>89,90</sup> At Farley, cracking occurred in the heat affected zone (HAZ) of the weld between the first elbow and the horizontal pipe, ≈0.9 m (36 in.) from the RCS cold-leg nozzle. At Tihange, the crack was located in the base metal of an elbow, ≈0.6 m (24 in.) from the RCS hot-leg nozzle. At the Genkai plant, cracking occurred in the RHR suction line at the weld between the first elbow downstream of the hot-leg nozzle and the horizontal pipe section. Cracking due to thermal fatigue also occurred in the safety injection system at Dampierre 1 and 2 plants, and in the chemical and volume control system (CVCS) in Obrigheim plant. In all cases, thermal cycling was caused by interaction of hot RCS fluid from turbulent penetration at the top of the pipe, and cold valve leakage fluid that stratified at the bottom of the pipe. At Genkai, the valve internals alternately shrunk and expanded causing periodic leakage of hot fluid through the stem packing and leak-off line into the elbow.

Thermal stratification, however, can occur even in the absence of valve leakage. The results of fatigue monitoring indicate that many PWR plants measured thermal-stratification cycling in the RHR suction line because of turbulence penetration of the hot leg fluid extending into the horizontal pipe section, which then stratified due to normal convection.<sup>87</sup> For thermal stratification, the length of the vertical pipe section of the RHR suction line must be short enough for the hot fluid to reach the horizontal pipe section, and the length of the horizontal pipe section must be long enough to cause sufficient heat losses for stratification to develop. A

typical temperature gradient of 49°C (120°F) was observed for typical cases of stratification, and temperature gradients as high as 177°C (350°F) were measured in some plants.

Non-isolable leaks due to thermal-stratification cycling also occurred in reactor coolant loop drain lines, excess letdown lines, and makeup/high pressure injection lines at the Three Mile Island (TMI), Loviisa 2, Mihama, and Oconee plants.<sup>87,88</sup> A leak in the cold-leg drain line [1.5 in. or 2 in. National Pipe Size (NPS)] occurred in the weld between the first elbow downstream of the loop nozzle and the horizontal pipe section at TMI, and in the elbow extrados at Oconee. In both cases, thermal stratification was caused by turbulence penetration of the RCS fluid periodically extending into the horizontal section and, because the pipe was not insulated, it stratified due to heat loss. The same mechanism caused a leak in the 2 in. NPS excess letdown line at Mihama. Whereas the Mihama line was insulated, stratification still occurred because the length of the horizontal section to the isolation valve was very long, resulting in significant heat loss.

Thermal fatigue caused leaks in a connecting pipe and shell of the regenerative heat exchanger in the CVCS at Tsuruga 2,<sup>91,92</sup> and in a 250-mm pipe section of the heat exchanger bypass on the RHR system at Civaux 1.<sup>76</sup> Thermal-hydraulic mock-up tests indicate that at Tsuruga, superposition of low-frequency temperature gradients due to changes in the flow pattern and high frequency temperature fluctuations due to mixing of the bypass flow and main flow caused thermal fatigue.<sup>91,92</sup>

Cracking also occurred in austenitic SS channel heads in an experimental test loop used for stress corrosion cracking studies in a simulated PWR environment.<sup>94</sup> Cracks were observed in a region that was subjected to temperature fluctuations between 170 and 190°C at a frequency of 0.05 Hz. The cracks initiated on the inner surface; the cracking morphology was essentially transgranular with fatigue-like striations visible in some regions of the fracture surface. Thermal fatigue, with possible effects of the PWR coolant environment, was concluded to be the root cause of these failures.<sup>94</sup>

Such cracking in non-isolable pipe sections due to thermal cycling was generally termed as high-cycle fatigue, i.e., it occurs at stress levels that correspond to allowable fatigue cycles of  $10^5$  or higher. The current understanding of turbulent penetration is not sufficient to accurately predict the frequency of thermal cycling associated with that phenomenon. Environmental effects on fatigue crack initiation may be significant in low-DO water at stress levels above the threshold value and at strain rates less than 0.4 %/s.

Lenz et al.<sup>85</sup> showed that in feedwater lines, the strain rates are  $10^{-3}$ – $10^{-5}$ %/s due to thermal stratification and  $10^{-1}$ %/s due to thermal shock. They also reported that thermal stratification is the primary cause of crack initiation due to SICC. Stephan and Masson<sup>95</sup> subjected a full-scale mock-up of the steam generator feedwater system to various regimes of stratification. After 4000 cycles of applied loading, destructive examination performed between two locations where stable states of stratification occurred revealed small cracks, 1.4–2.0 mm deep, in the weld region. The fatigue usage factors calculated with elastic and cyclic elastic-plastic computations gave values of 1.3–1.9. Because the average DO level in the water was approximately 5 ppb, which corresponds to the maximum admissible value under normal operating conditions (power greater than 25% nominal power) in French PWRs, environmental effects on life were expected to be minimal and environmental correction factors were not applied in the computations of the fatigue usage factor.

Full-scale mock-up tests to generate thermal stratification in a pipe in a laboratory confirmed the applicability of laboratory data to component behavior.<sup>96</sup> The material, loading, and

environmental conditions were simulated on a 1:1 scale using only thermo-hydraulic effects. Under the conditions of strain rate and strain range typical of thermal stratification in these piping systems, the coolant environment has a significant effect on fatigue crack initiation.<sup>12,29,30</sup>

Finally, a study conducted on SS pipe bend specimens in simulated PWR primary water at 240°C concluded that reactor coolant environment has a significant effect on the fatigue life of SSs.<sup>97-99</sup> Relative to fatigue lives in an inert environment, lives in a PWR environment at strain amplitudes of 0.4% and 0.6% were decreased by factors of 2.9 and 1.4 at strain rates of 0.0005 %/s and 0.01 %/s, respectively. These values show very good agreement with the values predicted from the Argonne National Laboratory (ANL) models presented later in this report for incorporating environmental effects into the ASME Code Section III fatigue evaluations.

### 1.3.2 Effects of Neutron Irradiation

The potential effects of neutron irradiation on the fatigue life of reactor structural materials such as low-alloy pressure vessel steel, austenitic stainless steels, and Ni-Cr-Fe alloys and their weld metals are not fully characterized. Irradiation effects were not included in the ASME Code Section III fatigue evaluations performed for reactor core support structures and reactor internal components. The majority of the existing data on the effects of neutron irradiation resulted from fatigue crack growth tests on austenitic SSs that were irradiated in fast reactors [primarily Experimental Breeder Reactor II (EBR-II)] at test temperatures of 427 (800°F) and 593°C (1100°F).<sup>100-104</sup> The CGR test results indicated that for Type 304 and 316 SS irradiated at 405-410°C (760-770°F) to  $1.2 \times 10^{22}$  n/cm<sup>2</sup> ( $E > 0.1$  MeV) fluence, the fatigue CGRs at 427°C (800°F) were up to a factor of 2 higher than those for unirradiated material at low values of stress intensity factor range ( $\Delta K$ ) [less than 40 ksi in.<sup>1/2</sup> (43.9 MPa m<sup>1/2</sup>)], but were lower for higher  $\Delta K$  values. These observations were reversed at 593°C (1100°F). Crack growth rates were comparable or lower at higher values of  $\Delta K$ . A similar behavior was observed for Type 316 weld metal. Tests on Type 304 and 316 SS irradiated in a thermal reactor [Advanced Test Reactor (ATR)] at 288°C (550°F) to  $1.8 \times 10^{21}$  n/cm<sup>2</sup> ( $E > 0.1$  MeV) and tested at 427°C (800°F) showed superior resistance to crack growth; CGRs were 25 to 50% lower than those for unirradiated material.<sup>105</sup> Based on these studies EPRI concluded,<sup>106</sup> “The work of several researchers suggest that neutron irradiation does not result in a further reduction in fatigue properties and in some cases suggest an improvement.”

Other limited fatigue  $\epsilon$ - $N$  data on materials irradiated under LWR conditions and tested at LWR operating temperatures also showed significant differences in the microstructure and microchemistry of LWR irradiated materials, and materials irradiated in fast neutron test reactors. Specifically, cavities and helium (He) bubbles were observed in austenitic SSs irradiated at a temperature of 320°C (608°F) to high neutron fluence levels in PWRs. Such microstructures could lead to embrittlement of the material.<sup>107</sup> Therefore, fatigue data on LWR irradiated materials should be developed to further quantify the effects of neutron irradiation on fatigue lives.

Fatigue  $\epsilon$ - $N$  data on irradiated Type 308 SS weld metals showed moderate decreases in fatigue lives in the low-cycle regime and superior fatigue lives in the high-cycle regime.<sup>108</sup> Similar effects from neutron irradiation were also observed on the room-temperature fatigue  $\epsilon$ - $N$  behavior of Type 347 SSs irradiated in the Engineering Test Reactor (ETR) at 60°C (140°F) to total integrated fast flux ( $> 1$  MeV) exposures of  $5.5 \times 10^{25}$ ,  $1.1 \times 10^{26}$ , and  $1.6 \times 10^{26}$  n/m<sup>2</sup>, as shown in Fig. 2a.<sup>109</sup> Neutron irradiation decreased the room-temperature fatigue lives of Type 347 SSs at high strain amplitudes (above 0.35%) and had beneficial effects on fatigue lives at low strain amplitudes (below 0.25%). The decreases in fatigue lives increased with increased

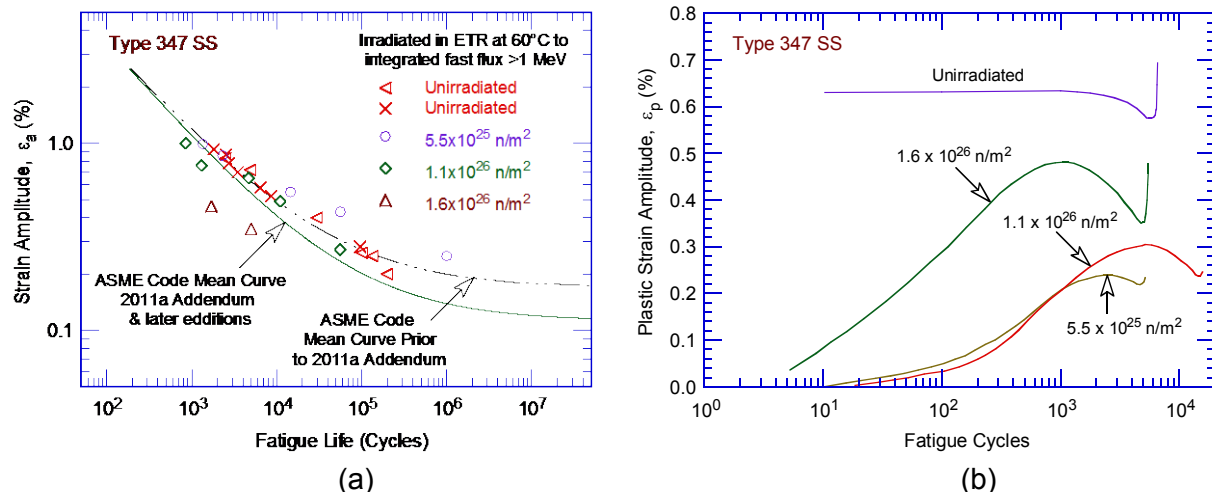


**Figure 2. The effects of neutron irradiation on fatigue lives of Type 347 SSs at room temperature: (a) the fatigue  $\epsilon$ -N behavior, and (b) variations in plastic strain amplitude as a function of fatigue cycles (Ref. 109).**

total neutron doses. The reductions in fatigue lives were likely related to the irradiation-induced decreases in ductility of the materials.

The fatigue test results also indicated significant differences in the cyclic hardening behavior of the irradiated materials relative to unirradiated materials. Typically, at room temperature, austenitic SSs exhibited strain softening after the initial cyclic hardening during the first ten cycles. For the irradiated Type 347 SSs, although total strain was held constant, the plastic strain varied significantly during the fatigue tests, as shown in Fig. 2b. The plastic strains were insignificant initially and increased gradually during the fatigue tests due to strain softening until a later stage where plastic strains started to decrease due to secondary strain hardening and formation of fatigue cracks in the specimens. The extent of strain softening increased with increased neutron doses (Fig. 2b). The rapid increases in plastic strains near the end of the tests were associated with specimen fracture. In contrast, the unirradiated Type 347 SSs exhibited slight strain hardening and plastic strain decreased at a very low rate; later, the materials also showed faster decreases in plastic strains because of secondary strain hardening and formation of fatigue cracks. Thus, the impact of irradiation on fatigue life is not readily apparent from these data because of several competing factors.

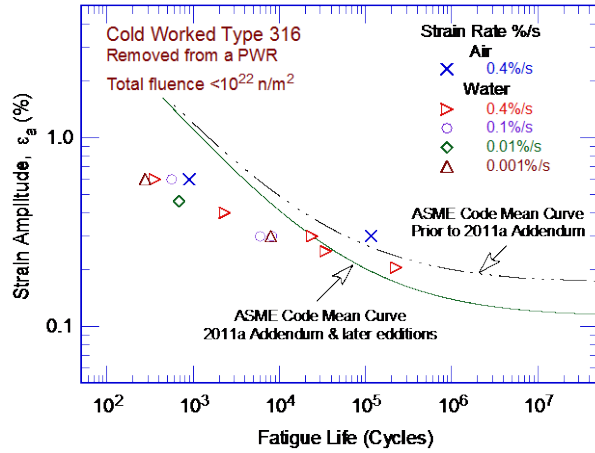
The fatigue  $\epsilon$ -N data on cold-worked (CW) Type 316 SS tube materials and solution-annealed Type 304 bar materials removed from an operating PWR are shown in Figs. 3 and 4, respectively.<sup>110</sup> The data were obtained in simulated PWR water at 325°C (617°F) on CW Type 316 SS tube specimens with a 6.48 mm outer diameter and a 0.71 mm wall thickness. The tube specimens were irradiated to fluence values of less than  $10^{22}$ ,  $2 - 6 \times 10^{25}$ , and greater than  $3 \times 10^{26}$  n/m<sup>2</sup> ( $E > 0.1$  MeV), while the 5.08-mm diameter cylindrical specimens of Type 304 SS were irradiated to fluence levels ranging from  $5 \times 10^{25}$  to  $10^{26}$  n/m<sup>2</sup> ( $E > 0.1$  MeV). However, the baseline fatigue data for the unirradiated materials for the same heats of SSs were not available. To determine the possible effects of specimen configuration (i.e., solid cylindrical vs. thin-walled tube specimens), fatigue tests using the two specimen geometries were conducted on another heat of CW Type 316 SS in air at 325°C. The results indicated that the fatigue strengths of the solid specimens were 1.4 times those of the cylindrical tube specimens. The ASME Code Section III best-fit mean air curves for austenitic SSs are shown in the plots in Figs. 3 and 4 for comparison. Based on these test results, the authors concluded, "The fatigue life of irradiated SS was longer than that of unirradiated SS in the range of this research, that is,



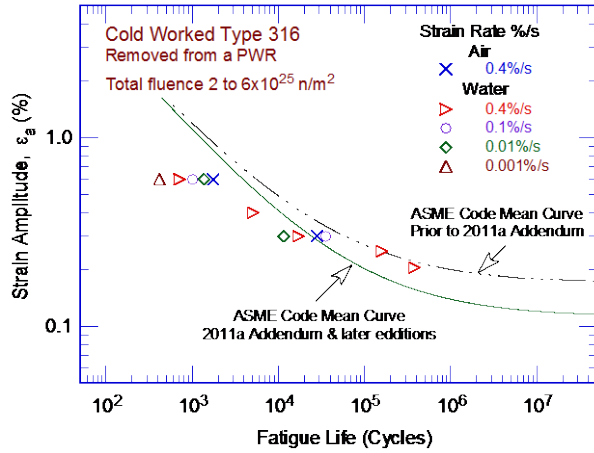
strain amplitude was less than 0.6%. This increase in fatigue strength was considered due to an increase of tensile strength after irradiation.”

In the absence of sufficient baseline fatigue data on unirradiated materials, the above conclusion that the fatigue lives of irradiated materials are longer than those of unirradiated materials is not fully justified. For example, the fatigue lives of irradiated Type 304 SSs in air are close to the ASME Code Section III best-fit mean curves. However, the effects of neutron irradiation are not available because there is insufficient fatigue  $\epsilon$ -N data in air on unirradiated materials for these heats of Type 304 SSs. The fatigue data for irradiated CW Type 316 SSs were obtained on thin-walled tube specimens, and were not consistent with the ASME Code Section III mean air curve for austenitic SSs because the majority of the data were obtained from solid cylindrical specimens. The experimental  $\epsilon$ -N behavior showed a lower  $\epsilon$ -N slope than that for the ASME Code Section III mean curve (Fig. 3). Even after adjusting by a factor of 1.4 on strain to account for the effect of specimen geometry, the fatigue lives in air at 0.3% strain amplitude fall to the right of the ASME Code Section III mean curve, whereas, the fatigue lives at 0.6% strain amplitude are significantly to the left. The primary reason for this inconsistency is likely caused by inadequate specimen size (tube specimens with 0.71-mm thick wall) for fatigue tests performed at high strain amplitudes. However, the fatigue data in Figs. 3 and 4 show that fatigue lives of austenitic SSs were decreased in a PWR primary water environment. Except for the data on CW Type 316 SSs irradiated to a fluence greater than  $3 \times 10^{26}$  n/m<sup>2</sup>, the data for irradiated materials and the data for irradiated Type 304 SSs show lower fatigue lives in PWR primary water environment compared to those in air. The effects of the environment increase with decreasing strain rates.

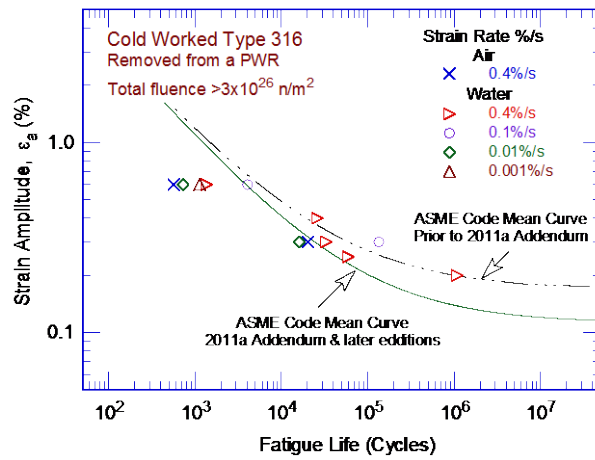
The limited available data are inconclusive with regard to the impact of irradiation on the fatigue lives of materials exposed to LWR environments. Although some small-scale laboratory fatigue  $\epsilon$ -N test data indicate that neutron irradiation decreases the fatigue lives of austenitic SSs, particularly at high strain amplitudes, it is not possible to quantify the impact of irradiation on the prediction of fatigue lives based on the limited data currently available. Additional fatigue data on reactor structural materials irradiated under LWR operating conditions are needed to determine whether there are measurable effects of neutron irradiation on the fatigue lives of these materials and, if so, to better define how those impacts may be quantified. In the absence of such data, the methods described in this report are considered appropriate for application to materials exposed to significant levels of irradiation, such as SS reactor internals components, when mandated by regulation or required by the current licensing basis.



(a)



(b)



(c)

Figure 3.

Strain amplitude vs. fatigue life data in 325°C air or simulated PWR primary water environments for CW Type 316 SS irradiated to (a) less than  $10^{22}$ , (b)  $2\text{--}6 \times 10^{25}$ , and (c) greater than  $3 \times 10^{26}$  n/m<sup>2</sup> ( $E > 1.0$  MeV) (Ref. 110).

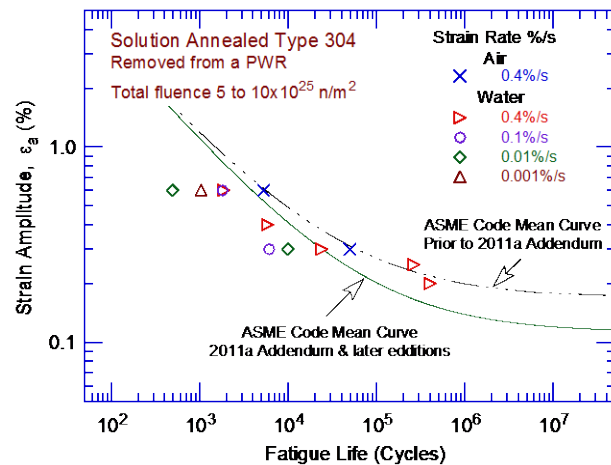


Figure 4.

Strain amplitude vs. fatigue life data in 325°C air and simulated PWR primary water environments for Type 304 SS irradiated to  $5 \times 10^{25}$ – $10 \times 10^{25}$  n/m<sup>2</sup> ( $E > 0.1$  MeV) (Ref. 110).

## 1.4 Modeling of Environmental Effects

In 1991, the U.S. Nuclear Regulatory Commission (NRC) issued a draft Branch Technical Position (BTP) for fatigue evaluation of nuclear plant components for license renewal. The BTP raised a concern about the adequacy of the ASME Code in addressing environmental effects on fatigue resistance of materials for operating PWRs and boiling water reactors (BWRs), whose primary-coolant pressure boundary components were constructed as specified in Section III of the ASME Code. In 1993, the Commission directed the NRC staff to treat fatigue as a potential safety issue within the existing regulatory process for operating reactors. The staff developed a Fatigue Action Plan (FAP) to resolve three principal issues: (a) adequacy of fatigue resistance of older vintage plants designed to the United States of America Standard B31.1 Code that did not require an explicit fatigue analysis of components, (b) effect of LWR environments on the fatigue resistance of primary pressure boundary materials, and (c) appropriate corrective action required when ASME Code fatigue allowable limits are exceeded, i.e., when the CUF is greater than unity.

The Idaho National Engineering Laboratory (INEL) assessed the significance of ANL-developed interim fatigue design curves, by performing fatigue evaluations of a sample of components in the reactor coolant pressure boundary.<sup>111</sup> In all, six locations were evaluated from facilities designed by each of the four U.S. nuclear steam supply system vendors. Selected components from older vintage plants designed according to the B31.1 Code were also included in the evaluation. Conservatism in the original fatigue evaluations, e.g., actual loading cycles instead of assumed cycles, was removed, and fatigue usage was evaluated with a fatigue design curve that considered the effects of the coolant environment. The results indicated that most of the locations had a CUF of less than the ASME Code limit of 1.0 for 40 years. The risk to reactor-coolant pressure boundary components from failure due to fatigue was assessed under Generic Safety Issue (GSI) 78, "Monitoring of Fatigue Transient Limits for the Reactor Coolant System," and GSI-166, "Adequacy of Fatigue Life of Metal Components."<sup>112</sup> Based on these studies, it was concluded<sup>113</sup> that no immediate action was necessary to address the three fatigue issues identified in the FAP. A risk study indicated that fatigue failure of piping was not a significant contributor to core damage frequency. Based on the risk assessment, a backfit to incorporate environmental effects into the fatigue analyses of operating plants was not justified.<sup>114</sup>

However, because the NRC studies were less certain that the conservatism in the original fatigue calculations could be used to account for an additional 20-years of operation, the NRC staff recommended that environmental effects be considered by evaluating the sample locations in the INEL study (NUREG/CR-6260)<sup>111</sup> for plants pursuing license renewal. These recommendations were documented in GSI-190, "Fatigue Evaluation of Metal Components for 60-year Plant Life."<sup>112</sup> Based on probabilistic analyses and sensitivity studies, interactions with the industry, and various programs available to licensees to manage the effects of aging, it was concluded that no generic regulatory action was required. For some components, although cumulative probabilities of crack initiation and through-wall cracks approached 1.0 for the renewal period, the maximum failure rate was generally low, in the range of  $10^{-2}$  through-wall cracks per year.

In addition, the predicted failure rates were generally associated with high CUF locations and components with thin walls; in most cases, any leakage that might result from these through-wall cracks was estimated to be small and not likely to lead to core damage. However, the calculations that supported the resolution of this issue indicated the potential for an increase in the frequency of pipe leaks as plants continue to operate. Thus, the NRC staff recommended that aging-management programs for license renewal should address component fatigue, including the effects of the reactor coolant environment. It should, however, be noted that when

the INEL study was performed, it was not known that the effects of high-temperature reactor coolant environment on fatigue cracking of austenitic SSs are greater in low-DO environments than in high-DO environments. Thus, the six sample locations evaluated in the INEL study may not necessarily be the bounding locations for some plants, and additional plant-specific component locations than those considered in NUREG/CR-6260 should be included in the fatigue CUF evaluations, including the effects of environment.

In 1991, the ASME Board on Nuclear Codes and Standards (BNCS) requested the Pressure Vessel Research Council (PVRC) to examine the existing worldwide  $\epsilon$ -N data and develop recommendations for the ASME. The PVRC compiled and evaluated fatigue  $\epsilon$ -N data related to the effects of LWR coolant environments on the fatigue life of pressure boundary materials; the results were summarized by Van Der Sluys and Yukawa.<sup>115,116</sup> The staff agreed with the concept of using an environmental correction factor ( $F_{en}$ ) approach to obtain fatigue usage reflecting environmental effects for ASME Code Section III fatigue evaluations. This information was forwarded to the appropriate ASME Code committee.<sup>117</sup>

An analysis of the existing fatigue  $\epsilon$ -N data and the procedures for incorporating environmental effects into ASME Code Section III fatigue evaluations was presented in several review articles<sup>115,116,118-126</sup> and ANL reports.<sup>10,12,13,45-47</sup> The fatigue  $\epsilon$ -N data in air and LWR environments were also examined from the standpoint of fracture mechanics and CGR data.<sup>127</sup> Further details are presented in the next section of this report. The key material, loading, and environmental parameters that influence the fatigue lives of carbon, low-alloy, and austenitic stainless steels were identified, and the range of these key parameters where environmental effects are significant, was defined. Two approaches were proposed for incorporating the environmental effects into ASME Section III fatigue evaluations for primary pressure boundary components in operating nuclear power plants: (a) develop new fatigue design curves for LWR applications, or (b) use an environmental fatigue correction factor to account for the effects of the coolant environment.

In the first approach, following the same procedures used to develop the fatigue design curves in ASME Code Section III, environmentally adjusted fatigue design curves were developed from fits to experimental data obtained in LWR environments. Interim fatigue design curves that address environmental effects on the fatigue life of carbon, low-alloy, and austenitic stainless steels were first proposed by Majumdar et al.<sup>129</sup> However, as mentioned above, the "interim" fatigue design curve for austenitic SSs was based on little or no data in low-DO environments. As a result, at the time of the development of the interim design curves, it was not known that the effects of high-temperature reactor coolant environment on fatigue lives are greater in low-DO environments than in high-DO environments. Fatigue design curves based on a more rigorous statistical analysis of experimental data were developed by Keisler et al.<sup>130</sup> These design curves were subsequently revised based on updated ANL models.<sup>10,12,45,46</sup> However, in LWR environments, the fatigue life of carbon and low-alloy steels, Ni-Cr-Fe alloys, and austenitic SSs depends on several loading and environmental parameters. Therefore, such an approach requires development of several design curves to cover all possible environmental conditions encountered during plant operation. Depending on the number of such design curves for the desired loading and environmental conditions, development of additional curves may be a significant undertaking.

The second approach, proposed by Higuchi and Iida in 1991,<sup>19</sup> considers the effects of reactor coolant environments on fatigue life in terms of an environmental fatigue correction factor,  $F_{en}$ , that is defined as the ratio of fatigue life in air at room temperature to that in water under reactor operating conditions. To incorporate environmental effects into fatigue evaluations, this approach required that the fatigue usage factor for a specific stress cycle or load set pair, based

on the ASME Code Section III design fatigue curves, be multiplied by the environmental fatigue correction factor. Specific expressions for  $F_{en}$ , based on the ANL fatigue life models, were developed.<sup>10,45</sup> Such an approach is relatively simple for application to previously-developed fatigue analyses and is recommended in this report. A similar methodology was also developed in Japan by the Environmental Fatigue Data (EFD) Committee of the Thermal and Nuclear Power Engineering Society (TENPES) under the Project on Environmental Fatigue Testing (EFT). The EFT was also supported by the Japan Power Engineering and Inspection Corporation (JAPEIC) and the Japan Nuclear Energy Safety (JNES) Organization, and some utilities.<sup>131-135</sup> Updated technical results were published in a JNES report,<sup>136</sup> JNES-SS-1005 “Environmental Fatigue Evaluation Method for Nuclear Power Plants.” All of that data were considered in the results documented in this report.

In 2007, the original version of NUREG/CR-6909,<sup>137</sup> which is the technical basis document for NRC Regulatory Guide (RG) 1.207, Revision 0, “Guidelines for Evaluating Fatigue Analyses Incorporating the Life Reduction of Metal Components Due to the Effects of the Light Water Reactor Environment for New Reactors,” presented an overview of the existing fatigue  $\epsilon$ -N data for carbon and low-alloy steels, Ni-Cr-Fe alloys, and wrought and cast austenitic SSs in air and LWR environments. The existing fatigue  $\epsilon$ -N data were evaluated to (a) identify the various material, environmental, and loading parameters that influence fatigue cracking, and (b) establish the effects of key parameters on the fatigue lives of these steels. Fatigue life models, presented in earlier reports for estimating fatigue life as a function of material, loading, and environmental conditions were updated using the fatigue  $\epsilon$ -N database available at that time. The report also described the  $F_{en}$  approach for incorporating effects of LWR environments into ASME Section III fatigue evaluations, and presented a critical review of the ASME Code fatigue adjustment factors of 2 on stress (or strain) and 20 on life to assess the possible conservatism in the choice of adjustment factors. The  $F_{en}$  methodology was identified as applicable to all reactor coolant pressure boundary components exposed to reactor water that require an ASME Section III fatigue CUF calculation.

This report presents a revision to the original version of NUREG/CR-6909 in its entirety. The  $F_{en}$  expressions were updated using a much larger fatigue  $\epsilon$ -N database. The additional data include the JNES data summarized in JNES-SS-1005 on carbon and low-alloy steels, wrought and cast austenitic SSs, and Ni-Cr-Fe alloys, and their associated weld metals, tested in air and LWR environments,<sup>136</sup> and fatigue  $\epsilon$ -N test results from the open literature on several heats of carbon and low-alloy steels tested in BWR environments.<sup>138-146</sup> we have not used any bending tests in our environmental effects analysis. Most of the data evaluated for this report were obtained from completely reversed, axial, strain-controlled tests on small laboratory specimens. The results from a small number of bending tests were also considered for austenitic stainless steels in air (see Table 6 in Section 3.2.1), Ni-Cr-Fe alloy steels in air (see Table 9 in Section 3.3), and carbon and low-alloy steels in water (see Table 10 in Section 4.1.1). These data were included to improve the best fit evaluation of the fatigue life data. Section 3.2.2 includes figures that support the use of these bending test data for austenitic stainless steels, which show that the bending test data points fall evenly on both side of the best fit curve of all the data. Only a small number of high-cycle fatigue tests conducted in load control were considered.

The updated environmental fatigue expressions in this report also address comments from interested stakeholders related to: (a) the constants in the  $F_{en}$  expressions that results in a  $F_{en}$  value of approximately 2 even when the strain rate is very high or temperature is very low, (b) the temperature dependence of  $F_{en}$  for carbon and low-alloy steels, and (c) the dependence of  $F_{en}$  on water chemistry for austenitic SSs. Finally, the updated methodology described in this report applies to any component exposed to the LWR environment that requires an ASME CUF

calculation as part of its design, or if required by the safety basis for the component, or if required by the plant current licensing basis, unless otherwise justified.

In addition, the appropriateness of a strain threshold and the possible effects of hold periods were also evaluated. The potential effects of dynamic strain aging (DSA) on cyclic deformation and environmental effects are discussed.<sup>147-153</sup> The  $F_{en}$  methodology proposed in this report was validated by comparing the results of five different experimental data sets obtained from fatigue tests that simulate actual plant conditions with estimates of fatigue usage adjusted for environmental effects using the updated  $F_{en}$  expressions. The five data sets represent fatigue tests with (a) changing strain rate and/or temperature,<sup>154</sup> (b) complex loading (actual PWR transient),<sup>155-157</sup> (c) spectrum loading (random strain amplitudes),<sup>158,159</sup> (d) thermal fatigue of a stepped pipe,<sup>160</sup> and (e) pipe U-bend tests.<sup>98,99</sup> Appendix C of this report presents a sample application of the  $F_{en}$  methodology that is intended to address by example some of the practical issues identified by interested stakeholders associated with the  $F_{en}$  calculations.<sup>161</sup>

## 2. MECHANISM OF FATIGUE

### 2.1 Formation of an Engineering Crack in Air

Deformation and microstructural changes in the surface grains of metals are responsible for fatigue cracking. During cyclic straining, the irreversibility of dislocation glide leads to the development of surface roughness. Strain localization in persistent slip bands (PSBs) results in the formation of extrusions and intrusions. With continued cycling, microcracks ultimately form in PSBs or at the edges of slip-band extrusions. At high strain amplitudes, microcracks form in notches that develop at grain, twin, or phase boundaries (e.g., ferrite/pearlite) or by cracking of second-phase particles (e.g., sulfide or oxide inclusions).

Once a microcrack forms, it continues to grow along its primary slip plane or a PSB as a Mode II (shear) crack in Stage I growth (where the orientation of the crack is usually at  $45^\circ$  to the stress axis). At low strain amplitudes, a Stage I crack may extend across several grain diameters before the increasing stress intensity of the crack promotes slip on planes other than the primary slip plane. A dislocation cell structure normally forms at the crack tip. Because slip is no longer confined to planes at  $45^\circ$  to the stress axis, the crack begins to propagate as a Mode I (tensile) crack, normal to the stress axis in Stage II growth. At high strain amplitudes, the stress intensity is quite large and the crack propagates entirely by the Stage II process. Stage II crack propagation continues until the crack reaches an engineering size. The two stages of fatigue crack growth in smooth specimens are shown in Fig. 5.

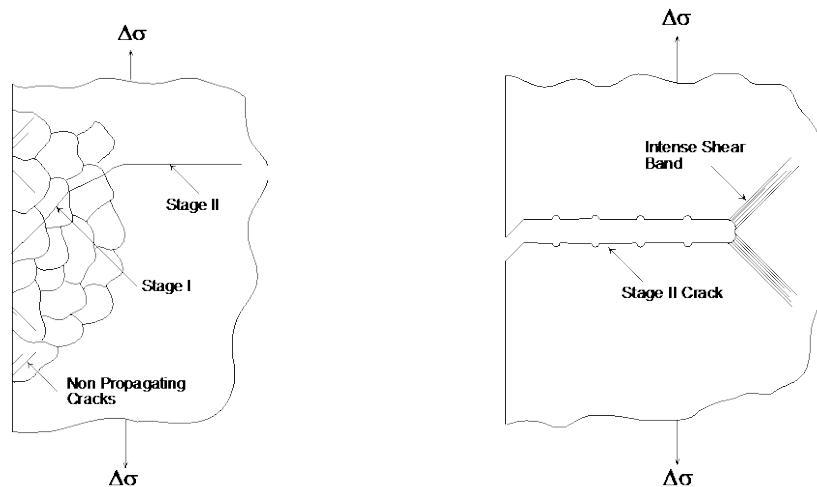


**Figure 5. Two stages of fatigue crack growth in smooth test specimens.**

In air or mildly corrosive environments, Stage II cracking is characterized by fatigue striations. The process of Stage II fatigue crack growth and formation of fatigue striations<sup>162</sup> is illustrated in Fig. 6. As tensile load is applied, slip bands form at the double notch or “ears” of the crack tip (Fig. 6b). The slip bands widen with further straining, causing blunting of the crack tip (Fig. 6c). Crack surfaces close during compressive loading and slip is reversed, producing ears at the edges of the blunt crack tip (Figs. 6d and 6e). The ears are observed as fatigue striations on the fracture surface. However, there is not necessarily a 1:1 correlation between striation spacing and fatigue cycles. At high strain amplitudes, several striations may be created during one cycle, whereas at low strain amplitudes, one striation may represent several cycles.

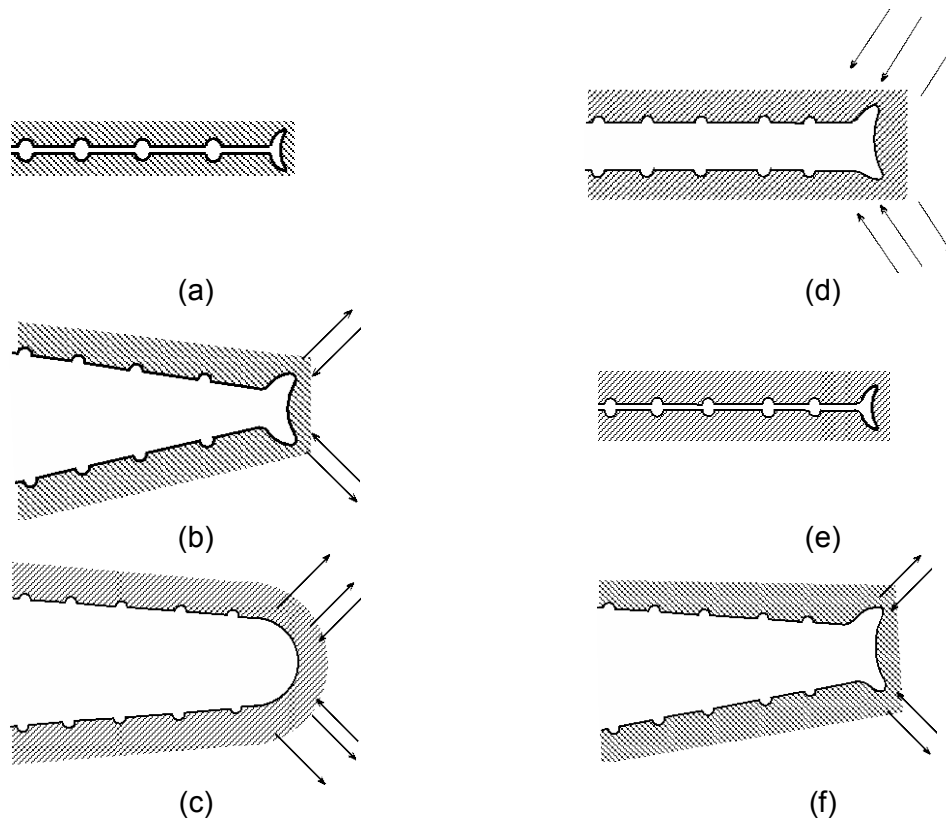


**Figure 6. Schematic illustration of the plastic blunting process of fatigue crack growth in Stage II: (a) zero load; (b) small tensile load; (c) maximum tensile load, widening of slip bands; (d) crack closure, and formation of “ears” at crack tip; (e) maximum compressive load; (f) small tensile load in the subsequent cycle.**

Thus, the formation of surface cracks and their growth as shear and tensile cracks (Stages I and II growth) to an “engineering” size (e.g., a 3-mm-deep) crack constitute the fatigue life of a material, which is represented by the fatigue  $\epsilon$ - $N$  curves. Fatigue life is conventionally divided into two stages: initiation, expressed as the number of cycles required to form microcracks on the surface; and propagation, expressed as the number of cycles required to propagate the surface cracks to an engineering size. Thus, the definition of a CUF value of unity, as described in Section 1.1, conventionally includes both initiation and some amount of propagation.

An alternative approach considers fatigue life of engineering structures and components to be entirely composed of the growth of short fatigue cracks, i.e., cracks less than “engineering” size.<sup>163,164</sup> For polycrystalline materials, the time for the formation of surface cracks is negligible. During cyclic loading, surface cracks, 5  $\mu\text{m}$  or longer, form early in life at surface irregularities either already in existence or produced by slip bands, grain boundaries, second-phase particles, etc. (Fig. 7).<sup>11,165-167</sup> Thus, fatigue life may be considered to constitute propagation of cracks from 10 to 3000  $\mu\text{m}$  long, and fatigue damage in a material may be considered as the current size of the fatigue crack.<sup>164</sup> However, the growth rates of short cracks cannot be predicted accurately from fracture mechanics methodology based on the range of stress intensity factor ( $\Delta K$ ) alone. Under the same  $\Delta K$  loading, short fatigue cracks (i.e., cracks having lengths comparable to the unit size of the microstructure) grow at a faster rate than longer fatigue cracks.<sup>168</sup> In addition, shorter cracks can grow at  $\Delta K$  values below those predicted from linear elastic fracture mechanics (LEFM). The differences between the



growth rates of short and long cracks are attributed to interactions with microstructural features, contributions of crack closure with increasing crack length, effects of mixed mode crack propagation, and an inadequate characterization of the crack tip stress/strain fields associated with short cracks.

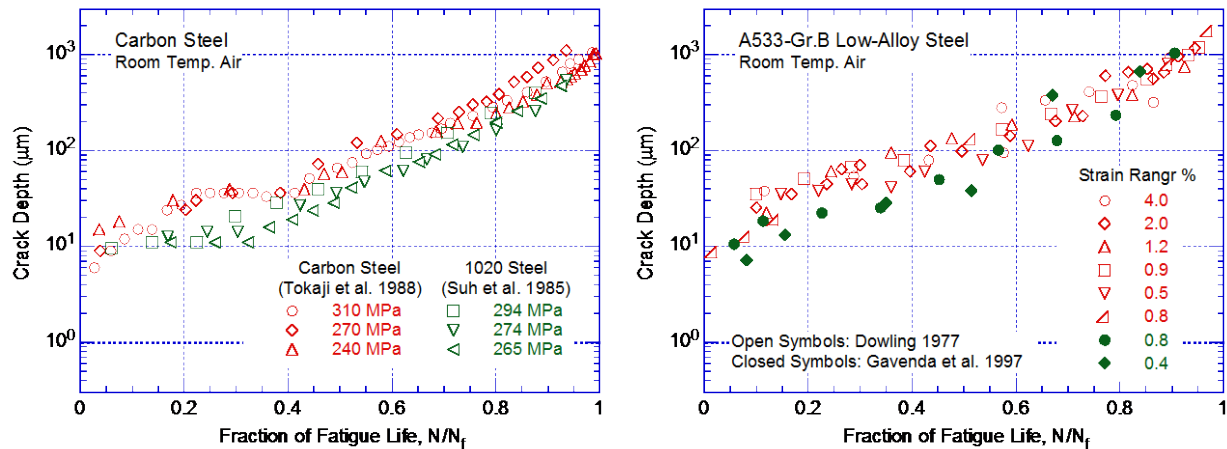


**Figure 7. Crack depth plotted as a function of fractional life for carbon and low-alloy steels tested in air (Refs. 11,165-167).**

A schematic illustration of the two stages of fatigue crack growth including (a) initiation, and (b) propagation, is shown in Fig. 8. The initiation stage involves growth of “microstructurally small cracks” (MSCs), characterized by decelerating crack growth (Region AB in Fig. 8a). The propagation stage involves growth of “mechanically small cracks,” characterized by accelerating crack growth (Region BC in Fig. 8a). The MSCs correspond to Stage-I cracks and grow along slip planes as shear cracks in the early stage of growth. The growth of the MSCs is very sensitive to microstructure.<sup>11,166-171</sup> For MSCs, microstructural effects are strong because of Stage I growth, i.e., crystallographic growth. The growth rates are markedly decreased by grain boundaries, triple points, and phase boundaries. In ferritic-pearlitic steels, fatigue cracks initiate and propagate preferentially in the ferrite phase that forms as long allotriomorphs at prior austenite phase boundaries.<sup>166,170,171</sup> The ferrite/pearlite phase boundaries act as strong barriers to crack propagation, and growth rates decrease significantly when small cracks grow into the pearlite from the ferrite.<sup>166</sup> Limited data suggest that microstructural effects are more pronounced at negative stress ratios; the compressive component of the applied load plays an important role in the formation of Stage I facets and formation of cracks.<sup>169</sup>

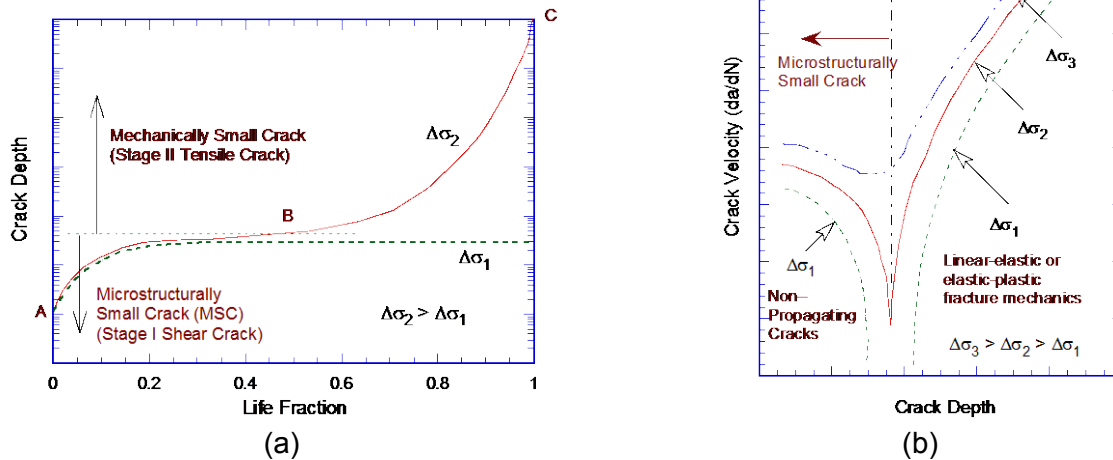


**Figure 8. Schematic illustration of (a) growth of short cracks in smooth specimens as a function of fatigue life fraction, and (b) crack velocity as a function of crack depth.**

Fatigue cracks greater than a critical size, show little or no influence of microstructure and are considered mechanically small cracks.<sup>169</sup> Mechanically small cracks correspond to Stage II (tensile) cracks, which are characterized by striated crack growth, with the fracture surface normal to the direction of maximum principal stress. The growth of mechanically small cracks is characterized in terms of the J-integral range,  $\Delta J$ , and CGR data in air and LWR environments. The CGRs estimated from smooth specimen  $\varepsilon$ -N data show good agreement with CGRs obtained on fracture mechanics compact tension (CT) specimens in air and water environments.<sup>13</sup>

Various criteria, summarized in Section 5.4.1 of Ref. 12, are used to define the crack depth for transition from microstructurally to mechanically small cracks. The transition crack depth is a function of applied stress ( $\sigma$ ) and the microstructure of the material. For completely reversed fatigue straining, the transition from a MSC to a mechanically small crack for several materials is estimated to be approximately 8 times the unit size of the microstructure;<sup>169</sup> actual values may range from 150 to 250  $\mu\text{m}$ .

At low stress levels ( $\Delta\sigma_1$ ) (Fig. 8a), the transition from MSC growth to accelerating crack growth does not occur. This circumstance represents the fatigue limit for a smooth specimen. Although cracks can form below the fatigue limit, they grow to engineering size only at stresses greater than the fatigue limit. The fatigue limit for a material is applicable only for constant loading conditions. Under variable loading conditions, MSCs can grow at high stresses ( $\Delta\sigma_3$ ) (Fig. 8b) to depths larger than the transition crack depth, and then continue to grow at stress levels below the fatigue limit ( $\Delta\sigma_1$ ).

As discussed in Section 1.1, fatigue life is described in this report as the number of cycles of a specified strain amplitude that a specimen can sustain before the formation of a 3-mm-deep crack (i.e., an “engineering crack”). This is assumed throughout this report to equate to crack initiation in an actual component. Using this definition, a calculated fatigue CUF less than unity provides reasonable assurance that a fatigue crack has not formed in a component, and indicates that the probability of forming a crack in the component is low.

## 2.2 Fatigue Cracking in LWR Environments

The available small-scale laboratory fatigue test data indicate a significant decrease in fatigue life of reactor structural materials in LWR environments. The extent of environmental effects depends on the applied strain, temperature, strain rate, DO in the water, and for carbon and low-alloy steels, the sulfur content in the steel. Although the structure and cyclic hardening behavior of carbon and low-alloy steels are distinctly different, there is little or no difference in susceptibility to environmental degradation of fatigue life of these steels. Reduction in fatigue life in LWR coolant environments may arise from easy formation of surface microcracks consisting of the growth of MSCs (i.e., the initiation stage) and/or an increase in growth of mechanically small cracks (i.e., propagation stage). The formation and growth characteristics of fatigue cracks are discussed in detail for carbon and low-alloy steels and wrought and cast austenitic SSs in the following sections. Similar information for Ni-Cr-Fe alloys is very limited.

### 2.2.1 Carbon and Low-Alloy Steels

Carbon and low-alloy steels tested in air show slight discoloration, while those tested in water develop a gray/black corrosion scale and are covered with magnetite ( $\text{Fe}_3\text{O}_4$ ) at all DO levels. Hematite ( $\alpha\text{-Fe}_2\text{O}_3$ ) forms on these materials at DO levels above 200 parts per billion (ppb).<sup>20,22,172</sup> The amount of hematite increases with increasing DO levels in the water.<sup>20</sup> Studies on the pitting behavior of carbon and low-alloy steels<sup>173,174</sup> in high-purity water indicate that pitting corrosion does not occur in these steels at reactor operating temperatures in low-DO PWR environments [typically less than 0.01 parts per million (ppm) DO], and at temperatures above 200°C in water that contains 0.1–0.2 ppm DO, which represents normal BWR water chemistry. However, even under these conditions, micropits form in both types of steels due to dissolution of manganese sulfide (MnS) inclusions<sup>18</sup> or by anodic reaction in the S contaminated matrix<sup>175</sup> close to sulfide inclusions. These micropits and cavities can act as stress raisers and provide preferred sites for the formation of fatigue cracks.

#### 2.2.1.1 Effects of Surface Micropits

The strain rate effects in water are such that fatigue life decreases with decreasing strain rate. These effects are often explained by a higher density of micropits at lower strain rates. Some investigators argue that the longer test durations for slow strain rate tests result in a higher density of micropits and, therefore, shorter periods for the formation of surface microcracks.<sup>18</sup> However, if the presence of micropits was responsible for the reduction in fatigue lives of carbon and low-alloy steels in LWR environments, then specimens pre-exposed to high-DO water followed by testing in air should also show a decrease in fatigue life.

Figure 9 shows a comparison of the fatigue lives of carbon and low-alloy steels tested in high-DO water at 288°C with the fatigue lives of carbon and low-alloy steels preoxidized at 288°C for 30–100 hours in water with 0.6–0.8 ppm DO and then tested in either air or low-DO water with less than 0.01 ppm DO.<sup>40,41,176</sup> The fatigue lives of the preoxidized specimens were identical to those of the unoxidized specimens; life was expected to decrease if surface micropits facilitate the formation of fatigue cracks. Only a moderate decrease in life was observed for both preoxidized and unoxidized specimens tested in low-DO water. Furthermore, if micropits were responsible for the decrease in fatigue lives in LWR environments, then the fatigue limit of these steels should be lower in water than in air.

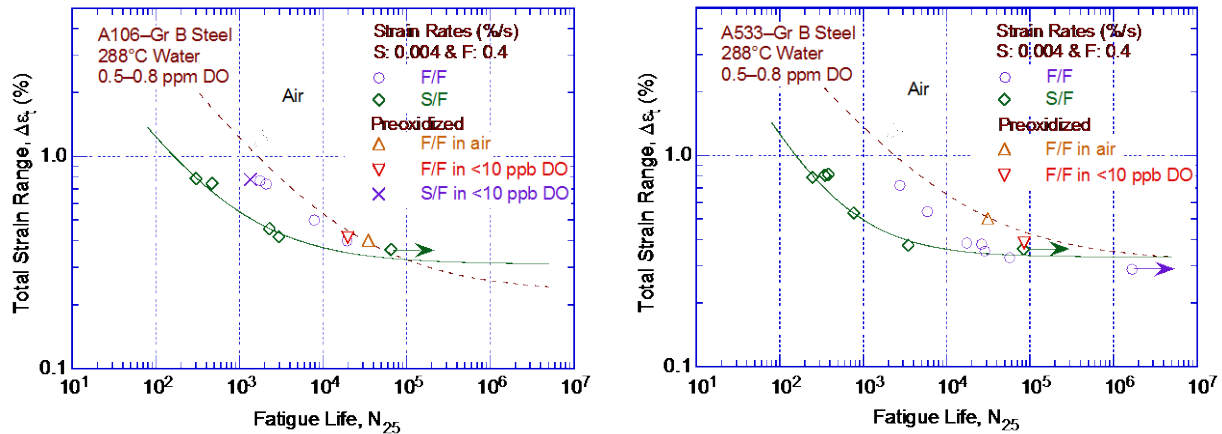


**Figure 9. Fatigue life of carbon and low-alloy steel specimens in high-DO water at 288°C compared with the fatigue life of specimens preoxidized in high-DO water and tested in either air or low-DO water at 288°C (Refs. 40,41,176).**

The extent of fatigue cracking, as measured by the number of cracks with depths greater than 10  $\mu\text{m}$ , along longitudinal sections of carbon and low-alloy steel specimens as a function of strain range in air, simulated PWR, and high-DO water was also investigated.<sup>176</sup> The results indicated that, with the exception of low-alloy steel tested in simulated PWR water, the water environment had no effect on the frequency (number per unit gauge length) of cracks. For similar loading conditions, the number of cracks in the specimens tested in air and high-DO water was identical, although fatigue lives were lower by a factor of approximately 8 in water. If the reduction in life was caused by enhanced crack nucleation, the specimens tested in high-DO water should have shown a higher number of cracks. Detailed metallographic evaluations of the fatigue test specimens<sup>176</sup> also indicated that, irrespective of environment, cracks in carbon and low-alloy steels nucleated along slip bands, carbide particles, or at the ferrite/pearlite phase boundaries.<sup>11,176</sup>

#### 2.2.1.2 Mechanisms of Corrosion Fatigue

The environmental enhancement of fatigue crack growth in pressure vessel steels in high-temperature oxygenated water and the effects of sulfur content, loading rate, and flow velocities are well documented.<sup>177-189</sup> Dissolution of MnS inclusions changes the water chemistry near the crack tip, making it more aggressive. This results in enhanced crack growth rates because either (a) the dissolved sulfides decrease the repassivation rate, which increases the amount of metal dissolution for a given oxide rupture rate;<sup>189</sup> or (b) the dissolved sulfide poisons the recombination of hydrogen (H) atoms liberated by corrosion, which enhances H uptake by the steel at the crack tip.

The enhanced CGRs in LWR environments are attributed to either slip oxidation/dissolution<sup>189-193</sup> or hydrogen-induced cracking mechanisms.<sup>194-196</sup> For the slip oxidation/dissolution mechanism, a critical concentration of sulfide ( $\text{S}^{2-}$ ) or hydrosulfide ( $\text{HS}^-$ ) ions, which are produced by the dissolution of sulfide inclusions in the steel, is required at the crack tip for environmental effects to occur. The crack tip is supplied with  $\text{S}^{2-}$  and  $\text{HS}^-$  ions as the advancing crack intersects the sulfide inclusions, and the inclusions dissolve in the high-temperature water environment. Sulfide ions are removed from the crack tip by one or more of the following processes: (a) diffusion due to a concentration gradient, (b) ion transport due to an electrochemical potential (ECP) gradient, (c) pumping action due to cyclic loading on the crack, and/or (d) fluid flow induced within the crack due to the flow of coolant outside the crack. The

morphology, size, and distribution of sulfide inclusions and the probability of advancing the crack to intercept the sulfide inclusions are important parameters affecting growth rates of carbon and low-alloy steels in LWR environments.<sup>183,185-188</sup>

The requirements for a slip dissolution model are that a protective oxide film is thermodynamically stable to ensure that a crack will propagate with a high aspect ratio without degrading into a blunt pit, and that a strain increment occurs to rupture that film and thereby expose the underlying matrix to the environment, Fig. 10. Once the passive oxide film is ruptured, crack extension is controlled by dissolution of freshly exposed surfaces and by the oxidation characteristics. The effect of the environment increases with decreasing strain rate. The mechanism assumes that environmental effects do not occur during the compressive load cycle because during that period water does not have access to the crack tip. Ford, Andresen, et al.<sup>191,192</sup> proposed that the average environmentally assisted crack growth rate,  $\bar{V}_t$  (centimeters/second), is related to the crack tip strain rate,  $\dot{\epsilon}_{ct}$ , by the relationship

$$\bar{V}_t = A(\dot{\epsilon}_{ct})^n, \quad (13)$$

where the constants A and n depend on the material and environmental conditions at the crack tip. There is a lower limit of crack propagation rate associated either with blunting when the crack tip cannot keep up with the general corrosion rate of the crack sides, or with the fact that a critical level of sulfide ions cannot be maintained at the crack tip. For example, the latter condition may occur when the crack growth rate falls below a critical value such that a high concentration of sulfide ions cannot be maintained at the crack tip. The critical crack growth rate at which this transition occurs depends on the DO level, flow rate, and S content of the steel.

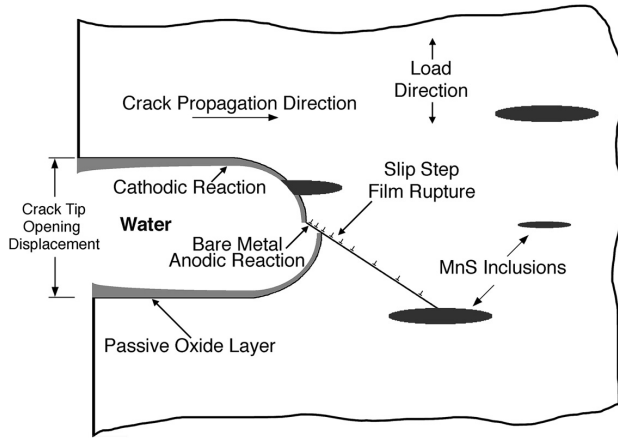


**Figure 10.**  
**Schematic illustration of slip**  
**oxidation/dissolution process.**

The average critical velocity,  $\bar{V}_{in}$  (millimeters/second), for initiation or cessation of environmentally assisted cracking (EAC), was shown to depend on the balance between sulfide supply rate and mass transport away from the crack tip.<sup>178,182</sup> Initiation of EAC requires a critical concentration of sulfide ions at the crack tip, which is supplied with sulfide ions as the advancing crack intersects the sulfide inclusions, and the inclusions dissolve in the high-temperature water. Crack growth studies in high-temperature, low-DO environment (i.e., less than 0.05 ppm DO) indicate that  $\bar{V}_{in}$  is given by

$$\bar{V}_{in} = \frac{1.27 \times 10^{-6}}{a}, \quad (14)$$

where  $a$  is the crack depth (mm). Thus, for a 2.54 mm crack depth, a minimum average crack velocity of  $5 \times 10^{-7}$  millimeters/second is required to produce the sulfide ion concentration for environmental effects on crack growth to be pronounced.<sup>182</sup> In addition, the critical velocity must be maintained for a minimum crack extension of 0.33 mm to achieve the concentration of sulfide ions needed for initiating environmental enhancement of growth rates.<sup>178</sup> Equation 14 indicates that the minimum crack velocity to initiate environmental effects increases with decreasing crack depth. For crack depths between 0.01 and 3 mm, crack velocities in the range of  $1.27 \times 10^{-4}$  to  $4.23 \times 10^{-7}$  millimeters/second are required to cause a measurable reduction in fatigue lives of carbon and low-alloy steels in low-DO water. For smooth cylindrical fatigue specimens, these growth rates are not achieved under the loading conditions typically used for fatigue  $\epsilon$ - $N$  data, which suggests that environmental effects on fatigue lives in low-DO environments are not significant. This behavior is consistent with the existing fatigue  $\epsilon$ - $N$  data; for most compositions of carbon and low-alloy steels, only moderate reductions in fatigue life (less than a factor of 2) are observed in 288°C water containing less than 0.01 ppm DO, which is within the data scatter.

In addition, consistent with the slip dissolution mechanism assumption mentioned previously, it is assumed that environmental enhancement of crack propagation does not occur during the compressive load cycle because, during that period, the water does not have access to the crack tip due to crack closure. The total crack advance during a fatigue cycle is given by the summation of crack advance in air due to mechanical factors, and crack advance during the tensile load cycle (i.e., increasing strain) from a slip-dissolution mechanism, once the tensile strain increment exceeds the fracture strain of the oxide.

Hydrogen-induced cracking (Fig. 11) of carbon and low-alloy steels is caused by hydrogen produced by the oxidation reaction at the crack tip that is partly absorbed into the metal; it interacts with MnS inclusions and leads to the formation of cleavage cracks at the inclusion matrix interface. Crack extension occurs by linkage of the cleavage cracks. Other hydrogen-induced fracture processes may also enhance growth rates in LWR environments. According to the decohesion mechanism, significant accumulation of hydrogen at or near the crack tip decreases the cohesive interatomic strength of the lattice.<sup>197</sup> Hydrogen-induced bond rupture ahead of the crack tip links up with the main crack resulting in discontinuous, but enhanced crack growth. Furthermore, adsorbed hydrogen lowers the surface energy of the metal, thus facilitating crack growth at a lower fracture stress level. In addition, hydrogen can cause localized crack tip plasticity by reducing the stress required for dislocation motion.<sup>198</sup> Note that the hydrogen produced at the crack tip by this mechanism is not related to the hydrogen content of the bulk fluid; as a result, hydrogen content of the bulk fluid is not a parameter in the  $F_{en}$  expressions.

Both the slip-oxidation/dissolution and hydrogen-induced cracking mechanisms are dependent on oxide rupture rates, passivation rates, and liquid diffusion rates. Therefore, it is difficult to differentiate between the two mechanisms or to establish their relative contribution to crack growth rates in LWR environments. However, fatigue crack morphologies in test specimens indicate that both the slip-oxidation/dissolution and hydrogen-induced cracking mechanisms are important for environmental effects of the fatigue lives of carbon and low-alloy steels in LWR environments. A change in fracture appearance from ductile striations in air to brittle facets or cleavage-like fracture in LWR environments lends the greatest support for hydrogen-induced cracking.<sup>142,143,187,195,196</sup>

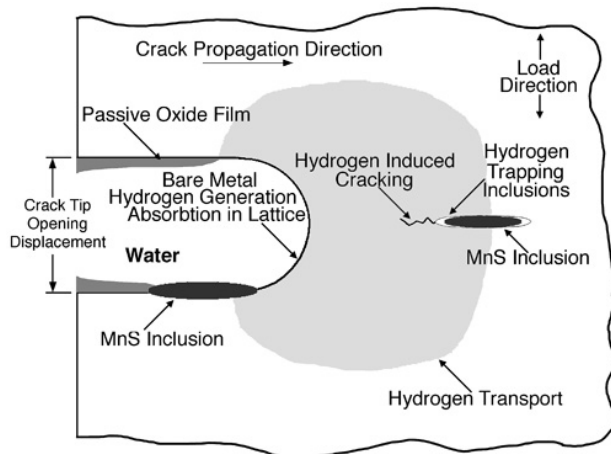


**Figure 11.**  
**Schematic illustration of**  
**hydrogen-induced cracking**  
**of low-alloy steel.**

The fatigue crack morphologies of carbon and low-alloy steels in a BWR environment also show a strong dependence and change with strain rate. At high strain rates, surface crack morphology is predominantly a zigzag pattern and inclined to the loading axis, whereas entirely straight crack morphology normal to the loading axis is observed at slow strain rates.<sup>10,139,143</sup> The surface crack morphology in A106-Gr. B carbon steel tested in air and high-DO water at 288°C is shown in Fig. 12. In addition, high strain rates lead to a rough fracture surface with the typical fan-like or quasi-cleavage cracking pattern, and slow strain rates result in a flat, nondescript fracture surface.<sup>139,142</sup> The propagation of fatigue cracks in A106-Gr. B carbon steel is shown in Fig. 13. In air, fatigue cracks grow along relatively soft ferrite regions and avoid the hard pearlite regions. In contrast, in a high-DO BWR environment, fatigue cracks appear to grow straight, normal to the stress axis, and through both the soft ferrite and the hard pearlite regions. Such crack growth characteristics are consistent with the slip-oxidation/dissolution mechanism and crack extension by anodic dissolution of the matrix in a corrosive environment.

Wu and Katada<sup>142</sup> attributed the change in crack morphology to a change in the corrosion fatigue mechanism from hydrogen-induced cracking to a slip-oxidation/dissolution mechanism with decreasing strain rate. The authors reasoned that, during cyclic loading in high temperature water, plastic deformation induces slip bands at the crack tip along the maximum shear or preferred slip directions. The extrusion of slip bands may rupture the protective oxide film at the crack tip. The slip bands are the favored path for hydrogen transportation and the interfaces between the matrix and inclusions or precipitations in the region of maximum hydrostatic tension are the preferred traps for hydrogen. Thus, hydrogen tends to accumulate at these sites and embrittle them. As a result, at high strain rates, fatigue cracking preferentially occurs along the slip bands or preferred slip directions as well as the matrix/inclusions interfaces, which results in macroscopically tortuous fatigue cracks and a rough fracture surface. However, at low strain rates, fatigue crack growth in high-temperature water is controlled by the film-rupture/oxidation-dissolution mechanism, which results in macroscopically straight fatigue cracks and a relatively flat, featureless fracture surface.



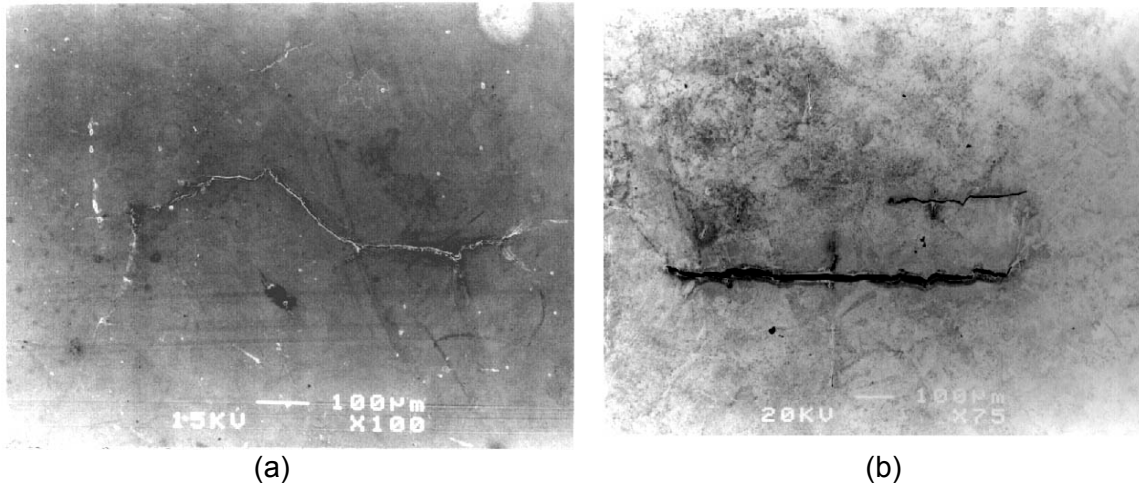


**Figure 12. Fatigue cracks on gauge surfaces of A106-Gr. B carbon steel tested in (a) air and (b) high-DO water at 288°C (Ref. 10).**

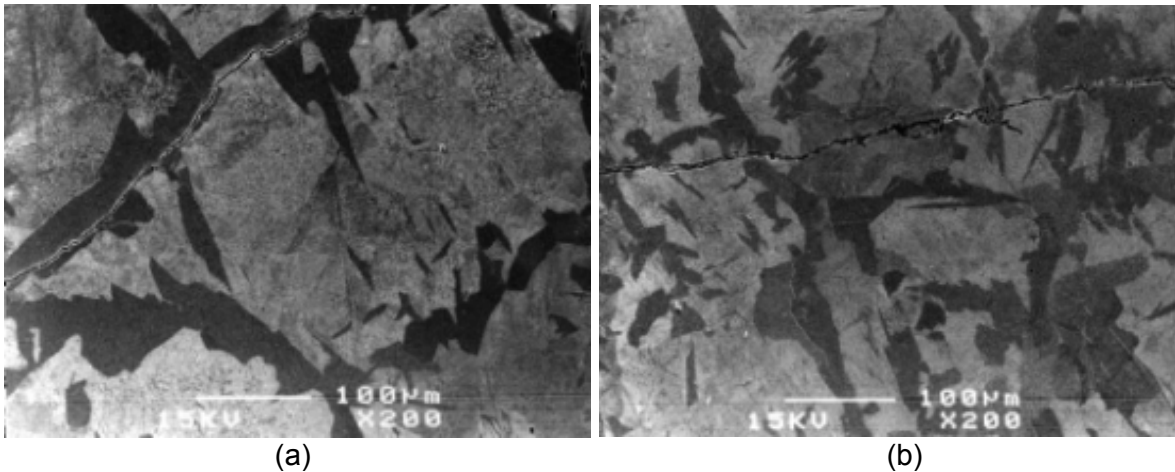


**Figure 13. Fatigue cracks along longitudinal sections of A106-Gr. B carbon steel tested in (a) air and (b) high-DO water at 288°C (Ref. 10).**

#### 2.2.1.3 Effects of Dynamic Strain Aging (DSA)

Several studies showed that DSA may play a significant role in the cyclic deformation process of carbon and low-alloy steels in LWR environments.<sup>147-151</sup> DSA occurs in alloys containing solutes that segregate strongly to dislocations resulting in strong interactions between the solute and the stress-strain field of the dislocations, which leads to dislocation pinning, Fig. 14. In carbon and low-alloy steels, DSA occurs due to interstitial elements such as nitrogen and carbon. DSA is sufficiently rapid to occur during fatigue straining and produces a variety of inhomogeneous deformations such as serrated yielding, jerky or serrated flow, etc. These effects depend on temperature and strain rate.



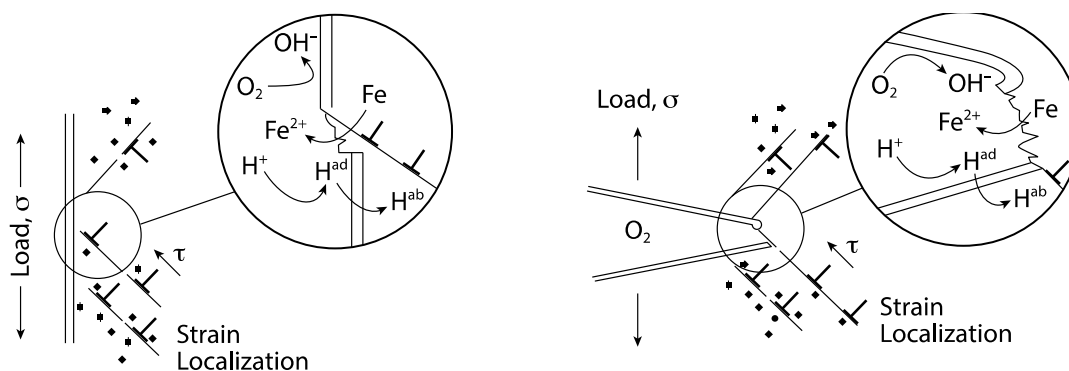


**Figure 14. (a) Fatigue crack initiation and (b) crack growth in DSA susceptible low-alloy steel exposed to high-temperature water environment (Ref. 147).**

Under certain combinations of temperature and strain rate conditions, DSA may significantly affect the EAC behavior of carbon and low-alloy steels by increasing the yield and tensile strength, the strain hardening exponent, the creep rate, and the crack-tip strain and strain rate.<sup>149</sup> DSA also results in planar deformation, an increase in dislocation density and inhomogeneous localization of deformation. These factors favor brittle crack extension and rupture of the protective oxide film, thereby enhancing crack advance by either anodic dissolution or hydrogen embrittlement processes. In high-temperature water, the synergistic interactions between EAC and DSA during fatigue straining may be rationalized as follows:<sup>149</sup>

- Hydrogen vacancies produced by the corrosion reaction at the crack tip enter the steel and hydrogen diffuses to strong trapping sites inside the crack-tip maximum hydrostatic stress region (e.g., MnS inclusions) ahead of the crack tip.
- These sites act as initiation sites for local quasi-cleavage cracking, as well as void formation, and these microcracks link with the main crack.
- In addition, at a given macroscopic strain due to external loads, the microscopic strain in steels that are susceptible to DSA is higher because of strain localization to small areas, which leads to higher rates and larger steps of oxide film rupture. As a result, the slip oxidation/dissolution process enhances fatigue crack initiation or fatigue crack growth rates.
- Such interactions, however, occur only under certain conditions of temperature, strain rate, and DO level in the environment.

In carbon and low-alloys steels, the interaction of nitrogen and dislocations during plastic deformation reduces plasticity, which causes strain localization in the material.<sup>147</sup> Small areas can deform plastically adjacent to areas that might be blocked by nitrogen/dislocation interactions. For a given macroscopic strain, the microscopic strain is higher due to strain localization in steels that are susceptible to DSA. Thus, because of strain localization, stress concentrations at active slip planes lead to higher rates and larger steps of oxide rupture and, simultaneously, to a decreased repassivation rate.<sup>147,148</sup> Consequently, both crack initiation and growth rates may be enhanced in carbon and low-alloy steels.

### 2.2.1.4 Crack Growth Rates in Smooth Fatigue Specimens

Studies on the formation and growth characteristics of short cracks in smooth fatigue specimens in LWR environments indicated that the decrease in fatigue life in LWR environments is caused primarily by the effects of the environment on the growth of MSCs (i.e., cracks less than 200  $\mu\text{m}$  deep) and, to a lesser extent, on the growth of mechanically small cracks.<sup>10,11</sup> Measured crack lengths as a function of fatigue cycles and fraction of fatigue life for smooth cylindrical specimens of A533-Gr B low-alloy steel in air, simulated PWR environment, and high-DO water are shown in Fig. 15. An example of the growth of a surface crack in A533-Gr. B steel tested in air at room temperature, and the fracture surface and probable crack front for the crack, are shown in Fig. 16. The results indicate that, for this example, three cracks merged to form the final fracture surface. The primary crack initiated near an inclusion and reached a surface length of approximately 100  $\mu\text{m}$  after 3,062 cycles (i.e., approximately 50% of the fatigue life). Two secondary cracks merged with the primary crack after approximately 5,700 and 6,000 cycles. Crack depth was determined by dividing the surface crack length by pi ( $\pi$ ).

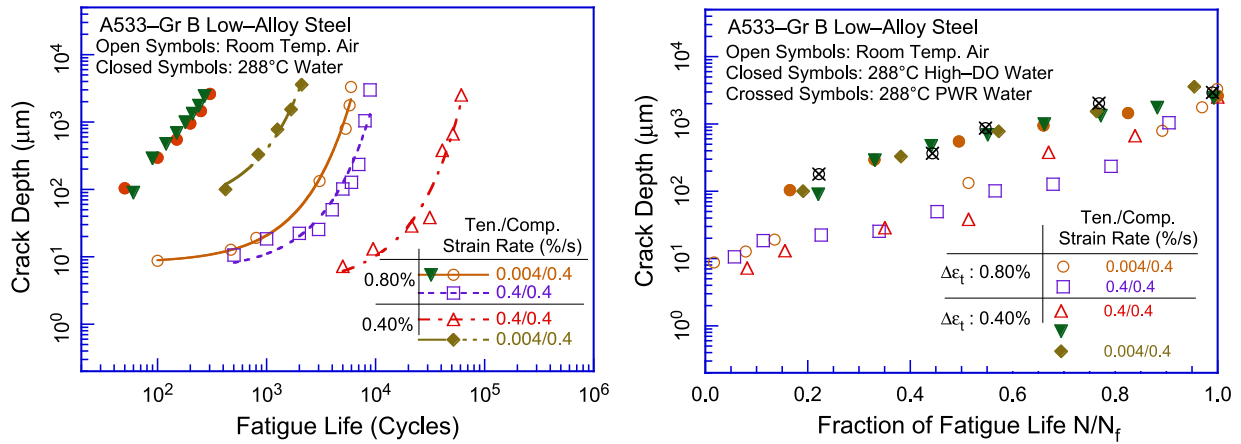


**Figure 15.** Depth of largest crack plotted as a function of (a) fatigue cycles and (b) fraction of fatigue life for A533-Gr B low-alloy steel in air and water environments (Ref. 11).

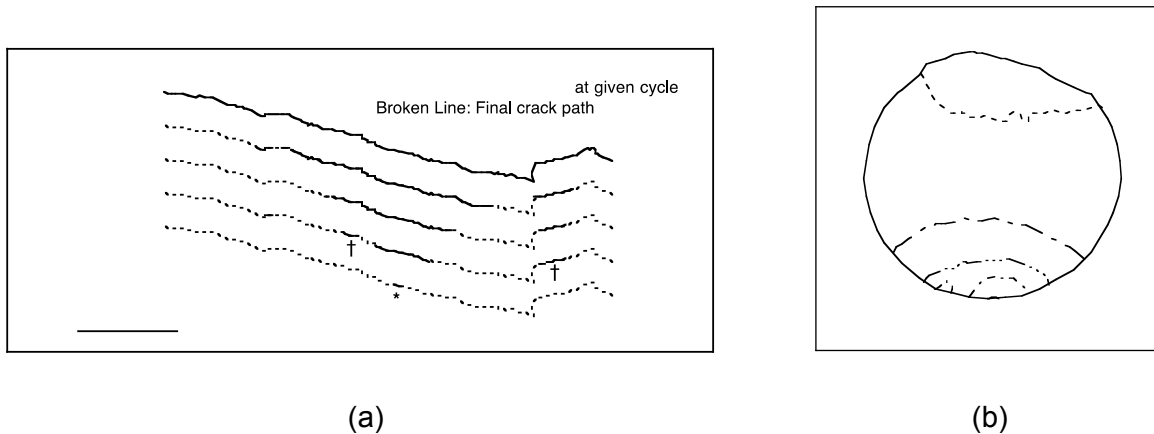


**Figure 16.** (a) Morphology and length of surface crack after various numbers of cycles for A533-Gr. B steel in air at room temperature, and (b) fracture surface and probable crack front for surface cracks shown in (a) (Ref. 11).

The crack growth rates corresponding to the data shown in Fig. 15 are plotted as a function of crack depth in Fig. 17. The results indicate that, in LWR environments, the period spent in the growth of MSCs is decreased. At approximately 0.8% strain range, only 30-50 cycles are needed to form a 100- $\mu\text{m}$  crack in high-DO water, whereas approximately 450 cycles are required to form a 100- $\mu\text{m}$  crack in a low-DO PWR environment and more than 3,000 cycles in air. These values correspond to average growth rates of approximately 2.5, 0.22, and 0.033  $\mu\text{m}/\text{cycle}$  in high-DO water, low-DO PWR environment, and air, respectively. The results also indicate that, relative to air, CGRs in high-DO water are nearly two orders of magnitude higher during the initial stages of fatigue life (i.e., for crack sizes less than 100  $\mu\text{m}$ ), and are one order of magnitude higher for crack sizes greater than 100  $\mu\text{m}$ .

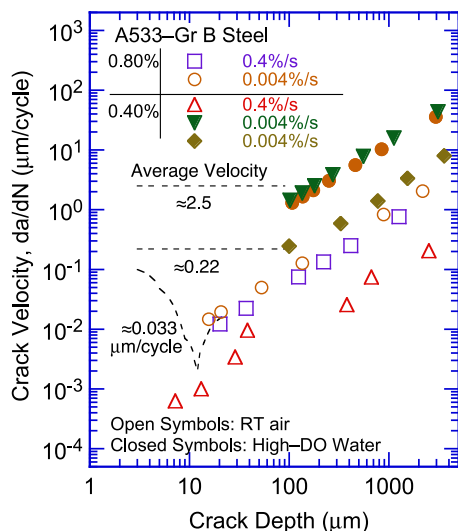


**Figure 17.**  
Crack growth rates plotted as a function of crack depth for A533-Gr B low-alloy steel tested in air and water environments (Ref. 11).

The surface crack and fracture surface morphologies of the test specimens indicate that, in high-temperature, high-DO water with slow strain rates, the surface cracks appear to grow entirely in Stage II growth as Mode I tensile cracks normal to the stress axis (Figs. 12 and 13). In air and low-DO PWR environments, both Stage I and Stage II growths are observed. Surface cracks grow initially as Mode II (shear) cracks along planes 45° to the stress axis and, when the stress intensities are large enough to promote slip on axes other than the primary slip axis, they grow as Mode I (tensile) cracks normal to the stress axis. Also, for A106-Gr. B carbon steel, Stage I crack growth in air and low-DO water occurs entirely along the soft ferrite grains, whereas in high-DO water, cracks propagate across both ferrite and pearlite regions. These results are consistent with the slip-oxidation/dissolution mechanism in high-DO water.

## 2.2.2 Austenitic Stainless Steels

Austenitic SSs exposed to LWR environments develop an oxide film that consists of two layers: a fine-grained, tightly-adherent, chromium-rich inner layer, and a crystalline, nickel-rich outer layer composed of large and intermediate-sized particles. Photomicrographs of the gauge surface of Type 316NG specimens tested in simulated PWR water and high-DO water are shown in Fig. 18. The inner layer forms by solid-state growth, whereas the crystalline outer layer forms by precipitation or deposition from the solution. A schematic representation of the surface oxide film is shown in Fig. 19.

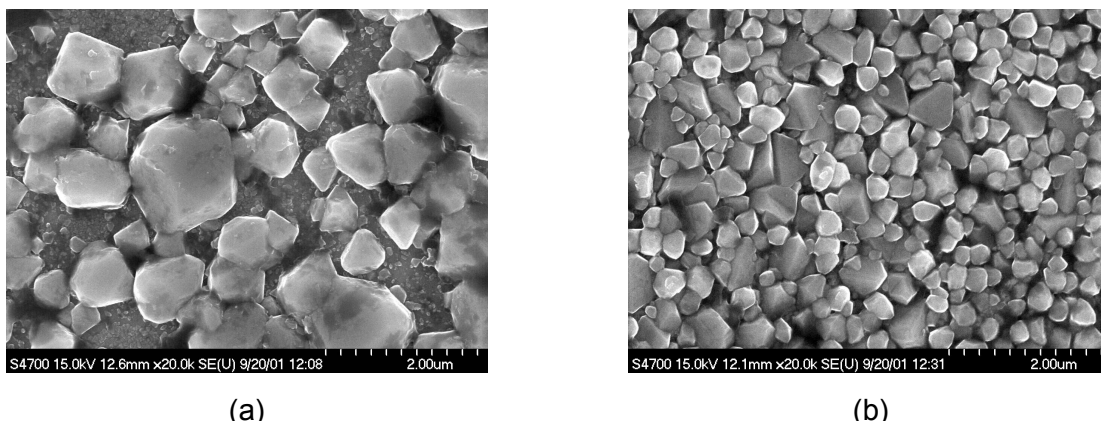


Figure 18. Photomicrographs of oxide films that formed on Type 316NG stainless steel in (a) simulated PWR water and (b) high-DO water (Ref. 13).

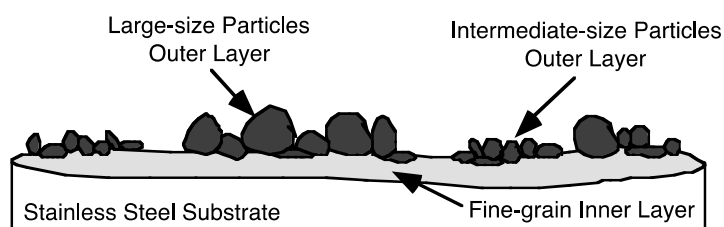


Figure 19. Schematic of the corrosion oxide film formed on austenitic stainless steels in LWR environments.

Several studies characterized the oxide films that form on austenitic SSs in LWR environments.<sup>199-205</sup> The inner layer consists of chromium-rich spinel ( $\text{Ni}_x\text{Cr}_y\text{Fe}_{3-x-y}\text{O}_4$ ) with a nonstoichiometric composition; the actual composition of spinels varies with environmental conditions. Da Cunha Belo, et al.<sup>203</sup> determined that the inner layer that formed on Type 316L SS in a PWR environment at 350°C consisted of mixed chromium oxides ( $\text{Cr}_2\text{O}_3 + \text{FeCr}_2\text{O}_4$ ) and  $\text{Fe}_3\text{O}_4$ . Nakayama and Oshida<sup>205</sup> characterized the oxide film on SSs exposed to high-DO (8 ppm) water at 300°C as chiefly composed of  $\text{NiO} \cdot (\text{Cr,Fe})_2\text{O}_3$  and/or  $\text{NiFe}_2\text{O}_4$ , which may be formed by a solid reaction between  $\text{NiO}$  and  $(\text{Cr,Fe})_2\text{O}_3$  or  $\alpha\text{-Fe}_2\text{O}_3$ . Kim<sup>199,200</sup> identified the  $\text{FeCr}_2\text{O}_4$  spinel chromite (or  $\text{Fe}_x\text{Cr}_{3-x}\text{O}_4$ ), along with  $\text{NiFe}_2\text{O}_4$ , in the inner layer formed on Types 304 and 316 SSs exposed at 288°C under BWR normal water chemistry (NWC) or BWR hydrogen water chemistry (HWC) conditions. Kim also noted that the inner oxide layer formed in a NWC BWR environment contained a lower concentration of chromium than that formed in a HWC low-DO environment. Such differences were attributed to chromium oxidation in high-DO water.

The structure and composition of the crystalline outer layer vary with the water chemistry. In BWR environments, the large particles in the outer layer are primarily composed of  $\gamma\text{-Fe}_2\text{O}_3$  hematite in NWC, and  $\text{Fe}_3\text{O}_4$  magnetite in HWC.<sup>199,200</sup> The intermediate particles in the outer layer are composed of  $\alpha\text{-Fe}_2\text{O}_3$  in NWC and  $\text{Fe}_3\text{O}_4$  in HWC. The structure of the outer layer varies when the water chemistry is cycled between NWC and HWC. In PWR environments, the large particles were identified as  $\text{Ni}_{0.75}\text{Fe}_{2.25}\text{O}_4$  spinel and the intermediate particles as  $\text{Ni}_{0.75}\text{Fe}_{2.25}\text{O}_4 + \text{Fe}_3\text{O}_4$ .<sup>203</sup> The possible effects of minor differences in the surface oxide film on fatigue crack initiation are discussed in the next section.

### 2.2.2.1 Effects of Surface Micropits

The characteristics of the surface oxide films that form on austenitic SSs in LWR coolant environments influence the mechanism and kinetics of corrosion processes and thereby influence the initiation stage, i.e., the growth of MSCs. As discussed earlier, the reduction of fatigue lives in high-temperature water may be due to the presence of surface micropits. To investigate the effect of surface micropits, fatigue tests were conducted on Type 316NG (Heat P91576) specimens that were pre-exposed to either low-DO or high-DO water and then tested in air or water environments.<sup>13</sup> The results of these tests, as well as data obtained earlier on this heat and Heat D432804 of Type 316NG SS in air and low-DO water at 288°C, are plotted in Fig. 20. The fatigue lives of specimens preoxidized in high-DO water and then tested in low-DO water were identical to those of specimens tested without preoxidation. Also, fatigue lives of specimens preoxidized at 288°C in low-DO water and then tested in air were identical to those of unoxidized specimens (Fig. 20). If micropits were responsible for the reduction in life, the pre-exposed specimens should have shown a decrease in life. Furthermore, the fatigue limit of these steels should have also been lower in water than in air, but the data indicated this limit was the same in both water and air environments. These results indicate that surface micropits or minor differences in the composition or structure of the surface oxide film had little or no effect on the formation of fatigue cracks.

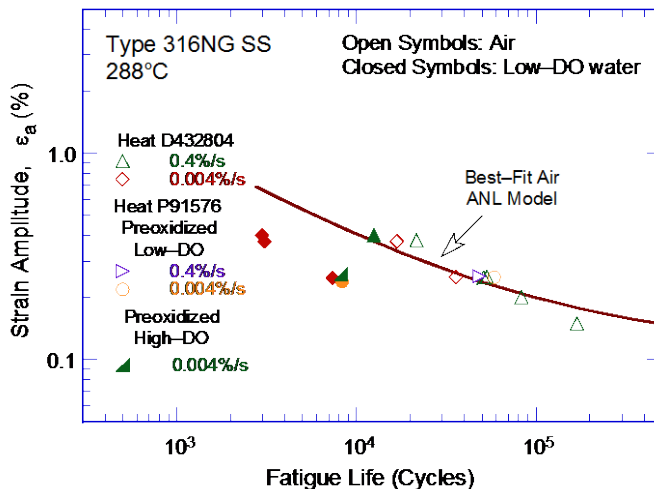


**Figure 20.** Effects of environment on formation of fatigue cracks in Type 316NG SS in air and low-DO water at 288°C. Preoxidized specimens were exposed for 10 days at 288°C in water that contained either less than 5 ppb DO and approximately 23 cm<sup>3</sup>/kg dissolved H<sub>2</sub> or approximately 500 ppb DO and no dissolved H<sub>2</sub> (Ref. 13).

### 2.2.2.2 Mechanisms of Corrosion Fatigue

Both the slip oxidation/dissolution and the hydrogen-induced cracking mechanisms depend on the rates of oxide rupture, passivation, and liquid diffusion. Therefore, it is difficult to differentiate between the two processes or to establish their relative contribution to fatigue cracking in LWR environments. However, for austenitic SSs, lower fatigue lives in low-DO water versus high-DO water are difficult to reconcile in terms of the slip oxidation/dissolution mechanism, which assumes that crack growth rates increase with increasing DO in the water. Metallographic examination of fatigue test specimens suggested that hydrogen-induced cracking may have played an important role in environmentally assisted reduction in fatigue lives of austenitic SSs.<sup>47</sup> For example, hydrogen can cause localized crack tip plasticity by reducing the stress required for dislocation motion, which leads to higher rates and larger steps of oxide film rupture. Thus, fatigue lives may be decreased, not because of increased growth rates, but because of increased film rupture frequency.

A detailed metallographic evaluation of austenitic SS fatigue test specimens was performed to characterize the crack and fracture morphology of the various heats under various heat treatment conditions.<sup>47</sup> Photomicrographs of the crack morphology of Type 304 SS specimens under all test and environmental conditions are presented in Fig. 21. In all cases, the tensile axis was vertical (parallel to the plane of each photomicrograph). For austenitic SSs, the fatigue crack surface morphology was similar to that observed for carbon and low-alloy steels. In an air environment, fatigue cracks were more likely to be oblique, approaching 45° with respect to the tensile axis. By contrast, the cracks that formed in either BWR or PWR environments tended to be perpendicular to the tensile axis.

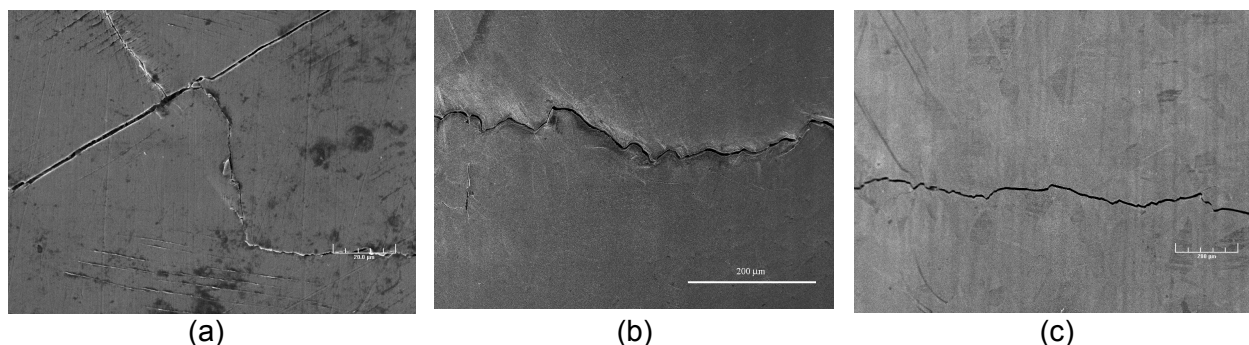
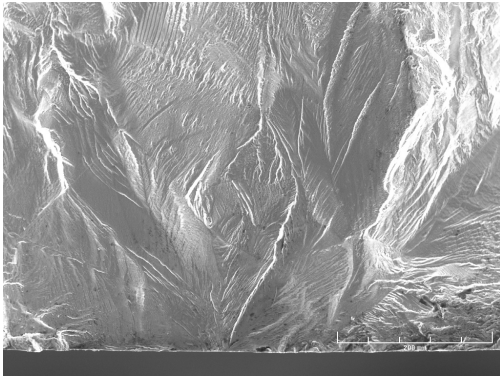


**Figure 21. Photomicrographs of the fatigue crack morphology of Type 304 SS in (a) air, (b) high-DO BWR water, and (c) low-DO PWR water at 289°C (Ref. 47).**

Photomicrographs of the crack morphology of Type 304 SS under all test and environmental conditions are presented in Fig. 22. In air, the fracture mode for crack initiation (i.e., crack depths up to 200  $\mu\text{m}$ ) and crack propagation (i.e., crack depths greater than 200  $\mu\text{m}$ ) was transgranular (TG), most likely along crystallographic planes, leaving behind relatively smooth surfaces. With an increasing degree of sensitization, cleavage-like, or stepped, TG fracture and ridge structures were observed on the smooth surfaces. In simulated NWC BWR environments, the initial crack appeared intergranular (IG) under all heat treatment conditions, implying a weakening of the grain boundaries. The extent of IG fracture increased with the degree of sensitization. Nevertheless, for crack depths beyond 200  $\mu\text{m}$ , the initial IG mode transformed into a TG mode with cleavage-like features. In simulated PWR environments, however, fatigue cracks initiated and propagated in a TG mode irrespective of the degree of sensitization. Prominent features of the fracture surfaces included highly angular, cleavage-like fracture facets that exhibited well-defined “river” patterns.<sup>47</sup> Intergranular facets were rarely observed, but when they were found, it was mostly in the more heavily sensitized alloys.

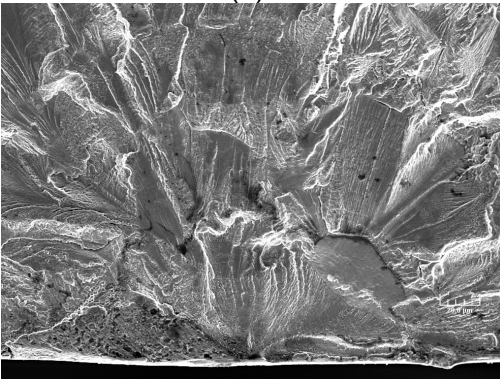
In addition, fatigue striations normal to the crack advance direction were clearly visible beyond approximately 200- $\mu\text{m}$ -crack depths on the fracture surfaces of all materials under all environmental conditions. An example of the fatigue striations observed in Type 304 SS in different environments is shown in Fig. 23. Striations were found on both the TG and IG facets of the samples tested under BWR NWC conditions, or co-existing with the “river” patterns specific to the samples tested in the PWR environments. However, the striations on specimens tested in PWR water were quite faint compared to those tested in NWC BWR water. Furthermore, examination of the specimens after chemical cleaning suggested that some striations were produced by rupture of the surface oxide film rather than the formation of double notches or “ears” at the crack tip.



(a)

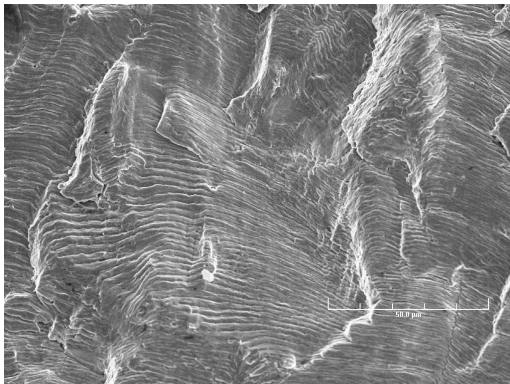


(b)

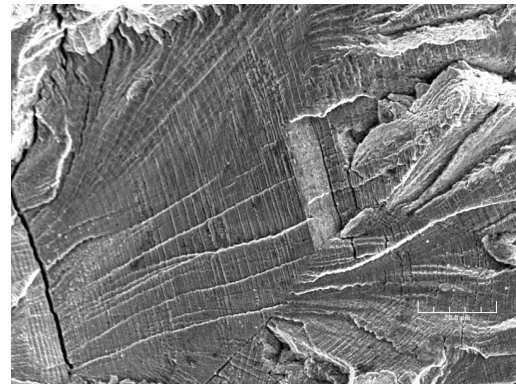


(c)

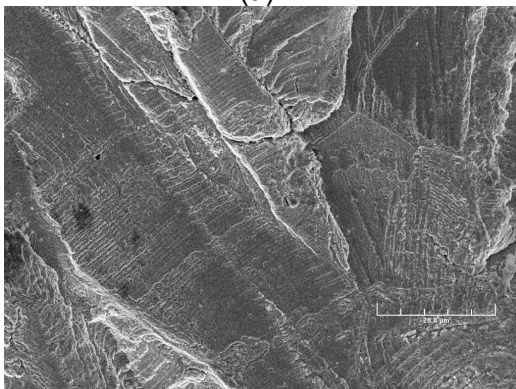
**Figure 22.**  
Photomicrographs showing sites of fatigue crack initiation on fracture surfaces of Type 304 SS tested at 289°C in (a) air, (b) high-DO BWR water, and (c) low-DO PWR water (Ref. 47).



(a)



(b)



(c)

**Figure 23.**  
Photomicrographs showing fatigue striations on fracture surfaces of Type 304 SS tested at 289°C in (a) air, (b) high-DO BWR water, and (c) low-DO PWR water (Ref. 47).



The characterization of surface cracks and fracture morphology in austenitic SSs suggests that, in LWR environments, although film rupture was apparent, the formation and growth of fatigue cracks were primarily caused by hydrogen-induced cracking.

#### 2.2.2.3 Effects of Dynamic Strain Aging (DSA)

DSA was observed in austenitic SSs in air at strain rates below 0.3 %/s and temperatures in the range of 300-600°C; the peak effects occurred at 500-600°C.<sup>206</sup> The fatigue life of a heat of Type 316LN SS at low strain rates was greater at 600°C than at 500°C. Typically at temperatures above 400°C, the fatigue life of austenitic SSs decreased with an increase in temperature or a decrease in strain rate.<sup>57</sup> DSA increased the dislocation density at slow strain rates, which enhanced the degree of inhomogeneity of deformation during fatigue loading.

DSA was also observed in Type 304L SS under LWR operating conditions. At 0.4 %/s strain rate, the fatigue life and fatigue limit in air were higher at 300°C than at 150°C (due to secondary strain hardening at 300°C).<sup>58</sup> A similar behavior was observed for this heat of SS in PWR water. At 0.4 %/s, fatigue life decreased in PWR water relative to that in air at 150°C, but not at 300°C. This difference was identified as secondary hardening at 300°C, which was not observed at 150°C. The secondary hardening at 300°C may be due to DSA, although the temperature was relatively low.

#### 2.2.2.4 Crack Growth Rates in Smooth Fatigue Specimens

Studies on the formation and growth characteristics of short cracks in smooth fatigue specimens of austenitic SSs in LWR environments indicated that, although the growth rates of mechanically small cracks were greater in water than in air, the decrease in fatigue lives was caused predominantly by the effects of the environment on the growth of MSCs.<sup>44</sup> The growth of the largest crack in austenitic SSs with respect to fatigue cycles, in air and water environments, is shown in Fig. 24. In the figure, the crack length for the test in air at 288°C and 0.75% strain range was measured only near the end of the test. The data obtained by Orbtlik, et al.<sup>207</sup> for Type 316L SS in air at 25°C and approximately 0.2% strain range were used to estimate the crack growth in air at 0.75% strain range. Similar studies on carbon and low-alloy steels indicate<sup>11,165-167</sup> that the fatigue crack size at various life fractions was independent of strain range, strain rate, and temperature; consequently, the depth of the largest crack at various life fractions was approximately the same at strain ranges of 0.75% and 0.2%. The curve for the test in air at 0.75% (shown as a dashed line in Fig. 24) was calculated from the best-fit equation of the experimental data for Type 316L SS at 0.2% strain range; the estimated crack lengths at 0.75% strain range show very good agreement with the measured values. The results showed that, at the same number of cycles, the crack length was longer in low-DO (PWR) water than in air, e.g., after 1,500 cycles, the crack length in air, high-DO (BWR) water, and PWR water was approximately 40, 300, and 1,100  $\mu\text{m}$ , respectively. The growth of cracks during the initiation stage, i.e., growth of MSCs, was enhanced in water; the fatigue cycles needed to form a 500- $\mu\text{m}$  crack were a factor of approximately 12 lower in low-DO water than in air. Figure 24 shows that the number of cycles required to produce a 500- $\mu\text{m}$  crack is 800, 3,000, and 9,000 in low-DO (PWR) water, high-DO (BWR) water, and air environments, respectively; thus, the number of cycles was more than a factor of 10 lower in low-DO water than in air.

The CGRs during the propagation stage, i.e., growth of mechanically small cracks, in air and water environments are plotted as a function of crack length in Fig. 25; they were calculated from the best fit of the data in Fig. 24. The CGRs in high-DO water for the specimen with a 24-hour soak period (closed diamonds in Fig. 25) were determined from measurements of fatigue striations. The CGRs were a factor of 2–6 higher in water than in air. Growth rates in



PWR water or high-DO water with a 24-hour soak period were higher than those in high-DO water with a 120-hour soak period. At a crack length of approximately 1,000  $\mu\text{m}$ , the CGRs in air, high-DO water, and low-DO water were 0.30, 0.64, and 1.05  $\mu\text{m}/\text{cycle}$ , respectively. For the 0.75% strain range and 0.004%/s strain rate, these values corresponded to growth rates of approximately  $1.6 \times 10^{-9}$ ,  $3.4 \times 10^{-9}$ , and  $5.6 \times 10^{-9}$  meters/second in air, high-DO water, and low-DO water, respectively. Thus, growth rates were a factor of 3.5 greater in low-DO water than in air.

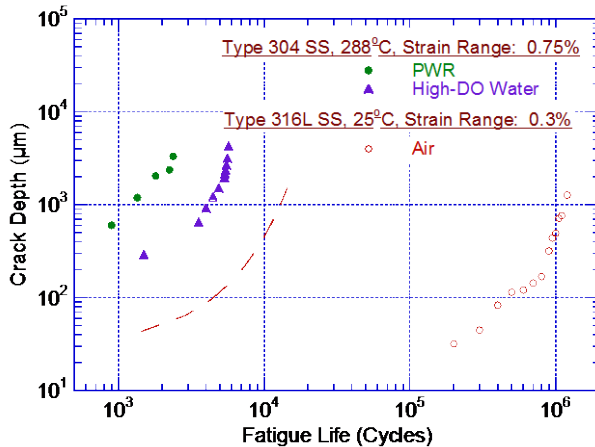
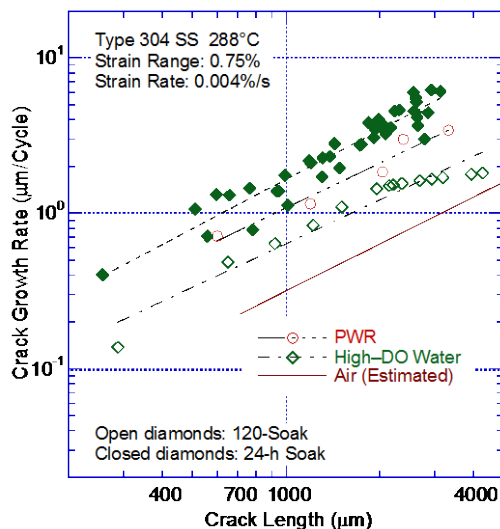
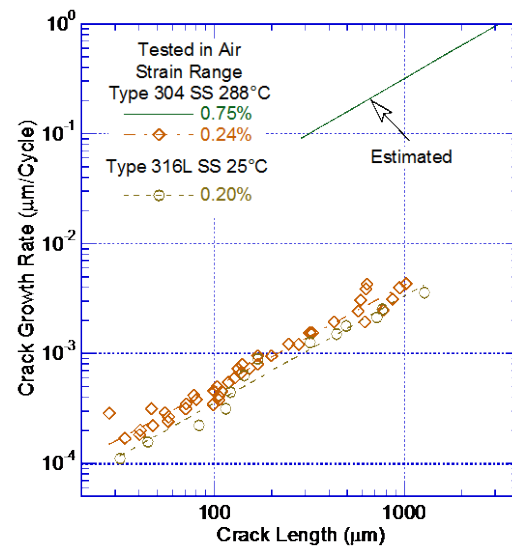


**Figure 24.** Depth of largest crack plotted as a function of fatigue cycles for austenitic stainless steels in air and water (Refs. 13,207).



(a)



(b)

**Figure 25.** Crack growth rates plotted as a function of crack length for austenitic stainless steels in (a) water and (b) air environments (Refs. 13,44,207).

The existing fatigue crack growth ( $da/dN$ ) data obtained from fracture-mechanics tests on CT specimens of wrought and cast SSs in LWR environments were compiled by Shack and Kassner.<sup>208</sup> The results indicated significant enhancement of CGRs in high-DO water; at CGRs of less than  $10^{-10}$  meters/second in air, the rates in BWR NWC conditions exceeded the air curve in Section III of the ASME Code by a factor of approximately 20–30. The experimental CGRs for sensitized Type 304 SS in high-DO water and those predicted in air for the same mechanical loading conditions are plotted in Fig. 26a. The fatigue CGRs in air,  $\dot{a}_{\text{air}}$  (meters/second), were determined from a correlation at 288°C given by

$$\dot{a}_{\text{air}} = 3.43 \times 10^{-12} S(R) \Delta K^{3.3}/T_R, \quad (15)$$

where the function  $S(R)$  is expressed as

$$\begin{aligned} S(R) &= 1.0 & R &\leq 0 \\ S(R) &= 1.0 + 1.8R & 0 < R &\leq 0.79 \\ S(R) &= -43.35 + 57.97R, & 0.79 < R &< 1.0, \end{aligned} \quad (16)$$

and  $T_R$  is the rise time (seconds) of the loading waveform,  $R$  is the load ratio ( $K_{\min}/K_{\max}$ ), and  $\Delta K$  is  $K_{\max} - K_{\min}$ . The fatigue CGR in water [ $\dot{a}_{\text{env}}$  (meters/second)] with 0.2 ppm DO (i.e., BWR NWC) is expressed in terms of the fatigue CGR in air ( $\dot{a}_{\text{air}}$ ) by the relationship

$$\dot{a}_{\text{env}} = \dot{a}_{\text{air}} + 4.5 \times 10^{-5} (\dot{a}_{\text{air}})^{0.5}. \quad (17)$$

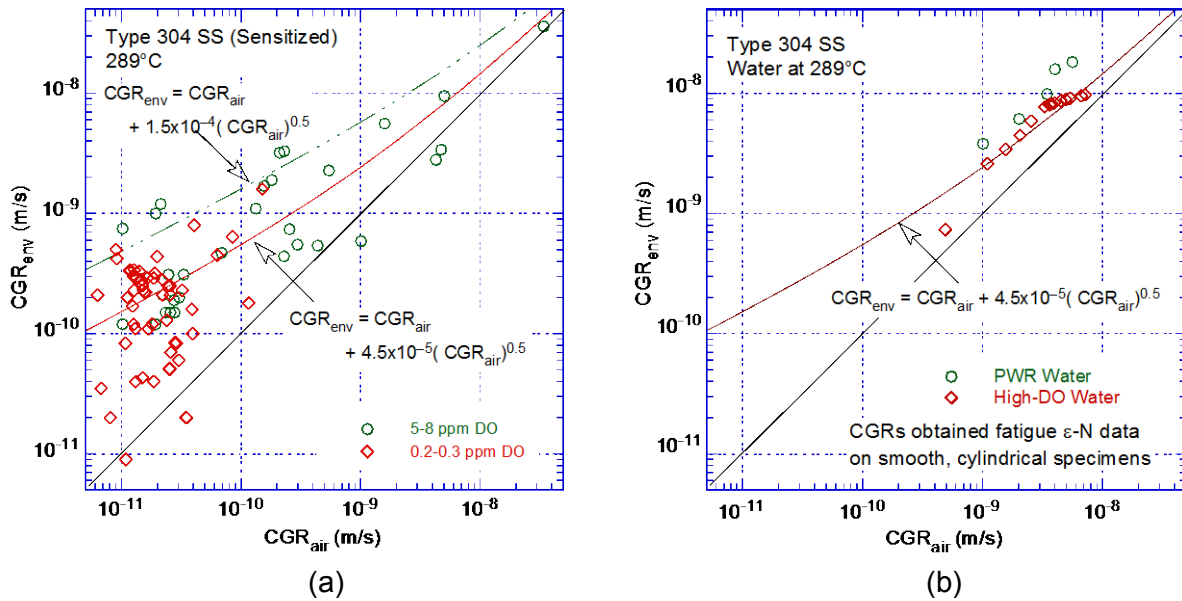


**Figure 26. Crack growth rate data for Type 304 SS in high temperature water determined from (a) fracture mechanics CT specimens and (b) smooth cylindrical fatigue specimens (Ref. 208).**

The CGR data from fracture-mechanics tests in low-DO PWR environments are sparse, particularly at rates that are less than  $10^{-9}$  meters/second. At high CGRs, the observed enhancement in both low- and high-DO environments was relatively small, and the magnitude of the enhancement under the same loading conditions was comparable in the two environments. Until further data become available at low CGRs in simulated PWR water, Shack and Kassner<sup>208</sup> recommended that the environmental enhancement represented by Eq. 17 for 0.2 ppm DO water should also be considered for PWR environments.

The CGRs determined from fatigue  $\varepsilon$ -N tests on smooth, cylindrical specimens in high-DO and low-DO (PWR) water environments at 289°C, are plotted in Fig. 26b. The rates in high-DO and low-DO (PWR) water represent the measured values shown as open diamonds and circles, respectively, from Fig. 25a. The CGRs in air for the same loading conditions (i.e., the same crack length) were determined from the estimated rates in air, shown by the solid line in Fig. 25 a. The results from fatigue  $\varepsilon$ -N tests showed good agreement with the data obtained from the

fracture-mechanics tests. The CGRs in high-DO water were consistent with the trend predicted from Eq. 17. The rates in low-DO water were slightly higher.

The large reductions in fatigue life of austenitic SSs in PWR environments cannot be explained entirely on the basis of enhanced CGRs during the propagation stage, i.e., growth of mechanically small cracks. For example, the CGRs in low-DO water are a factor of 1.6 greater than those in high-DO water, but fatigue lives are approximately a factor of 4 lower in low-DO water than in high-DO water. As indicated by the results shown in Fig. 25a, the decrease in fatigue lives of austenitic SSs in PWR environments was caused predominantly by the effects of environment on the growth of MSCs.

It should also be noted that, if enhanced CGRs alone were responsible for the environmentally assisted decrease in fatigue lives of materials in LWR environments, environmental effects on the fatigue lives of Alloy 600 and austenitic SSs in LWR environments should be comparable. In air, the fatigue  $\epsilon$ -N behavior of Alloy 600 is comparable to that of austenitic SSs.<sup>61</sup> Fatigue CGR data indicate that the enhancement of CGRs of Alloy 600 and austenitic SSs in LWR environments is also comparable.<sup>209</sup> However, the fatigue  $\epsilon$ -N behaviors of Alloy 600 and austenitic SSs in water differ significantly; only moderate effects of environment are observed for Alloy 600 base material and welds both in low-DO and high-DO water. For example, the fatigue life of Alloy 600 weld metal in water with less than 0.005 ppm DO at 325°C and 0.6% strain amplitude decreased by a factor of approximately 2.5 when the strain rate was decreased from 0.4 to 0.001 %/s. Under similar environmental and loading conditions, the fatigue lives of austenitic SSs were decreased by a factor of approximately ten.



### 3. FATIGUE STRAIN VS. LIFE ( $\epsilon$ -N) BEHAVIOR IN AIR

---

During 1990s, the existing fatigue  $\epsilon$ -N data developed at various establishments and research laboratories worldwide were compiled by the PVRC Working Group on  $\epsilon$ -N Curve and Data Analysis. The database used in the ANL studies, and presented in the initial revision to NUREG/CR-6909, was an extended version of the PVRC database. The reanalysis of the fatigue  $\epsilon$ -N data presented in this report is based on a much larger fatigue  $\epsilon$ -N database. The additional data include the JNES data summarized in JNES-SS-1005 on carbon and low-alloy steels, wrought and cast austenitic SSs, Ni-Cr-Fe alloys, and their associated weld metals tested in air and LWR environments,<sup>136</sup> and fatigue  $\epsilon$ -N test results from the open literature on several heats of carbon and low-alloy steels tested in BWR environments.<sup>138-146</sup> Nearly 60% of the data in the more recent JNES database were included the old JNUFAD<sup>210</sup> database. The JNUFAD database formed a portion of the PVRC database, which was used in the original revision to NUREG/CR-6909 report.

Unless otherwise mentioned, the fatigue database was obtained from smooth cylindrical gauge specimens that were tested under strain control with fully reversed loading, i.e., strain ratio, R, of  $-1$ . Tests on notched specimens or at R values other than  $-1$  were excluded from the fatigue  $\epsilon$ -N data analysis performed for this report. For the previous fatigue testing performed at ANL, the estimated uncertainty in the strain measurements was about 4% of the reported values. For the data obtained in other laboratories, the uncertainty in the reported values of strain is unknown, but was assumed to be small enough such that the results were not significantly impacted.

In nearly all tests, fatigue life was defined as the number of cycles necessary for the tensile stress to drop 25% from its peak or steady-state value,  $N_{25}$ . As discussed in Section 1.1, for the specimen sizes used in these studies, e.g., 5.1–9.5 mm (0.2–0.375 in.) diameter cylindrical specimens, failure corresponds to an approximately 3-mm-deep crack. Some of the earlier tests in air were carried out to complete failure of the specimens, and in some other tests, fatigue lives were defined as the number of cycles for peak tensile stresses to decrease by 10 or 50%. Fatigue lives defined by a criterion other than a 25% load drop were therefore converted to consistent  $N_{25}$  values according to the following formula:

$$N_{25} = N_X / (0.947 + 0.00212X), \quad (18)$$

where X is the failure criterion (e.g., 10, 50 or 100% decrease in peak tensile stress).<sup>10</sup> The estimated uncertainty in fatigue life determined by this procedure is about 2%, which is within the strain measurement uncertainty.

The 25% load drop criterion was not used for the tests that were performed using tube specimens. For tube specimens, fatigue lives were represented by the number of cycles to develop a leak because, with the exception of a few specimens, all tube specimens had 3-mm wall thicknesses.

#### 3.1 Carbon and Low-Alloy Steels and Weld Metals

##### 3.1.1 Experimental Data

The primary sources of fatigue  $\epsilon$ -N data for carbon and low-alloy steels are the tests performed by General Electric Co. (GE) in a test loop at the Dresden 1 reactor;<sup>14,15</sup> work sponsored by EPRI at GE;<sup>16,17</sup> the work of Terrell at Materials Engineering Associates (MEA);<sup>48-50</sup> the work at

ANL on fatigue of pressure vessel and piping steels;<sup>10–13,40–47</sup> the large JNES database<sup>136</sup> “Environmental Fatigue Evaluation Method for Nuclear Power Plants,” studies at Ishikawajima-Harima Heavy Industries (IHI), Hitachi, and Mitsubishi Heavy Industries (MHI) in Japan;<sup>18–36</sup> and the studies at Kraftwerk Union Laboratories (KWU) and Materialprüfungsanstalt (MPA) in Germany.<sup>55,56</sup> From these sources, the total database for fatigue tests in air is composed of 684 tests; 254 tests on carbon steels and 430 tests on low-alloy steels. Carbon steels include 19 heats of A106–Grades B and C, A333–Grade 6, A508–Grade 1, and A333–Grade 6 weld metals. Low-alloy steels include 22 heats of A302–Grade B, A508–Grade 2 and 3, and A533–Grade B steel. A summary of the sources included in the updated database used for the present analyses, as categorized by material type and test environment, is presented in Table 1. Other material information such as chemical composition, heat treatment, and room temperature tensile properties of the various types and heats of materials is given in Appendix B.

**Table 1. Sources of the fatigue  $\epsilon$ –N data on carbon and low-alloy steels in air environment.**

ANL Mat. ID	Material Specification	Sulfur Content (wt.%)	Test Temperature (°C)	Number of Data Points	Source	Applicable Reference
<u>Carbon Steels</u>						
1	A106-Gr.B	0.015	25, 288	3, 17	ANL	10
3	A106-Gr.B	0.020	25, 288	13, 12	MEA	48-50
4	A106-Gr.C (STS480)	0.006	25	5	JNES (Kanasaki)	136
-	A106-Gr.C (STS480)	0.003	25	2	JNES (Kanasaki)	136
6	A106-Gr.B (STS49)	0.007	25	9	JNES (Higuchi)	136
9	A333-Gr.6 (STS42)	0.015	25, 250, 290	13, 7, 3	JNES (Higuchi)	136
10	A333-Gr.6 (STS42)	0.014	25	7 <sup>a</sup>	JNES (Higuchi)	136
11	A333-Gr.6	0.006	288	1	JNES (Higuchi)	136
12	A333-Gr.6 (STS410)	0.012	25, 100, 200, 288	5, 4, 4, 2	JNES (Nakao), ANL	136, 10
13	A333-Gr.6	0.030	25, 288	7, 6	GE	14-17
14	A333-Gr.6 (STS410)	0.008	25, 289	24, 10	JNES (Hirano)	136
15	A333-Gr.6 (STS410)	0.016	25, 289	12, 5	JNES (Hirano)	136
18	A508-Gr.1 (SFVC2B)	0.004	25, 289	6, 5	JNES (Hirano)	136
19	A508-Gr.1 <sup>b</sup>	0.008	25	14	JNES (PLEX)	136
24	CS	-	25, 170	10, 28	MPA	55,56
<u>Carbon Steel Weld Metals</u>						
-	A336-Gr.6 (STS410)	0.001	25, 288	6, 4	JNES (Hirano)	136
-	A336-Gr.6 (STS410)	0.010	25, 289	5, 5	JNES (Hirano)	136
<u>Low-alloy Steels</u>						
1	A302-Gr.B	0.027	288	7	ANL	10
2	A508-Gr.2	0.003	25	9	JNES (Nakao/Higuchi)	136
6	A508-Gr. 3 (SFVV3)	0.003	25, 288	6, 14	JNES (Nagata)	136
7	A508-Gr. 3 (SFVV3)	0.002	25, 288	7, 8	JNES (Narumoto)	136
8	A508-Gr. 3 (SFVV3)	0.003	25	8	JNES (Narumoto)	136
9	A508-Gr. 3 (SFVV3)	0.005	25, 200	31, 2	JNES (Ikemoto, Iwadate, Kou, Nihei, Fukakura)	136
10	A508-Gr. 3 (SFVV3)	0.003	150, 200, 290	18, 15, 13	JNES (Kou, Fukakura, Iida)	136
11	A508-Gr. 3 (SFVV3)	0.003	25, 200, 290	11, 17,	JNES (Nihei, Kou,	136

ANL Mat. ID	Material Specification	Sulfur Content (wt.%)	Test Temperature (°C)	Number of Data Points	Source	Applicable Reference
12	A508-Gr. 3 (SFVV3)	0.003	25	24	Fukakura, Iwadate,)	
13	A508-Gr. 3 (SFVV3)	0.008	25	10	JNES (Higuchi, Endou)	136
14	A508-Gr. 3	0.002	25	8 <sup>b</sup>	JNES (Kanasaki)	136
16	A533-Gr. B	0.012	288	14	Wu & Katada	141
17	A533-Gr. B (SQV2A)	0.007	25, 288	6, 16	ANL	10,11,12
18	A533-Gr. B (SQV2A)	0.001	25, 288	14, 14	JNES (Nagata), Wu & Katada	136,141
19	A533-Gr. B (SQV2A)	0.003	25, 350	34, 10	JNES (Kazuo Toyam)	136
20	A533-Gr. B (SQV2A)	0.002	25, 300	6, 6	JNES (Narumoto)	136
21	A533-Gr. B (SQV2A)	0.010	25, 286	9, 8	JNES (Narumoto)	136
22	A533-Gr. B (SQV2A)	0.008	25	18 <sup>c</sup>	JNES (Iida)	136
			25, 150, 200, 250, 289	19, <sup>b</sup> 1, 1, 1, 4	JNES (Hirano)	136
23	A533-Gr. B	0.013	288	7	Wu & Katada	143
28	A533-Gr. B	0.014	270	2	MPA	55,56
29	LAS	-	25, 170	16, 16	MPA	55,56
31	17MnMoV64	0.018	200	3	S/KWU	55,56

<sup>a</sup> Six tests performed under load control were excluded.

<sup>b</sup> Includes test results for thermally aged materials.

<sup>c</sup> Tests performed using a sine waveform, and data include results for thermally aged materials.

In air, the fatigue lives of both carbon and low-alloy steels depend on steel type, temperature, and for some compositions, applied strain rate and sulfide morphology. Fatigue  $\epsilon$ -N data from various investigations on carbon and low-alloy steels are shown in Fig. 27. The best-fit air curves based on the ANL models (Eqs. 24 and 25 from Section 3.1.6) and the ASME Section III mean-data air curves at room temperature (Eqs. 7 and 8 from Section 1.2) are also included in the plots in this figure. The results indicate that, although significant scatter is apparent due to material variability, the fatigue lives of these steels are comparable at less than  $5 \times 10^5$  cycles, and those of low-alloy steels are greater than carbon steels for greater than  $5 \times 10^5$  cycles. In addition, the fatigue life at  $10^6$  cycles of low-alloy steels is higher than that of carbon steels.

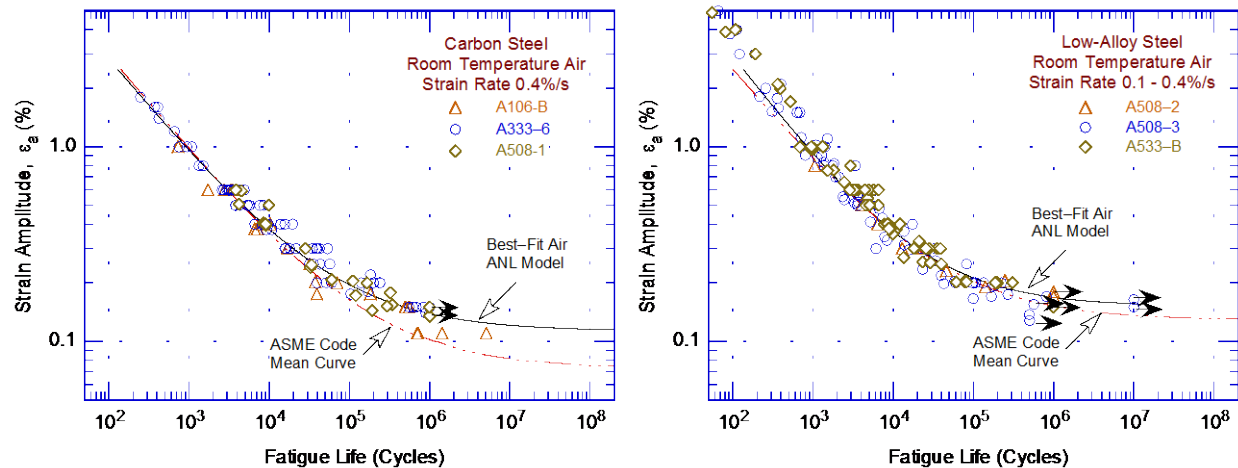


**Figure 27. Fatigue strain vs. life data for carbon and low-alloy steels in air at room temperature (JNUFAD database and Refs. 10,18,19,48).**

The results also indicate that the existing fatigue  $\varepsilon$ - $N$  data for low-alloy steels are in good agreement with the ASME mean data curve. The existing data for carbon steels are consistent with the ASME mean data curve for fatigue lives below  $5 \times 10^5$  cycles, and are above the ASME mean data curve at longer lives. Thus, for carbon steels above  $5 \times 10^5$  cycles, the ASME mean data curve is conservative with respect to the existing fatigue  $\varepsilon$ - $N$  data.

- The ASME Code mean data air curves for carbon and low-alloy steels (Eqs. 7 and 8) are either consistent with the existing fatigue  $\varepsilon$ - $N$  data or are somewhat conservative under some conditions.

### 3.1.2 Temperature

In air, the fatigue lives of both carbon and low-alloy steels decrease with increasing temperature; however, the effect is relatively small (less than a factor of 1.5). The existing fatigue  $\varepsilon$ - $N$  data in air at 25–290°C are shown in Fig. 28. As discussed in Section 3.1.1 for each grade of steel, the data represent several heats of material. The solid lines in the plots represent the temperature dependence defined by Eq. 22 in Section 3.1.6. The results indicate a factor of approximately 1.5 decrease in fatigue lives of both carbon and low-alloy steels as the temperature is increased from room temperature to 300°C.

- Variations in the fatigue lives in air due to the effects of temperature for carbon and low-alloy steels were accounted for in the subfactor for “data scatter and material variability.”

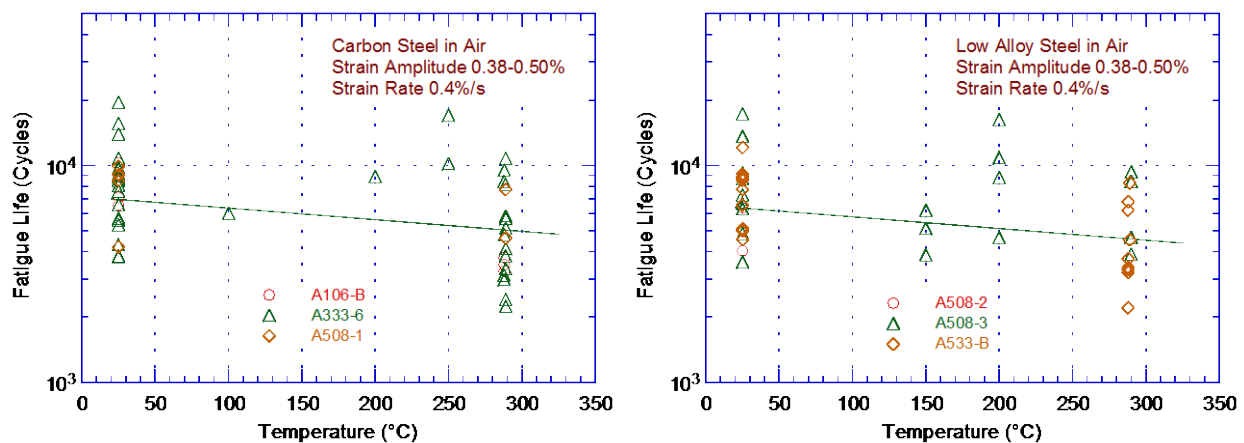


**Figure 28.** The change in fatigue lives of carbon and low-alloy steels in air as a function of temperature.

### 3.1.3 Strain Rate

The effect of strain rate on the fatigue lives of carbon and low-alloy steels in air appears to depend on the material composition. The existing data indicate that in the temperature range of dynamic strain aging (200–370°C), some heats of carbon and low-alloy steels were sensitive to strain rate; with decreasing strain rate, the fatigue lives in air were either unaffected,<sup>10</sup> decreased for some heats,<sup>211</sup> or increased for others.<sup>212</sup> The carbon and nitrogen contents in the steel are considered to have an important influence on strain rate effects. Inhomogeneous plastic deformation can result in localized plastic strains. This localization retards blunting of propagating cracks that is usually expected when plastic deformation occurs and can result in higher crack growth rates.<sup>211</sup> The increases in fatigue lives were attributed to retardation of



CGRs due to crack branching and suppression of the plastic zone.<sup>212</sup> Furthermore, as discussed earlier, the formation of cracks may be enhanced in the presence of DSA.

- *Variations in fatigue lives in air due to the effects of strain rate for carbon and low-alloy steels were accounted for in the subfactor for “data scatter and material variability.”*

### 3.1.4 Sulfide Morphology

Some high-sulfur steels exhibit very poor fatigue properties in certain orientations because of structural factors such as the distribution and morphology of sulfides in the steel. For example, fatigue tests on a high-sulfur heat of A302–Gr. B steel in three orientations\* in air at 288°C indicated that the fatigue life and fatigue limit in the radial (T2) orientation are lower than those in the rolling (R) and transverse (T1) orientations.<sup>10</sup> At low strain rates, fatigue lives in the T2 orientation were nearly one order of magnitude lower than in the R orientation. In the orientation with poor fatigue resistance, crack propagation occurred preferentially along the sulfide stringers and is facilitated by sulfide cracking.

- *Variations in fatigue lives in air due to differences in sulfide morphology for carbon and low-alloy steels were accounted for in the subfactor for “data scatter and material variability.”*

### 3.1.5 Cyclic Strain Hardening Behavior

The cyclic stress-strain response of carbon and low-alloy steels varies with steel type, temperature, and strain rate. In general, these steels show initial cyclic hardening, followed by cyclic softening or a saturation stage at all strain rates. Carbon steels, with a pearlite and ferrite structure and low yield stress, exhibit significant initial hardening. Low-alloy steels, with a tempered bainite and ferrite structure and a relatively high yield stress, show little or no initial hardening and may exhibit cyclic softening with continued cycling. For both steels, the maximum stress increases as applied strain increases and generally decreases as temperature increases. However, at 200–370°C, these steels exhibited DSA, which resulted in enhanced cyclic hardening, a secondary hardening stage, and negative strain rate sensitivity.<sup>211,212</sup> The temperature range and extent of DSA varied with composition and structure.

The effects of strain rate and temperature on the cyclic stress response of A106–Gr B carbon steel and A533–Gr B low-alloy steel are shown in Fig. 29. For both steels, cyclic stresses were higher at 288°C than at room temperature. At 288°C, all steels exhibited greater cyclic and secondary hardening because of DSA. The extent of hardening increased as the applied strain rate decreased.

- *Cyclic strain hardening behavior influenced the fatigue limits of materials; variations in fatigue lives in air due to the effects of strain hardening for carbon and low-alloy steels were accounted for in the subfactor for “data scatter and material variability.”*

---

\*The three orientations were represented by the direction that was perpendicular to the fracture plane. Both transverse (T1) and radial (T2) directions were perpendicular to the rolling direction, but the fracture plane was across the thickness of the plate in the transverse orientation and parallel to the plate surface in the radial orientation.

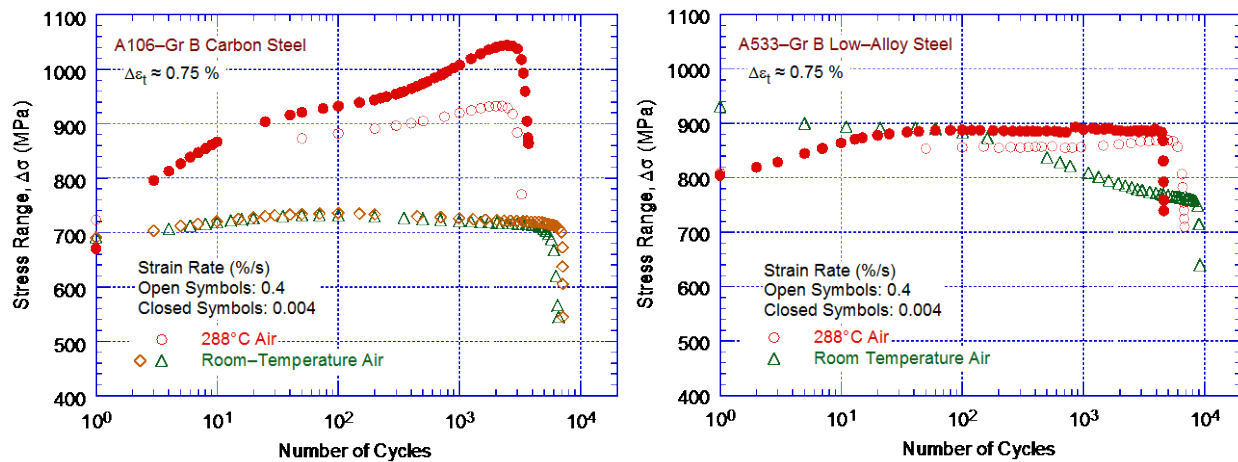


**Figure 29. Effect of strain rate and temperature on cyclic stress of carbon and low-alloy steels.**

### 3.1.6 Fatigue Life Model

ASTM Standard E 739, “Standard Practice for Statistical Analysis of Linear or Linearized Stress–Life ( $S-N$ ) and Strain–Life ( $\epsilon-N$ ) Fatigue Data,”<sup>4</sup> treats fatigue life,  $N$  (or the logarithm of the fatigue life), as the dependent variable, and the controlled variables, e.g., stress or strain, as the independent variable. The coefficients of a “linear” model are commonly established through least-squares curve-fitting of the data using fatigue life as the dependent variable. An optimization program sets the coefficients to minimize the sum of the square of the residual errors, which are the differences between the predicted and actual values of  $N$  or  $\ln(N)$ . However, such an approach may not adequately determine the optimum coefficients for a nonlinear expression such as the Langer curve (Eq. 6), which includes a constant term,  $C$ , related to the fatigue limit. The model does not address the fact that at low strain amplitudes, most of the error in life is due to uncertainty associated with either measurement of stress or strain or variation in threshold strain caused by material variability. A predictive model based on a least-squares fit on  $N$  or  $\ln(N)$  is biased for low strain amplitude ( $\epsilon_a$ ); also, data obtained at strain amplitudes less than the constant  $C$  in Eq. 6 cannot be included in the analysis. On the other hand, a least-squares fit on  $\epsilon_a$  does not work well for higher strain amplitudes. The two kinds of models are transformations of each other, although the precise values of the coefficients differ.

In the statistical model presented in Refs. 130 and 10, the two approaches were combined by minimizing the sum of the squared Cartesian distances from the data points to the predicted curve (Fig. 30). For low  $\epsilon_a$ , this is very close to optimizing the sum of squared errors in predicted  $\epsilon_a$ ; at high  $\epsilon_a$ , this is very close to optimizing the sum of squared errors in predicted life; and at medium  $\epsilon_a$ , this model combines both factors. Therefore, the use of this model addresses the weaknesses identified previously for the model based on residual errors alone. To perform this alternate optimization, it was necessary to normalize the  $x$  and  $y$  axes by assigning relative weights that are used in combining the error in life and strain amplitude because the  $x$  and  $y$ -axes are not in comparable units. In this analysis, errors in strain amplitude (%) were weighted 20 times as heavily as errors in  $\ln(N)$ . A value of 20 was selected for two related reasons. First, this factor led to approximately equal weighting of low and high strain amplitude data in the least-squared error computation of model coefficients. Second, when the factor was applied to the model to generate probability curves, it yielded a standard deviation on strain amplitude comparable to that obtained from the best fit of the high cycle fatigue data to Eq. 1.<sup>130</sup> Because there was judgment applied in the selection of this value, a sensitivity analysis was performed that demonstrated that the coefficients of the model do not

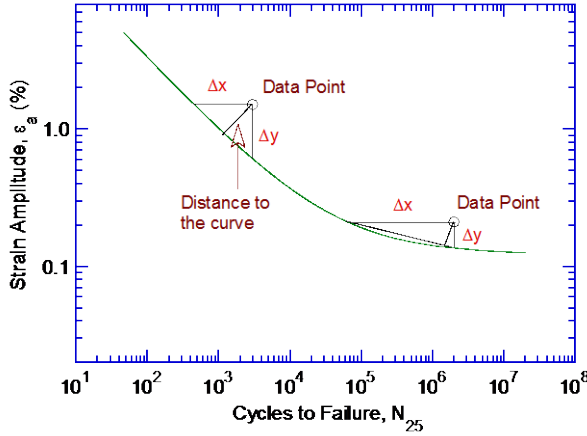


**Figure 30.**  
Schematic diagram of the best-fit of the experimental data by minimizing the distance between the data point and the S-N curve.

change significantly for weight factors between 10 and 25. The normal distance from the best-fit curve was estimated as

$$D = \left\{ (x - \hat{x})^2 + [k(y - \hat{y})]^2 \right\}^{1/2}, \quad (19)$$

where  $\hat{x}$  and  $\hat{y}$  represent predicted values, and  $k = 20$ . Although R-squared is only applicable for linear regression, an approximate value for combined R-squared was derived for illustrative purposes. The combined R-squared was defined as

$$1 - \left( \frac{\sum D^2}{\sum Z^2} \right), \quad (20)$$

$$\text{where } Z = \left\{ (x - x')^2 + [k(y - y')]^2 \right\}^{1/2} \quad (21)$$

and  $x'$  and  $y'$  represent the 25th percentile of  $x$  and  $y$ , respectively. The 25th percentile is selected instead of the mean because the mean values are exaggerated due to the nonlinearity of the equations, and because higher values are less influential to the model. The value from Eq. 20 is not a true R-squared value, but often falls between the  $x$ -based R-squared and the  $y$ -based R-squared values; therefore, it is considered to be a better qualitative measure of the model's predictive accuracy because it is not distorted in the way  $x$ -based R-squared and  $y$ -based R-squared measures would be.

Fatigue life models presented in the original version of NUREG/CR-6909 for estimating the fatigue lives in air of carbon and low-alloy steels in air were developed at ANL as best fits of a Langer curve to an updated version of the PVRC database.<sup>10,46</sup> From those best fits, the fatigue lives,  $N$ , of carbon steels was represented by

$$\ln(N) = 6.614 - 0.00124 T - 1.975 \ln(\epsilon_a - 0.113), \quad (22)$$

and that of low-alloy steels by

$$\ln(N) = 6.480 - 0.00124 T - 1.808 \ln(\epsilon_a - 0.151), \quad (23)$$

where  $\varepsilon_a$  is applied strain amplitude (%), and  $T$  is the test temperature ( $^{\circ}\text{C}$ ). Thus, in room-temperature ( $25^{\circ}\text{C}$ ) air, the fatigue lives of carbon steels was expressed as

$$\ln(N) = 6.583 - 1.975 \ln(\varepsilon_a - 0.113), \quad (24)$$

and that of low-alloy steels, by

$$\ln(N) = 6.449 - 1.808 \ln(\varepsilon_a - 0.151). \quad (25)$$

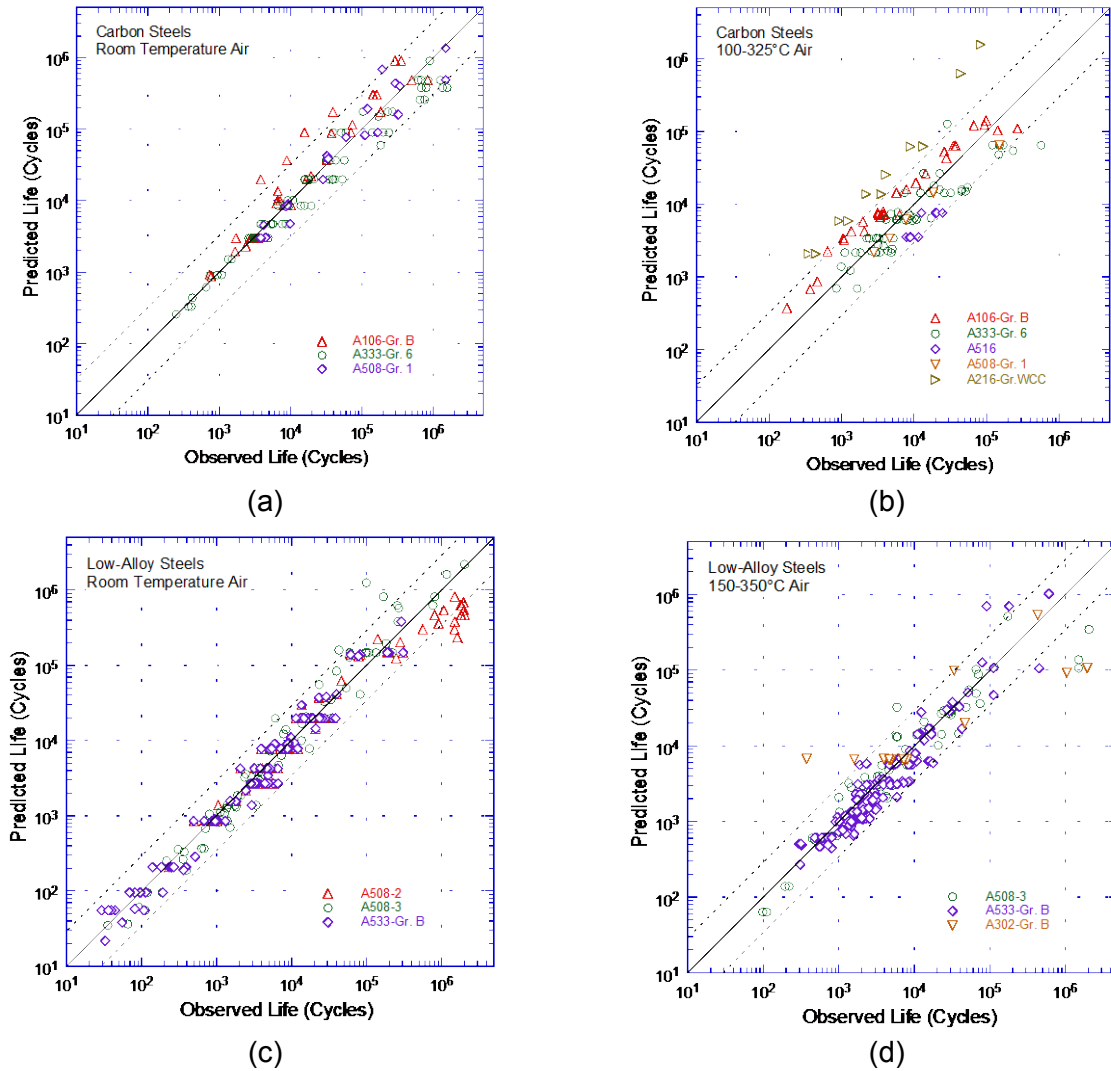


**Figure 31. Experimental and predicted fatigue lives of (a, b) carbon steels and (c, d) low-alloy steels in air.**

Note that Eqs. 24 and 25 were based on incorporation of additional fatigue data and the analysis presented in Section 4.1.7 of Ref. 137; the values of the constant  $A$  in the equations were updated from the values reported in NUREG/CR-6583<sup>10</sup> and NUREG/CR-6815.<sup>46</sup> The heat-to-heat variability of these equations is discussed further in Section 3.1.7 of this report. Relative to the models presented in NUREG/CR-6583, the fatigue lives predicted by the models in the original revision to NUREG/CR-6909 were approximately 2% higher for carbon steel and approximately 16% lower for low-alloy steels. The predicted fatigue lives showed good

agreement with the experimental values; the experimental and predicted values were within a factor of 3. The experimental and predicted fatigue lives of carbon and low-alloy steel data using the expressions defined by Eqs. 24 and 25 are shown in Fig. 31. As discussed in Section 3.1.7, the greater-than-observed fatigue lives for A106-Gr B steel at room temperature and for A216-Gr. WCC at 325°C appear to be due to heat-to-heat variability and not temperature effects.

- *The fatigue life models for carbon and low-alloy steels represent mean values of fatigue lives in air for specimens tested under fully reversed strain-controlled loading. The effects of parameters (such as mean stress, surface finish, size and geometry, and loading history) known to influence fatigue lives were accounted for in the several subfactors that were applied to the mean data air curve to obtain the fatigue design air curve.*

### 3.1.7 Heat-to-Heat Variability

Several factors, such as small differences in material composition and structure, can change the tensile and fatigue properties of materials. The effect of interstitial element content on DSA and the effect of sulfide morphology on fatigue lives are discussed in Sections 3.1.5 and 3.1.4, respectively. The effect of tensile strength on fatigue lives was included in the expression for the ASME mean data air curve described in the Section III criteria document, i.e., constant  $A_f$  in Eq. 2. In addition, the material fatigue limit was correlated with tensile strength, e.g., the fatigue limit increases with increasing tensile yield stress.<sup>213</sup>

The effects of material variability and data scatter must be included in the data evaluation to ensure that the resulting design curves not only describe the available test data adequately, but also adequately describe the fatigue lives of the much larger number of heats of material that are found in the field compared to the limited number of heats used for testing. The effects of material variability and data scatter are often evaluated by comparing the experimental data to a specific model for fatigue crack initiation, e.g., the best fit (in some sense) to the data. The adequacy of the evaluation depends on the sample of data used in the analysis. For example, if most of the data were obtained from a heat of material that has poor resistance to fatigue damage or under loading conditions that show significant environmental effects, the results may be conservative for most of the materials or service conditions of interest. Conversely, if most data are from a heat of material with a high resistance to fatigue damage, the results may be nonconservative for many heats in service.

Another method to assess the effect of material variability and data scatter is to consider the best-fit curves determined from tests on individual heats of materials or loading conditions as samples of a much larger population of heats of materials and service conditions of interest. To do this, the fatigue behavior of each of the heats or loading conditions was characterized by the value of the constant  $A$  in Eq. 6. The values of  $A$  for the various data sets were rank-ordered, and median ranks were used to estimate the cumulative distribution of  $A$  for the population.<sup>214,215</sup> The distributions were fit to lognormal curves. No rigorous statistical evaluation was performed for these curves, but the fits appeared reasonable and described the observed variability adequately. The data were normalized to room-temperature values using Eqs. 22 and 23 (Section 3.1.6). The median value of the constant  $A$ , reported in the original revision of NUREG/CR-6909, was 6.583 and 6.449, respectively, for the fatigue lives of carbon steels and low-alloy steels in room-temperature air. The estimated cumulative distributions of constant  $A$  in the ANL model for fatigue lives for heats of carbon and low-alloy steels included in the original revision of NUREG/CR-6909 and those included in this report are shown in Fig. 32.

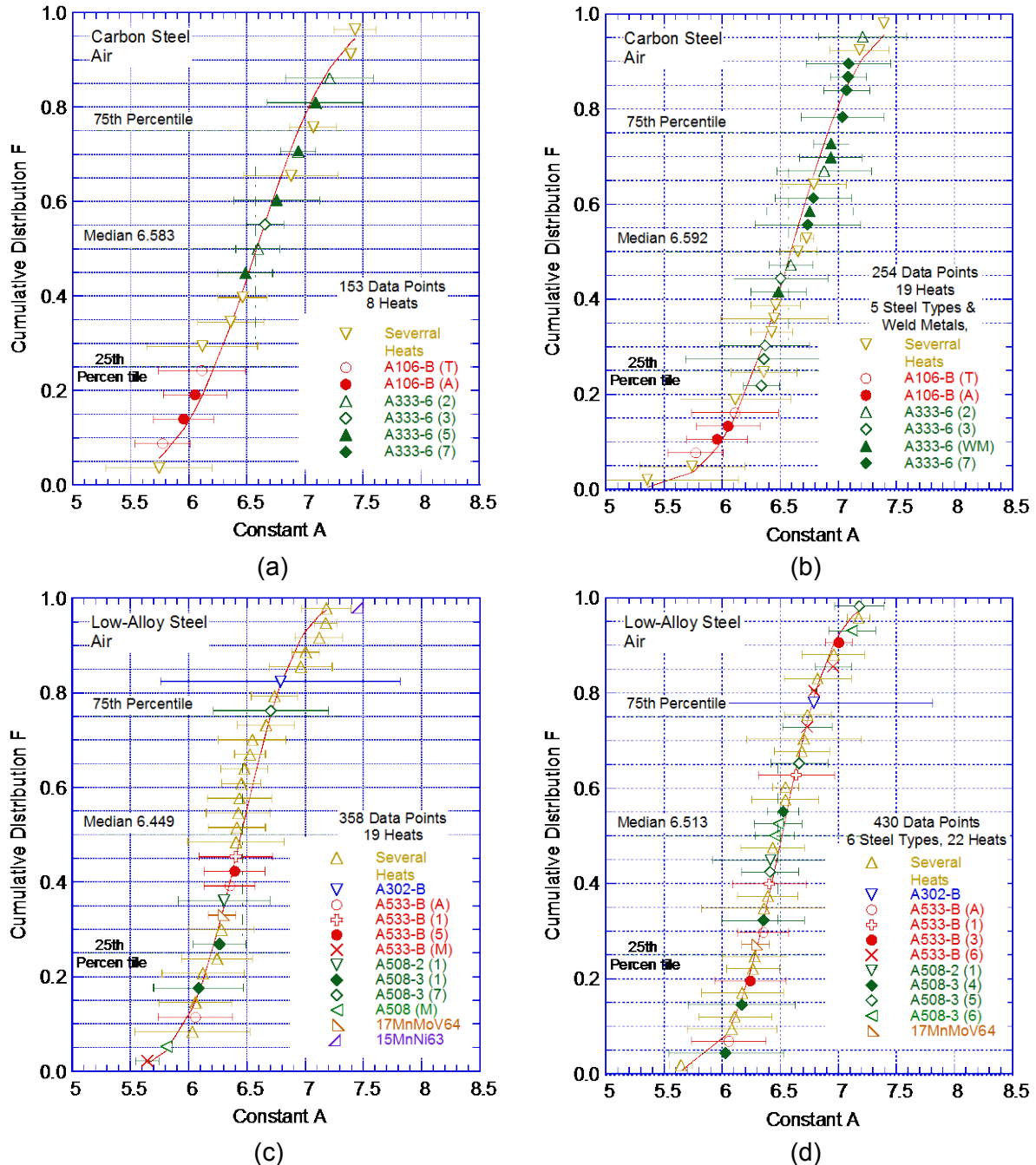


**Figure 32. Estimated cumulative distribution of constant A in the ANL models for fatigue life data in the original revision of NUREG/CR-6909 (a, c) and this report (b, d); (a, b) for heats of carbon steels and (c, d) low-alloy steels in air.**

The results indicate that the ANL fatigue models presented in the original revision of NUREG/CR-6909 for predicting fatigue lives of carbon and low alloy steels in air remain valid. In spite of a significant increase in the number of data points, the median value of the constant A in Eq. 6 did not change significantly for carbon steels (changed from 6.583 to 6.593) or for low-alloy steels (changed from 6.449 to 6.513). Note that the two heats of A106-Gr B carbon steel were in the 10<sup>th</sup> to 25<sup>th</sup> percentile of the data, i.e., the fatigue lives of these heats were much lower than the average value for carbon steels. Also, the average value of the constant A for the A216-Gr. WCC steel at 325°C (after adjusting for temperature effects) was 4.899, which

is significantly lower than the median value of 6.583 for carbon steels. Therefore, it was not included in the reanalysis of the updated fatigue  $\epsilon$ -N database, and the value of the constant A for A216-Gr. WCC is not shown in Fig. 32.

As discussed in the original revision of NUREG/CR-6909, the A values that describe the 5th percentile of these distributions give fatigue  $\epsilon$ -N curves that are expected to bound the fatigue lives of 95% of the heats of the materials tested. The cumulative distributions of A values in Fig. 32 contain two potential sources of error. The means and standard deviations of the populations must be estimated from the means and standard deviations of the samples,<sup>216</sup> and confidence bounds must be obtained on the population means and standard deviations in terms of the sample means and standard deviations. Secondly, even these conditions did not fully address the uncertainties in the distributions because of the large uncertainties in the sample values themselves, i.e., the “horizontal” uncertainty in the actual value of A for a heat of material, as indicated by the error bars in Fig. 32. Therefore, a Monte Carlo analysis was performed to address both sources of uncertainty. The results for the median values and standard deviations of the constant A from the Monte Carlo analysis did not differ significantly from those determined directly from the experimental values.

The results for carbon and low-alloy steels are summarized in Tables 2 and 3, respectively, in terms of values for the constant A that provide bounds for the portion of the population and the confidence that is desired in the estimates of the bounds. In air, the 5<sup>th</sup> percentile value of constant A at a 95% confidence level was 5.559 for carbon steels and 5.689 for low-alloy steels. From Fig. 32. Since the reanalysis did not change the constants significantly, the median values of the constant A for carbon and low-alloy steels were not changed in this report. Thus, constant A for the sample remains 6.583 for carbon steels and 6.449 for low-alloy steels, and the 95/95 values of the factor to account for material variability and data scatter are 2.8 and 2.1 on life for carbon and low-alloy steels, respectively. These factors provide 95% confidence that the resultant lives are greater than those observed for 95% of the materials of interest.

- *The mean data air curves for carbon and low-alloy steels used to develop the fatigue design air curves represented the average fatigue behavior; heat-to-heat variability was included in the subfactor that was applied to the mean data air curve to obtain the fatigue design air curve to account for “data scatter and material variability.”*

**Table 2. Values of constant A in the ANL fatigue life model for carbon steels in air and the factors on life as a function of confidence level and percentage of population bounded.**

Confidence Level	Percentage of Population Bounded (Percentile Distribution of A)				
	95 (5)	90 (10)	75 (25)	67 (33)	50 (50)
Values of Constant A					
50	5.798	5.971	6.261	6.373	6.583
75	5.700	5.883	6.183	6.295	6.500
95	5.559	5.756	6.069	6.183	6.381
Factors on Life					
50	2.2	1.8	1.4	1.2	1.0
75	2.4	2.0	1.5	1.3	1.1
95	2.8	2.3	1.7	1.5	1.2

**Table 3. Values of constant A in the ANL fatigue life model for low-alloy steels in air and the factors on life as a function of confidence level and percentage of population bounded.**

Confidence Level	Percentage of Population Bounded (Percentile Distribution of A)				
	95 (5)	90 (10)	75 (25)	67 (33)	50 (50)
Values of Constant A					
50	5.832	5.968	6.196	6.284	6.449
75	5.774	5.916	6.150	6.239	6.403
95	5.689	5.840	6.085	6.175	6.337
Factors on Life					
50	1.9	1.6	1.3	1.2	1.0
75	2.0	1.7	1.3	1.2	1.0
95	2.1	1.8	1.4	1.3	1.1

### 3.1.8 Fatigue $\epsilon$ -N Behavior of Weld Metals

Available fatigue  $\epsilon$ -N data for carbon and low-alloy steel weld metals in air at room temperature and 289°C are plotted in Fig. 33. The results indicated that, in air, the fatigue lives of carbon and low-alloy steel weld metals were slightly lower than the mean  $\epsilon$ -N behavior of non-welded carbon or low-alloy steel test specimens. Except for one data set for CM US-56B/MF-27 weld metal for which fatigue lives were a factor 2 lower than the mean data curves, the fatigue lives of the other data sets were marginally lower. The results also indicated that the fatigue lives at 289°C were slightly lower than at room temperature. Despite these observations, the available fatigue  $\epsilon$ -N data for carbon and low-alloy steel weld metals were insufficient to accurately establish their fatigue behavior relative to the mean data air curve for carbon steels or low-alloy steels, respectively.

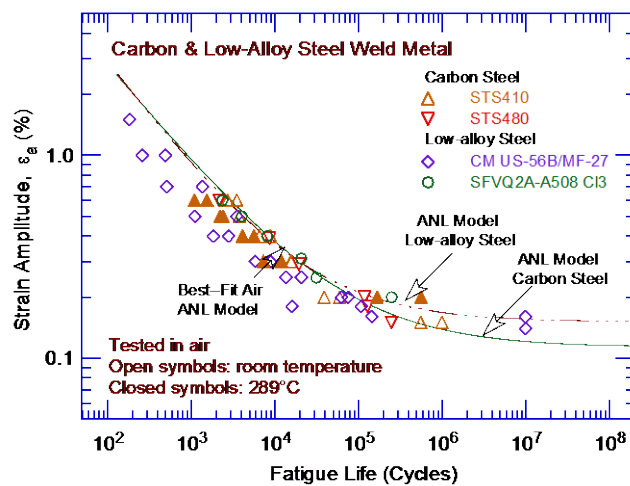


**Figure 33.**  
**Fatigue  $\epsilon$ -N behavior for carbon and low-alloy steel weld metals in air at room temperature and 289°C (Ref. 136).**

- *Until additional fatigue  $\epsilon$ -N data for carbon and low-alloy steel weld metals are available, the fatigue mean air curves for carbon steel or low-alloy steels may also be used for weld metals.*

### 3.1.9 Surface Finish

The effect of surface finish was considered to account for the difference in fatigue lives expected in an actual component with an industrial-grade surface finish compared to the smooth polished surface of test specimens. Fatigue lives are sensitive to surface finish; cracks can initiate at surface irregularities that are normal to the axis of applied stress. The height,



spacing, shape, and distribution of surface irregularities are important for crack initiation. The most common measure of roughness is average surface roughness,  $R_a$ , which is a measure of the height of the irregularities. Investigations of the effects of surface roughness on the low-cycle fatigue of Type 304 SS in air at 593°C indicated that fatigue lives decreased as surface roughness increased.<sup>217,218</sup> The effect of roughness on crack initiation,  $N_i(R)$ , is given by

$$N_i(R) = 1012 R_q^{-0.21}, \quad (26)$$

where the root-mean-square (RMS) value of surface roughness,  $R_q$ , is in  $\mu\text{m}$ . Typical values of  $R_a$  for surfaces finished by different metalworking processes in the automotive industry<sup>219</sup> indicated that a value of  $R_a$  of 3  $\mu\text{m}$  (or an  $R_q$  of 4  $\mu\text{m}$ ) represented the maximum surface roughness for drawing/extrusion, grinding, honing, and polishing processes, and a mean value for the roughness range for milling or turning processes. For carbon or low-alloy steels, an  $R_q$  of 4  $\mu\text{m}$  in Eq. 26 would decrease fatigue life by a factor of 3.7 (the  $R_q$  of a smooth polished specimen is approximately 0.0075  $\mu\text{m}$ ).<sup>217</sup>

A fatigue test was conducted on a A106-Gr B carbon steel specimen that was intentionally roughened in a lathe, under controlled conditions, with 50-grit sandpaper to produce circumferential scratches with an average roughness of 1.2  $\mu\text{m}$  and an  $R_q$  of 1.6  $\mu\text{m}$  (approximately 62 micro in.).<sup>46</sup> The results for smooth and roughened specimens are shown in Fig. 34. In air, the fatigue life of a roughened A106-Gr B specimen was a factor of approximately 3 lower than that of smooth specimens. Another study of the effect of surface finish on the fatigue lives of carbon steels in room-temperature air showed a factor of 2 decrease in life when  $R_a$  was increased from 0.3 to 5.3  $\mu\text{m}$ .<sup>220</sup> These results are consistent with Eq. 26. Thus, a factor of 2 to 3 on cycles is necessary to account for surface finish effects on the fatigue lives of carbon and low-alloy steels.

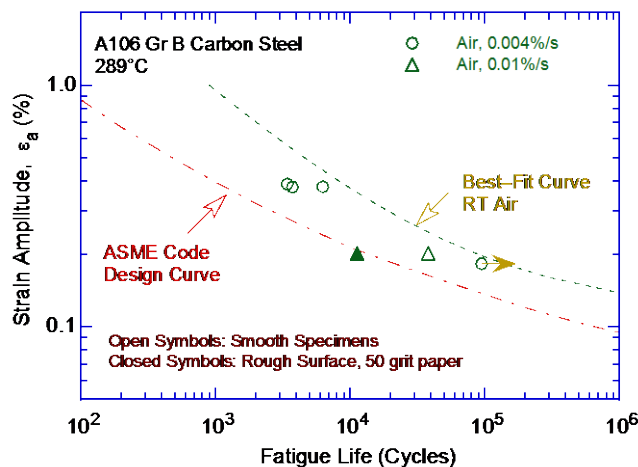


**Figure 34.**  
Effect of surface finish on the  
fatigue life of A106-Gr B carbon  
steel in air at 289°C (Ref. 46).

- The effect of surface finish was included as part of the “surface finish and environment” subfactor that was applied to the mean data air curves to obtain the fatigue design air curves for carbon and low-alloy steels.

### 3.1.10 Extension of the Best-Fit Mean Curve from $10^6$ to $10^{11}$ Cycles

The experimental fatigue  $\epsilon$ - $N$  air curves that were used to develop the 2011 ASME Code Section III fatigue design air curve for carbon and low-alloy steels were based on low-cycle fatigue data (less than  $2 \times 10^5$  cycles). The design air curves proposed in this report were

developed from a larger database that included fatigue lives up to  $10^8$  cycles. Both the ASME mean air curves and the ANL models in this report used the modified Langer equation to express the best-fit mean air curves; they are not recommended for estimating fatigue lives beyond the range of the experimental data, i.e., in the high-cycle fatigue regime.

An extension of the current high-cycle fatigue design curves in Section III and Section VIII, Division 2 of the ASME Code for carbon and low-alloy steels from  $10^6$  to  $10^{11}$  cycles was proposed by W. J. O'Donnell to the ASME Section III Subgroup on Fatigue Strength.\* In the high-cycle regime at temperatures not exceeding  $371^\circ\text{C}$  ( $700^\circ\text{F}$ ), the stress amplitude vs. life relationship is expressed as

$$S_a = E\varepsilon_a = C_1 N^{-0.05}, \quad (27)$$

where  $\varepsilon_a$  is applied strain amplitude,  $E$  is the elastic modulus,  $N$  is the fatigue life, and  $C_1$  is a constant. A fatigue life exponent of -0.05 was selected based on the fatigue stress range vs. fatigue life data on plain plates, notched plates, and typical welded structures given in Welding Research Council (WRC) Bulletin 398.<sup>221</sup> Because the data were obtained from load-controlled tests with an  $R$  ratio of zero, they take into account the effect of maximum mean stresses and may over-estimate the effect of mean stress under strain-controlled loading conditions. In addition, the fatigue data presented in WRC Bulletin 398 extend only up to  $5 \times 10^6$  cycles; extrapolation of the results to  $10^{11}$  cycles using a fatigue life exponent of -0.05 may yield overly conservative estimates of fatigue life. Finally, ASME received feedback from the evaluation of plant trouble reports, laboratory tests of socket welded joints, and plant operating experience that supported their use of Eq. 27.

Manjoine and Johnson<sup>213</sup> developed fatigue design curves up to  $10^{11}$  cycles for carbon steels and austenitic SSs from inelastic and elastic strain relationships, which were correlated with ultimate tensile strength. The log-log plots of the elastic strain amplitudes vs. fatigue life data were represented by a bilinear curve. In the high-cycle regime, the elastic-strain-vs.-life curve had a small negative slope instead of a fatigue limit.<sup>213</sup> For carbon steel data at room temperature and  $371^\circ\text{C}$  ( $700^\circ\text{F}$ ) and fatigue lives extending up to  $4 \times 10^7$  cycles, Manjoine and Johnson obtained an exponent of -0.01. The fatigue  $\varepsilon$ - $N$  data used in this report at room temperature and with fatigue lives up to  $10^8$  cycles yielded a fatigue life exponent of approximately -0.007 for both carbon and low-alloy steels. Because the data are limited, the more conservative exponent value (i.e., -0.01) obtained by Manjoine and Johnson<sup>213</sup> was used in the initial edition of NUREG/CR-6909 report. In the high-cycle regime, the applied stress amplitude was expressed by the relationship

$$S_a = E\varepsilon_a = C_2 N^{-0.01}. \quad (28)$$

In the initial edition of the NUREG/CR-6909, Eq. 28 was used to extend the best-fit mean air curves beyond  $10^6$  cycles (in the high-cycle regime); thus, the mean stress-life curves exhibited a small negative slope instead of the fatigue limit predicted by the modified Langer equation. The selection of a smaller value for the fatigue life exponent to extend the best-fit curve was based on evaluation of thermal fatigue data, which are bounded by Eq. 28. However, the high-cycle thermal fatigue data are limited, and the data do not consider mechanical fatigue (i.e., vibration).

---

\*W. J. O'Donnell, "Proposed Extension of ASME Code Fatigue Design Curves for Carbon and Low-Alloy Steels from  $10^6$  to  $10^{11}$  Cycles for Temperatures not Exceeding  $700^\circ\text{F}$ ," presented to ASME Subgroup on Fatigue Strength, December 4, 1996.

As discussed earlier in this report, the classical fatigue limit for ferrous alloys is a consequence of performing fatigue tests at constant cyclic stress or strain range and determining the threshold range below which cracks cannot propagate beyond microstructural barriers and fatigue failures do not occur. Miller and O'Donnell<sup>222</sup> discussed the causes that lead to elimination of the fatigue limit, including the introduction of transitory cyclic processes or time-dependent mechanisms that permit a previously nonpropagating crack to grow across microstructural barriers. The authors argued that the most probable significant condition for engineering plants designed to last beyond  $10^6$  cycles is the introduction of very low cyclic stress vibrations at high mean stress levels, with or without other mechanisms such as corrosion or time-dependent mechanisms. Therefore, in this report, to better accommodate the vibration data (e.g., Ref. 221), the extension of the fatigue stress or strain-life curves beyond  $10^6$  cycles is based on the more conservative Eq. 27 rather than Eq. 28, i.e., an exponent of -0.05 is used. The value of constant  $C_1$  was determined from the value of strain amplitude at which the slope of the curve expressed by Eq. 27 is the same as that of the fatigue  $\epsilon$ -N curve expressed by Eq. 24 for carbon steels or Eq. 25 for low-alloy steels.

- *The fatigue design air curves for carbon and low-alloy steels were extended beyond  $10^6$  cycles using Eq. 27, which is consistent with the methodology used to develop the fatigue design air curve for carbon and low-alloy steels in the 2011 Addenda of ASME Code Section III.*

### 3.1.11 Fatigue Design Curves

Although the two equations for the ASME Code mean air curves for carbon and low-alloy steels (i.e., Eqs. 7 and 8) are significantly different (because the mean stress correction is much larger for the low-alloy steels), the differences between the curves are much smaller when mean stress corrections are considered. Thus, ASME Code, Section III provides one common fatigue design air curve for both carbon and low-alloy steels. The ASME Code fatigue design air curves for carbon and low-alloy steels were obtained from the best-fit curves in air (i.e., Eqs. 7 and 8, respectively) by first correcting for mean stress effects by using the modified Goodman relationship, followed by reducing the mean-stress adjusted curves by factors of 2 on stress or 20 on cycles, whichever was more conservative. The discussions presented in Section 7.5 of the original edition of NUREG/CR-6909 indicated that the current ASME Code requirement of a factor of 20 on cycles, to account for the effects of material variability and data scatter, specimen size, surface finish, and loading history, was conservative by at least a factor of 1.7 for these steels. To reduce this conservatism, separate fatigue design air curves based on the ANL models for carbon and low-alloy steels were developed using factors of 12 on life and 2 on stress. The fatigue design air curves developed following this approach for carbon and low-alloy steels are shown in Fig. 35. The difference between the design air curves based on the ANL models and the ASME Code design air curve is due to the difference in the factor on life used to obtain these curves i.e., 20 for the ASME Code curve and 12 for the ANL curves. In addition, for the carbon steel design air curve, the conservatism in the high-cycle regime was corrected in the ANL models.

The ASME Code fatigue design air curve for carbon and low-alloy steels with ultimate tensile strength (UTS) less than 552 MPa (80 ksi) included an extension of the design curve to  $10^{11}$  cycles, which was proposed by W. J. O'Donnell and was based on Eq. 27 in this report. In the initial edition of NUREG/CR-6909, the fatigue design air curves developed based on the ANL fatigue  $\epsilon$ -N models were extended in the high-cycle regime beyond  $10^6$  cycles using Eq. 28 instead of Eq. 27. However, as discussed in Section 3.1.10, and to better accommodate the field vibration data, the extension of the fatigue design curves beyond  $10^6$  cycles is based on Eq. 27. The values of stress amplitude ( $S_a$ ) vs. cycles for the ASME Code Section III fatigue

design air curve with O'Donnell's extension, and the design curve based on Eq. 27 and the ANL fatigue life models from Eq. 24 for carbon steels and Eq. 25 for low-alloy steels, are listed in Table 4. The corresponding fatigue design air curves are shown in Figs. 36 and 37, respectively, for carbon and low-alloy steels. The values of stress amplitude vs. cycles presented in the initial edition of NUREG/CR-6909 for the fatigue design air curves based on the ANL fatigue  $\epsilon$ -N models and Eq. 28 are presented in Table 5 for comparison.

- *Separate fatigue design air curves were developed for carbon and low-alloy steels. These curves were developed from the ANL models using factors of 12 on life and 2 on stress. The results indicated that the ASME Code Section III fatigue design air curve for carbon and low-alloy steels for ultimate tensile strengths less than 552 MPa (80 ksi) was conservative with respect to the existing fatigue  $\epsilon$ -N data, particularly for carbon steels. In this report, the extension of the fatigue design air curves beyond  $10^6$  cycles was based on Eq. 27 instead of Eq. 28 used in the initial revision to NUREG/CR-6909.*

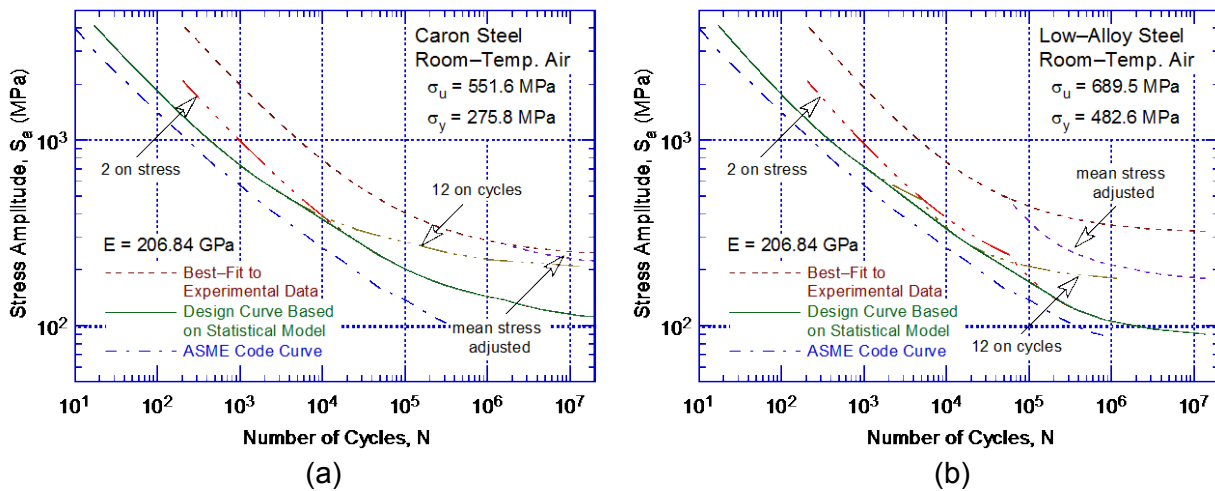


**Figure 35. Fatigue design curves based on the ANL model for (a) carbon steels and (b) low-alloy steels in air.**

**Table 4. Fatigue design curves for carbon and low-alloy steels including proposed updated extension to  $10^{11}$  cycles.**

Cycles	Stress Amplitude (MPa/ksi)			Cycles	Stress Amplitude (MPa/ksi)		
	ASME Code Curve	Eqs. 24 & 27 Carbon Steel	Eqs. 25 & 27 Low-Alloy Steel		ASME Code Curve	Eqs. 24 & 27 Carbon Steel	Eqs. 25 & 27 Low-Alloy Steel
1 E+01	3999 (580)	5355 (777)	5467 (793)	2 E+05	114 (16.5)	176 (25.5)	141 (20.5)
2 E+01	2827 (410)	3830 (556)	3880 (563)	5 E+05	93.1 (13.5)	154 (22.3)	116 (16.8)
5 E+01	1896 (275)	2510 (364)	2438 (354)	1 E+06	86.2 (12.5)	142 (20.6)	106 (15.4)
1 E+02	1413 (205)	1820 (264)	1760 (255)	2 E+06		130 (18.9)	98 (14.2)
2 E+02	1069 (155)	1355 (197)	1300 (189)	5 E+06		120 (17.4)	94 (13.6)
5 E+02	724 (105)	935 (136)	900 (131)	1 E+07	76.8 (11.1)	115 (16.7)	91 (13.2)
1 E+03	572 (83)	733 (106)	720 (104)	2 E+07		110 (16.0)	88 (12.7)
2 E+03	441 (64)	584 (84.7)	576 (83.5)	5 E+07		105 (15.2)	84 (12.2)
5 E+03	331 (48)	451 (65.4)	432 (62.7)	1 E+08	68.5 (9.9)	101 (14.7)	81 (11.8)
1 E+04	262 (38)	373 (54.1)	342 (49.6)	1 E+09	61.1 (8.8)	90 (13.1)	72.3 (10.5)
2 E+04	214 (31)	305 (44.2)	276 (40.0)	1 E+10	54.4 (7.9)	81 (11.7)	64.4 (9.3)
5 E+04	159 (23)	238 (34.5)	210 (30.5)	1 E+11	48.5 (7.0)	72 (10.4)	57.4 (8.3)
1 E+05	138 (20.0)	201 (29.2)	172 (24.9)				

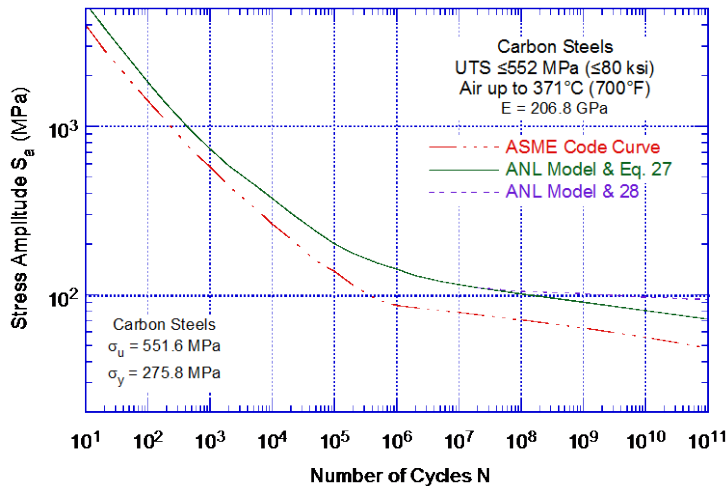


**Figure 36.**  
Fatigue design curve for carbon steels in air. The curve developed from the ANL model is based on factors of 12 on life and 2 on stress.

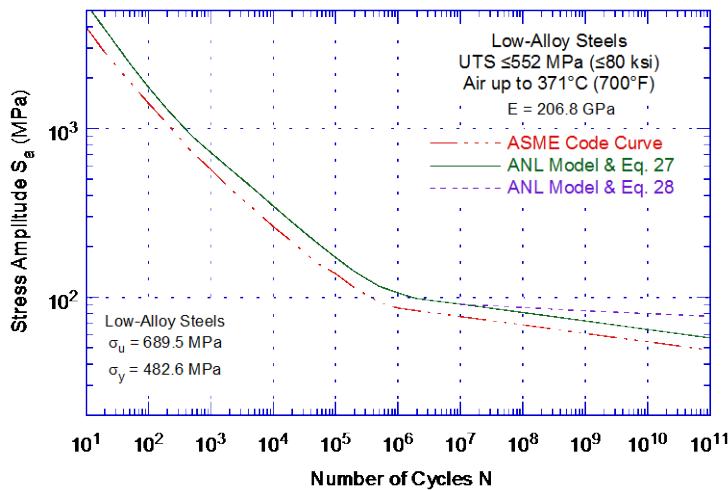


**Figure 37.**  
Fatigue design curve for low-alloy steels in air. The curve developed from the ANL model is based on factors of 12 on life and 2 on stress.

**Table 5. Fatigue design curves for carbon and low-alloy steels and the extension to 10<sup>11</sup> cycles proposed in the initial revision to NUREG/CR-6909.**

Stress Amplitude (MPa/ksi)				Stress Amplitude (MPa/ksi)			
Cycles	ASME	Eqs. 24 & 28	Eqs. 25 & 28	Cycles	ASME	Eqs. 24 & 28	Eqs. 25 & 28
	Code Curve	Carbon Steel	Low-Alloy Steel		Code Curve	Carbon Steel	Low-Alloy Steel
1 E+01	3999 (580)	5355 (777)	5467 (793)	2 E+05	114 (16.5)	176 (25.5)	141 (20.5)
2 E+01	2827 (410)	3830 (556)	3880 (563)	5 E+05	93 (13.5)	154 (22.3)	116 (16.8)
5 E+01	1896 (275)	2510 (364)	2438 (354)	1 E+06	86 (12.5)	142 (20.6)	106 (15.4)
1 E+02	1413 (205)	1820 (264)	1760 (255)	2 E+06		130 (18.9)	98 (14.2)
2 E+02	1069 (155)	1355 (197)	1300 (189)	5 E+06		120 (17.4)	94 (13.6)
5 E+02	724 (105)	935 (136)	900 (131)	1 E+07	76.5 (11.1)	115 (16.7)	91 (13.2)
1 E+03	572 (83)	733 (106)	720 (104)	2 E+07		110 (16.0)	90 (13.1)
2 E+03	441 (64)	584 (84.7)	576 (83.5)	5 E+07		107 (15.5)	88 (12.8)
5 E+03	331 (48)	451 (65.4)	432 (62.7)	1 E+08	68.3 (9.9)	105 (15.2)	87 (12.6)
1 E+04	262 (38)	373 (54.1)	342 (49.6)	1 E+09	60.7 (8.8)	102 (14.8)	83 (12.0)
2 E+04	214 (31)	305 (44.2)	276 (40.0)	1 E+010	54.5 (7.9)	97 (14.1)	80 (11.6)
5 E+04	159 (23)	238 (34.5)	210 (30.5)	1 E+011	48.3 (7.0)	94 (13.6)	77 (11.2)
1 E+05	138 (20.0)	201 (29.2)	172 (24.9)				

## 3.2 Wrought and Cast Austenitic Stainless Steels and Weld Metals

### 3.2.1 Experimental Data

The relevant fatigue  $\epsilon$ -N data used to evaluate wrought and cast austenitic SSs in air include the large JNES database;<sup>136</sup> data developed at ANL<sup>45</sup> and GE;<sup>14,15</sup> results of Keller,<sup>63</sup> and the data<sup>64,65,70,73</sup> compiled by Jaske and O'Donnell<sup>61</sup> for developing fatigue design criteria for pressure vessel alloys. The database is composed of 770 tests from which 622 data points were obtained; 332 tests (267 data points) on Type 304 SS, 315 tests (244 data points) on Type 316 SS, 96 tests (77 data points) on SS weld metals (34 tests (23 data points) on Type 304 SS and 62 tests (54 data points) on Type 316 SS weld metals), and 37 tests (34 data points) for CF-8M grade of cast austenitic SSs. Both low-carbon and high-carbon grades of Types 304 and 316 SS are included in the database. Out of these, 432 data points were obtained at room temperature, 7 data points were obtained at 100-200°C, and 183 data points were obtained at 250-325°C. Another 70 data points obtained at temperatures of 400°C and above were not included in the present reanalysis to verify the fatigue  $\epsilon$ -N expression for austenitic SSs in air because they were outside of the temperature range experienced in LWRs. As discussed in Section 3.2.4, the fatigue  $\epsilon$ -N data for austenitic SSs shows some temperature dependence above 460°C. A summary of the points included in the updated database used for the present analyses, as categorized by material type and test environment, is presented in Table 6. Other material information such as chemical composition, heat treatment, and room temperature tensile properties of the various types and heats of materials is given in Appendix B.

**Table 6. Sources of the fatigue  $\epsilon$ -N data on wrought and cast austenitic stainless steels in an air environment.**

ANL Mat. ID	Material Heat Designation <sup>a</sup>	Carbon Content (wt.%)	Test Temperature (°C)	No. of Data Points	Source	Applicable Reference
<u>Type 304 Stainless Steels</u>						
1	304-1	0.050	288	10	JNES (Tokimasa)	136
2	304-30, 31	0.050	25	10, 4	JNES (Yamanaka),	136
3	304-3H	0.060	25	8	JNES (Enomoto),	136
4	304-4B	0.050	25	10	JNES (Kitigawa)	136
5	304-5B	0.060	25	3	JNES (Sakamoto)	136
6	304-6B	0.060	25	11	JNES (Tsunenari)	136
7	304-7B	0.059	25	10	JNES (Kasahara)	136
8	304-8B	0.060	25	6	JNES (Ichihara)	136
10	304-10, 10H	0.060	25, 300, 100	2, 7, 2	JNES (Usami)	136
11	304-11H	0.070	25	7	JNES (Yamanaka)	136
12	304-12	-	25	11	JNES (Nishijima)	136
13	304-13	0.026	21	10	Jaske & O'Donnell	64
14	304-14	0.026	21	9	Jaske & O'Donnell	64
15	304-15	-	21	6	Jaske & O'Donnell	63
16	304-16	0.060	21	8	Jaske & O'Donnell	70
17	304-17	-	21	6	Jaske & O'Donnell	65
18	304-18	0.020	27	8	Jaske & O'Donnell	73
20	304-G	0.060	25, 260	9, 9 <sup>b</sup>	GE	14,15
21	304-A2	0.060	288	4	ANL	45
22	304-21, 21T	0.060	25, 325	2, 7	JNES (Kanasaki, Tsutsumi)	136

ANL Mat. ID	Material Heat Designation <sup>a</sup>	Carbon Content (wt.%)	Test Temperature (°C)	No. of Data Points	Source	Applicable Reference
23	304-32	0.070	300	3	JNES (Endo)	136
24	304-35	0.070	25, 289	8, <sup>c</sup> 5	JNES (Hirano)	136
26	304HP-1	0.050	25	6	JNES (Nishijima)	136
27	304HP-2	0.060	25	17, <sup>c</sup> 14 <sup>c,d</sup>	JNES (Nishijima)	136
28	304L-E	0.039	150,300	5, 11	Solomon	58-60
29	304L-1	0.017	25	5	JNES (Hirano)	136
30	304L-G	0.022	260	7	GE	14,15
31	304L	0.013	25	9	JNES (Suzuki)	136
<u>Type 316 Stainless Steels</u>						
32	316-1H	0.055	25, 290	7, 8	JNUFAD (Tokimasa)	210
33	316-2	0.050	25	6	JNES (Kaneo)	136
34	316-3H	0.040	25	6	JNES (Ikemoto)	136
35	316-4	0.060	21	4	Jaske & O'Donnell	63
38	316-7	-	21	8	Jaske & O'Donnell	61
39	316-8	-	22	3	Jaske & O'Donnell	61
40	316-9	-	21	5	Jaske & O'Donnell	61
41	316-10	-	21	4	Jaske & O'Donnell	61
42	316-12T, 25T	0.060	325, 25	7, 5	JNES (Kanasaki, Tsutsumi)	136
45	316-25, -25, -27T	0.040, 0.060	25, 325, 25	4, 6, 6	JNES (EFT, PLEX)	136
46	316-26T	0.057	25	10 <sup>e</sup>	JNES (EFT)	136
47	316-1H, 316L-1H	0.055, 0.015	25, 290	7, 7	JNES (Tokimasa)	136
48	316N-1	0.010	25, 288	25 <sup>b</sup> , 18 <sup>b</sup>	JNES (Yamauchi, Matsuno, Tokimasa)	136
50	316N-3H	0.012	25, 290	7, 7	JNES (Tokimasa)	136
51	316N-6	0.007	25	12	JNES (Higuchi)	136
52	316N-7	0.008	25, 290	25, 14	JNES (Utsunomiya, Nagata, Higuchi, Kanasaka, Ogawa)	136
53	316N-8	0.011	25, 289	5, 8	JNES (Hirano)	136
54	316N-A	0.013	22, 288, 320	12, 6, 3	ANL	45
<u>Stainless Steel Weld Metals</u>						
55	304HP-WM-1	0.058	25	7 <sup>d</sup> , 10	JNES (Nishijima)	136
56	304-WM-2	0.034	25	6	JNES (Kanasaki)	136
57	316-WM	0.020	25	6 <sup>f</sup>	JNES (EFT)	136
58	316N-WM-1	0.018	25, 290	13, 11	JNES (Ogawa, Nagata)	136
59	316N-WM-2	0.017	25, 289	10, 7	JNES (Hirano)	136
60	316N-WM-3	0.002	25	7	JNES (Kanasaki)	136
<u>Cast Austenitic Stainless Steels</u>						
61	CF-8M-1	0.053	325	12	JNES (Tsutsumi)	136
62	CF-8M-2	0.050	25	10	JNES (Hirano)	136
63	CF-8M-3	0.050	25	6	JNES (Kanasaki)	136
68	CF-8M-8	0.064	288	5 <sup>b</sup>	ANL	45
69	CF-8M-9	0.065	288	1 <sup>b</sup>	ANL	45

<sup>a</sup> The last letter at the end of the material heat designation refers to the following: H = hourglass specimens, T = tube specimens, and B = bending tests.

<sup>b</sup> Includes thermally aged specimens.

<sup>c</sup> Half the tests performed on hourglass specimens.

<sup>d</sup> Tests performed in axial load-control using a sinusoidal waveform.

<sup>e</sup> Five tests each performed on solid cylindrical specimens and tube specimens.

<sup>f</sup> Tests performed on tube specimens.

The fatigue  $\epsilon$ - $N$  data for Types 304, 304L, 316, and 316NG SSs in air at temperatures between room temperature and 400°C are shown in Fig. 38. The best-fit air curve based on the updated ANL fatigue life model (Eq. 29 in Section 3.2.6) and the mean-data air curve from ASME Code Section III prior to the 2009b Addenda are included in the plots in this figure. The results indicate that the fatigue lives of Types 304, 304L, and 316 SS are comparable and show excellent agreement with the ANL model with respect to the mean data air curve. The fatigue lives of Type 316NG are slightly higher than those for Types 304, 304L, and 316 SS at high strain amplitudes. However, all of the data are evenly distributed within the scatter band along the ANL mean air curve for austenitic SSs. Some of the tests on Type 316 SS in room-temperature air were conducted in load-control mode at stress levels in the range of 190–230 MPa. The data are shown as triangles in Fig. 38, with strain amplitudes of 0.1–0.12% and fatigue lives in the range of  $7 \times 10^4$  to  $3 \times 10^7$  cycles. For these tests, the strain amplitude was calculated only as elastic strain rather than also including the portion of the strain from plastic loading. When plastic strain was considered, based on cyclic stress-vs.-strain correlations for Type 316 SS,<sup>45</sup> actual strain amplitudes for these tests ranged from 0.23 to 0.32%. Therefore, these results were excluded from the analysis of the fatigue  $\epsilon$ - $N$  data to develop the model for estimating the fatigue lives of these steels in air so as not to interject an inconsistent bias in the evaluation.

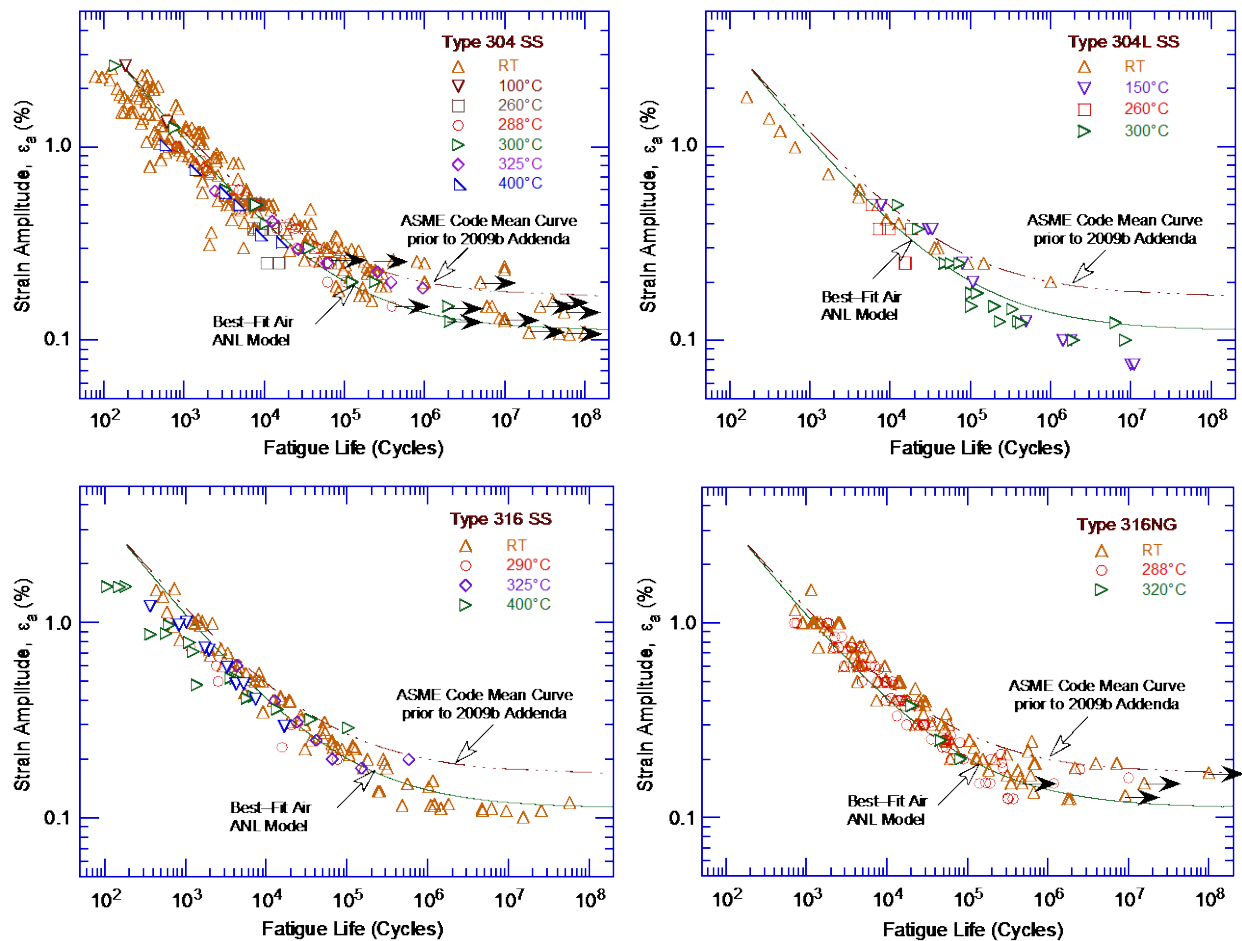


**Figure 38.** Fatigue  $\epsilon$ - $N$  behavior for Types 304, 304L, 316, and 316NG SS austenitic stainless steels in air at various temperatures up to 400°C (Refs. 13,42-47, 61,136).



The results in Fig. 38 indicated that the mean-data air curve in Section III of the ASME Code prior to the 2009b Addenda was not consistent with the existing fatigue  $\epsilon$ -N data for austenitic SSs. At strain amplitudes less than 0.3% [stress amplitudes less than 585 MPa (84.9 ksi)], the ASME Code mean air curve predicted significantly longer fatigue lives than those observed experimentally for several heats of austenitic SSs with compositions and tensile strengths within the ASME specifications. The difference between the ASME Code Section III mean air curve and the best-fit of the available experimental data was caused by differences in the tensile strengths of the steels. The ASME Code Section III mean air curve represents SSs with relatively high tensile strengths; the fatigue  $\epsilon$ -N data obtained during the last 30 years were obtained on SSs with lower tensile strengths. Furthermore, for the mean air curve from Section III of the ASME Code prior to the 2009b Addenda, the  $10^6$ -cycles fatigue limit (i.e., the stress amplitude at a fatigue life of  $10^6$  cycles) was 389 MPa, which is greater than the monotonic yield strength of austenitic SSs most commonly used (approximately 303 MPa). Consequently, the fatigue design air curve for austenitic SSs in Section III of the ASME Code did not include a mean stress correction for fatigue lives below  $10^6$  cycles. Studies by Wire et al.<sup>223</sup> and Solomon, et al.,<sup>58</sup> on the effects of residual stress on fatigue lives demonstrated that mean stress decreased the  $10^6$ -cycles fatigue limits of materials; the extent of these effects depended on the cyclic hardening behavior of the materials and the resultant decreases in strain amplitudes developed during load-controlled cycling. Strain hardening is more pronounced at high temperatures (e.g., 288-320°C) or at high mean stress values (e.g., greater than 70 MPa); therefore, as observed by Wire et al. and Solomon et al., fatigue lives for load-controlled tests with mean stress were actually increased at high temperatures or large values of mean stress. In both studies, under load controlled conditions, mean stress effects were observed at low temperatures (150°C) or at relatively low mean stress values (less than 70 MPa).

Wire et al.<sup>223</sup> performed fatigue tests on two heats of Types 304 SS to establish the effects of mean stress under both strain controlled and load controlled conditions. The strain-controlled tests indicated “an apparent reduction of up to 26% in strain-amplitude occurred in the low and intermediate cycle regime ( $<10^6$  cycles) for a mean stress of 138 MPa.” However, the results were affected by both mean stress and cold work. Although the composition and vendor-supplied tensile strengths for the two heats of Type 304 SS were within ASME Code specifications, the measured mechanical properties showed much larger variations than indicated by the vendor properties. Wire et al. stated, “at 288°C, yield strength varied from 152-338 MPa. These wide variations are attributed to variations in [cold] working from the surface to the center of the thick cylindrical forgings.” After separating the individual effects of mean stress and cold work, the Wire et al. results indicated a 12% decrease in strain amplitude for a mean stress of 138 MPa. These results were consistent with the predictions based on conventional mean stress models such as the Goodman correlation.

The current ASME Code Section III fatigue design air curve (i.e., 2009b Addenda or later editions of the ASME Code) is based on the ANL model presented in Eq. 29. This curve is consistent with the extensive fatigue  $\epsilon$ -N data analyzed in this report. Additional details of the analysis are presented in Section 3.2.6.

- *The ASME Code Section III fatigue design air curve is now based on the ANL model and is consistent with the existing fatigue  $\epsilon$ -N data for austenitic SSs.*

### 3.2.2 Specimen Geometry and Type of Loading

The influence of specimen geometry (hourglass vs. gauge length specimens) on the fatigue lives of Types 304 and 316 SS is shown in Fig. 39. At temperatures up to 300°C, specimen geometry had little or no effect on the fatigue lives of austenitic SSs; the fatigue lives of hourglass specimens were comparable to those of gauge specimens.

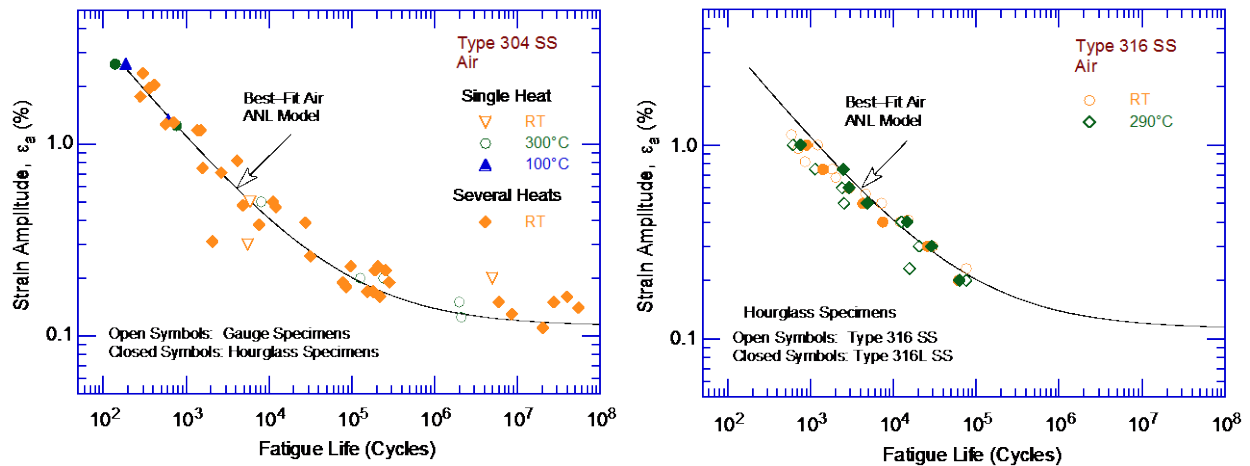


**Figure 39. Influence of specimen geometry on fatigue lives of Types 304 and 316 stainless steels (JNUFAD data).**

Figure 40 shows the results of strain-controlled bending fatigue tests tested on rectangular bar specimens of Type 304 SS in room-temperature air. Although all of the fatigue tests were performed at high strain amplitudes (i.e., producing fatigue lives less than  $10^4$  cycles), the bending-test data were evenly distributed along the ANL mean data air curve for austenitic SSs.

- *Fatigue  $\epsilon$ - $N$  data obtained on hourglass specimens, straight gauge specimens, or bending test specimens may be used to develop the fatigue design air curves.*

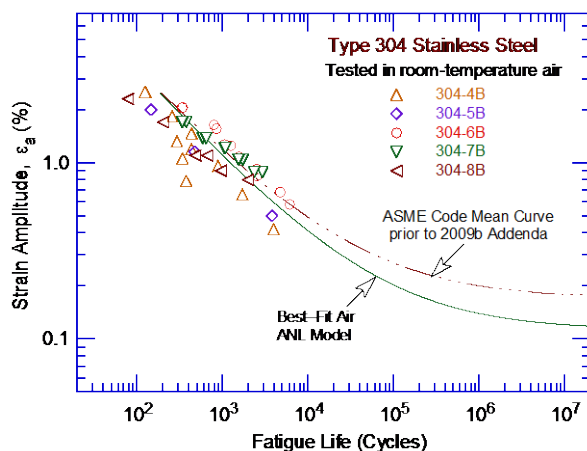


**Figure 40. Influence of bending loading on fatigue lives of Types 304 and 316 stainless steels (JNUFAD data).**

### 3.2.3 Strain Rate

A statistical analysis of the fatigue  $\epsilon$ -N data presented in Ref. 45 indicated that the fatigue lives of austenitic SSs in an air environment decreased with decreasing strain rate at temperatures between 400 and 430°C. However, studies at EdF in France indicated that variations in strain rate in the range of 0.4–0.008%/s had no effect on the fatigue lives of SSs at temperatures up to 400°C.<sup>57</sup> Thus, for the fatigue data analysis presented in this report, strain rate effects on fatigue lives in air were considered insignificant.

- *Effects of strain rate on the fatigue lives of austenitic SSs in air were considered insignificant.*

### 3.2.4 Temperature

The fatigue lives of austenitic SSs in air at temperatures between room temperature and 400°C are plotted in Fig. 38. The results indicated that the fatigue lives of Types 304, 304L, 316, and 316NG SS did not show any dependence on temperature from room temperature up to 400°C. These results are consistent with the observation of Amzallag et al. (Ref. 57).

Additional fatigue data at temperatures between 427 and 456°C are plotted in Fig. 41.<sup>61-63</sup> The results indicated that the fatigue  $\epsilon$ -N data at temperatures between 400 and 460°C were evenly distributed along the ANL best-fit air curve. Furthermore, for austenitic SSs, DSA is typically observed at temperatures of 500–600°C.<sup>206</sup> Therefore, based on these results, the fatigue  $\epsilon$ -N data for austenitic SSs in air was represented by a single curve for temperatures from room temperature up to 450°C.

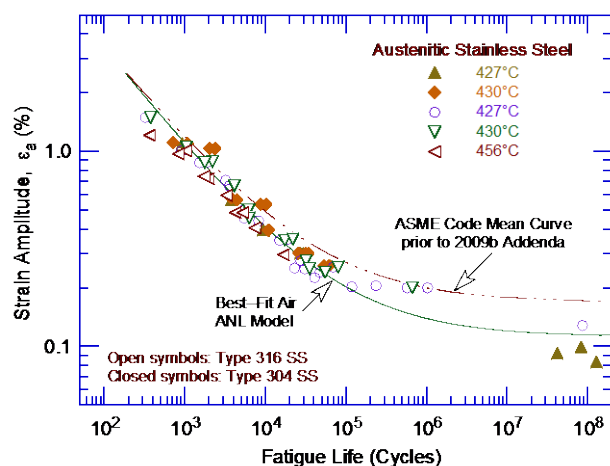


**Figure 41.**  
**Influence of temperature on fatigue lives of austenitic stainless steels in air (Ref. 61-63).**

However, studies at GE by Solomon et al. indicate that temperature influenced the fatigue limit of austenitic SSs because of differences in the secondary hardening behavior of the material.<sup>60</sup> Secondary hardening is the transformation of retained austenite to martensite causing an increase in hardness. This frequently occurs in high alloy steels due to precipitation of carbides during the tempering process. For a heat of Type 304L SS, the fatigue limit was higher at 300°C than at 150°C because of significant secondary hardening at 300°C.

- *Temperature had no significant effect on the fatigue lives of austenitic SSs in air at temperatures from room temperature up to 450°C. Variations in fatigue lives due to the effects of secondary hardening behavior were accounted for in the factor applied on stress that was applied to obtain the design air curve from the mean data air curve.*

### 3.2.5 Cyclic Strain Hardening Behavior

Under cyclic loading, austenitic SSs exhibited rapid hardening during the first 50–100 cycles; as shown in Fig. 42, the extent of hardening increased with increasing strain amplitude and decreasing temperature and strain rate.<sup>45</sup> The initial hardening was followed by a softening and saturation stage at high temperatures and by continuous softening at room temperature.

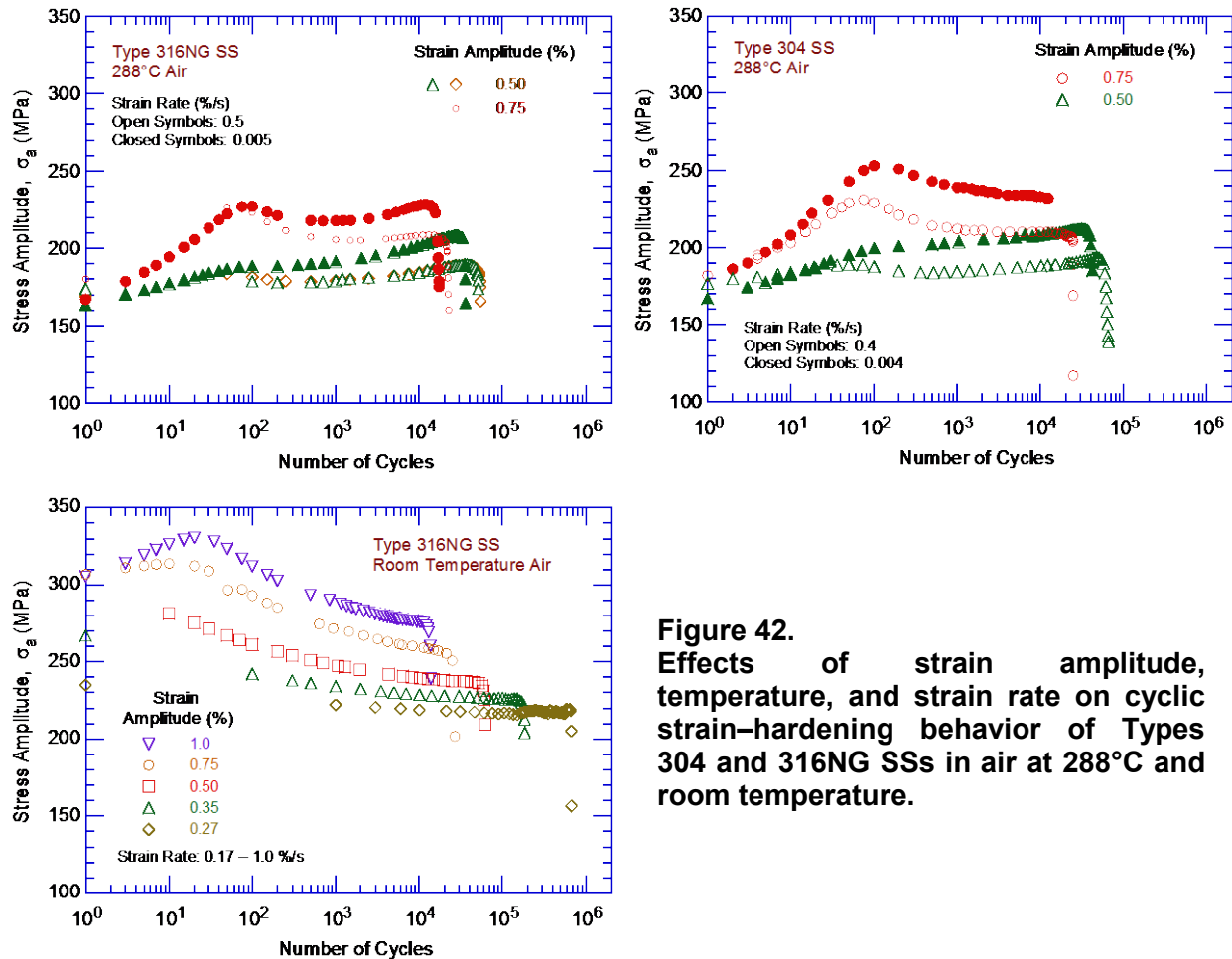


**Figure 42.**  
Effects of strain amplitude, temperature, and strain rate on cyclic strain-hardening behavior of Types 304 and 316NG SSs in air at 288°C and room temperature.

The cyclic stress–vs.–strain curves for Types 316, 304, and 316NG SS at room temperature and 288°C are shown in Fig. 43; cyclic stress corresponds to the value at half-life at a strain rate of 0.4%/s. For the various steels, cyclic stresses increased in magnitude in the following order: Types 316NG, 304, and 316.<sup>45</sup>

- *Cyclic strain hardening behavior influenced the fatigue lives of SS materials; variations in fatigue lives due to such effects were accounted for in the factor of 2 on stress that was applied to obtain the design air curve from the mean data air curve.*

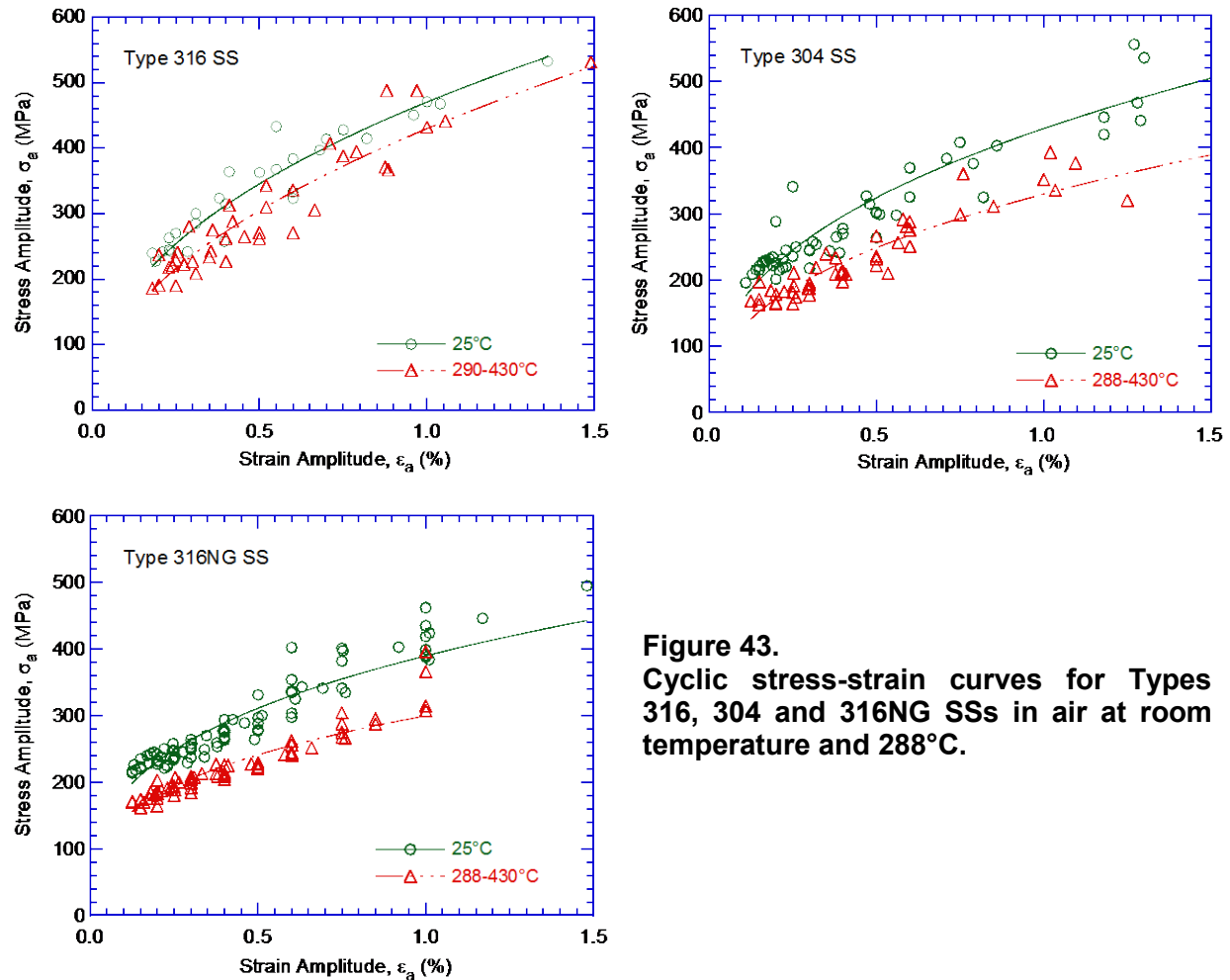


**Figure 43.**  
Cyclic stress-strain curves for Types 316, 304 and 316NG SSs in air at room temperature and 288°C.

### 3.2.6 Fatigue Life Model

In the initial revision of NUREG/CR-6909,<sup>137</sup> an updated version of the PVRC database was used to develop the best-fit mean air curve for austenitic SSs. The sources were listed in Table 1 of the report. The data were obtained on smooth specimens tested under strain-controlled conditions with fully reversed loading (i.e.,  $R = -1$ ) in compliance with consensus standard approaches used for the development of such data. The database consisted of 520 tests on Types 304, 316, 304L, 316L and 316NG SSs; approximately 220 of the tests were for Type 304 SS; 150 tests were for Type 316 SS; and 150 tests were for Types 316NG, 304L, and 316L SSs. The austenitic SSs used in these studies complied with the compositional and strength requirements of ASME Code specifications. The best-fit methodology described in Section 3.1.6 for carbon and low-alloy steels was also used for the analysis of the fatigue  $\epsilon$ -N data for austenitic SSs.

Several different best-fit mean  $\epsilon$ -N curves for austenitic SSs were previously proposed in the literature. Examples include Jaske and O'Donnell,<sup>61</sup> Diercks,<sup>224</sup> Chopra,<sup>45</sup> Tsutsumi et al.,<sup>34</sup> and Solomon and Amzallag.<sup>225</sup> These curves differ by up to 50%, particularly in the  $10^4$  to  $10^7$  cycles regime. The constant  $C$  in Eq. 6 (related to the fatigue limit of the material) varied from a value of 0.110 proposed by Tsutsumi and 0.112 by Jaske and O'Donnell to a value of 0.167 proposed in the original ASME Code Section III mean air curve. The differences primarily

occurred because different databases were used in developing these models for the mean  $\varepsilon$ -N curves. The analyses by Jaske and O'Donnell and by Diercks were based on Jaske and O'Donnell's data.

Tsutsumi et al. used the JNUFAD data, which are included in the JNES database.<sup>136</sup> In the initial revision of NUREG/CR-6909, the updated PVRC data were analyzed to develop the ANL model for austenitic SSs; the updated PVRC data included the JNUFAD database. In addition, unlike the earlier ANL reports that proposed separate expressions for high-carbon and low-carbon grades of SSs, a single expression was developed for the fatigue  $\varepsilon$ -N behavior of austenitic SSs. The model assumed that fatigue lives in air were independent of temperature and strain rate. Consistent with the models proposed by Tsutsumi<sup>34</sup> and by Jaske and O'Donnell,<sup>61</sup> the value of the constant C in the modified Langer equation (Eq. 6) was lower than that in earlier reports (i.e., 0.112 instead of 0.126). The proposed curve yielded an  $R^2$  value of 0.851 when compared with the updated PVRC data; the  $R^2$  values for the mean curves derived by Tsutsumi et al., Jaske and O'Donnell, and the ASME Code were 0.839, 0.826, and 0.568, respectively.

In air at temperatures up to 400°C, the fatigue lives for Types 304, 304L, 316, 316L, and 316NG SSs were represented by the expression:

$$\ln(N) = 6.891 - 1.920 \ln(\varepsilon_a - 0.112) \quad (29)$$

where  $\varepsilon_a$  is applied strain amplitude (%). The experimental values of fatigue lives and those predicted by Eq. 29 for austenitic SSs in air are plotted in Fig. 44. The predicted lives showed good agreement with the experimental values; for most tests, the differences between the experimental and predicted values were within a factor of 3. For some tests, the observed fatigue lives at low strain amplitudes (i.e., amplitudes that yielded fatigue lives greater than  $5 \times 10^4$  cycles) were significantly longer than the predicted values.

- *The ANL fatigue life model for austenitic SSs represents mean values of fatigue lives in air. The effects of parameters (such as mean stress, surface finish, size and geometry, and loading history) known to influence fatigue lives were accounted for in the factors of 12 on life and 2 on stress that were applied to the mean data air curve to obtain the fatigue design air curve.*

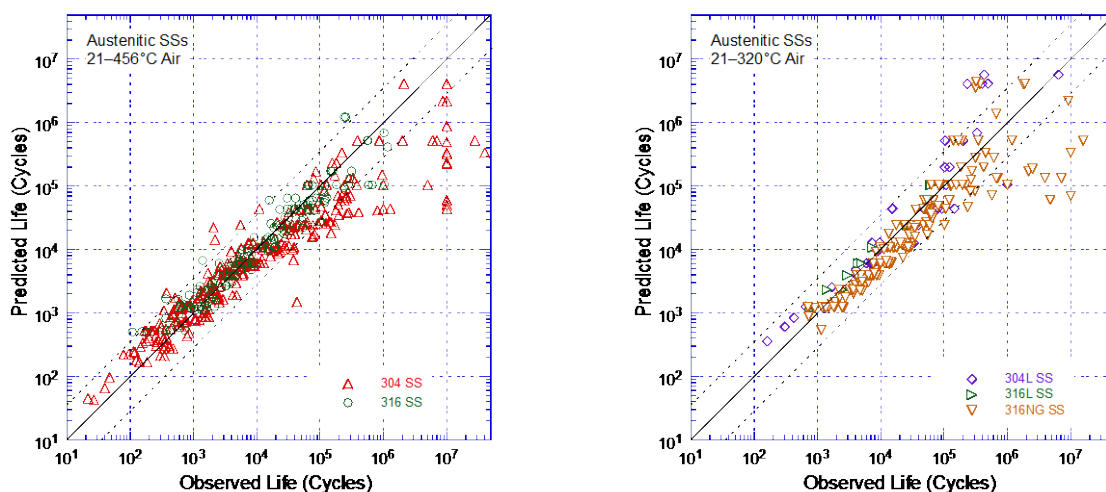


**Figure 44. Experimental and predicted fatigue lives (using the ANL model) for austenitic SSs in air.**

### 3.2.7 Heat-to-Heat Variability

The effects of material (heat-to-heat) variability and data scatter were included in the fatigue model to ensure that the design curves describe the available test data adequately, and adequately describe the fatigue lives of the much larger number of heats of materials found in the field compared to the limited numbers of heats tested in the laboratory. As mentioned earlier for carbon and low-alloy steels, heat-to-heat variability and data scatter in the fatigue  $\epsilon$ -N data for austenitic SSs were also evaluated by considering the best-fit curves determined from tests on individual heats of materials or loading conditions as samples of the much larger population of heats of materials and service conditions of interest. The fatigue lives of each of the heats or loading conditions were characterized by the value of the constant A in Eq. 6. The values of A for the various data sets were rank-ordered, and median ranks were used to estimate the cumulative distribution of A for the population. The distributions were fit to lognormal curves. The estimated cumulative distributions of constant A in the ANL model for fatigue lives of heats of wrought and cast austenitic SSs included in the initial revision of NUREG/CR-6909 and those included in this report are shown in Fig. 45. Note that the new updated database used in this report consisted of 622 data points; a significant increase (74%) compared to the 357 data points used in the initial revision of NUREG/CR-6909. The data were obtained on 5 types of austenitic SSs, 4 types of associated SS weld metals, and one type of cast austenitic SS. There are a total of 86 different heats of these materials.

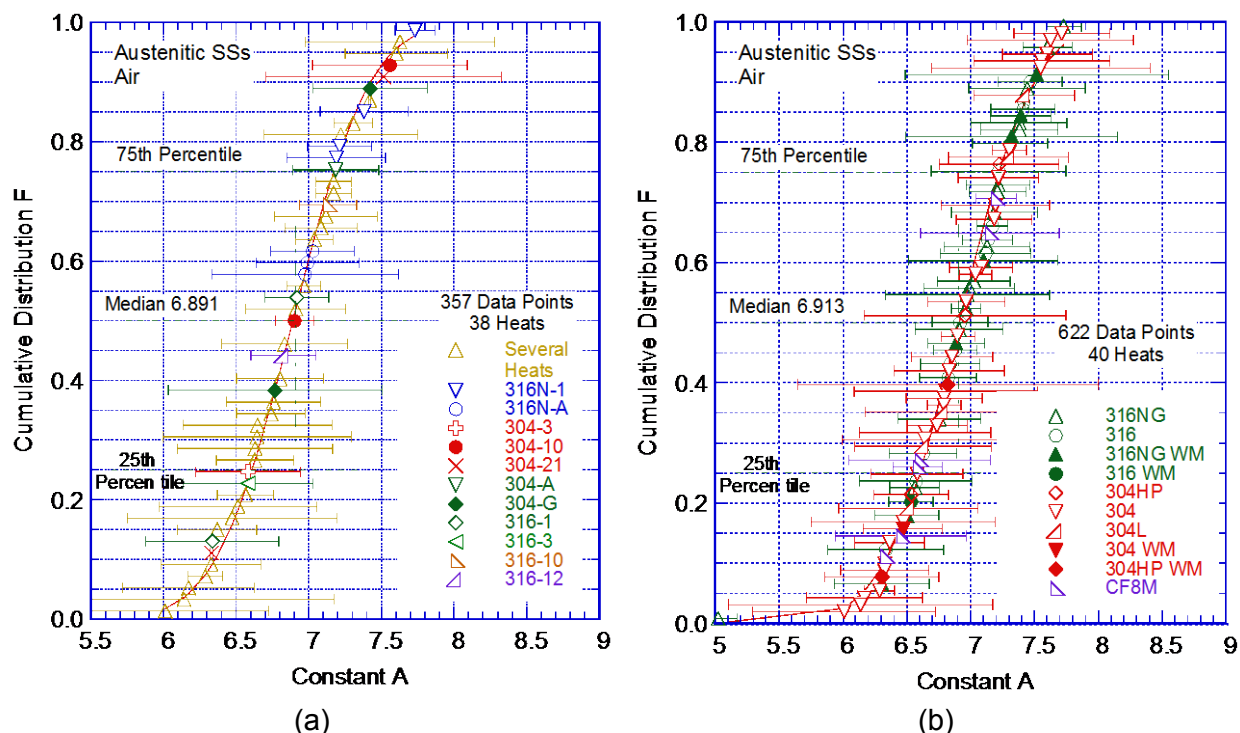


**Figure 45. Estimated cumulative distribution of constant A in the ANL model for fatigue lives for heats of austenitic SSs in air included in (a) the initial revision of NUREG/CR-6909 and (b) those included in this report.**

The results of the reanalysis indicated that the ANL fatigue model presented in the initial revision of NUREG/CR-6909 for predicting fatigue lives of austenitic SSs in air was adequate and remains representative of the updated (larger) database. Despite the significant increase in data, the reanalysis of the much larger updated database yielded an insignificant change in the median value of the constant A in Eq. 6. The constant A increased from 6.891 to 6.917. In



addition, Fig. 45 indicates that the various heats of wrought austenitic SSs and the associated SS weld metals were evenly distributed about the median value of constant A. The few heats of CF-8M cast austenitic SS were in the 15<sup>th</sup> – 30<sup>th</sup> percentile of the data, i.e., the fatigue lives of the heats of CF-8M were lower than the average values for austenitic SSs. However, this does not necessarily indicate that cast CF-8M materials have marginally lower fatigue lives than the average wrought SS material. This behavior is representative for this specific sample. Additional fatigue  $\epsilon$ -N data are needed on cast austenitic SSs to better establish the typical fatigue behavior of cast SS materials.

The values of the constant A that describe the 5<sup>th</sup> percentile of the statistical distributions produced a fatigue  $\epsilon$ -N curve that bounded the fatigue lives of 95% of the heats of austenitic SSs. A Monte Carlo analysis was performed to address the data uncertainties in the median value and standard deviation of the sample used for the analysis. For austenitic SSs, the values for A that provided bounds for the portion of the population and the confidence that was desired in the estimates of the bounds are summarized in Table 7. From Fig. 45, since the reanalysis did not change the constant A significantly, the median value of the constant A for austenitic SSs was not changed in this report. Thus, the median value of A for the sample remains 6.891. From Table 7, the 95/95 value of the factor to account for material variability and data scatter is 2.3 on life. This factor is needed to provide reasonable confidence that the resultant lives are greater than those observed for 95% of the SS materials of interest.

**Table 7. Values of constant A in the ANL fatigue life model for austenitic SSs and the factors on fatigue lives for austenitic SSs in air as a function of confidence level and percentage of population bounded.**

Confidence Level	Percentage of Population Bounded (Percentile Distribution of A)				
	95 (5)	90 (10)	75 (25)	67 (33)	50 (50)
<u>Values of Constant A</u>					
50	6.205	6.356	6.609	6.707	6.891
75	6.152	6.309	6.569	6.668	6.851
95	6.075	6.241	6.510	6.611	6.793
<u>Factors on Life</u>					
50	2.0	1.7	1.3	1.2	1.0
75	2.1	1.8	1.4	1.2	1.0
95	2.3	1.9	1.5	1.3	1.1

- *The mean data air curve for austenitic SSs used to develop the fatigue design air curve represented the average fatigue behavior; heat-to-heat variability was included in the subfactor that was applied to the mean data air curve to obtain the fatigue design air curve to account for “data scatter and material variability.”*

### 3.2.8 Fatigue $\epsilon$ -N Behavior of Cast Austenitic Stainless Steels

Available fatigue  $\epsilon$ -N data<sup>29,34,43,45</sup> indicated that the fatigue lives of cast CF-8M SSs in air were similar to those of wrought austenitic SSs. The fatigue  $\epsilon$ -N data for CF-8M cast austenitic SS in air, at temperatures between room temperature and 325°C, are plotted in Fig. 46. The results indicated that the fatigue lives of cast SSs were evenly distributed along the ANL best-fit curve for the mean data for wrought austenitic SSs.



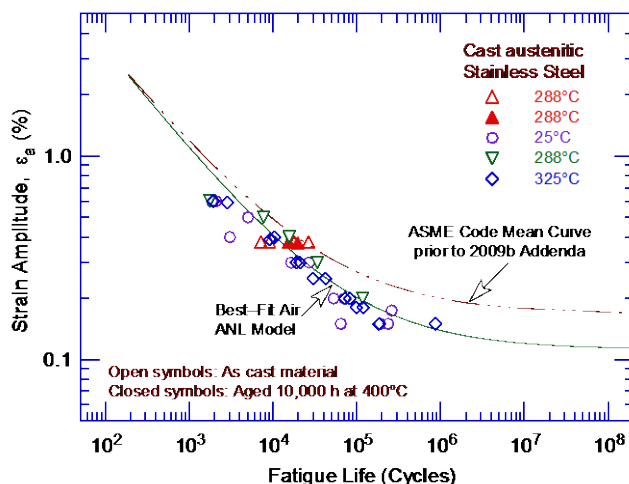


**Figure 46.**  
Fatigue  $\epsilon$ -N behavior for  
several heats of CF-8M cast  
austenitic SSs in air at various  
temperatures.

The effects of thermal aging at 250–400°C on the fracture toughness properties of cast austenitic SSs are well established. Fracture toughness decreased significantly after thermal aging because of the spinodal decomposition of the ferrite phase to form a Cr-rich  $\alpha'$  phase.<sup>229-232</sup> The cyclic-hardening behavior of cast austenitic SSs was also influenced by thermal aging.<sup>45</sup> The spinodal decomposition of the ferrite phase during thermal aging at 400°C strengthened the ferrite phase and increased cyclic hardening. At 288°C, cyclic stresses of cast SSs aged for 10,000 h at 400°C were higher than for unaged material or wrought SSs. The existing data were too sparse to establish the effects of thermal aging on strain-rate effects on the fatigue lives of cast SSs in air.

- *The fatigue mean data air curve for wrought austenitic SSs may be used for cast austenitic SSs.*

### 3.2.9 Fatigue $\epsilon$ -N Behavior of Weld Metals

Available fatigue  $\epsilon$ -N data for Types 304, 340HP (i.e., high purity), 316, and 316NG weld metals in air at room temperature are plotted in Fig. 47. The results indicated that the fatigue lives of SS weld metals were slightly lower than the mean  $\epsilon$ -N air curve for austenitic SSs in the low-cycle fatigue regime (i.e., fatigue lives less than  $10^4$  cycles), and generally longer in the high-cycle regime. However, the weld metal data were within the scatter band for the various grades and heats of austenitic SSs.

- *The limited fatigue  $\epsilon$ -N air data indicate that the mean data air curve for wrought austenitic SSs may be used for SS weld metals.*

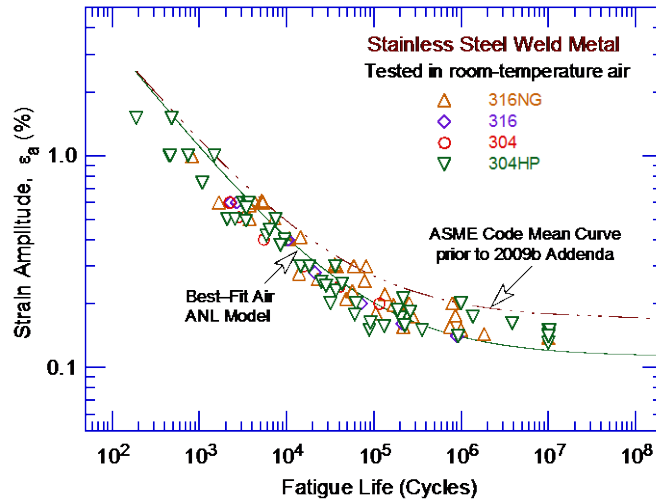


Figure 47.  
Fatigue  $\epsilon$ -N behavior for  
austenitic SS weld metals  
in air at room temperature.

### 3.2.10 Surface Finish

Fatigue tests were conducted on Types 304 and 316NG SS specimens that were intentionally roughened in a lathe, under controlled conditions, with 50-grit sandpaper to produce circumferential scratches with an average surface roughness of  $1.2 \mu\text{m}$ .<sup>46</sup> The results are shown for Types 316NG and 304 SS in Figs. 48a and b, respectively. For both steels, the fatigue lives of the roughened specimens were a factor of approximately 3 lower than those of the smooth specimens.

- *The effect of surface finish was included as part of the “surface finish and environment” subfactor that was applied to the mean data air curve to obtain the fatigue design air curve for austenitic SSs.”*

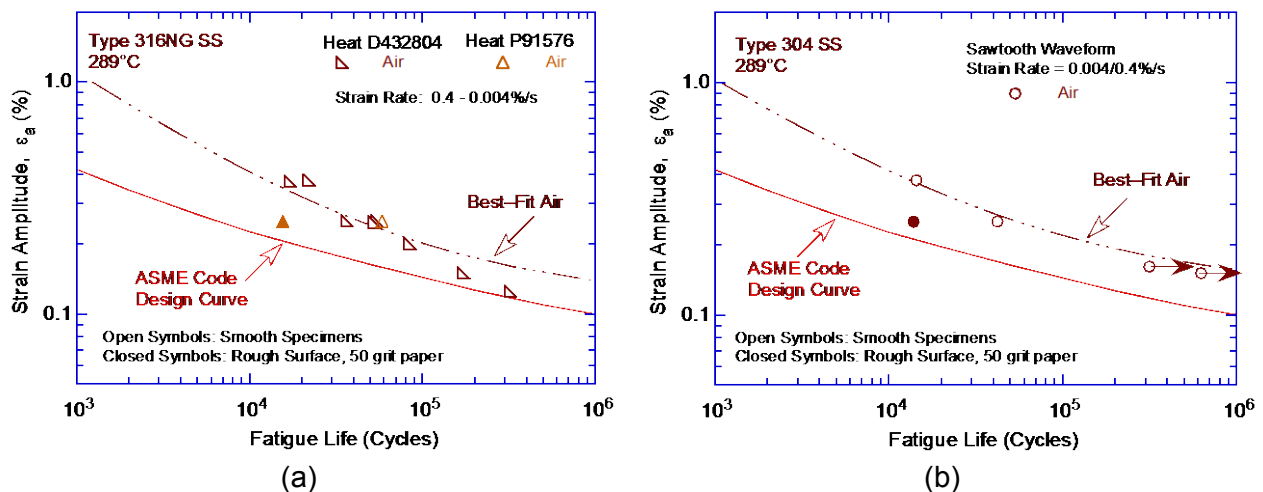


Figure 48. Effects of surface roughness on fatigue lives of (a) Type 316NG and (b) Type 304 SSs in air (Ref. 46).

### 3.2.11 Fatigue Design Curve

As discussed in Section 3.2.1, the ASME Code mean-data that were used to develop the current ASME Code Section III fatigue design air curve were not consistent with the existing fatigue  $\epsilon$ -N data. Therefore, a fatigue design air curve that was consistent with the existing database was derived from the ANL model (Eq. 29) by following the same procedure that was used to develop the ASME Code Section III fatigue design air curve. The discussions presented in Section 5.5 indicated that the current ASME Code Section III requirement for a factor of 20 on cycles to account for the effects of material variability and data scatter, specimen size, surface finish, and loading history was conservative by at least a factor of 1.7. Therefore, to reduce this conservatism, an fatigue design air curve based on the ANL model for austenitic SSs (Eq. 29) was developed by correcting for mean stress effects using the modified Goodman relationship and then lowering the mean-stress-adjusted curve by a factor of 2 on stress and 12 on cycles, whichever was more conservative. The resulting fatigue design air curve and the fatigue design air curve in ASME Code Section III prior to the 2009b Addenda were presented in the original revision of NUREG/CR-6909. The two fatigue design air curves were identical beyond  $10^8$  cycles. In 2009, the new fatigue design air curve based on the ANL model for austenitic SSs was adopted into Mandatory Appendix I of Section III of the ASME Code. Both of the ASME Code Section III air fatigue design air curves are shown in Fig. 49, and the values of stress amplitude vs. cycles for the current and the proposed design air curves are given in Table 8. In 2005, a new fatigue design air curve was also proposed for austenitic SSs and Alloy 600 and 800 materials by the ASME Section III Subgroup on Fatigue Strength.<sup>125</sup>

- *A new fatigue design air curve for austenitic SSs that is consistent with the existing data was developed from the ANL model using factors of 12 on life and 2 on stress. This curve is the same as the ASME Code Section III fatigue design air curve implemented in 2009.*

**Table 8. The ASME Code fatigue design curves for austenitic SSs in air.**

No. of Applied Cycles	Stress Amplitude MPa (ksi)		No. of Applied Cycles	Stress Amplitude MPa (ksi)	
	ASME Code Design Curve	ASME Code Design Curve Prior to 2009		ASME Code Design Curve	ASME Code Design Curve Prior to 2009
1 E+01	6000 (870)	4881 (708)	2 E+05	168 (24.4)	248 (35.9)
2 E+01	4300 (624)	3530 (512)	5 E+05	142 (20.6)	214 (31.0)
5 E+01	2748 (399)	2379 (345)	1 E+06	126 (18.3)	195 (28.3)
1 E+02	1978 (287)	1800 (261)	2 E+06	113 (16.4)	157 (22.8)
2 E+02	1440 (209)	1386 (201)	5 E+06	102 (14.8)	127 (18.4)
5 E+02	974 (141)	1020 (148)	1 E+07	99 (14.4)	113 (16.4)
1 E+03	745 (108)	820 (119)	2 E+07		105 (15.2)
2 E+03	590 (85.6)	669 (97.0)	5 E+07		98.6 (14.3)
5 E+03	450 (65.3)	524 (76.0)	1 E+08	97.1 (14.1)	97.1 (14.1)
1 E+04	368 (53.4)	441 (64.0)	1 E+09	95.8 (13.9)	95.8 (13.9)
2 E+04	300 (43.5)	383 (55.5)	1 E+10	94.4 (13.7)	94.4 (13.7)
5 E+04	235 (34.1)	319 (46.3)	1 E+11	93.7 (13.6)	93.7 (13.6)
1 E+05	196 (28.4)	281 (40.8)	2 E+10		

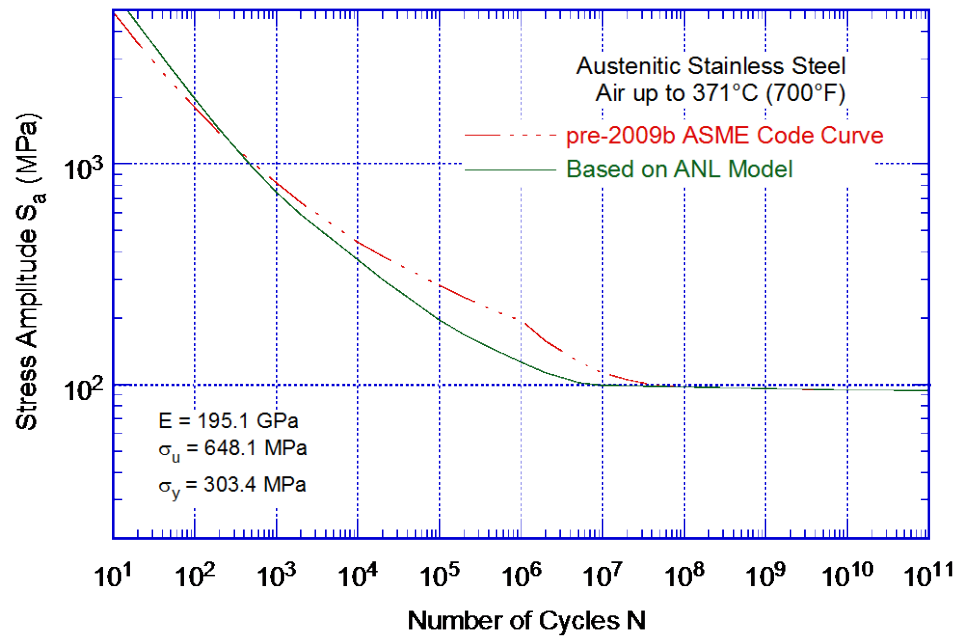


**Figure 49. Fatigue design curves for austenitic SSs in air.**

### 3.3 Ni-Cr-Fe Alloys and Weld Metals

The relevant fatigue  $\epsilon$ -N data for Ni-Cr-Fe alloys and their welds in air environments include the data compiled by Jaske and O'Donnell<sup>61</sup> for developing fatigue design criteria for pressure vessel alloys; the JNES database from Japan, which included studies at MHI, IHI, and Hitachi;<sup>39,136,210</sup> studies at Bettis Atomic Power Laboratory,<sup>70</sup> Knolls Atomic Power Laboratory,<sup>67,68</sup> NASA;<sup>73</sup> Battelle's Columbus Laboratories<sup>69</sup> and GE;<sup>14,71,72</sup> work sponsored by EPRI at Westinghouse Electric Corporation;<sup>66</sup> and the tests performed by Van Der Sluys et al.<sup>75</sup> The database was composed of 588 tests from which 559 data points were obtained; 191 data points for 17 heats of Alloy 600, 17 data points for 3 heats of Alloy 690, 23 data points for 2 heats of Alloy 800, 196 data points for 7 heats of Alloy 718; and 140 tests of Ni-Cr-Fe weld metals from which 132 data points were obtained for 1 heat of Alloy 690 weld metal, 5 heats of Alloy 82 weld metal, 4 heats of Alloy 182 weld metal, and 6 heats of other Ni-Cr-Fe weld metals. Out of these, 427 data points were obtained from tests conducted at room temperature, 40 data points were obtained from tests conducted at 260–316°C, and 92 data points were obtained from tests conducted at 427°C. A summary of the sources included in the updated database used for this report, as categorized by material type and test environment, is presented in Table 9. Other material information such as chemical composition, heat treatment, and room temperature tensile properties of these Ni-Cr-Fe alloys and associated weld metals is given in Appendix B.

**Table 9. Sources of the fatigue  $\epsilon$ -N data on Ni-Cr-Fe alloys and their weld metals in an air environment.**

ANL Mat. ID	Material Heat Designation <sup>a</sup>	Yield Strength (MPa)	Test Temperature (°C)	No. of Data Points	Source	Applicable Reference
<u>Alloy 600</u>						
1	Alloy 600-1	310	25	12	JNES (Higuchi)	136
2	Alloy 600-2	294	25	9	JNES (Nakao),	136
3	Alloy 600-3	-	25	6	JNES (Hirano),	136
4	Alloy 600-4	289	25	6	JNES (Hirano)	136
5	Alloy 600-5	264	25	11	JNES (Hirano)	136
6	Alloy 600-6	303	25	6	JNES (Kanasaki)	136
7	Alloy 600-7	253	24, 93, 204, 316	5, 5, 10, 7	KAPL (Dinerman)	67
8	Alloy 600-8	-	24	8 <sup>a</sup>	KAPL (Mowbray)	68
9	Alloy 600-9	-	24	10 <sup>a</sup>	KAPL (Mowbray)	68
10	Alloy 600-10	-	24	8 <sup>a</sup>	KAPL (Mowbray)	68
11	Alloy 600-11	-	24	13 <sup>a</sup>	KAPL (Mowbray)	68
12	Alloy 600-12	-	24	7 <sup>a</sup>	KAPL (Mowbray)	68
13	Alloy 600-13	-	24, 316	9, 9	EPRI (Jacko)	66
14	Alloy 600-14	-	21	19	Bettis (McGowan&Faber)	70
15	Alloy 600-15	386	260	6	GE (Hale)	14
16	Alloy 600-16	-	21	15	Jaske & O'Donnell	61
17	Alloy 600-17	-	24, 83	5, 5	Jaske & O'Donnell	61
<u>Alloy 690</u>						
20	Alloy 690-1	280	25	6	JNES (Kanasaki)	136
21	Alloy 690-2	-	25	5	PVP (Higuchi)	39
22	Alloy 690-3	-	315	6	PVP (Van der Sluys)	75
<u>Alloy 800</u>						
25	Alloy 800-1	-	21	7	BMI (Jaske et al.)	69
26	Alloy 800-2	-	427	6, 10	BMI (Jaske et al.), GE (Conway)	69,71
<u>Alloy 718</u>						

ANL Mat. ID	Material Heat Designation <sup>a</sup>	Yield Strength (MPa)	Test Temperature (°C)	No. of Data Points	Source	Applicable Reference
30	Inconel 718-1	-	21	18	ASME Data File	210
31	Inconel 718-2	-	21	4	J. Miller (J of Mat.)	72
32	Inconel 718-3	-	24, 427	17, 31	ASME Data File	61
33	Inconel 718-4	-	24, 427	30, 10	ASME Data File	61
34	Inconel 718-5	-	21, 427	34, 4	ASME Data File	61
35	Inconel 718-6	-	27, 427	12, 8	ASME Data File, NASA (Natchigall)	61,73
36	Inconel 718-7	-	22, 427	5, 23	ASME Data File	61
<u>Ni-Cr-Fe Alloy Weld Metals</u>						
38	Alloy 690 WM	431	25	6	JNES (Kanasaki)	136
39	Alloy 62	-	24	9 <sup>a</sup>	KAPL (Mowbray)	68
40	Alloy 82-1	-	24	8 <sup>b</sup>	KAPL (Mowbray)	68
41	Alloy 82-2	-	24	8 <sup>a</sup>	KAPL (Mowbray)	68
42	Alloy 82-3	-	24	17 <sup>a</sup>	KAPL (Mowbray)	68
43	NiCrFe WM-1	-	24	9	Higuchi, Iida	SGFS 1988
44	Arcaloy 8N12	-	24	6 <sup>a</sup>	KAPL (Mowbray)	68
45	NiCrFe WM-2	-	25	9, 5	JNUFAD (Higuchi, Nakao)	210
46	Alloy 82-4	322	260	7	KAPL (Mowbray)	68
47	Alloy 182-1	-	25	13	PVP (Higuchi)	39
48	Alloy 182-2	456	290	7	JNES (Higuchi)	136
49	Alloy 182-3	405	25	5	JNES (Nakao)	136
50	Alloy 182-4	409	25	6	JNES (Kanasaki)	136
51	Alloy 82-5	339	315	5	PVP (Van der Sluys)	75
52	Alloy 152	-	25	6	PVP (Higuchi)	39
53	Alloy 132	-	25	6	PVP (Higuchi)	39

<sup>a</sup> Tests performed under bending fatigue.

<sup>b</sup> Six tests performed under bending fatigue and four under rotating bending.

### 3.3.1 Experimental Data

The fatigue  $\epsilon$ -N data for Alloys 600, 690, and 800 in air at temperatures between room temperature and 427°C are shown in Fig. 50, and those for Alloys 62, 82, 132, 152, 182, and other Ni-Cr-Fe alloy weld metals in air at temperatures between room temperature and 315°C are shown in Fig. 51. The fatigue  $\epsilon$ -N data for Inconel 718 in air at room temperature and 427°C is shown in Fig. 52. Fatigue CUF evaluations for Ni-Cr-Fe alloy components were performed using the fatigue design air curve for austenitic SSs because there is not a separate curve for Ni-Cr-Fe materials in Section III of the ASME Code. Therefore, the best-fit air curve for austenitic SSs based on the ANL model (Eq. 29 in Section 3.2.6) is included in these three figures. The results indicate that, although the data for Alloys 690 and 800 are limited, the fatigue lives of these alloys were comparable to those of Alloy 600 (Fig. 50). The fatigue  $\epsilon$ -N data for Ni-Cr-Fe alloy weld metals indicated that the fatigue lives of the various weld metals were comparable, although the data for Alloy 82 at 260 to 315°C showed significant scatter

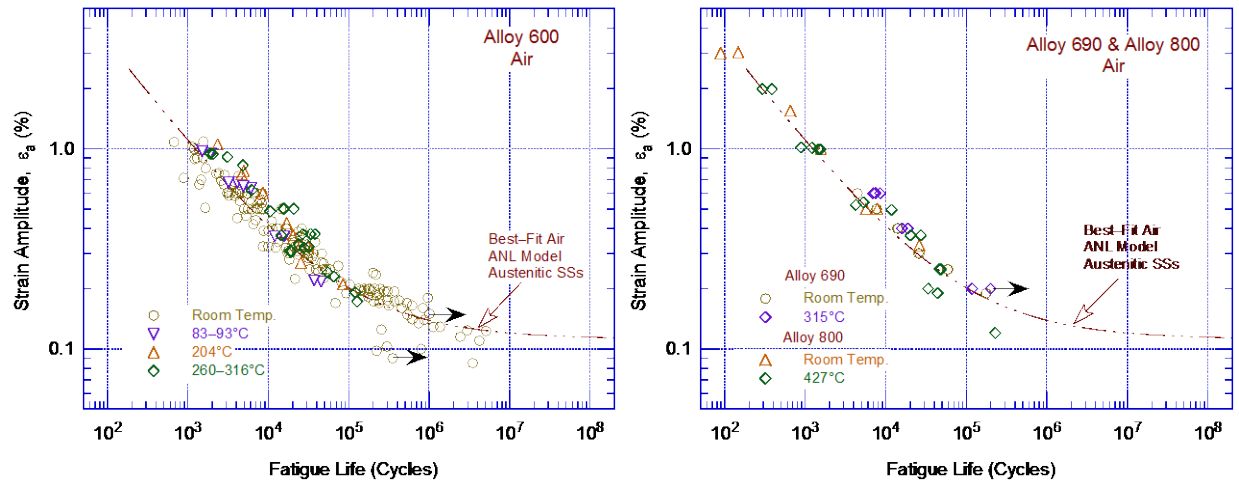


Figure 50. Fatigue  $\epsilon$ -N behavior for Alloys 600, 690 and 800 in air at temperatures between room temperature and 315°C (Refs. JNUFAD data, 61,66-75).

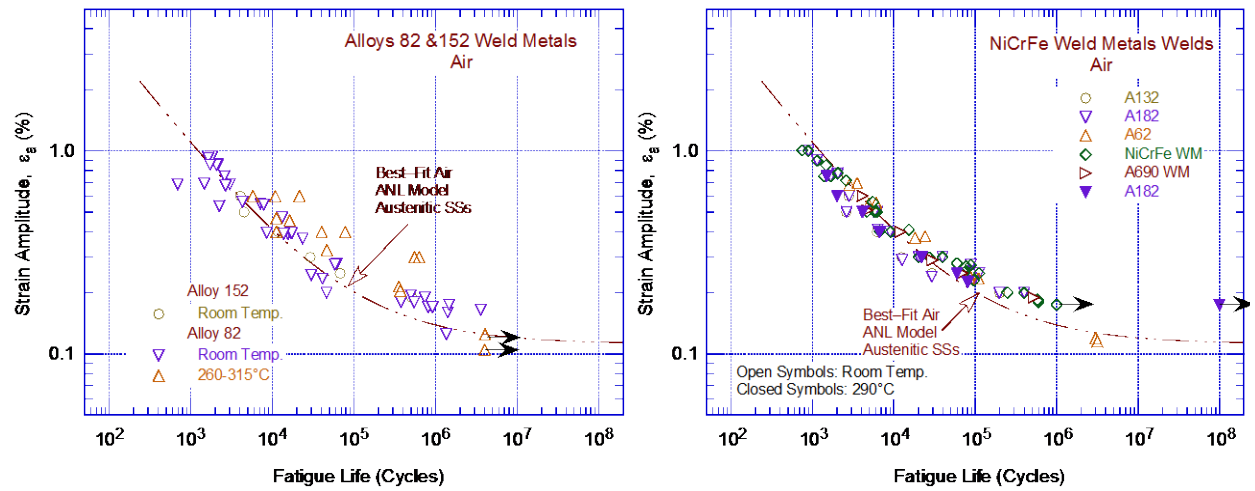


Figure 51. Fatigue  $\epsilon$ -N behavior for Alloys 62, 82, 132, 152, and 182 welds in air at various temperatures (Refs. JNUFAD data,61,66-75).

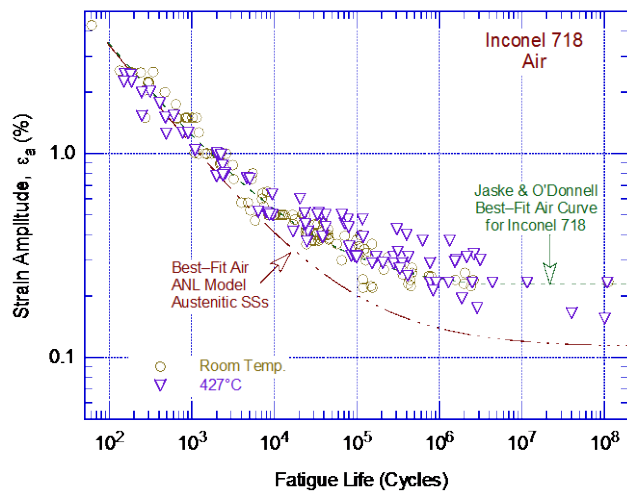


Figure 52. Fatigue  $\epsilon$ -N behavior for Inconel 718 in air at room temperature and 427°C (Refs. 61,72,73,136 ,210).

(Fig. 51). The fatigue lives of the Ni-Cr-Fe alloy weld metals were comparable to those of the wrought Alloys 600 and 690 in the low-cycle regime (i.e., less than  $10^5$  cycles) and were slightly superior to the lives of wrought materials in the high-cycle regime. The results also indicated that the fatigue limit for the weld metals was higher than that for wrought materials. Overall, the available fatigue  $\epsilon$ -N data indicated that the fatigue lives of Ni-Cr-Fe alloys was represented by the fatigue design air curve for austenitic SSs; however, fatigue evaluations for Ni-Cr-Fe weld metals were conservative under this assumption.

The fatigue  $\epsilon$ -N data in Fig. 52 indicate that the fatigue lives of Inconel 718 were longer than those for austenitic SSs or other Ni-Cr-Fe alloys and their weld metals, particularly at strain amplitudes less than 0.5% (i.e., in the high-cycle regime). The fatigue limit for Inconel 718 was much higher than that of austenitic SSs. Therefore, fatigue analyses for Inconel 718 that used the fatigue design air curve for austenitic SSs yielded conservative estimates of fatigue usage. To avoid this conservatism, a separate fatigue design air curve is appropriate for Inconel 718. Jaske and O'Donnell proposed the following expression for fatigue lives of Inconel 718 in air,

$$\ln(N) = 6.859 - 2.0 \ln(\epsilon_a - 0.210). \quad (30)$$

The Jaske and O'Donnell best-fit air curve for Inconel 718 is also shown in Fig. 52.

The available fatigue  $\epsilon$ -N data for Ni-Cr-Fe alloys also indicated that, unlike austenitic SSs that do not show temperature dependencies of fatigue lives under LWR operating conditions, the fatigue lives of Alloy 600 were generally longer at high temperatures compared to those at room temperature, particularly for Alloy 82 weld metal (Fig. 51a).<sup>66-68</sup> A similar behavior was observed for Inconel 718 (Fig. 52). However, limited data for Alloy 690 (Fig. 50b) and Alloys 62, 132, 182, and 690 weld metals (Fig. 51b), indicated little or no effects of temperature on their fatigue lives. The existing data were insufficient to adequately determine the effect of strain rate on the fatigue lives of Ni-Cr-Fe alloys.

Overall, the results indicated that the best-fit mean air curve for austenitic SSs represented slightly conservative estimates of the fatigue lives for Ni-Cr-Fe alloys in the high-cycle regime (fatigue lives greater than  $5 \times 10^4$  cycles), particularly for Ni-Cr-Fe alloy weld metals. However, the best-fit mean data curve for austenitic SSs yielded very conservative estimates of fatigue lives for Inconel 718 for fatigue lives greater than  $10^4$  cycles. To reduce this conservatism, the fatigue behavior of Inconel 718 should be represented by a separate fatigue  $\epsilon$ -N curve.

- *For Ni-Cr-Fe alloys and their welds, the ANL fatigue life air model proposed in this report for austenitic SSs (Eq. 29) was either consistent or conservative with respect to the fatigue  $\epsilon$ -N data.*

### 3.3.2 Fatigue Life Model

For Ni-Cr-Fe alloys, fatigue evaluations are based on the fatigue design air curve for austenitic SSs because there is not a separate curve for Ni-Cr-Fe materials in Section III of the ASME Code. However, the rather limited fatigue  $\epsilon$ -N data for Ni-Cr-Fe alloys (such as Alloys 600, 690, and 800 and their welds) were consistent with the best-fit mean air curve for austenitic SSs for fatigue lives less than  $10^4$  cycles. The data also showed longer fatigue lives than the estimated values for fatigue lives greater than  $10^4$  cycles. The data were comparable or slightly conservative with respect to the ANL model for austenitic SSs, e.g., Eq. 29. Estimates of the cumulative distribution of Constant A in the fatigue  $\epsilon$ -N curve for the various heats of Alloys 600, 690, and 800, and their associated weld metals, yielded a median value of 7.129. This value was slightly greater than the value of Constant A derived for austenitic SSs. In other



words, the fatigue lives of these Ni-Cr-Fe alloys were approximately 25% greater than those for austenitic SSs. Based on these findings, the current ASME Code Section III fatigue design air curve for austenitic SSs, which is the same as the ANL model presented in Fig. 49 and Table 8, adequately represented the fatigue  $\epsilon$ -N behavior of Ni-Cr-Fe alloys and their welds.

However, the fatigue design air curve for austenitic SSs yielded very conservative estimates of fatigue lives for Inconel 718. A detailed analysis of the cumulative distribution of Constant A for the various data sets available for Inconel 718 was not performed because the Constants B (the slope of the curve) and C (the constant associated with the fatigue limit) in the fatigue  $\epsilon$ -N curve were significantly different than those for austenitic SSs. For Inconel 718, the slope of the fatigue  $\epsilon$ -N curve was flatter and the fatigue limit (i.e., fatigue life at  $10^6$  cycles) was higher.

- *The ASME Code Section III fatigue design air curve for austenitic SSs, which is the same as the ANL air model for austenitic SSs, may also be used for Ni-Cr-Fe alloys and their welds. The current design fatigue air curve for austenitic SSs yielded conservative estimates of fatigue lives for Inconel 718.*



## 4. FATIGUE $\epsilon$ -N BEHAVIOR IN LWR ENVIRONMENTS

An analysis of the existing fatigue  $\epsilon$ -N data and the procedures for incorporating environmental effects into ASME Code fatigue evaluations was presented in several review articles<sup>118-126</sup> and ANL topical reports.<sup>10,12,13,45-47</sup> The key material, loading, and environmental parameters that influenced the fatigue lives of carbon and low-alloy steels and austenitic stainless steels were identified, and the ranges of these key parameters where environmental effects were significant were defined. How various material, loading, and environmental parameters affected fatigue lives and how these effects are incorporated into the ASME Code fatigue evaluations are discussed in detail for carbon and low-alloy steels, wrought and cast SSs, and Ni-Cr-Fe alloys in the following three sections of this chapter.

### 4.1 Carbon and Low-Alloy Steels

Fatigue-life models for estimating the fatigue life of carbon and low-alloy steels in LWR environments presented in the initial revision of NUREG/CR-6909 were based on the updated PVRC database available at that time. The effects of key parameters, such as temperature, strain rate, DO content in water, and sulfur content in the steel, were included in the correlations. The functional forms for the effects of strain rate, temperature, DO level in water, and sulfur content in the steel, were based on the data trends. For both carbon and low-alloy steels, the model assumed threshold and saturation values of 1.0 and 0.001%/s, respectively, for strain rate; 0.001 and 0.015 wt.%, respectively, for sulfur; and 0.04 and 0.5 ppm, respectively, for DO. The model also considered a threshold value of 150°C for temperature below which environmental effects were considered to be insignificant. The fatigue  $\epsilon$ -N data in LWR environments were fitted to a modified version of Eq. 6 expressed as

$$\ln(N) = A - B \ln(\epsilon_a - C) - D S^* T^* O^* \dot{\epsilon}^*, \quad (31)$$

where  $S^*$ ,  $T^*$ ,  $O^*$ , and  $\dot{\epsilon}^*$  are transformed sulfur content, temperature, DO level, and strain rate, respectively, defined in Eqs. 35-38, and  $D$  is a constant. The slope,  $B$ , of the fatigue  $\epsilon$ -N behavior in LWR environments was considered to be the same as in air, and the constant  $C$  was also considered the same because, as discussed in Section 4.1.3, environmental effects on fatigue were not observed below a threshold strain level. The constants  $A$  and  $D$  were determined from the best-fit of the fatigue  $\epsilon$ -N data in LWR environments. The constant  $A$  in the ANL models presented in the initial revision of NUREG/CR-6909 differed from the value reported earlier in NUREG/CR-6583 and NUREG/CR-6815. Relative to the earlier model, the fatigue lives predicted by the updated model in the initial revision of NUREG/CR-6909 were approximately 6% lower for carbon steels and approximately 2% higher for low-alloy steels.

The effects of reactor coolant environments on fatigue lives were expressed in terms of an environmental fatigue correction factor,  $F_{en}$ , which was defined as the ratio of life in air at room temperature,  $N_{RTair}$ , to that in water at the service temperature,  $N_{water}$ . Values of  $F_{en}$  were obtained from the ANL fatigue life models, where

$$\ln(F_{en}) = \ln(N_{RTair}) - \ln(N_{water}). \quad (32)$$

The environmental fatigue correction factor for carbon steels was given by

$$F_{en} = \exp(0.632 - 0.101 S^* T^* O^* \dot{\epsilon}^*), \quad (33)$$

and for low-alloy steels, by

$$F_{en} = \exp(0.702 - 0.101 S^* T^* O^* \dot{\epsilon}^*), \quad (34)$$

where  $S^*$ ,  $T^*$ ,  $O^*$ , and  $\dot{\epsilon}^*$  are transformed sulfur content ( $S$ )<sup>†</sup>, temperature, DO level, and strain rate, respectively, defined as:

$$\begin{aligned} S^* &= 0.015 & (\text{DO} > 1.0 \text{ ppm}) \\ S^* &= 0.001 & (\text{DO} \leq 1.0 \text{ ppm and } S \leq 0.001 \text{ wt.}\%) \\ S^* &= S & (\text{DO} \leq 1.0 \text{ ppm and } 0.001 < S \leq 0.015 \text{ wt.}\%) \\ S^* &= 0.015 & (\text{DO} \leq 1.0 \text{ ppm and } S > 0.015 \text{ wt.}\%) \end{aligned} \quad (35)$$

$$\begin{aligned} T^* &= 0 & (T \leq 150^\circ\text{C}) \\ T^* &= T - 150 & (150 < T \leq 350^\circ\text{C}) \end{aligned} \quad (36)$$

$$\begin{aligned} O^* &= 0 & (\text{DO} \leq 0.04 \text{ ppm}) \\ O^* &= \ln(\text{DO}/0.04) & (0.04 \text{ ppm} < \text{DO} \leq 0.5 \text{ ppm}) \\ O^* &= \ln(12.5) & (\text{DO} > 0.5 \text{ ppm}) \end{aligned} \quad (37)$$

$$\begin{aligned} \dot{\epsilon}^* &= 0 & (\dot{\epsilon} > 1\%/s) \\ \dot{\epsilon}^* &= \ln(\dot{\epsilon}) & (0.001 \leq \dot{\epsilon} \leq 1\%/s) \\ \dot{\epsilon}^* &= \ln(0.001) & (\dot{\epsilon} < 0.001\%/s). \end{aligned} \quad (38)$$

These models were recommended for predicting fatigue lives of less than or equal to  $10^6$  cycles. It was also noted that, as discussed in Section 4.2.7 of the initial revision of NUREG/CR-6909, because the effect of sulfur on the fatigue lives of carbon and low-alloy steels depended on the DO level in water, an environmental correction factor  $F_{en}$  determined from Eqs. 33–38 probably yielded nonconservative estimates of fatigue life for low-sulfur (less than 0.005 wt.%) steels in high-temperature water with greater than 1 ppm DO. However, this behavior is associated with laboratory test data and not likely to be applicable to LWR operating conditions.

During the time since the publication of the initial revision of NUREG/CR-6909, the NRC received several comments from interested stakeholders on the fatigue life models proposed therein. These comments have focused on the constants (i.e., 0.632 and 0.702 in Eqs. 33 and 34, respectively), which result in  $F_{en}$  values of approximately 2 even at temperatures below  $150^\circ\text{C}$  or at very high strain rates. Although this behavior seems inconsistent with the mechanisms that were proposed for environmental fatigue effects (because the calculated CUF step increases at the time environmental effects are applied), the constants were appropriate based on analyses of the fatigue  $\epsilon$ -N data and assumed constraints that were applied in the data reduction and analysis. The fatigue  $\epsilon$ -N behavior for carbon and low-alloy steels in air at room temperature and high-purity water at temperatures below  $150^\circ\text{C}$  is shown in Fig. 53. These results indicated that in both low-DO PWR and NWC BWR environments, the fatigue lives of carbon and low-alloy steels were a factor of two lower, thereby indicating the need for the constant terms in Eqs. 33 and 34. Another comment received from interested stakeholders was in regards to the temperature range specified in Eq. 36. The maximum temperature limit was specified as  $350^\circ\text{C}$  even though there were sparse data on carbon and low-alloys steels at temperatures above  $300^\circ\text{C}$ .

In this report, the  $F_{en}$  expressions (i.e., Eqs. 33–38) for incorporating environmental effects on the fatigue lives of carbon and low-alloy steels were updated to address the stakeholders comments using a much larger database that is described in Section 4.1.1. In LWR environments, the fatigue lives of carbon and low-alloy steels remains dependent on strain rate,

<sup>†</sup> In the expressions for  $F_{en}$ , the letter S is used for the metal sulfur content in the transformed sulfur term  $S^*$ .

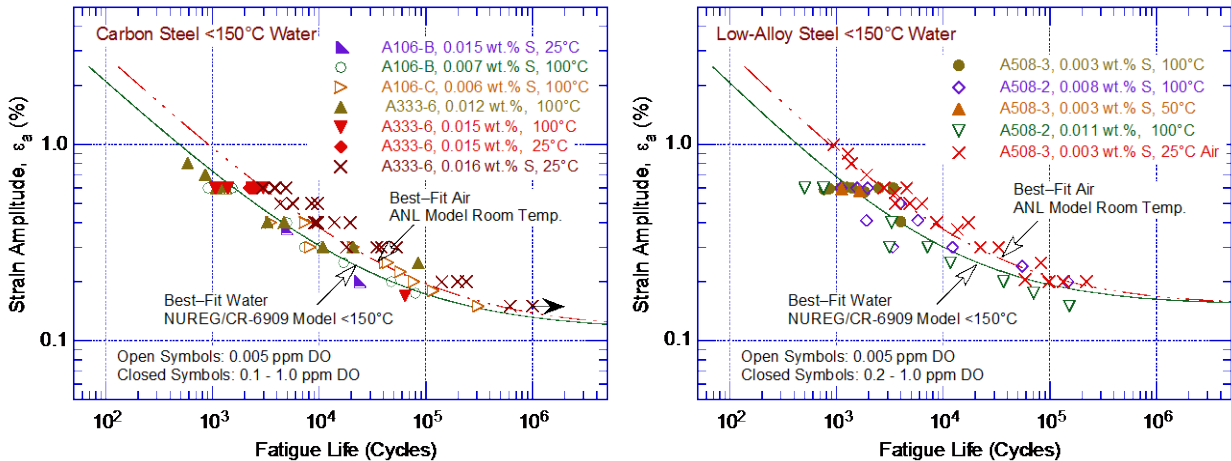


**Figure 53. Fatigue  $\epsilon$ -N behavior for carbon and low-alloy steels in air at room temperature and high-purity water at temperatures below 150°C (Ref. 137).**

DO level, temperature, and sulfur content of the steel; the effects of these and other parameters on the fatigue lives of these materials are discussed in the following sections.

#### 4.1.1 Experimental Data

The primary sources of fatigue  $\epsilon$ -N data for carbon and low-alloy steels in LWR environments are the tests performed by GE in a test loop at the Dresden 1 reactor;<sup>14,15</sup> the work of Terrell at MEA;<sup>48-50</sup> the work at ANL on fatigue of pressure vessel and piping steels;<sup>10-13,40-47</sup> the large JNES database<sup>136</sup> that includes studies at IHI, Hitachi, and MHI in Japan,<sup>18-36</sup> the work at KWU and MPA in Germany;<sup>55,56</sup> and some recent investigations by Wu and Katada.<sup>138-144</sup> The database in LWR environments used in this report was composed of a total of 1,174 tests, which represented 638 tests on carbon steels and 536 tests on low-alloy steels. The carbon steel tests included 21 heats of A106-Grades B and C, A333-Grade 6, A508-Grade 1, A226 Cl. 4, A516-G70, and A516-KC70 steels. The low-alloy steel tests included 20 heats of A302-Grade B, A508-Grades 2 and 3, A533-Grade B, 15MnNi63, and 17MnMoV64 steels. A summary of the data sources for the updated database used in this report, as categorized by material type and test environment, is shown in Table 10. Other material information, such as chemical composition, heat treatment, and room temperature tensile properties, for the various types and heats of materials is given in Appendix B.

A sampling of fatigue  $\epsilon$ -N data on carbon and low-alloy steels in air and high-DO water at 288°C are shown in Fig. 54. The curves based on the ANL air models (Eqs. 24 and 25 in Section 3.1.6) are also included in the figures. The fatigue data in LWR environments indicated a significant decrease in fatigue lives for carbon and low-alloy steels when four key threshold conditions were satisfied simultaneously, viz., applied strain range, service temperature, and DO in the water were above a minimum threshold level, and the loading strain rate was below a threshold value. The sulfur content of the steel was also an important parameter for environmental effects on the fatigue lives for carbon and low-alloy steels. Although the microstructures and cyclic-hardening behavior of carbon and low-alloy steels were significantly different, environmental degradation of the fatigue lives for these steels was nearly identical. As shown in Fig. 53, for both steels, environmental effects on the fatigue lives were moderate (i.e., a factor of approximately 2 lower) if any one of the key threshold conditions was not satisfied.

**Table 10. Sources of the fatigue  $\epsilon$ -N data for carbon and low-alloy steels in LWR environments.**

ANL Mat. ID	Material Specifications	Sulfur Content (wt.%)	Dissolved Oxygen (ppm)	Test Temperature (°C)	No. of Data Points	Source	Applicable Reference
<u>Carbon Steels</u>							
1	A106-Gr.B <sup>a</sup>	0.015	0.001-8.0	288	35	ANL, JNES (Higuchi)	10-13, 136
2	A106-Gr.B	0.007	0.005	100, 290	8, 7	JNES (Kanasaki)	136
3	A106-Gr.B	0.020	0.01	288	18	MEA	48
4	A106-Gr.C (STS480)	0.006	0.005	100, 290	12, 9	JNES (Tsutsumi)	136
5	A106-Gr.C (STS480)	0.020	0.005	290	4	JNES (Tsutsumi)	136
7	A226-Cl.4 (SFVC2B)	0.004	0.05-8.0	289	15	JNES (Hirano)	136
8	A333-Gr.6 (STS42)	0.015	8.0	250	8	JNES (Ishihara)	136
9	A333-Gr.6 (STS42)	0.015	0.01-8.0	100, 150, 200, 250, 290	6, 12, 11, 32, 13	JNES (Higuchi)	136
10	A333-Gr.6 (STS42)	0.014	0.2	288	12	JNES (Higuchi, Emnomoto)	136
11	A333-Gr.6 (STS410)	0.006	8.0	288	5	JNES (Higuchi)	136
12	A333-Gr.6 (STS410) <sup>b</sup>	0.012	0.01-8.0	25, 50, 100, 150, 200, 250, 288/290	1, 3, 18, 19, 22, 13, 62	JNES (Higuchi, Hirano, Kanasaki, Nakao), ANL	136, 10-13
14	A333-Gr.6 (STS410)	0.008	0.01-8.0	50, 100, 150, 200, 250, 289/290	2, 1, 5, 5, 5, 105	JNES (Abe, Higuchi, Kanasaki, Hirano)	136
15	A333-Gr.6 (STS410)	0.016	0.01-8.0	100, 200, 250, 289/290	7, 12, 4, 91	JNES (Hirano, Higuchi, Kanasaki)	136
16	A333-Gr.6 (STS410)	0.026	0.05-8.0	289	12	JNES (Hirano)	136
17	A508-Gr.1 (SFVV1)	0.008	8.0	300	14	JNES (Kitagawa)	136
21	A516-KC70	0.033	0.2	260	14 <sup>c</sup>	GE	14, 15
22	A516-G70 (SGV480)	0.002	8.0	290	3	JNES (Higuchi)	136
23	CS tube	0.025	0.01-8.0	240	13	S/KWU	55,56
<u>Low-Alloy Steels</u>							
1	A302-Gr.B	0.027	0.001-0.9	288	9	ANL	10-13
2	A508-Gr.2	0.003	0.2	288	21 <sup>d</sup>	JNES (Nakao, Higuchi)	136
4	A508-Gr.2 <sup>e</sup>	0.008	0.05-8.0	200, 250, 289	6, 9, 39	JNES (Hirano)	136
5	A508-Gr.2 <sup>e</sup>	0.008	0.005	100, 150, 200, 250, 290	10, 2, 10, 2, 13	JNES (Nomura)	136
6	A508-Gr. 3 (SFVV3)	0.003	0.1	288	9	JNES (Nagata)	136
12	A508-Gr. 3 (SFVV3)	0.003	0.05-8.0	50, 100, 150, 200, 250, 283/	2, 12, 29, 27, 8,	JNES (Endou, Kasai, Higuchi)	136

ANL Mat. ID	Material Specifications	Sulfur Content (wt.%)	Dissolved Oxygen (ppm)	Test Temperature (°C)	No. of Data Points	Source	Applicable Reference
				288/290	60		
14	A508-Gr. 3	0.002	0.1	288	16	Wu & Katada	141, 143
15	A508-Gr. 3	0.018	0.5	285	3	MPA	55,56
16	A533-Gr. B	0.012	0.001-0.9	288	30	ANL	10-13
17	A533-Gr. B (SQV2A)	0.007	0.1, (0.01-4.0)	288, (20, 100, 147/150, 200, 250, 288)	8, (1, 4, 2, 2, 1, 23)	JNES (Nagata), Wu & Katada	136, (141, 143)
21	A533-Gr. B (SQV2A)	0.010	0.2-8.0	288/290	53 <sup>e</sup>	JNES (Nakao, Higuchi)	136
23	A533-Gr. B	0.013	0.1	288	27	Wu & Katada	139, 142, 143
24	A533-Gr. B	0.025	0.1	288	6	Wu & Katada	143
25	A533-Gr. B	0.038	0.1, 2.0	200, 288	6, 13	Wu & Katada	139
26	A533-Gr. B (SQV2A)	0.021	0.05-1.0	200, 289	5, 29	JNES (Higuchi)	136
27	A533-Gr. B Cl. 2	<0.001	1.0	289	3	JNES (Hirano)	136
28	A533-Gr. B	0.003, 0.005, 0.014	2.0	285	3, 2, 5	MPA	55,56
30	15MnNi63	0.003	0.4, 8.0	240	1, 4	MPA	55,56
31	17MnMoV64	0.018	0.45	210	21	S/KWU	55,56

<sup>a</sup> This material was tested at ANL and IHI (Higuchi).

<sup>b</sup> This material was also tested at ANL.

<sup>c</sup> Tests performed on rectangular bars under bending fatigue.

<sup>d</sup> Four tests performed under load control using sine waveform.

<sup>e</sup> Data include results for thermally aged materials.

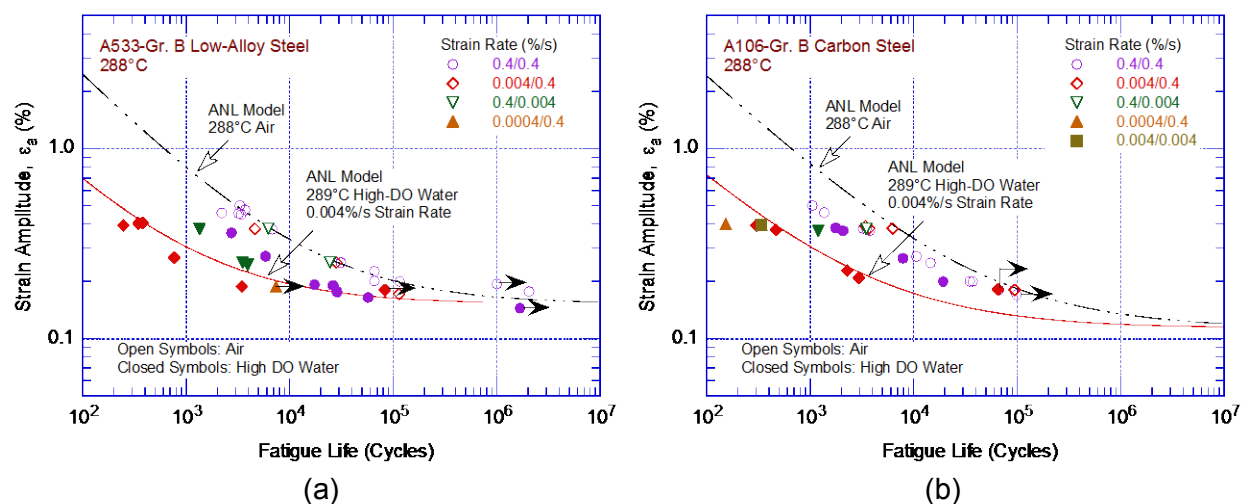


**Figure 54. Strain amplitude vs. fatigue life data for (a) A533-Gr B and (b) A106-Gr B steels in air and high-dissolved-oxygen water at 288°C (Ref. 10).**

The existing fatigue data indicated that slow strain rates applied during tensile–loading cycles were primarily responsible for environmentally assisted reduction in the fatigue lives of these steels.<sup>10</sup> The mechanism of environmentally assisted reduction in the fatigue lives of carbon and low-alloy steels was termed SICC.<sup>78,85,86</sup> Slow strain rates applied during both the tensile–load and compressive–load portions of load cycles (i.e., slow/slow strain rate test) did not further decrease the fatigue lives, e.g., refer to the solid diamond and solid square symbols in Fig. 54b for A106–Gr B carbon steel. Limited data from fast/slow tests indicated that slow strain rates during compressive load cycles also decreased fatigue lives. However, the decrease in life was relatively small; for fast/slow strain rate tests, the major contribution of environment occurred during slow compressive loading near peak tensile loads. For example, the fatigue lives of A533–Gr B low-alloy steels at 288°C, 0.7 ppm DO, and approximately 0.5% strain range decreased by factors of 5, 8, and 35 for the fast/fast, fast/slow, and slow/fast tests, respectively, i.e., refer to the solid circle, diamond, and inverted triangle symbols in Fig. 54a. Similar results were observed for A333–Gr. 6 carbon steel;<sup>23</sup> relative to the fast/fast test, the fatigue lives for the slow/fast and fast/slow tests at 288°C, 8 ppm DO, and 0.6% strain amplitude decreased the fatigue lives by factors of 7.4 and 3.4, respectively.

Environmental effects on the fatigue lives of carbon and low-alloy steels were consistent with the slip oxidation/dissolution mechanism for crack propagation, particularly at slow strain rates.<sup>189,190</sup> A critical concentration of sulfide ( $S^{2-}$ ) or hydrosulfide ( $HS^-$ ) ions, which is produced by the dissolution of sulfide inclusions in the steel, is required at the crack tip for environmental effects to occur. For this mechanism, a model for the initiation or cessation of EAC of these steels in low-DO PWR environments was also proposed.<sup>182</sup> Initiation of EAC requires a critical concentration of sulfide ions at the crack tip, which is supplied with the sulfide ions as the advancing crack intersects the sulfide inclusions, and the inclusions dissolve in the high-temperature water. Thus, environmental fatigue is controlled by the synergistic effects of sulfur content, environmental conditions, and flow rate. The EAC initiation/cessation model was used to determine the minimum crack extension and CGRs that are required to maintain the critical sulfide ion concentration at the crack tip and sustained environmental enhancement of growth rates.

- *LWR environments have significant effects on the fatigue lives of carbon and low-alloy steels; such effects were not considered in the original ASME Code fatigue design curves. Environmental effects for carbon and low-alloy steels may be incorporated into ASME Code fatigue evaluations using the  $F_{en}$  expression given in Eq. 41 (Section 4.1.11).*

#### 4.1.2 Strain Rate

The effects of strain rate on the fatigue lives of carbon and low-alloy steels in LWR environments were determined to be significant when other key threshold conditions, e.g., strain amplitude, temperature, and DO content, were satisfied. When any one of the threshold conditions was not satisfied, e.g., if low–DO PWR environments or temperatures less than 150°C were not present, the effects of strain rate were consistent with those observed in air.

When all threshold conditions were satisfied, the fatigue lives of carbon and low-alloy steels decreased logarithmically with decreasing strain rate. The fatigue lives of A106–Gr B and A333–Gr. 6 carbon steels and A533–Gr B low-alloy steel<sup>10,23</sup> are plotted as a function of strain rate in Fig. 55. The lines in this figure represent the predicted fatigue lives determined from the updated  $F_{en}$  expressions presented later in Section 4.1.10 (for water for the two DO values identified on each plot) and either Eqs. 24 or 25 (for air). Only a moderate decrease in fatigue lives was observed in simulated (low–DO) PWR water, e.g., at DO levels of less than or equal to 0.04 ppm. For the heats of A106–Gr. B and A333–Gr. 6 carbon steel and A533–Gr. B low-alloy



steel, the effects of strain rate on fatigue lives saturated between values of 0.004 and 0.0004 %/s strain rate. Although the data for A333–Gr. 6 carbon steel at 250°C and 8 ppm DO did not indicate saturation for strain rates up to 0.0001%/s, the results were comparable to those for the other two steels. The  $F_{en}$  expressions proposed by JNES for incorporating environmental effects on the fatigue lives of carbon and low-alloy steels recommended a saturation strain rate of 0.0004 %/s for DO levels up to 0.7 ppm and 0.0001 %/s above 0.7 ppm. Based on the data shown in Fig. 55, the saturation strain rate in the ANL model was also changed to 0.0004 %/s for all DO levels.

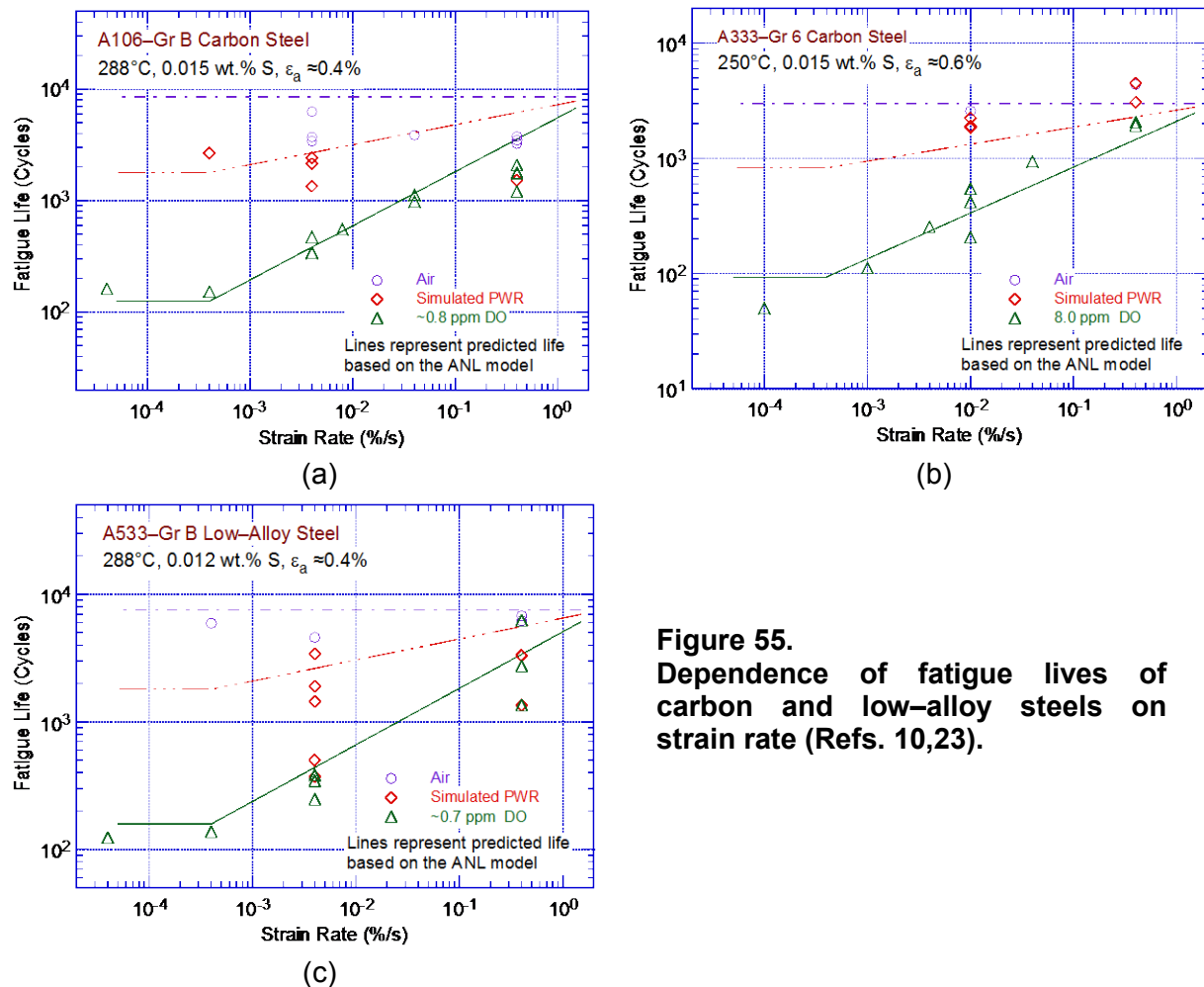


**Figure 55.**  
Dependence of fatigue lives of carbon and low-alloy steels on strain rate (Refs. 10,23).

For carbon and low-alloy steels, the potential effects of DSA are also likely to affect fatigue lives. The strain-rate dependence of fatigue life of A533-B low-carbon steel at 288°C and 200°C in high-purity water with 0.1 and 2.0 ppm DO is shown in Fig. 56. The lines represent the predicted fatigue lives based on the revised  $F_{en}$  expressions given in Eq. 41. The results indicated that the predicted fatigue lives at 0.001 %/s strain rate were greater than the experimental values, particularly at 200°C (i.e., the ANL models yielded nonconservative estimates for these environmental and loading conditions). This behavior was attributed to DSA. However, the difference between the estimated and experimental values was a factor of 2, which is within the range of data scatter for the fatigue  $\epsilon$ -N data for carbon and low-alloy steels in LWR environments. Therefore, no additional adjustments were made to accommodate DSA effects in the revised ANL model for carbon and low-alloy steels.

The methodology for calculating  $F_{en}$  under conditions where temperature and strain rate are changing (i.e., actual load transients) is discussed in Section 4.1.14, and guidance is provided for defining the strain rate for a specific load cycle or load set pair.

- The effect of strain rate on the fatigue lives of carbon and low-alloy steels in LWR environments were explicitly considered in the  $F_{en}$  expression given in Eq. 41 (Section 4.1.11); the saturation strain rate limit was changed from the value of 0.001 %/s, specified in the original revision of NUREG/CR-6909, to 0.0004 %/s to more appropriately reflect the data in the updated database.

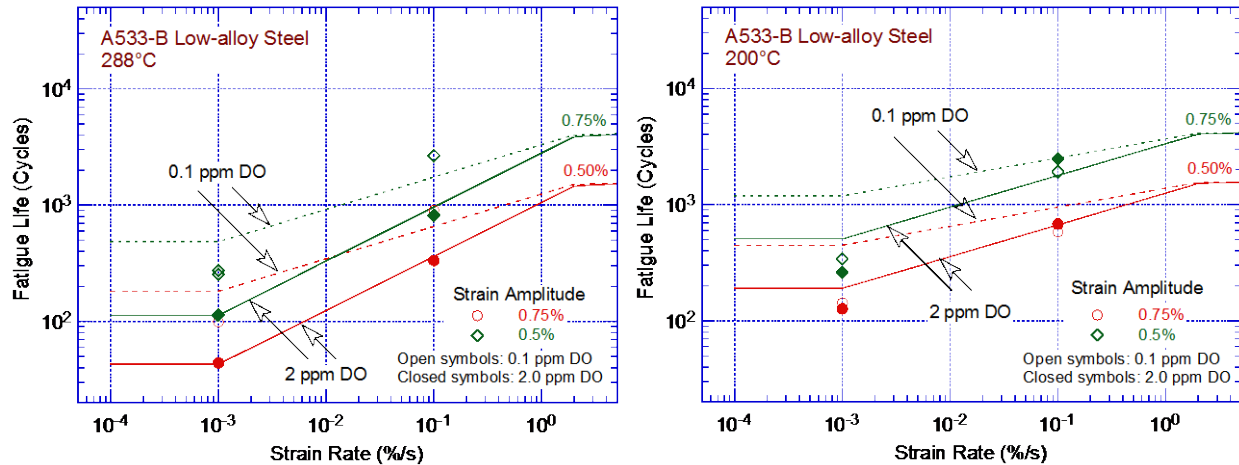


Figure 56. Fatigue life of A533–Gr. B low-alloy steel as a function of strain rate in high purity water with 0.1 or 2.0 ppm dissolved oxygen (Refs. 141,143).

#### 4.1.3 Strain Amplitude

The fatigue lives of carbon and low-alloy steels in LWR environments were observed to be lower than those in air. However, limited data indicated that at strain amplitudes below 0.3%, the fatigue lives of A533-B and A508-3 low-alloy steels were greater than those in air (Fig. 57). The reasons for this behavior were not clear. However, under the environmental and loading conditions that resulted in such behavior, estimates of fatigue lives of low-alloy steels were

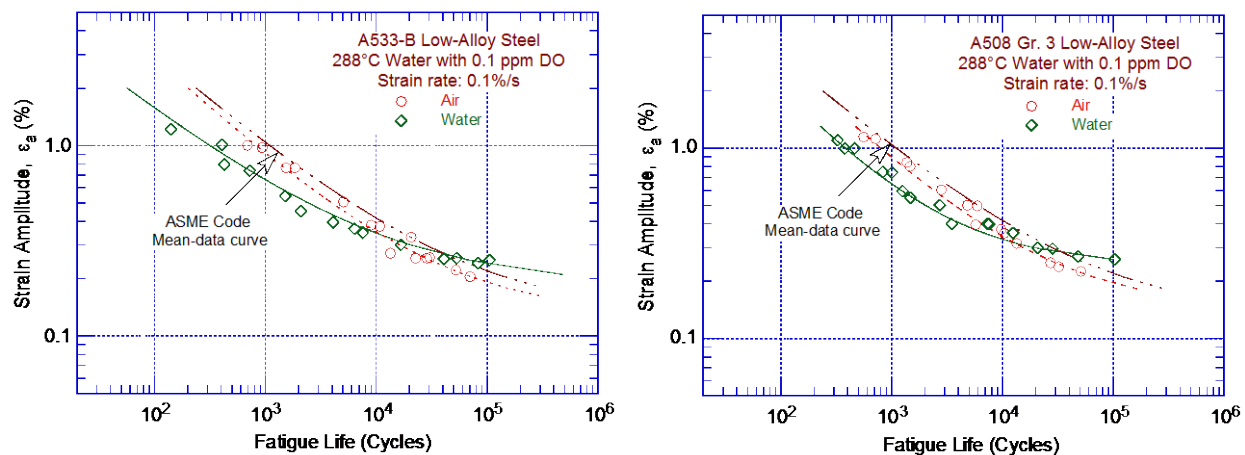
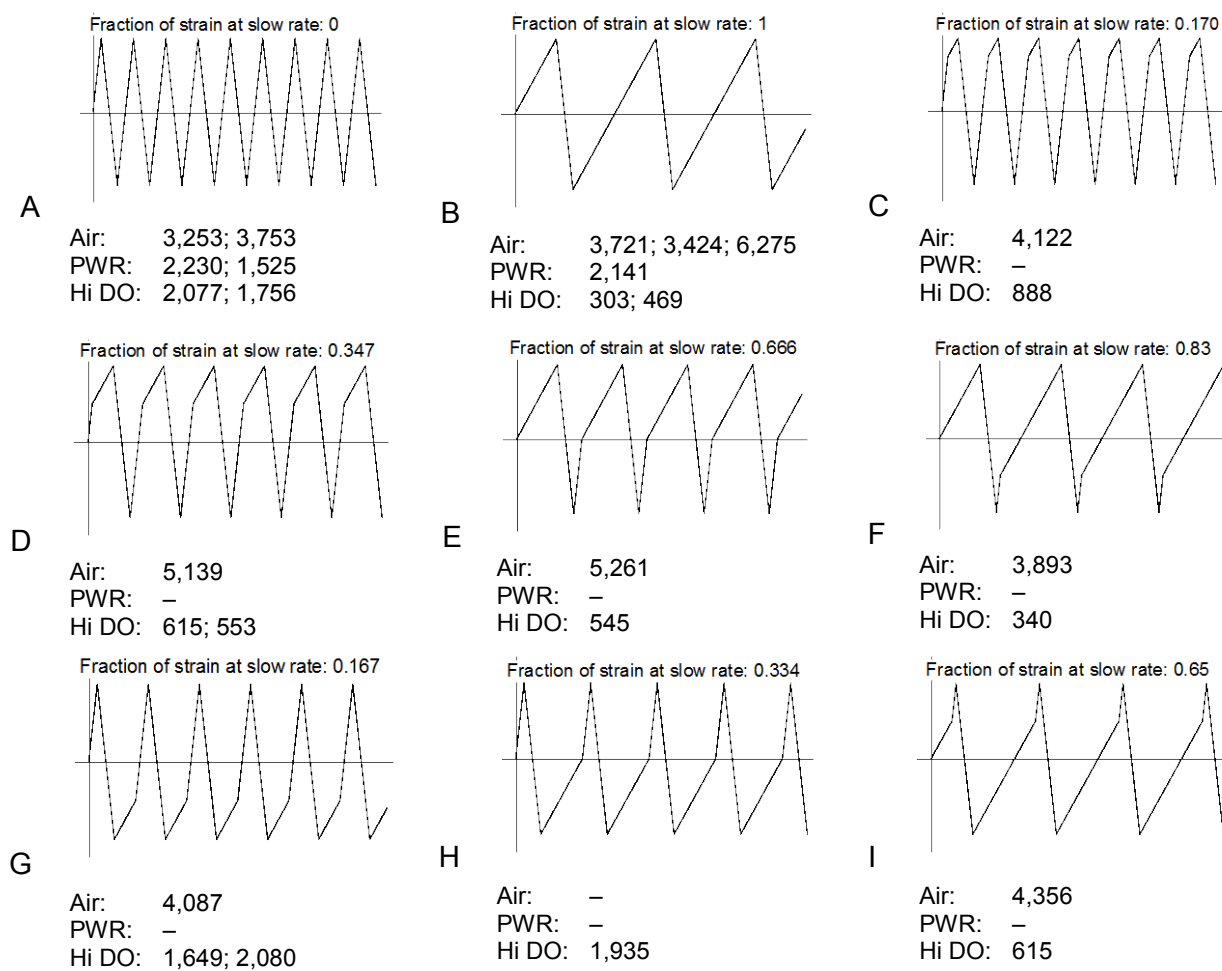


Figure 57. Fatigue strain-life behavior of A533–Gr. B and A508–Gr. 3 low-alloy steels at 288°C in air and high-purity water with 0.1 ppm dissolved oxygen (Ref. 151).

conservative. Therefore, in this report, this behavior was not explicitly addressed in the  $F_{en}$  methodology for estimating environmental effects on fatigue lives.

The available small-scale laboratory fatigue test data indicated that a minimum threshold strain range was required to cause an environmentally assisted decrease in fatigue lives, i.e., LWR coolant environments had no effect on the fatigue lives of these steels at strain ranges below the threshold value. The fatigue lives of A533–Gr B and A106–Gr B steels in high–DO water at 288°C and various strain rates<sup>10</sup> are shown in Fig. 54. Fatigue tests at low strain amplitudes were rather limited. Because environmental effects on fatigue lives increased with decreasing strain rates, fatigue tests at low strain amplitudes and strain rates that would result in significant environmental effects are restrictively time consuming. For the limited data that were available, the threshold strain amplitude (one-half the threshold strain) was slightly above the fatigue limits for these steels.

Exploratory fatigue tests with changing strain rate were conducted to determine the threshold strain ranges beyond which environmental effects were significant. The tests were performed with waveforms in which slow strain rates were applied during a portion of the tensile loading cycles.<sup>10,24</sup> The results for A106–Gr B steel tested in air and low– and high–DO environments at 288°C and approximately 0.75% strain range are summarized in Fig. 58. The loading waveforms implemented in the tests consisted of segments of loading and unloading at fast and



**Figure 58. Fatigue life of A106–Gr B carbon steel at 288°C and 0.75% strain range in air and water environments under different loading waveforms (Ref. 10).**

slow strain rates. The variation in fatigue lives of two heats of carbon steel and one heat of low-alloy steel<sup>10,24</sup> is plotted as a function of the fraction of the loading strain at slow strain rate in Fig. 59. Open symbols indicate tests where the slow strain rate loading occurred near the maximum tensile strain, and closed symbols indicate tests where the slow strain rate loading occurred near the maximum compressive strain. If the relative damage was the same at all strain levels, fatigue lives should have decreased linearly from A to C along the chain-dot lines in Fig. 59. Instead, the results indicated that, during a strain cycle, the relative damage due to slow strain rate occurred only after the strain level exceeded a threshold value. The threshold strain range for these steels was in the range of 0.32–0.36%.

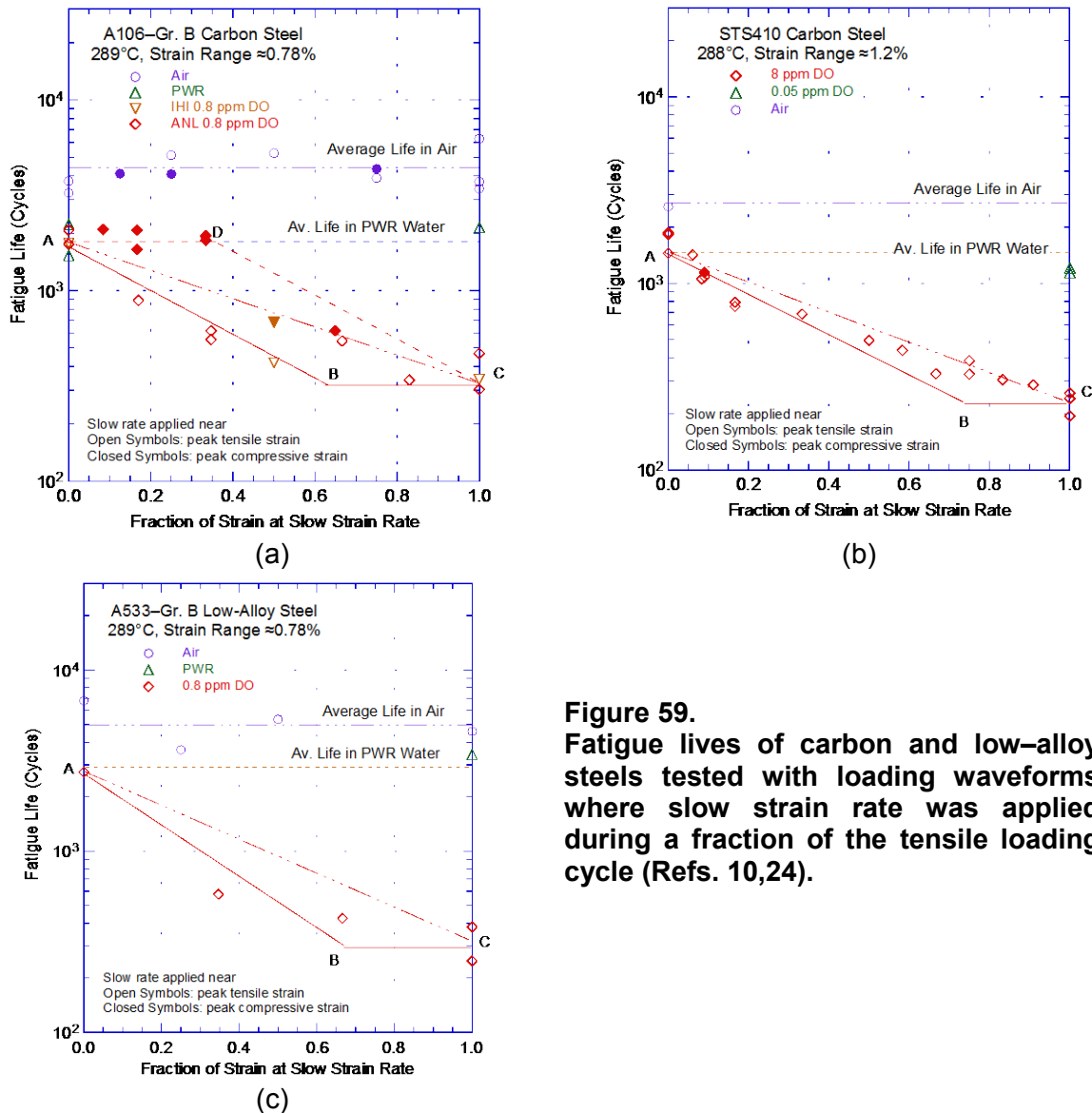


**Figure 59.** Fatigue lives of carbon and low-alloy steels tested with loading waveforms where slow strain rate was applied during a fraction of the tensile loading cycle (Refs. 10,24).

Loading histories with slow strain rate applied near the maximum tensile strain (i.e., waveforms C, D, E, or F in Fig. 58) showed continuous decreases in fatigue lives (lines AB in Fig. 59), followed by saturation when a portion of the slow strain rate occurred at strain levels below the threshold value (lines BC in Fig. 59). In contrast, loading histories with slow strain rates applied near the maximum compressive strain (i.e., waveforms A, G, H, or I in Fig. 58) did not produce any fatigue damage (line AD in Fig. 59a) until the fraction of the strain was sufficiently large such that the slow strain rates occurred at strain levels greater than the threshold value.

However, tests with such loading histories often showed lower fatigue lives than the predicted values, e.g., the solid inverted triangle or solid diamond symbols in Fig. 59a. The fatigue  $\varepsilon$ -N data presented in Fig. 54 indicated that the threshold strain was between 0.25 and 0.40 %. As discussed in Section 4.2.2, similar tests on austenitic SSs in PWR environments also showed the existence of a strain threshold below which the material was insensitive to environmental effects.<sup>35</sup> The threshold strain range,  $\Delta\varepsilon_{th}$ , was independent of material type (weld metal or base metal) and temperature in the range of 250–325°C, but it tended to decrease as the strain range was decreased. For austenitic SSs, the threshold strain was expressed in terms of the applied strain range,  $\Delta\varepsilon$  (Eq. 56). At a low strain amplitude (e.g., 0.3%), the proposed expression yielded a strain threshold of approximately 0.28%. Since the contribution of strain threshold was more significant at low strain amplitudes, a value of 0.28% was proposed in the initial revision of NUREG/CR-6909. After applying a factor of 2 on strain to account for the uncertainties associated with material variability and experimental scatter, a threshold “*strain amplitude*” of 0.07% [or a stress amplitude of 145 MPa (21 ksi)] was specified in the initial revision of NUREG/CR-6909 for use when performing ASME Code fatigue CUF evaluations for both carbon and low-alloy steels. The modified rate approach, described in Section 4.1.14, was used to predict the results from tests on A106-B and A333-6 carbon steels and A533-B low-alloy steel, conducted with changing strain rate in high-DO water (0.8–8.0 ppm DO) at 289°C.<sup>136</sup>

The experimental values of fatigue lives and those predicted from the modified rate approach, with and without the consideration of a threshold strain, are shown in Fig. 60. Most of the scatter in the data was due to heat-to-heat variations. The results indicated that estimates of fatigue lives based on the modified rate approach, without the consideration of a strain threshold, were in good agreement with the experimental values for A106-B and A333-6 carbon steels (Fig. 60a). However, the data for A533-B low-alloy steel (shown as circular symbols in Fig. 60) show an unusual behavior. First, the material showed a very strong dependence of environmental effects on applied strain amplitude. For example, for the tests with no strain-rate change (shown by closed symbols), the fatigue lives at 0.6% strain amplitude (i.e., fatigue lives in the range of 100 to 800 cycles) showed excellent agreement with the experimental values.

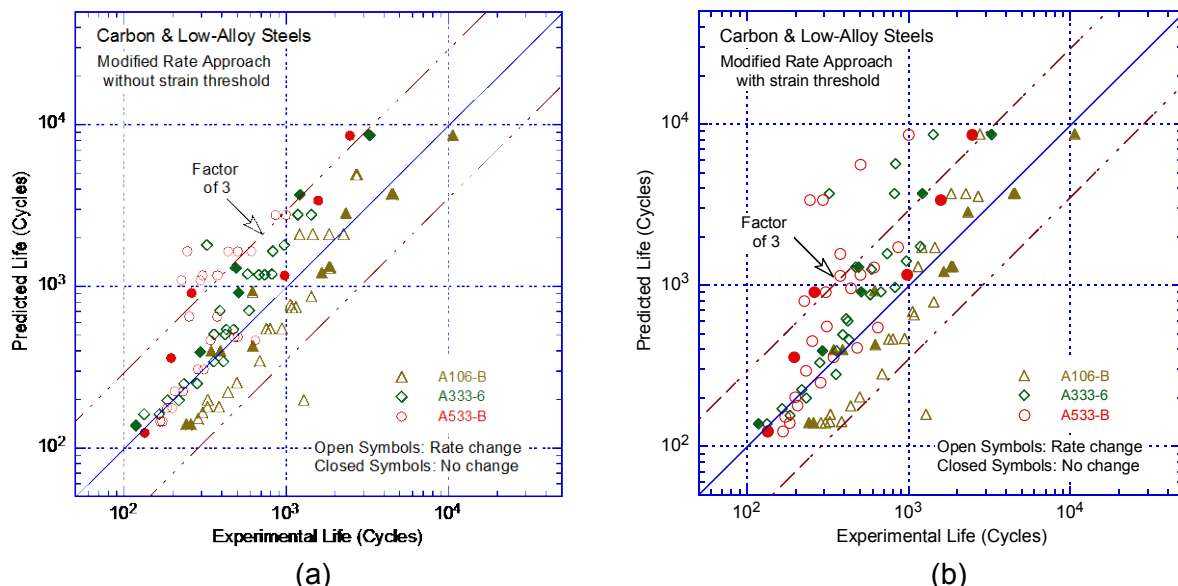


**Figure 60. Experimental values of fatigue life and those predicted from the modified rate approach (a) without and (b) with consideration of a threshold strain (Ref. 136).**

However, the predicted fatigue lives at 0.4% strain amplitude (i.e., fatigue lives in the range of 250 to 1,500 cycles) were a factor of 2 higher; and, at 0.3% strain amplitude (i.e., fatigue lives in the range of 350 to 3,300 cycles) the predicted fatigue lives were more than a factor of 3 higher. In addition, nearly all fatigue tests where slow strain rates were applied near the compressive-strain peak, particularly the tests at 0.4% or 0.3% strain amplitudes, exhibited unusually low fatigue lives. The reasons for such a dependence of environmental effects on applied strain amplitude are not understood.

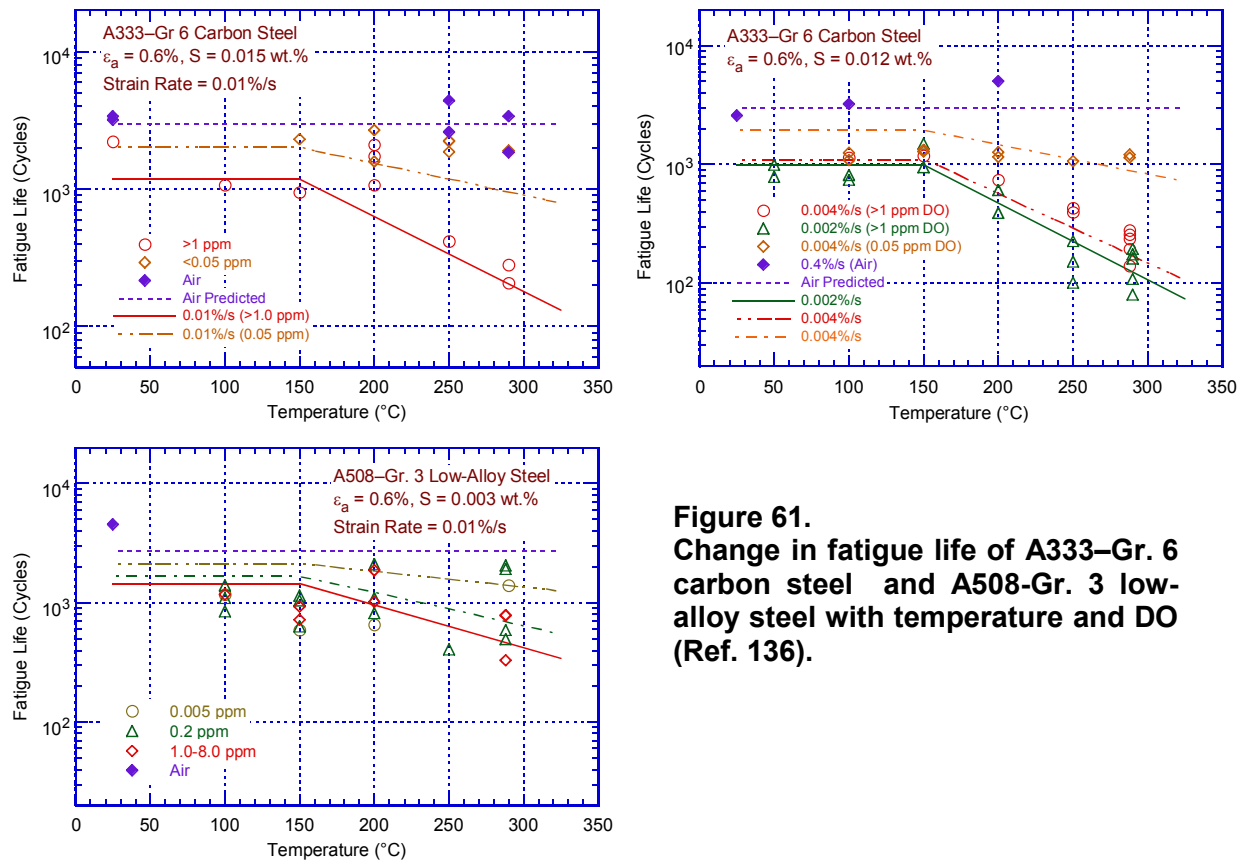
The results shown in Fig. 60b included a threshold strain of 0.28%. It was assumed that, during a strain cycle beginning from the peak compressive strain, environmental effects on fatigue lives occurred only when the strain exceeded the strain threshold (the  $F_{en}$  was determined in accordance with the modified rate approach defined by Eq. 50). Once again, the results for A106-B and A333-6 carbon steel either showed little or no changes in the resulting fatigue lives, or they showed better agreement with the experimental values, but the data for A533-B low-alloy steel, particularly for tests with slow strain rate imposed at the peak compressive strain, exhibited an unusual behavior. These results indicated that the modified rate approach, without consideration of a strain threshold, yielded the best estimates of fatigue lives of carbon and low-alloy steels in LWR environments.

- *The procedure for calculating  $F_{en}$  in LWR coolant environments is defined in Eq. 41 (Section 4.1.11) and Eqs. 49 or 50 (Section 4.1.14), where the equations may consider a threshold strain below which environment has no effect on fatigue lives (i.e.,  $F_{en} = 1$ ). However, while using the modified rate approach to determine  $F_{en}$  for a stress cycle or load set pair (Eq. 50 in Section 4.1.14), inclusion of a threshold strain may yield nonconservative estimates for fatigue lives.*

#### 4.1.4 Temperature

The change in fatigue lives of two heats of A333-Gr. 6 carbon steel<sup>18,19,22</sup> as a function of test temperature at different levels of DO and strain rates is shown in Fig. 61. The sulfur content of the two heats of A333-Gr. 6 carbon steel was 0.015% and 0.012 wt. %. For all these tests, the strain amplitude was 0.6%, which is above the threshold strain limit for environmental effects. In air, both heats had a fatigue life of 2,993 cycles. The results indicated a threshold temperature of 150°C, above which the environment decreased the fatigue life if the DO content in the water was also above the critical level of 0.05 ppm. An artificial neural network (ANN) was used to find patterns and identify the threshold temperature below which environmental effects were moderate.<sup>226</sup> The main benefits of the ANN approach were that estimates of lives were based purely on the data and not on preconceptions, and by learning trends; the network interpolated effects where data were not present. The factors that affected fatigue lives had synergistic effects on one another. The neural network detected and utilized these effects in its predictions. The training of the neural network was all based on the same data set, but the order in which the data were presented to the ANN for training was varied, and the initial ANN weights were randomized to guard against overtraining and to ensure that the network did not arrive at a solution that was a local minimum. The results indicated that at high strain rates (0.4%/s), fatigue lives were relatively insensitive to temperature. At low strain rates (0.004%/s), fatigue lives decreased with an increase in temperature beyond a threshold value of approximately 150°C.<sup>226</sup> The precision of the data indicated that this trend was present in the data used to train the ANN. Only a moderate decrease in fatigue lives was observed in water at temperatures below the threshold value of 150°C or at DO levels less than or equal to 0.05 ppm. Under these conditions, fatigue lives in water were a factor of approximately 2 lower than in air; Fig. 61 shows an average life of approximately 2,000 cycles for the 0.015 wt.% sulfur steel, and approximately 1,200 cycles for the 0.012 wt.% sulfur steel.





At temperatures above  $150^\circ\text{C}$ , the logarithm of fatigue life decreased linearly with temperature; the decrease in fatigue life was greater at higher temperatures and DO levels. However, as mentioned earlier, the temperature range specified in the initial revision of NUREG/CR-6909 for environmental effects for carbon and low-alloy steels in LWR environments extended beyond the range of actual fatigue  $\epsilon$ -N data. An insignificant amount of fatigue  $\epsilon$ -N data were available at temperatures above  $290^\circ\text{C}$ . Consequently, in this report, the maximum temperature limit was set at  $325^\circ\text{C}$  as a reasonable bound to cover all anticipated LWR operating conditions. This is adequate for all expected operating LWR conditions considering the use of average temperature (as discussed in Section 4.1.11 and shown in Fig. 81).

Nearly all of the fatigue  $\epsilon$ -N data available for evaluation for this report were obtained under loading histories with constant strain rates, temperatures, and strain amplitudes. However, the operating experience for U.S. LWRs indicates that the actual loading histories encountered during normal operation involves variable loading and environmental conditions. Some fatigue tests were conducted in Japan on 12-mm outside diameter tube specimens (1- and 3-mm wall thicknesses) of A333-Gr. 6 carbon steel in oxygenated water under combined mechanical and thermal cycling.<sup>21</sup> Triangular waveforms were used for both strain and temperature cycling. Two sequences were selected for temperature cycling (Fig. 62): an in-phase sequence in which the temperature cycling was synchronized with the mechanical strain cycling, and another sequence in which the temperature and strain cycling were out of phase, i.e., the maximum temperature occurred at the time of minimum strain level and vice versa. Three temperature ranges,  $50$ – $290^\circ\text{C}$ ,  $50$ – $200^\circ\text{C}$ , and  $200$ – $290^\circ\text{C}$ , were selected for the tests. The results are shown in Fig. 63; an average temperature was used to plot the thermal cycling tests. Because environmental effects on fatigue lives were moderate and independent of temperature below  $150^\circ\text{C}$ , the temperatures for the tests cycled in the ranges of  $50$ – $290^\circ\text{C}$  or  $50$ – $200^\circ\text{C}$  were

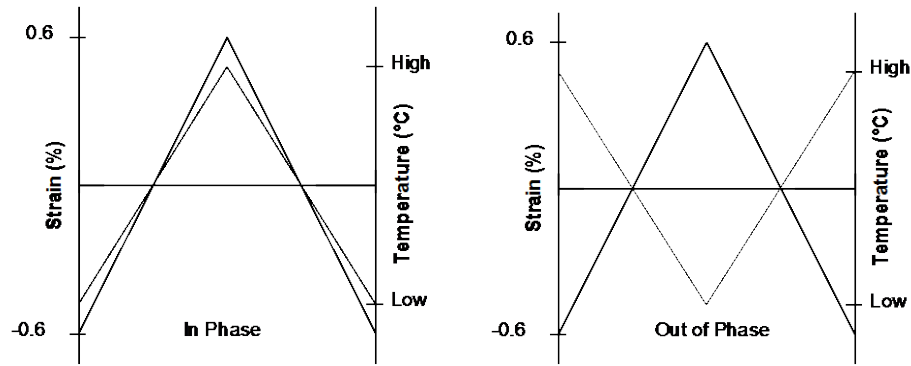


**Figure 62. Waveforms for changes in temperatures and strains during exploratory fatigue tests (Ref. 21).**

determined from the average of the threshold temperature of 150°C and the maximum temperature of the test (i.e., 220°C and 175°C, respectively). The results (Fig. 63) indicated that load cycles involving variable temperature conditions represented by an average temperature, e.g., the fatigue lives from variable-temperature tests were comparable with those from constant-temperature tests.

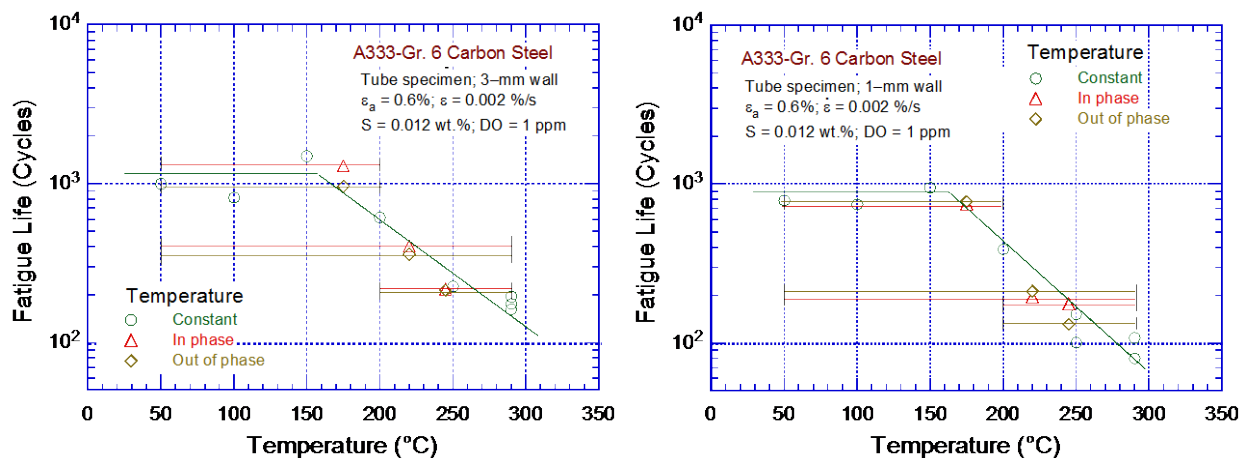


**Figure 63. Fatigue lives of A333-Gr. 6 carbon steel tube specimens under varying temperature conditions, as indicated by horizontal bars (Ref. 21).**

However, nearly identical fatigue lives were obtained from the in-phase and out-of-phase tests. Assuming that the tensile-load cycle was primarily responsible for the observed environmentally assisted reductions in fatigue lives, and that the applied strains and temperatures must be above a minimum threshold value for environmental effects to occur, then the fatigue lives obtained from the out-of-phase tests were expected to be longer than those obtained from the in-phase tests. This expectation was based on the premise that the applied strains above the threshold strain occurred at temperatures above 150°C for the in-phase tests, whereas the applied strains above the threshold strain occurred at temperatures below 150°C for the out-of-phase tests. Under the assumption that environmental effects on fatigue lives were considered to be minimal below the 150°C temperature and 0.28 % strain threshold values, the average temperatures for the out-of-phase tests at 50–290°C, 50–200°C, and 200–290°C were 195, 160, and 236°C, respectively, instead of 220, 175, and 245°C, as plotted in Fig. 63. Thus, the fatigue lives from out-of-phase tests were expected to be at least 50% higher than those from the in-phase tests. Such differences in environmental conditions were therefore assumed to be offset by the difference in the cyclic hardening behavior of the material for the out-of-phase and



in-phase tests. From those observations, it was concluded that estimates of fatigue lives for actual nuclear power plant transients based on an average temperature may yield nonconservative estimates.

- *The effects of temperature on the fatigue lives of carbon and low-alloy steels in LWR environments were explicitly considered in  $F_{en}$  defined in Eq. 41 (Section 4.1.11). For simple, linear transients, an average temperature that considers the threshold temperature of 150°C may be used to calculate  $F_{en}$  for a specific stress cycle or load set pair. Complex thermal transients that have multiple increasing and decreasing temperature excursions should be evaluated using the maximum temperature for the specific stress cycle or load set pair unless information is available to justify the use of an average temperature.*

#### 4.1.5 Dissolved Oxygen

The dependence of fatigue lives of carbon and low-alloy steels on the DO content in water is shown in Fig. 64.<sup>18,19,22</sup> For the tests summarized in this figure, the temperatures, applied strain amplitudes, and sulfur contents in the steels tested were above, and the strain rates were below, the critical threshold values. The results indicated a minimum DO level of 0.04 ppm above which the environment decreased the fatigue lives of the steels tested. The effect of DO content on fatigue lives saturated at 0.5 ppm, i.e., increases in DO levels above 0.5 ppm did not cause further decreases in fatigue lives. In Fig. 64, for DO levels between 0.04 and 0.5 ppm, fatigue lives decreased logarithmically with DO. Estimates of fatigue lives from the trained ANN also showed a similar effect of DO on the fatigue lives of carbon steels and low-alloy steels.

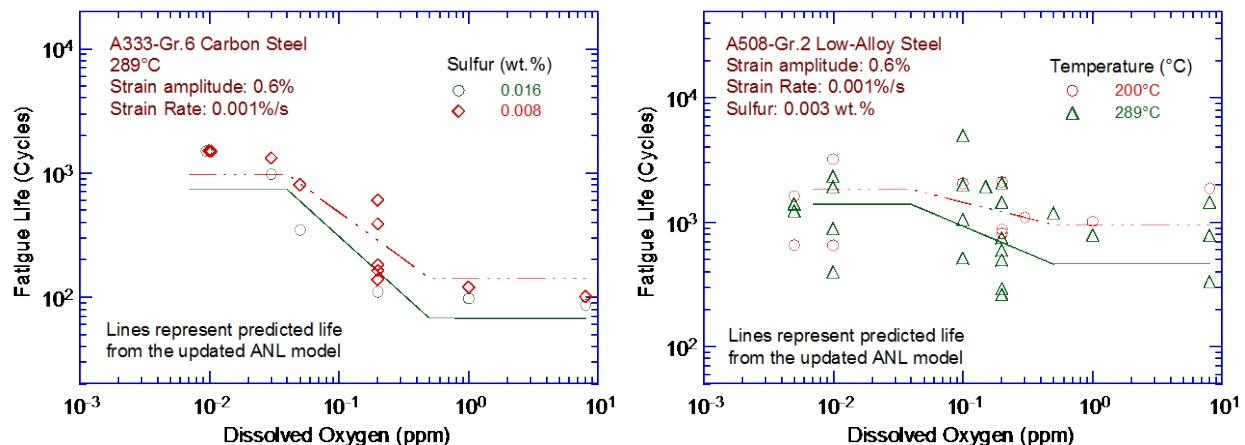


**Figure 64. Dependence on DO of the fatigue lives of carbon and low alloy steels in high-purity water (Ref. 18, 19, 22).**

Environmental effects on the fatigue lives of carbon and low-alloy steels were minimal at DO levels below 0.04 ppm, i.e., in low-DO PWR or HWC BWR environments. In contrast, environmental enhancement of CGRs was observed in low-alloy steels even in low-DO water.<sup>182</sup> This apparent inconsistency of fatigue  $\epsilon$ -N data with the CGR data was attributed to differences in the environmental conditions locally at the crack tip. As discussed earlier in Section 2.2.1.2, environmentally assisted enhancement of CGRs in low-alloy steels required a critical level of sulfides at the crack tip.<sup>182</sup> The development of this critical sulfide concentration required a minimum crack extension of 0.33 mm and CGRs in the range of  $1.3 \times 10^{-4}$  to  $4.2 \times 10^{-7}$  millimeters/second. These conditions were not achieved under the majority of the available  $\epsilon$ -N tests. Thus, environmental effects on fatigue lives are expected to be insignificant in low-DO environments for carbon and low-alloy steels.

- The effects of DO levels on the fatigue lives of carbon and low-alloy steels in LWR environments were explicitly considered in the  $F_{en}$ , defined in Eq. 41 (Section 4.1.11).

#### 4.1.6 Water Conductivity

In most of the studies reviewed for this report, the DO level in water was considered as the key environmental parameter that affected the fatigue lives of materials in LWR environments. Studies on the effects of the concentration of anionic impurities in water (expressed as the overall conductivity of water) were limited. The limited data indicated that the fatigue lives of WB36 low-alloy steel at 177°C in water with approximately 8 ppm DO decreased by a factor of approximately 6 when the conductivity of the water was increased from 0.06 to 0.5  $\mu\text{S}/\text{cm}$ .<sup>78,227</sup> Similar behavior was also observed in another study of the effects of conductivity on the initiation of short cracks.<sup>228</sup>

- U.S. LWRs are unlikely to accumulate significant fatigue cycles during off-normal water chemistry conditions. Thus, the effects of water conductivity on fatigue lives were not considered in the determination of  $F_{en}$  for carbon and low-alloy steels.

#### 4.1.7 Sulfur Content in Steel

Sulfur content and morphology were the most important material-related parameters that determined susceptibility of low-alloy steels to environmentally enhanced fatigue CGRs.<sup>184–188</sup> A critical concentration of  $\text{S}^{2-}$  or  $\text{HS}^-$  ions was required at crack tips for environmental effects to occur. The corrosion fatigue CGRs and threshold stress intensity factor,  $\Delta K_{th}$ , were both a function of the sulfur content in the range 0.003–0.019 wt.%.<sup>187</sup> The probability of environmental enhancement of fatigue CGRs in precracked specimens of low-alloy steels, diminished markedly for sulfur contents less than 0.005 wt. %.

The available fatigue  $\epsilon$ -N data for carbon and low-alloy steels also indicated a dependence of fatigue lives on sulfur content. When all the threshold conditions were satisfied, the environmental effects on the fatigue lives of these materials increased with increased sulfur content. The fatigue lives of A508–Cl. 3 low-alloy steels with 0.003 and 0.008 wt.% sulfur and A333–Gr. 6 carbon steels with 0.008 and 0.016 wt.% sulfur were plotted as a function of strain rate, as shown in Fig. 65. The available data sets were too sparse to establish a functional form

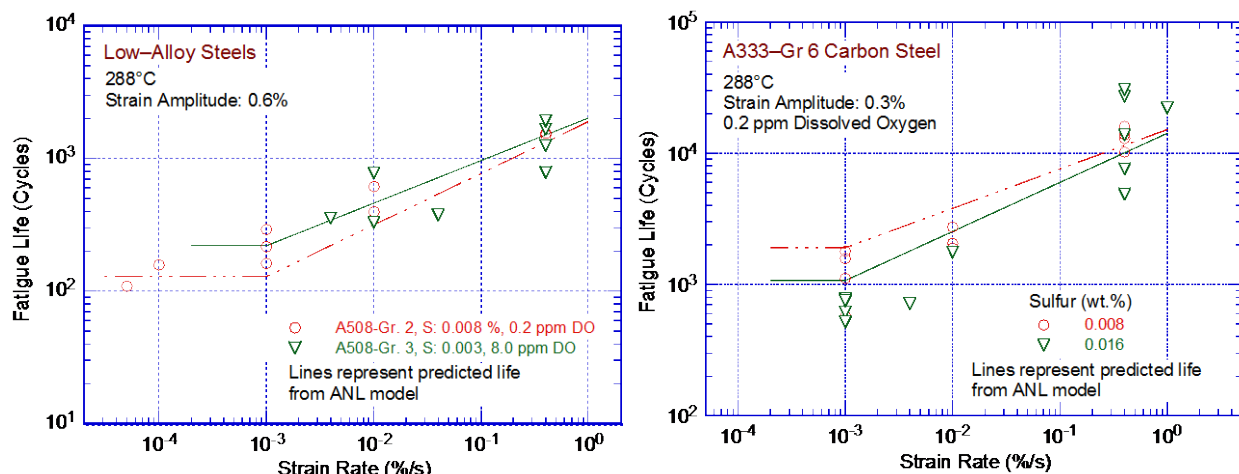


**Figure 65. Effect of strain rate on fatigue life of low-alloy steels with different sulfur contents (Refs. 10, 136).**

for dependence of fatigue lives on sulfur content and to define either a threshold for sulfur content below which environmental effects were unimportant or an upper limit above which the effects of sulfur on fatigue lives may saturate. A linear dependence of fatigue life versus sulfur content was assumed in proposed correlations for estimating the fatigue lives of carbon steels and low-alloy steels in LWR environments.<sup>10,118</sup> The limited data indicated that in high-purity water with 0.2 ppm DO at 289°C, the fatigue lives of carbon steels with 0.016 and 0.026 wt.% sulfur at 0.001 %/s strain rate and 0.3 % strain amplitude were comparable. Similar behavior was observed for low-alloy steels with greater than 0.0125 wt.% sulfur. Therefore, fatigue lives of carbon and low-alloy steels were assumed to saturate at sulfur contents above 0.015 wt.%.<sup>10</sup>

The existing fatigue  $\epsilon$ -N data also indicated significant reductions in fatigue lives for some heats of carbon steels with sulfur levels as low as 0.002 wt.%. The fatigue lives of several heats of A333-Gr. 6 carbon steels with sulfur contents of 0.002–0.016 wt.% in high-DO water at 288°C and 0.6% strain amplitude were plotted as a function of strain rate, as shown in Fig. 66.<sup>10</sup> Environmental effects on the fatigue lives of these steels were independent of sulfur contents in the range of 0.002–0.015 wt.%. The fatigue lives of carbon steel in air-saturated water (approximately 8 ppm DO) were relatively insensitive to sulfur contents in very high DO water. Under these conditions, the effects of DO dominated fatigue lives.

- *The effects of steel sulfur content on the fatigue lives of carbon and low-alloy steels in LWR environments were explicitly considered in the  $F_{en}$ , defined in Eq. 41 (Section 4.1.11). Evaluation of experimental data on low-sulfur steels (less than 0.005 wt.% sulfur) in water with more than 1 ppm DO should be performed with caution because, in some cases, the effects of sulfur were observed to be larger than those predicted by Eq. 41.*

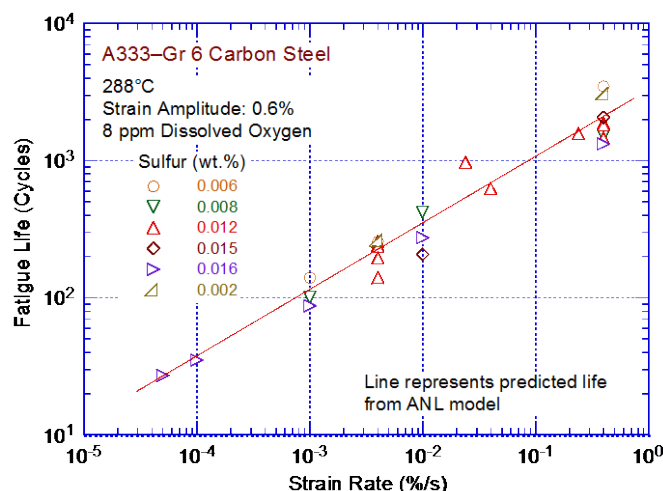


**Figure 66.**  
Effect of strain rate on the fatigue lives of A333-Gr. 6 carbon steels with different sulfur contents (Ref. 10).

#### 4.1.8 Hold Periods

Fatigue tests conducted using trapezoidal loading waveforms indicated that hold periods at peak tensile strains decreased the fatigue lives of carbon steels in high-DO water at 289°C.<sup>10,24</sup> However, examination of the data indicated that these results were caused by limitations of the test procedures or by frequency effects. Loading waveforms, hysteresis loops, and fatigue lives for the tests on A106-Gr B carbon steel in air and water environments were plotted, as shown in Fig. 67.<sup>10</sup> A 300-s hold period was sufficient to reduce fatigue lives by approximately 50% (approximately 2,000 cycles without a hold period and approximately 1,000 cycles with a hold period); a longer hold period of 1800 s resulted in lower fatigue lives than those obtained with a 300-s hold period. For example, two 300-s hold tests at 288°C and approximately 0.78% strain

range in oxygenated water with 0.7 ppm DO yielded fatigue lives of 1,007 and 1,092 cycles; the fatigue life from a 1,800-s hold test was 840 cycles. These tests were conducted in stroke-control mode and were different from conventional hold-time tests in a strain-controlled mode where the total strain in the sample was held constant during the hold period. However, a portion of the elastic strain was converted to plastic strain because of stress relaxation. In the stroke-controlled tests, there were additional plastic strains in the samples due to relaxation of elastic strains from the load trains (Fig. 67). Consequently, significant strain changes occurred during the hold periods; the measured plastic strains during the hold periods were approximately 0.028% from relaxation of the gauge and 0.05–0.06% from relaxation of the load trains. These conditions resulted in strain rates of 0.005–0.02%/s during the hold periods. The reductions in fatigue lives were attributed to slow strain rates during the hold periods. Also, frequency effects decreased the fatigue lives obtained from hold time tests, e.g., in air, the fatigue lives of stroke-controlled tests with hold periods were approximately 50% lower than those without the hold periods.

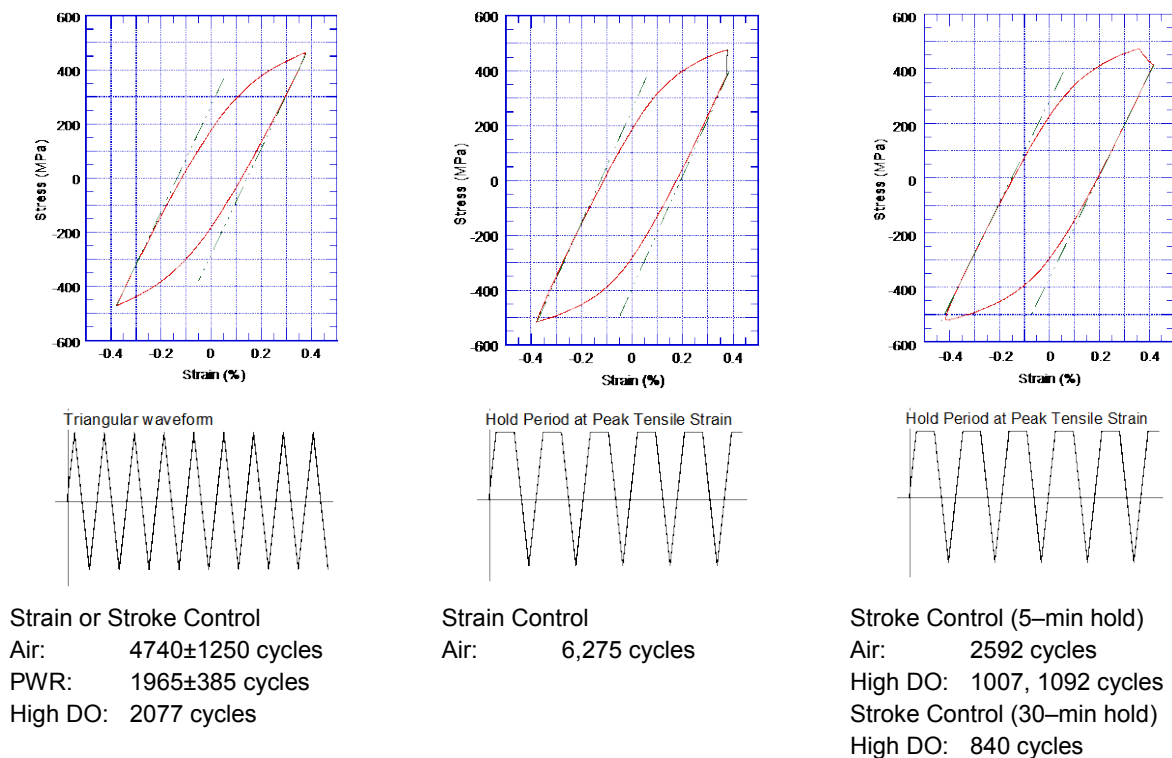


**Figure 67. Fatigue lives of A106-Gr B steel in air and water environments at 288°C, 0.78% strain range, and hold periods at peak tensile strain (Ref. 10). Hysteresis loops are for tests in air.**

Hold-time tests were also conducted on STS410 carbon steel at 289°C in water with 1 ppm DO (Fig. 68).<sup>24</sup> The most significant observation was that, for strain hold periods at peak tensile strain, reduction in fatigue lives were significant in tests that were conducted at fast strain rates, e.g., at 0.4%/s. The reduction in fatigue lives with hold periods decreased at lower strain rates with insignificant reductions in fatigue lives at 0.004 %/s strain rate. The results also indicated that the decrease in fatigue lives with extended hold periods saturated at values that were comparable to fatigue lives at slow strain rates (e.g., 0.004 %/s).

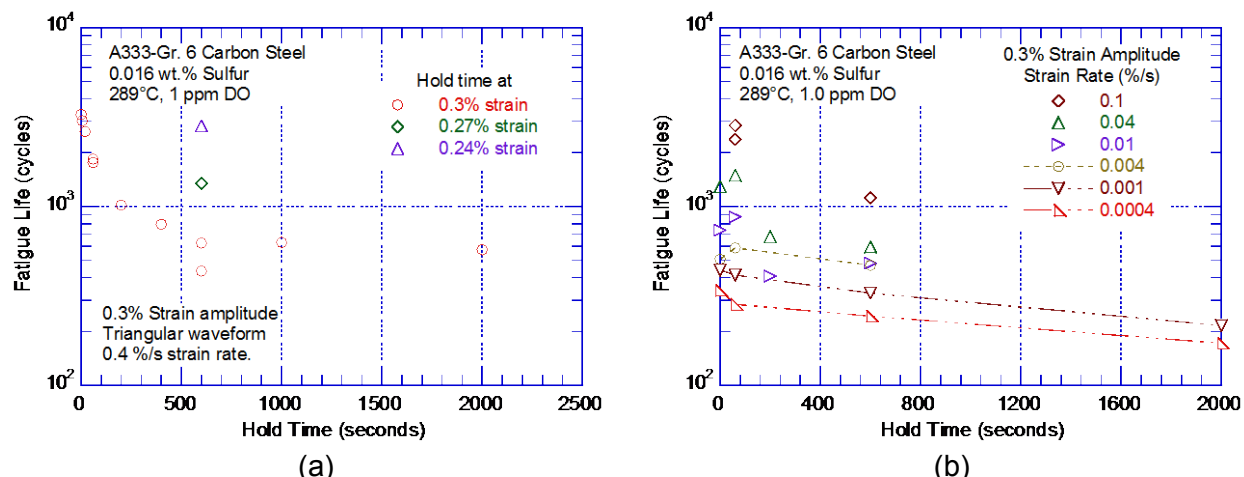


**Figure 68. Effect of hold periods on the fatigue lives of A333-Gr. 6 carbon steel at 289°C in water with 1 ppm DO (Ref. 24).**

The most significant observation of this data was that little or no decreases in fatigue lives were observed when the hold periods were below the peak strain during the decreasing strain portions of the fatigue cycles (i.e., 0.06% below the peak strain of 0.24%). Based on these results, Higuchi et al.<sup>24</sup> concluded that the procedures for calculating  $F_{en}$  did not need revision.

The JNES report<sup>136</sup> investigated hold time effects and reported that, in the high temperature water environments, the fatigue lives of carbon and low-alloy steels were reduced due to strain hold times at the peak (local maximum value). Fatigue life reductions due to strain hold times at the peak were significant at higher strain rates, but they were reduced as the strain rate decreased. There were little or no observed fatigue life reductions at strain rates of 0.004%/s or less. JNES concluded that the extent of fatigue life reduction depended on the length of the hold time, and that fatigue life reductions tended to be saturated as the hold time became longer. A threshold was observed at a strain rate of 0.004%/s. For carbon steels, the effects of strain hold times were negligible at strain rates of 0.004%/s or lower. Fatigue life reductions due to strain hold times in low-alloy steels were smaller than those in carbon steels. Although fatigue lives were reduced due to strain hold times at the peak (local maximum value), when strain was held at 0.06% below the peak strain after overshoot showed no reductions in fatigue lives, although tensile stresses corresponding to the yield point still remained. From these results, JNES concluded that the effects of strain hold times in the actual components was not necessary since the peak thermal stress generated by actual operating thermal transients is not considered to exceed the yield stress significantly but, for strain rates exceeding 0.004%/s, evaluations should be performed assuming a threshold strain rate of 0.004%/s while considering fatigue life reduction due to strain holding when the strain is at the peak and held under the internal pressure condition that accompanies elastic follow-up.

As discussed in Section 4.1.11, the differences in fatigue lives observed in the JNES tests were generally within the data scatter for the fatigue  $\epsilon$ - $N$  data in LWR environments. Thus, the effects of hold time from available data are inconclusive and, until such time as sufficient data are available, these effects were not explicitly addressed in the updated  $F_{en}$  methodology. Further research of these effects is recommended.

- The available  $\epsilon$ - $N$  data investigated in this report were not fully conclusive with respect to the effects of hold time periods on the fatigue lives of carbon and low-alloy steels in LWR environments. Thus, hold time effects were not explicitly addressed in the updated  $F_{en}$  methodology.

#### 4.1.9 Flow Rate

Nearly all of the laboratory fatigue  $\epsilon$ - $N$  data for LWR environments were obtained at very low water flow rates. Recent test data indicated that, under the environmental conditions typical for operating BWRs, environmental effects on the fatigue lives of carbon steels were lower at high flow rates (7 meters/second) compared to the fatigue lives under very low flow rate conditions similar to those flow rates where most of the data were obtained.<sup>25,26,55</sup> The effects of water flow rate on the fatigue lives of high- and low-sulfur A333-Gr. 6 carbon steel and A533-Gr. B low-alloy steel in high-purity water at 289°C tested at different strain amplitudes and strain rates are shown in Fig. 69.

The results indicated that the effects of increased flow rates were modest. The benefits were greater for high-sulfur steels at high strain amplitudes and high strain rates (e.g., 0.4%/s).<sup>25,26</sup> At 0.3% strain amplitude and 0.01%/s strain rate, and for all DO levels, fatigue lives were increased by a factor of approximately 2 when the flow rate was increased from approximately  $10^{-5}$  to 7 meters/second. At 0.6% strain amplitude and 0.001%/s strain rate, fatigue lives were increased by a factor of approximately 6 in water with 0.2 ppm DO and by a factor of

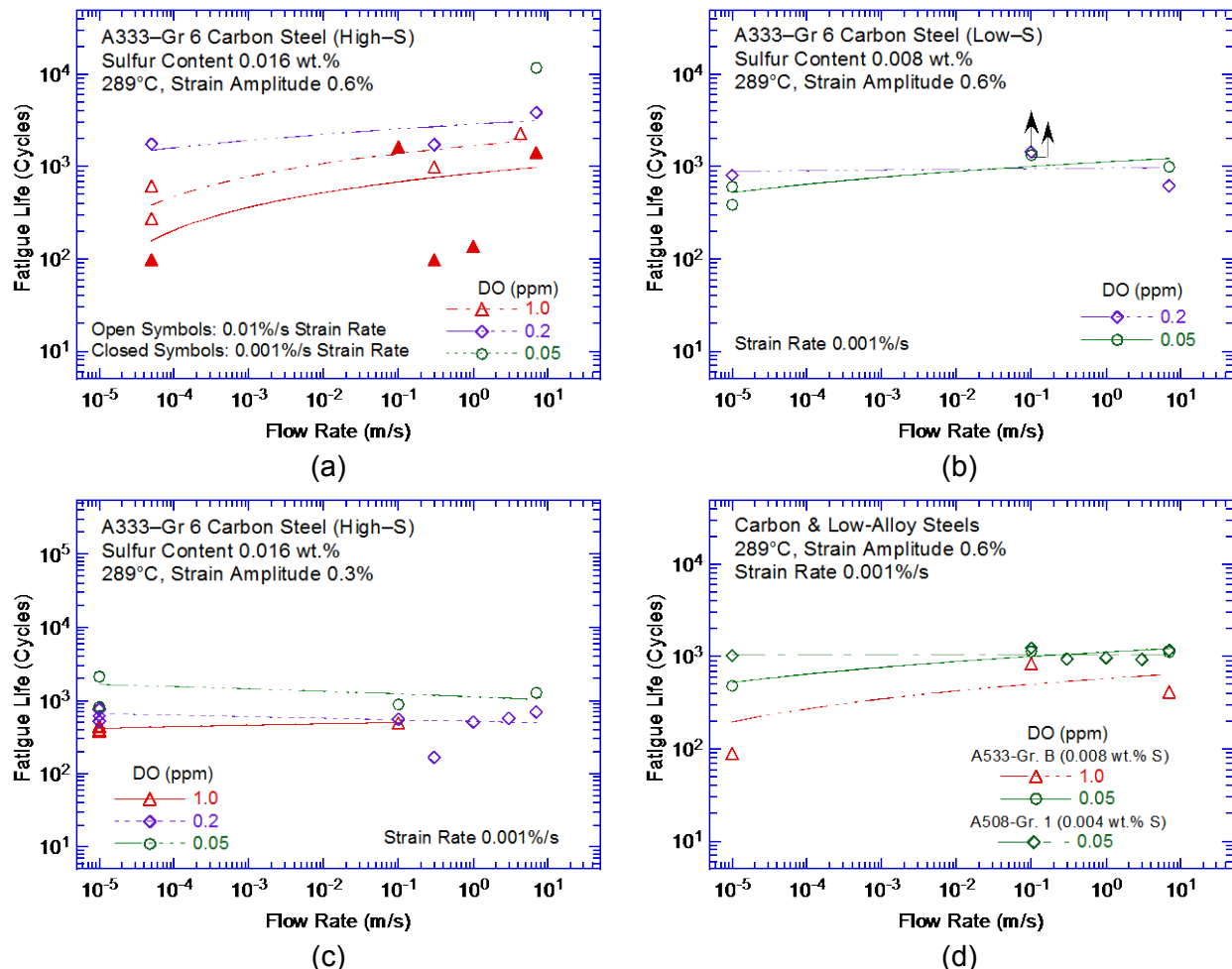


**Figure 69.** Effects of water flow rate on fatigue lives of A333-Gr. 6 and A508-Gr. 1 carbon steels and A533-Gr. B low-alloy steel at 289°C and 0.3 or 0.6% strain amplitudes and various strain rates (Ref. 25,26).



approximately 3 in water with 1.0 or 0.05 ppm DO. Under similar loading conditions, i.e., 0.6% strain amplitude and 0.001%/s strain rate, a low-sulfur (0.008 wt.%) heat of A333-Gr. 6 carbon steel showed a factor of approximately 2 increase in fatigue life with increased flow rates. Note that the beneficial effects of flow rate were determined from a single test on each material at very low flow rates; data scatter in LWR environments is typically a factor of approximately 2. A factor of 2 increase in fatigue lives was observed (Fig. 70) at KWU during component tests with 180° bends of carbon steel tubing (0.025 wt.% sulfur) when internal flow rates of up to 0.6 meters/second were established.<sup>55</sup> The tests were conducted at 240°C in water that contained 0.2 ppm DO.

- *Because of the uncertainties in the flow conditions at or near the locations of crack initiation, the beneficial effects of flow rates on the fatigue lives of carbon and low-alloy steels were not explicitly considered in the updated  $F_{en}$  methodology.*

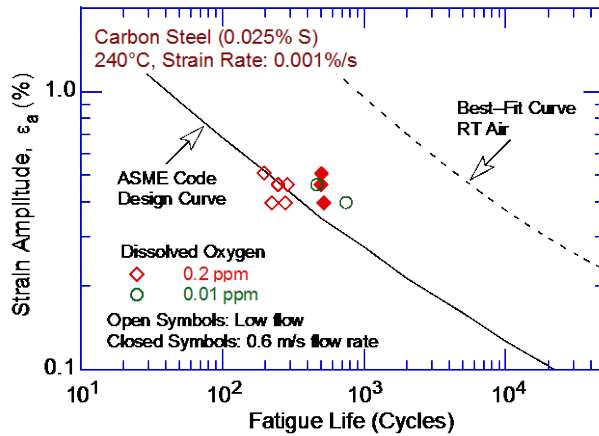


**Figure 70.**  
Effect of flow rate on low-cycle fatigue of carbon steel tube bends in high-purity water at 240°C (Ref. 55). RT = room temperature.

#### 4.1.10 Fatigue Life Model

As discussed in the beginning of Section 4.1, the fatigue-life models for estimating the fatigue lives of carbon and low-alloy steels in LWR environments presented in the original revision of NUREG/CR-6909 were based on an analysis of the updated PVRC database. For this report, more recently available data were fit to a modified version of the Langer equation expressed by Eq. 6, which included a term for environmental effects on fatigue lives. The environmental term included the effects of key parameters, such as temperature, strain rate, DO content in the water, and sulfur content in the steel on the fatigue lives of carbon and low-alloy steels, and also considered revised constraints based on stakeholder comments and experience with implementation of the  $F_{en}$  methodology in industry analyses. The functional forms of these dependencies and constraints were based on the observed data trends. In LWR environments, the analysis concluded that the fatigue life,  $N$ , of carbon steels was best represented by

$$\ln(N) = 5.951 - 1.975 \ln(\varepsilon_a - 0.113) + 0.101 S^* T^* O^* \dot{\varepsilon}^*, \quad (39)$$

and that of low-alloy steels, by

$$\ln(N) = 5.747 - 1.808 \ln(\varepsilon_a - 0.151) + 0.101 S^* T^* O^* \dot{\varepsilon}^*, \quad (40)$$

where  $S^*$ ,  $T^*$ ,  $O^*$ , and  $\dot{\varepsilon}^*$  represent the terms for transformed sulfur content, temperature, DO level, and strain rate, respectively, that are defined by Eqs. 35-38. These equations for carbon

and low-alloy steels remain unchanged from those specified in the initial revision to NUREG/CR-6909. The predicted fatigue lives showed good agreement with the experimental values; the experimental and predicted values differed by a factor of 3 or less. A threshold strain amplitude (one-half of the applied strain range) was also defined, below which LWR coolant environments have an insignificant effect on fatigue lives, i.e.,  $F_{en} = 1$ . The threshold strain amplitude was specified as 0.07%, or a 145 MPa (21 ksi) stress amplitude for both carbon and low-alloy steels.

- *The ANL fatigue life models for carbon and low-alloy steels represent the mean values of fatigue life as a function of applied strain amplitude, temperature, strain rate, DO level in the water, and sulfur content of the steel. The effects of parameters (such as mean stress, surface finish, size and geometry, and loading history) known to influence fatigue lives were not included in the models; the effects of these parameters were considered in the development of the fatigue design curves, as discussed in Chapter 5.*

#### 4.1.11 Environmental Fatigue Correction Factor

To incorporate environmental effects into ASME Code Section III fatigue evaluations, the initial revision to NUREG/CR-6909 specified that the fatigue usage for a specific stress cycle or load set pair based on the current ASME Code Section III fatigue design curves was multiplied by the environmental correction factor,  $F_{en}$ , given by Eqs. 33 and 34, respectively, for carbon steels and low-alloy steels. Further details for incorporating environmental effects into fatigue evaluations were presented in Appendix A of the initial revision to NUREG/CR-6909.

The previous  $F_{en}$  expressions for carbon and low-alloy steels (i.e., Eqs. 33 and 34) were updated in this report using the larger fatigue  $\epsilon$ -N database described in Table 10 to remove some of the conservatism in the  $F_{en}$  methodology and to reflect the additional data available since the initial publication of NUREG/CR-6909. As discussed previously, an additional objective of the reevaluation was to investigate the significance of the constant terms in the previous expressions. The updated evaluation addressed stakeholders' concerns related to: (a) the constants in the  $F_{en}$  expressions that result in  $F_{en}$  values of approximately 2 even when strain rate is very high or temperature is very low, and (b) the temperature dependence of  $F_{en}$  for carbon and low-alloy steels.

The available fatigue  $\epsilon$ -N data for carbon and low-alloy steels were reanalyzed using a different dependence of fatigue lives on strain rate, dissolved oxygen, and temperature, such that  $F_{en}$  is equal to 1 at high strain rates (i.e., greater than 2.2%/s). A single  $F_{en}$  expression was developed for both carbon and low-alloy steels. The functional form of the new  $F_{en}$  expression and for the dependence of  $F_{en}$  on the sulfur content in the steel were comparable to the expressions proposed by the JNES.<sup>136</sup> In addition, a maximum temperature limit was selected at 325°C as a reasonable extension to cover all anticipated LWR operating conditions. This is adequate for all expected operating LWR conditions considering the use of average temperature (as discussed in Section 4.1.11 and shown in Fig. 81). In addition, the limit for the saturation strain rate was decreased from 0.001 to 0.0004%/s. A best fit of the experimental data yielded the following expression for  $F_{en}$  for both carbon and low-alloy steels,

$$F_{en} = \exp((0.003 - 0.031 \dot{\epsilon}^*) S^* T^* O^*), \quad (41)$$

where  $S^*$ ,  $T^*$ ,  $O^*$ , and  $\dot{\epsilon}^*$  are the transformed sulfur content, temperature, DO level, and strain rate, respectively, defined as:



$$\begin{aligned} S^* &= 2.0 + 98 S & (S \leq 0.015 \text{ wt.}\%) \\ S^* &= 3.47 & (S > 0.015 \text{ wt.}\%) \end{aligned} \quad (42)$$

$$\begin{aligned} T^* &= 0.395 & (T < 150^\circ\text{C}) \\ T^* &= (T - 75)/190 & (150^\circ\text{C} \leq T \leq 325^\circ\text{C}) \end{aligned} \quad (43)$$

$$\begin{aligned} O^* &= 1.49 & (DO < 0.04 \text{ ppm}) \\ O^* &= \ln(DO/0.009) & (0.04 \text{ ppm} \leq DO \leq 0.5 \text{ ppm}) \\ O^* &= 4.02 & (DO > 0.5 \text{ ppm}) \end{aligned} \quad (44)$$

$$\begin{aligned} \dot{\epsilon}^* &= 0 & (\dot{\epsilon} > 2.2\%/s) \\ \dot{\epsilon}^* &= \ln(\dot{\epsilon}/2.2) & (0.0004\%/s \leq \dot{\epsilon} \leq 2.2\%/s) \\ \dot{\epsilon}^* &= \ln(0.0004/2.2) & (\dot{\epsilon} < 0.0004\%/s). \end{aligned} \quad (45)$$

The experimental values of fatigue lives compared to those predicted by Eq. 41 and Eqs. 33 or 34 were plotted, as shown in Figs. 71 and 72 for carbon and low-alloy steels, respectively. The results indicate that the new  $F_{en}$  expressions represent a better fit of the experimental data relative to the fit for the expressions in the original revision of NUREG/CR-6909; the regression

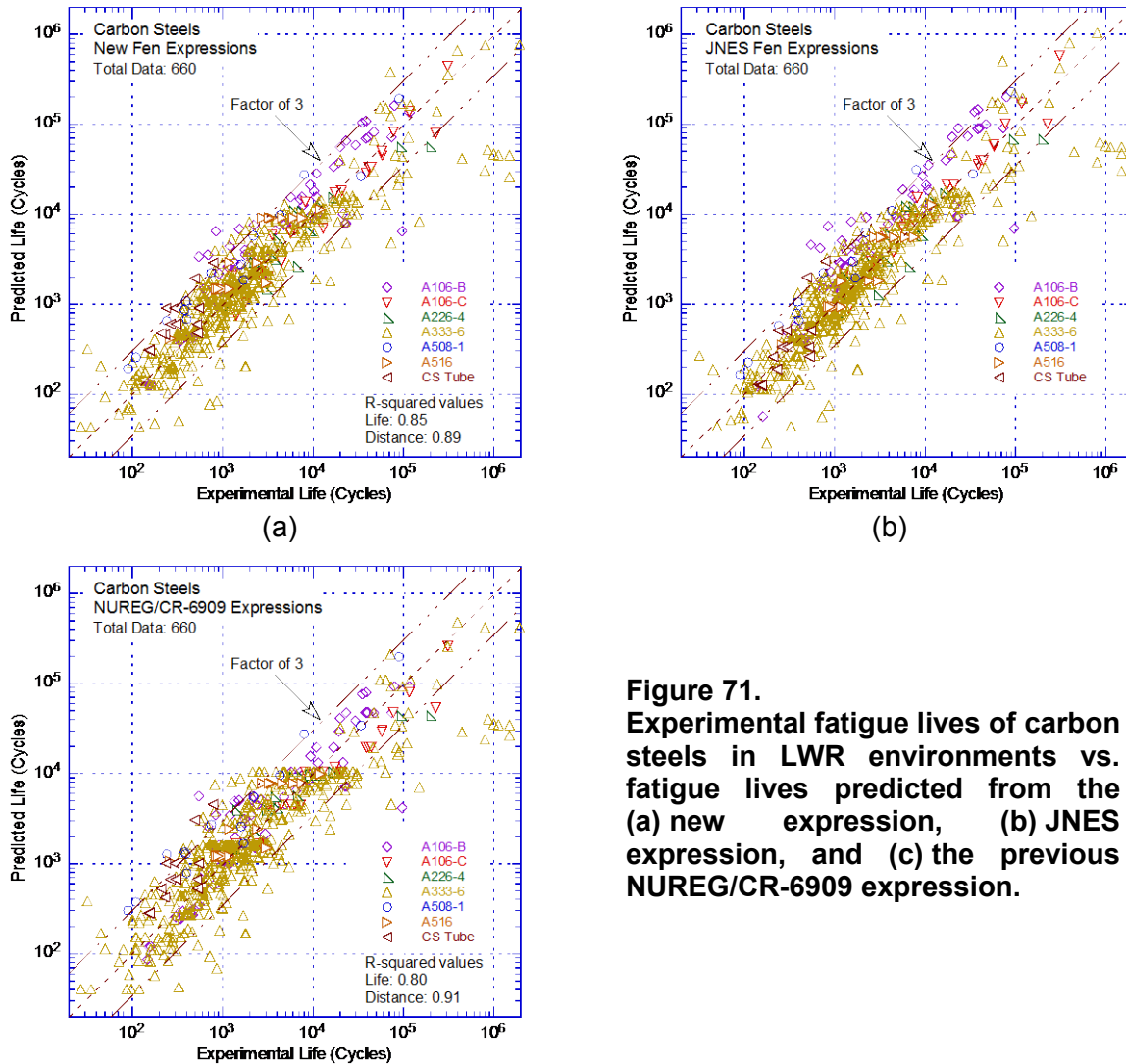


**Figure 71.**  
Experimental fatigue lives of carbon steels in LWR environments vs. fatigue lives predicted from the (a) new expression, (b) JNES expression, and (c) the previous NUREG/CR-6909 expression.

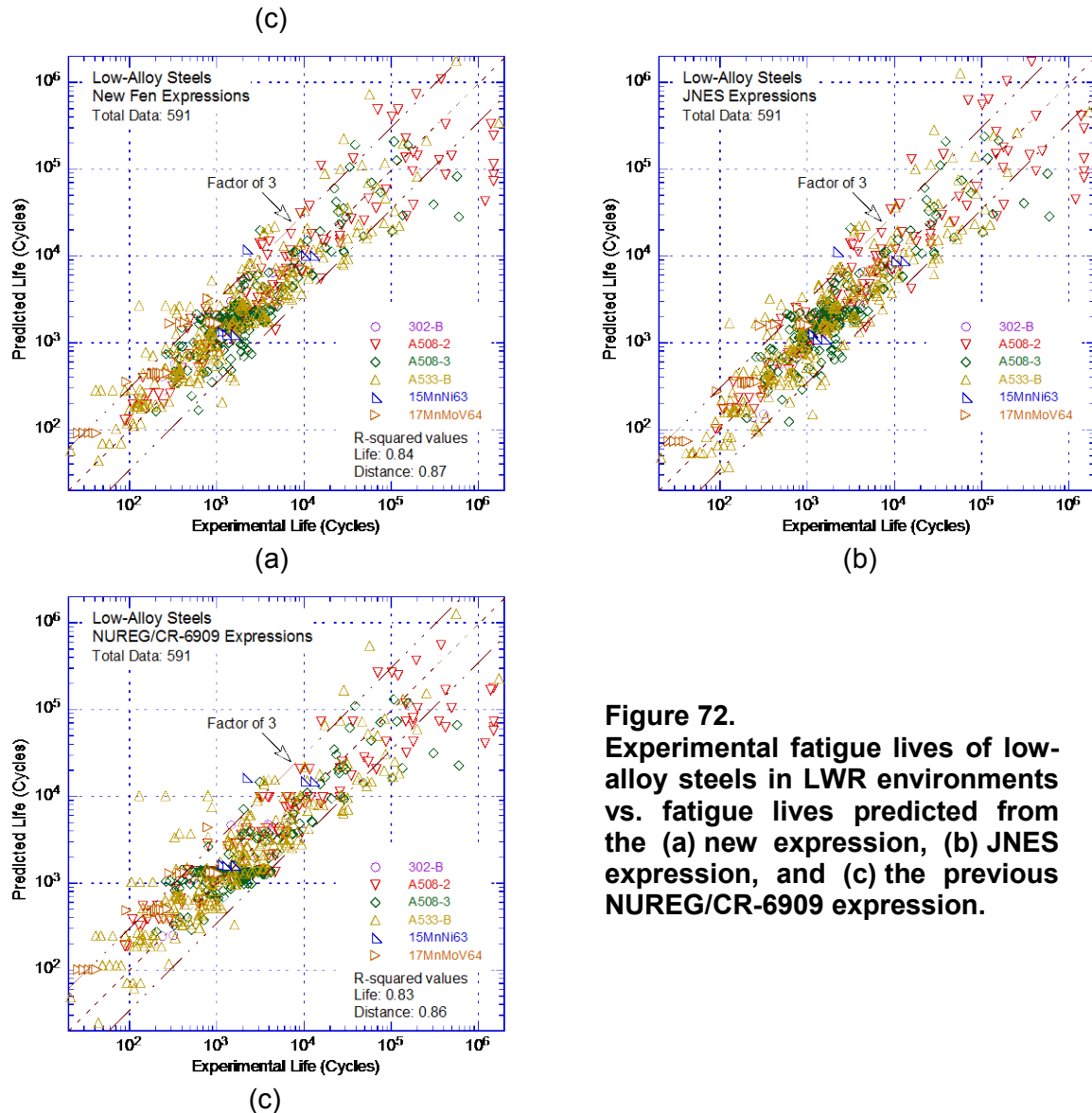


**Figure 72.**  
Experimental fatigue lives of low-alloy steels in LWR environments vs. fatigue lives predicted from the (a) new expression, (b) JNES expression, and (c) the previous NUREG/CR-6909 expression.

(R-squared) values increased from 0.80 to 0.85 for carbon steels and from 0.83 to 0.84 for low-alloy steels. The new expressions typically underestimated environmental effects for operating conditions that resulted in very large  $F_{en}$  values (i.e., greater than 40) and in the high-cycle fatigue regime (i.e., fatigue lives above 50,000 cycles). However, such conditions are not typical of the thermal transients encountered during reactor operation or evaluated in most ASME Code CUF calculations.

A comparison was made of the fatigue lives predicted for carbon and low-alloy steels using the new  $F_{en}$  expressions and the JNES  $F_{en}$  expressions, and is shown in Fig. 73. In general,  $F_{en}$  values calculated from the new ANL expression were marginally lower than those obtained from the JNES expression in Ref. 136; the fatigue lives predicted by the new ANL expressions were either comparable to or slightly longer than those predicted from the JNES expressions. However, there were a few data points for carbon steels and several data points for low-alloy steels for which the fatigue lives predicted by the JNES expression were significantly lower than those predicted by the new ANL expression (bottom left corner of the plots in Fig. 73). As discussed previously, the new ANL  $F_{en}$  expression was optimized under environmental and

loading conditions that are anticipated during reactor operation (i.e., conditions that yield  $F_{en}$  values less than 40). This optimization limitation explains the differences observed between the two expressions, as the predicted  $F_{en}$  values for nearly all of these data points were above 60. The tests associated with these points were conducted in air-saturated water (8 ppm DO) at very low strain rates. Considering this, the ANL and JNES expressions are in very good agreement, which is remarkable given that the development approaches used were different.

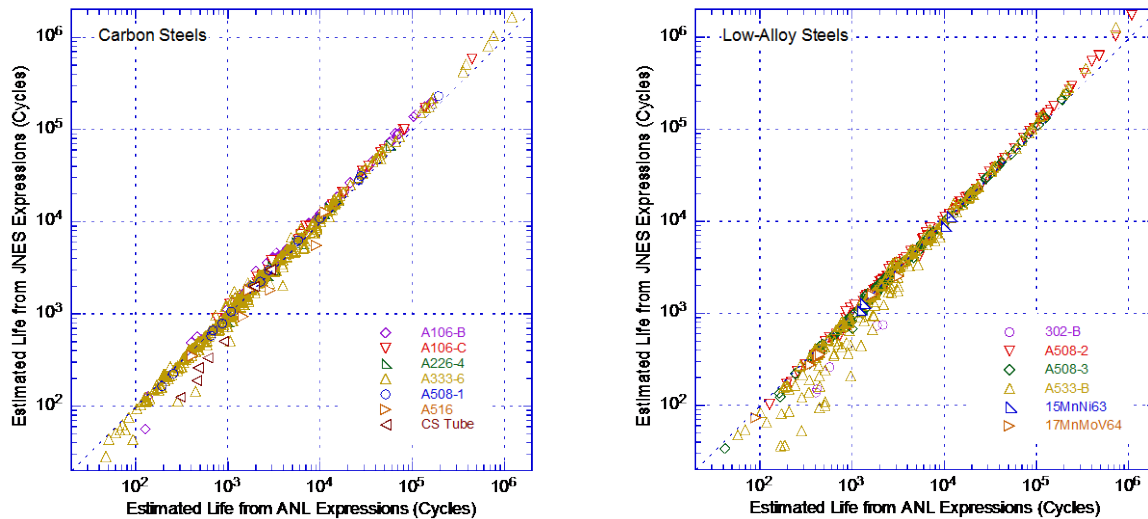


**Figure 73. Comparison of the fatigue lives of carbon and low-alloy steels predicted from the new  $F_{en}$  expression and the JNES  $F_{en}$  expression.**

Upon completion of the modeling phase, the residual errors (i.e., the Cartesian distance of each data point from the mean prediction curve) did not show significant patterns, such as heteroskedasticity (changing variance), or a nonzero slope. The residual errors for each variable, grouped by steel type, were plotted and are shown in Figs. 74 and 75 for carbon and low-alloy steels, respectively. The residuals were determined from the difference between the logarithms of the estimated lives and predicted lives. Thus, negative residual errors indicated conservative estimates of fatigue lives and positive residual errors indicated nonconservative estimates of fatigue lives (i.e., predicted lives were greater than the observed fatigue lives). However, if the residuals for a specific heat were not evenly distributed about zero, it did not necessarily indicate any deficiency in the predictive models. Such results indicated that the specific heat was either superior or inferior to the average behavior predicted by the model. For example, a positive residual indicated that the heat was inferior (i.e., the constant  $A$  from Eq. 6 for the heat was smaller than the median value of  $A$  determined for the model) and a negative residual indicated that the heat was superior to the average behavior for the material. This behavior is discussed further in Section 4.1.13.

The results presented in Figs. 74 and 75 did not show any unexplained patterns. In general, high variance tended to be associated with longer lives and lower strain amplitudes. Furthermore, biases were traceable to heat-to-heat variations. For example, the heats of A108-Gr. B, A508-Gr. 1, and A516-KC70 had inferior fatigue resistances and two heats of A333-Gr. 6 (ANL Material IDs 8 and 10 in Table 10) had superior fatigue resistances compared to the average behavior represented by the fatigue  $\epsilon$ -N model (Eqs. 39 and 40).

Some of the heats of carbon and low-alloy steels were also tested in air. The residual errors for the best fit of the fatigue  $\epsilon$ -N data for carbon and low-alloy steels in air were plotted as a function of the ANL Material ID, as shown in Fig. 76. Most of the data subsets for fatigue tests

in air followed the same trends observed in LWR environments; data subsets that yielded positive residuals in LWR environments also showed positive residuals in air, and vice versa.

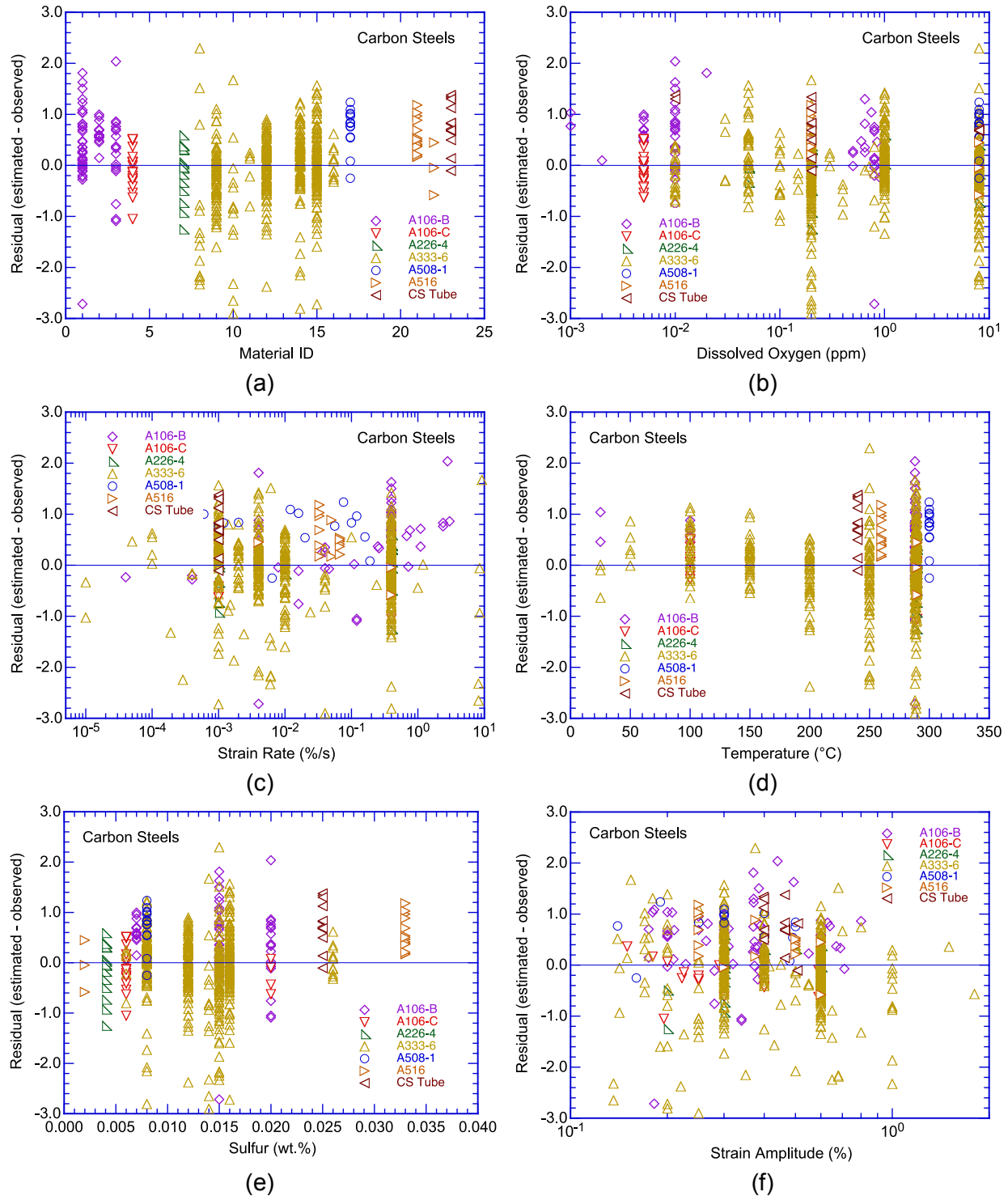


**Figure 74. Residuals for predicted fatigue lives of carbon steels as a function of (a) Material ID, (b) water dissolved oxygen content, (c) strain rate, (d) temperature, (e) steel sulfur content, and (f) strain amplitude.**

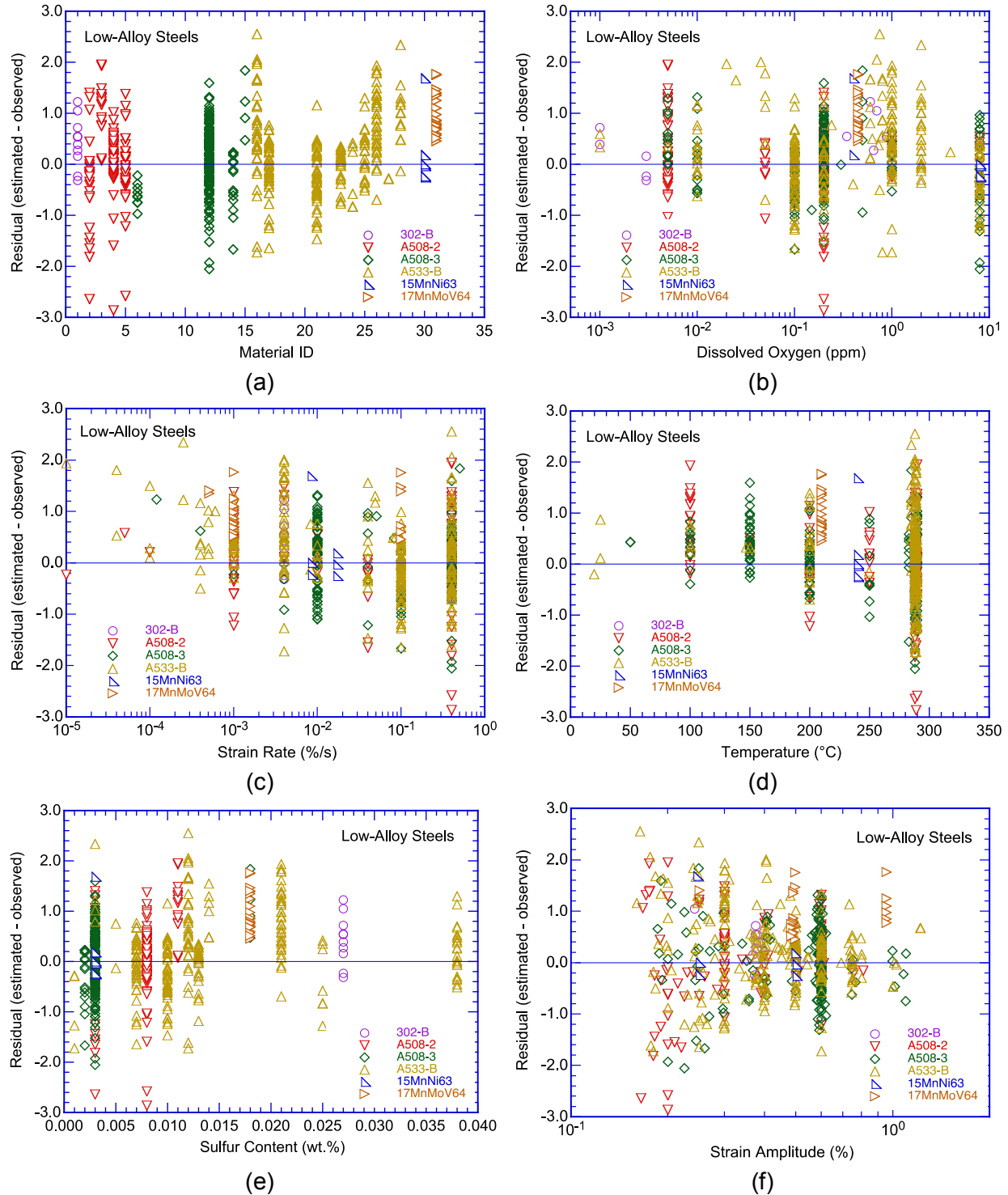


**Figure 75.** Residuals for predicted fatigue lives of low-alloy steels as a function of (a) Material ID, (b) water dissolved oxygen content, (c) strain rate, (d) temperature, (e) steel sulfur content, and (f) strain amplitude.

The exception was ANL Material ID 21, which yielded a positive residual in an LWR environment but a negative residual in an air environment. However, the total data in air were quite limited for this heat of A516-KC70 carbon steel, so quantitative conclusions were not made.

- The  $F_{en}$  approach should be used to incorporate environmental effects into ASME Code, Section III fatigue evaluations for carbon and low-alloy steels. Appendix C of this report presents a sample application of the  $F_{en}$  methodology.

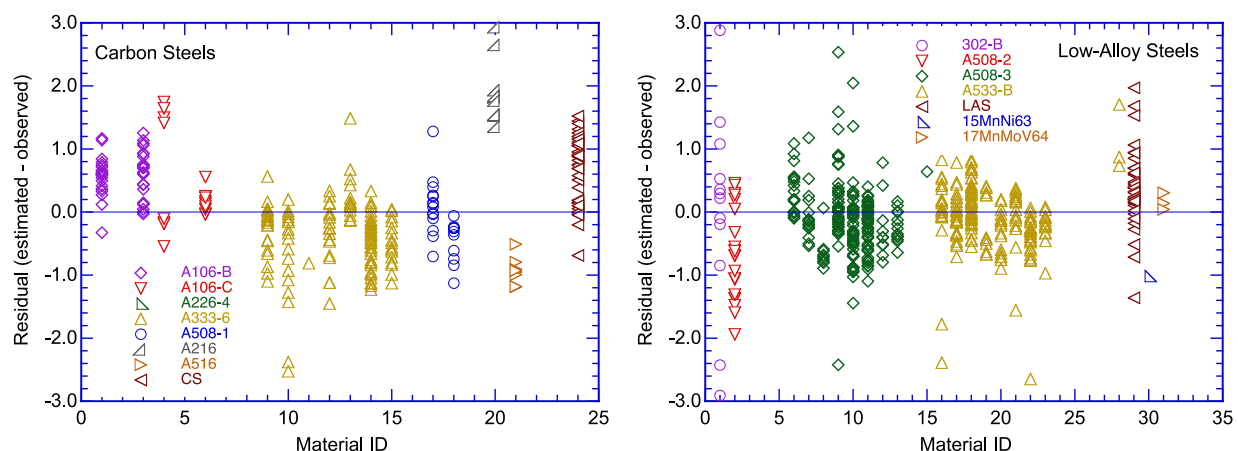


**Figure 76. Residuals for predicted fatigue lives in air of carbon and low-alloy steels as a function of Material ID.**

#### 4.1.12 Surface Finish

Fatigue tests were conducted on specimens of carbon and low-alloy steels that were intentionally roughened in a lathe, under controlled conditions, with 50-grit sandpaper to produce circumferential scratches with an average roughness,  $R_a$ , of  $1.2 \mu\text{m}$  and a root-mean-square,  $R_q$ , of  $1.6 \mu\text{m}$  (approximately 62 micro in.).<sup>46</sup> The results for A106-Gr B carbon steel and A533-Gr B low-alloy steel are shown in Fig. 77. In air, the fatigue lives of rough A106-Gr B specimens were a factor of 3 lower than that of smooth specimens, and, in high-DO water, were the same as those of smooth specimens. In low-DO water, the fatigue lives of the roughened A106-Gr B specimen were slightly lower than those for smooth specimens. The effects of surface finish on the fatigue lives of A533-Gr B low-alloy steel were similar to those for A106-Gr B carbon steel; in high-DO water, the fatigue lives of both rough and smooth specimens were the same. The results in water were consistent with a mechanism of growth by a slip oxidation/dissolution process, which was not affected by surface finish. Surface roughness is expected to influence fatigue lives because environmental effects were moderate in low-DO water.



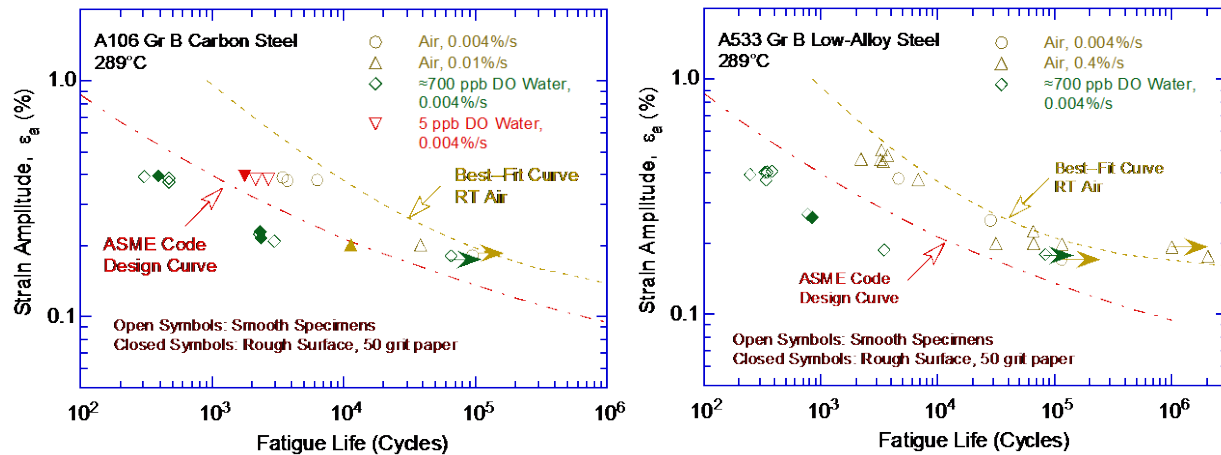


**Figure 77. Effect of surface finish on the fatigue lives of (a) A106–Gr B carbon steel and (b) A533 low–alloy steel in air and high–purity water at 289°C (Ref. 46).**

The potential additional impact of strain rate on the observed surface finish effects on the fatigue lives of low-alloy steels were also investigated (Fig. 78).<sup>144</sup> The results showed a strong influence of strain rate on surface finish effects. At high strain rates, relative to smooth specimens, the fatigue lives of A533-B low-alloy steel decreased significantly even with slight increases in surface roughness, whereas at low strain rates, since fatigue lives were already low, any further decrease in fatigue lives occurred only for very rough surfaces. The different behavior was attributed to the differences in the mechanism for corrosion fatigue of carbon and low-alloy steels in LWR environments. As discussed in Section 2.2.1.2, the corrosion fatigue mechanism changed from hydrogen-induced cracking to a slip-oxidation/dissolution mechanism with decreasing strain rates. During cyclic loading in high-temperature water, plastic deformation induced slip bands at the crack tip along the maximum shear directions or the preferred slip directions, which ruptured the protective oxide film at the crack tip. Furthermore, the slip bands were the favored paths for hydrogen transportation and the matrix/inclusion interfaces were the preferred traps for hydrogen. As a result, at high strain rates, fatigue cracking preferentially occurred along the slip bands as well as the matrix/inclusions interfaces, which resulted in macroscopically tortuous fatigue cracks and a rough fracture surface. However, at low strain rates, fatigue crack growth in high-temperature water was controlled by

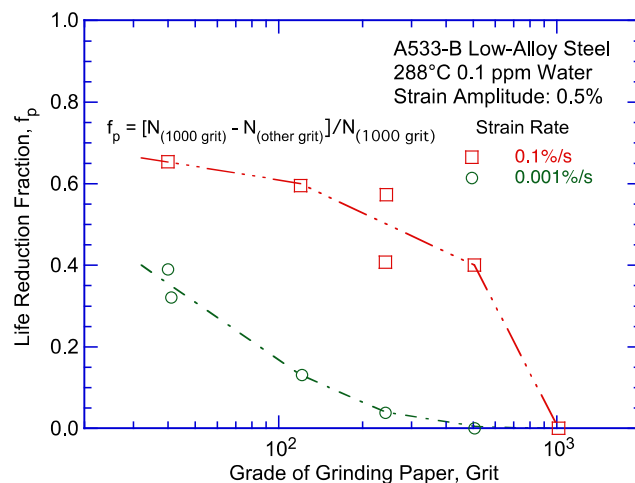


**Figure 78. Relationship between surface finish and fatigue life reduction fraction for A533-Gr. B low-alloy steel in water at 288°C (Ref. 144).**

the film-rupture/oxidation-dissolution mechanism, which resulted in a macroscopically straight, and relatively flat, featureless fracture surface.

The results in Fig. 77 were also observed to be consistent with strain rate effects; the surface finish of the specimens that were tested at slow strain rates were not sufficiently rough to further decrease the fatigue lives.

- *The effects of surface finish were not explicitly included in the environmental fatigue correction factor for carbon and low-alloy steels; instead, they were included in the subfactor for “surface finish and environment” that was applied to the mean data air curve to develop the fatigue design curve in air.*

#### 4.1.13 Heat-to-Heat Variability

The effects of material heat-to-heat variability and data scatter on the fatigue lives of carbon and low-alloy steels was evaluated for LWR environments. The fatigue behavior of each of the heats or loading conditions was characterized by the value of the constant A in the ANL models for carbon steels given by

$$\ln(N) = A - 1.975 \ln(\varepsilon_a - 0.113) - \ln(F_{en}), \quad (46)$$

and in the ANL model for low-alloy steels by

$$\ln(N) = A - 1.808 \ln(\varepsilon_a - 0.151) - \ln(F_{en}), \quad (47)$$

where  $F_{en}$  was determined from Eq. 41. The values of A, determined from Eqs. 46 and 47 for the various data sets in the larger, updated fatigue  $\varepsilon$ -N database used in this report were ordered, and median ranks were used to estimate the cumulative distribution of A for the population. The estimated cumulative distribution of constant A for heats of carbon and low-alloy steels in water environments were plotted, and are shown in Fig. 79. The median value of constant A in water was slightly lower than that in air; the values of constant A in LWR and air environments, respectively, were 6.503 and 6.583 for carbon steels and 6.358 and 6.449 for low-alloy steels. The results of the analysis of the larger, updated fatigue  $\varepsilon$ -N database indicated that an increase in the fatigue data of more than 60% had an insignificant impact on the parameters in the ANL models for the fatigue lives of carbon and low-alloy steels.

The results also demonstrated that the  $F_{en}$  expression given in Eq. 41 adequately captured the effects of LWR environments on the fatigue lives of carbon and low-alloy steels. Since the actual heats of carbon and low-alloy steels that were tested in air and LWR environments were different, the location (percentile) of a specific heat on the distribution curve differed between the two environments. However, the estimated cumulative distribution of most of the heats of carbon steel and low-alloy steels that were tested in both air and LWR environments were comparable. However, a few exceptions showed significant differences. For example, for ANL heat designation A333-Gr. 6-3 (0.014 wt. % sulfur, ANL Material ID 10 in Tables 1 and 10), the updated ANL model underestimated environmental effects and the material ranked in the 97<sup>th</sup> percentile in LWR environment and the 50<sup>th</sup> percentile in air. In contrast, for ANL heat designation A333-Gr. 6-7 (0.008 wt. % sulfur, ANL Material ID 14 in Tables 1 and 10), the model overestimated environmental effects and the material ranked 40<sup>th</sup> percentile in LWR environment and the 55<sup>th</sup> percentile in air. A similar contrasting behavior was observed in two heats of low-alloy steels, e.g., the environmental effects were overestimated for A302-Gr. B (0.027 wt. % sulfur, ANL Material ID 1 in Tables 1 and 10) and underestimated for A508-Gr. 3-1 (0.003 wt. % sulfur, ANL Material ID 6 in Tables 1 and 10).



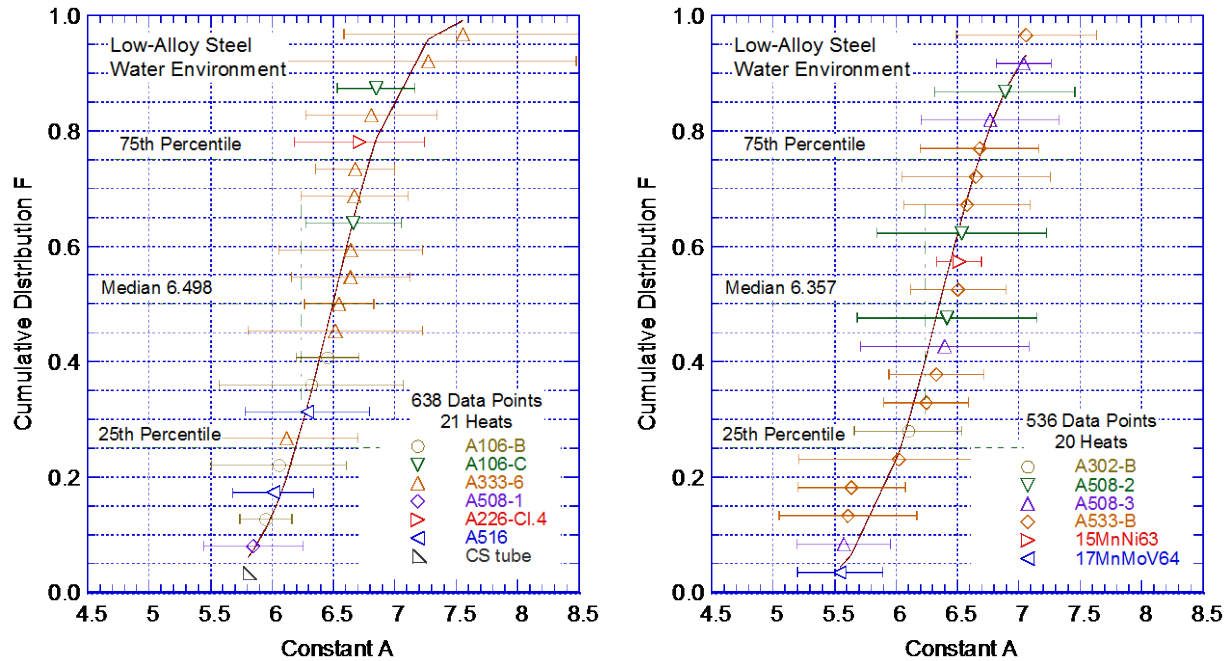


**Figure 79. Estimated cumulative distribution of parameter A in the ANL model for fatigue lives for heats of carbon and low-alloy steels in LWR environments.**

These results and evaluation indicated that, for carbon and low-alloy steels, the heat-to-heat variation in LWR environments were essentially the same as that established in air and presented in Section 3.1.7. Thus, the 95/95 values of the factors to account for material variability and data scatter were the same in air (i.e., presented in Tables 2 and 3 for carbon and low-alloy steels, respectively). These factors were required to provide 95% confidence that the resultant lives were greater than those observed for 95% of the materials of interest.

- *The effects of heat-to-heat variability were not explicitly included in the environmental fatigue correction factor for carbon and low-alloy steels; instead, they were included in the subfactor for “data scatter and material variability” that was applied to the mean data air curve to develop the fatigue design curve in air.*

#### 4.1.14 Modified Rate Approach

Most of the available fatigue  $\epsilon$ – $N$  data evaluated in this report were obtained under loading histories with constant strain rate, temperature, and strain amplitude. The actual loading histories encountered during service of nuclear power plants are far more complex. Exploratory fatigue tests were conducted with loading waveforms in which the test temperature and strain rate were varied.<sup>10,21,24</sup> The results of such tests provided limited guidance for developing procedures and rules for fatigue evaluation of components under complex loading histories.

The modified rate approach was proposed to predict fatigue lives under changing test conditions.<sup>37,38</sup> This approach provided methods for calculating  $F_{en}$  under conditions where temperature and strain rate were varied. In this approach, the correction factor,  $F_{en}(\dot{\epsilon}, T)$ , is assumed to increase linearly from a minimum value of 1.0 with increments of strain from a minimum value,  $\epsilon_{min}$  (%), to a maximum value,  $\epsilon_{max}$  (%). Increments of  $F_{en}$ ,  $dF_{en}$ , during increments of increasing strain,  $d\epsilon$ , are calculated from

$$dF_{en} = (F_{en} - 1) d\epsilon / (\epsilon_{max} - \epsilon_{min}). \quad (48)$$

Integration of Eq. 48 from  $\varepsilon_{\min}$  to  $\varepsilon_{\max}$  (portion of loading where strain is increasing) provides the environmental fatigue correction factor under changing temperature and strain rate. The application of the modified rate approach to an increasing strain transient is illustrated in Fig. 80; at each strain increment,  $d\varepsilon$ , the associated  $F_{\text{en}}(\dot{\varepsilon}, T)$  value for carbon and low-alloy steels is determined from Eq. 41. Thus,  $F_{\text{en}}$  for the total increasing strain transient is given by

$$F_{\text{en}} = \sum_{k=1}^n F_{\text{en},k}(\dot{\varepsilon}_k, T_k) \frac{\Delta \varepsilon_k}{\varepsilon_{\max} - \varepsilon_{\min}}, \quad (49)$$

where  $n$  is the total number of strain increments, and  $k$  is the subscript for the  $k^{\text{th}}$  incremental segment.

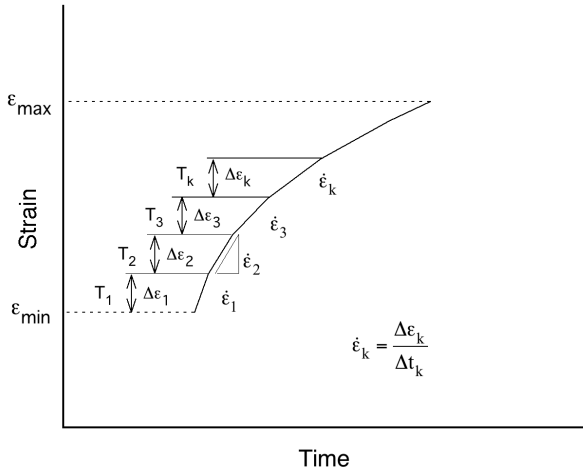


**Figure 80.**  
Application of the modified rate approach to determine the environmental fatigue correction factor  $F_{\text{en}}$  during the increasing strain portion of a transient.

As discussed in Section 4.1.3, a minimum threshold strain,  $\varepsilon_{\text{th}}$  (one-half of the strain threshold of 0.14% strain for carbon and low-alloy steels considering a factor of 2 for data scatter), was required for an environmentally assisted decrease in fatigue life. Consideration of a strain threshold assumes that during a strain cycle, environmental effects are significant only after the applied strain level exceeds the threshold value. In application of the modified rate approach when a threshold strain,  $\varepsilon_{\text{th}}$ , is considered,  $F_{\text{en}}$  for the total strain transient is given by

$$F_{\text{en}} = \sum_{k=1}^n F_{\text{en},k}(\dot{\varepsilon}_k, T_k) \frac{\Delta \varepsilon_k}{\varepsilon_{\max} - (\varepsilon_{\min} + \varepsilon_{\text{th}})}. \quad (50)$$

The modified rate approach was used to evaluate fatigue lives under cyclic loading conditions where both temperature and strain rate were varied during the test.<sup>24,37,38</sup> The studies demonstrated the applicability of the modified rate approach to variable loading conditions such as those that are typically present during actual plant transients. The following significant conclusions were made from those studies.

(a) The use of a strain threshold,  $\varepsilon_{\text{th}}$ , for calculating  $F_{\text{en}}$  by the modified rate approach (i.e., Eq. 50) was not necessary because it did not improve the accuracy of estimation.<sup>38</sup> As discussed in Section 4.1.3, application of the modified rate approach, without the consideration of a strain threshold, gave the best estimates of fatigue lives.

(b) Under load cycles that involved variable strain rates, estimates of  $F_{\text{en}}$  based on an average strain rate [i.e., in Fig. 80, total strain  $(\varepsilon_{\max} - \varepsilon_{\min})$  divided by the total time between  $\varepsilon_{\min}$  and

( $\epsilon_{\max}$ ) were the most conservative when the maximum transient temperature was used.<sup>24</sup> Thus, calculations of  $F_{en}$  based on an average strain rate for the transient are expected to yield conservative estimates of fatigue lives provided that appropriate temperatures are selected for use in the calculations.

- (c) An average temperature for the transient, considering the threshold temperature of 150°C, may be used to estimate  $F_{en}$  during a load cycle, i.e., average of the maximum temperature for the transient and the higher of the threshold temperature for the material under consideration and the minimum temperature for the transient. However, some limited NRC calculations indicated that using either an average transient temperature or an average of the transient maximum temperature and the  $F_{en}$  threshold temperature did not always yield a conservative  $F_{en}$  estimate when compared to the results obtained from an integrated  $F_{en}$  using the modified rate approach, as shown in Fig. 81. If the integration time step is sufficiently small, there is an insignificant difference in  $F_{en}$  results for the modified rate approach when either average or maximum temperatures are used.

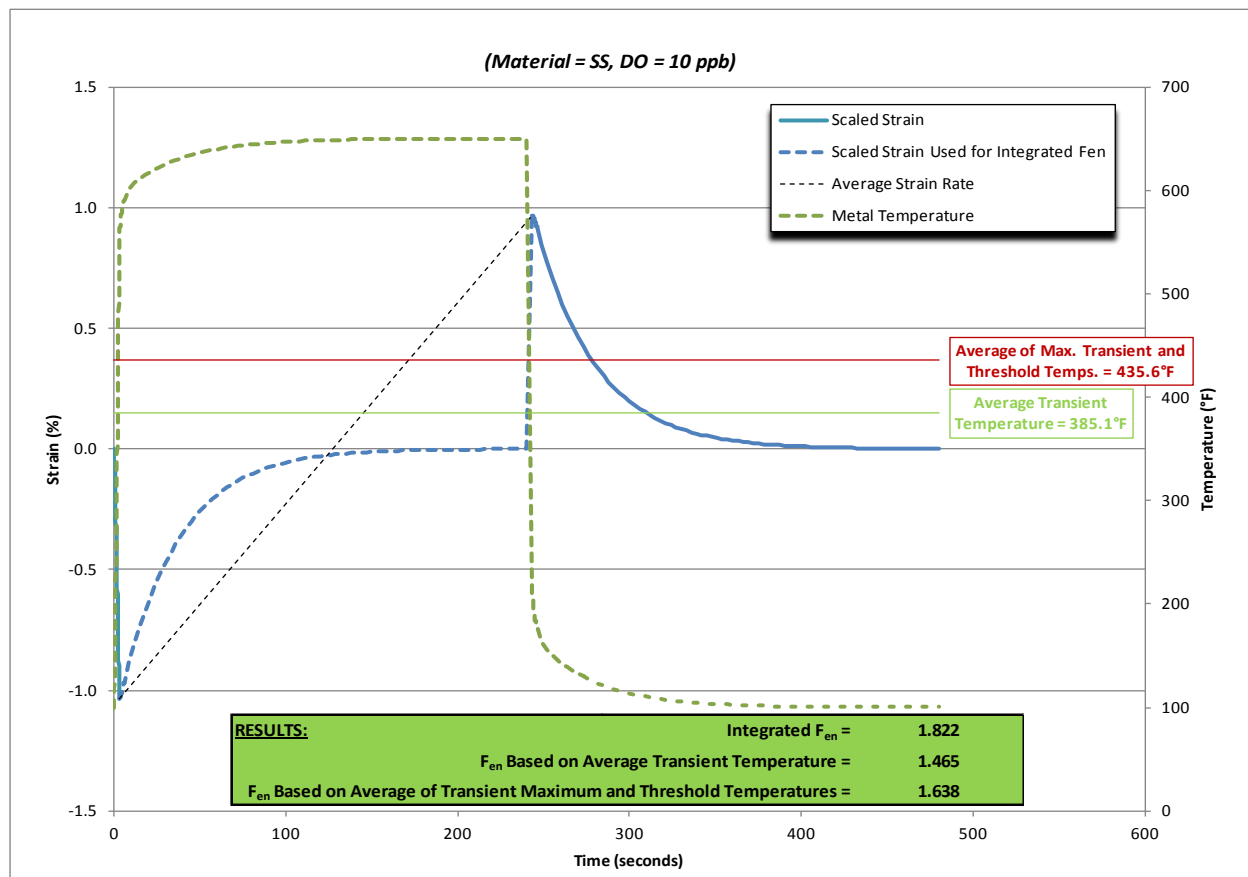


**Figure 81. Example showing  $F_{en}$  values computed using average temperatures compared to the  $F_{en}$  computed using an integrated (modified rate) approach.**

- Where information is available regarding the transients associated with a specific stress cycle or load set pair, the modified rate approach may be used to determine  $F_{en}$  using Eq. 49.

## 4.2 Wrought and Cast Austenitic Stainless Steels

Fatigue-life models for estimating the fatigue lives of wrought and cast austenitic SSs in LWR environments presented in the initial revision of NUREG/CR-6909 were based on the updated PVRC database available at that time. The effects of key parameters, such as temperature, strain rate, and the DO content in water were included in the correlations. The functional forms for the effects of these parameters were based on the observed data trends. For both wrought and cast austenitic SSs, the model assumed threshold and saturation values of 0.4 and 0.0004%/s, respectively, for strain rate and a threshold value of 150°C for temperature. In addition, because of a lack of relevant fatigue data, the dependence of environmental effects on the DO level was not defined in the initial revision of NUREG/CR-6909. Lacking sufficient data to establish the effects of DO level on fatigue lives, those effects were assumed to be the same in low- and high-DO water for both wrought and cast austenitic SSs. The fatigue  $\epsilon$ -N data for austenitic SSs in LWR environments were fitted to a modified version of Eq. 6 and expressed as

$$\ln(N) = A - B \ln(\epsilon_a - C) - T' O' \dot{\epsilon}', \quad (51)$$

where  $T'$ ,  $O'$ , and  $\dot{\epsilon}'$  are the transformed temperature, water DO level, and strain rate, respectively, which are defined in Eqs. 53-55. The least-squares fit of the experimental data in LWR environments yielded a steeper slope for the  $\epsilon$ -N curve than the slope of the curve obtained in air.<sup>45,121</sup> These results indicated that, for austenitic SSs, environmental effects were less pronounced with increasing strain amplitudes above the threshold value of strain amplitude. Differing slopes for the  $\epsilon$ -N curves in air and water environments added complexity to the determination of the environmental fatigue correction factor,  $F_{en}$ . Therefore, the slope,  $B$ , of the  $\epsilon$ -N curve was assumed to be the same in LWR and air environments (i.e., the value of constant  $B$  was assumed to be 1.920 for both environments), and the constant  $C$  was also considered the same for both environments (i.e., constant  $C$  was assumed to be 0.112). A value of 6.157 for the constant  $A$  was determined from the best fit of the fatigue  $\epsilon$ -N data in LWR environments. Note that the constant  $A$  in the ANL model for austenitic SSs presented in the initial revision of NUREG/CR-6909 differed from the values reported earlier in NUREG/CR-5704, NUREG/CR-6815, and NUREG/CR-6878 because relative to the earlier expressions, the environmental fatigue correction factor,  $F_{en}$ , determined in the initial revision of NUREG/CR-6909 was 45–60% lower. Thus, the environmental fatigue correction factor for wrought and cast austenitic SSs was given by

$$F_{en} = \exp(0.734 - T' \dot{\epsilon}' O'), \quad (52)$$

where  $T'$ ,  $\dot{\epsilon}'$ , and  $O'$  were defined as the transformed temperature, strain rate, and water DO level, respectively, as follows:

$$\begin{aligned} T' &= 0 & (T < 150^\circ\text{C}) \\ T' &= (T - 150)/175 & (150 \leq T < 325^\circ\text{C}) \\ T' &= 1 & (T \geq 325^\circ\text{C}) \end{aligned} \quad (53)$$

$$\begin{aligned} \dot{\epsilon}' &= 0 & (\dot{\epsilon} > 0.4\%/s) \\ \dot{\epsilon}' &= \ln(\dot{\epsilon}/0.4) & (0.0004 \leq \dot{\epsilon} \leq 0.4\%/s) \\ \dot{\epsilon}' &= \ln(0.0004/0.4) & (\dot{\epsilon} < 0.0004\%/s) \end{aligned} \quad (54)$$

$$O' = 0.281 \quad (\text{all DO levels}). \quad (55)$$

The model was recommended for predicted fatigue lives equal to or less than  $10^6$  cycles. Note that Eq. 52 was based on the ANL model for austenitic SSs in air (Eq. 29) and the analysis

presented in Section 5.2.11 of the initial revision of NUREG/CR-6909. A single expression was specified for Types 304, 304L, 316, 316L, and 316NG SSs. Equations 52–55 were also applicable to cast austenitic SSs such as CF-3, CF-8, and CF-8M. The initial revision of NUREG/CR-6909 noted that, because the influence of DO level on the fatigue lives of austenitic SSs were influenced by the material composition and heat treatment, the ANL fatigue life model was somewhat conservative for some SSs in high-DO water.

Since the initial publication of NUREG/CR-6909, comments received from stakeholders focused on two areas. First, the constant value of 0.734 in the  $F_{en}$  expression, which resulted in an  $F_{en}$  of approximately 2.5 even at very low temperatures (i.e., below the threshold temperature of 150°C) or at very high strain rates (e.g., during seismic or similar loadings). The other area concerned the absence of DO dependence on environmental effects. As a result, the  $F_{en}$  expression given by Eq. 52 yielded conservative estimates of  $F_{en}$  for some materials (e.g., for low-carbon or nonsensitized high-carbon wrought SSs).

In this report, the  $F_{en}$  expressions (i.e., Eqs. 52-55) for incorporating environmental effects on the fatigue life of wrought and cast austenitic SSs were updated to address the stakeholder comments as well as to incorporate data from the much larger database described in Section 4.2.1. In addition, the dependence of environmental effects on the DO level in the reactor coolant environment was included in the revised expression.

#### 4.2.1 Experimental Data

The relevant fatigue  $\epsilon$ - $N$  data for wrought and cast austenitic SSs in LWR environments include the large JNES database;<sup>136</sup> tests performed by GE in a test loop at the Dresden 1 reactor;<sup>14,15</sup> work sponsored by EPRI at GE;<sup>58-60</sup> and the data developed at ANL.<sup>45</sup> The data that was used in the evaluation consisted of 683 tests; 193 tests on 11 heats of Type 304 SS, 255 tests on 8 heats of Type 316 SS, 115 tests on 7 heats of CF-8M cast austenitic SSs, and 120 tests on 6 compositions of SS weld metals. Both low-carbon and high-carbon grades of Types 304 and 316 SSs were included in the database. For all of the SS data, 15% of the tests were conducted at temperatures of 100-200°C, 39% at 250–290°C, 44% at 300–325°C, and 1% (10 tests) at 360°C. A summary of the data sources for the updated database used in this report, as categorized by material type and test environment, is shown in Table 11. Other material information such as chemical composition, heat treatment, and room temperature tensile properties of the various types and heats of materials is given in Appendix B.

The data indicated that the fatigue lives of austenitic SSs were decreased in LWR environments; an example of environmental effects on the fatigue lives of Types 304 and 316NG SSs in high-purity water at 288°C is shown in Fig. 82. The  $\epsilon$ - $N$  curves based on the ANL model (Eqs. 29 and 52) are also included in this figure. The fatigue lives were decreased significantly when three threshold conditions were satisfied simultaneously, viz., when both the applied strain range and the service temperature were above minimum threshold levels, and the loading strain rate was below a threshold value. The DO level in the water and, to some extent, the composition and heat treatment of the steel were important parameters for environmental effects on fatigue lives. For some steels, fatigue lives were longer in high-DO water than in low-DO PWR environments. Although the fatigue lives in air of Type 316NG SSs were slightly longer than those of Types 304 and 316 SSs, the effects of LWR environments were comparable for wrought Types 304, 316, and 316NG SSs. In addition, as discussed later in Section 4.2.13, available data indicated that the fatigue lives of cast austenitic SSs in both low-DO and high-DO environments were comparable to those of wrought SSs in low-DO environments.

**Table 11. Sources of the fatigue  $\epsilon$ -N data for cast and austenitic stainless steels in LWR environments.**

ANL Mat. ID <sup>a</sup>	Material Heat Designation <sup>a</sup>	Carbon Content (wt.%)	Dissolved Oxygen (ppm)	Test Temperature (°C)	No. of Data Points	Source	Applicable Reference
<u>Type 304 Stainless Steels</u>							
1	304-1	0.050	0.02, 8.0	288	12, 5	JNES (Hasegawa, Fukakura)	136
3	304-3	0.060	0.2	288	7	JNES (Enomoto),	136
9	304-9T	0.070	8.0	300	22 (15 aged)	JNES (Endo)	136
20	304-G	0.070	0.2	260	7	GE	14,15
21	304-A2	0.060	0.003, 0.8	288	14, 5 <sup>b</sup>	ANL	45
22	304-21T	0.060	0.005	100-360	58 (4 aged), 6	JNES (Kanasaki, Tsutsumi)	136
24	304-35	0.070	0.01-0.2	289	15 (4 aged)	JNES (Hirano)	136
25	304-36T	0.050	0.005	325	4	JNES (Nomura)	136
28	304L-E	0.039	0.09	150, 300	8, 20	Solomon	58-60
29	304L-1	0.017	0.01-0.2	289	6	JNES (Hirano)	136
30	304L-G	0.017	0.2	260	4	GE	14,15
<u>Type 316 Stainless Steels</u>							
42	316-12T	0.060	0.005, 8.0	100-325	45, 6	JNES (Kanasaki, Tsutsumi)	136
43	316-13T	0.070	0.005	325	4	JNES (Tsutsumi)	136
44	316-14T	0.060	0.005	325	8 (4 aged)	JNES (Tsutsumi)	136
45	316-15T	0.040	0.005	100-325	61 <sup>c</sup>	JNES (EFT)	136
48	316N-1	0.010	0.01-0.2, 8.0	150-289, 288	65, 30	JNES (Nakao, Higuchi, Hirano, Fukakura)	136
49	316N-2	0.009	0.2	288	9	JNES (Asano)	136
51	316N-4	0.008	0.01, 8.0	290	11	JNES (Higuchi)	136
54	316N-A	0.013	0.004-0.75	288	16	ANL	45
<u>Stainless Steel Weld Metals</u>							
56a	308-WM-1	0.050	0.005	100, 200, 325	6, 6, 14	JNES (Tsutsumi)	136
56b	308-WM-2	0.034	0.005	325	9	JNES (Nomura)	136
57a	316 WM	0.039	0.005	100, 200, 325	4, 4, 24 <sup>d</sup>	JNES (Tsutsumi)	136
57c	316TP-WM	0.070	0.005	100, 200, 325	3, 3, 11	JNES (Nomura)	136
58	316N-WM-1	0.018	0.01, 8.0	290	4, 8	JNES (Higuchi)	136
59	316N-WM-2	0.017	0.01-8.0	150-289	24	JNES (Hirano)	136
<u>Cast Austenitic Stainless Steels</u>							
61	CF-8M-1	0.050	0.01-1.0	289	26 (4 aged)	JNES (Hirano)	136
62	CF-8M-2T	0.050	0.005	325	36 (21 aged)	JNES (Tsutsumi)	136
63	CF-8M-3T	0.050	0.005	325	4	JNES (Tsutsumi)	136
64	CF-8M-4T	0.050	0.005	325	4	JNES (Tsutsumi)	136
65	CF-8M-5T	0.050	0.005	325	38 (4 aged)	JNES (Nomura)	136
68	CF-8M-8	0.064	0.006-1.0	288	5	ANL	45
69	CF-8M-9	0.065	0.008-1.0	288	2	ANL	45

<sup>a</sup> T at the end of the number designates a tube specimen.

<sup>b</sup> Six specimens were sensitized.

<sup>c</sup> Twelve specimens had 2% mean strain.

<sup>d</sup> Six specimens were aged for 25,200 h at 465°C.

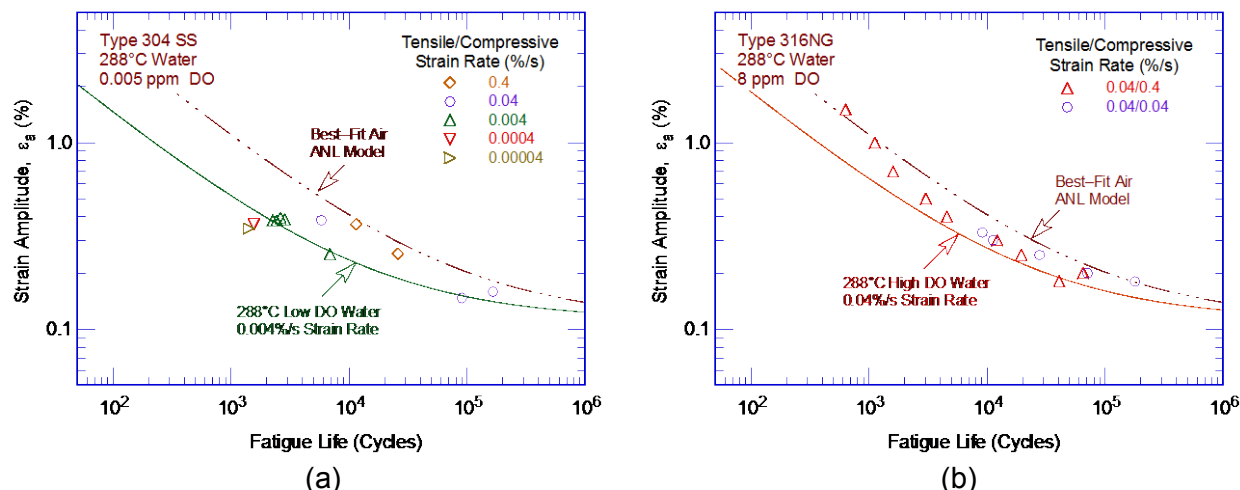


**Figure 82. Strain amplitude vs. fatigue life data for (a) Type 304 and (b) Type 316NG SSs in water at 288°C (JNUFAD and Refs. 13,45).**

Furthermore, the existing fatigue data indicated that a slow strain rate applied during the tensile-loading cycle (i.e., up-ramp with increasing strain) was primarily responsible for the environmentally assisted reduction in fatigue lives. Slow loading rates applied during both tensile- and compressive-loading cycles (i.e., up- and down-ramps) did not further decrease fatigue lives compared with those observed for tests with only slow tensile-loading cycles (Fig. 82b). Consequently, loading and environmental conditions during the tensile-loading cycle (strain rate, temperature, and DO level) are important for environmentally assisted reduction of the fatigue lives of these steels.

It is important to note for evaluation of experimental fatigue  $\epsilon$ -N data that although most of the data were obtained from strain-controlled fatigue tests, some data, particularly at low strain amplitudes, were obtained from load-controlled fatigue tests. Caution should be exercised when comparing such data to the ASME Code fatigue design curve for austenitic SSs. For example, the applied stress amplitude vs. fatigue life data from load-controlled tests on Type 304L SSs, with or without a 100 MPa mean stress, in air and PWR primary water environments at 150 and 300°C are shown in Fig. 83. The results indicated that, for tests conducted at applied stress amplitudes of 80-170 MPa with 100 MPa mean stress, the fatigue lives in PWR water relative to fatigue lives in air were significantly decreased at 150°C, while the fatigue lives were increased at 300°C. Some investigators have incorrectly interpreted these results and indicated that a combination of mean stress and PWR environment decreased the  $10^7$  cycles fatigue limit of austenitic SSs at 150°C.

As discussed earlier, the ASME Code fatigue design curves were based on fully reversed (i.e., R ratio equal to -1) strain-controlled fatigue tests. The stress amplitude used to develop the stress-life (S-N) fatigue design curves was a pseudo-stress defined as  $S_a = E \epsilon_a$ , where E is the elastic modulus. Therefore, for all fatigue tests conducted at strain amplitudes beyond the elastic limit (i.e., with some plastic strain), the experimental stress amplitudes were lower than the stress amplitudes plotted for use in developing the ASME Code fatigue design curves. Furthermore, as discussed earlier, at low strain amplitudes, based on the chemical composition of the material, the effects of DSA may affect the cyclic hardening behavior of austenitic SSs. Therefore, depending on the temperature and strain rate, the cyclic stress amplitudes during strain-controlled tests or total strain amplitudes during load-controlled tests, may vary significantly during tests. These differences have significant effects of the fatigue lives of SS materials.



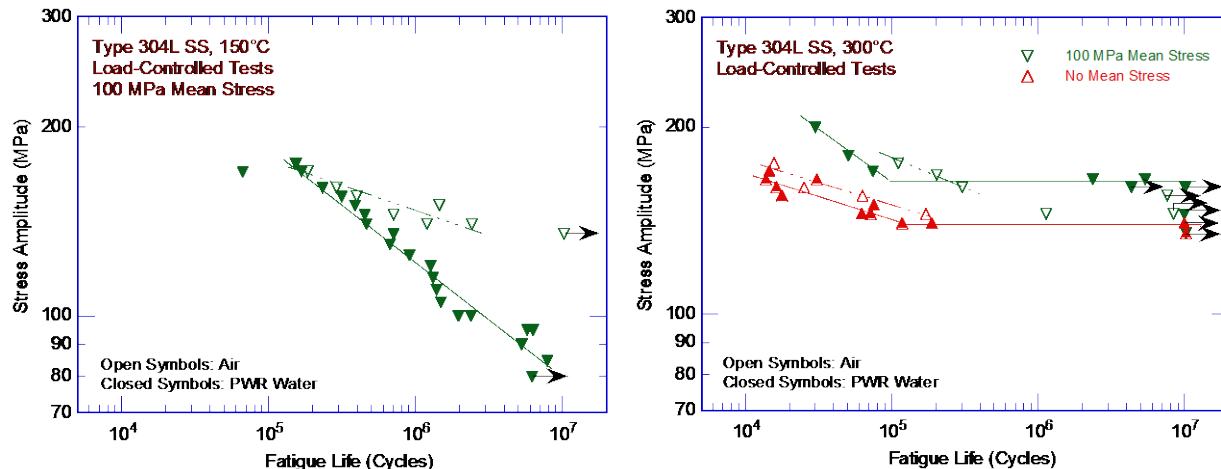


**Figure 83. Fatigue stress - life data from load-controlled tests on Type 304L SSs, with and without mean stress, in air and PWR water (Ref. 60).**

The fatigue lives of some load-controlled tests were plotted as a function of total strain amplitude in Fig. 84. Note that these results may also be plotted as stress amplitude,  $S_a$  vs. fatigue life, where  $S_a$  is obtained by multiplying the total strain amplitudes by the elastic modulus,  $E$ . The best-fit air curve and the mean-stress adjusted curve of the fatigue  $\epsilon$ -N data and the ASME Code Section III fatigue design curve are also shown in the figure. Fatigue  $\epsilon$ -N data from other strain-controlled-tests performed by the same authors on Type 304L SSs are also included for comparison.<sup>60</sup> The results indicated that the load-controlled data show excellent agreement with the strain-controlled test results. Unfortunately, data for the load-controlled tests that showed significant reductions in fatigue lives (i.e., tests with 100 MPa mean stress in PWR water at 150°C) were not included in this comparison because the actual strain amplitudes for these tests were not specified. In general, at a strain rate of 0.4%, environmental effects decreased fatigue lives at 300°C, and had insignificant effects at 150°C.

The results also indicated that, for Type 304L SSs, the slope of the fatigue  $\epsilon$ -N curve was steeper than that of the best-fit air curve based on the ANL model for austenitic SSs. This behavior was consistent with the best-fit curves developed in NUREG/CR-5704 for Types 304316, and 316NG SSs. In general, the slope of the curve for low-carbon grades of austenitic SSs (e.g., Type 316NG or 304L) was steeper than the slope of the curve for high-carbon SSs (Types 304 or 316). For fatigue lives greater than  $10^5$  cycles, the fatigue data for Type 304L SSs were all below the best-fit air curve. The fatigue lives of tests in air at 150 or 300°C with 100 MPa mean stress were significantly below those predicted using the mean-stress adjusted curve. However, all data were above the ASME Code Section III fatigue design curve, without adjusting for environmental effects. Consequently, the potential effects of differences in the cyclic hardening behavior of austenitic SSs, particularly at low strain amplitudes, should be considered while establishing the factors in the ASME Code Section III fatigue design curves to account for the effects of data scatter, heat-to-heat variability, component size and geometry, and surface roughness.

- *When interpreting load-controlled fatigue tests, care should be taken, particularly when comparing the experimental stress amplitudes from such tests to stress amplitudes from the ASME Code Section III fatigue design curve. In addition, the potential effects of differences in the cyclic hardening behavior should be considered when establishing the factors in ASME Code Section III fatigue design curves.*



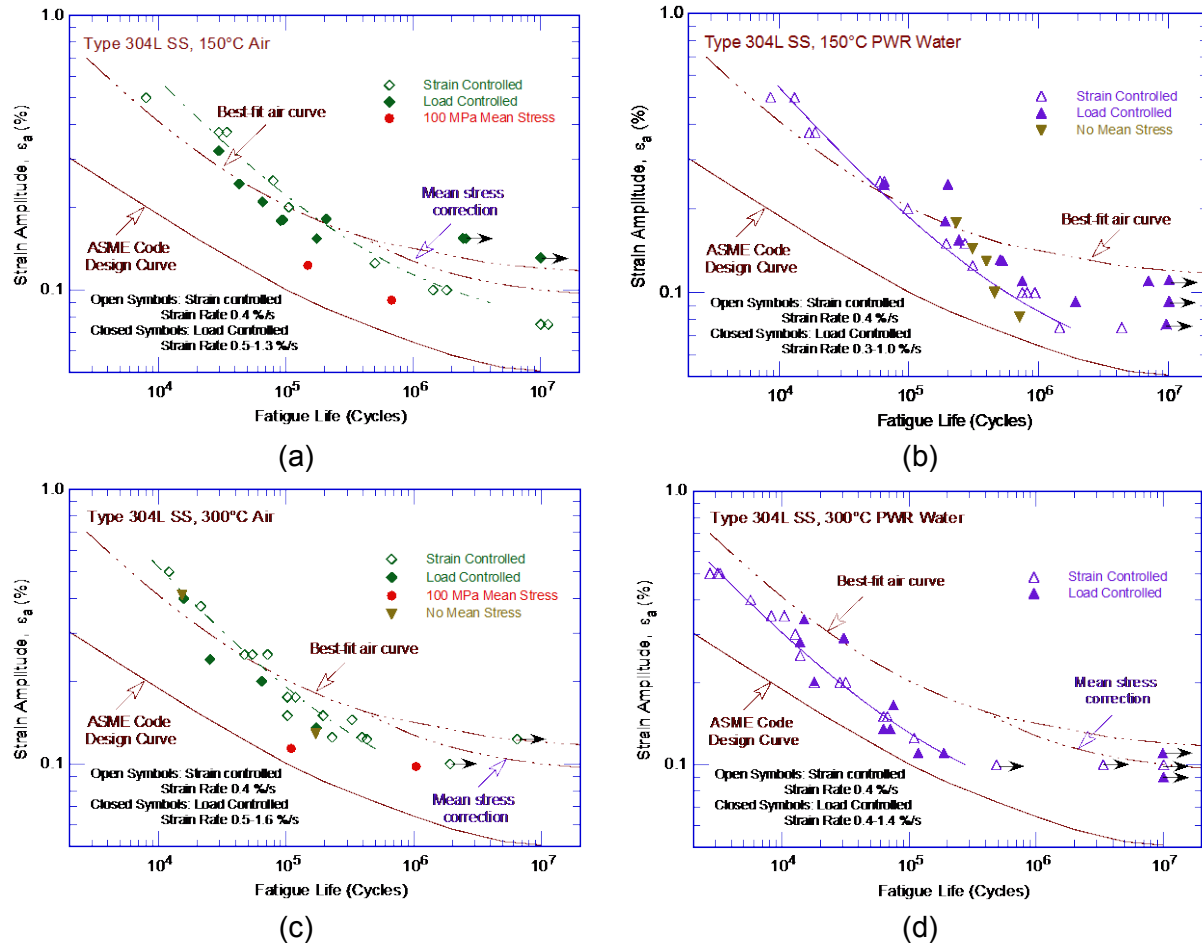


**Figure 84. Fatigue strain - life data from load-controlled tests on Type 304L SSs, with and without mean stress, in air (a, c) and PWR water (b, d) (Refs. 58,60).**

#### 4.2.2 Strain Rate

The fatigue lives of Types 304L and 316 SSs in low-DO water were plotted as a function of tensile strain rate, as shown in Fig. 85. The lines in the two plots of this figure were based on the best-fit air curve for austenitic SSs given by Eq. 29 and the  $F_{en}$  expressions given in Eqs. 61 and 58-60. The results of the reanalysis of the larger database indicated that in low-DO PWR environments, the fatigue lives of austenitic SSs decreased with decreasing strain rates below approximately 10%/s; the effects of environment on fatigue lives saturated at approximately 0.0004%/s (Fig. 85).<sup>13,24,27-31,34,35,45-47</sup> Environmental effects did not occur at strain rates greater than 10%/s (i.e.,  $F_{en} = 1$ ). Decreases in the strain rate from 10 to 0.0004%/s reduced the fatigue lives by more than a factor of 10.

In high-DO water at 288°C, the effects of strain rate were less pronounced than in low-DO water (Fig. 86). For example, for Heat 30956 of Type 304 SS, strain rate had no effect on the fatigue lives in high-DO water, whereas fatigue lives decreased linearly with strain rate in low-DO water (Fig. 86a). For Heat D432804 of Type 316NG, some effect of strain rate was observed in high-DO water, although it was smaller than that in low-DO water (Fig. 86b).

- The effects of strain rate on the fatigue lives of austenitic SSs in LWR environments were explicitly considered in the  $F_{en}$  expression defined in Eq. 61 (Section 4.2.13).

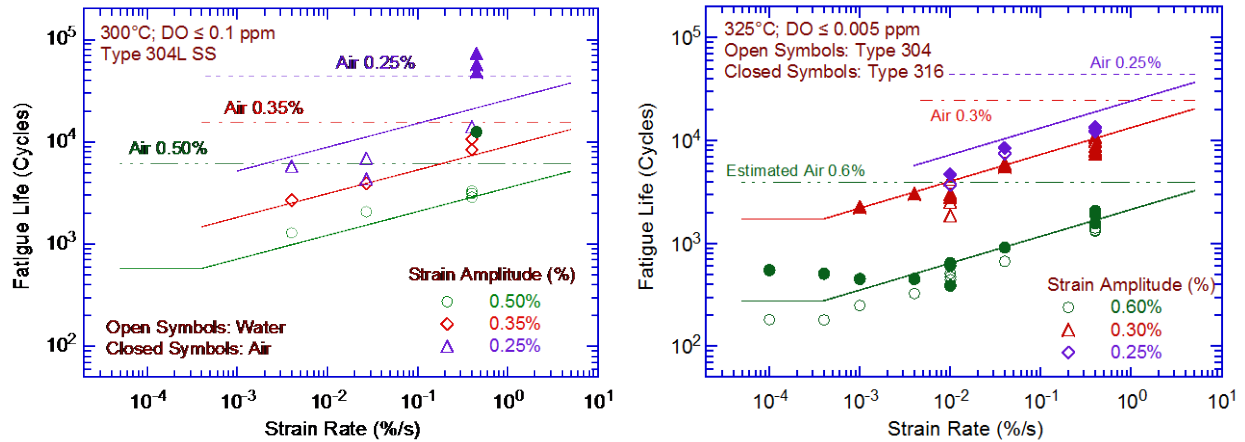


**Figure 85.** Dependence of fatigue lives of austenitic stainless steels on strain rate in low-DO water (Refs. 13,45,47,60).

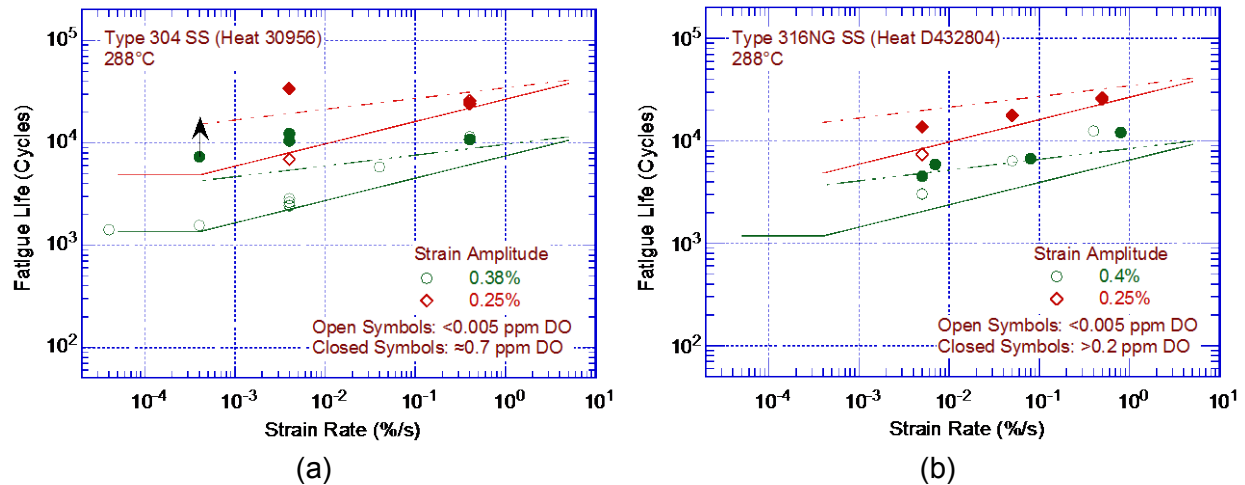


**Figure 86.** Dependence of fatigue lives of Types (a) 304 and (b) 316NG SSs on strain rate in high- and low-DO water at 288°C (Ref. 13,45,47).

#### 4.2.3 Strain Amplitude

As in the case of the carbon and low-alloy steels, a minimum threshold strain range was required for the environmentally induced decrease in fatigue lives of SSs to occur. Exploratory fatigue tests were conducted on austenitic SSs to determine the threshold strain range beyond which environmental effects were significant during a fatigue cycle.<sup>30,35</sup> The tests were performed with loading waveforms in which the slow strain rate was applied during only a fraction of the tensile loading cycle. The results indicated that a minimum threshold strain was necessary to produce an environmentally assisted decrease in the fatigue lives of SSs (Fig. 87). The threshold strain range,  $\Delta\varepsilon_{th}$ , was independent of material type (weld or base metal) and temperature in the range of 250–325°C, but it tended to decrease as the strain range was decreased.<sup>30,35</sup> The threshold strain range was expressed in terms of the applied strain range,  $\Delta\varepsilon$ , by the equation

$$\Delta\varepsilon_{th}/\Delta\varepsilon = -0.22 \Delta\varepsilon + 0.65. \quad (56)$$

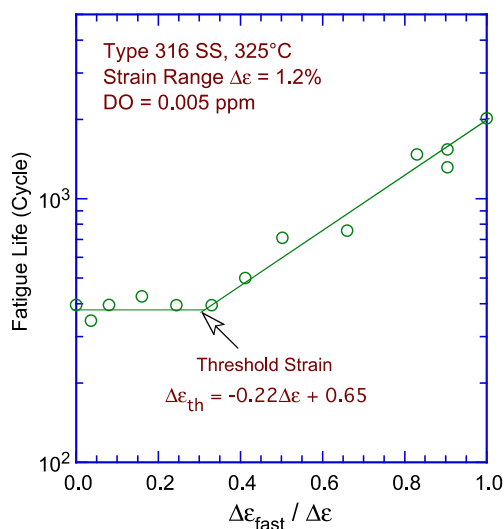


**Figure 87.**  
Results of strain rate change tests on Type 316 SSs in low-DO water at 325°C. Low strain rate was applied during only a fraction of the tensile loading cycle. Fatigue life is plotted as a function of fraction of strain at high strain rate (Refs. 30,35).

The results suggested that the threshold strain range,  $\Delta\epsilon_{th}$ , was related to the elastic strain range of the test, and it did not correspond to the strain at which the crack closed. The threshold value was attributed to the rupture strain of the surface oxide film; limited data suggested that the threshold strain was between 0.32 and 0.36%. The above expression yields a value of 0.31% at a strain range of 0.6%.

Since the contribution of strain threshold was relatively more significant at low strain amplitudes, a strain threshold value of 0.32% (or a strain amplitude of 0.16%) was identified in the original version of NUREG/CR-6909. This value was adjusted for the effects of mean stress and uncertainties due to material and loading variability. The threshold strain amplitude was decreased by approximately 10% to account for mean stress effects and by a factor of 1.5 to account for uncertainties in fatigue lives associated with material and loading variability. Thus, a threshold strain amplitude of 0.10% (stress amplitude of 195 MPa, or 28.3 ksi) was selected, below which environmental effects on fatigue lives were considered insignificant.

Some stakeholders identified that the strain amplitude threshold of 0.10% was based on a factor of 1.7 on strain instead of the factor of 2 proposed in the criteria document for developing the ASME Code Section III fatigue design curves.<sup>8</sup> The threshold value of 0.10% was endorsed by the PVRC Steering Committee for Cyclic Life Environmental Effects (CLEE).<sup>\*</sup> Based on experimental data, the CLEE proposed a strain threshold for environmental effects; a lower strain amplitude below which environmental effects were considered to be insignificant, a slightly higher strain amplitude above which environmental effects decreased fatigue lives, and a linear variation between these two values. The two strain amplitudes were 0.10 and 0.11% for both wrought and cast austenitic SSs. For simplicity, in the initial revision of NUREG/CR-6909, a single value of 0.10% was proposed for the strain amplitude threshold.

The same procedure is appropriate for defining a value of strain threshold that maintains the factor of 2 on strain proposed by ASME Code Section III. However, since the effects of mean stress on fatigue lives are accounted for in the mean-stress adjustment to the best-fit mean data curve using the Modified Goodman relation, only the effects of material and loading variability were addressed in defining the strain threshold for environmental effects to avoid double counting mean stress effects.

<sup>\*</sup> Welding Research Council Progress Report, Vol. LIX No. 5/6, May/June 1999.

- The procedure for calculating  $F_{en}$ , defined in Eq. 61 (Section 4.2.13), includes a threshold strain amplitude of 0.10% below which LWR coolant environments do not affect fatigue lives, i.e.,  $F_{en} = 1$ . However, this threshold strain amplitude should not be considered when the modified rate approach is used to determine  $F_{en}$  for a stress cycle or a load set pair.

#### 4.2.4 Temperature

The changes in fatigue lives of austenitic SSs with test temperatures at two strain amplitudes and two strain rates were plotted and are shown in Fig. 88. The results indicated a threshold temperature of 100°C, above which the environment decreased fatigue lives in low-DO water if the strain rate was below the threshold value. In the range of 100–325°C, the logarithm of fatigue life decreased linearly with temperature. Environmental effects either did not occur or were insignificant at temperatures below the threshold value of 100°C.

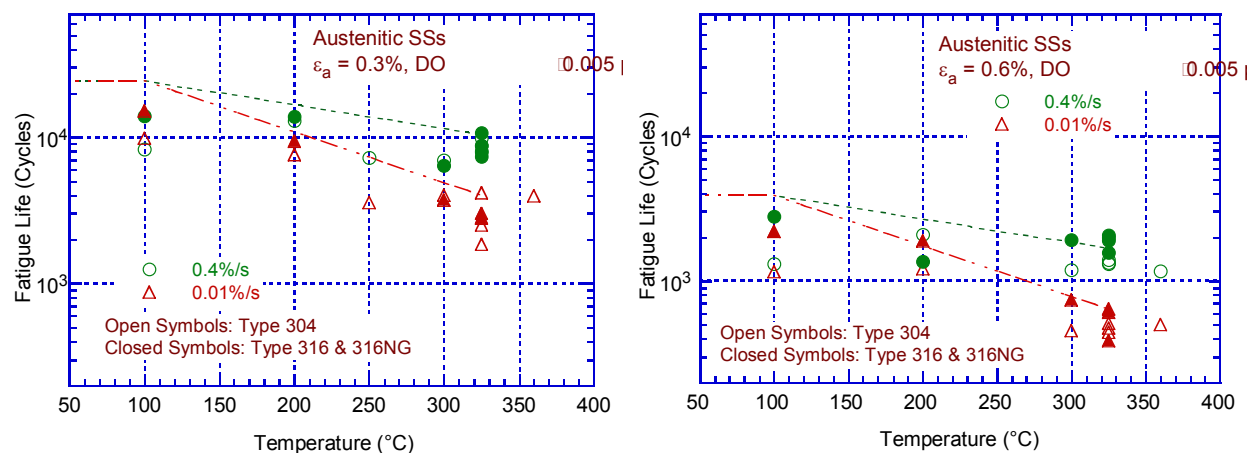


**Figure 88. Change in fatigue lives of austenitic stainless steels in low-DO water with temperature (Refs. 13,29–31,34,45–47).**

Fatigue tests were conducted at MHI in Japan on Type 316 SSs under combined mechanical and thermal cycling.<sup>29,30</sup> Triangular waveforms were used for both strain and temperature cycling. The strain rate for the tests was 0.002%/s. Two sequences were selected for temperature cycling: (i) an in-phase sequence, in which temperature cycling was synchronized with mechanical strain cycling, and (ii) a sequence in which temperature and strain were out of phase, i.e., maximum temperature occurred at minimum strain level and vice versa. Two temperature ranges, 100–325°C and 200–325°C, were selected for the tests. The results are shown in Fig. 89, along with data obtained from tests at constant temperature at a strain rate of 0.01%/s. An average temperature was used in Fig. 89 for the thermal cycling tests. The average temperature was determined by considering that environmental effects were insignificant below threshold values of 100°C for temperature and 0.32% for strain. Thus, the average temperature for the thermal cycling tests was determined from the higher value between 100°C and the temperature at the threshold strain for the in-phase tests, and the lower value between the maximum temperature and the temperature at the threshold strain for the out-of-phase tests. The solid and chain-dash lines in the figure were based on the best-fit air curve (Eq. 29) and the updated  $F_{en}$  expression for austenitic SSs (Eq. 61).

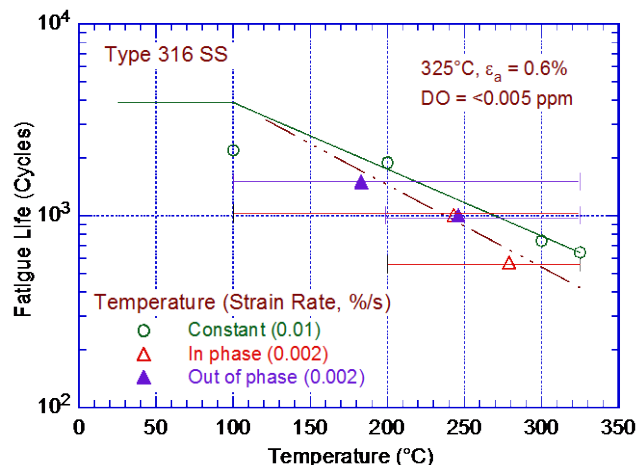


**Figure 89.**  
Fatigue lives of Type 316 SSs  
under constant and varying  
test temperatures (Ref. 29,30).

The results in Fig. 89 indicated that for the variable temperature tests, fatigue lives estimated using an average temperature, determined by taking into consideration the threshold values of temperature and strain, showed good agreement with the experimental fatigue lives. As expected, the predicted fatigue lives of the in-phase tests were shorter than those for the out-of-phase tests. The reason fatigue lives were longer for out-of-phase tests compared to in-phase tests was that applied strains above the threshold strain occurred at higher temperatures for the in-phase tests, whereas they occurred at lower temperatures for the out-of-phase tests. The results from the thermal cycling tests (triangles) agreed well with the estimated values shown by the chain-dash line, and those from the constant-temperature tests (open circles) agreed well with the estimated values shown by the solid line.

Another study conducted by JNES on Type 316 SSs under combined mechanical and thermal cycling in PWR water showed similar results; the in-phase tests had lower fatigue lives than the out-of-phase tests.<sup>36,38</sup> These results indicated that load cycles involving simple linear temperature transients were represented by an average temperature determined by taking into consideration the threshold values of temperature and strain. However, the use of an average temperature for more complex temperature transients requires verification.

- *The effects of temperature on the fatigue lives of austenitic SSs in LWR environments were explicitly considered in  $F_{en}$ , defined in Eq. 61 (Section 4.2.13). In addition, guidance was developed to define the temperature used to calculate  $F_{en}$  for actual reactor transients.*

#### 4.2.5 Dissolved Oxygen

In contrast to the behavior of carbon and low-alloy steels, the fatigue lives of austenitic SSs decreased significantly in low-DO (i.e., less than 0.05 ppm DO) water. In low-DO water, the fatigue lives were not influenced by the material composition or heat treatment. The fatigue lives, however, continued to decrease with decreasing strain rate in the range of 10 – 0.0004%/s and increasing temperature in the range of 100 – 325°C.<sup>13,24,29–31,34,35,45–47</sup> As discussed in Sections 4.2.2 and 4.2.4, environmental effects saturated at a strain rate of 0.0004%/s and a temperature of 325°C.

In high-DO water, the fatigue lives of austenitic SSs were either comparable to<sup>29,34</sup> or, in some cases, higher<sup>13,45,47</sup> than those in low-DO water, i.e., for some SSs, environmental effects were lower in high-DO water compared to low-DO water. The results (Figs. 86a and 86b) indicated that, in high-DO water, environmental effects on the fatigue lives of austenitic SSs were influenced by the material composition and heat treatment. For example, for high-carbon Type

304 SS, environmental effects in high-DO water were insignificant for mill-annealed (MA) material (Fig. 86a), whereas the effects of environment were the same for sensitized material in high- and low-DO water. For low-carbon Type 316NG SSs, some effects of strain rate were apparent in high-DO water, although they were smaller than those in low-DO water (Fig. 86b). The effects of material heat treatment on the fatigue lives of Type 304 SSs is discussed further in Section 4.2.7.

- *The effects of DO on the fatigue lives of austenitic SSs in LWR environments were explicitly considered in  $F_{en}$ , defined in Eq. 61 (Section 4.2.13). In high-DO water, the material composition and heat treatment affected the fatigue lives of austenitic SSs.*

#### 4.2.6 Water Conductivity

The studies performed at ANL indicated that, for fatigue tests in high-DO water, the conductivity of water and the ECP of steel were important parameters that must be held constant.<sup>13,45,47</sup> During laboratory tests, the time to reach stable environmental conditions depended on the autoclave volume, DO level, flow rate, etc. In the ANL test facility, fatigue tests on austenitic SSs in high-DO water required a soaking period of 5–6 days for the ECP of the steel to stabilize. The steel ECP increased from zero or a negative value to above 150 mV during this period. The results shown in Fig. 86a for Type 304 MA Heat 30956 SS in high-DO water (closed circular symbols) were obtained for specimens that were soaked for 5–6 days prior to testing. The same material tested in high-DO water after soaking for 24 h showed a significant reduction in fatigue life, as indicated by Fig. 90. At conductivity values of 0.05–0.1  $\mu\text{S}/\text{cm}$ , the fatigue lives of specimens that were soaked for 24 h (shown as solid symbols) were a factor of approximately 3 lower than those of specimens soaked for 120 h (shown as open symbols).

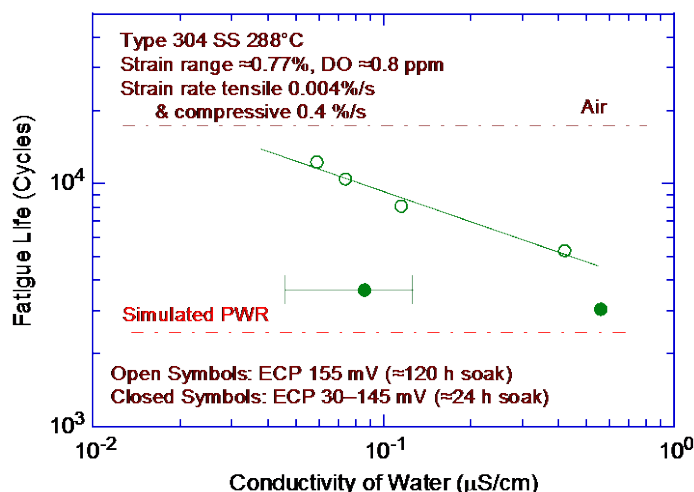


**Figure 90.**  
Effects of water conductivity and soaking period on fatigue lives of Type 304 SSs in high-DO water (Ref. 13,45).

The effects of water conductivity and the ECP of the steel on the fatigue lives of austenitic SSs were determined, as shown in Fig. 90. In high-DO water, the fatigue lives were decreased by a factor of approximately 2 when the conductivity of the water was increased from approximately 0.05 to 0.4  $\mu\text{S}/\text{cm}$ . Note that environmental effects appeared more significant for the specimens that were soaked for only 24 h. For these tests, the ECP of the steel was initially very low and increased during testing (i.e., the DO level in the test autoclave was lower than the target DO level of 0.7 ppm).

- *The effects of water conductivity on the fatigue lives of austenitic SSs were not explicitly included in the determination of the environmental fatigue correction factor,  $F_{en}$ . Additional*



guidance was therefore not included to address excursions from normal water chemistry conditions.

#### 4.2.7 Material Heat Treatment

Limited small-scale laboratory fatigue test data indicated that, although heat treatment had little or no effects on the fatigue lives of austenitic SSs in low-DO and air environments, fatigue lives in high-DO environments were longer for nonsensitized or slightly sensitized SSs.<sup>47</sup> The effects of heat treatment on the fatigue lives of Type 304 SSs in air, BWR, and PWR environments are shown in Fig. 91. Fatigue lives were plotted as a function of EPR (electrochemical potentiodynamic reactivation) values for various material conditions. The results indicated that heat treatment had little or no effects on the fatigue lives of Type 304 SSs in air and PWR environments. In a BWR environment, fatigue lives were lower for the sensitized SSs; fatigue lives decreased with increasing EPR values.

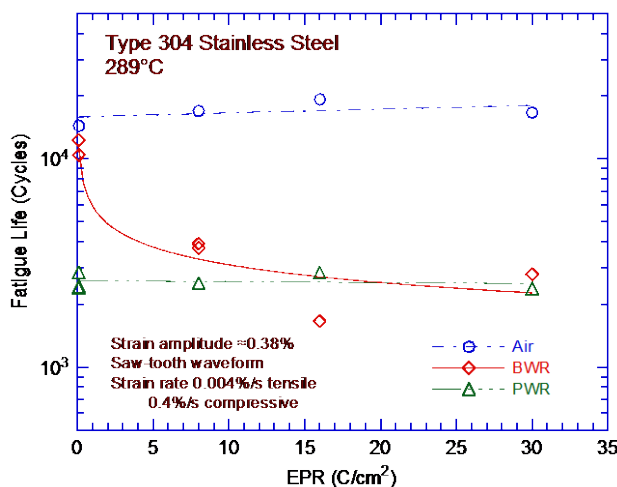


**Figure 91.**  
The effects of material heat treatment on fatigue lives of Type 304 SSs in air, BWR and PWR environments at 289°C, approximately 0.38% strain amplitude, sawtooth waveform loading, and 0.004%/s tensile strain rate (Ref. 47).

These results are consistent with the data obtained at MHI on solution-annealed and sensitized Types 304 and 316 SSs.<sup>27,31</sup> In low-DO (less than 0.005 ppm) water at 325°C, sensitization annealing had no effects on the fatigue lives of these steels. In high-DO (8 ppm) water at 300°C, the fatigue lives of sensitized Type 304 SSs were a factor of approximately 2 lower than those of solution-annealed steels. However, sensitization annealing had little or no effect on the fatigue lives of low-carbon Type 316NG SSs in high-DO water at 288°C, and the fatigue lives of solution-annealed and sensitized Type 316NG SSs were comparable.

- The effects of heat treatment was not explicitly included in the environmental fatigue correction factor; estimates of  $F_{en}$  based on Eq. 61 (Section 4.2.13) are therefore conservative for some SSs in high-DO water.

#### 4.2.8 Cast Austenitic Stainless Steels

The fatigue lives of cast austenitic SSs were lower in LWR coolant environments. The available data also indicated that the fatigue lives of cast SSs in high-DO water were the same as those in low-DO water. The fatigue lives of CF-8M cast austenitic SSs in high-purity water at 289°C and 0.3 and 0.6% strain amplitudes were plotted as a function of DO (Fig. 92). The results showed no fatigue life dependency on water DO levels. In both NWC and HWC BWR environments, the fatigue lives of cast austenitic SSs were well represented by the  $F_{en}$  expressions for wrought austenitic SSs in low-DO PWR environments.

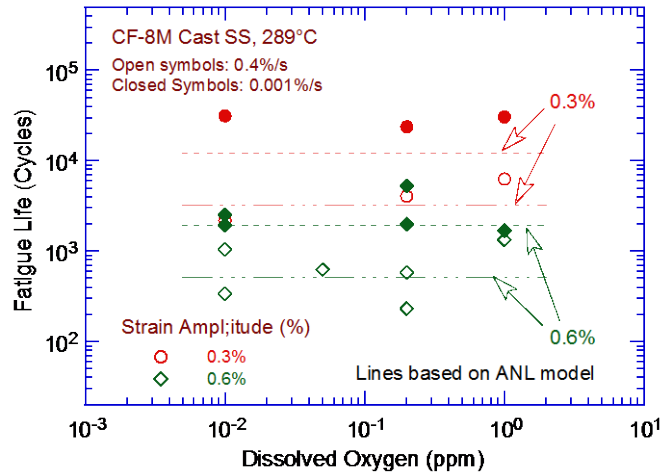


**Figure 92.**  
Fatigue lives of cast austenitic SSs in high-purity water at 289°C and 0.3% and 0.6% strain amplitude plotted as a function of DO content (Ref. 136).

In addition, the existing data indicated that the fatigue lives of cast austenitic SSs were relatively insensitive to changes in ferrite content in the range of 12–28%.<sup>29,34</sup> The fatigue  $\epsilon$ -N data for a heat of CF-8M cast SS (with 19.7% ferrite) at 325°C in PWR water containing 0.005 ppm DO were plotted (Fig. 93) at various strain rates. The best-fit air curve at room temperature and the estimated fatigue lives for the tests at 0.4 and 0.01%/s strain rates were also included. The results showed a gradual decrease in fatigue lives with decreasing strain rates. The results also indicated that thermal aging for 25,200 h at 465°C had little or no effect on fatigue lives. The experimental data showed good agreement with the estimated fatigue  $\epsilon$ -N curves. However,

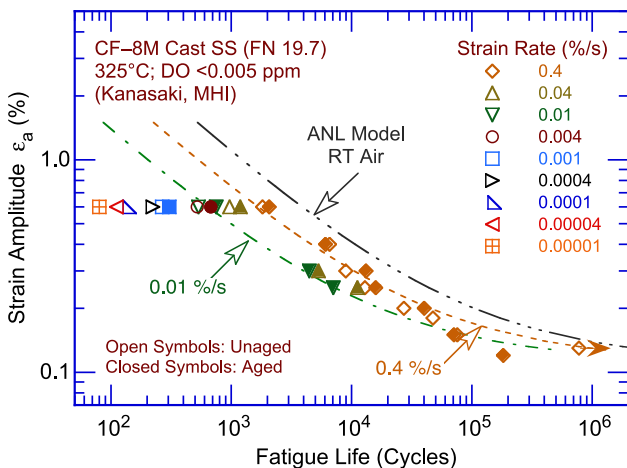


**Figure 93.**  
Strain amplitude vs. fatigue life data for cast austenitic SSs at 325°C and various strain rates in water with 0.005 ppm DO content (Ref. 29,34).

the fatigue  $\epsilon$ -N data for unaged and aged (for 10,000 h at 400°C) material from two heats of CF-8M cast SSs, shown in Fig. 94a, indicated potential effects of thermal aging. Some of the data shown in Fig. 93 were plotted as a function of strain rate (Fig. 94a). The limited data for Heat CF8M-8 (shown as open and closed circular symbols in Fig. 94a) indicated that, unlike the thermal aging effects of cast SSs aged at 450°C or higher, thermal aging for 10,000 h at 400°C decreased the fatigue lives of the material by a factor of 2.<sup>45</sup>



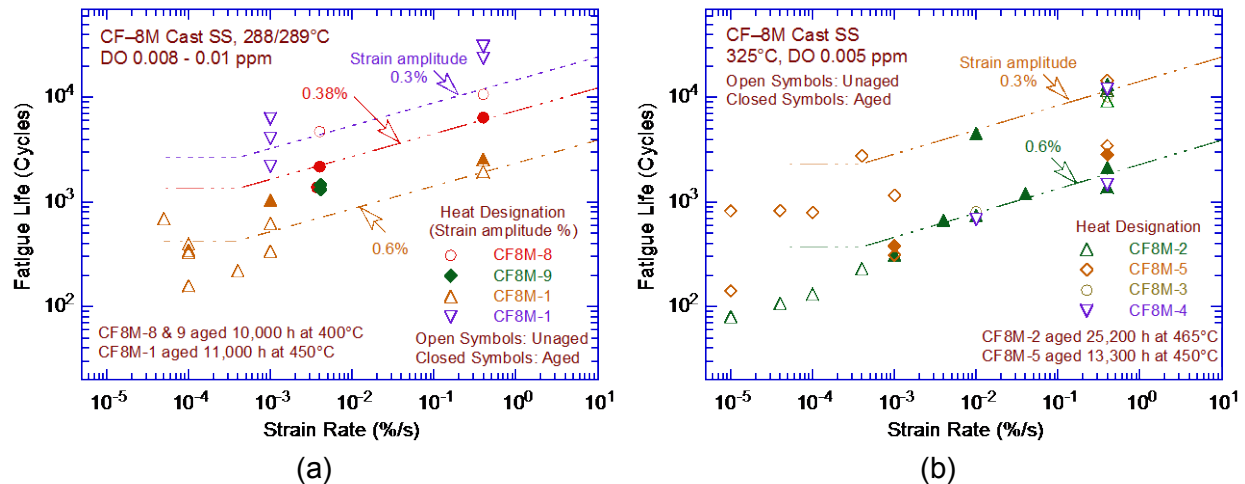


**Figure 94. Dependence of fatigue lives of CF-8M cast SSs on strain rate in low-DO water at various strain amplitudes (Refs. 136,43,45).**

The different thermal aging effects observed for the cast austenitic SSs in Figs. 94a are attributed to differences in the microstructure produced after thermal aging at 400°C as opposed to 465°C. Available data indicated that thermal aging at temperatures between 300 and 400°C resulted in a spinodal decomposition of the ferrite phase which strengthened the ferrite phase and increased cyclic hardening.<sup>229-232</sup> In contrast, thermal aging at 465°C resulted in the nucleation and growth of large  $\alpha'$  particles and other phases such as a sigma phase, which did not change the tensile or cyclic hardening properties of the material.<sup>230</sup>

The results also showed that the effects of strain rate on the fatigue lives of cast SSs were similar to those for wrought SSs. However, for the cast SS unaged Heat CF8M-2, environmental effects on life did not appear to saturate even at strain rates as low as 0.00001%/s.<sup>29,34</sup> Similar results were also reported for unaged CF-8M steels in low-DO water at 325°C.<sup>233</sup> Based on these results, JNES<sup>136</sup> recommended a lower threshold value for the saturation strain rate for cast austenitic SSs. The saturation strain rate of 0.0004%/s, recommended for wrought SSs, was decreased to 0.00004%/s for cast SSs.

As shown in Fig. 94, the fatigue data obtained at 289°C were in good agreement with estimates based on the  $F_{en}$  expressions for wrought austenitic SSs. Even the data at 325°C at strain rates equal to or greater than 0.001%/s were in agreement with the estimated curves. However, the strain rate dependence of the data obtained on unaged material at low strain rates increased at strain rates below 0.0005%/s (i.e., the slope of the log-log plot of fatigue lives vs. strain rates was steeper). The reasons for this behavior of the unaged cast austenitic SSs were not determined. Until more data are available, the effects of strain rate on the fatigue lives of cast austenitic SSs were assumed similar to those for wrought SSs in low-DO PWR environments. Furthermore, strain rates less than 0.0004%/s are either not expected for typical reactor operation, or the total strain accumulated under these transients is expected to be insignificant.

Limited data indicated that the effects of temperature on the fatigue lives of cast austenitic SSs were also similar to those for wrought SSs in low-DO PWR environments, as shown in Fig. 95. The data showed good agreement with the estimated values.

- The effects of LWR environments on the fatigue lives of cast austenitic SSs was represented by the same  $F_{en}$  expression (i.e., Eq. 61 in Section 4.2.13) developed for wrought SSs in low-DO PWR environments.

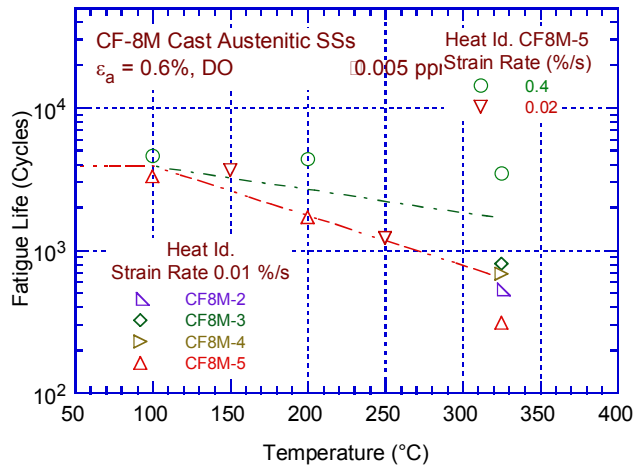


**Figure 95.**  
Change in fatigue lives of cast austenitic SSs in low-DO water with temperature (Ref. 136).

#### 4.2.9 Stainless Steel Weld Metals

As discussed in Section 3.2.9, the available fatigue  $\epsilon$ -N data indicated that the best-fit mean data curve for wrought austenitic SSs in air may be used for the fatigue  $\epsilon$ -N behavior of SS weld metals. In addition, the plots of the estimated cumulative distribution of constant A for the mean data curve for wrought SSs in air (i.e., Fig. 45) showed that the constant A for the few heats of SS weld metals for which fatigue data were available were evenly distributed about the median value of constant A. The available fatigue  $\epsilon$ -N data for austenitic SS weld metals also indicated that environmental effects in LWR environments could be estimated from the  $F_{en}$  expression given by Eq. 61 in Section 4.2.13 for cast and wrought austenitic SSs. The fatigue  $\epsilon$ -N data for Type 308 and 316TP SS weld metals at 325°C in PWR water containing 0.005 ppm DO were plotted, and are shown in Fig. 96 at various strain rates. The fatigue lives estimated from Eqs. 29 (Section 3.2.6) and 61 (Section 4.2.13) for the tests at various strain rates were also included as shown in the figure. The experimental fatigue lives were in good agreement with the estimated  $\epsilon$ -N curves; the fatigue lives decreased gradually with decreasing strain rates.

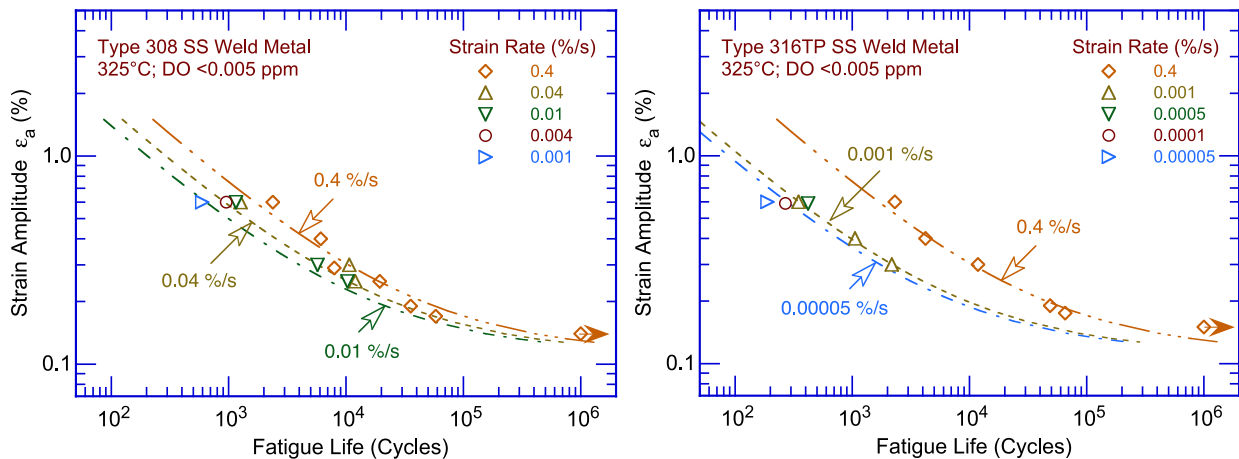


**Figure 96.** Strain amplitude vs. fatigue lives for Types 308 and 316TP SS weld metals at 325°C and various strain rates in water with 0.005 ppm DO content (Ref. 136).

The experimental fatigue lives of SS weld metals at 0.6% strain amplitude were compared with the estimated fatigue lives (using Eqs. 29 and 61) at various strain rates and temperatures, as

shown in Fig. 97. The results indicated that the estimates based on the expressions for wrought austenitic SSs yielded either comparable or slightly lower fatigue lives compared to the experimental values. The fatigue  $\epsilon$ -N data also indicated that changes in the water DO content had little or no effects on fatigue lives; the fatigue lives in 8 or 0.2 ppm water were comparable to those in 0.005 ppm water.

- The effects of LWR environments on the fatigue lives of austenitic SS weld metals were represented by the same  $F_{en}$  expression (i.e., Eq. 61 in Section 4.2.13) developed for wrought SSs in low-DO PWR environments.

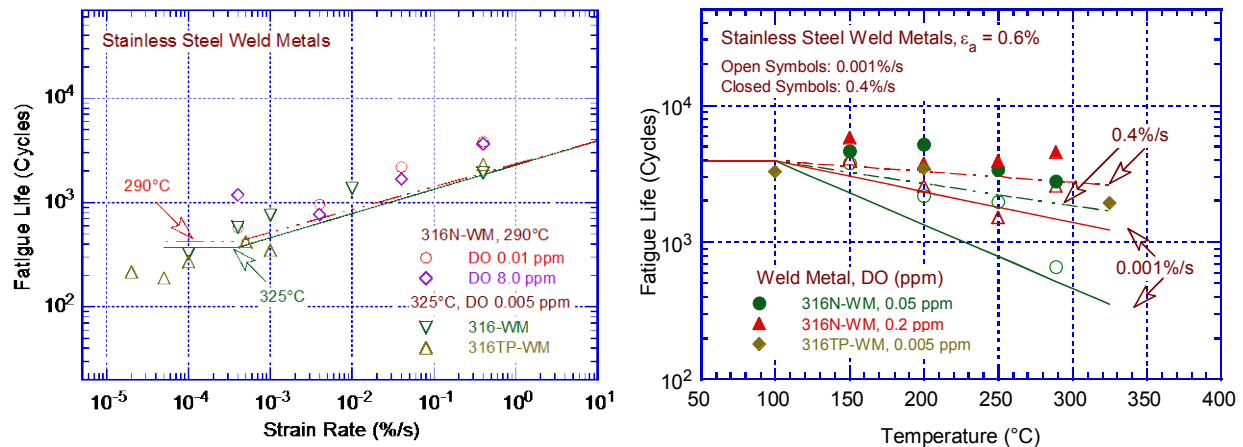


**Figure 97. Change in fatigue lives of SS weld metals in LWR environments with strain rate and temperature (Ref. 136).**

#### 4.2.10 Hold Periods

Environmental effects on fatigue lives occurred primarily during tensile-loading cycles and at strain levels greater than the threshold strain value. Information on the effects of hold periods on the fatigue lives of austenitic SSs in water was limited. In high-DO water, the fatigue lives of Type 304 SSs tested with a trapezoidal waveform (i.e., hold periods at peak tensile and compressive strain)<sup>14</sup> were comparable to those tested with a triangular waveform,<sup>31</sup> as shown in Fig. 98. As discussed in Section 4.1.8, a similar behavior was observed for carbon and low-alloy steels: the data showed little or no effects of hold periods on fatigue lives of the steels in

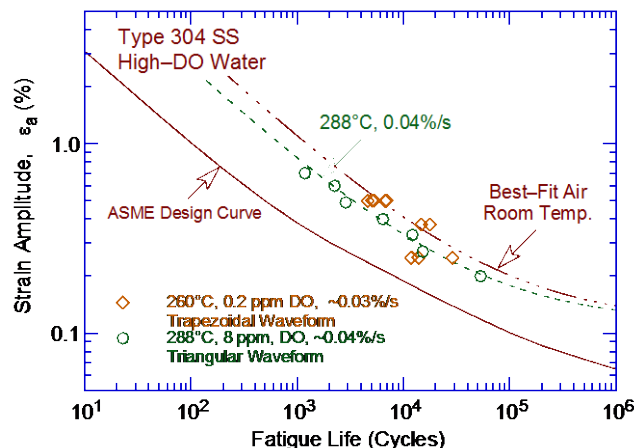


**Figure 98. Fatigue lives of Type 304 SSs tested in high-DO water at 260–288°C with trapezoidal or triangular waveform loadings (Refs. 14,31).**

high-DO water. The effects of hold periods as long as 2,000 s at peak tensile strains are shown in Fig. 99. The results indicated little or no effects of hold periods at peak tensile strains on the fatigue lives of austenitic SSs.

- The available fatigue  $\varepsilon$ -N data did not demonstrate that hold periods at peak tensile strains affected the fatigue lives of austenitic SSs in LWR environments. Therefore, the effects of hold times were not explicitly included in the  $F_{en}$  expression (i.e., Eq. 61 in Section 4.2.13) developed for austenitic SSs.

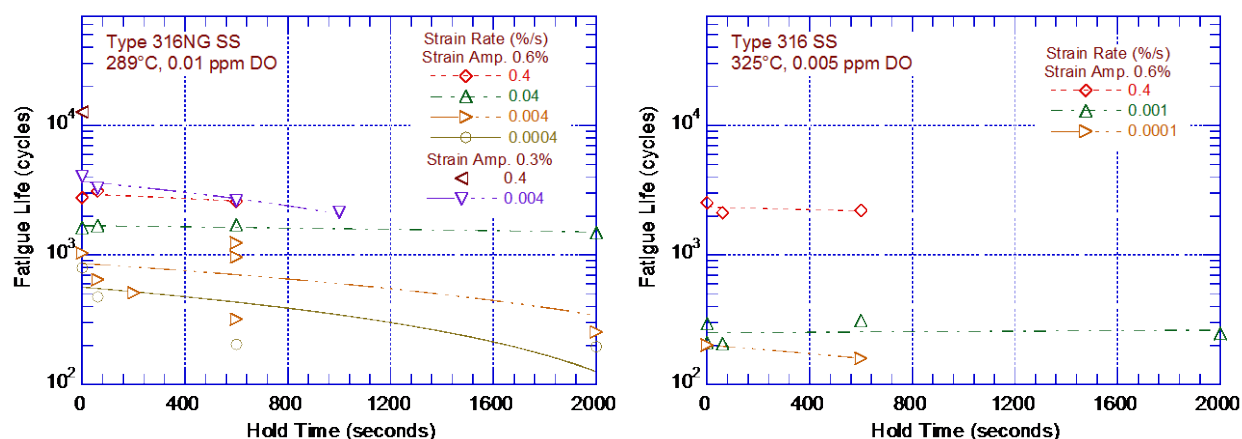


**Figure 99. Effect of hold periods on the fatigue lives of Types 316NG and 316 SSs in LWR environments at various strain rates (Ref. 136).**

#### 4.2.11 Flow Rate

Flow rate affects the fatigue lives of LWR materials because it causes differences in local environmental conditions in the enclaves of the microcracks formed during the early stages of a fatigue  $\varepsilon$ -N test. As discussed in Section 4.1.9, data obtained under typical operating conditions for BWRs indicated that environmental effects on the fatigue lives of carbon steels were a factor of approximately 2 lower at high flow rates (7 meters/second) compared to those at low flow rates (0.3 meters/second or lower).<sup>25,26</sup> However, similar tests in both low-DO and high-DO environments indicated that increasing flow rates had either no effects or detrimental effects on the fatigue lives of austenitic SSs. The potential effects of water flow rate on the fatigue lives of Types 304, 304L, and 316NG wrought austenitic SSs and CF-8M cast austenitic SSs at 289°C in high-purity water containing 0.05 to 0.2 ppm DO were plotted, and are shown in Fig. 100. Similarly, the effects of flow rate on the fatigue lives of austenitic SSs in PWR primary water environment at 325°C were plotted, and are shown in Fig. 101. Under all test conditions, the fatigue lives of these steels were either the same or slightly lower at high flow rates compared to those at lower rates or semi-stagnant conditions.

Fatigue tests conducted on SS pipe bend specimens in simulated PWR primary water at 240°C also indicated that water flow rate had no effects on the fatigue lives of austenitic SSs.<sup>131</sup> Increasing the flow rate from 0.005 meters/second to 2.2 meters/second had no effects on fatigue crack initiation in approximately 26.5-mm diameter tube specimens. These results were consistent with the notion that, in LWR environments, the mechanism of fatigue crack initiation in austenitic SSs differs from that in carbon and low-alloy steels.

- Because of the uncertainties in the flow conditions at or near the locations of crack initiation and the observations of the insignificant effects of flow rate, flow rate effects were not explicitly included in the  $F_{en}$  expression (i.e., Eq. 61 in Section 4.2.13) developed for austenitic SSs.

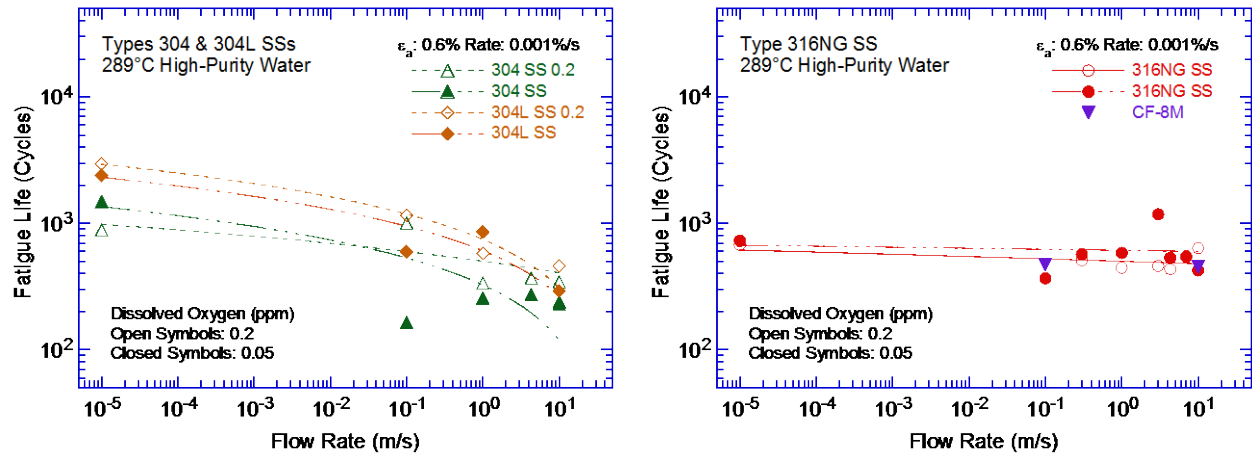


**Figure 100. Effects of water flow rate on the fatigue lives of Types 304, 304L, 316NG and CF-8M cast SSs in high-purity water at 289°C (Ref. 136).**

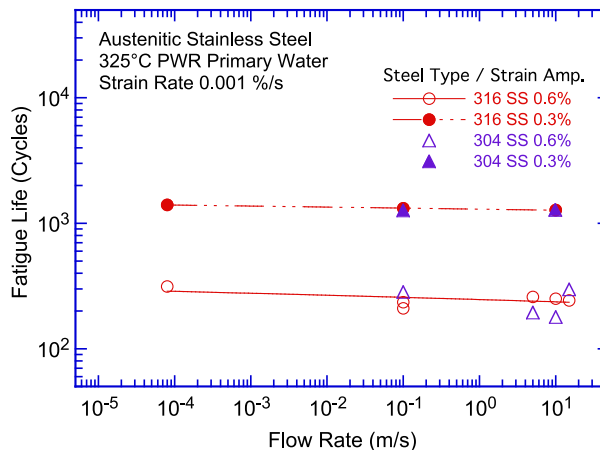


**Figure 101. Effects of water flow rates on the fatigue lives of Type 304 and 316 austenitic SSs in PWR primary water at 325°C (Ref. 136).**

#### 4.2.12 Fatigue Life Model

The fatigue life models for estimating the fatigue lives of austenitic SSs in LWR environments were presented in the initial revision of NUREG/CR-6909, and were based on an analysis of the updated PVRC database. The data were fitted to a modified version of the Langer equation expressed by Eq. 6, which included a term for environmental effects. The environmental term included the effects of key parameters, such as strain rate, water DO content, and temperature. The functional forms of these dependencies were based on the data trends. For both wrought and cast austenitic SSs, the model assumed threshold and saturation values of 0.4 and 0.0004%/s, respectively, for strain rate and a threshold value of 150°C for temperature. However, because of insufficient data, the dependencies of environmental effects on water DO

content were not included. The results of the analysis indicated that the fatigue lives of austenitic SSs in LWR environments were best represented by the following expression

$$\ln(N) = A - 1.920 \ln(\epsilon_a - 0.112) + T' \epsilon' O', \quad (57)$$

where constant A was determined to be 6.157 and the transformed temperature,  $T'$ , the transformed strain rate,  $\epsilon'$ , and the transformed DO content,  $O'$ , were defined by Eqs. 53-55. The experimental and predicted values differed by a factor of less than 3 for most heats of austenitic SSs. The experimental fatigue lives for a few tests on Type 304 SSs were up to a factor of approximately 4 lower than the predicted values; all of these tests were on tube specimens with 1- or 3-mm wall thicknesses. A threshold strain amplitude (one-half of the applied strain range) was defined, below which LWR coolant environments had no effects on fatigue lives, i.e.,  $F_{en} = 1$ . The threshold strain amplitude was specified as 0.10%, or a 195 MPa (28.3 ksi) stress amplitude for wrought and cast austenitic SSs.

- *The ANL model represented the mean values of fatigue lives as a function of applied strain amplitude, temperature, strain rate, and water DO content. The effects of parameters such as mean stress, surface finish, size and geometry, and loading history, which are known to influence fatigue lives, were not included in the model; the effects of these parameters were considered in the development of the fatigue design curve, as discussed in Chapter 5.*

#### 4.2.13 Environmental Correction Factor

As discussed at the beginning of Section 4.2, the ANL model for incorporating environmental effects on the fatigue lives of austenitic SSs (i.e., Eq. 57) resulted in approximately a factor of 2.5 decrease in fatigue lives relative to those in air, even when the environmental term of the expression is neglected (i.e., when either the temperature was below the threshold value of 150°C or the strain rate was above the threshold strain rate value). In addition, Eq. 57 did not consider the dependence of environmental effects on DO and the temperature dependency was not consistent with the available fatigue  $\epsilon$ -N data. As discussed in Section 4.2.5, the fatigue lives of austenitic SSs were decreased significantly in low-DO water, whereas in high-DO water they were either comparable or, for some steels, lower than those in low-DO water. In high-DO water, the material composition and heat treatment influenced the magnitude of environmental effects on austenitic SSs (refer to Section 4.2.7). Therefore, the  $F_{en}$  expression given by Eq. 52 yielded very conservative estimates of  $F_{en}$  for some materials (e.g., for low-carbon or nonsensitized high-carbon wrought SSs).

The fatigue life model for incorporating environmental effects on the fatigue lives of wrought and cast austenitic SSs in LWR environments was updated in this report to address the foregoing concerns using a much larger database that is described in Section 4.2.1. As discussed earlier, in the initial revision of NUREG/CR-6909, the least-squares fit of the experimental data for austenitic SSs in LWR environments yielded a steeper slope for the  $\epsilon$ -N curve compared to the slope of the curve obtained in air.<sup>45,121</sup> These results indicated that environmental effects may be more pronounced at low strain amplitudes compared to high strain amplitudes. However, differing slopes for the  $\epsilon$ -N curves in air and water environments added complexity to the determination of the environmental fatigue correction factor,  $F_{en}$ . Therefore, the ANL model slope of the  $\epsilon$ -N curve was assumed to be the same in both LWR and air environments. Furthermore, the reevaluation of the fatigue  $\epsilon$ -N data assumed that the constant A under environmental conditions was also the same as the value in air.

In addition, a review of the updated fatigue database indicated that the results from the EdF-sponsored study at GE on Type 304L SSs tested in PWR water at 150°C showed significant



environmental effects in the high-cycle regime (i.e., greater than  $10^4$  cycles). However, the  $F_{en}$  expression in the initial revision of NUREG/CR-6909 included a temperature threshold of  $150^\circ\text{C}$  below which environmental effects were considered insignificant. The  $F_{en}$  expressions developed by JNES did not consider a temperature threshold. Therefore, to better represent the existing fatigue  $\varepsilon$ -N data, the temperature dependence relationships in the  $F_{en}$  expression was modified and the temperature threshold was decreased from 150 to  $100^\circ\text{C}$ . In addition, a maximum temperature limit was selected at  $325^\circ\text{C}$  as a reasonable extension to cover all anticipated LWR operating conditions. This is adequate for all expected operating LWR conditions considering the use of average temperature (as discussed in Section 4.1.11 and shown in Fig. 81). The dependency of fatigue lives on strain rate was also modified, and the threshold strain rate below which environmental effects were significant was increased from 0.4 to 10%/s. In addition, the dependence of environmental effects on water DO content was also included; it was based on the material composition and heat treatment.

Using Eq. 51 and values of constants A, B, and C that are the same as those obtained for the best-fit air curve for austenitic SSs (i.e., Eq. 29), a least-squared fit of the much larger fatigue  $\varepsilon$ -N database in LWR environments yielded the following expressions for the transformed parameters  $T'$ ,  $\dot{\varepsilon}'$ , and  $O'$ :

$$\begin{aligned} T' &= 0 & (T < 100^\circ\text{C}) \\ T' &= (T - 100)/250 & (100^\circ\text{C} \leq T \leq 325^\circ\text{C}) \end{aligned} \quad (58)$$

$$\begin{aligned} \dot{\varepsilon}' &= 0 & (\dot{\varepsilon} > 10\%/s) \\ \dot{\varepsilon}' &= \ln(\dot{\varepsilon}/10) & (0.0004\%/s \leq \dot{\varepsilon} \leq 10\%/s) \\ \dot{\varepsilon}' &= \ln(0.0004/10) & (\dot{\varepsilon} < 0.0004\%/s) \end{aligned} \quad (59)$$

$$\begin{aligned} &\text{For DO less than 0.1 ppm, i.e., PWR of BWR HWC water,} \\ O' &= 0.29 & (\text{all wrought and cast SSs and heat treatments and SS weld metals}) \\ &\text{For DO greater than or equal to 0.1 ppm, i.e., NWC BWR water,} \\ O' &= 0.29 & (\text{sensitized high-carbon wrought and cast SSs}) \\ O' &= 0.14 & (\text{all wrought SSs except sensitized high-carbon SSs}). \end{aligned} \quad (60)$$

The reevaluation of the updated fatigue  $\varepsilon$ -N data for austenitic SSs using the updated expressions yielded a good fit of the data, particularly in the low-cycle regime. The R-squared values for the best fit of the data to minimize the error in the values of fatigue lives and the values of the shortest distance between the data points and the best fit  $\varepsilon$ -N curve improved from 0.83 to 0.86 and 0.92 to 0.93, respectively. This updated model is recommended for predicting fatigue lives up to  $10^6$  cycles. A single expression was used for Types 304, 304L, 316, 316L, and 316NG SSs, and Eqs. 57–60 also apply to cast austenitic SSs such as CF-3, CF-3M, CF-8, and CF-8M as well as SS weld metals.

The effects of reactor coolant environments on fatigue lives were expressed in terms of a fatigue life correction factor,  $F_{en}$ , which was defined as the ratio of fatigue life in air at room temperature to that in water at the service temperature. The  $F_{en}$  for austenitic SSs in LWR environments is given by

$$F_{en} = \exp(-T' \dot{\varepsilon}' O'), \quad (61)$$

where the constants  $T'$ ,  $\dot{\varepsilon}'$ , and  $O'$  are defined in Eqs. 58–60. To incorporate environmental effects into an ASME Code Section III fatigue evaluation, the fatigue usage in air for a specific stress cycle is multiplied by the environmental correction factor,  $F_{en}$ . Further details for incorporating environmental effects into fatigue evaluations are presented in Appendix A.

Comparisons of the experimental fatigue lives of wrought and cast austenitic SSs, as well as their associated weld metals in LWR environments, were compared to those predicted by the updated  $F_{en}$  expression (i.e., from Eqs. 61 and 29), the JNES expression,<sup>136</sup> and the expression in the initial revision of NUREG/CR-6909, as shown in Fig. 102. The results indicated that the updated  $F_{en}$  expression represented a better fit to the larger experimental database relative to the fit for the expression in the initial revision of NUREG/CR-6909. Typically, for fatigue lives less than  $3 \times 10^4$  cycles, the predicted values were within a factor of 3 to the experimental values. Also, compared to the estimates based on the expressions in the initial revision of NUREG/CR-6909, the R-squared values for the best-fit of the data were slightly higher.

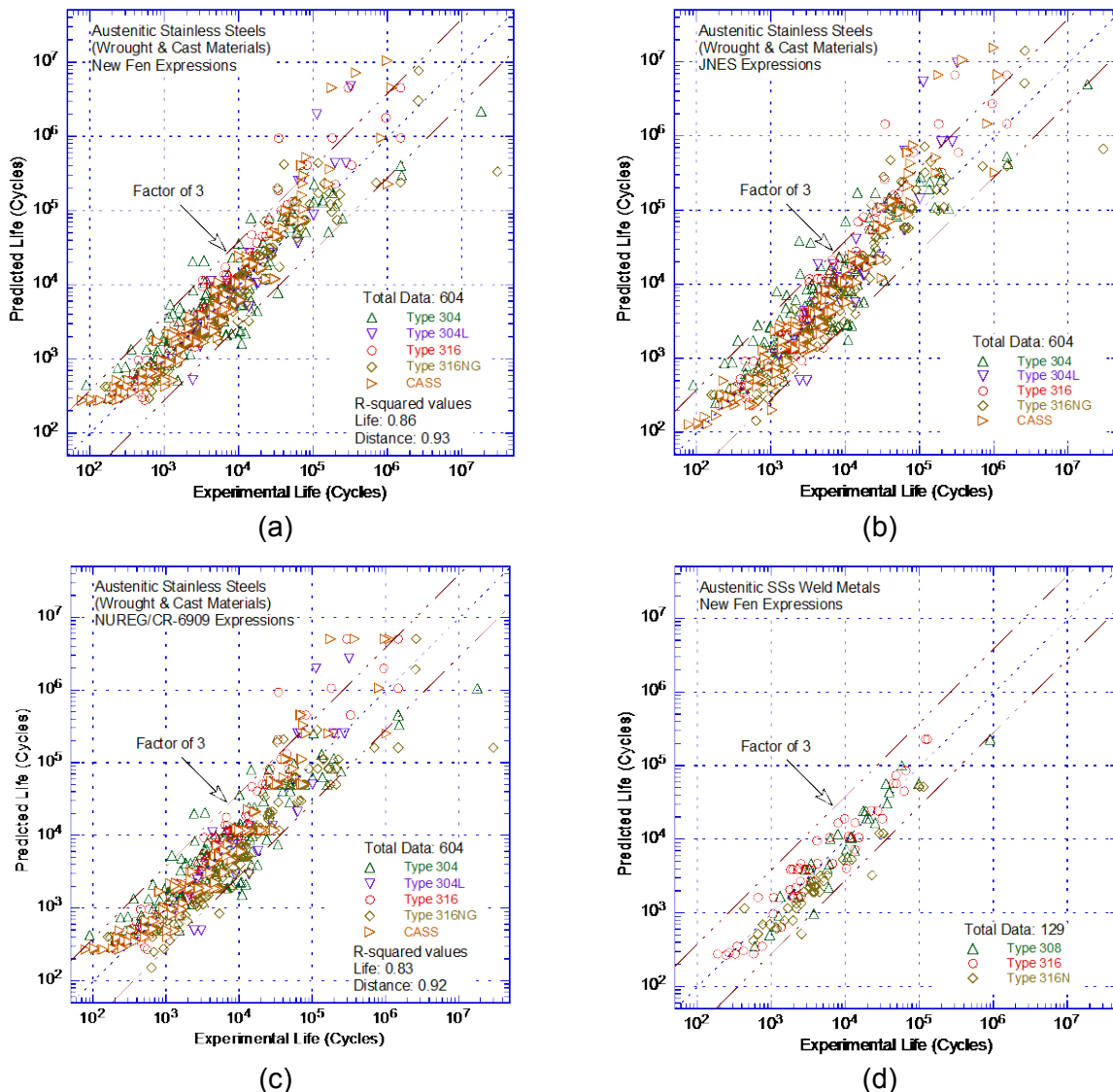


**Figure 102.** Experimental fatigue lives of wrought and cast austenitic SSs in LWR environments vs. fatigue lives predicted from (a) the updated ANL expression, (b) the JNES expression, (c) the previous NUREG/CR-6909 expression, and (d) fatigue lives of SS weld metals predicted from the updated ANL expression.



A comparison of the fatigue lives predicted using the updated  $F_{en}$  expression and the JNES  $F_{en}$  expression was also made, as shown in Fig. 103. In general, the  $F_{en}$  values calculated from the updated expression were marginally lower for fatigue lives less than  $10^4$  cycles and slightly longer than those predicted from the JNES expression for fatigue lives greater than  $10^4$  cycles. Some significant differences remain in the predicted lives obtained from the updated  $F_{en}$  expression for SS compared to those obtained from the JNES expression for BWR environments. The reasons for these differences are not fully understood, but appear to be predominantly associated with the DO and temperature relationships. Further investigation of these differences is recommended as a part of any future research activities.

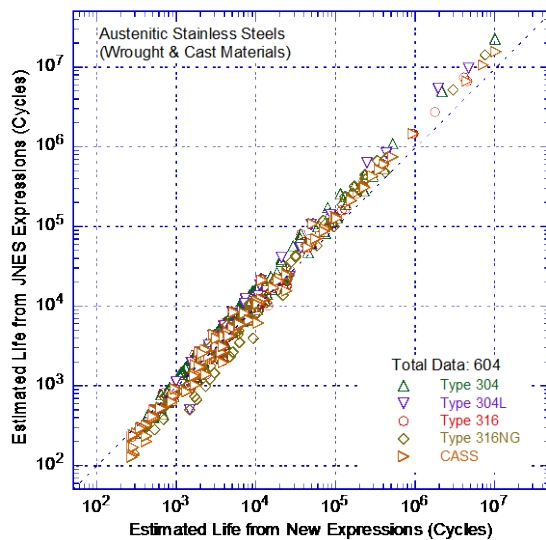


**Figure 103.**  
Fatigue lives of wrought and cast austenitic SSs in LWR environments estimated from the new  $F_{en}$  expressions vs. those estimated from the JNES expression.

The experimental fatigue lives were compared with the estimated values using the updated  $F_{en}$  expression and the JNES expression for a smaller dataset of Types 304L and 316N SSs and cast and wrought austenitic SSs in water containing greater than 0.1 ppm DO, as shown in Figs. 104 and 105, respectively. The results indicated that, in general, the estimates based on the updated expression were slightly better than those from the JNES expression. However, the data scatter for high-carbon Type 304 SSs in high-DO water (i.e., greater than 0.1 ppm DO in water) is larger than that for the other grades of SSs.

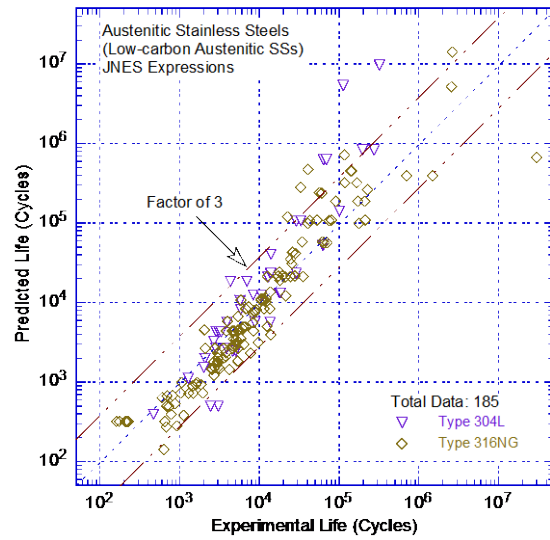
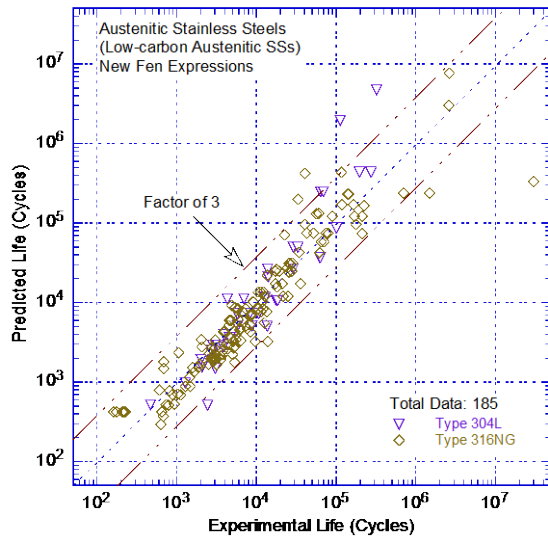


Figure 104. Experimental fatigue lives of Types 304L and 316N austenitic SSs in LWR environments vs. fatigue lives predicted from (a) the updated ANL expression and (b) the JNES expression.

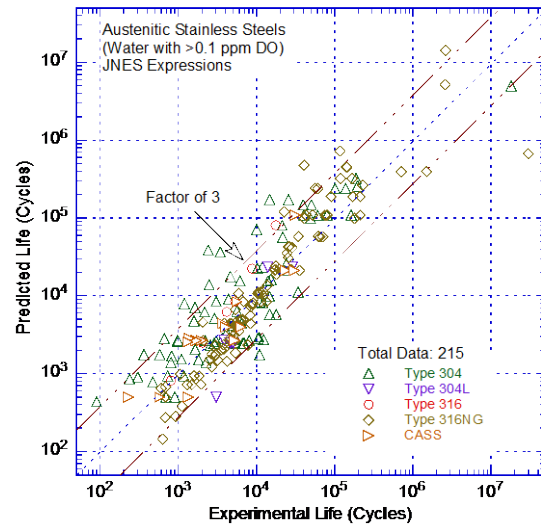
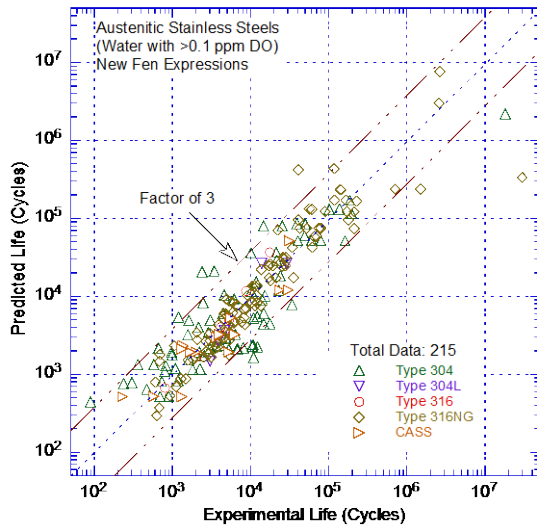
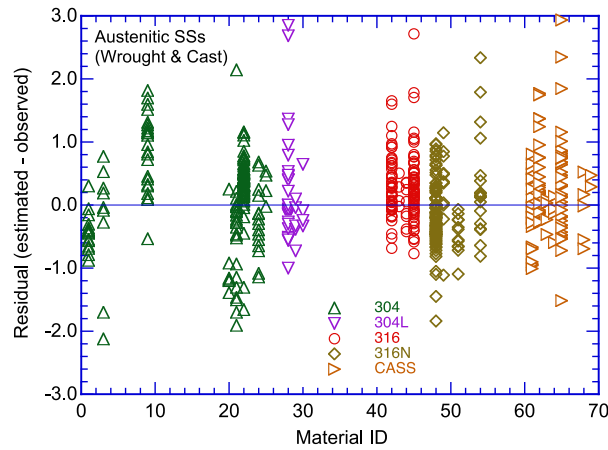


Figure 105. Experimental fatigue lives of wrought and cast austenitic SSs in water containing greater than 0.1 ppm DO vs. fatigue lives predicted from (a) the updated ANL expression and (b) the JNES expression.

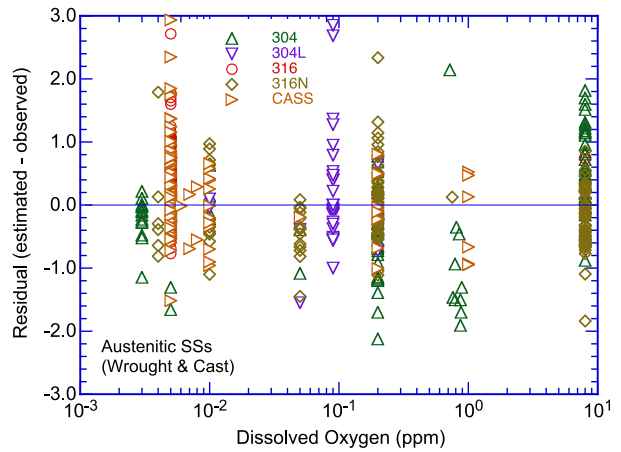
As observed in Section 4.1.11 for carbon and low-alloy steels, upon completion of the modeling phase, the residual errors did not show significant patterns, such as changing variance or a nonzero slope. The residual errors for each variable, grouped by steel type, were plotted, as shown in Fig. 106 for wrought and cast austenitic SSs in LWR environments. The residuals were determined from the difference between the logarithms of the estimated lives and predicted lives. Thus, negative residual errors corresponded to conservative estimates of fatigue lives and positive residual errors corresponded to nonconservative estimates of fatigue lives (i.e., predicted lives were greater than observed fatigue lives). However, predominantly positive or negative residuals did not necessarily indicate any deficiency in the predictive models. Such results indicated that the specific heat was either superior or inferior to the average behavior predicted by the model. For example, a positive residual indicated that the heat was inferior (i.e., the constant A for the heat was smaller than the median value of constant A in the model) and a negative residual indicated that the heat was superior to the average behavior for the material. This behavior is discussed further in Section 4.2.15.

The results presented in Fig. 106 did not reveal any unexplained patterns. In general, high observed variances tended to be associated with longer lives and lower strain amplitudes. Furthermore, any observed biases were traceable to heat-to-heat variations. For example, heats of Type 304 SSs with Mat. ID #9, Type 316 SSs with Mat. ID #49, and cast austenitic SSs with Mat. ID #61 had inferior fatigue resistance, and heats of Type 304 SSs with Mat. ID #1 and 21 and of Type 316 SSs with Mat. ID #51 had superior fatigue resistance than the average behavior represented by the fatigue  $\epsilon$ -N model (Eqs 61 and 29).

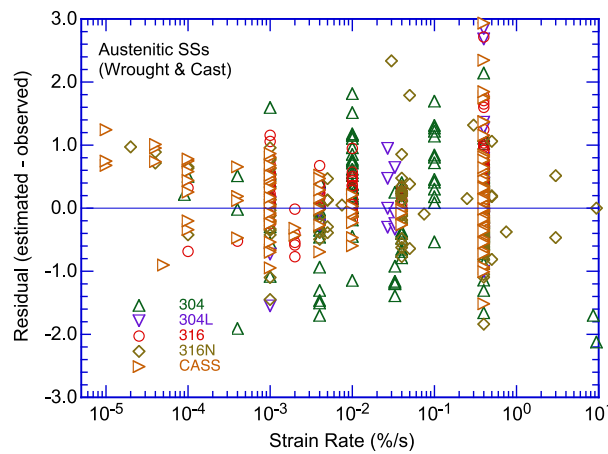
Some of the heats of austenitic SSs that were tested in LWR environments were also tested in air. The residual errors for the best fit of the fatigue  $\epsilon$ -N data for austenitic SSs in air were plotted as a function of the ANL Material ID, as shown in Fig. 107. Most of the data subsets for fatigue tests in air followed the same trends as those observed in LWR environments. For example, data subsets for Mat. ID #21 and 51 yielded predominantly negative residuals in both environments and predominantly positive residuals for Mat. ID #61. The one exception was material ID #9, which yielded positive residuals in air and marginally negative residuals in LWR environments. These results indicated that environmental effects on fatigue lives in LWR environments were accurately estimated by the updated  $F_{en}$  expression.



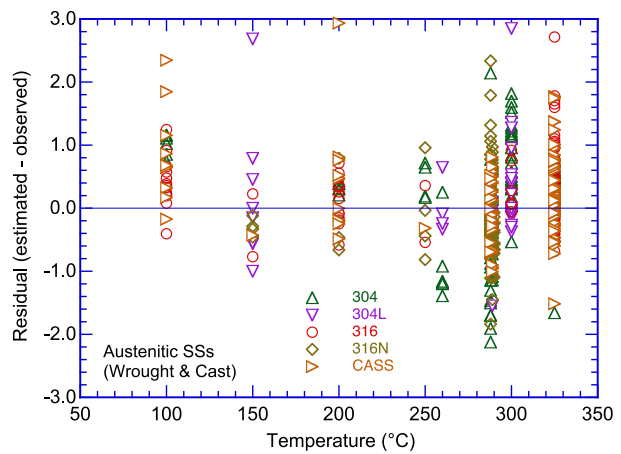
(a)



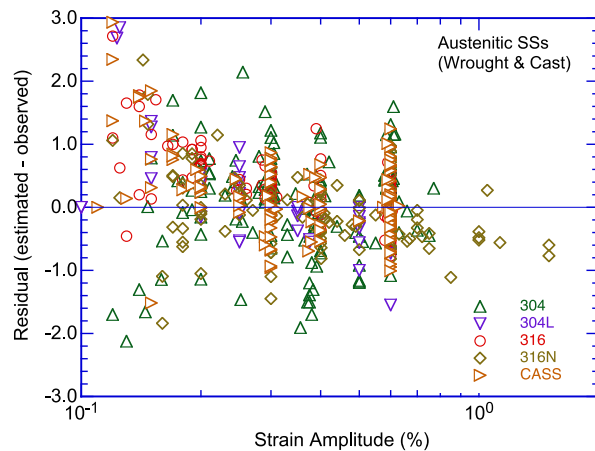
(b)



(c)



(d)



(e)

**Figure 106.**  
Residuals for predicted fatigue lives of wrought and cast austenitic SSs as a function of (a) ANL Material ID, (b) water DO content, (c) strain rate, (d) temperature, and (e) strain amplitude.

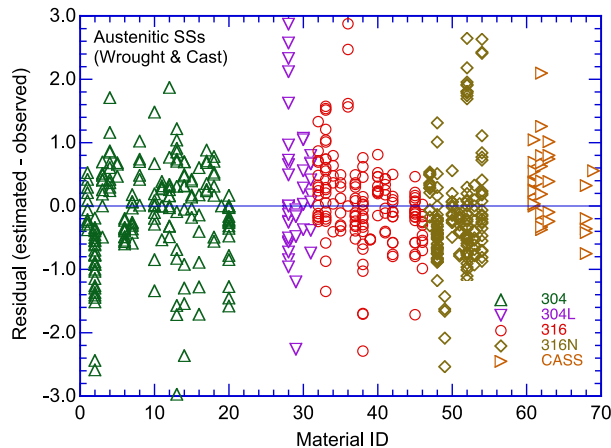


**Figure 107.**  
Residuals for predicted fatigue lives of wrought and cast austenitic SSs in air as a function of ANL Material ID.

- The  $F_{en}$  approach should be used to incorporate environmental effects into ASME Code Section III fatigue evaluations for cast and wrought austenitic SSs and their associated weld metals. Appendix C of this report presents a sample application of the  $F_{en}$  methodology.

#### 4.2.14 Surface Finish

Austenitic SSs tended to develop a corrosion scale in high-temperature water thereby eliminating any apparent effects of surface finish in LWR environments. Therefore, the fraction of the adjustment factor related to surface finish that was applied to the best-fit mean data curve to obtain the fatigue design curve was assumed to be 1.5 or lower. Fatigue tests were conducted on Types 304 and 316NG SSs that were intentionally roughened in a lathe, under controlled conditions, with 50-grit sandpaper to produce circumferential cracks with an average surface roughness of 1.2  $\mu\text{m}$ . The results are shown in Fig. 108 for Types 316NG and 304 SSs. For both steels, the fatigue lives of roughened specimens were up to a factor of 3 lower than those of the smooth specimens in both air and low-DO water environments. However, the results of a single test on Heat P91576 of Type 316NG in high-DO water did not show any effects of surface finish; the fatigue lives were the same for rough and smooth specimens (shown as open and closed diamond symbols in Fig. 108a).

Similar tests conducted on Type 304L SSs in air and PWR water environments<sup>155-157</sup> also indicated a factor of approximately 2 decrease in fatigue lives of the ground specimens relative to those of the polished specimens, as shown in Fig. 109. The tests were conducted with a triangular waveform loading with a strain rate of 0.4%/s and a complex waveform loading that simulated a PWR safety injection transient. The tests were conducted under strain control and the strain rates associated with the safety injection transient ranged from 0.08 to 0.00013%/s. Note that the strain accumulated under specific strain rates decreased with decreasing strain rates.

Thus, the available small-scale laboratory fatigue  $\epsilon$ -N data indicated decrease in fatigue lives of up to a factor of up to 2.5 for the roughened specimens relative to the lives of polished specimens in both air and LWR environments. Limited data also indicated that for some low-carbon heats of austenitic SSs, surface finish did not have any effects on the fatigue lives of SSs in LWR environments. However, the data were very limited, so additional data are needed to validate this behavior.

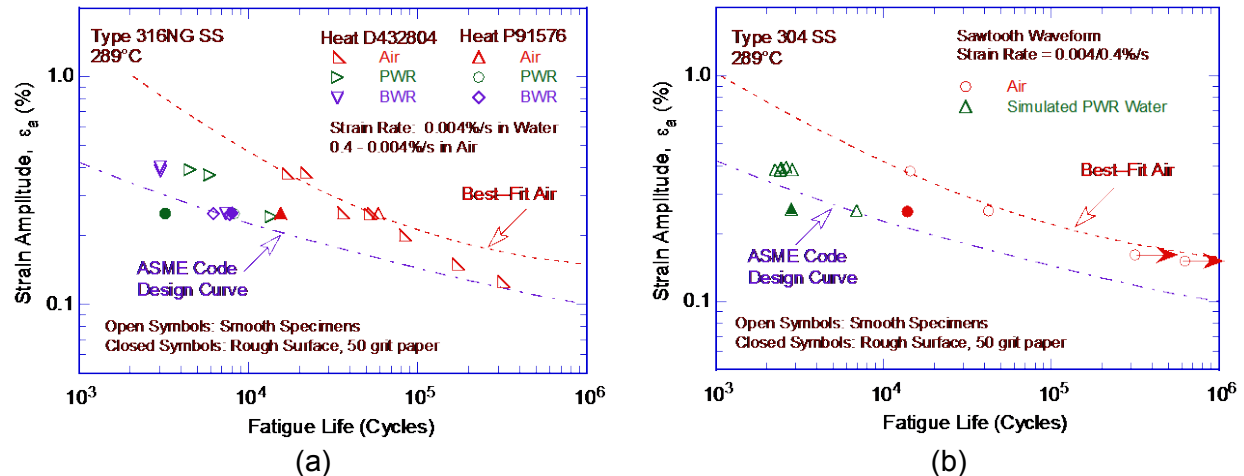


Figure 108. Effect of surface finish on fatigue life of (a) Type 316NG and (b) Type 304 stainless steels in air and high-purity water at 289°C.

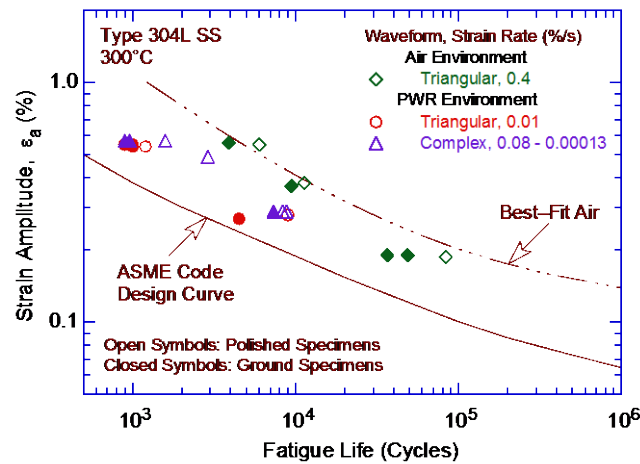


Figure 109. Effects of surface finish on the fatigue lives of Type 304L SSs in air and PWR primary water environments at 300°C (Refs. 155,157).

- The effects of surface finish were not explicitly included in the environmental fatigue correction factor; instead, they were included in the subfactor for “surface finish and environment,” which was applied to the mean data air curve to develop the fatigue design curve in air.

#### 4.2.15 Heat-to-Heat Variability

The effects of material variability and data scatter on the fatigue lives of austenitic SSs were evaluated for data in LWR environments. The fatigue behavior of each of the heats or loading conditions was characterized by the value of the constant  $A$  in the ANL model (e.g., Eq. 6). The values of  $A$  were determined from Eq. 57 for the various data sets in the larger, updated fatigue  $\epsilon$ - $N$  database used in this report. The values of constant  $A$  were ordered, and median ranks were used to estimate the cumulative distribution of  $A$  for the population. If the  $F_{en}$  expression given in Eq. 57 adequately captured the effects of LWR environments on the fatigue lives of wrought and cast austenitic SSs, the reanalysis should have yielded a median value of constant  $A$  that is the same as in an air environment.

The estimated cumulative distribution of constant A is shown in Fig. 110. The results yielded a median value of A of 6.800 for all the data sets for cast and wrought austenitic SSs and their associated weld metals, and a value of 6.749 without the datasets for weld metals. These values of constant A are slightly lower than that in air (e.g., the difference is less than 10%). These results demonstrate that the  $F_{en}$  expressions for cast and wrought austenitic SSs adequately capture the environmental effects in LWR environments.

The heat-to-heat variation in LWR environments differed insignificantly from that in air and presented in Section 3.2.7. The 95/95 values of the factors to account for material variability and data scatter were the same in air (i.e., presented in Table 7 for austenitic SSs). These factors provide 95% confidence that the resultant lives are greater than those observed for 95% of the materials of interest.

- *Heat-to-heat variability was not explicitly included in the environmental fatigue correction factor for austenitic SSs; instead, it was included in the subfactor for “data scatter and material variability” that was applied to the room-temperature mean data air curve to develop the fatigue design curve in air.*

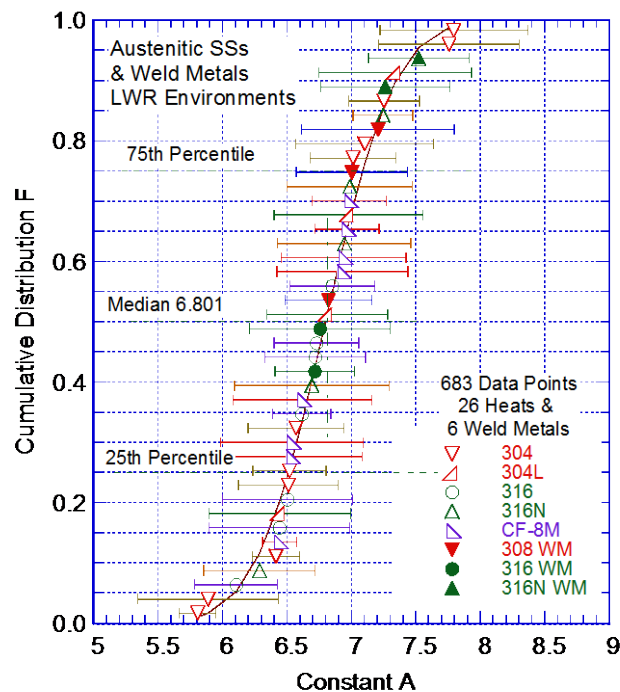


**Figure 110.**  
Estimated cumulative distribution of constant A in the ANL model for fatigue lives of heats of austenitic SSs in LWR environments.

### 4.3 Ni-Cr-Fe Alloys

The relevant fatigue  $\epsilon$ -N data for Ni-Cr-Fe alloys and associated weld metals in LWR environments evaluated in this report included the data compiled in the JNES database from Japan<sup>136</sup> and the tests performed by Van Der Sluys et al.<sup>75</sup> The database was composed of 162 tests; 87 tests on 5 heats of Alloy 600, 21 tests on 2 heats of Alloy 690, and 54 tests on 6 heats of Ni-Cr-Fe alloy weld metals, which included Alloys 82, 182, 132, 152, and 690. Out of these, 7 tests were conducted at 100°C (one at 54°C), 10 tests at 200°C, 88 tests at 288/289°C, 10 tests at 315°C, and 47 tests at 325°C. A summary of the data sources for the updated database used in this report, as categorized by material type and test environment, is shown in Table 12. Other material information such as chemical composition, heat treatment, and room temperature tensile properties for the Ni-Cr-Fe alloys and associated weld metals evaluated is given in Appendix B.

**Table 12. Sources of the fatigue  $\epsilon$ -N data for Ni-Cr-Fe alloys and their weld metals in LWR environments.**

ANL Mat. ID	Material Heat Designation	Carbon Content (wt.%)	Dissolved Oxygen (ppm)	Test Temperature (°C)	No. of Data Points	Source	Applicable Reference
<u>Alloy 600</u>							
1	Alloy 600-1	0.07	0.2	288	12	JNES (Higuchi)	39, 136
2	Alloy 600-2	0.07	0.2	288	16	JNES (Nakao)	136
5	Alloy 600-3	0.01	0.01, 0.05, 0.2, 8.0	289 (4 at 200)	11, 1, 14, 4	JNES (Hirano)	136
3	Alloy 600-4	0.07	0.01, 0.2	289	2, 6	JNES (Hirano)	136
4	Alloy 600-5	0.03	0.005	100, 200, 325	6, 6, 9	JNES (Nomura)	136
<u>Alloy 690</u>							
9	Alloy 690-1	0.03	0.005	325	20	JNES (Nomura)	136
12	Alloy 690-3	0.02	0.01	315	1	PVP (Van der Sluys)	75
<u>Ni-Cr-Fe Alloy Weld Metals</u>							
10	Alloy 152 WM	0.037	0.005	325	9	JNES (Kanasaki)	136
6	Alloy 182-1	0.06	0.2	288	14	JNES (Higuchi)	136
7	Alloy 182-2	0.038	0.2	288	12	JNES (Nakao)	136
11	Alloy 82-5	0.04	0.01, 0.007	315	4, <sup>a</sup> 5	PVP (Van der Sluys)	75
8	Alloy 132	0.04	0.005	325	9	JNES (Nomura)	136
13	Alloy 152-2	0.032	0.01	315	1	PVP (Van der Sluys)	75

<sup>a</sup> One test in 0.01 ppm DO water was performed at 54°C.

#### 4.3.1 Experimental Data

Similar to carbon, low-alloy and austenitic SSs, the fatigue lives of Ni-Cr-Fe alloys and their welds were also decreased in LWR environments; the fatigue  $\epsilon$ -N data for various Ni-Cr-Fe alloys in simulated BWR water at approximately 289°C and PWR water at 315-325°C are shown in Figs. 111 and 112, respectively. The  $\epsilon$ -N air curve based on the ANL model for austenitic SSs (Eq. 29 discussed in Section 3.2.6) is also included on the plots in these figures. The results indicated that environmental effects on the fatigue lives of Ni-Cr-Fe alloys were also dependent on key parameters such as strain rate, temperature, and the DO level in the water. Similar to SSs, the effects of coolant environments on the fatigue lives of Ni-Cr-Fe alloys were



greater in low-DO PWR environments than they were in the high-DO BWR environments. However, under similar loading and environmental conditions, the extent of the effects of environment was considerably less for the Ni-Cr-Fe alloys compared to that for austenitic SSs. In general, environmental effects on fatigue lives were the same for wrought and weld Ni-Cr-Fe alloys.

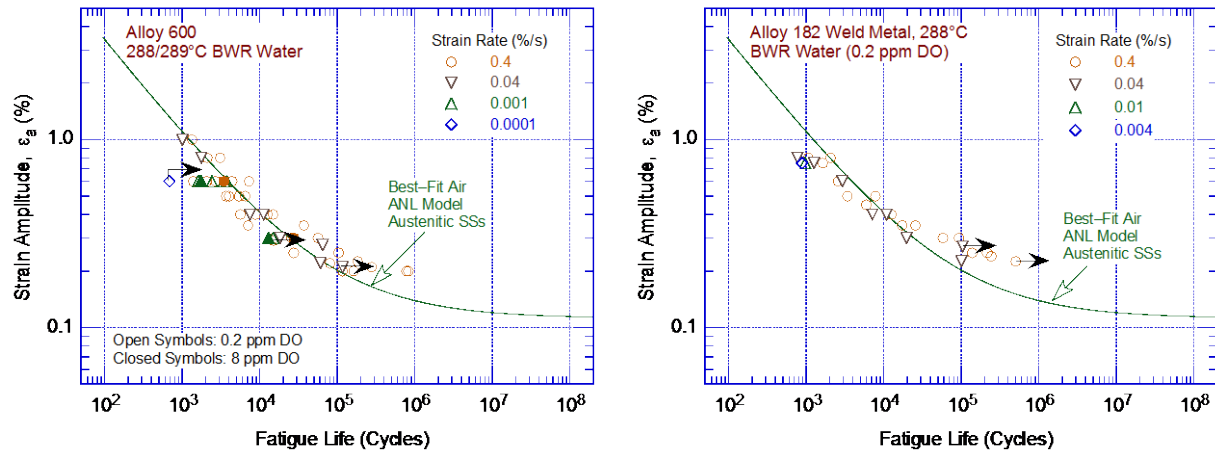


**Figure 111. Fatigue  $\epsilon$ -N behavior for Alloy 600 and its weld alloys in simulated BWR water at approximately 289°C (Refs. 136, 39).**

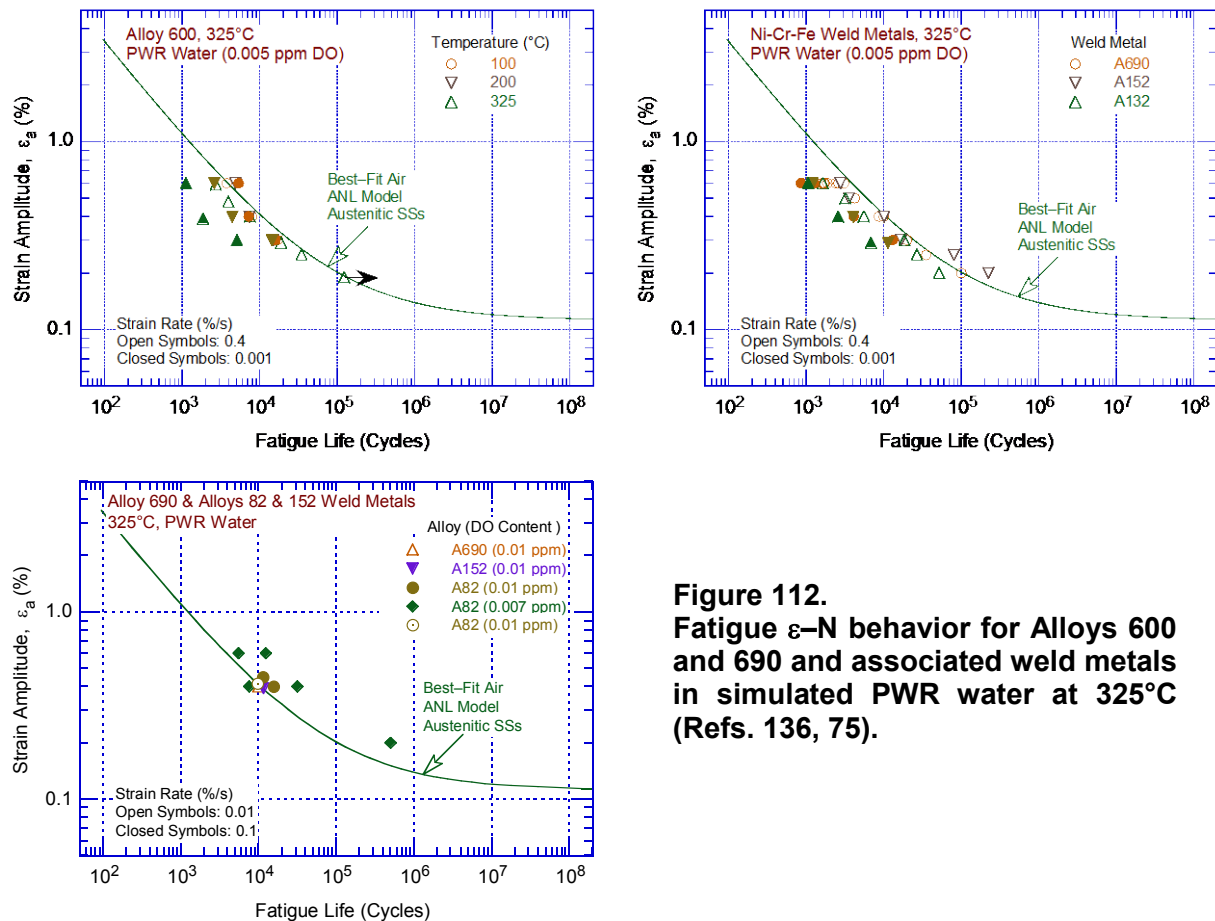


**Figure 112. Fatigue  $\epsilon$ -N behavior for Alloys 600 and 690 and associated weld metals in simulated PWR water at 325°C (Refs. 136, 75).**

### 4.3.2 Effects of Key Parameters

The effects of the key loading and environmental parameters (e.g., strain rate, temperature, and DO level) on the fatigue lives of Ni-Cr-Fe alloys in LWR environments were evaluated using the limited fatigue  $\varepsilon$ -N data that were available. The fatigue lives of Alloys 600 and 690 and their weld metals (e.g., Alloys 132 and 152) in simulated PWR and BWR water at different strain amplitudes were plotted as a function of strain rate, as shown in Fig. 113. The fatigue lives of these alloys decreased logarithmically with decreasing strain rate. Since there were little or no data at strain rates below 0.001%/s, the effects of strain rate on Ni-Cr-Fe alloys were assumed to be similar to those for austenitic SSs. The effects were assumed to saturate at a strain rate of 0.0004%/s.

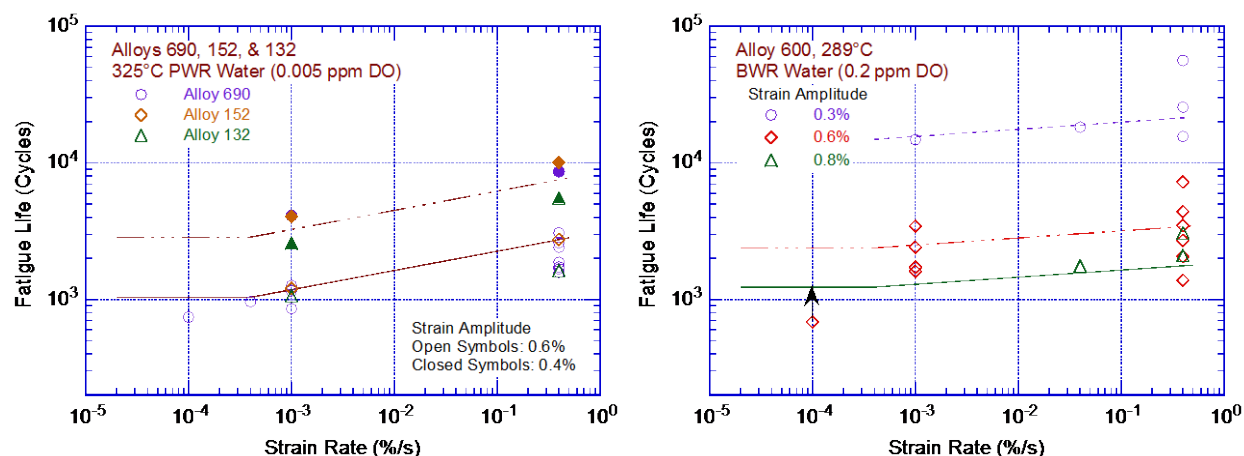


**Figure 113. Dependence of fatigue lives of Alloys 690 and 600 and associated weld metals on strain rate in PWR and BWR environments (Refs. 39, 75, 136).**

Furthermore, the threshold strain rate below which environmental effects were insignificant could not be sufficiently determined from the available data. Higuchi et al.<sup>39</sup> defined a threshold strain rate of 1.8%/s in high-DO BWR water and 26.1%/s in low-DO PWR water. As discussed in the next section, an average threshold value of 5%/s provided good estimates of fatigue lives of Ni-Cr-Fe alloys in LWR environments. The results also indicated that the effects of environment were greater in low-DO PWR water than in high-DO BWR water. For example, a three-orders-of-magnitude decrease in strain rate decreased the fatigue lives of these alloys by a factor of approximately 3 in PWR water and by a factor of approximately 2 in BWR water.

The fatigue lives of Alloy 600 in PWR environments at three different strain amplitudes were plotted as a function of temperature, as shown in Fig. 114. The results indicated a decrease in fatigue lives with increasing temperature. Because of very limited fatigue data for Ni-Cr-Fe alloys, the effects of temperature on the fatigue lives of these materials were also assumed to be similar to those observed in austenitic SSs. Environmental effects on fatigue lives were considered to be insignificant below a threshold temperature of 50°C. In addition, it was assumed that a slow strain rate applied during the tensile-loading cycle (i.e., up-ramp with increasing strain) was primarily responsible for the environmentally assisted reduction in fatigue lives. Slow rates applied during both tensile- and compressive-loading cycles (i.e., up- and down-ramps) did not further decrease fatigue lives compared with those observed for tests with only a slow tensile-loading cycle. Thus, loading and environmental conditions during the tensile-loading cycle were important for an environmentally assisted reduction in the fatigue lives of Ni-Cr-Fe alloys. The available fatigue  $\varepsilon$ -N data for Ni-Cr-Fe alloys in LWR environments

were inadequate to define the threshold strain amplitude below which environmental effects on fatigue lives did not occur.

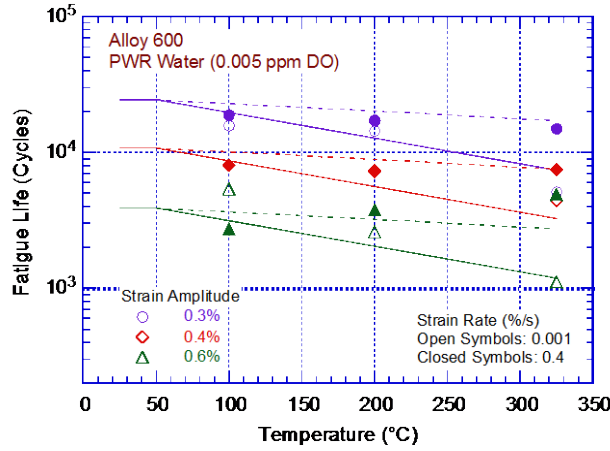


**Figure 114.**  
Dependence of fatigue lives of Alloy 600 on temperature in a PWR environment (Refs. 39, 75, 136).

As discussed in Section 4.2.13, some significant differences remain in the predicted lives obtained from the updated  $F_{en}$  expression for austenitic SSs compared to those obtained from the JNES expression for BWR environments. These differences may also impact the relations for Ni-Cr-Fe alloys. The reasons for these differences are not fully understood, but appear to be predominantly associated with the DO and temperature relationships. Further investigation of these differences is recommended as a part of any future research activities.

### 4.3.3 Environmental Correction Factor

The effects of reactor coolant environments on the fatigue lives of Ni-Cr-Fe alloys were also expressed in terms of a fatigue life correction factor,  $F_{en}$ . The available fatigue data were very limited to develop a fatigue life model for Ni-Cr-Fe alloys in LWR environments. However, as discussed in Section 4.3.2, environmental effects for these alloys showed the same trends as those observed for austenitic SSs. Environmental effects increased with increasing temperature and decreasing strain rate. Based on the available fatigue  $\epsilon$ -N data, the effects of temperature on the fatigue lives were considered to be insignificant below 50°C and saturated at 325°C. A maximum temperature limit was selected at 325°C as a reasonable extension to cover all anticipated LWR operating conditions. This is adequate for all expected operating LWR conditions considering the use of average temperature (as discussed in Section 4.1.11 and shown in Fig. 81). Similarly, the effects of strain rate were considered insignificant at strain rates above 5%/s and they saturated at 0.0004%/s. Thus, the  $F_{en}$  relationship for Ni-Cr-Fe alloys was expressed as

$$F_{en} = \exp(-T' \dot{\epsilon}' O'), \quad (62)$$

where  $T'$ ,  $\dot{\epsilon}'$ , and  $O'$  are transformed temperature, strain rate, and DO, respectively. The functional forms for these transformed parameters were obtained from the best fit of the experimental data and were defined as follows:

$$\begin{aligned} T' &= 0 & (T < 50^\circ\text{C}) \\ T' &= (T-50)/275 & (50^\circ\text{C} \leq T \leq 325^\circ\text{C}) \end{aligned} \quad (63)$$

$$\begin{aligned} \dot{\epsilon}' &= 0 & (\dot{\epsilon} > 5.0\%/s) \\ \dot{\epsilon}' &= \ln(\dot{\epsilon}/5.0) & (0.0004\%/s \leq \dot{\epsilon} \leq 5.0\%/s) \\ \dot{\epsilon}' &= \ln(0.0004/5.0) & (\dot{\epsilon} < 0.0004\%/s) \end{aligned} \quad (64)$$

$$\begin{aligned}
 O' &= 0.06 && (\text{NWC BWR water, i.e., } \geq 0.1 \text{ ppm DO}) \\
 O' &= 0.14 && (\text{PWR or HWC BWR water, i.e., } < 0.1 \text{ ppm DO}). \quad (65)
 \end{aligned}$$

The fatigue lives of Ni-Cr-Fe alloys in LWR environments were estimated from Eqs. 29 and 62–65. The experimental fatigue lives of various Ni-Cr-Fe alloys in BWR NWC (i.e.,  $\geq 0.1$  ppm DO) and PWR or HWC BWR (i.e.,  $< 0.1$  ppm DO) environments estimated using the updated  $F_{en}$  expression, the original NUREG/CR-6909 expression, and the JNES expression were plotted, as shown in Figs. 115–117, respectively. The results indicated that the updated expression represented a better fit to the larger database compared to the expression in the initial revision of NUREG/CR-6909. The R-squared values for the best-fit of the data were slightly higher for the updated expression compared to those obtained from the original NUREG/CR-6909  $F_{en}$  expression. In general, the estimated values were either comparable (within a factor of 2) or longer (conservative) than those observed experimentally.

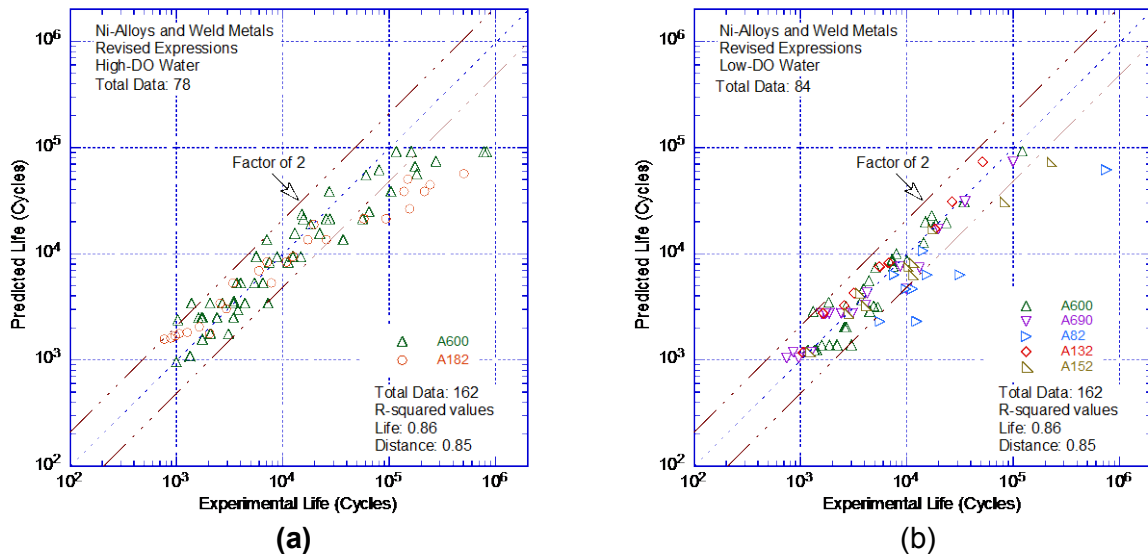


**Figure 115. Experimental fatigue lives vs. fatigue lives predicted from the updated  $F_{en}$  expression for Ni-Cr-Fe alloys and weld metals in simulated (a) BWR and (b) PWR environments.**

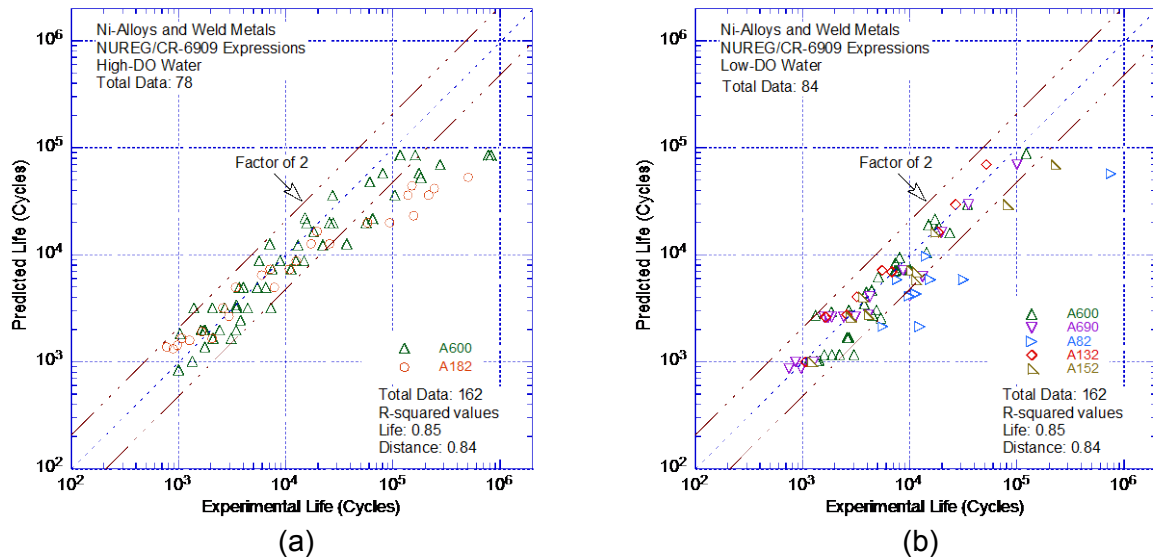


**Figure 116. Experimental fatigue lives vs. fatigue lives predicted from the  $F_{en}$  expression in the original revision of NUREG/CR-6909 for Ni-Cr-Fe alloys and weld metals in simulated (a) BWR and (b) PWR environments.**

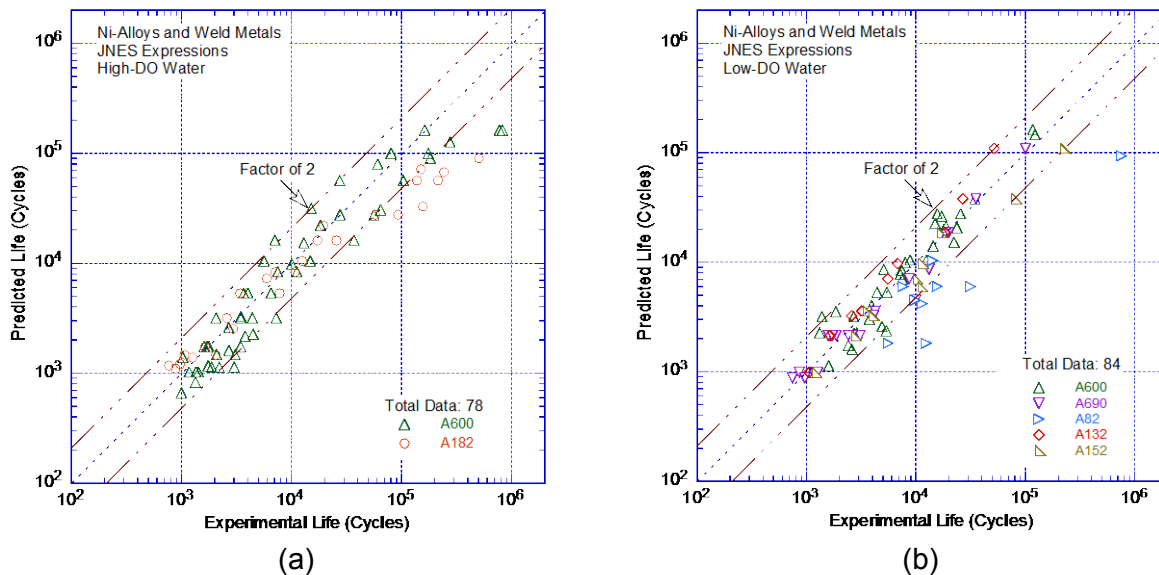


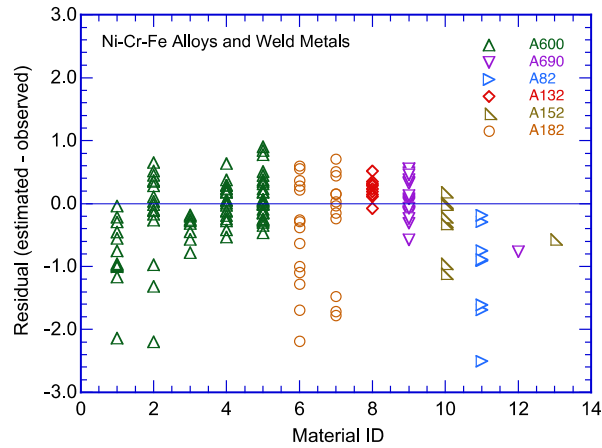
**Figure 117. Experimental fatigue lives vs. fatigue lives predicted from the JNES  $F_{en}$  expression for Ni-Cr-Fe alloys and associated weld metals in simulated (a) BWR and (b) PWR environments.**

For Ni-Cr-Fe alloys, the residual errors did not show significant patterns such as changing variances or nonzero slopes. The residual errors for each variable, grouped by steel type, were plotted, as shown in Fig. 118 for Ni-Cr-Fe wrought and weld alloys in LWR environments. The residuals were determined from the difference between the logarithms of the estimated lives and the predicted lives. Therefore, negative residual errors corresponded to conservative estimates of fatigue lives and positive residual errors corresponded to nonconservative estimates of fatigue lives. The results did not reveal any unexplained patterns. In general, high observed variances tended to be associated with longer lives and lower strain amplitudes. Furthermore, any observed biases were traceable to heat-to-heat variations. For example, the

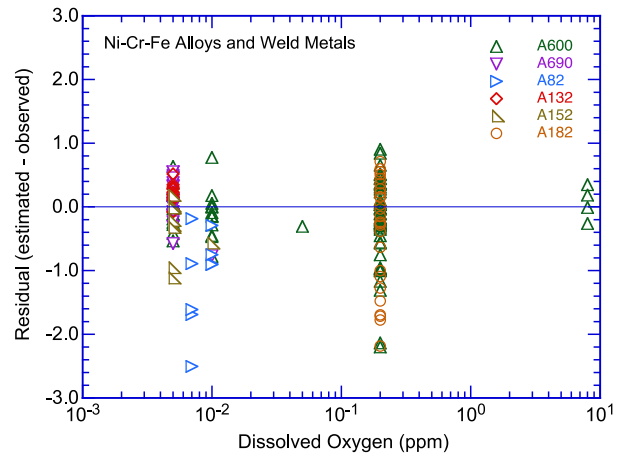
negative residuals for Alloy 82 weld metal were likely due to superior fatigue properties of the material relative to that of Alloy 600. Most of the compositions of Ni-Cr-Fe alloys that were tested in LWR environments were also tested in air. The residual errors for the best fit of the fatigue  $\epsilon$ -N data for Ni-Cr-Fe alloys in air were plotted as a function of the material ID, as shown in Fig. 119. Most of the data subsets for fatigue tests in air followed the same trends as those observed in LWR environments. For example, except for the data subset associated with Material ID #42, the other four data subsets for Alloy 82, including Material ID #51, yielded predominantly negative residuals in air. These results indicated that environmental effects on the fatigue lives of Ni-Cr-Fe alloys in LWR environments were reasonably estimated by the updated  $F_{en}$  expression.

A threshold strain amplitude (one-half of the applied strain range) was also defined, below which LWR coolant environments had insignificant effects on fatigue lives, i.e.,  $F_{en} = 1$ . The threshold value for strain amplitude was assumed to be the same as that for austenitic SSs, or 0.10% (195 MPa, or 28.3 ksi). Further details for incorporating environmental effects into fatigue evaluations for Ni-Cr-Fe materials are presented in Appendix A.

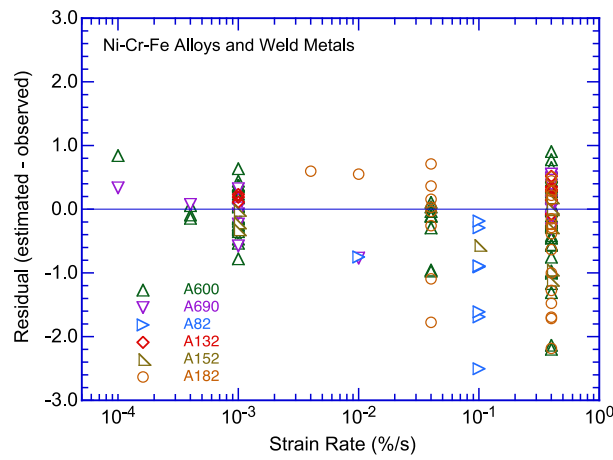
- *Due to significantly less available data for Ni-Cr-Fe materials compared to carbon and low-alloy steels and austenitic SSs, the updated austenitic SS  $F_{en}$  expression may be used to incorporate environmental effects into ASME Code Section III fatigue evaluations for Ni-Cr-Fe materials. The modified rate approach may also be used for Ni-Cr-Fe materials. Appendix C of this report presents a sample application of the  $F_{en}$  methodology.*



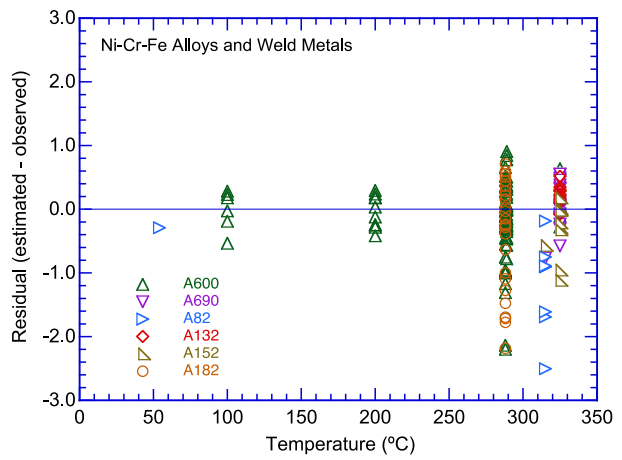
(a)



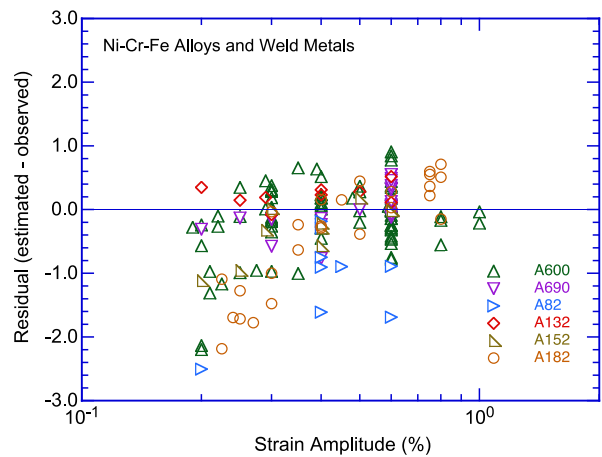
(b)



(c)



(d)



(e)

**Figure 118.**  
Residuals for predicted fatigue lives of Ni-Cr-Fe alloys and associated weld metals as a function of (a) material ID, (b) water DO content, (c) strain rate, (d) temperature, and (e) strain amplitude.

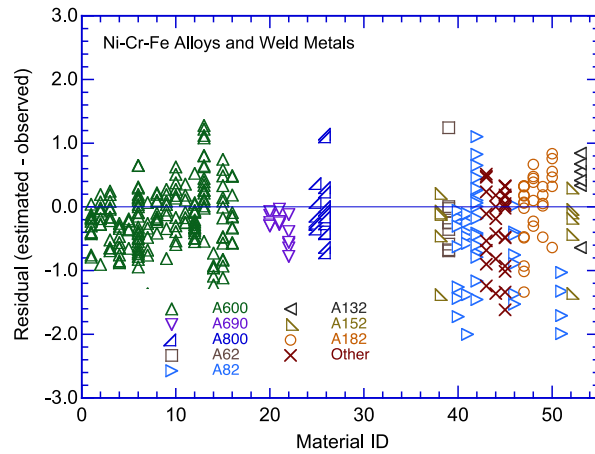


**Figure 119.**  
Residuals for predicted fatigue lives of Ni-Cr-Fe alloys and associated weld metals in air as a function of ANL Material ID.



## 5 ADJUSTMENT FACTORS IN ASME CODE FATIGUE DESIGN CURVES

---

Conservatisms in ASME Code Section III fatigue evaluations typically arise from (a) the fatigue evaluation procedures and assumptions implemented by the analyst, and/or (b) the fatigue design curves. The overall conservatisms in ASME Code Section III fatigue evaluations were demonstrated in fatigue tests on components.<sup>234,235</sup> Mayfield et al.<sup>234</sup> showed that, in air, the factors on the number of cycles to failure for elbows and tees ranged from 40 to 310 and 104 to 510, respectively, for austenitic SSs and 118 to 2,500 and 123 to 1,700, respectively, for carbon steels. The factors for girth butt welds were significantly lower, ranging from 6 to 77 for SSs and from 14 to 128 for carbon steels. Data obtained by Heald and Kiss<sup>235</sup> on 26 piping components at room temperature and 288°C showed that the adjustment factors for cracking exceeded a factor of 20, and for most of the components, it was greater than a factor of 100. In these tests, fatigue lives were expressed as the number of cycles for the crack to penetrate through the wall thickness of the test specimens, which ranged in thicknesses from 6 to 18 mm. Consequently, depending on the wall thickness, the actual factors to initiate a finite crack (e.g., to form a 3-mm-deep crack) were estimated to be a factor of 2 to 3 lower.

Deardorff and Smith<sup>236</sup> discussed the types and extent of conservatisms present in ASME Code Section III fatigue evaluation procedures and the effects of LWR environments on fatigue adjustment factors. The sources of conservatisms in the procedures included (a) the use of design transients that were significantly more severe than those experienced in service, (b) conservative grouping of transients, and (c) the use of simplified elastic-plastic analyses that led to higher stresses. The authors estimated that the ratio of the CUFs computed with the mean experimental air fatigue curve for test specimen data in air to those obtained using more accurate values of the stresses and calculated CUFs using the ASME Code Section III air fatigue design curve were approximately 60 and 90, respectively, for PWR and BWR nozzles. The reductions in these factors caused by environmental effects were estimated to be factors of 5.2 and 4.6 for PWR and BWR nozzles, respectively. Thus, Deardorff and Smith<sup>236</sup> argued that, after accounting for environmental effects, factors of 12 and 20 on life for PWR and BWR nozzles, respectively, were available to account for uncertainties due to material variability, surface finish, size, mean stress, and loading sequence.

However, other studies on piping and components indicated that the ASME Code Section III fatigue design procedures do not always contain large conservatisms.<sup>237,238</sup> Southwest Research Institute performed fatigue tests in room-temperature water on 0.91-m (36-in) diameter carbon and low-alloy steel vessels.<sup>237</sup> In the low-cycle regime, approximately 5-mm (0.2-in) deep cracks were initiated slightly above the number of cycles predicted by the ASME Code Section III fatigue design curve (Fig. 120a). Battelle-Columbus conducted tests on 203-mm (8.0-in) and 914-mm (36.0-in) carbon steel pipe welds at room temperature in an inert environment, and Oak Ridge National Laboratory (ORNL) performed four-point bend tests on a 406-mm (16.0-in) diameter Type 304 SS pipe removed from the C-reactor at the Savannah River site.<sup>238</sup> The results showed that the number of cycles to produce leaks was lower than predicted from calculations using the ASME Code Section III fatigue design curves (Fig. 120). In the case of the ORNL “tie-in” and flawed “test” welds, the specimens cracked completely through the 12.7-mm (0.5-in) wall thickness, and the number of cycles to initiate a 3-mm crack was shorter than the cycles predicted using the ASME Code Section III fatigue design curve. These and other similar tests indicate that other factors, such as environmental effects, may eliminate much of the conservatism that may be present in ASME Code calculations.

Much of the margin in ASME Code Section III fatigue evaluations arises from design procedures (e.g., stress analysis rules and assumptions) that, as discussed by Deardorff and Smith,<sup>236</sup> are

quite conservative. However, the Section III of the ASME Code is not fully prescriptive, so there is a wide variation in the specific procedures that are applied to fatigue evaluations by different analysts. For example, modern computer capabilities, particularly modern finite element methods, fatigue monitoring, and improved  $K_e$  factors, allow for evaluation refinements that significantly decrease the conservatisms traditionally applied in fatigue evaluation procedures performed in the past.

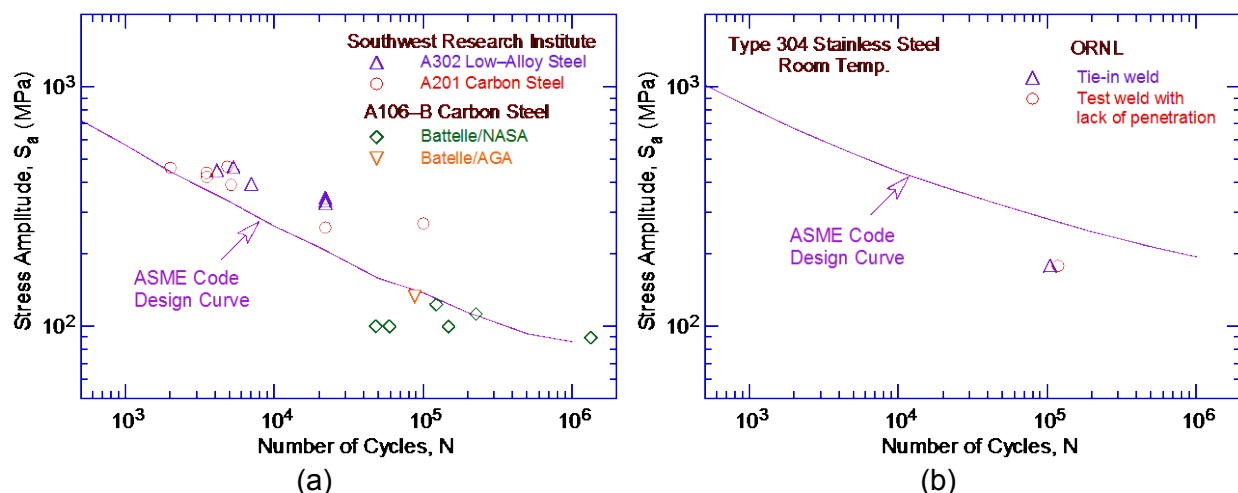


**Figure 120. Fatigue data for (a) carbon and low-alloy steel and (b) Type 304 stainless steel components (Refs. 237,238).**

The factors of 2 on stress and 20 on cycles used in the ASME Code Section III air fatigue design curves were intended to cover the effects of variables that influence fatigue lives but were not investigated in the laboratory tests that provided the data for the curves. It is therefore not clear how much conservatism is embedded in the particular values of 2 and 20. A study sponsored by the PVRC to assess the factors of 2 and 20 used in the development of the ASME Code Section III air fatigue design curves concluded that these factors should not be changed due to their being too many unknowns.<sup>239</sup>

The variables that can affect fatigue lives in air and LWR environments are broadly classified into three groups:

- (a) Material
  - (i) Composition
  - (ii) Metallurgy: grain size, inclusions, orientation within a forging or plate
  - (iii) Processing: cold work, heat treatment
  - (iv) Size and geometry
  - (v) Surface finish: fabrication surface condition
  - (vi) Surface preparation: surface work hardening
- (b) Loading
  - (i) Strain rate: rise time
  - (ii) Sequence: cycle counting, linear damage summation or Miner's rule
  - (iii) Mean stress
  - (iv) Biaxial effects: constraints
- (c) Environment
  - (i) Water chemistry: DO, lithium hydroxide, boric acid concentrations
  - (ii) Temperature
  - (iii) Flow rate

The existing fatigue  $\epsilon$ -N database covers an adequate range of material parameters (a(i-iii)), one loading parameter (b(i)), and environmental parameters (c(i-ii)); therefore, the variability and uncertainty in fatigue lives due to these parameters were incorporated into the revised ANL models described in Chapter 4. The existing data are conservative with respect to the effects of surface preparation because the fatigue  $\epsilon$ -N data were obtained for specimens that were free of surface cold work, which tends to improve fatigue performance due to the introduction of favorable compressive surface residual stresses. Fabrication procedures for fatigue test specimens generally followed American Society for Testing and Materials (ASTM) guidelines, which required that the final polishing of the specimens avoided surface work-hardening. Biaxial effects were covered by design procedures and were not considered in the ASME Code Section III fatigue design curves.

As discussed in Sections 4.1.9 and 4.2.11, under conditions that were typical of operating BWRs, environmental effects on the fatigue lives were a factor of approximately 2 lower at high flow rates (7 meters/second) compared to those at very low flow rates (0.3 meters/second or lower) for carbon and low-alloy steels and were independent of flow rate for austenitic SSs.<sup>25,26</sup> However, because of the uncertainties in the flow conditions at or near the locations of crack initiation, the beneficial effects of flow rate on the fatigue lives of carbon and low-alloy steels was not included in the revised ANL models described in Chapter 4.

Thus, the contributions of four groups of variables, namely, material variability and data scatter, specimen size and geometry, surface finish, and loading sequence (Miner's rule), were considered in the ANL investigations for developing revised fatigue design curves applicable to components.

## 5.1 Material Variability and Data Scatter

The effects of material variability and data scatter were included in the ANL investigations to ensure that the design curves encompass the available test data well and adequately describe the fatigue lives of the much larger number of heats of material that are found in the field. The effects of material variability and data scatter were evaluated for various materials by considering the best-fit curves determined from tests on individual heats of materials or loading conditions as samples of the much larger population of heats of materials and service conditions of interest. The fatigue behaviors of each of the heats or loading conditions were characterized by the values of the constant A in Eq. 6. The values of A for the various data sets were ordered, and median ranks were used to estimate the cumulative distribution of A for the entire population. The distributions were fit to lognormal curves. Further details of heat-to-heat variability of fatigue lives in air and LWR environments are discussed, respectively, in Sections 3.1.7 and 4.1.13 for carbon and low-alloy steels and in Sections 3.2.7 and 4.2.15 for cast and wrought austenitic SSs. The results indicated that the revised  $F_{en}$  expressions presented in this report adequately capture the effects of LWR environments on the fatigue lives of carbon and low-alloy steels and austenitic SSs. After accounting for the environmental effects from the experimental fatigue lives in LWR environments, the resultant fatigue lives showed good agreement with the fatigue lives that are expected for the materials in air. The results also indicated that the statistical data presented in the original revision to NUREG/CR-6909 remain valid and were therefore not updated.

The median values of A and the standard deviations for the sample of data available for each material that were presented in the original version of NUREG/CR-6909 are listed in Table 13. These values did not change significantly based on the reevaluation of the larger database used for this report so they were not changed. The 95/95 values of the factors on the median values to account for material variability and data scatter for the samples of heats of materials used in

the present evaluation were determined as 2.8, 2.1, and 2.3 for carbon steels, low-alloy steels, and austenitic SSs, respectively. These factors applied to the mean values of fatigue lives determined from the ANL models provide 95% confidence that the fatigue lives of the 95<sup>th</sup> percentile of the materials of interest were greater than the resultant values estimated from the ANL model.

**Table 13. Statistical information for the constant A used to evaluate material variability and data scatter.**

	Air Environment		
	Median Value of A	Standard Deviation	Number of Data Sets
Carbon Steel	6.583	0.477	17
Low-Alloy Steel	6.449	0.375	32
Stainless Steel	6.891	0.417	51

## 5.2 Size and Geometry

The effect of specimen size on fatigue lives were reviewed in earlier reports.<sup>12,46</sup> Various studies concluded that “size effects” are not significant in the design curve factors when the fatigue curves were based on data from axial strain controlled specimens rather than bending test specimens. No intrinsic size effects were observed for smooth specimens tested in axial loading or plain bending. However, size effects did occur in rotating bending test specimens; the fatigue endurance limits decreased by approximately 25% if the specimen sizes were increased from 2 to 16 mm, but the limits did not decrease further with larger sizes. Also, some effects of size and geometry were observed on small-scale-vessel tests conducted at the Ecole Polytechnique in conjunction with the large-size-pressure-vessel tests carried out by the Southwest Research Institute.<sup>237</sup> The tests at the Ecole Polytechnique were conducted in room-temperature water on 19-mm (0.75-in) thick shells with a 305-mm (12.0-in) inner diameter that contained nozzles made of machined bar stock. The results indicated that the fatigue lives determined from tests on the small-scale-vessels were 30–50% lower than those obtained from tests on small, smooth fatigue specimens. However, the differences in fatigue lives in these tests were not attributed to specimen size alone; rather, they were attributed to the effects of both size and surface finish.

During cyclic loading, cracks generally form at surface irregularities either already in existence or produced by slip bands, grain boundaries, second phase particles, etc. In smooth specimens, formation of surface cracks is affected by the specimen size; crack initiation is easier in larger specimens because of the increased surface areas and, therefore, an increased numbers of sites for crack initiations. However, specimen sizes are not likely to influence crack initiation in specimens with rough surfaces because cracks already initiate at existing irregularities on the rough surface. As discussed in the next section, surface roughness has large effects on fatigue lives. Consequently, for rough surfaces, the effects of specimen sizes are not appropriate for consideration in the factor of 12 applied to the fatigue design curves developed in this report. Therefore, considering all of the foregoing, a factor ranging from 1.0 to 1.4 on fatigue lives was used to incorporate size effects on fatigue lives in the low-cycle regime. This range is slightly improved over the range used in the original revision to NUREG/CR-6909 (1.2 to 1.4) to account for the fact that, in some cases, size effects were observed to be negligible.

### 5.3 Surface Finish

The effects of surface finish were considered to account for the differences in fatigue lives expected in actual components with industrial-grade surface finishes compared to the smooth polished surfaces of test specimens. Fatigue lives are sensitive to surface finish; cracks are more likely to initiate at surface irregularities that act as stress risers. The height, spacing, shape, and distribution of surface irregularities are important for crack initiation. The effects of surface finish on crack initiation are expressed by Eq. 26 in terms of the RMS value of surface roughness ( $R_q$ ).

The roughnesses of machined surfaces or natural finishes typically range from approximately 0.8 to 6.0  $\mu\text{m}$ .<sup>219</sup> Typical surface finishes for various machining processes are in the range of 0.2 to 1.6  $\mu\text{m}$  for cylindrical grinding, 0.4 to 3.0  $\mu\text{m}$  for surface grinding, 0.8 to 3.0  $\mu\text{m}$  for finish turning and drilling, and 1.6 to 4.0  $\mu\text{m}$  for milling. For fabrication processes, roughnesses range from 0.8 to 3.0  $\mu\text{m}$  for extrusion and 1.6 to 4.0  $\mu\text{m}$  for cold rolling. Thus, from Eq. 26, the fatigue lives of components with such surface roughnesses can be a factor of 2 to 3.5 lower than those of smooth specimens.

Limited data in LWR environments on specimens that were intentionally roughened indicated that the effects of surface roughness on fatigue lives were the same in air and water environments for austenitic SSs, but were insignificant in water for carbon and low-alloy steels, particularly in NWC BWR environments. However, the results for surface finish effects on carbon and low-alloy steels were limited. Therefore, additional data are needed to better define surface finish effects for carbon and low alloy steels in LWR environments. Until additional data are available to verify that surface finish effects for carbon and low-alloy steels are insignificant in LWR environments, a factor of 2.0 to 3.5 was used in the ANL investigations to account for the effects of surface finish on the fatigue lives of carbon and low-alloy steels and wrought and cast austenitic SSs. This range is slightly improved over the range used in the original revision to NUREG/CR-6909 (2.0 to 3.5) to account for the fact that, in some cases, surface finish effects of as low as a factor of 1.5 have been observed.

### 5.4 Loading Sequence

The effects of variable amplitude loading of smooth specimens were also reviewed in an earlier report.<sup>46</sup> A few cycles at high strain amplitude loading introduced into a small strain amplitude load history resulted in significantly lower fatigue lives compared to constant-amplitude loading, i.e., the fatigue limits of the materials were lower under variable loading histories.

As discussed in Section 2.1, fatigue life is conventionally divided into two stages: initiation, expressed as the number of cycles required to form MSCs on the surface, and initial propagation, expressed as the number of cycles required to propagate the MSCs to engineering size ( $\approx 3\text{ mm}$ ) – the depth at which most crack propagation analyses take over and crack initiation is considered complete. The transition from the initiation stage to the propagation stage strongly depends on the applied stress amplitude; at stress levels above the fatigue limit of the material, tests showed that the transition from the initiation stage to the propagation stage occurred at crack depths in the range of 150 to 250  $\mu\text{m}$ . However, under constant loading at stress levels below the fatigue endurance limit of the material ( $\Delta\sigma_1$  in Fig. 8), although microcracks approximately 10  $\mu\text{m}$  formed early in life, they did not grow to an engineering size. Under the variable loading conditions typically encountered during the operation of nuclear power plants, cracks created by growth of MSCs at high stresses ( $\Delta\sigma_3$  in Fig. 8) with depths larger than the transition crack depth grew to an engineering size even at continued stress levels below the fatigue limit of the material tested. Therefore, because the fatigue  $\epsilon$ -N data

used to develop the ASME Code Section III fatigue design curves were obtained from fatigue tests at constant strain amplitudes, the effects of loading sequence on the fatigue lives and the fatigue limits of materials were included in the ASME air design curves. These effects were also included in the ANL air design curves.

Studies on fatigue damage in Type 304 SS under complex loading histories<sup>240</sup> indicated that the loading sequences for decreasing strain levels (i.e., high strain levels followed by low strain levels) were more damaging than those of increasing strain levels. The fatigue lives of the steels at low strain levels decreased by factors of 2 to 4 under decreasing strain sequences. In another study, the fatigue endurance limits of medium carbon steels were lowered even after low-stress high-cycle fatigue; higher applied stresses caused greater decreases in the fatigue thresholds.<sup>241</sup> A study on Type 316NG and Ti-stabilized Type 316 SS on strain-controlled tests in air and PWR environments with constant or variable strain amplitudes reported factors of 3 or more decreases in fatigue lives under variable amplitude loading compared with constant amplitude loading.<sup>158</sup> Although the strain spectrum used in the study was not intended to be representative of actual operating plant transients, it represented a generic loading case and demonstrated the effects of variable strain amplitudes on the fatigue lives of materials.

Because variable loading histories primarily influence fatigue lives at low strain levels, the mean fatigue  $\epsilon$ -N curves were lowered to account for damaging cycles that occur below the constant-amplitude fatigue limits of the materials tested. Factors ranging from 1.0 to 2.0 were used to incorporate the possible effects of variable strain amplitudes on fatigue lives in the low-cycle regime. This range is slightly improved over the range used in the original revision to NUREG/CR-6909 (1.2 to 2.0) to account for the fact that, in some cases, loading sequence effects were observed to be negligible.

## **5.5 Air Fatigue Design Curve Adjustment Factors Summarized**

The ASME Code Section III air fatigue design curves were obtained from the mean data curves by first adjusting for the effects of mean stress using the modified Goodman relationship, and then reducing the life at each point of the adjusted curve by a factor of 2 on strain or 20 on life, whichever was more conservative. The factors on strain were needed to account for the variation in the fatigue limit of the material caused by material variability and data scatter, component size, surface finish, and load history. Because these variables affect life through their influence on the growth of short cracks (less than 100  $\mu\text{m}$ ), the adjustment on strain to account for such variations is typically not cumulative. Thus, the adjustment on strain is controlled by the variable that has the largest effect on fatigue life. In relating the fatigue lives of laboratory test specimens to those of actual reactor components, the factor of 2 on strain used to develop the ASME Code Section III air design curves was adequate to account for the uncertainties associated with material variability, component size, surface finish, and load history.

The factors on life are needed to account for variations in fatigue lives in the low-cycle regime. Based on the previous discussions, the effects of various material, loading, and environmental parameters on fatigue lives may be summarized as follows:

- (a) The results presented in Table 13 were used to determine the factors that were applied to the mean value of fatigue life to ensure that the resultant value of fatigue life bounded the 95<sup>th</sup> percentile of the materials and loading conditions of interest.
- (b) For rough surfaces, specimen size does not significantly influence fatigue lives. However, specimen size does, in some cases, significantly affect fatigue lives for smooth specimens.

Absent additional test data that indicate otherwise, factors ranging from 1.0 to 1.4 on fatigue lives were used in the reanalysis of the larger fatigue database to incorporate size effects on fatigue lives.

- (c) Factors ranging from 1.5 to 3.5 were used to incorporate the effects of surface finish on fatigue lives in air. Limited data indicate that, for carbon and low-alloy steels, the effects of surface roughness on fatigue lives may be insignificant in LWR environments. Therefore, a lower factor of 2.0 was used for carbon and low-alloy steels in water environments instead of the factors ranging from 1.5 to 3.5 that were used for these steels in air. A factor of 2.0 was used for austenitic SSs in both air and water environments for surface finish effects.
- (d) Variable loading histories primarily influence fatigue lives at low strain levels (i.e., in the high-cycle regime), so the mean air fatigue  $\epsilon$ -N curves were adjusted by a factor of 2.0 on strain to account for damaging cycles that occur below the constant-strain fatigue limit of the material. Factors ranging from 1.0 to 2.0 were used to incorporate the possible effects of load histories on fatigue lives in the low-cycle regime.

The subfactors needed to account for the effects of the various material, loading, and environmental parameters on fatigue lives are summarized in Table 14. The total adjustment on life varies from 4.7 to 27.4. However, because the maximum value represents relatively poor heats of materials and assumes the maximum effects of size, surface finish, and loading history, the maximum value of 27.4 is overly conservative to apply depending on the confidence bounds desired. A value of 12 was used to develop the air design curves from the mean-data air curves to be consistent with the initial version of this report. However, based on Monte Carlo statistical evaluation, a value of 10 was justified as discussed below.

**Table 14. Factors on life applied to the mean fatigue  $\epsilon$ -N air curve to account for the effects of various material, loading, and environmental parameters.**

Parameter	Section III Criterion Document	Present Report
Material Variability and Data Scatter		
(minimum to mean)	2.0	2.1–2.8
Size Effect	2.5	1.0–1.4
Surface Finish, etc.	4.0	1.5–3.5
Loading History	–	1.0–2.0
Total Adjustment	20	4.7–27.4

To determine the most appropriate value for the adjustment factor on fatigue life, Monte Carlo simulations were performed using the material variability and data scatter results given in Table 13, and the factors needed to account for the effects of size, surface finish, and loading history listed in Table 14. A lognormal distribution was assumed for the effects of size, surface finish, and loading history, and 5th and 95th percentile values were assumed to represent the minimum and maximum values of the adjustment factors (i. e., 1.0 and 1.4 for size, 1.5 and 3.5 for surface finish, and 1.0 and 2.0 for loading history, respectively). A total of 25,000 simulations were performed for each material. The median value, standard deviation, and 95<sup>th</sup> percentile values for the factor were, respectively, 5.037, 3.159, and 10.233 for carbon steels, 4.830, 2.558, and 9.037 for low-alloy steels, and 4.932, 2.864, and 9.643 for austenitic SSs. The 95<sup>th</sup> percentile values for the factors that were applied to the best-fit mean air data curves to obtain the design fatigue  $\epsilon$ -N air curves are given in Table 15. The factor that was applied to the mean data curves for test specimens to obtain component curves that bounded 95% of the population ranged from 9.0 to 10.2 for carbon, low-alloy, and austenitic stainless steels,

respectively, as shown in Table 15. Plots of the cumulative distribution of the values of constant A for best-fit mean data air curves and for the adjusted design air curves are shown in Fig. 121 for carbon, low-alloy, and austenitic stainless steels.

The average value for the factor for application to the best-fit mean air curves for the three materials to obtain air fatigue design curves that are applicable for reactor components is 9.6. Note that the selection of 95<sup>th</sup> percentile value for the factor was arbitrary, but is consistent with NRC practice. As a comparison, the corresponding 98<sup>th</sup> percentile values for the factors are 11.5, 10.1, and 10.8, respectively, for carbon, low-alloy, and austenitic stainless steels (or an average value of 10.8).

The results of the reanalysis of the fatigue adjustment factors indicate that, for all materials, the current ASME Code Section III use of a factor of 20 on cycles to account for the effects of material variability and data scatter, as well as specimen size, surface finish, and loading history, may contain as much as a factor of 2.0 conservatism (i.e., 20/10 considering the average factor of 9.6 obtained from Table 15). To reduce this conservatism, fatigue design air curves were derived from the mean data curves by first correcting for mean stress effects using the modified Goodman relationship, and then reducing the mean-stress adjusted curve by a factor of 2 on stress and 12 on cycles, whichever was more conservative. Fatigue design curves that were developed from the ANL fatigue life models using this procedure for carbon and low-alloy steels are presented in Section 3.1.11 and for wrought and cast austenitic SSs in Section 3.2.11. The selection of bounding the 95th percentile of the population for a design curve was made under the presumption that the design curve controls fatigue initiation, not failure. The choice also recognized that there were conservatisms implied in the choice of log normal distributions, which have infinite tails, and in the identification of values of the effects as 95th percentile values. Finally, the results of the present analysis indicate that the conservatism in the ASME Code Section III fatigue design air curves may be further reduced by using a factor of 10 on life instead of the factor of 12 on life used in the fatigue design air curves presented in this report for carbon, low-alloy, and wrought and cast austenitic stainless steels.

**Table 15. Factor applied to the mean values of fatigue life to bound 95% of the data population.**

Material	Air Environment
Carbon Steels	10.2
Low-Alloy Steels	9.0
Austenitic Stainless Steels	9.6



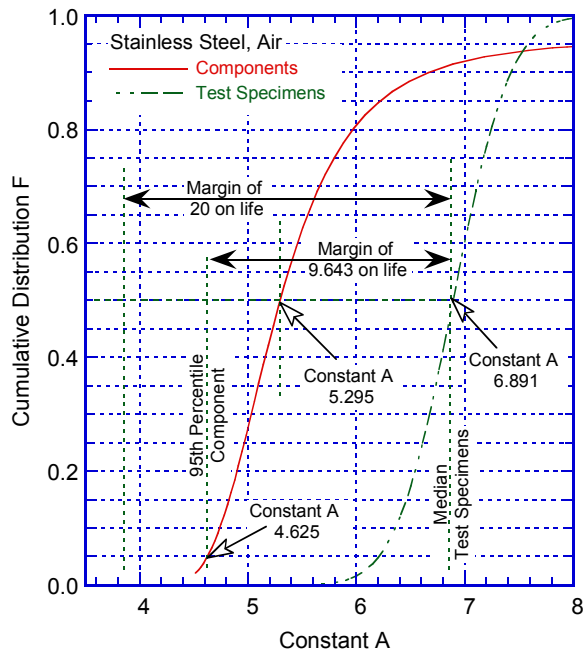
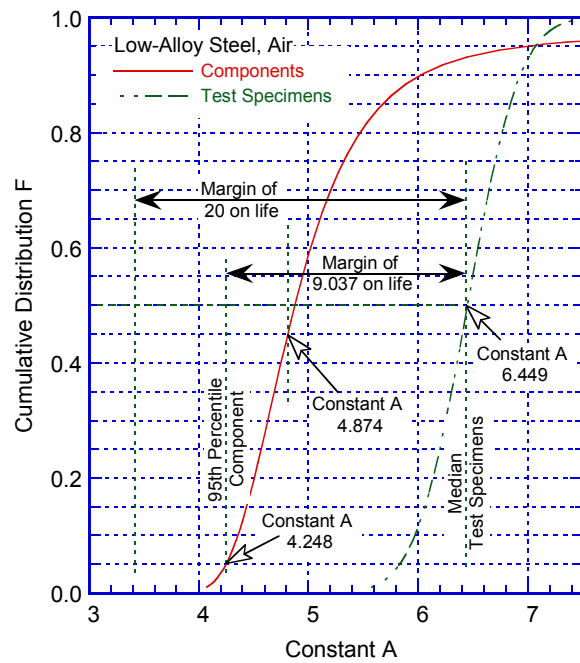
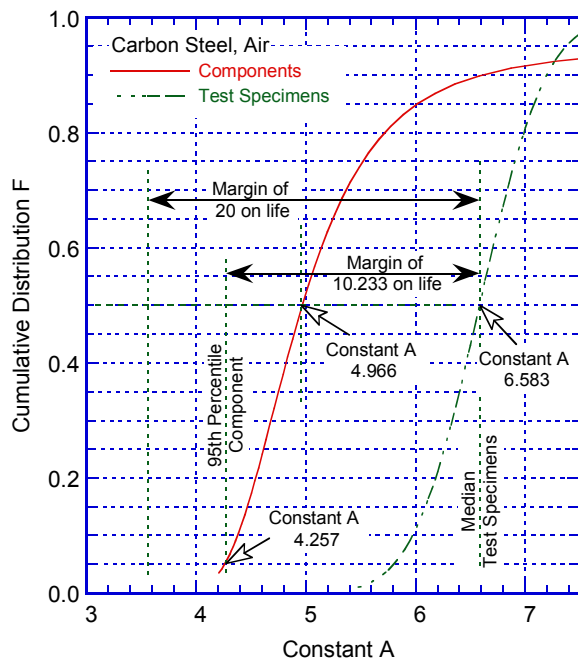


**Figure 121.**  
Estimated cumulative distribution of parameter A in the ANL models that represent the fatigue lives of test specimens and actual components in air.



## 6. VALIDATION OF $F_{en}$ EXPRESSIONS

The updated  $F_{en}$  expressions were validated by comparing calculated results from six experimental data sets with estimates of fatigue lives based on the updated  $F_{en}$  expressions. The intent of the calculations was only to validate the accuracy of the revised  $F_{en}$  expressions. The experimental data sets evaluated included the following:

1. Tests with changing strain rates within each strain cycle.<sup>136</sup>
2. Tests performed by VTT on small specimens with either constant or spectrum strain cycling (i.e., an amplitude sequence of a narrow band randomized block of 50 strain cycles that was repeated until specimen failure).<sup>158,159</sup>
3. Tests performed by Areva on small specimens with triangular and complex strain cycles of cold and hot thermal shock associated with a simulated safety injection transient.<sup>155-157</sup>
4. EPRI U-bend tests in inert (dry nitrogen) and PWR environments.<sup>97-99</sup>
5. Tests with changing strain rate and temperature within each strain cycle.<sup>154</sup>
6. Bettis laboratory thermal fatigue tests of a stepped pipe of differing thicknesses exposed to temperature cycles between 38 and 343°C (100 and 650°F).<sup>160</sup>

Since the experimental data sets were tested to crack initiation (i.e., CUF greater than unity), the goal of these evaluations was to benchmark the  $F_{en}$  methodology against the predictions of failures and, if warranted, make appropriate adjustments to the  $F_{en}$  expressions. In the tests evaluated, fatigue failure was defined as the number of cycles to (a) form a finite crack or (b) decrease the cyclic tensile stress by 25% from its peak (steady-state) value. The following three methods were used to calculate the environmental correction factor,  $F_{en}$ , which was applied to the number of loading cycles in air to estimate the number of loading cycles in the environment.

*Strain-Integrated Method:* In this method, the applied strain cycle was divided into small time intervals, and the environmental correction factor,  $F_{en}$ , was determined at each time interval using the modified rate approach and the updated  $F_{en}$  expressions. In addition,  $F_{en}$  was calculated using expressions presented in the initial version of NUREG/CR-6909 for comparative purposes. In these calculations, the overall integrated  $F_{en}$  was expressed as

$$F_{en} = \frac{\sum F_{enj}(\epsilon_i - \epsilon_{i-1})}{(\epsilon_{max} - \epsilon_{min})}, \quad (66)$$

where  $\epsilon_{min}$  and  $\epsilon_{max}$ , respectively, are the minimum and maximum values of strain, and  $\epsilon_i$  and  $F_{en,i}$  are the strain and  $F_{en}$  at the  $i^{th}$  increment of strain. The summation was only applied when the strain increment was positive. In addition, a threshold strain,  $\epsilon_{th}$ , was also considered to compute the overall  $F_{en}$ . Consideration of a threshold strain assumes that, during a strain cycle, environmental effects are significant only after the applied strain exceeds the threshold value. Thus,

$$F_{en} = \frac{\sum F_{enj}(\epsilon_i - \epsilon_{i-1})}{\epsilon_{max} - (\epsilon_{min} + \epsilon_{th})}. \quad (67)$$

*Simplified Method:* In this method the overall  $F_{en}$  was determined for the entire period of the strain cycle where the strain rate was greater than zero (i.e., increasing strain) and used the average temperature and average strain rate for the interval. The average values were determined using an average (i.e., straight line) from the valley to adjacent peak strain. As

before, the overall  $F_{en}$  was computed from both the updated  $F_{en}$  expressions and the expressions in the initial version of NUREG/CR-6909.

**Multi-Linear Strain Based Method:** This method is a modified version of the simplified method. Depending on the strain-time profile, the applied strain cycle was divided into two or more linear ramps within which the strain rate was positive. The overall  $F_{en}$  was determined for each ramp using the updated and the original NUREG/CR-6909  $F_{en}$  expressions. Also, average values of temperature and strain rate were used in the  $F_{en}$  calculations for each ramp. The overall  $F_{en}$  was defined as

$$F_{en} = \frac{(F_{en,1}\Delta\varepsilon_1 + F_{en,2}\Delta\varepsilon_2 + \dots)}{(\Delta\varepsilon_1 + \Delta\varepsilon_2 + \dots)}, \quad (68)$$

where  $\Delta\varepsilon_1$  and  $\Delta\varepsilon_2$  are the first and second strain increments, and  $F_{en,1}$  and  $F_{en,2}$  are the  $F_{en}$  values for the first and second strain increments. Overall  $F_{en}$  values were calculated for each dataset using the foregoing three methods. The results were compared with the experimental values to benchmark the revised  $F_{en}$  methodology and to provide insights as to which computational methods yielded the most consistent and reliable results. The results associated with the changing strain rates within each cycle were presented in Section 4.1.3 as a part of the discussion associated with the threshold strain amplitude and, therefore, are not duplicated in this section. In addition, the assessments to estimate the overall  $F_{en}$  for the thermal fatigue tests of a stepped pipe indicated that the reported estimates of the total applied strain (elastic and plastic) were not reliable. NRC was not able to complete additional finite element analyses to provide meaningful thermal strain values for use in the evaluation. As a result, the dataset for the stepped pipe thermal fatigue tests was not considered further and those results are not included in this report. The results of the remaining four datasets are discussed in the following sections.

## 6.1 Spectrum Straining

Low-cycle, strain-controlled, completely-reversed fatigue tests were conducted on Type 316NG and Ti-stabilized 316 (O8X8H10T steel) austenitic SSs in air and simulated PWR environments using cylindrical specimens with a 4-mm diameter and a 10-mm gage length.<sup>158</sup> Test specimens were fabricated from a 12-mm diameter round bar of Type 316NG SS. A 300-mm diameter, 16-mm thickness pipe was fabricated from the Ti-stabilized 316 material. The test specimens were smooth, but not polished. The chemical composition and tensile properties of the two materials are given Table 16. Pneumatic bellows, designed and developed by Valtion Teknillinen Tutkimuskeskus (VTT), which is the Technical Research Centre of Finland, were used for accurate control of strain. Fatigue tests were conducted on the Type 316NG SS specimens in a simulated PWR environment at 320°C. For the Ti-stabilized 316 SS specimens, fatigue tests were conducted in a simulated Voda-Vodyanoi Energetichesky Reaktor (VVER) Russian reactor environment at 293°C. Both steels were also tested in air at room temperature (25°C). Further details of the environmental conditions are given in Table 17.

**Table 16. Chemical composition and tensile strength of test materials for the constant and spectrum strain amplitude fatigue tests.**

Material	Chemical Composition (wt. %)									Min. YS (MPa)	Min. UTS (MPa)	Min. Elong. (%)
	C	Si	Mn	Ni	Cr	Mo	V	Cu	Ti			
316NG	0.01	0.60	1.40	11.2	16.9	2.60	-	-	-	250	570	-
Ti-stab.	0.08	0.39	1.36	10.5	18.2	0.17	0.05	0.18	0.62	330	595	-

**Table 17. Environmental conditions for the constant and spectrum strain amplitude fatigue tests.**

Test Condition	For Type 316NG SS	For Ti-Stabilized 316 SS
Temperature	320°C	293°C
Pressure	125 bar	100 bar
pH at RT	5.1	7.2
Conductivity	2 to 40 µmho/cm	80 to 90 µmho/cm
Dissolved Oxygen	< 0.01 ppm	< 0.01 ppm
Chlorides	< 0.15 ppm	< 0.05 ppm
Fluorides	< 0.15 ppm	< 0.01 ppm
Dissolved Hydrogen	25 to 35 cm <sup>3</sup> /kg	30 to 35 cm <sup>3</sup> /kg
Boric Acid	2500 ppm	2750 ppm
To adjust pH 7.0	Lithium	Kalium

Constant and variable strain amplitude fatigue tests were performed using a sinusoidal waveform. For spectrum loading, an amplitude sequence of a narrow-band, randomized block of 50 strain cycles, as shown in Fig. 122, was repeated until specimen failure occurred, which was defined as a 25% decrease in load from the steady state value. The spectrum straining data were transformed to equivalent constant amplitude  $\epsilon$ -N data as follows:

$$\epsilon_{a,eq} = \frac{\sum \{n_i D_i (\epsilon_{a,i})\}}{\sum \{n_i D_i\}}, \quad N_{eq} = \sum \left\{ n_i \left( \frac{D_i}{D_i(\epsilon_{a,eq})} \right) \right\}, \quad (69)$$

where  $N_{eq}$  and  $\epsilon_{a,eq}$  are, respectively, the equivalent number of cycles and strain amplitude under constant strain loading, and  $n_i$  is the number of cycles at strain amplitude  $\epsilon_{a,i}$  under spectrum loading and  $D_i$  is an arbitrary damage function associated with that fatigue loading, and is given by

$$D_i = \frac{1}{N_f} = f(\epsilon_a). \quad (70)$$

**Figure 122.**  
**Schematic of the repeated sequence of randomized block of 50 strain cycles (Ref. 158).**

The results yielded an equivalent strain amplitude at the mean damage level representative of the spectrum straining and the number of equivalent cycles that provided an identical damage sum (i.e., usage factor) for the equivalent straining and the original spectrum straining. Thus, the results were directly comparable and, therefore, were plotted on common graphs. The test conditions and a summary of the results are given in Table 18. The fatigue  $\epsilon$ -N data on Type

316NG and Ti-stabilized 316 SSs in air and PWR environments using constant and spectrum strain amplitude loading are shown in Fig. 123.

**Table 18. The conditions and results of fatigue tests on austenitic SSs obtained under constant and spectrum strain amplitude loading.**

Environment	Strain Rate (%/s)	$\epsilon_a$ (%)	Equiv. $\epsilon_a$ (%)	$N_f$	$N_{eq}$	Estimated <sup>a</sup> $N_{air}$	Estimated $F_{en}$	Predicted <sup>b</sup> $N_f$
<u>Type 316NG SS</u>								
Air 25°C	1.020	0.510	0.510	6,120	6,120	5,767	-	9,227
Air 25°C	0.620	0.310	0.310	47,000	47,000	22,036	-	35,257
Air 100°C	0.170	0.420	0.420	15,600	15,600	9,434	-	15,095
Air 25°C	0.800	0.20-0.80	0.535	9,650	3,260	5,130	-	4,104
PWR 320°C	0.020	0.508	0.508	1,400	1,400	5,823	4.88	1,908
PWR 320°C	0.016	0.040	0.400	2,650	2,650	10,732	5.17	3,321
PWR 320°C	0.013	0.315	0.315	6,660	6,660	21,005	5.45	6,165
PWR 320°C	0.013	0.315	0.315	7,800	7,800	21,005	5.45	6,165
PWR 320°C	0.065	0.19-0.78	0.529	1,250	384	5,273	3.62	1,167
PWR 320°C	0.039	0.11-0.48	0.359	4,600	883	14,413	4.12	2,799
<u>Ti-Stabilized 316 SS</u>								
Air 25°C	1.000	0.500	0.500	4,590	4,590	6,056	-	9,689
Air 25°C	0.980	0.350	0.350	26,700	26,700	15,477	-	24,764
Air 25°C	0.920	0.230	0.230	362,900	362,900	59,526	-	95,242
Air 25°C	1.000	0.20-0.80	0.536	6,900	2,282	5,107	-	4,086
Air 25°C	1.000	0.12-0.50	0.359	21,900	4,367	14,413	-	11,530
Air 25°C	1.000	0.12-0.50	0.372	36,350	7,250	13,061	-	10,449
Air 25°C	1.000	0.072-0.30	0.238	450,000	84,437	52,482	-	41,986
VVER 293°C	0.020	0.500	0.500	1,734	1,734	6,056	4.02	2,410
VVER 293°C	0.011	0.283	0.283	12,256	12,256	29,199	4.60	10,165
VVER 293°C	0.060	0.18-0.77	0.523	2,150	641	5,422	3.14	1,380
VVER 293°C	0.030	0.09-0.39	0.302	14,400	2,492	23,852	3.67	5,197
VVER 293°C	0.024	0.08-0.31	0.247	95,500	17,847	45,971	3.86	9,529

<sup>a</sup> Fatigue lives estimated using Eq. 29.

<sup>b</sup> For constant strain amplitude loading, fatigue lives were determined from the estimated lives in air by multiplying by a factor of 1.6 to account for heat-to-heat variability. For fatigue lives in a PWR environment, the adjusted values were divided by  $F_{en}$ . For spectrum loading, the effects of loading sequence were also included by dividing the values determined for the constant strain amplitude loading by a factor of 2.

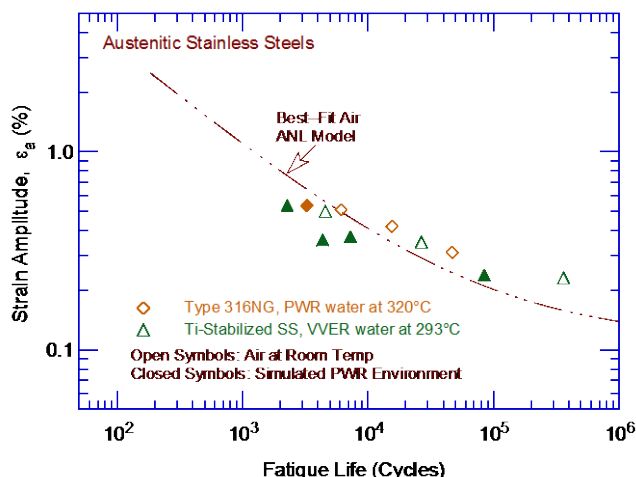


**Figure 123.**  
Fatigue strain-life data for Type 316NG SS in PWR water at 320°C and for Ti-stabilized 316 SS in VVER water at 293°C (Refs. 158,159).

The results indicated that, for the two heats of Type 316NG and Ti-stabilized 316 SSs tested, the slope of the fatigue  $\epsilon$ -N data obtained under the constant strain amplitude loading was less steep than that of the ANL best-fit mean data curve. For fatigue lives greater than  $10^4$  cycles, the experimental fatigue lives were greater than those estimated from the ANL best fit air curve. For the Ti-stabilized steel, the experimental fatigue life was a factor of 6 greater than the fatigue life estimated using the best-fit mean data curve. For both steels, the measured fatigue lives at strain amplitudes between 0.3 and 0.5% were approximately 60% greater than the estimated values. Thus, a subfactor of 1.6 was used to account for heat-to-heat variability. Note that, since all tests were conducted on smooth rather than polished specimens, this subfactor included some effects of surface finish.

The results also indicated that the fatigue  $\epsilon$ -N data obtained under spectrum strain amplitude loading were up to a factor of 5 lower than those obtained under constant strain amplitude loading. The actual differences between spectrum and constant strain amplitude loading in air and PWR environments, respectively, were factors of 2.4 and 4.4 for Type 316NG, and 3.4 and 5.2 for Ti-stabilized 316 SS. The differences were greater for a PWR environment, most likely because these tests were conducted using a sine wave loading and the estimated values were based on average strain rates. Therefore, the environmental effects were likely underestimated. However, these results demonstrated the potential effects of loading sequence, which are discussed in Section 5.4.

The predicted fatigue lives for the constant and spectrum strain loading fatigue tests are listed in the last column of Table 18. These values were determined from the fatigue lives in air ( $N_{air}$ ) estimated from Eq. 29 (seventh column of Table 18). Since these tests were conducted at constant strain rate and temperature, the predicted fatigues lives were determined by multiplying  $N_{air}$  by a factor of 1.6 to account for heat-to-heat variability (and potential effects of surface finish), and dividing the adjusted values by  $F_{en}$  to account for environmental effects. Furthermore, for spectrum loading, the effects of loading sequence were included by dividing the values determined for the constant strain amplitude loading by a factor of 2, which is the maximum subfactor proposed in Table 14 (Section 5.5) to account for the effects of loading sequence. A subfactor of 2 was used instead of the values of 3.4–5.2 measured in these tests because these tests were conducted using a sinusoidal waveform instead of a triangular waveform. Therefore, the experimental environmental effects were greater because of differences in strain rates. The subfactor to account for the effects of surface finish was not used to determine the fatigue lives, even though the test specimens were “smooth” but not polished, because the effects of surface finish were already included in the heat-to-heat

adjustment factor of 1.6 used to determine the predicted fatigue lives from the best-fit mean data curve.

The measured fatigue lives,  $N_{eq.}$ , and the predicted fatigue lives for the constant and spectrum strain loading tests are plotted in Fig. 124. The results for the constant strain amplitude loading showed very good agreement with the experimental values; the predicted fatigue lives were within a factor of 2 (i.e., within the factor for data scatter). The predicted fatigue lives for the spectrum strain amplitude loading were generally greater than the measured values because of differences in the loading waveform (sinusoidal or triangular waveforms).

- *The predicted fatigue lives showed very good agreement with the experimental values. The loading sequence effects observed in the spectrum loading tests were greater than those proposed in this study; the differences were attributed to differences in the loading waveform (e.g., sinusoidal or triangular waveforms) and the methods used to determine equivalent strain amplitude and fatigue lives.*

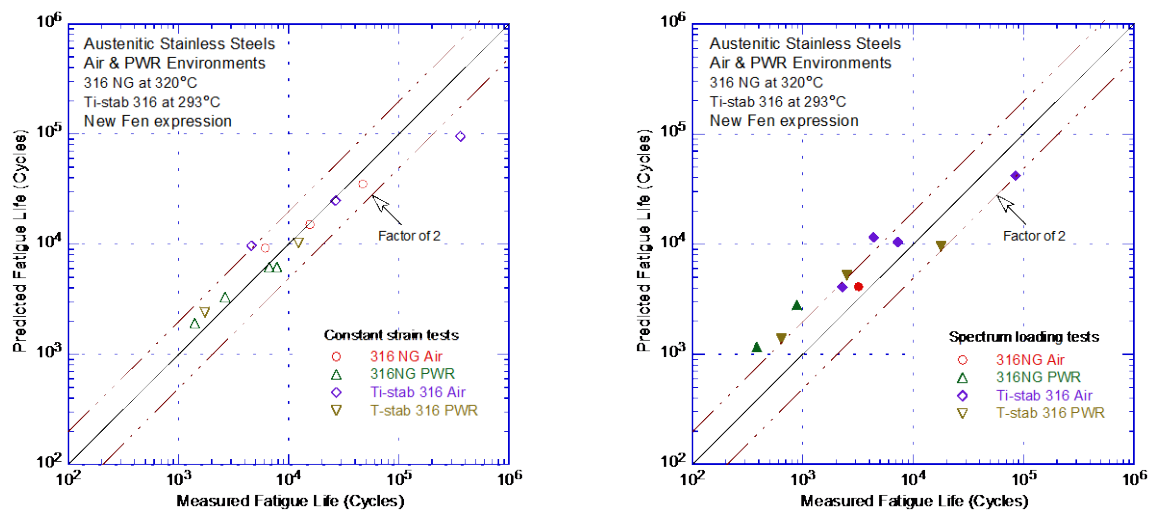


**Figure 124. Experimental and estimated fatigue lives for Type 316NG and Ti-stabilized 316 SS tested with constant and spectrum strain loading (Refs. 158,159).**

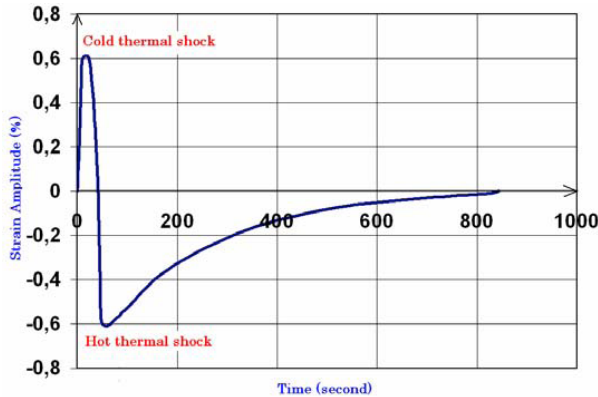
## 6.2 Complex Loading – Safety Injection Transient

Low-cycle, strain-controlled, completely-reversed fatigue tests were conducted on Type 304L austenitic SSs in a simulated PWR environment using cylindrical specimens with a 9-mm diameter and a 13.5-mm gage length.<sup>155-157</sup> The test specimens were fabricated from a 590 x 450 x 103 mm rolled plate that was water quenched. The chemical composition and tensile properties of the Type 304L SS are given Table 19. Fatigue tests were conducted on both polished and ground specimens in air and the simulated PWR environment at 300°C using a triangular loading waveform and a waveform that simulated the typical strain history of cold and hot thermal shocks associated with a PWR safety injection transient. The actual strain cycle used in this study is shown in Fig. 125. The specimen surface finish was specified as 40  $\mu\text{m}$ , which corresponded to the material surface height between the maximum peak and minimum valley measured over a length of 4 mm. The authors noted that the machining process induced a superficial hardened layer which was not totally removed by the polishing process. The environmental conditions for the tests in the PWR environment are given in Table 20.



**Table 19. Chemical composition and tensile strength of Type 304L SS.**

Material	Chemical Composition (wt. %)									Min. YS (MPa)	Min. UTS (MPa)	Min. Elong. (%)
	C	Si	Mn	Ni	Cr	Mo	V	Cu	Ti			
304L	0.025	0.37	1.687	9.12	18.3	0.38	-	0.217	-	255	573	64

**Figure 125.**  
Typical strain cycle of cold and hot thermal shocks corresponding to a PWR safety injection transient (Ref. 155).**Table 20. Environmental conditions for fatigue tests in simulated PWR environment.**

Test Condition	Value
Temperature	300°C
Pressure	140 bar
Conductivity	2 to 40 $\mu\text{S}/\text{cm}$
Dissolved Oxygen	< 0.1 ppm
Chlorides, Fluorides	< 0.15 ppm
Dissolved Hydrogen	25 to 35 $\text{cm}^3/\text{kg}$
Boron	1000 ppm (adjusted by boric acid)
Lithium	~ 2 ppm (adjustment for pH)

Strain-controlled fatigue tests were conducted in both air and the PWR environment at 300°C using a triangular waveform to obtain the baseline data for the Type 304L SS material.<sup>155-157</sup> The results are shown on Fig. 126. The tests in air were used to establish the heat-to-heat variation of the material and surface finish effects, and the tests in the PWR environment were used to validate the estimates of fatigue lives calculated using the updated  $F_{en}$  expressions. The results indicated a small heat-to-heat variation; the fatigue lives for the heat of Type 304L SS used for these tests were 12% lower than those predicted by the best-fit mean data curve. The results also indicated that in air, fatigue lives of the ground specimens relative to those of polished specimens were decreased by a factor of 1.7.

In addition, the effects of the PWR environment on the fatigue lives of Type 304L SS at 300°C and 0.01%/s strain rate were determined from a comparison of the fatigue  $\epsilon$ -N behavior of the polished specimens in air versus those in the PWR environment. The experimental data yielded a  $F_{en}$  of 3.62 (i.e., the fatigue lives in the PWR environment were decreased by a factor of 3.62 relative to those in air). The experimental data also indicated that surface finish effects were smaller in the PWR environment than those in air. For example, the reductions in the fatigue lives of the ground specimens in a PWR environment compared to those in an air environment were a factor of 2.90 instead of the factor of 3.62 obtained for the polished specimens.

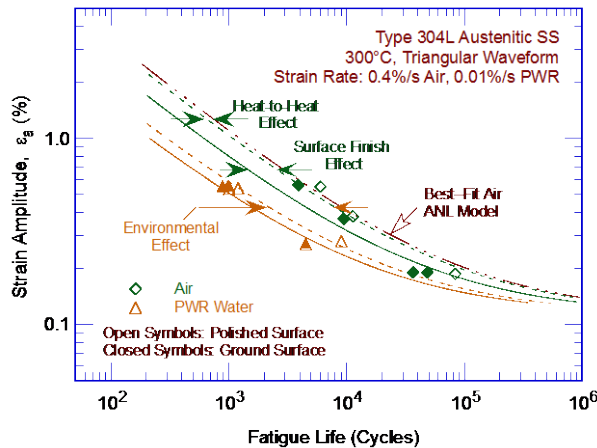


**Figure 126.**  
Fatigue strain-life data for Type 304L SS in air and PWR environments at 300°C (Refs. 155-157).

For the tests performed with a complex strain loading cycle,  $F_{en}$  values were determined using the three methods and the modified rate approach as described previously. The test conditions and results for these tests are given in Table. 21. The predicted fatigue lives were determined from the estimated fatigue lives in air (using Eq. 29) by multiplying the values by 0.88 to account for the effects of heat-to-heat variability, dividing by 1.7 to account for the effects of surface finish, and dividing by  $F_{en}$  to account for environmental effects. The overall  $F_{en}$  values were computed using the strain-integrated method (i.e., Eqs. 66 and 67 for the values without and with a strain threshold of 0.32%, respectively).

The measured fatigue lives and the predicted fatigue lives for the triangular and complex loading tests are plotted in Fig. 127. The results indicate that the predicted fatigue lives from the tests with a triangular loading waveform were in good agreement with the experimental values. The differences were within a factor of 2 (i.e., within data scatter). The predicted fatigue lives for the tests with the complex strain loading cycle were approximately a factor of 2.5 lower than the experimental values; this difference was less than a factor of 2 when the strain threshold was included in the computation of  $F_{en}$ . This behavior is considered unique to this specific strain loading cycle. Fatigue tests with other strain loading cycle profiles should be conducted to provide a better understanding of possible effects of complex loading patterns on the fatigue lives of materials. However, although the predicted lives were generally lower, the estimated values were within the range of data scatter.

For the PWR safety injection transient, the predicted fatigue lives estimated using the simplified method were 25% lower than those obtained from the modified rate approach. The predicted lives estimated using the multi-linear method (using 3 ramps) were marginally (3%) lower.

- *The predicted fatigue lives were generally lower than the experimental values; however, the values were within the range of data scatter.*

**Table 21. The conditions and results of fatigue tests on Type 304L austenitic SS at 300°C in air and PWR environments using a triangular or complex strain cycle.**

Environment / Surface Finish	Strain Rate (%/s)	$\varepsilon_a$ (%)	Measured $N_f$	Estimated <sup>a</sup> $N_{air}$	Without Strain Threshold		With Strain Threshold	
					Estimated $F_{en}$	Predicted <sup>b</sup> $N_f$	Estimated $F_{en}$	Predicted $N_f$
Triangular Waveform								
Air, Polished	0.40	0.550	6,000	4,798	1.00	4,223	-	-
Air, Polished	0.40	0.380	11,325	12,323	1.00	10,844	-	-
Air, Polished	0.40	0.187	83,500	142,104	1.00	125,051	-	-
Air, Ground	0.40	0.560	3,891	4,595	1.00	2,379	-	-
Air, Ground	0.40	0.370	9,464	13,256	1.00	6,862	-	-
Air, Ground	0.40	0.190	36,552	131,796	1.00	68,224	-	-
Air, Ground	0.40	0.190	48,717	131,796	1.00	68,224	-	-
PWR, Polished	0.01	0.540	1,002	5,016	4.97	889	-	-
PWR, Polished	0.01	0.540	1,200	5,016	4.97	889	-	-
PWR, Polished	0.01	0.280	9,000	30,209	4.97	5,353	-	-
PWR, Ground	0.01	0.550	890	4,798	4.97	500	-	-
PWR, Ground	0.01	0.550	1,000	4,798	4.97	500	-	-
PWR, Ground	0.01	0.270	4,500	33,986	4.97	3,543	-	-
Complex Strain Cycle								
PWR, Polished	variable	0.570	1,588	4,404	5.92	655	5.37	722
PWR, Polished	variable	0.570	1,936	4,404	5.92	655	5.37	722
PWR, Polished	variable	0.490	2,900	6,367	6.10	919	5.35	1,047
PWR, Polished	variable	0.290	8,318	27,034	6.73	3,535	4.35	5,469
PWR, Polished	variable	0.290	8,810	27,034	6.73	3,535	4.35	5,469
PWR, Ground	variable	0.570	895	4,404	5.92	385	4.60	425
PWR, Ground	variable	0.570	960	4,404	5.92	385	3.14	425
PWR, Ground	variable	0.290	7,330	27,034	6.73	2,079	3.86	3,217

<sup>a</sup> Fatigue lives estimated using Eq. 29.

<sup>b</sup> The predicted fatigue lives were obtained from the estimated lives in air by multiplying by a factor of 0.88 to account for heat-to-heat variability, dividing by 1.7 to account for surface finish effects, and dividing by  $F_{en}$  to include environmental effects. The differences between the  $F_{en}$  values in 6<sup>th</sup> and 8<sup>th</sup> columns are due to the consideration of a threshold strain value of 0.32% as part of the calculation of the  $F_{en}$  values shown in the 8<sup>th</sup> column.

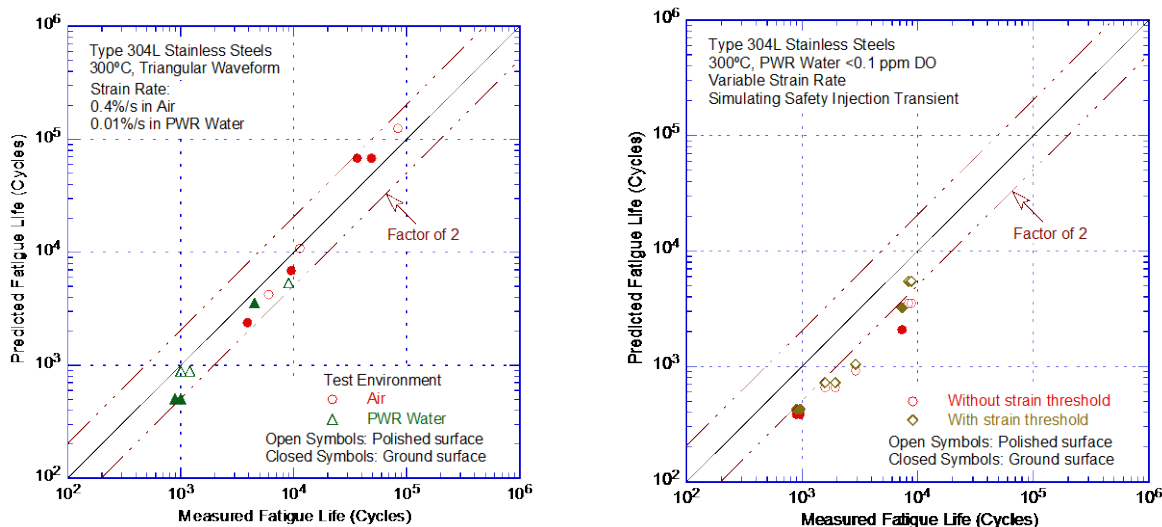


**Figure 127. The experimental and estimated fatigue lives for Type 304L SS tested at 300°C in air and a PWR environment using triangular and complex loading that simulated a PWR safety injection transient (Refs. 155-157).**

### 6.3 U-Bend Tests in Inert and PWR Water Environments

Low-cycle, corrosion-fatigue tests were conducted on Type 304L SS tube U-bend specimens in an inert (pressurized nitrogen) environment and a simulated PWR primary water environment at 240°C.<sup>97-99</sup> The primary focus of the tests was to study the effects of flow rate on fatigue crack initiation. Initially straight tubing of nominal 33.4 mm outer diameter (OD) and 3.38 mm wall thickness was used for the tests. The tubing was manufactured by cold rolling followed by solution annealing at 1100°C and water quenching. The tubing was subsequently subjected to a pickling and passivation process. The tubing material was procured from Tubacex, Spain, meeting the compositional and mechanical property requirements of SA 312 Grade Type 304L low-carbon austenitic SS. A qualified, reproducible bending procedure was used by Babcock and Wilcox, Canada, to deform the tubing into a 180° U-bend using a cold die bend with an internal mandrel. A total of ten U-bend test specimens were fabricated. A typical, as-received U-bend test specimen and the nomenclature adopted for the orientation around the circumference at the apex of the bend are shown in Fig. 128. The tensile yield strength, ultimate tensile strength, and total elongation of the material were, respectively, 245 MPa, 607 MPa, and 76.5% at room temperature and 168 MPa, 476 MPa, and 41.5% at 240°C.

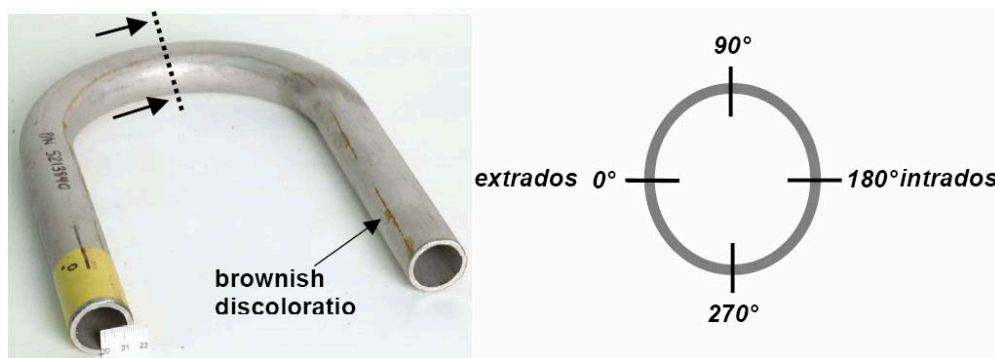


**Figure 128. U-bend test specimen and nomenclature (Ref. 97).**

Measurements made to characterize the as-received condition indicated that, as expected, the U-bend specimens exhibited a non-uniform wall thickness that was thinner at the extrados (0° circumferential position) and thicker at the intrados (180° position) in the apex region. The “neutral” bend positions (90° and 270°) retained the original wall thickness of the tubing. Furthermore, the stress-states at all locations along the outer surface of the bend were predominantly tensile in nature with the exception of the circumferential stress at the intrados, which was compressive throughout most of the evaluation depth. This stress state implied tensile residual stress for this location at the water-wetted, internal surface. The macroscopic external and internal surface condition of the bends was generally good, except for some shallow linear indications. Both the outer and internal surfaces exhibited mild pickling attack. For some tests, the outer surface was mechanically polished and the inside surface was electropolished. All U-bend specimens were pre-conditioned by lengthy exposure to simulated PWR primary water before testing.

Low-cycle fatigue tests were carried out using fully-reversed cycling ( $R = -1$ ) and a triangular loading waveform. Both load and axial strain gauge response at the 0, 90 and 180° positions were continuously monitored during the cycling. All fatigue tests were allowed to continue until failure, defined as a through-wall crack leading to a loss of internal pressure within the U-bend specimens. Strain control was used for the first 12 loading cycles to allow for shakedown, with the remainder of the test performed under displacement control. An axial strain gauge at the bend intrados was used as the leading strain gauge to establish the desired strain amplitudes of

either 0.6% or 0.4%. A series of baseline tests involving U-bends instrumented with numerous strain gauges were carried out in an inert environment at both room temperature and 240°C to establish both the basic fatigue behavior of the bend specimens and the appropriate load control sequence for subsequent testing in a simulated PWR primary water environment.

The simulated PWR primary water environment consisted of high purity water with less than 10 ppb DO, 1200 ppm boron as boric acid, and 2 ppm Li as LiOH. The combined chloride, fluoride, and sulfate impurities in water were less than 100 ppb. The tests were performed with either a low flow rate of 0.005 meters/second (10 liters/hour) or a high flow rate of 2.2 meters/second (4400 liters/hour) for the 26.5-mm internal diameter (ID) tube. To facilitate proper evaluation of interim fatigue results, the following loading considerations were originally expected to be appropriate for the U-bend tests:

- The bend test was effectively strain controlled, with the axial strain at the outside surface of the bend intrados (180° position) acting as the control strain.
- Despite the reduced wall thickness from fabrication at the bend extrados (0° position), axial strains at the outer surface of that location were anticipated to be considerably smaller than at the intrados because of bend radius effects.
- Under the push-pull of the bend legs, compressive/tensile, cyclic, axial strains were also created at the inside surface of the intrados, but their maximum values were expected to be about 35% lower than the control strain at the outer surface.
- As a result of ovalization at the apex of the bend during cycling, the circumferential strains expected at the inside surface in the 90° and 270° locations were estimated to be approximately 75% of the axial control strain, and slightly higher than the circumferential strains at the outer surface.
- The strains resulting from cyclic loading at the various locations around the bend apex were not expected to be entirely symmetrical because of factors such as “out-of-roundness” and wall thickness variations arising from the tube manufacturing and bending processes, as well as the bend residual stress.

From these considerations, mechanically-dominated fatigue was expected to lead to circumferential cracking, starting at the outside surface of the intrados, whereas environmental effects were expected to manifest themselves primarily as axial cracking at the inside surface in the “neutral” bend positions (i.e., 90° and 270°) at the apex of the test specimens. The key conditions and results of the U-bend tests are summarized in Table 22. All tests were conducted at a strain rate of 0.01 %/s, except Tests 3a and 3b, which were performed at a strain rate of 0.0005 %/s. The dominant failures were through-wall cracks that led to a loss of internal pressure in the U-bend tube specimens. The results also showed that fatigue cracks on the outer surfaces were typically circumferential and on the inner surfaces were axial. An overview of the extent and location of the fatigue cracking in the U-bend tests at strain amplitude of 0.6 and 0.4% is presented in Figs. 129 and 130, respectively.

The predicted fatigue lives for the U-bend tests were obtained by dividing the estimated fatigue lives in air,  $N_{air}$  (determined from Eq. 29) by  $F_{en}$  to account for environmental effects. Furthermore, since the tests were conducted using constant strain rate and temperature, the modified rate approach was not considered and the  $F_{en}$  was determined using the simplified method. However, since the estimates of fatigue lives based on Eq. 29 represent small, polished test specimens, and the U-bend test results were obtained on larger U-bend tube specimens with a mechanically polished or pickled surface, the U-bend test results were adjusted for the effects of surface finish, size, and heat-to-heat variability. An adjustment for loading sequence was not included because all tests were conducted at constant strain amplitude. A value of 2.3 for the combined adjustment factor to account for the effects of

surface finish, size, and heat-to-heat variability was determined by comparing the predicted fatigue lives with the results for the two tests in the inert environment (i.e., tests BLT2 and BLT3). The estimated fatigue lives were further adjusted by dividing by a factor of 2.3 to obtain the predicted fatigue lives for the various U-bend test datasets.

**Table 22. Summary of the key conditions and results of the U-bend tests at 240°C.**

Test	Strain amplitude (%)	Displacements (mm)	Surface Condition		Flow Rate	N <sub>f</sub>	Failure location & mechanism	Striation spacing mid fracture area		Crack depth 180° position	Crack depth 90° position
			Outer	Internal				Env.	Mech. <sup>(1)</sup>		
BLT2	0.60	+6.90 -4.70	As pickled		Stagnant N <sub>2</sub>	1705	180° OD mechanical	- (2)	2.0 μm	- (2)	- (2)
2a	0.60	+6.50 -4.85	As pickled		Low	1520	180° OD mechanical	1 μm	5.0 μm	>1000 μm	N/A <sup>(3)</sup>
2b	0.60	+7.15 -5.40	As pickled		High	1238 at notch	180° OD mechanical	1 μm	2.5 μm	400 μm	N/A <sup>(3)</sup>
BLT3	0.40	+4.90 -4.92	Mech. polished	As pickled	Stagnant N <sub>2</sub>	4995	180° OD mechanical	- (2)	3.0 μm	- (2)	- (2)
4a	0.40	+4.82 -5.25	As pickled		Low	3609	270° ID environ.	3 μm	1 μm (180°)	580 μm	1700 μm
4a'	0.40	+4.91 -5.07	Mech. polished	As pickled	Low	3437	270° ID environ.	1 μm	N/A <sup>(3)</sup> (180°)	500 μm	1050 μm
4b	0.40	+5.07 -5.08	Mech. polished	As pickled	High	3616	270° ID environ.	1 μm	- (2)	1000 μm	750 μm
4d	0.40	+4.83 -5.03	Mech. polished	electro polished	High	3835	270° ID environ.	1 μm	N/A <sup>(3)</sup> (180°)	680 μm	2600 μm
3a	0.40	+4.88 -5.07	Mech. polished	As pickled	Low	1939	270° ID environ.	2 μm	- (2)	200 μm	2900 μm
3b	0.40	+4.67 -4.71	Mech. polished	As pickled	High	1517	270° ID environ.	2 μm	- (2)	210 μm	Through wall

<sup>1</sup> OD crack initiation.

<sup>2</sup> Crack did not exist.

<sup>3</sup> Crack existed but was not examined.

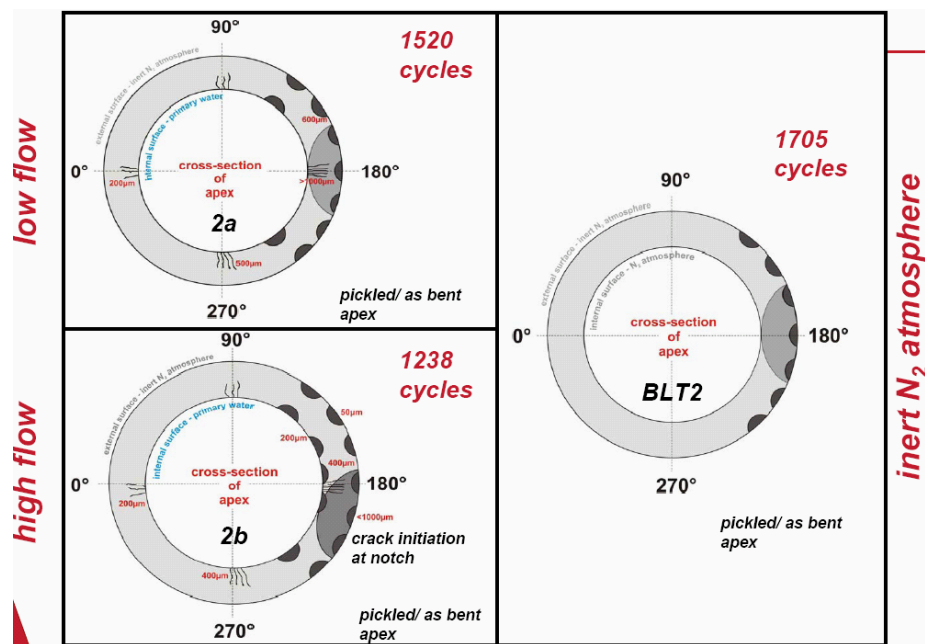


**Figure 129. Overview of the extent and location of fatigue cracking in U-bend tests at strain amplitude of 0.6% (Ref. 97).**



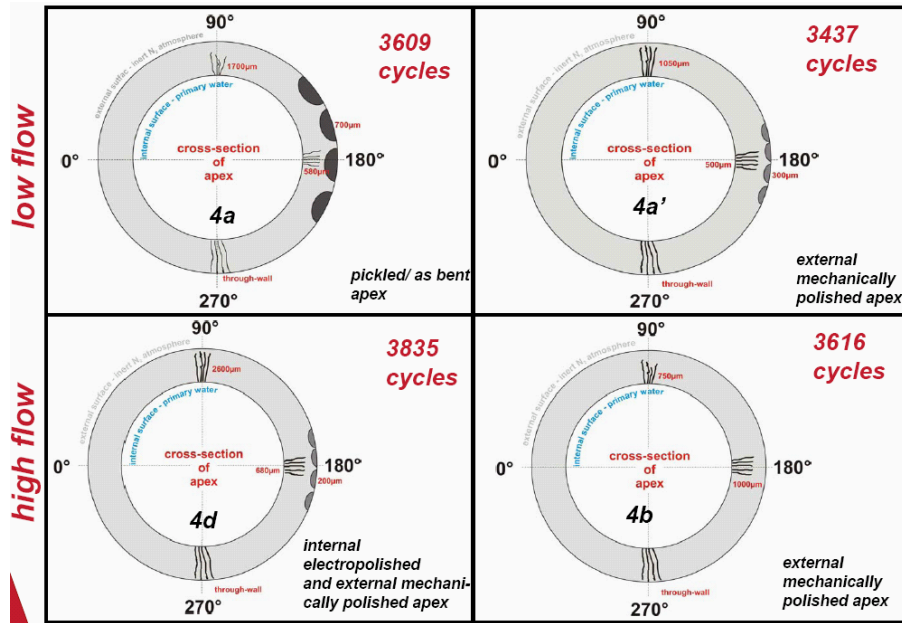


**Figure 130. Overview of the extent and location of fatigue cracking in U-bend tests at strain amplitude of 0.4% (Ref. 97).**

The experimental and predicted fatigue lives for the Type 304L SS U-bend specimens at 240°C in inert and simulated PWR primary water environments are plotted in Fig. 131. As mentioned before, the data in an inert environment (stagnant  $N_2$ ) were used to determine the adjustment factor to account for the effects of surface finish, size, and heat-to-heat variability on fatigue life. Consequently, the data in the inert environment (solid circles in Fig. 131) lie on the diagonal line, as expected. The results indicated that the predicted fatigue lives for axial cracks that initiated at the neutral bend positions (90° and 270°) in the PWR primary water environment showed very good agreement compared to the experimental fatigue lives. The predicted lives were within a factor of  $\pm 1.5$  compared to the measured values. However, in the PWR environment, the predicted lives for the cracks at the intrados position (180°) were significantly lower than the experimental values. The lack of agreement for these cracks was most likely related to the concurrent dominant mechanical cracking from the OD at the same location. This is observed from the information presented in Fig. 130 for Tests 4a, 4a', and 4d where several 200 to 700-mm deep circumferential cracks initiated at the OD intrados position.

The U-bend test results also indicated that, in contrast to the results for carbon steels, no beneficial effects of higher flow rates on fatigue lives were observed for Type 304L austenitic SS. The fatigue lives at high flow rates were lower than those at low flow rates for some tests and greater for other tests (diamonds and triangle symbols in Fig. 131). Furthermore, the results indicated little or no effects of electro-polished and pickled surface finishes on fatigue lives; the fatigue lives of U-bend specimens with pickled surfaces (Test 4b) or electro-polished surfaces were comparable.

- *The predicted fatigue lives were within a factor of  $\pm 1.5$  of the experimental values (i.e., within the range of data scatter). The results did not indicate any beneficial effects of higher flow rates on the fatigue lives of austenitic SSs.*

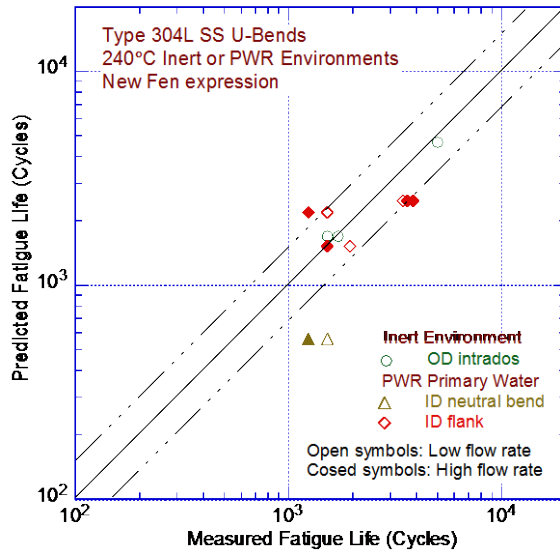


**Figure 131.**  
The experimental and predicted fatigue lives for Type 304L SS U-bend specimens at 240°C in inert and PWR environments (Refs. 97-99).

## 6.4 Simulation of Actual Plant Conditions

As discussed in Section 4.1.14, a modified rate approach was proposed for estimating fatigue lives of materials in LWR environments under varying temperature and strain rate conditions. The applicability of the modified rate approach was validated using fatigue  $\epsilon$ -N data obtained under varying temperature and strain rate conditions. However, actual operating plant transients involve not only varying temperatures and strain rates, but also varying strain amplitudes. Therefore, to validate the applicability of the modified rate approach together with CUF evaluations that account for varying strain amplitudes, fatigue tests were conducted in a simulated PWR environment by combining loading cycle blocks of different strain amplitudes, which included changes in both temperature and strain rate.

Tests were conducted on Type 316 austenitic SS hollow, cylindrical specimens with a 12 mm outside diameter, a 3 mm wall thickness and a 24 mm gauge length. The material was obtained from a Type 316 SS pipe with a 355.7 mm outside diameter and a 35.7 mm wall thickness. The material was heat treated for 30 minutes at 1055°C, followed by water quenching. The chemical composition and mechanical properties are given in Table 23.

**Table 23. Chemical composition and tensile strength of Type 316 SS material.**

Material	Chemical Composition (wt. %)									Min. YS (MPa)	Min. UTS (MPa)	Min. Elong. (%)
	C	Si	Mn	Ni	Cr	Mo	V	Cu	Ti			
316 SS	0.04	0.37	1.55	12.55	16.5	2.10	-	-	-	247	531	54

The tubular specimens were machined from the piping material such that the specimen gauge lengths were in the axial direction of the pipe. The outer and inner surfaces of the specimens were polished in the axial direction using emery papers up to 800 grit to remove machining scratches. All fatigue tests were conducted in a simulated PWR primary water environment under axial strain control using an extensometer attached to the outer surface of the specimens. The test environment consisted of 500 ppm boron added as boric acid, 2 ppm Li added as LiOH, less than 0.005 ppm DO, and dissolved hydrogen was maintained at 30 cc/kg of water. The fatigue loading consisted of two blocks of differing strain amplitude and temperature ranges, in which either the strain rate changed in response to the temperature or the

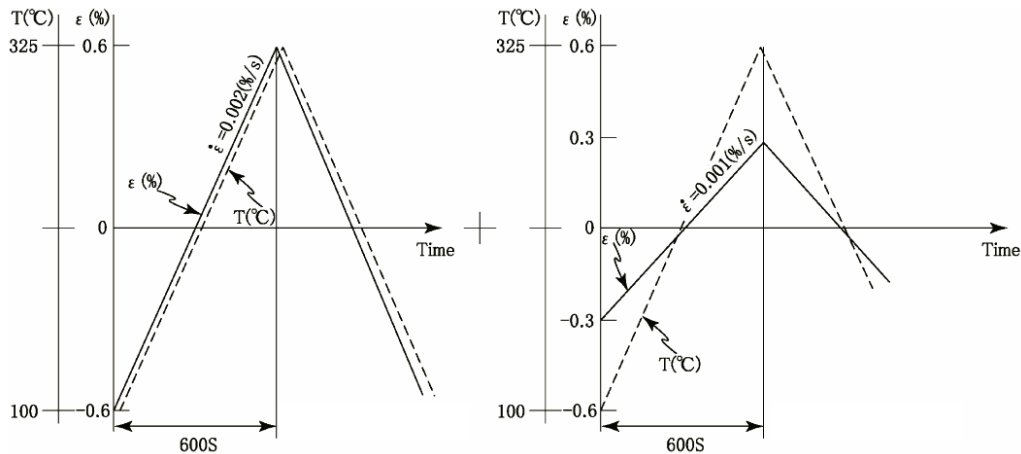


temperature was changed in response to strain rate (in phase or out-of-phase). Examples of the loading cycles are shown in Fig. 132. The test matrix for the combined two-block cumulative fatigue damage test is given in Table 24. Fatigue life was defined as the number of cycles at which a fatigue crack penetrated through the wall thickness of the specimen,  $N_{leak}$ .

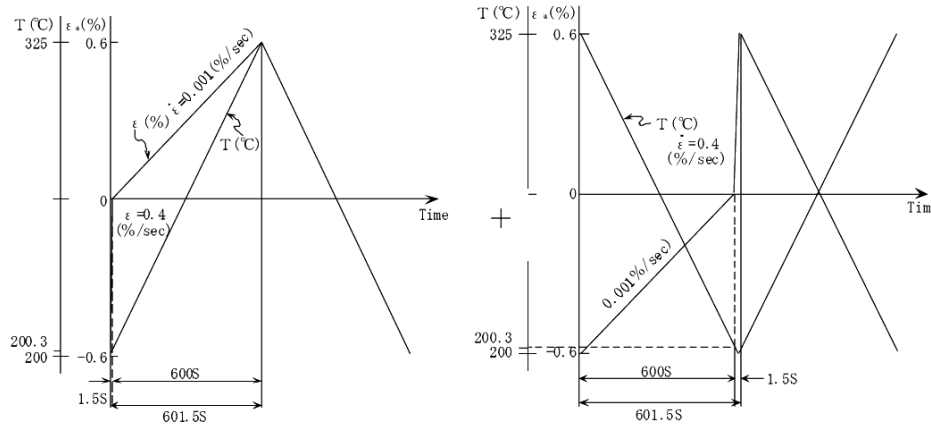
The measured fatigue lives and the predicted fatigue lives for the simulated actual plant conditions tests are plotted in Fig. 133. The predicted fatigue lives for these tests were obtained by dividing the estimated fatigue lives in air,  $N_{air}$  (determined from Eq. 29), by  $F_{en}$  to account for environmental effects. In addition, since the tests were conducted using linear changes in strain rate and temperature, the multi-linear method was used to determine the  $F_{en}$ . The predicted and experimental fatigue lives and the associated number of number of blocks and  $F_{en}$  values are listed in Table 25. The fatigue usage per block was determined from the ratio of cycles per block and the predicted fatigue life for the loading and environmental conditions for that block.

The results show very good agreement between the predicted and experimental fatigue lives for all tests; the difference is within a factor of  $\pm 2$  (i.e., within the range of material variability and data scatter).

- The predicted fatigue lives for all block loading tests were within a factor of  $\pm 2.0$  of the experimental values (i.e., within the range of material variability and data scatter).



Test No. 1



Block 1

Block 2

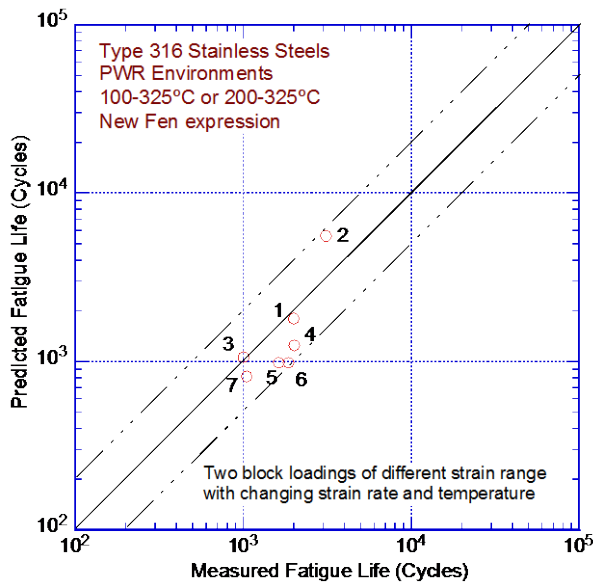
Test No. 7

Figure 132. Loading waveforms for Fatigue Test Nos. 1 and 7 (Ref. 154).

**Table 24. Test matrix for the two blocks fatigue damage tests.**

Test No.	Block 1					Block 2				
	$\varepsilon_a$ (%)	Pattern	Temp. (°C)	Strain Rate (%/s)	Cycles /Block	$\varepsilon_a$ (%)	Pattern	Temp. (°C)	Strain Rate (%/s)	Cycles /Block
1	0.6	In phase	100-325	0.002	275	0.3	In phase	100-325	0.001	379 <sup>a</sup>
2	0.6	In phase	100-325	0.002	27	0.3	In phase	100-325	0.001	379
3	0.6	Out of phase	100-325	0.002	311	0.6	In phase	200-325	0.002	152
4	0.6	Out of phase	100-325	0.002	311	0.6	In phase	200-325	0.002	15
5	0.6	In phase	200-325	0.4-0.001	77	0.6	In phase	200-325	0.001-0.4	70
6	0.6	Out of phase	200-325	0.4-0.001	70	0.6	Out of phase	200-325	0.001-0.4	77
7	0.6	In phase	200-325	0.4-0.001	77	0.6	Out of phase	200-325	0.001-0.4	77

<sup>a</sup> The second block stopped after 129 cycles.



**Figure 133.**  
The experimental and predicted fatigue lives of Type 316 SS tested in PWR primary water using two blocks of fatigue cycles of different strain amplitudes and varying temperature and strain rate (Ref. 154).

**Table 25. Results of the two blocks fatigue damage tests.**

Test No.	$\varepsilon_a$ (%)	Temp. (°C)	Strain Rate (%/s)	Cycles /Block	N <sub>leak</sub> (cycles)		N <sub>air</sub> (cycles)	F <sub>en</sub>	Usage /Block	Predicted Blocks	N <sub>estd</sub> (cycles)	
					Partial	Total					Partial	Total
1	0.6	100-325	0.002	275	1,108	1,995	3,899	3.039	0.214	3.302	908	1,795
	0.3	100-325	0.001	379	887		24,341	3.327	0.052		887	
2	0.6	100-325	0.002	27	216	3,100	3,899	3.039	0.021	13.729	378	5,574
	0.3	100-325	0.001	379	2,884		24,341	3.327	0.052		5,196	
3	0.6	100-325	0.002	311	699	1,003	3,899	3.039	0.242	2.291	757	1,061
	0.6	200-325	0.002	152	304		3,899	4.980	0.194		304	
4	0.6	100-325	0.002	311	1,915	2,005	3,899	3.039	0.242	3.823	1,201	1,246
	0.6	200-325	0.002	15	90		3,899	4.980	0.019		45	
5	0.6	200-325	0.4-0.001	77	1,001	1,857	3,899	4.779	0.094	6.695	539	984
	0.6	200-325	0.001-0.4	70	856		3,899	3.063	0.055		445	
6	0.6	200-325	0.4-0.001	70	777	1,624	3,899	3.063	0.055	6.695	490	984
	0.6	200-325	0.001-0.4	77	847		3,899	4.779	0.094		494	
7	0.6	200-325	0.4-0.001	77	539	1,046	3,899	4.779	0.094	5.298	431	816
	0.6	200-325	0.001-0.4	77	507		3,899	4.779	0.094		385	

## 7. SUMMARY

---

The comprehensive review of the available fatigue  $\epsilon$ -N data for nuclear power plant piping and pressure vessel steels presented in the original version of NUREG/CR-6909 was reevaluated using a much larger database, and the results were updated to address feedback from interested stakeholders regarding the  $F_{en}$  methodology for incorporating environmental effects into ASME Code Section III fatigue CUF evaluations.

In this report, fatigue life is described as the number of cycles of a specified strain amplitude that a specimen can sustain before the formation of a 3-mm-deep crack (i.e., an “engineering crack”). This equates to a 25% load drop in test specimens, and is assumed to equate to crack initiation in an actual component. Using this definition, a calculated fatigue CUF less than unity provides reasonable assurance that a fatigue crack has not formed in a component, and indicates that the probability of forming a crack in the component is low.

In the original version of NUREG/CR-6909, the existing fatigue  $\epsilon$ -N data for carbon and low-alloy steels, wrought and cast austenitic SSs, and Ni-Cr-Fe alloys were evaluated to identify the various material, environmental, and loading parameters that influenced fatigue crack initiation, and to establish the effects of key parameters on the fatigue lives of these steels. The fatigue lives of these materials were decreased in LWR environments; the magnitude of the reduction depended on temperature, strain rate, DO level in the water, and, for carbon and low-alloy steels, the sulfur content of the steel. For all steels, environmental effects on fatigue lives were significant only when critical parameters (temperature, strain rate, DO level, and strain amplitude) met certain threshold values. Environmental effects were moderate, e.g., less than a factor of 2 decrease in lives, when any one of the threshold conditions was not satisfied. The threshold values of the critical parameters and the effects of other parameters (such as water conductivity, water flow rate, and material heat treatment) on the fatigue lives of the steels were also discussed. In this updated report, all of these evaluations were updated and reevaluated, and the results are summarized below.

### Carbon and Low-Alloy Steels

In air, the fatigue lives of carbon and low-alloy steels depended on steel type, temperature, specimen orientation, and strain rate. The fatigue lives of carbon steels were a factor of approximately 1.5 lower than those of low-alloy steels. For both steels, fatigue lives decreased with an increase in temperature. Some heats of carbon and low-alloy steels exhibited effects of strain rate and specimen orientation. For these heats, fatigue lives decreased with decreasing strain rate. In addition, the data indicated significant heat-to-heat variation; the distribution and morphology of sulfides had a significant effect on the fatigue lives of these materials. The results also indicated that, in room-temperature air, the ASME Code Section III mean curve for low-alloy steels was in good agreement with the available experimental data, and the mean curve for carbon steels was somewhat conservative in the high-cycle regime (i.e., fatigue lives greater than  $10^4$  cycles). Revised fatigue design curves based on the ANL models were developed in the initial version of NUREG/CR-6909. Those curves extended up to  $10^{11}$  cycles. In the present report, the extension of the fatigue design curves beyond  $10^6$  cycles was modified to be consistent with the current ASME Code Section III fatigue design air curve to better accommodate the field vibration data.

The fatigue lives of both carbon and low-alloy steels were decreased in LWR environments; the amount of reduction depended on temperature, strain rate, DO level in the water, and sulfur content of the steel. The results indicated that a minimum threshold strain was required for an environmentally-assisted decrease in the fatigue lives of these steels. In addition,

environmental effects occurred primarily during the tensile-loading cycles and at strain levels greater than a threshold value. The fatigue lives were decreased significantly when all four conditions were satisfied simultaneously, viz., the strain amplitude, temperature, and DO in the water were above minimum levels, and the strain rate was below a threshold value. The sulfur content in the steel was also important; its effect on fatigue lives depended on the DO level in the water.

Although the microstructures and cyclic-hardening behavior of carbon and low-alloy steels differed significantly, environmental degradation of the fatigue lives of these steels was very similar. The available fatigue  $\epsilon$ - $N$  data were reviewed to establish the critical parameters that influenced fatigue lives and updated definitions were developed for their threshold and limiting values within which environmental effects were significant. In the original version of NUREG/CR-6909, the  $F_{en}$  expressions for both steels predicted a moderate decrease in fatigue lives (i.e., by about a factor of 2) when any one of the threshold conditions was not satisfied, e.g., a low-DO BWR HWC or PWR environment, temperatures less than 150°C, or vibratory fatigue. In the present report, the  $F_{en}$  expressions for carbon and low-alloy steels were revised so that the value of  $F_{en}$  was 1 (i.e., no environmental effects) when any one of the threshold conditions was not satisfied. The impact of this revision on fatigue CUF values relative to the  $F_{en}$  expressions in the original version of NUREG/CR-6909 is that the updated  $F_{en}$  values are generally lower under certain environmental and loading conditions compared to the previous expressions.

#### Austenitic Stainless Steels

In air, the fatigue lives of Types 304 and 316 SS were comparable; those of Type 316NG were superior to those of Types 304 and 316 SS at high strain amplitudes (i.e., the slope of the fatigue  $\epsilon$ - $N$  curve was steeper). The fatigue lives of austenitic SSs in air were independent of temperature in the range from room temperature to 427°C. Also, variations in strain rate in the range of 0.4–0.008%/s had no effect on the fatigue lives of SSs at temperatures up to 400°C. The fatigue  $\epsilon$ - $N$  behavior of cast SSs was similar to that of wrought austenitic SSs. The results indicated that the experimental data at strain amplitudes less than 0.5% or 975 MPa (141 ksi) were not consistent with the mean-data curve for SSs corresponding to the fatigue design curves in editions of Section III of the ASME Code prior to the 2009b Addenda; the ASME Code Section III mean air curve predicted significantly longer lives than those observed experimentally. The fatigue design air curve in editions of Section III of the ASME Code later than the 2009b Addenda was based on the ANL model and is consistent with the available fatigue  $\epsilon$ - $N$  data.

The fatigue lives of cast and wrought austenitic SSs decreased in LWR environments compared to those in air. The decrease depended on the strain rate, the DO level in the water, and temperature. Similar to the behavior of carbon and low-alloy steels, a minimum threshold strain was required for environmental effects on fatigue lives of SSs to occur, and this strain was independent of material type (weld or base metal) and temperature in the range of 250–325°C. Furthermore, environmental effects were significant only during the tensile-loading cycles. Strain rates and temperatures had strong effects on fatigue lives in LWR environments. Fatigue lives decreased with decreasing strain rates below 0.4%/s; the effects saturated at 0.0004%/s. In the original version of NUREG/CR-6909, a threshold temperature of 150°C was defined below which environmental effects were insignificant; in the range of 150–325°C, the logarithm of fatigue lives decreased linearly with temperature. However, to better represent all of the more recently available fatigue  $\epsilon$ - $N$  data, the temperature dependence relationships in the  $F_{en}$  expressions were modified and the temperature threshold decreased from 150 to 100°C. The dependency of fatigue lives on strain rate was also modified, and the threshold strain rate above

which environmental effects were considered insignificant was increased from 0.4 to 10%/s. The impact of these revisions on fatigue CUF values relative to the  $F_{en}$  expressions in the original version of NUREG/CR-6909 was that  $F_{en}$  values using the updated expressions are lower under many environmental and loading conditions, but are marginally higher for some conditions.

The effects of DO levels were different for different steels. In low-DO water (i.e., less than 0.01 ppm DO), the fatigue lives for all wrought and cast austenitic SSs were decreased significantly; compositions or heat treatments of the steels had little or no effects on fatigue lives. However, in high-DO water, the environmental effects on fatigue lives were influenced by the composition and heat treatment of the steels. For example, for high-C Type 304 SSs, environmental effects were significant only for sensitized steels. For low-C Type 316NG SSs, some effects of environment were observed even for mill-annealed (nonsensitized) steels in high-DO water, although the effects were smaller than those observed in low-DO water. Limited fatigue  $\epsilon$ -N data indicated that the fatigue lives of cast SSs were approximately the same in low- and high-DO water and were comparable to those observed for wrought SSs in low-DO water. As such, in the initial version of NUREG/CR-6909, environmental effects on the fatigue lives of wrought and cast austenitic SSs were considered to be identical in high-DO and low-DO environments. However, based on the more recently available fatigue  $\epsilon$ -N data, the dependency of environmental effects on water DO content was included in this report; that dependency was based on the material composition and heat treatment.

#### Ni-Cr-Fe Alloy Steels

The available fatigue  $\epsilon$ -N data for Ni-Cr-Fe alloys indicated that, although the data for Alloys 690 and 800 were very limited, the fatigue lives of these alloys were comparable to those of Alloy 600. In addition, the fatigue lives of the Ni-Cr-Fe alloy weld metals were comparable to those of the wrought Alloy 600 and 690 materials in the low-cycle regime (i.e., less than  $10^5$  cycles), and were slightly superior in the high-cycle regime. The data for Ni-Cr-Fe alloys also indicated that the fatigue resistance of Inconel 718 was superior to that of Alloy 600, 690, and 800 materials. For Inconel 718, the slope of the fatigue  $\epsilon$ -N curve was flatter and the fatigue limit (i.e., fatigue life at  $10^6$  cycles) was higher than those for austenitic SSs.

The available laboratory fatigue data for Ni-Cr-Fe alloys in LWR environments were very limited. However, the available data indicated that the effects of key loading and environmental parameters on fatigue lives are similar to those for austenitic SSs. For example, the fatigue lives of these steels decreased logarithmically with decreasing strain rates. Also, the effects of environment were greater in low-DO PWR water compared to those in high-DO BWR water. However, environmental effects on the fatigue lives of Ni-Cr-Fe alloys were lower than those for austenitic SSs. Therefore, in this report, the temperature dependency of the  $F_{en}$  expression for Ni-Cr-Fe alloys was revised; the effects of temperature on fatigue lives of these materials were considered to be insignificant below 50°C and they saturated at temperatures above 325°C. The impact of this revision on fatigue evaluations is that updated  $F_{en}$  values are typically lower relative to those based on  $F_{en}$  expressions in the initial version of NUREG/CR-6909.

#### Model Validation

The updated  $F_{en}$  methodology proposed in this revised report was validated by comparing evaluation of the results of several experimental data sets obtained from fatigue tests that simulated actual plant conditions with estimates of fatigue usage using the updated  $F_{en}$  expressions. The data sets represented fatigue tests with changing strain rates and/or temperatures, complex loadings that simulated a PWR safety injection transient, spectrum

loadings (i.e., random strain amplitudes), and pipe U-bend tests. In all cases, the results indicated that the predicted fatigue lives were in good agreement with the experimental values; the differences between the experimental and predicted fatigue lives were within a factor of 2, which is within data scatter. However, the predicted fatigue lives for the tests with the complex strain loading cycles were all lower than the experimental values by a factor of about 2. The reason for this one exception was not clear. This behavior may have been unique to the specific strain loading cycles used in the test. Fatigue tests with other strain loading cycle profiles are recommended to provide further understanding of possible effects of complex loading patterns on the fatigue lives of materials. Nonetheless, although the predicted lives were lower, the estimated values were within the range of data scatter.

### *Fatigue Design Curve Adjustment Factors*

This updated report also presented a critical review of the ASME Code Section III fatigue adjustment factors of 2 on stress and 20 on life, and assessed the possible conservatisms in the choice of these adjustment factors. These factors covered the effects of variables that influence fatigue lives, but were not investigated in the tests that provided the data for the ASME Code Section III air design curves. These variables included material variability and data scatter, size, surface finish, and loading sequence. Although the factors of 2 and 20 used by ASME were intended to be conservative, they are not considered to be safety margins because they were intended to account for variables that are known to affect fatigue lives. Data available in the literature were reviewed to evaluate the factors on cycles and stress that are needed to account for the differences and uncertainties caused by the four parameters that were not considered in the fatigue test data. Monte Carlo simulations were performed to determine the factor on cycles needed to obtain fatigue design air curves that provide conservative estimates of the number of cycles to initiate a fatigue crack in reactor components.

The results presented in the initial version of NUREG/CR-6909 indicated that, for carbon and low-alloy steels and austenitic SSs, the current ASME Code Section III requirements for a factor of 20 on cycles to account for the effects of material variability and data scatter, as well as size, surface finish, and loading history, were conservative by at least a factor of 1.7. Thus, to reduce this conservatism, fatigue design curves were developed from the ANL model by first correcting for mean stress effects, and then reducing the mean-stress adjusted curve by a factor of 2 on stress and 12 on cycles, whichever was more conservative. In this updated report, the range of the subfactors for material variability and data scatter, size, surface finish, and loading sequence were examined and modified, and Monte Carlo simulations were performed to determine the factor on cycles needed to obtain fatigue design air curves with 95% confidence bounds. The results indicated that for these materials, a factor of 2 on stress and 10 on cycles were adequate to develop the fatigue design curves from the best-fit mean air curves. However, until these results are further validated with applicable fatigue data  $\epsilon$ -N data, the fatigue design curves presented in this report were based on factors of 2 on stress and 12 on life.

A detailed procedure for incorporating environmental effects into ASME Code Section III fatigue evaluations is presented in Appendix A. The methodology is identical to that presented in the initial version of NUREG/CR-6909, except that the  $F_{en}$  expressions were updated based on the analyses presented in this report. In addition, the updated methodology described in this report applies to any component exposed to the LWR environment that requires an ASME CUF calculation as part of its design, or if required by the safety basis for the component, or if required by the plant current licensing basis, unless otherwise justified. Appendix C of this report presents a sample application of the  $F_{en}$  methodology.

## 8. REFERENCES

---

1. ASTM Designation E 1823-09a, "Standard Terminology Relating to Fatigue and Fracture Testing," American Society for Testing and Materials, Philadelphia, PA, March 2009.
2. ASTM Designation E 606-04, "Standard Practice for Strain-Controlled Fatigue Testing," American Society for Testing and Materials, Philadelphia, PA, July 2005.
3. ASTM Designation E 468-90, "Standard Practice for Presentation of Constant Amplitude Fatigue Test Results for Metallic Materials," Philadelphia, PA, October 2004.
4. ASTM Designation E 739-91, "Standard Practice for Statistical Analysis of Linear or Linearized Stress-Life (S-N) and Strain-Life ( $\epsilon$ -N) Fatigue Data," American Society for Testing and Materials, Philadelphia, PA, May 2006.
5. Rice, R. C., "Fatigue Data Analysis," Metals Handbook, Vol. 8, American Society for Metal, Materials Park, OH, pp. 695-720, 1985.
6. ASTM Designation E 1823-09a, "Standard Terminology Related to Fatigue and Fracture Testing," American Society for Testing and Materials, Philadelphia, PA, March 2009.
7. Langer, B. F., "Design of Pressure Vessels for Low-Cycle Fatigue," ASME J. Basic Eng. 84, 389-402, September 1962.
8. "Criteria of the ASME Boiler and Pressure Vessel Code for Design by Analysis in Sections III and VIII, Division 2," The American Society of Mechanical Engineers, New York, 1969.
9. Cooper, W. E., "The Initial Scope and Intent of the Section III Fatigue Design Procedure," Welding Research Council, Inc., Technical Information from Workshop on Cyclic Life and Environmental Effects in Nuclear Applications, Clearwater, Florida, Jan. 22-21, 1992.
10. Chopra, O. K., and W. J. Shack, "Effects of LWR Coolant Environments on Fatigue Design Curves of Carbon and Low-Alloy Steels," NUREG/CR-6583, ANL-97/18, March 1998.
11. Gavenda, D. J., P. R. Luebbbers, and O. K. Chopra, "Crack Initiation and Crack Growth Behavior of Carbon and Low-Alloy Steels," Fatigue and Fracture 1, Vol. 350, S. Rahman, K. K. Yoon, S. Bhandari, R. Warke, and J. M. Bloom, eds., American Society of Mechanical Engineers, New York, pp. 243-255, 1997.
12. Chopra, O. K., and W. J. Shack, "Environmental Effects on Fatigue Crack Initiation in Piping and Pressure Vessel Steels," NUREG/CR-6717, ANL-00/27, May 2001.
13. Chopra, O. K., "Mechanisms and Estimation of Fatigue Crack Initiation in Austenitic Stainless Steels in LWR Environments," NUREG/CR-6787, ANL-01/25, Aug. 2002.
14. Hale, D. A., S. A. Wilson, E. Kiss, and A. J. Giannuzzi, "Low-Cycle Fatigue Evaluation of Primary Piping Materials in a BWR Environment," GEAP-20244, U.S. Nuclear Regulatory Commission, Sept. 1977.
15. Hale, D. A., S. A. Wilson, J. N. Kass, and E. Kiss, "Low Cycle Fatigue Behavior of Commercial Piping Materials in a BWR Environment," J. Eng. Mater. Technol. 103, 15-25, 1981.

16. Ranganath, S., J. N. Kass, and J. D. Heald, "Fatigue Behavior of Carbon Steel Components in High-Temperature Water Environments," BWR Environmental Cracking Margins for Carbon Steel Piping, EPRI NP-2406, Appendix 3, Electric Power Research Institute, Palo Alto, CA, May 1982.
17. Ranganath, S., J. N. Kass, and J. D. Heald, "Fatigue Behavior of Carbon Steel Components in High-Temperature Water Environments," Low-Cycle Fatigue and Life Prediction, ASTM STP 770, C. Amzallag, B. N. Leis, and P. Rabbe, eds., American Society for Testing and Materials, Philadelphia, pp. 436-459, 1982.
18. Nagata, N., S. Sato, and Y. Katada, "Low-Cycle Fatigue Behavior of Pressure Vessel Steels in High-Temperature Pressurized Water," *ISIJ Intl.* 31 (1), 106-114, 1991.
19. Higuchi, M., and K. Iida, "Fatigue Strength Correction Factors for Carbon and Low-Alloy Steels in Oxygen-Containing High-Temperature Water," *Nucl. Eng. Des.* 129, 293-306, 1991.
20. Katada, Y., N. Nagata, and S. Sato, "Effect of Dissolved Oxygen Concentration on Fatigue Crack Growth Behavior of A533 B Steel in High Temperature Water," *ISIJ Intl.* 33 (8), 877-883, 1993.
21. Kanasaki, H., M. Hayashi, K. Iida, and Y. Asada, "Effects of Temperature Change on Fatigue Life of Carbon Steel in High Temperature Water," *Fatigue and Crack Growth: Environmental Effects, Modeling Studies, and Design Considerations*, PVP Vol. 306, S. Yukawa, ed., American Society of Mechanical Engineers, New York, pp. 117-122, 1995.
22. Nakao, G., H. Kanasaki, M. Higuchi, K. Iida, and Y. Asada, "Effects of Temperature and Dissolved Oxygen Content on Fatigue Life of Carbon and Low-Alloy Steels in LWR Water Environment," *Fatigue and Crack Growth: Environmental Effects, Modeling Studies, and Design Considerations*, PVP Vol. 306, S. Yukawa, ed., American Society of Mechanical Engineers, New York, pp. 123-128, 1995.
23. Higuchi, M., K. Iida, and Y. Asada, "Effects of Strain Rate Change on Fatigue Life of Carbon Steel in High-Temperature Water," *Fatigue and Crack Growth: Environmental Effects, Modeling Studies, and Design Considerations*, PVP Vol. 306, S. Yukawa, ed., American Society of Mechanical Engineers, New York, pp. 111-116, 1995; also *Proc. of Symp. on Effects of the Environment on the Initiation of Crack Growth*, ASTM STP 1298, American Society for Testing and Materials, Philadelphia, 1997.
24. Higuchi, M., K. Iida, and K. Sakaguchi, "Effects of Strain Rate Fluctuation and Strain Holding on Fatigue Life Reduction for LWR Structural Steels in Simulated PWR Water," *Pressure Vessel and Piping Codes and Standards*, PVP Vol. 419, M. D. Rana, ed., American Society of Mechanical Engineers, New York, pp. 143-152, 2001.
25. Hirano, A., M. Yamamoto, K. Sakaguchi, T. Shoji, and K. Iida, "Effects of Water Flow Rate on Fatigue Life of Ferritic and Austenitic Steels in Simulated LWR Environment," *Pressure Vessel and Piping Codes and Standards - 2002*, PVP Vol. 439, M. D. Rana, ed., American Society of Mechanical Engineers, New York, pp. 143-150, 2002.



26. Hirano, A., M. Yamamoto, K. Sakaguchi, and T. Shoji, "Effects of Water Flow Rate on Fatigue Life of Carbon and Stainless Steels in Simulated LWR Environment," *Pressure Vessel and Piping Codes and Standards – 2004*, PVP Vol. 480, American Society of Mechanical Engineers, New York, pp. 109–119, 2004.
27. Fujiwara, M., T. Endo, and H. Kanasaki, "Strain Rate Effects on the Low–Cycle Fatigue Strength of 304 Stainless Steel in High–Temperature Water Environment, Fatigue Life: Analysis and Prediction," *Proc. Intl. Conf. and Exposition on Fatigue, Corrosion Cracking, Fracture Mechanics, and Failure Analysis*, ASM, Metals Park, OH, pp. 309–313, 1986.
28. Mimaki, H., H. Kanasaki, I. Suzuki, M. Koyama, M. Akiyama, T. Okubo, and Y. Mishima, "Material Aging Research Program for PWR Plants," *Aging Management Through Maintenance Management*, PVP Vol. 332, I. T. Kisisel, ed., American Society of Mechanical Engineers, New York, pp. 97–105, 1996.
29. Kanasaki, H., R. Umehara, H. Mizuta, and T. Suyama, "Fatigue Lives of Stainless Steels in PWR Primary Water," *Trans. 14th Intl. Conf. on Structural Mechanics in Reactor Technology (SMiRT 14)*, Lyon, France, pp. 473–483, 1997.
30. Kanasaki, H., R. Umehara, H. Mizuta, and T. Suyama, "Effects of Strain Rate and Temperature Change on the Fatigue Life of Stainless Steel in PWR Primary Water," *Trans. 14th Intl. Conf. on Structural Mechanics in Reactor Technology (SMiRT 14)*, Lyon, France, pp. 485–493, 1997.
31. Higuchi, M., and K. Iida, "Reduction in Low–Cycle Fatigue Life of Austenitic Stainless Steels in High–Temperature Water," *Pressure Vessel and Piping Codes and Standards*, PVP Vol. 353, D. P. Jones, B. R. Newton, W. J. O'Donnell, R. Vecchio, G. A. Antaki, D. Bhavani, N. G. Cofie, and G. L. Hollinger, eds., American Society of Mechanical Engineers, New York, pp. 79–86, 1997.
32. Hayashi, M., "Thermal Fatigue Strength of Type 304 Stainless Steel in Simulated BWR Environment," *Nucl. Eng. Des.* 184, 135–144, 1998.
33. Hayashi, M., K. Enomoto, T. Saito, and T. Miyagawa, "Development of Thermal Fatigue Testing with BWR Water Environment and Thermal Fatigue Strength of Austenitic Stainless Steels," *Nucl. Eng. Des.* 184, 113–122, 1998.
34. Tsutsumi, K., H. Kanasaki, T. Umakoshi, T. Nakamura, S. Urata, H. Mizuta, and S. Nomoto, "Fatigue Life Reduction in PWR Water Environment for Stainless Steels," *Assessment Methodologies for Preventing Failure: Service Experience and Environmental Considerations*, PVP Vol. 410-2, R. Mohan, ed., American Society of Mechanical Engineers, New York, pp. 23–34, 2000.
35. Tsutsumi, K., T. Dodo, H. Kanasaki, S. Nomoto, Y. Minami, and T. Nakamura, "Fatigue Behavior of Stainless Steel under Conditions of Changing Strain Rate in PWR Primary Water," *Pressure Vessel and Piping Codes and Standards*, PVP Vol. 419, M. D. Rana, ed., American Society of Mechanical Engineers, New York, pp. 135–141, 2001.

36. Tsutsumi, K., M. Higuchi, K. Iida, and Y. Yamamoto, "The Modified Rate Approach to Evaluate Fatigue Life under Synchronously Changing Temperature and Strain Rate in Elevated Temperature Water," Pressure Vessel and Piping Codes and Standards – 2002, PVP Vol. 439, M. D. Rana, ed., American Society of Mechanical Engineers, New York, pp. 99–107, 2002.
37. Higuchi, M., T. Hirano, and K. Sakaguchi, "Evaluation of Fatigue Damage on Operating Plant Components in LWR Water," Pressure Vessel and Piping Codes and Standards – 2004, PVP Vol. 480, American Society of Mechanical Engineers, New York, pp. 129–138, 2004.
38. Nomura, Y., M. Higuchi, Y. Asada, and K. Sakaguchi, "The Modified Rate Approach Method to Evaluate Fatigue Life under Synchronously Changing Temperature and Strain Rate in Elevated Temperature Water in Austenitic Stainless Steels," Pressure Vessel and Piping Codes and Standards – 2004, PVP Vol. 480, American Society of Mechanical Engineers, New York, pp. 99–108, 2004.
39. Higuchi, M., K. Sakaguchi, A. Hirano, and Y. Nomura, "Revised and New Proposal of Environmental Fatigue Life Correction Factor ( $F_{en}$ ) for Carbon and Low-Alloy Steels and Nickel Alloys in LWR Water Environments," Proc. of the 2006 ASME Pressure Vessels and Piping Conf., July 23–27, 2006, Vancouver, BC, Canada, paper # PVP2006-ICPVT-93194.
40. Chopra, O. K., and W. J. Shack, "Evaluation of Effects of LWR Coolant Environments on Fatigue Life of Carbon and Low-Alloy Steels," Effects of the Environment on the Initiation of Crack Growth, ASTM STP 1298, W. A. Van Der Sluys, R. S. Piascik, and R. Zawierucha, eds., American Society for Testing and Materials, Philadelphia, pp. 247–266, 1997.
41. Chopra, O. K., and W. J. Shack, "Low-Cycle Fatigue of Piping and Pressure Vessel Steels in LWR Environments," Nucl. Eng. Des. 184, 49–76, 1998.
42. Chopra, O. K., and D. J. Gavenda, "Effects of LWR Coolant Environments on Fatigue Lives of Austenitic Stainless Steels," J. Pressure Vessel Technol. 120, 116–121, 1998.
43. Chopra, O. K., and J. L. Smith, "Estimation of Fatigue Strain-Life Curves for Austenitic Stainless Steels in Light Water Reactor Environments," Fatigue, Environmental Factors, and New Materials, PVP Vol. 374, H. S. Mehta, R. W. Swindeman, J. A. Todd, S. Yukawa, M. Zako, W. H. Bamford, M. Higuchi, E. Jones, H. Nickel, and S. Rahman, eds., American Society of Mechanical Engineers, New York, pp. 249–259, 1998.
44. Smith, J. L., and O. K. Chopra, "Crack Initiation in Smooth Fatigue Specimens of Austenitic Stainless Steel in Light Water Reactor Environments," in Operations, Applications, and Components – 1999, PVP Vol. 395, I. T. Kisisel, ed., American Society of Mechanical Engineers, New York, pp. 235–242, 1999.
45. Chopra, O. K., "Effects of LWR Coolant Environments on Fatigue Design Curves of Austenitic Stainless Steels," NUREG/CR-5704, ANL-98/31, 1999.
46. Chopra, O. K., and W. J. Shack, "Review of the Margins for ASME Code Design Curves – Effects of Surface Roughness and Material Variability," NUREG/CR-6815, ANL-02/39, Sept. 2003.

47. Chopra, O. K., B. Alexandreanu, and W. J. Shack, "Effect of Material Heat Treatment on Fatigue Crack Initiation in Austenitic Stainless Steels in LWR Environments," NUREG/CR-6878, ANL-03/35, July 2005.
48. Terrell, J. B., "Fatigue Life Characterization of Smooth and Notched Piping Steel Specimens in 288°C Air Environments," NUREG/CR-5013, EM-2232 Materials Engineering Associates, Inc., Lanham, MD, May 1988.
49. Terrell, J. B., "Fatigue Strength of Smooth and Notched Specimens of ASME SA 106-B Steel in PWR Environments," NUREG/CR-5136, MEA-2289, Materials Engineering Associates, Inc., Lanham, MD, Sept. 1988.
50. Terrell, J. B., "Effect of Cyclic Frequency on the Fatigue Life of ASME SA-106-B Piping Steel in PWR Environments," J. Mater. Eng. 10, 193-203, 1988.
51. O'Donnell, W. James and W. John O'Donnell, "Temperature Dependence of Reactor Water Environmental Fatigue Effects on Carbon, Low-Alloy and Austenitic Stainless Steels," Proc. of the 2008 ASME Pressure Vessels and Piping Division Conf., July 27-31, 2008, Chicago, IL, paper # PVP2008-61917.
52. Takahashi, Y. and T. Nakamura, "Statistical Analyses of In-Air and In-Water Fatigue Test Data of Austenitic Stainless Steels and Ferritic Steels," Pressure Vessel and Piping Codes and Standards - 2003, PVP Vol. 453, American Society of Mechanical Engineers, New York, pp. 113-122, 2003, paper # PVP2003-1775.
53. Nomura, Y., S. Asada, T. Nakamura, and M. Tanaka, "Effects of Continuous Strain Rate Changing on Environmental Fatigue for Stainless Steels in PWR Environment," Proc. of the ASME 2010 Pressure Vessels and Piping Division/K-PVP Conf., July 18-22, 2010, Bellevue, Washington, DC, paper # PVP2010-25194.
54. Le Duff, J. A., A. Lefrancois, J. P. Vernot, and D. Bossu, "Effect of Loading Signal Shape and of Surface Finish on the Low Cycle Fatigue Behavior of 304L Stainless Steel in PWR Environment," Proc. of the ASME 2010 Pressure Vessels and Piping Division/K-PVP Conf., July 18-22, 2010, Bellevue, Washington, DC, paper # PVP2010-26027.
55. Lenz, E., N. Wieling, and H. Muenster, "Influence of Variation of Flow Rates and Temperature on the Cyclic Crack Growth Rate under BWR Conditions," Environmental Degradation of Materials in Nuclear Power Systems - Water Reactors, The Metallurgical Society, Warrendale, PA, 1988.
56. Garud, Y. S., S. R. Paterson, R. B. Dooley, R. S. Pathania, J. Hickling, and A. Bursik, "Corrosion Fatigue of Water Touched Pressure Retaining Components in Power Plants," EPRI TR-106696, Final Report, Electric Power Research Institute, Palo Alto, Nov. 1997.
57. Amzallag, C., P. Rabbe, G. Gallet, and H.-P. Lieurade, "Influence des Conditions de Sollicitation Sur le Comportement en Fatigue Oligocyclique D'aciers Inoxydables Austénitiques," Memoires Scientifiques Revue Metallurgie Mars, pp. 161-173, 1978.
58. Solomon, H. D., C. Amzallag, A. J. Vallee, and R. E. De Lair, "Influence of Mean Stress on the Fatigue Behavior of 304L SS in Air and PWR Water," Proc. of the 2005 ASME Pressure Vessels and Piping Conf., July 17-21, 2005, Denver, CO, paper # PVP2005-71064.

59. Solomon, H. D., C. Amzallag, R. E. De Lair, and A. J. Vallee, "Comparison of the Fatigue Life of Type 304L SS as Measured in Load and Strain Controlled Tests," Proc. of the 12<sup>th</sup> Intl. Conf. on Environmental Degradation of Materials in Nuclear Power Plants – Water Reactors, T. R. Allen, P. J. King, and L. Nelson, eds., The Minerals, Metals and Materials Society, 2004.
60. Solomon, H. D., C. Amzallag, R. E. De Lair, and A. J. Vallee, "Strain Controlled Fatigue of Type 304L SS in Air and PWR Water," Proc. Third Intl. Conf. on Fatigue of Reactor Components, Seville, Spain, Oct. 3–6, 2004.
61. Jaske, C. E., and W. J. O'Donnell, "Fatigue Design Criteria for Pressure Vessel Alloys," Trans. ASME J. Pressure Vessel Technol. 99, 584–592, 1977.
62. Conway, J. B., R. H. Stentz, and J. T. Berling, "Fatigue, Tensile, and Relaxation Behavior of Stainless Steels," TID–26135, U.S. Atomic Energy Commission, Washington, DC, 1975.
63. Keller, D. L., "Progress on LMFBR Cladding, Structural, and Component Materials Studies During July, 1971 through June, 1972, Final Report," Task 32, Battelle–Columbus Laboratories, BMI–1928, 1977.
64. Smith, R. W., M. H. Hirschberg, and S. S. Manson, "Fatigue Behavior of Materials Under Strain Cycling in Low and Intermediate Life Range," NASA TN D-1574, Lewis Research Center, April 1963.
65. Krempl, E., "Low Cycle Fatigue Crack Initiation in the Presence of Stress/Strain Concentration," in Reactor Primary Coolant System Rupture Study, Quarterly Progress Report No. 3, GEAP-5082, General Electric, San Jose, CA, pp. 6-6 to 6-23, Jan. 1966.
66. Jacko, R. J., "Fatigue Performance of Ni–Cr–Fe Alloy 600 under Typical PWR Steam Generator Conditions," EPRI NP–2957, Electric Power Research Institute, Palo Alto, CA, March 1983.
67. Dinerman, A. E., "Cyclic Strain Fatigue of Inconel at 75 to 600°F," KAPL–2084, Knolls Atomic Power Laboratory, Schenectady, NY, August 1960.
68. Mowbray, D. F., G. J. Sokol, and R. E. Savidge, "Fatigue Characteristics of Ni–Cr–Fe Alloys with Emphasis on Pressure–Vessel Cladding," KAPL–3108, Knolls Atomic Power Laboratory, Schenectady, NY, July 1965.
69. Jaske, C. E., H. Mindlin, and J. S. Perrin, "Low-Cycle Fatigue of Incoloy Alloy 800," Topical Report BMI-1921, Battelle's Columbus Laboratories, Feb. 1972.
70. McGowan, E. J., and J. W. Faber, "Effects of Electric Discharge and Electrochemical Machining on the Fatigue Strength of Selected Structural Materials," WAPD-TM-787, Bettis Atomic Power Laboratory, Jan. 1969.
71. Conway, J. B., "Short Term tensile and Low-Cycle Fatigue Studies of Incoloy 800," GEMP-732, General Electric Company, Dec. 1969.
72. Miller, J., "Low Cycle Fatigue Under Biaxial Strain Controlled Conditions," J. of Materials, Vol. 7, No. 3, 307-314, Sept. 1972.

73. Nachtigall, A. J., "Strain Cycling Fatigue Behavior of Ten Structural Metals Tested in Liquid Helium (4K), in Liquid Nitrogen (78K), and in Ambient Air (300K)," NASA TN D-7532, Lewis Research Center, Feb. 1974.
74. Brinkman, C. R., and G. E. Korth, "Strain Fatigue and Tensile Behavior of Inconel 718 from Room Temperature to 650°C," J. of Testing and Evaluation, Vol. 2, No. 4, 249-259, July 1974.
75. Van Der Sluys, W. A., B. A. Young, and D. Doyle, "Corrosion Fatigue Properties on Alloy 690 and Some Nickel-Based Weld Metals," Assessment Methodologies for Preventing Failure: Service Experience and Environmental Considerations, PVP Vol. 410-2, R. Mohan, ed., American Society of Mechanical Engineers, New York, pp. 85-91, 2000.
76. Faidy, C., T. Le Courtois, E. de Fraguier, J-A Leduff, A. Lefrancois, and J. Dechelotte, "Thermal Fatigue in French RHR System," Int. Conf. on Fatigue of Reactor Components, Napa, CA, July 31-August 2, 2000.
77. Kusmaul, K., R. Rintamaa, J. Jansky, M. Kemppainen, and K. Törrönen, "On the Mechanism of Environmental Cracking Introduced by Cyclic Thermal Loading," in IAEA Specialists Meeting, Corrosion and Stress Corrosion of Steel Pressure Boundary Components and Steam Turbines, VTT Symp. 43, Espoo, Finland, pp. 195-243, 1983.
78. Hickling, J., "Strain Induced Corrosion Cracking of Low-Alloy Reactor Pressure Vessel Steels under BWR Conditions," Proc. 10th Intl. Symp. on Environmental Degradation of Materials in Nuclear Power Systems – Water Reactors, F. P. Ford, S. M. Bruemmer, and G. S. Was, eds., The Minerals, Metals, and Materials Society, Warrendale, PA, CD-ROM, paper 0156, 2001.
79. Hickling, J., "Research and Service Experience with Environmentally Assisted Cracking of Low-Alloy Steel," Power Plant Chem., 7 (1), 4-15, 2005.
80. Iida, K., "A Review of Fatigue Failures in LWR Plants in Japan," Nucl. Eng. Des. 138, 297-312, 1992.
81. NRC IE Bulletin No. 79-13, "Cracking in Feedwater System Piping," U.S. Nuclear Regulatory Commission, Washington, DC, June 25, 1979.
82. NRC Information Notice 93-20, "Thermal Fatigue Cracking of Feedwater Piping to Steam Generators," U.S. Nuclear Regulatory Commission, Washington, DC, March 24, 1993.
83. Kusmaul, K., D. Blind, and J. Jansky, "Formation and Growth of Cracking in Feed Water Pipes and RPV Nozzles," Nucl. Eng. Des. 81, 105-119, 1984.
84. Gordon, B. M., D. E. Delwiche, and G. M. Gordon, "Service Experience of BWR Pressure Vessels," Performance and Evaluation of Light Water Reactor Pressure Vessels, PVP Vol.-119, American Society of Mechanical Engineers, New York, pp. 9-17, 1987.
85. Lenz, E., B. Stellwag, and N. Wieling, "The Influence of Strain-Induced Corrosion Cracking on the Crack Initiation in Low-Alloy Steels in HT-Water – A Relation Between Monotonic and Cyclic Crack Initiation Behavior," in IAEA Specialists Meeting Corrosion and Stress Corrosion of Steel Pressure Boundary Components and Steam Turbines, VTT Symp. 43, Espoo, Finland, pp. 243-267, 1983.

86. Hickling, J., and D. Blind, "Strain-Induced Corrosion Cracking of Low-Alloy Steels in LWR Systems – Case Histories and Identification of Conditions Leading to Susceptibility," Nucl. Eng. Des. 91, 305–330, 1986.
87. Hirschberg, P., A. F. Deardorff, and J. Carey, "Operating Experience Regarding Thermal Fatigue of Unisolable Piping Connected to PWR Reactor Coolant Systems," Int. Conf. on Fatigue of Reactor Components, Napa, CA, July 31–August 2, 2000.
88. Shah, V. N., M. B. Sattison, C. L. Atwood, A. G. Ware, G. M. Grant, and R. S. Hartley, "Assessment of Pressurized Water Reactor Primary System Leaks," NUREG/CR-6582, INEEL/EXT-97-01068, Dec. 1998.
89. NRC Information Notice 88-01, "Safety Injection Pipe Failure," U.S. Nuclear Regulatory Commission, Washington, DC (Jan. 27, 1988).
90. NRC Bulletin No. 88-08, "Thermal Stresses in Piping Connected to Reactor Coolant Systems," U.S. Nuclear Regulatory Commission, Washington, DC, June 22; Suppl. 1, June 24; Suppl. 2, Aug. 4, 1988; Suppl. 3, April 1989.
91. Sakai, T., "Leakage from CVCS Pipe of Regenerative Heat Exchanger Induced by High-Cycle Thermal Fatigue at Tsuruga Nuclear Power Station Unit 2," Int. Conf. on Fatigue of Reactor Components, Napa, CA, July 31–August 2, 2000.
92. Hoshino, T., T. Ueno, T. Aoki, and Y. Kutomi, "Leakage from CVCS Pipe of Regenerative Heat Exchanger Induced by High-Cycle Thermal Fatigue at Tsuruga Nuclear Power Station Unit 2," Proc. 8th Intl. Conf. on Nuclear Engineering, 1.01 Operational Experience/Root Cause Failure Analysis, Paper 8615, American Society of Mechanical Engineers, New York, 2000.
93. NRC Bulletin No. 88-11, "Pressurizer Surge Line Thermal Stratification," U.S. Nuclear Regulatory Commission, Washington, DC, Dec. 20, 1988.
94. Daret, J., J. M. Boursier, and J. M. Olive, "Cracking of Stainless Steel Channel Heads in a Primary Water Experimental Loop," in Proc. Tenth Intl. Symp. on Environmental Degradation of Materials in Nuclear Power Systems – Water Reactors, The Metallurgical Society, Warrendale, PA, Paper #0089, Lake Tahoe, NV, Aug. 5-9, 2001.
95. Stephan, J.-M., and J. C. Masson, "Auxiliary Feedwater Line Stratification and Coufast Simulation," Int. Conf. on Fatigue of Reactor Components, Napa, CA, July 31–August 2, 2000.
96. Lenz, E., A. Liebert, and N. Wieling, "Thermal Stratification Tests to Confirm the Applicability of Laboratory Data on Strain-Induced Corrosion Cracking to Component Behavior," in 3rd IAEA Specialists Meeting on Sub-Critical Crack Growth, Moscow, pp. 67–91, 1990.
97. Kilian, R., J. Hickling, and R. Nickell, "Environmental Fatigue Testing of Stainless Steel Pipe Bends in Flowing, Simulated PWR Primary Water at 240°C," Third Intl. Conf. Fatigue of Reactor Components (MRP-151), EPRI Report 1011958, Electric Power Research Institute, Palo Alto, CA, Aug. 2005.

98. Kilian, R., "Environmental Fatigue Testing of Type 304L Stainless Steel U-Bends in Simulated PWR Primary Water (MRP-188)," Materials Reliability Program, EPRI Report 1013028, Electric Power Research Institute, Palo Alto, CA, Jan. 2006.
99. Hickling, J., R. Kilian, L. Spain, and J. Carey, "Environmental Fatigue Testing of Type 304L Stainless Steel U-Bends in Simulated PWR Primary Water," Proc. of the 2006 ASME Pressure Vessels and Piping Conf., July 23–27, 2006, Vancouver, BC, Canada, paper # PVP2006–ICPVT11–93318.
100. Shahinian, P., H. E. Watson, and H. H. Smith, "Effect of Neutron Irradiation on Fatigue Crack Propagation in Types 304 and 316 Stainless Steels at High Temperature," NRL Report 7446, Naval Research Laboratory, Washington, DC, July 1972.
101. James, L. A., and R. L. Knecht, "Fatigue-Crack Propagation in Fast-Neutron-Irradiated Types-304 and -316 Stainless Steels," Nucl. Technol. 19, 148–155, 1973.
102. James, L. A., "The Effect of Fast Neutron Irradiation Upon the Fatigue-Crack Propagation Behavior of Two Austenitic Stainless Steels," J. Nucl. Mater. 59, 183–191, 1975.
103. Michel, D. J., "Irradiation Effects on Fatigue Crack Propagation in Austenitic Stainless Steels," NRL Memorandum Report 3610, Naval Research Laboratory, Washington, DC, Sept. 1977.
104. Michel, D. J., and H. H. Smith, "Fatigue Crack Propagation in Neutron Irradiated Type 304 and Type 308 Stainless Steel Plate and Weld Materials," J. Nucl. Mater. 71, 173–177, 1977.
105. Shahinian, P., H. E. Watson, and H. H. Smith, "Neutron Irradiation Effects on Fatigue Crack Growth in Types 304 and 316 Stainless Steels," in Irradiation Effects on Reactor Structural Materials, Quarterly Progress Report 1 May – 31 July 1972, Section II Advance Reactor Materials (LMFBR), NRL Memorandum Report 2505, Naval Research Laboratory, Washington, DC, Aug. 1972.
106. Fyfe, S., H. Xu, K. Moore, and R. Gurdal, "PWR Internals Materials Aging Degradation Mechanism Screening and Threshold Values (MRP-175)," Materials Reliability Program, EPRI Report 1012081, Electric Power Research Institute, Palo Alto, CA, December 2005.
107. Edwards, D., E. Simonen, S. Bruemmer, and P. Efsing, "Microstructural Evolution in Neutron- Irradiated Stainless Steels: Comparison of LWR and Fast-Reactor Irradiations," Proc. 12th Intl. Conf. on Environmental Degradation of Materials in Nuclear Power System - Water Reactors, T. R. Allen, P. J. King, and L. Nelson, eds., Minerals, Metals, & Materials Society, pp. 419-428, 2005.
108. Korth, G. E., and M. D. Harper, "Fatigue and Creep-Fatigue Behavior of Irradiated and Unirradiated Type 308 Stainless Steel Weld Metal at Elevated Temperatures," Properties of Reactor Structural Alloys After Neutron or Particle Irradiation, ASTM STP 570, American Society for Testing and Materials, Philadelphia, PA 175-190, 1975.
109. Kangilaski, M., and F. R. Shober, "Effect of Neutron Irradiation on Mechanical Properties of AISI Type 347 Stainless Steel," Effects of Radiation on Structural Metals, ASTM STP 426, American Society for Testing and Materials, 487-510, 1967.

110. Kanasaki, H., I. Satoh, M. Koyama, T. Okubo, T. R. Mager, and R. G. Lott, "Fatigue and Stress Corrosion Cracking Behaviors of Irradiated Stainless Steels in PWR Primary Water," Proc. of the 5<sup>th</sup> Intl. Conf. on Nuclear Engineering (ICONE 5), Nice, France, May 26-30, 1997.
111. Ware, A. G., D. K. Morton, and M. E. Nitzel, "Application of NUREG/CR-5999 Interim Design Curves to Selected Nuclear Power Plant Components," NUREG/CR-6260, INEL-95/0045, March 1995.
112. NUREG-0933, Main Report with Supplements 1-34 "Resolution of Generic Safety Issues," Section 3 "New Generic Issues," Issues 78, 166, and 190, March 29, 2012.
113. SECY-95-245, "Completion of Fatigue Action Plan," Sept. 25, 1995.
114. Khaleel, M. A., F. A. Simonen, H. K. Phan, D. O. Harris, and D. Dedhia, "Fatigue Analysis of Components for 60-Year Plant Life," NUREG/CR-6674, PNNL-13227, June 2000.
115. Van Der Sluys, W. A., and S. Yukawa, "Status of PVRC Evaluation of LWR Coolant Environmental Effects on the S-N Fatigue Properties of Pressure Boundary Materials," Fatigue and Crack Growth: Environmental Effects, Modeling Studies, and Design Considerations, PVP Vol. 306, S. Yukawa, ed., American Society of Mechanical Engineers, New York, pp. 47-58, 1995.
116. Van Der Sluys, W. A., "PVRC's Position on Environmental Effects on Fatigue Life in LWR Applications," Welding Research Council Bulletin 487, Welding Research Council, Inc., New York, Dec. 2003.
117. Memorandum for W. Travers from A. Thadani, "Closeout of Generic Safety Issue 190, 'Fatigue Evaluation of Metal Components for 60-Year Plant Life,'" December 26, 1999.
118. Iida, K., T. Bannai, M. Higuchi, K. Tsutsumi, and K. Sakaguchi, "Comparison of Japanese MITI Guideline and Other Methods for Evaluation of Environmental Fatigue Life Reduction," Pressure Vessel and Piping Codes and Standards, PVP Vol. 419, M. D. Rana, ed., American Society of Mechanical Engineers, New York, pp. 73-81, 2001.
119. Chopra, O. K., and W. J. Shack, "Overview of Fatigue Crack Initiation in Carbon and Low-Alloy Steels in Light Water Reactor Environments," J. Pressure Vessel Technol. 121, 49-60, 1999.
120. Higuchi, M., "Revised Proposal of Fatigue Life Correction Factor  $F_{en}$  for Carbon and Low Alloy Steels in LWR Water Environments," Assessment Methodologies for Preventing Failure: Service Experience and Environmental Considerations, PVP Vol. 410-2, R. Mohan, ed., American Society of Mechanical Engineers, New York, pp. 35-44, 2000.
121. Leax, T. R., "Statistical Models of Mean Stress and Water Environment Effects on the Fatigue Behavior of 304 Stainless Steel," Probabilistic and Environmental Aspects of Fracture and Fatigues, PVP Vol. 386, S. Rahman, ed., American Society of Mechanical Engineers, New York, pp. 229-239, 1999.
122. Mehta, H. S., and S. R. Gosselin, "Environmental Factor Approach to Account for Water Effects in Pressure Vessel and Piping Fatigue Evaluations," Nucl. Eng. Des. 181, 175-197, 1998.



123. Mehta, H. S., and S. R. Gosselin, "An Environmental Factor Approach to Account for Reactor Water Effects in Light Water Reactor Pressure Vessel and Piping Fatigue," EPRI Report TR-105759, Electric Power Research Institute, Palo Alto, CA, Dec. 1995.
124. Mehta, H. S., "An Update on the Consideration of Reactor Water Effects in Code Fatigue Initiation Evaluations for Pressure Vessels and Piping," Assessment Methodologies for Preventing Failure: Service Experience and Environmental Considerations, PVP Vol. 410-2, R. Mohan, ed., American Society of Mechanical Engineers, New York, pp. 45–51, 2000.
125. O'Donnell, W. J., W. J. O'Donnell, and T. P. O'Donnell, "Proposed New Fatigue Design Curves for Austenitic Stainless Steels, Alloy 600, and Alloy 800," Proc. of the 2005 ASME Pressure Vessels and Piping Conf., July 17–21, 2005, Denver, CO, paper # PVP2005–71409.
126. O'Donnell, W. J., W. J. O'Donnell, and T. P. O'Donnell, "Proposed New Fatigue Design Curves for Carbon and Low-Alloy Steels in High Temperature Water," Proc. of the 2005 ASME Pressure Vessels and Piping Conf., July 17–21, 2005, Denver, CO, paper # PVP2005–71410.
127. Park, H. B., and O. K. Chopra, "A Fracture Mechanics Approach for Estimating Fatigue Crack Initiation in Carbon and Low-Alloy Steels in LWR Coolant Environment," Assessment Methodologies for Preventing Failure: Service Experience and Environmental Considerations, PVP Vol. 410-2, R. Mohan, ed., American Society of Mechanical Engineers, New York, pp. 3–11, 2000.
128. O'Donnell, T. P., and W. J. O'Donnell, "Stress Intensity Values in Conventional S-N Fatigue Specimens," Pressure Vessels and Piping Codes and Standard: Volume 1 – Current Applications, PVP Vol. 313–1, K. R. Rao and Y. Asada, eds., American Society of Mechanical Engineers, New York, pp. 191–192, 1995.
129. Majumdar, S., O. K. Chopra, and W. J. Shack, "Interim Fatigue Design Curves for Carbon, Low-Alloy, and Austenitic Stainless Steels in LWR Environments," NUREG/CR–5999, ANL–93/3, 1993.
130. Keisler, J., O. K. Chopra, and W. J. Shack, "Fatigue Strain–Life Behavior of Carbon and Low-Alloy Steels, Austenitic Stainless Steels, and Alloy 600 in LWR Environments," NUREG/CR–6335, ANL–95/15, 1995.
131. Higuchi, M., K. Sakaguchi, Y. Nomura, and A. Hirano, "Final Proposal of Environmental Fatigue Life Correction Factor ( $F_{en}$ ) for Structural Materials in LWR Water Environment," Proc. of the 2007 ASME Pressure Vessels and Piping Division Conf., July 22–26, 2007, San Antonio, TX, paper # PVP2007–26100.
132. Higuchi, M., "Comparison of Environmental Fatigue Evaluation Methods in LWR Water," Proc. of the 2008 ASME Pressure Vessels and Piping Division Conf., July 27–31, 2008, Chicago, IL, paper # PVP2008–61087.
133. Nakamura, T., M. Iwasaki, and S. Asada, "Optimization of Environmental Fatigue Evaluation (Step 1)," Proc. of the 2007 ASME Pressure Vessels and Piping Division Conf., July 22–26, 2007, San Antonio, TX, paper # PVP2007–26247.

134. Nomura, Y., K. Tsutsumi, T., Inoue, S. Asada, and T. Nakamura, "Optimization of Environmental Fatigue Evaluation (Step 2)," Proc. of the 2009 ASME Pressure Vessels and Piping Division Conf., July 26–30, 2009, Prague, Czech Republic, paper # PVP2009–77115.
135. Higuchi, M., T. Nakamura, and Y. Sugie, "Updated Knowledge Implemented to the Revision of Environmental Fatigue Evaluation Method for Nuclear Power Plants in JSME Code," Proc. of the 2009 ASME Pressure Vessels and Piping Division Conf., July 26–30, 2009, Prague, Czech Republic, paper # PVP2009–77077.
136. JNES-SS Report, "Environmental Fatigue Evaluation Method for Nuclear Power Plants," JNES-SS-1005, Nuclear Energy System Safety Division, Japan Nuclear Energy Safety Organization, March 2011.
137. Chopra, O. K., and W. J. Shack, "Effect of LWR Coolant Environments on the Fatigue Life of Reactor Materials – Final Report," NUREG/CR–6909, ANL–06/08, Feb. 2007.
138. Wu, X. Q., and Y. Katada, "Influence of Cyclic Strain Rate on Environmentally Assisted Cracking Behavior of Pressure Vessel Steel in High-Temperature Water," Mater. Sci. Eng. A379, 58–71, 2004.
139. Wu, X., and Y. Katada, "Corrosion Fatigue Behavior of Low-Alloy Pressure Vessel Steels in High Temperature Water under Multi-Factor Conditions," J. Pressure Vessel Technol. Trans. ASME, Vol. 126, 466–472, 2004.
140. Wu, Q. X., and Y. Katada, "Influence of Strain Rate Change on Corrosion Fatigue Behavior of A533B Steel in Simulated BWR Water," J. Mater. Sci. 39, 2519–2522, 2004.
141. Wu, Q. X., and Y. Katada, "Strain-Amplitude Dependent Fatigue Resistance of Low-Alloy Pressure Vessel Steels in High-Temperature Water," J. Mater. Sci. 40, 1953–1958, 2005.
142. Wu, X., and Y. Katada, "Strain-Rate Dependence of Low Cycle Fatigue Behavior in a Simulated BWR Environment," Corros. Sci. 47, 1415–1428, 2005.
143. Wu, X., E. Han, W. Ke, and Y. Katada, "Effects of Loading Factors on Environmental Fatigue Behavior of Low-Alloy Pressure Vessel Steels in Simulated BWR Water," Nucl. Eng. Des. 237, 1452–1459, 2007.
144. Wu, X., H. Guan, E. H. Han, W. Ke, and Y. Katada, "Influence of Surface Finish on Fatigue Cracking Behavior of Reactor Pressure Vessel Steel in High Temperature Water," Mater. Corros. 57 (11), 868–871, 2006.
145. Solomon, H. D., R. E. De Lair, and H. Hoffmann, "Influence of Environment and Strain Rate on the Low Cycle Fatigue Crack Initiation in Low Alloy Steel 15NiCuMoNb5 in High Temperature Water," Proc. of the 11<sup>th</sup> Intl. Conf. on Environmental Degradation of Materials in Nuclear Systems, Stevenson, WA, Aug. 10-14, 2004.
146. Roth, A., and J. Hickling, "Crack Initiation due to Environmentally Assisted Cracking in Carbon and Low-Alloy Steels Exposed to High-Temperature Water," Proc. of the 13<sup>th</sup> Intl. Conf. on Environmental Degradation of Materials in Nuclear Power Systems, Whistler, BC, Canada, Aug. 19-23, 2007.

147. Devrient, B., A. Roth, K. Kuster, U. Ilg, and M. Widera, "Effect of Dynamic Strain Ageing on the Environmentally Assisted Cracking of Low-Alloy Steels in Oxygenated High-Temperature Water," Proc. of the 13<sup>th</sup> Intl. Conf. on Environmental Degradation of Materials in Nuclear Power Systems, Whistler, BC, Canada, Aug. 19-23, 2007.
148. Devrient, B., A. Roth, K. Kuster, M. Widera, and U. Ilg, "Influence of Dynamic Strain Ageing on the Crack Growth Rates and Crack Tip Plasticity of Low-Alloy Steels in Oxygenated High-Temperature Water," Proc. of the 14<sup>th</sup> Intl. Conf. on Environmental Degradation of Materials in Nuclear Power Systems, Virginia Beach, VA, Aug. 23-27, 2009.
149. Hanninen, H., Y. Yagodzinskyy, O. Tarasenko, U. Ehrnsten, and P. Aaltonen, H.-P. Seifert, "Effects of Dynamic Strain Ageing on Environmentally Assisted Cracking of Low-Alloy Pressure Vessel and Piping Steels," Proc. of the Tenth Intl. Conf. on Environmental Degradation of Materials in Nuclear Power Systems – Water Reactors, The Metallurgical Society, Warrendale, PA, Paper #0047, Lake Tahoe, NV, Aug. 5-9, 2001.
150. Seifert, H.-P., and S. Ritter, "Strain-Induced Corrosion Cracking Behavior of Low-Alloy Steels under Boiling Water Reactor Conditions," J. Nucl. Mater. 378, 312–326, 2008.
151. Wu, Q. X., and Y. Katada, "Role of Dynamic Strain Aging in Corrosion Fatigue of Low-Alloy Pressure Vessel Steel in High Temperature Water," J. Mater. Sci. 42, 633–639, 2007.
152. Lee, B. H., and I. S. Kim, "Dynamic Strain Aging in High-Temperature Low-Cycle Fatigue of SA508 Cl. 3 Forging Steel," J. Nucl. Mater. 226, 216–225, 1995.
153. Huang, J. Y., J. R. Hwang, J. J. Yeh, C. Y. Chen, R. C. Kuo, and J. G. Huang, "Dynamic Strain Aging and Grain Size Reduction Effects on the Fatigue Resistance of SA533B3 Steels," J. Nucl. Mater. 324, 140–151, 2004.
154. Sakaguchi, Y. Nomura, S. Suzuki, and H. Kanasaki, "Applicability of the Modified Rate Approach Method Under Various Conditions Simulating Actual Plant Conditions," Proc. of the 2006 ASME Pressure Vessels and Piping Conf., July 23–27, 2006, Vancouver, BC, Canada, paper # PVP2006–ICPVT–11-93220.
155. Le Duff, J. A., A. Lefrancois, and J. P. Vernot, "Effect of Surface Finish and Loading Conditions on the Low Cycle Fatigue Behavior of Austenitic Stainless Steel in PWR Environment Comparison of LCF Test Results with NUREG/CR-6909 Life Estimates," Proc. of the 2008 ASME Pressure Vessels and Piping Division Conf., July 27–31, 2008, Chicago, IL, paper # PVP2008–61894.
156. Le Duff, J. A., A. Lefrancois, J. P. Vernot, and D. Bossu, "Effect of Loading Signal Shape and of Surface Finish on the Low Cycle Fatigue Behavior of 304L Stainless Steel in PWR Environment," Proc. of the 2010 ASME Pressure Vessels and Piping Division/K-PVP Conf., July 18–22, 2010, Bellevue, WA, paper # PVP2010–26027.
157. Le Duff, J. A., A. Lefrancois, and J. P. Vernot, "Effect of Surface Finish and Loading Conditions on the Low Cycle Fatigue Behavior of Austenitic Stainless Steel in PWR Environment for Various Strain Amplitude Levels," Proc. of the ASME 2009 Pressure Vessels and Piping Division Conf., July 26–30, 2009, Prague, Czech Republic, paper # PVP2009–78129.

158. Solin, J. P., "Fatigue of Stabilized SS and 316NG Alloy in PWR Environment," Proc. of the 2006 ASME Pressure Vessels and Piping Conf., July 23–27, 2006, Vancouver, BC, Canada, paper # PVP2006–ICPVT–93833.
159. Solin, J. P., S. Reese, and W. Mayinger, "Discussion on Fatigue Design Curves for Stainless Steels," Proc. of the ASME 2011 Pressure Vessels and Piping Division Conf., July 17–21, 2011, Baltimore, MD, paper # PVP2011–57943.
160. Jones, D. P., J. E. Holliday, T. R. Leax, and J. L. Gordon, "Analysis of a Thermal Fatigue Test of a Stepped Pipe," PVP Vol. 482, Computer Technology and Applications, July 25–29, 2004, San Diego, CA, paper # PVP2004–2748.
161. Stevens, G. L., and J. M. Davis, "Guidelines for Addressing Fatigue Environmental Effects in a License Renewal Application (MRP-47 Revision 1)," Industry Guidance Document TR-1012017, Electric Power Research Institute, Palo Alto, CA, April 2005.
162. Laird, C., "The Influence of Metallurgical Structure on the Mechanism of Fatigue Crack Propagation," in Fatigue Crack Propagation, ASTM STP 415, American Society for Testing and Materials, Philadelphia, PA, 131–180, 1967.
163. Miller, K. J., "Initiation and Growth Rates of Short Cracks," in Fundamentals of Deformation and Fracture, B. A. Bilby, K. J. Miller, and J. R. Willis, eds., Cambridge United Press, 476–500, 1984.
164. Miller, K. J., "Damage in Fatigue: A New Outlook," in Pressure Vessels and Piping Codes and Standard: Volume 1 – Current Applications, PVP Vol. 313–1, K. R. Rao and Y. Asada, eds., American Society of Mechanical Engineers, New York, 191–192, 1995.
165. Suh, C. M., R. Yuuki, and H. Kitagawa, "Fatigue Microcracks in a Low Carbon Steel," Fatigue Fract. Eng. Mater. Struct. 8, 193–203, 1985.
166. Tokaji, K., T. Ogawa, and S. Osako, "The Growth of Microstructurally Small Fatigue Cracks in a Ferritic–Pearlitic Steel, Fatigue Fract." Eng. Mater. Struct. 11, 331–342, 1988.
167. Dowling, N. E., "Crack Growth During Low–Cycle Fatigue of Smooth Axial Specimens," in Cyclic Stress–Strain and Plastic Deformation Aspects of Fatigue Crack Growth, ASTM STP 637, American Society for Testing and Materials, Philadelphia, PA, 97–121, 1977.
168. Suresh, S., and R. O. Ritchie, "Propagation of Short Fatigue Cracks," Int. Metals Reviews 29, 445–476, 1984.
169. Tokaji, K., and T. Ogawa, "The Growth of Microstructurally Small Fatigue Cracks in Metals," in Short Fatigue Cracks,ESIS 13, M. J. Miller and E. R. de los Rios, eds., Mechanical Engineering Publication, London, 85–99, 1992.
170. de los Rios, E. R., Z. Tang, and K. J. Miller, "Short Crack Fatigue Behavior in a Medium Carbon Steel," Fatigue of Engineering Materials and Structures 7, 97–108, 1984.
171. de los Rios, E. R., A. Navarro, and K. Hussain, "Microstructural Variations in Short Fatigue Crack Propagation of a C–Mn Steel," in Short Fatigue Cracks,ESIS 13, M. J. Miller and E. R. de los Rios, eds., Mechanical Engineering Publication, London, pp. 115–132, 1992.

172. Chopra, O. K., Michaud, W. F. and Shack, W. J., "Environmentally Assisted Cracking in Light Water Reactors, Semiannual Report, October 1992–March 1993," NUREG/CR–4667 Vol. 16, ANL–93/27, pp. 3–19, September 1993.
173. Mizuno, T., Pednekar, S., Smialowska, S. and Macdonald, D. D., "Corrosion Behavior of Carbon Steel in Oxygenated Water Environments," EPRI NP–2853, Electric Power Research Institute, Palo Alto, CA, Section 2, February 1983.
174. Choi, H., Smialowska, S. and Macdonald, D. D., "Stress Corrosion Cracking of ASME SA508–Cl2 Pressure Vessel Steel," EPRI NP–2853, Electric Power Research Institute, Palo Alto, CA, Section 4, February 1983.
175. Wranglen, G., "Pitting and Sulphide Inclusions in Steel," *Corr. Sci.* 14, 331–349 (1974).
176. Chopra, O. K., Michaud, W. F., Shack, W. J. and Soppet, W. K., "Environmentally Assisted Cracking in Light Water Reactors, Semiannual Report, April–September 1993," NUREG/CR–4667 Vol. 17, ANL–94/16, pp. 1–22, June 1994.
177. James, L. A., "The Effect of Temperature and Cyclic Frequency Upon Fatigue Crack Growth Behavior of Several Steels in Elevated Temperature Aqueous Environment," *J. Pressure Vessel Technol.* 116, 122–127, 1994.
178. James, L. A., "The Initiation of Environmentally–Assisted Cracking in Semi–Elliptical Surface Cracks," in *Pressure Vessel and Piping Codes and Standards*, PVP Vol. 353, T. C. Esselman, ed., American Society of Mechanical Engineers, New York, pp. 125–139, 1997.
179. Bulloch, J. H., "A Review of the Fatigue Crack Extension Behaviour of Ferritic Reactor Pressure Vessels Materials in Pressurized Water Reactor Environments," *Res. Mech.* 26, 95–172, 1989.
180. Lenz, E., N. Wieling, and H. Munster, "Influence of Variation of Flow Rates and Temperature on the Cyclic Crack Growth Rate under BWR Conditions," in *Proc. 3rd Int. Symp. on Environmental Degradation of Materials in Nuclear Power Systems – Water Reactors*, G. J. Theus and J. R. Weeks, eds., The Metallurgical Society, Warrendale, PA, pp. 283–288, 1988.
181. James, L. A., G. L. Wire, and W. H. Cullen, "The Effect of Water Flow Rate Upon the Environmentally–Assisted Cracking Response of a Low–Alloy Steel," *J. Pressure Vessel Technol.* 117 (3), 238–244, 1995.
182. Wire, G. L., and Y. Y. Li, "Initiation of Environmentally–Assisted Cracking in Low–Alloy Steels," *Fatigue and Fracture* Vol. 1, PVP Vol. 323, H. S. Mehta, ed., American Society of Mechanical Engineers, New York, pp. 269–289, 1996.
183. Van Der Sluys, W. A., and R. H. Emanuelson, "Environmentally Acceleration of Fatigue Crack Growth in Reactor Pressure Vessel Materials," EPRI Report TR-102796, Electric Power Research Institute, Palo Alto, CA, Aug. 1993.
184. Cullen, W. H., M. Kemppainen, H. Hänninen, and K. Törrönen, "The Effects of Sulfur Chemistry and Flow Rate on Fatigue Crack Growth Rates in LWR Environments," NUREG/CR–4121, 1985.

185. Van Der Sluys, W. A., and R. H. Emanuelson, "Environmental Acceleration of Fatigue Crack Growth in Reactor Pressure Vessel Materials and Environments," *Environmentally Assisted Cracking: Science and Engineering*, ASTM STP 1049, W. B. Lisagor, T. W. Crooker, and B. N. Leis, eds., American Society for Testing and Materials, Philadelphia, PA, pp. 117–135, 1990.
186. Atkinson, J. D., and J. E. Forrest, "The Role of MnS Inclusions in the Development of Environmentally Assisted Cracking of Nuclear Reactor Pressure Vessel Steels," in *Proc. 2nd Int. Atomic Energy Agency Specialists' Meeting on Subcritical Crack Growth*, NUREG/CP-0067, MEA-2090, Vol. 2, pp. 153–178, April 1986.
187. Atkinson, J. D., J. Yu, and Z.-Y. Chen, "An Analysis of the Effects of Sulfur Content and Potential on Corrosion Fatigue Crack Growth in Reactor Pressure Vessel Steels," *Corros. Sci.* 38 (5), 755–765, 1996.
188. Auten, T. A., S. Z. Hayden, and R. H. Emanuelson, "Fatigue Crack Growth Rate Studies of Medium Sulfur Low Alloy Steels Tested in High Temperature Water," *Proc. 6th Int. Symp. on Environmental Degradation of Materials in Nuclear Power Systems – Water Reactors*, R. E. Gold and E. P. Simonen, eds., The Metallurgical Society, Warrendale, PA, pp. 35–40, 1993.
189. Ford, F. P., and P. L. Andresen, "Stress Corrosion Cracking of Low-Alloy Pressure Vessel Steel in 288°C Water," *Proc. 3rd Int. Atomic Energy Agency Specialists' Meeting on Subcritical Crack Growth*, NUREG/CP-0112, Vol. 1, pp. 37–56, Aug. 1990.
190. Ford, F. P., "Overview of Collaborative Research into the Mechanisms of Environmentally Controlled Cracking in the Low Alloy Pressure Vessel Steel/Water System," *Proc. 2nd Int. Atomic Energy Agency Specialists' Meeting on Subcritical Crack Growth*, NUREG/CP-0067, MEA-2090, Vol. 2, pp. 3–71, April 1986.
191. Ford, F. P., D. F. Taylor, and P. L. Andresen, "Corrosion-Assisted Cracking of Stainless and Low-Alloy Steels in LWR Environments," EPRI NP-5064S, Electric Power Research Institute, Palo Alto, CA, Feb. 1987.
192. Ford, F. P., S. Ranganath, and D. Weinstein, "Environmentally Assisted Fatigue Crack Initiation in Low-Alloy Steels - A Review of the Literature and the ASME Code Design Requirements," EPRI Report TR-102765, Electric Power Research Institute, Palo Alto, CA, Aug. 1993.
193. Ford, F. P., "Prediction of Corrosion Fatigue Initiation in Low-Alloy and Carbon Steel/Water Systems at 288°C," *Proc. 6th Intl. Symp. on Environmental Degradation of Materials in Nuclear Power Systems – Water Reactors*, R. E. Gold and E. P. Simonen, eds., The Metallurgical Society, Warrendale, PA, pp. 9–17, 1993.
194. Hänninen, H., K. Törrönen, and W. H. Cullen, "Comparison of Proposed Cyclic Crack Growth Mechanisms of Low Alloy Steels in LWR Environments," in *Proc. 2nd Int. Atomic Energy Agency Specialists' Meeting on Subcritical Crack Growth*, NUREG/CP-0067, MEA-2090, Vol. 2, pp. 73–97, April 1986.
195. Hänninen, H., K. Törrönen, M. Kempainen, and S. Salonen, "On the Mechanisms of Environment Sensitive Cyclic Crack Growth of Nuclear Reactor Pressure Vessel Steels," *Corros. Sci.* 23, 663–679, 1983.

196. Törrönen, K., M. Kempainen, and H. Hänninen, "Fractographic Evaluation of Specimens of A533B Pressure Vessel Steel," EPRI Report NP-3483, Project 1325-7, May 1984.
197. Oriani, R. A., "A Mechanistic Theory of Hydrogen Embrittlement of Steels," *Ber. Bunsenges. Phys. Chem.* 76, 848-857, 1972.
198. Beachem, C. D., "A New Model for Hydrogen Assisted Cracking," *Met. Trans.* 3A (2), 437-451, 1972.
199. Kim, Y. J., "Characterization of the Oxide Film Formed on Type 316 Stainless Steel in 288°C Water in Cyclic Normal and Hydrogen Water Chemistries," *Corrosion* 51 (11), 849-860, 1995.
200. Kim, Y. J., "Analysis of Oxide Film Formed on Type 304 Stainless Steel in 288°C Water Containing Oxygen, Hydrogen, and Hydrogen Peroxide," *Corrosion* 55 (1), 81-88, 1999.
201. Tapping, R. L., Davidson, R. D., McAlpine, E. and Lister, D. H., "The Composition and Morphology of Oxide Films Formed on Type 304 Stainless Steel in Lithiated High-Temperature Water," *Corrosion Sci.* 26 (8), 563-576 (1986).
202. Lister, D. H., Davidson, R. D. and McAlpine, E., "The Mechanism and Kinetics of Corrosion Product Release from Stainless Steel in Lithiated High-Temperature Water," *Corrosion Sci.* 27 (2), 113-140 (1987).
203. Belo, M. Da Cunha, M. Walls, M., Hakiki, N. E., Corset, J., Picquenard, E., Sagon, G. and Neol, D., "Composition, Structure and Properties of the Oxide Films Formed on the Stainless Steel 316L in a Primary Type PWR Environment," *Corrosion Sci.* 40 (2/3), 447-463 (1998).
204. Stellwag, B., "The Mechanism of Oxide Film Formation on Austenitic Stainless Steels in High-Temperature Water," *Corrosion Sci.* 40 (2/3), 337-370 (1998).
205. Nakayama, T. and Oshida, Y., "Identification of the Initial Oxide Films on 18-8 Stainless Steel in High-Temperature Water," *Corrosion NACE* 24 (10), 336-337 (1968).
206. Srinivasan, V. S., M. Valsan, R. Sandhya, K. Bhanu Sankara Rao, M. L. Mannan, and D. H. Sastry, "High Temperature Time-Dependent Low Cycle Fatigue Behavior of a Type 316L(N) Stainless Steel," *Intl. J. Fatigue* 21, 11-21, 1999.
207. Obrtlík, K., J. Polák, M. Hájek, and A. Vasek, "Short Fatigue Crack Behavior in 316L Stainless Steel," *Intl. J. Fatigue* 19, 471-475, 1997.
208. Shack, W. J., and T. F. Kassner, "Review of Environmental Effects on Fatigue Crack Growth of Austenitic Stainless Steels," NUREG/CR-6176, ANL-94/1, May 1994.
209. Chopra, O. K., W. K. Soppet, and W. J. Shack, "Effects of Alloy Chemistry, Cold Work, and Water Chemistry on Corrosion Fatigue and Stress Corrosion Cracking of Nickel Alloys and Welds," NUREG/CR-6721, ANL-01/07, April 2001.
210. Private communication from M. Higuchi, Ishikawajima-Harima Heavy Industries Co. Japan, to M. Prager of the Pressure Vessel Research Council, 1992. The old database "FADAL" has been revised and renamed "JNUFAD."

211. Abdel-Raouf, H., A. Plumtree, and T. H. Topper, "Effects of Temperature and Deformation Rate on Cyclic Strength and Fracture of Low-Carbon Steel," *Cyclic Stress-Strain Behavior – Analysis, Experimentation, and Failure Prediction*, ASTM STP 519, American Society for Testing and Materials, Philadelphia, pp. 28–57, 1973.
212. Lee, B. H., and I. S. Kim, "Dynamic Strain Aging in the High-Temperature Low-Cycle Fatigue of SA 508 Cl. 3 Forging Steel," *J. Nucl. Mater.* 226, 216–225, 1995.
213. Manjoine, M. J., and R. L. Johnson, "Fatigue Design Curves for Carbon and Low Alloy Steels up to 700°F (371°C)," *Material Durability/Life Prediction Modeling: Materials for the 21st Century*, PVP–Vol. 290, American Society of Mechanical Engineers, New York, 1994.
214. Johnson, L. G., "The Median Ranks of Sample Values in Their Population with an Application to Certain Fatigue Studies," *Ind. Math.* 2, 1–9, 1951.
215. Lipson, C., and N. J. Sheth, "Statistical Design and Analysis of Engineering Experiments," McGraw Hill, New York, 1973.
216. Beck, J., and K. Arnold, "Parameter Estimation in Engineering and Science," J. Wiley, New York, 1977.
217. Maiya, P. S., and D. E. Busch, "Effect of Surface Roughness on Low-Cycle Fatigue Behavior of Type 304 Stainless Steel," *Met. Trans.* 6A, 1761–1766, 1975.
218. Maiya, P. S., "Effect of Surface Roughness and Strain Range on Low-Cycle Fatigue Behavior of Type 304 Stainless Steel," *Scripta Metall.* 9, 1277–1282, 1975.
219. Stout, K. J., "Surface Roughness – Measurement, Interpretation, and Significance of Data," *Mater. Eng.* 2, 287–295, 1981.
220. Iida, K., "A Study of Surface Finish Effect Factor in ASME B & PV Code Section III," *Pressure Vessel Technology*, Vol. 2, L. Cengdian and R. W. Nichols, eds., Pergamon Press, New York, pp. 727–734, 1989.
221. Stambaugh, K. A., D. H. Leeson, F. V. Lawrence, C. Y. Hou, and G. Banas, "Reduction of S-N Curves for Ship Structural Details," *Welding Research Council* 398, January 1995.
222. Miller, K. J. and W. J. O'Donnell, "The Fatigue Limit and its Elimination," *Fatigue Fract. Eng. Mater. Struct.* 22, 545-557, 1999.
223. Wire, G. L., T. R. Leax, and J. T. Kandra, "Mean Stress and Environmental Effects on Fatigue in Type 304 Stainless Steel," in *Probabilistic and Environmental Aspects of Fracture and Fatigues*, PVP Vol. 386, S. Rahman, ed., American Society of Mechanical Engineers, New York, pp. 213–228, 1999.
224. Diercks, D. R., "Development of Fatigue Design Curves for Pressure Vessel Alloys Using a Modified Langer Equation," *Trans. ASME J. Pressure Vessel Technol.* 101, 292–297, 1979.
225. Solomon, H. D., and C. Amzallag, "Comparison of Models Predicting the Fatigue Behavior of Austenitic Stainless Steels," *Proc. of the 2005 ASME Pressure Vessels and Piping Conf.*, July 17–21, 2005, Denver, CO, paper # PVP2005–71063.



226. Pleune, T. T., and O. K. Chopra, "Artificial Neural Networks and Effects of Loading Conditions on Fatigue Life of Carbon and Low-Alloy Steels," *Fatigue and Fracture* Vol. 1, PVP Vol. 350, S. Rahman, K. K. Yoon, S. Bhandari, R. Warke, and J. M. Bloom, eds., American Society of Mechanical Engineers, New York, pp. 413–423, 1997.
227. Solomon, H. D., R. E. DeLair, and A. D. Unruh, "Crack Initiation in Low-Alloy Steel in High-Purity Water," *Effects of the Environment on the Initiation of Crack Growth*, ASTM STP 1298, W. A. Van Der Sluys, R. S. Piascik, and R. Zawierucha, eds., American Society for Testing and Materials, Philadelphia, pp. 135–149, 1997.
228. Solomon, H. D., R. E. DeLair, and E. Tolksdorf, "LCF Crack Initiation in WB36 in High-Temperature Water," *Proc. 9th Intl. Symp. on Environmental Degradation of Materials in Nuclear Power Systems – Water Reactors*, F. P. Ford, S. M. Bruemmer, and G. S. Was, eds., The Minerals, Metals, and Materials Society, Warrendale, PA, pp. 865–872, 1999.
229. Chopra, O. K., "Estimation of Fracture Toughness of Cast Stainless Steels During Thermal Aging in LWR Systems," NUREG/CR-4513, ANL-93/22, Aug. 1994.
230. Chopra, O. K., and A. Sather, "Initial Assessment of the Mechanisms and Significance of Low-Temperature Embrittlement of Cast Stainless Steels in LWR Systems," NUREG/CR-5385, ANL-89/17, Aug. 1990.
231. Michaud, W. F., P. T. Toben, W. K. Soppet, and O. K. Chopra, "Tensile Property Characterization of Thermally Aged Cast Stainless Steels," NUREG/CR-6142, ANL-93/35, Feb. 1994.
232. Chopra, O. K., "Effect of Thermal Aging on Mechanical Properties of Cast Stainless Steels," in *Proc. of the 2nd Int. Conf. on Heat-Resistant Materials*, K. Natesan, P. Ganesan, and G. Lai, eds., ASM International, Materials Park, OH, pp. 479–485, 1995.
233. Higuchi, M., "Review and Consideration of Unsettled Problems on Evaluation of Fatigue Damage in LWR Water," *Proc. of the 2005 ASME Pressure Vessels and Piping Conf.*, July 17–21, 2005, Denver, CO, paper # PVP2005-71306.
234. Mayfield, M. E., E. C. Rodabaugh, and R. J. Eiber, "A Comparison of Fatigue Test Data on Piping with the ASME Code Fatigue Evaluation Procedure," ASME Paper 79-PVP-92, American Society of Mechanical Engineers, New York, 1979.
235. Heald, J. D., and E. Kiss, "Low Cycle Fatigue of Nuclear Pipe Components," *J. Pressure Vessel Technol.* 74, PVP-5, 1–6, 1974.
236. Deardorff, A. F., and J. K. Smith, "Evaluation of Conservatisms and Environmental Effects in ASME Code, Section III, Class 1 Fatigue Analysis," SAND94-0187, prepared by Structural Integrity Associates, San Jose, CA, under contract to Sandia National Laboratories, Albuquerque, NM, 1994.
237. Kooistra, L. F., E. A. Lange, and A. G. Pickett, "Full-Size Pressure Vessel Testing and Its Application to Design," *J. Eng. Power* 86, 419–428, 1964.

238. Scott, P. M., and G. M. Wilkowski, "A Comparison of Recent Full-Scale Component Fatigue Data with the ASME Section III Fatigue Design Curves," in *Fatigue and Crack Growth: Environmental Effects, Modeling Studies, and Design Considerations*, PVP Vol. 306, S. Yukawa, ed., American Society of Mechanical Engineers, New York, pp. 129–138, 1995.
239. Hechmer, J., "Evaluation Methods for Fatigue - A PVRC Project," in *Fatigue, Environmental Factors, and New Materials*, PVP Vol. 374, H. S. Mehta, R. W. Swindeman, J. A. Todd, S. Yukawa, M. Zako, W. H. Bamford, M. Higuchi, E. Jones, H. Nickel, and S. Rahman, eds., American Society of Mechanical Engineers, New York, pp. 191–199, 1998.
240. Manjoine, M. J., "Fatigue Damage Models for Annealed Type 304 Stainless Steel under Complex Strain Histories," *Trans. 6th Intl. Conf. on Structural Mechanics in Reactor Technology (SMiRT)*, Vol. L, 8/1, North-Holland Publishing Co., pp. 1–13, 1981.
241. Nian, L., and Du Bai-Ping, "The Effect of Low-Stress High-Cycle Fatigue on the Microstructure and Fatigue Threshold of a 40Cr Steel," *Int. J. Fatigue* 17 (1), 43–48, 1995.

## APPENDIX A INCORPORATING ENVIRONMENTAL EFFECTS INTO FATIGUE EVALUATIONS

---

### A1 Scope

This Appendix provides the environmental fatigue correction factor ( $F_{en}$ ) methodology that is considered acceptable for incorporating the effects of reactor coolant environments in fatigue usage factor evaluations of metal components. The methodology for performing fatigue evaluations for the four major categories of structural materials, e.g., carbon steels, low-alloy steels, wrought and cast austenitic stainless steels, and Ni-Cr-Fe alloys, is described.

### A2 Environmental Correction Factor ( $F_{en}$ )

The effects of reactor coolant environments on the fatigue lives of structural materials are expressed in terms of a nominal environmental fatigue correction factor,  $F_{en,nom}$ , which is defined as the ratio of fatigue life in air at room temperature ( $N_{air,RT}$ ) to that in water at the service temperature ( $N_{water}$ ):

$$F_{en,nom} = N_{air,RT}/N_{water} \quad (A.1)$$

The nominal environmental fatigue correction factor,  $F_{en,nom}$ , for both carbon and low-alloy steels is expressed as

$$F_{en,nom} = \exp((0.003 - 0.031 \dot{\epsilon}^*) S^* T^* O^*) \quad (A.2)$$

where  $S^*$ ,  $T^*$ ,  $O^*$ , and  $\dot{\epsilon}^*$  are transformed sulfur (S) content, material temperature, dissolved oxygen (DO) level, and strain rate, respectively, defined as:

$$\begin{aligned} S^* &= 2.0 + 98 S & (S \leq 0.015 \text{ wt. \%}) \\ S^* &= 3.47 & (S > 0.015 \text{ wt. \%}) \end{aligned} \quad (A.3)$$

$$\begin{aligned} T^* &= 0.395 & (T < 150 \text{ }^\circ\text{C}) \\ T^* &= (T - 75)/190 & (150^\circ\text{C} \leq T \leq 325 \text{ }^\circ\text{C}) \end{aligned} \quad (A.4)$$

$$\begin{aligned} O^* &= 1.49 & (DO < 0.04 \text{ ppm}) \\ O^* &= \ln(DO/0.009) & (0.04 \text{ ppm} \leq DO \leq 0.5 \text{ ppm}) \\ O^* &= 4.02 & (DO > 0.5 \text{ ppm}) \end{aligned} \quad (A.5)$$

$$\begin{aligned} \dot{\epsilon}^* &= 0 & (\dot{\epsilon}^* > 2.2\%/s) \\ \dot{\epsilon}^* &= \ln(\dot{\epsilon}^*/2.2) & (0.0004\%/s \leq \dot{\epsilon}^* \leq 2.2\%/s) \\ \dot{\epsilon}^* &= \ln(0.0004/2.2) & (\dot{\epsilon}^* < 0.0004\%/s) \end{aligned} \quad (A.6)$$

For carbon and low-alloy steels, a threshold value of 0.07% for strain amplitude (one-half the strain range for the cycle) is defined, below which environmental effects on the fatigue lives of these steels may not occur. Thus,

$$F_{en,nom} = 1 \quad (\epsilon_a \leq 0.07\%) \quad (A.7)$$

Note that the strain amplitude threshold should not be applied when using a modified rate approach, as it may yield non-conservative results.

For wrought and cast austenitic stainless steels,

$$F_{en,nom} = \exp(-T' O' \dot{\epsilon}') \quad (A.8)$$

where  $T'$ ,  $\dot{\epsilon}'$ , and  $O'$  are transformed temperature, strain rate, and DO level, respectively, defined as:

$$\begin{aligned} T' &= 0 & (T \leq 100^\circ\text{C}) \\ T' &= (T - 100)/250 & (100^\circ\text{C} \leq T < 325^\circ\text{C}) \end{aligned} \quad (A.9)$$

$$\begin{aligned} \dot{\epsilon}' &= 0 & (\dot{\epsilon}' > 10\%/s) \\ \dot{\epsilon}' &= \ln(\dot{\epsilon}/10) & (0.0004\%/s \leq \dot{\epsilon}' \leq 10\%/s) \\ \dot{\epsilon}' &= \ln(0.0004/10) & (\dot{\epsilon}' < 0.0004\%/s) \end{aligned} \quad (A.10)$$

For DO less than 0.1 ppm, i.e., for PWR or BWR HWC water:

$$O' = 0.29 \quad (\text{all wrought and cast SSs and heat treatments and SS weld metals})$$

For DO greater than or equal to 0.1 ppm (i.e., for BWR NWC water):

$$\begin{aligned} O' &= 0.29 & (\text{sensitized high-carbon wrought and cast SSs}) \\ O' &= 0.14 & (\text{all wrought SSs except sensitized high-carbon SSs}) \end{aligned} \quad (A.11)$$

For wrought and cast austenitic stainless steels, a threshold value of 0.10% for strain amplitude (one-half the strain range for the cycle) is defined, below which environmental effects on the fatigue lives of these steels do not occur. Thus,

$$F_{en,nom} = 1 \quad (\epsilon_a \leq 0.10\%) \quad (A.12)$$

Note that the strain amplitude threshold should not be applied when using a modified rate approach, as it may yield non-conservative results.

For Ni-Cr-Fe alloys,

$$F_{en,nom} = \exp(-T' \dot{\epsilon}' O') \quad (A.13)$$

where  $T'$ ,  $\dot{\epsilon}'$ , and  $O'$  are transformed temperature, strain rate, and DO, respectively, defined as:

$$\begin{aligned} T' &= 0 & (T < 50^\circ\text{C}) \\ T' &= (T - 50)/275 & (50^\circ\text{C} \leq T \leq 325^\circ\text{C}) \end{aligned} \quad (A.14)$$

$$\begin{aligned} \dot{\epsilon}' &= 0 & (\dot{\epsilon}' > 5.0\%/s) \\ \dot{\epsilon}' &= \ln(\dot{\epsilon}/5.0) & (0.0004\%/s \leq \dot{\epsilon}' \leq 5.0\%/s) \\ \dot{\epsilon}' &= \ln(0.0004/5.0) & (\dot{\epsilon}' < 0.0004\%/s) \end{aligned} \quad (A.15)$$

$$\begin{aligned} O' &= 0.06 & (\text{NWC BWR water, i.e., } \geq 0.1 \text{ ppm DO}) \\ O' &= 0.14 & (\text{PWR or HWC BWR water, i.e., } < 0.1 \text{ ppm DO}) \end{aligned} \quad (A.16)$$

For Ni-Cr-Fe alloys, a threshold value of 0.10% for strain amplitude (one-half the strain range for the cycle) is defined, below which environmental effects on the fatigue lives of these alloys do not occur. Thus,

$$F_{en,nom} = 1 \quad (\varepsilon_a \leq 0.10\%) \quad (A.17)$$

Note that the strain amplitude threshold should not be applied when using a modified rate approach, as it may yield non-conservative results.

For all materials, a maximum temperature limit was selected at 325°C as a reasonable extension to cover all anticipated LWR operating conditions. This is adequate for all expected operating LWR conditions considering the use of average temperature.

### A3 Fatigue Evaluation Procedure

The environmental fatigue evaluation method uses as its input the partial fatigue usage factors  $U_1, U_2, U_3, \dots, U_n$ , determined in fatigue evaluations. To incorporate environmental effects into the fatigue evaluation, the partial fatigue usage factor for a specific stress cycle or load set pair, based on the fatigue design curves, is multiplied by the environmental fatigue correction factor:

$$U_{en,1} = U_1 \cdot F_{en,1} \quad (A.18)$$

In the ASME Code Section III design-by-analysis (NB-3200) methods, the partial fatigue usage factors are calculated for each type of stress cycle in Subparagraph NB-3222.4(e)(5). For piping products designed using NB-3600 methods, Paragraph NB-3653 provides the procedures for the calculation of partial fatigue usage factors for each of the load set pairs. The partial usage factors are obtained from the fatigue design curves provided they are consistent, or conservative, with respect to the existing fatigue  $\varepsilon$ - $N$  data. For example, the ASME Code Section III fatigue design curve for austenitic SSs developed in the 1960s (i.e., the design curve in Code editions prior to 2009b Addenda) is not consistent with the fatigue database used to develop the environmental factors in this report and, therefore, may give non-conservative estimates of environmental fatigue usage factors for most heats of austenitic SSs used in the construction of nuclear reactor components. The current ASME Code fatigue design curve (i.e., the design curve in Code editions as of the 2009b Addenda) is consistent with the ANL fatigue life model (presented in Fig. 49), and is consistent with the fatigue  $\varepsilon$ - $N$  database used in this report. Examples of calculating partial usage factors are as follows:

- (1) For carbon and low-alloy steels with ultimate tensile strengths less than 552 MPa (80 ksi), the partial fatigue usage factors are obtained from the ASME Code fatigue design curve, i.e., Fig. I-9.1 of Mandatory Appendix I to Section III of the ASME Code. As an alternative, to reduce conservatism in the current Code fatigue design curve for carbon steel and the Code requirement of a factor of 20 on life, partial usage factors may be determined from the fatigue design curves developed from the ANL fatigue life model, i.e., Figs. A.1 and A.2 and Table A.1.
- (2) For wrought or cast austenitic SSs and Ni-Cr-Fe alloys, the partial fatigue usage factors are obtained from the fatigue design curve in the 2009b Addenda or later editions of the ASME Code, i.e., Fig. I-9.2 of Mandatory Appendix I to Section III of the ASME Code, which is the same as the ANL fatigue design curve. The ANL fatigue design curve is based on the ANL fatigue life model and was developed using a factor of 12 on life, i.e., Fig. A.3 and Table A.2.

The cumulative fatigue usage factor,  $U_{en}$ , considering the effects of reactor coolant environments is then calculated as follows:

$$U_{en} = U_1 \cdot F_{en,1} + U_2 \cdot F_{en,2} + U_3 \cdot F_{en,3} + U_i \cdot F_{en,i} \dots + U_n \cdot F_{en,n} \quad (A.19)$$

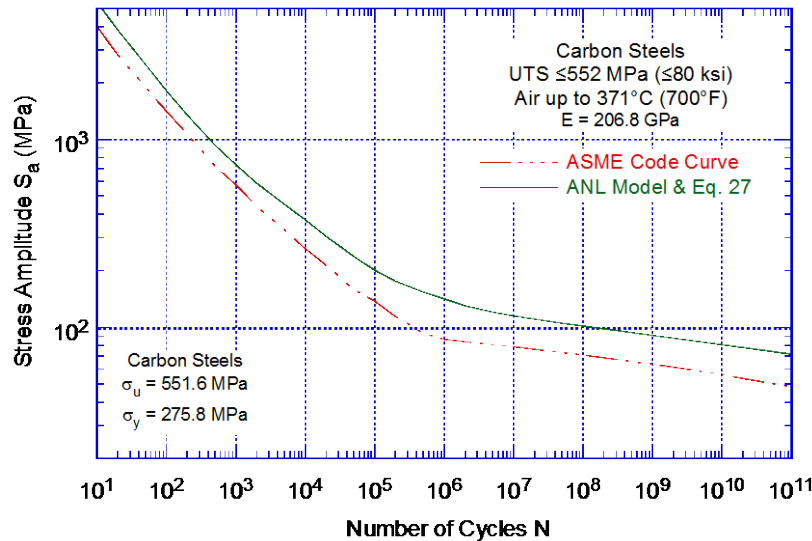


**Figure A.1.**  
Fatigue design curves for carbon steels in air. The curve developed from the ANL model is based on factors of 12 on life and 2 on stress.

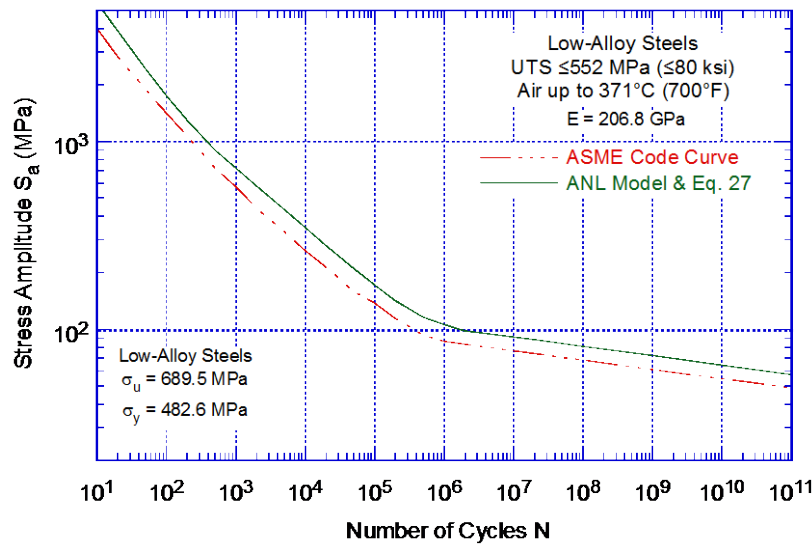


**Figure A.2.**  
Fatigue design curves for low-alloy steels in air. The curve developed from the ANL model is based on factors of 12 on life and 2 on stress.

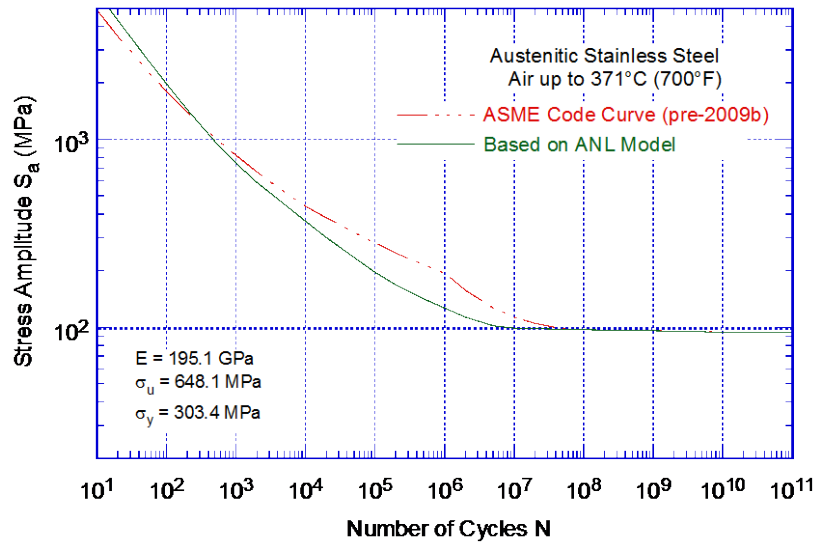


**Figure A.3.**  
Fatigue design curve for austenitic stainless steels in air. The curve developed from the ANL model is based on factors of 12 on life and 2 on stress.

**Table A.1. Fatigue design curves for carbon and low-alloy steels in air.**

Cycles	Stress Amplitude, MPa (ksi)			Cycles	Stress Amplitude, MPa (ksi)		
	ASME Code Curve	Carbon Steel	Low-Alloy Steel		ASME Code Curve	Carbon Steel	Low-Alloy Steel
1 E+01	3999 (580)	5355 (777)	5467 (793)	2 E+05	114 (16.5)	176 (25.5)	141 (20.5)
2 E+01	2827 (410)	3830 (556)	3880 (563)	5 E+05	93.1 (13.5)	154 (22.3)	116 (16.8)
5 E+01	1896 (275)	2510 (364)	2438 (354)	1 E+06	86.2 (12.5)	142 (20.6)	106 (15.4)
1 E+02	1413 (205)	1820 (264)	1760 (255)	2 E+06		130 (18.9)	98 (14.2)
2 E+02	1069 (155)	1355 (197)	1300 (189)	5 E+06		120 (17.4)	94 (13.6)
5 E+02	724 (105)	935 (136)	900 (131)	1 E+07	76.8 (11.1)	115 (16.7)	91 (13.2)
1 E+03	572 (83)	733 (106)	720 (104)	2 E+07		110 (16.0)	88 (12.7)
2 E+03	441 (64)	584 (84.7)	576 (83.5)	5 E+07		105 (15.2)	84 (12.2)
5 E+03	331 (48)	451 (65.4)	432 (62.7)	1 E+08	68.5 (9.9)	101 (14.7)	81 (11.8)
1 E+04	262 (38)	373 (54.1)	342 (49.6)	1 E+09	61.1 (8.8)	90 (13.1)	72.3 (10.5)
2 E+04	214 (31)	305 (44.2)	276 (40.0)	1 E+10	54.4 (7.9)	81 (11.7)	64.4 (9.3)
5 E+04	159 (23)	238 (34.5)	210 (30.5)	1 E+11	48.5 (7.0)	72 (10.4)	57.4 (8.3)
1 E+05	138 (20.0)	201 (29.2)	172 (24.9)				

**Table A.2. Fatigue design curves for austenitic stainless steels in air.**

Cycles	Stress Amplitude, MPa (ksi)	Cycles	Stress Amplitude, MPa (ksi)
	New Design Curve		New Design Curve
1 E+01	6000 (870)	2 E+05	168 (24.4)
2 E+01	4300 (624)	5 E+05	142 (20.6)
5 E+01	2748 (399)	1 E+06	126 (18.3)
1 E+02	1978 (287)	2 E+06	113 (16.4)
2 E+02	1440 (209)	5 E+06	102 (14.8)
5 E+02	974 (141)	1 E+07	99 (14.4)
1 E+03	745 (108)	1 E+08	97.1 (14.1)
2 E+03	590 (85.6)	1 E+09	95.8 (13.9)
5 E+03	450 (65.3)	1 E+10	94.4 (13.7)
1 E+04	368 (53.4)	1 E+11	93.7 (13.6)
2 E+04	300 (43.5)		
5 E+04	235 (34.1)		
1 E+05	196 (28.4)		

where  $F_{en,i}$  is the nominal environmental fatigue correction factor for the " $i^{th}$ " stress cycle (NB-3200) or load set pair (NB-3600). Because environmental effects on fatigue lives occur primarily during the tensile-loading cycle (i.e., up-ramp with increasing strain or stress), this calculation is performed only for the tensile stress producing portion of the stress cycle

constituting a load pair. Also, the values for key parameters such as strain rate, material temperature, DO in the water, and for carbon and low-alloy steels S content, are needed to calculate  $F_{en}$  for each stress cycle or load set pair. As discussed in Section 4 of this report, the following guidance may be used to determine these parameters:

- (1) An average strain rate for the transient typically yields a conservative estimate of  $F_{en}$ . For complex loading conditions, the strain rates used in the calculations should produce results that are consistent with the results that would be obtained using the modified rate approach described in Section 4.1.14 of this report. The lower bound or saturation strain rate of 0.0004%/s can be used to perform the most conservative evaluation.
- (2) For the case of a constant strain rate and a linear temperature response, an average temperature (i.e., average of the maximum temperature for the transient and the higher of the threshold temperature for the material under consideration and the minimum temperature for the transient) may be used to calculate  $F_{en}$ . In general, the “average” temperature used in the calculations should produce results that are consistent with the results that would be obtained using the modified rate approach described in Section 4.1.14 of this report. The maximum temperature can be used to perform the most conservative evaluation.
- (3) The DO value is obtained from each transient constituting the stress cycle. For carbon and low-alloy steels, the DO content associated with a stress cycle is the highest oxygen level in the transient, and for austenitic stainless steels, it is the lowest DO level in the transient. A value of 0.5 ppm for carbon and low-alloy steels and 0.05 ppm for austenitic stainless steels and Ni alloys can be used for the DO content to perform a conservative evaluation.
- (4) The sulfur content, S, in terms of weight percent might be obtained from the certified material test report or an equivalent source. If the sulfur content is unknown, then its value shall be assumed as the maximum value specified in the procurement specification or the applicable construction Code.

The detailed procedures for incorporating environmental effects into the Code fatigue evaluations have been presented in several articles and reports. The following are just two examples of such documents that may be used for guidance:

- (1) Mehta, H. S., “An Update on the Consideration of Reactor Water Effects in Code Fatigue Initiation Evaluations for Pressure Vessels and Piping,” Assessment Methodologies for Preventing Failure: Service Experience and Environmental Considerations, PVP Vol. 410-2, R. Mohan, ed., American Society of Mechanical Engineers, New York, pp. 45–51, 2000.
- (2) Nakamura, T., M. Higuchi, T. Kusunoki, and Y. Sugie, “JSME Codes on Environmental Fatigue Evaluation,” Proc. of the 2006 ASME Pressure Vessels and Piping Conf., July 23–27, 2006, Vancouver, BC, Canada, paper # PVP2006-ICPVT11-93305.

In addition, Appendix C of this report presents a sample application of the  $F_{en}$  methodology.



## APPENDIX B MATERIAL INFORMATION

The various grades, heat treatment, chemical composition, and mechanical properties of the carbon and low-alloy steels, austenitic stainless steels, and Ni-Cr-Fe alloy steels used in this report are provided in this appendix.

### B1 Carbon and Low-Alloy Steels Included in the Fatigue Database

The various grades, heat treatment, chemical composition, and mechanical properties of the carbon and low-alloy steels used in this report are listed in the following table.

Mat. ID	Heat Designation	Heat Treatment	Chemical Composition (wt.%)								YS (MPa)	UTS (MPa)	Elong. (%)	RA (%)	Reference	
			C	Si	Mn	P	S	Ni	Cr	Mo						
Carbon Steels																
1	A106-Gr.B-A	-	0.29	0.25	0.88	0.013	0.015	0.09	0.19	0.05	301	572	23.5	44.0	10	
2	A106-Gr.B-H	-	0.24	0.29	0.91	0.01	0.007	-	-	-	333	559	34.0	-	136	
3	A106-Gr.B-T	-	0.26	0.28	0.92	0.008	0.020	0.002	0.015	0.003	300	523	36.3	66.3	45	
4	A106-Gr.C-1	-	0.24	0.27	1.27	0.022	0.006	-	-	-	340	520	37.0	-	136	
5	A106-Gr.C-2	-	0.21	0.24	1.25	0.003	0.020	-	-	-	390	533	34.0	72.0	136	
6	A106-Gr.C-3	-	0.27	0.29	0.87	0.012	0.007	-	-	-	323	519	35.0	-	136	
7	A226-Cl.4	650°C×1.5hr	0.19	0.23	1.24	0.005	0.004	-	-	-	347	501	36.0	77.0	136	
8	A333-Gr.6-1	900°C×10hxA	0.16	0.14	1.2	0.026	0.015	-	-	-	353	539	36.0	-	136	
9	A333-Gr.6-2	900°C×0.5hxA	0.20	0.31	0.93	0.020	0.015	-	-	-	302	490	41.0	80.0	136	
10	A333-Gr.6-3	900°C ×2hxA	0.16	0.29	1.26	0.02	0.014	-	-	-	297	426	36.4	77.0	136	
11	A333-Gr.6-4	-	0.15	0.2	1.25	0.019	0.006	-	-	-	314	490	41.0	-	136	
12	A333-Gr.6-5	-	0.21	0.31	1.14	0.016	0.012	-	-	-	383	549	35.0	-	136	
13	A333-Gr.6-GE	-	0.12	0.23	1.05	0.010	0.030	-	-	-	309	427	-	-	17	
14	A333-Gr.6-7	As received	0.21	0.27	1.29	0.01	0.008	-	-	-	310	531	34.0	74.0	136	
15	A333-Gr.6-8	900°C×0.5hxA	0.20	0.26	1.14	0.01	0.016	-	-	-	348	509	36.0	76.0	136	
16	A333-Gr.6-9	650°C×1.5hr	0.21	0.27	1.29	0.011	0.026	-	-	-	278	524	36.0	73.0	136	
17	A508-Gr.1-1	870°C×6.0h×W, 620°C×1.0h×AC, 635°C×46.0h×FC	0.20	0.26	1.31	0.008	0.008	0.35	0.06	0.02	335	503	38.5	72.1	136	
18	A508-Gr.1-2	-	0.19	0.23	1.24	0.005	0.004	0.32	0.21	0.02	347	501	36.0	77.0	136	
19	A508-Gr.1-3	-	0.21	0.30	1.25	0.011	0.008	-	-	-	350	540	34.8	72.1	136	
20	A216-Gr.WCC	-	0.22	0.40	0.90	0.013	0.015	0.14	0.20	0.17	316	500	31.6	58.0	136	
21	A516-KC70-	-	0.26	0.28	0.95	0.017	0.033	-	-	-	331	514	31.0	-	14	
22	A516-G70	As received	0.23	0.24	1.11	0.012	0.002	-	0.05	-	330	526	30.0	-	136	
23	CS Tube	-	-	-	-	-	-	-	-	-	-	-	-	-	-	

Mat. ID	Heat Designation	Heat Treatment	Chemical Composition (wt.%)								YS (MPa)	UTS (MPa)	Elong. (%)	RA (%)	Reference
			C	Si	Mn	P	S	Ni	Cr	Mo					
24	CS	-	-	-	-	-	-	-	-	-	-	-	-	-	-
Low-Alloy Steels															
1	A302-Gr.B	899-927°Cx4hWQ to 538°Cx4.649-tempered @ 677°C:621-649°Cx6hxA	0.21	0.22	1.34	0.021	0.027	0.23	0.14	0.51	389	552	-	-	10
2	A508-Gr.2	880°CX4.5hXWC+665°CX4.3hXAC+620°CX46.2hXFC	0.21	0.25	0.88	0.007	0.003	0.86	0.42	0.66	521	673	22.9	72.5	136
3	A508-Gr.2	-	0.21	0.25	0.68	0.01	0.011	0.84	0.36	0.65	469	629	28	-	136
4	A508-Gr.2	880°CX6hXWC+660°CX10hXAC+620°CX45hXFC	0.18	0.31	0.77	0.008	0.008	0.74	0.36	0.6	510	637	27	74	136
5	A508-Gr.2	880°CXWC+660°CXAC+620°CXFC	0.20	0.26	0.94	0.006	0.008	0.78	0.36	0.6	583	655	24	76	136
6	A508-Gr.3	880°CX7hXWC+654°CX8hXWC	0.17	0.28	1.38	0.003	0.003	0.74	0.15	0.48	447	598	29.1	73	136
7	A508-Gr.3	900°Cx16.7hxA:650°Cx16.5hxF:890°Cx9.1hXW:660°Cx9.0hxA	0.20	0.26	1.42	0.004	0.002	0.74	0.11	0.5	453	605	30	69	136
8	A508-Gr.3	900°Cx8.3hxA:650°Cx8.0hx:880°Cx4.8hXW:660°Cx4.1hxA	0.23	0.27	1.5	0.004	0.003	0.77	0.13	0.52	503	637	26	69	141
9	A508-Gr.3	910°Cx8hxA:660°Cx7.0hxA:890°Cx8.0hXW:650°Cx8.0hxA	0.18	0.22	1.46	0.003	0.005	0.69	0.15	0.57	476	602	30.9	74.7	55.56
10	A508-Gr.3	910°CX8.0hXAC+660°CX7.0hXAC+890°CX8.0hXWC+650°CX8.0hXAC	0.20	0.29	1.45	0.003	0.003	0.68	0.12	0.55	476	611	29.9	74.4	10
11	A508-Gr.3	930°Cx8hxA:660°Cx5.0hxA:890°Cx6.0hXW:660°Cx8.0hxA	0.19	0.2	1.46	0.003	0.003	0.76	0.15	0.48	456	596	24.5	75.5	136,141
12	A508-Gr.3	910°Cx8hxA:660°Cx7.0hxA:890°Cx8.0hXW:650°Cx8.0hxA	0.20	0.29	1.45	0.003	0.003	0.68	0.12	0.55	476	611	29.9	74.4	136
13	A508-Gr.3	-	0.20	0.26	0.94	0.006	0.008	0.78	0.36	0.6	533	655	24	76	136
14	A508-Gr.3	880°C x 7h water quenching, 655°C x 9h air cooling	0.21	0.25	1.24	0.007	0.002	0.88	0.21	0.47	461	593	29	74	136
15	A508-Gr.3	-	-	-	-	-	0.018	-	-	-	-	-	-	-	136
16	A533-Gr.B	871-899°Cx5.5hxBQ:649-663°Cx5.5hxBQ:607°Cx23.8hxA	0.22	0.19	1.3	0.01	0.012	0.51	0.18	0.48	431	602	27.8	66.6	136
17	A533-Gr.B	880°CX0.0hXWC+660°CX5.0hXFC	0.19	0.24	1.28	0.008	0.007	0.64	0.19	0.45	454	601	29	68	136
18		900°Cx5.0hxA:640°Cx5.0hxA:880°Cx4.0hXW:660°Cx4.0hxA	0.17	0.27	1.32	0.004	0.001	0.65	0.13	0.55	518	647	26.8	72.8	136
19	A533-Gr.B	900°Cx8.0hxA:635°Cx12.3hxA:880°Cx8.0hXW:655°Cx6.2hxA	0.18	0.27	1.39	0.008	0.003	0.61	0.15	0.54	580	647	27	73	55.56
20	A533-Gr.B	900°Cx3.3hxA:880°Cx3.3hXW:655°Cx3.3hxA	0.18	0.22	1.42	0.004	0.002	0.69	0.09	0.49	443	597	31	74	55.56
21	A533-Gr.B	880°CX5.6hXWC+660°CX4.9hXAC+615°CX45.9hXFC	0.19	0.27	1.45	0.02	0.010	0.60	0.13	0.52	488	630	27.7	65.2	55.56

Mat. ID	Heat Designation	Heat Treatment	Chemical Composition (wt.%)								YS (MPa)	UTS (MPa)	Elong. (%)	RA (%)	Reference	
			C	Si	Mn	P	S	Ni	Cr	Mo						
22	A533-Gr.B	880°C x 5.6h x W: 660°C x 4.9h x A: 615°C x 4.5.9h x F: 375°C x 480.0h x F	0.18	0.31	0.77	0.008	0.008	0.008	0.74	0.36	0.6	510	637	27	74.0	136
23	A533-Gr.B	900°C x 3h water quenching, 660°C x 3h air cooling, then 600°C x 25h to relieve stress	0.17	0.25	1.39	0.003	0.013	0.013	0.59	0.004	0.46	483	584	23.5	58	136
24	A533-Gr.B	900°C x 3h water quenching, 660°C x 3h air cooling, then 600°C x 25h to relieve stress	0.17	0.24	1.38	0.003	0.025	0.025	0.60	0.004	0.47	488	582	21.5	52	55,56
25	A533-Gr.B	-	0.17	0.24	0.36	0.003	0.038	0.038	0.59	0.009	0.47	-	-	-	-	55,56
26	A533- Gr. B (SQV2A)	-	0.22	0.28	1.43	0.021	0.021	0.021	0.51	0.1	0.49	481	617	-	-	55,56
27	A533-Gr.B Cl.2	-	0.18	0.24	1.43	0.003	0.003	<0.001	0.66	-	0.57	548	679	26	75	136
28	A533-Gr.B	-	-	-	-	-	-	0.014	-	-	-	-	-	-	-	136
29	LAS	-	-	-	-	-	-	-	-	-	-	-	-	-	-	136
30	15MnNi63	-	-	-	-	-	-	-	-	-	-	-	-	-	-	136
31	17MnNiMoV64	-	-	-	-	-	-	-	-	-	-	-	-	-	-	136

## B2 Wrought and Cast Austenitic Stainless Steels and Welds

The various grades, heat treatment, chemical composition, and mechanical properties of the wrought and cast austenitic stainless steels and associated weld metals used in this report are listed in the following table.

Mat. ID	Heat Designation	Chemical Composition (wt.%)								YS (MPa)	UTS (MPa)	Elong. (%)	RA (%)	Reference
		C	Si	Mn	P	S	Ni	Cr	Mo					
Type 304 Stainless Steel														
1	304-1	0.050	0.50	1.52	0.028	0.001	9.45	18.35	-	253	570	66.3	78.6	136
2	304-2H	0.050	0.26	0.74	0.032	0.022	8.21	18.14	0.15	252	605	78.8	80.7	
3	304-3, 3H	0.060	0.50	1.55	0.023	0.001	9.35	18.35	-	260	573	59.7	81.7	136
4	304-4B	0.050	0.51	0.15	0.035	0.004	9.04	18.52	-	-	-	-	-	136
5	304-5B	0.060	0.54	0.11	0.027	0.008	8.87	18.51	-	-	-	-	-	136
6	304-6B	0.060	0.56	0.16	0.040	0.005	9.20	18.35	-	-	-	-	-	136
7	304-7B	0.059	0.69	0.08	0.025	0.005	8.89	18.28	-	-	-	-	-	136
8	304-8B	0.060	0.54	0.09	0.025	0.007	8.69	18.15	-	-	-	-	-	136
9	304-9T	0.070	0.27	1.69	0.033	0.009	8.15	18.16		223	602	63.0	79.8	136
10	304-10	0.060	0.50	0.80	0.032	0.010	8.82	18.35	0.19	222	667	72.9	77.6	136
11	304-11H	0.070	0.56	1.60	0.023	0.007	9.40	18.30	-	237	628	53.0	80.0	136
12	304-12	-	-	-	-	-	-	-	-	-	600	-	-	136
13	304-13	0.026	0.40	0.45	0.030	0.014	8.50	18.67	0.02	255	745	-	74.3	64
14	304-14	0.026	0.40	0.45	0.030	0.014	8.50	18.67	0.02	745	951	-	68.8	64
15	304-15	-	-	-	-	-	-	-	-	-	-	-	-	63
16	304-16	0.060	0.31	1.89	0.026	0.025	9.96	19.92	0.15	305	632	60.9	69.1	68
17	304-17	-	-	-	-	-	-	-	-	-	-	-	-	65
18	304-18	0.020	0.49	1.78	0.014	0.011	9.78	18.50	-	276.5	572.2	-	-	71
19	304-19	-	-	-	-	-	-	-	-	-	-	-	-	61
20	304-G	0.070	0.54	1.63	0.016	0.013	9.50	18.57	-	251	561	64.0	-	14,15
21	304-A2	0.060	0.48	1.54	0.019	0.007	8.00	18.99	0.44	-	-	-	-	45
22	304-21T	0.060	0.59	0.83	0.023	0.002	9.17	18.89	-	246	604	57.4	70.4	136
23	304-32	0.070	0.27	1.69	0.033	0.009	8.15	18.16	-	221	616	62.0	77.4	136
24	304-35	0.070	0.65	0.91	0.022	0.002	8.09	18.48	-	245	682	59.0	73.0	136
25	304-xxT	0.050	0.48	1.72	0.027	0.003	9.23	18.12	-	274	580	60.0	78.0	136,10
26	304HP-1	0.050	0.54	0.88	0.029	0.010	9.10	18.53	0.12	242	666	68.0	82.0	136
27	304HP-2	0.060	0.45	0.82	0.029	0.006	8.61	18.38	-	275	618	68.0	82.0	136

Mat. ID	Heat Designation	Chemical Composition (wt.%)										YS (MPa)	UTS (MPa)	Elong. (%)	RA (%)	Reference
		C	Si	Mn	P	S	Ni	Cr	Mo	N						
28	304L-E	0.039	0.36	1.82	0.030	0.006	10.38	18.50	0.06	0.055	-	-	-	-	58-60	
29	304L-1	0.017	0.29	1.19	0.024	0.002	9.15	18.05	-	-	245	574	61.0	84.0	136	
30	304L-G	0.017	0.51	1.72	0.018	0.013	10.16	19.09	-	-	259	339	63.3	65.2	14,15	
31	304L	0.013	0.61	0.90	0.020	0.080	9.30	18.50	-	0.090	235	588	65.0	75.0	136	
Type 316 Stainless Steel																
32	316-1H	0.055	0.52	1.51	0.027	0.005	13.20	16.25	2.12	-	177	465	43.5	75.5	210	
33	316-2	0.050	0.70	1.10	0.034	0.003	12.60	17.05	2.24	0.017	257	606	67	79	136	
34	316-3H	0.040	0.76	1.63	0.030	0.007	11.57	17.44	2.47	-	-	-	58	63.6	136	
35	316-4	0.060	0.40	1.72	0.012	0.007	13.30	17.30	2.33	-	-	-	-	-	63	
36	316-5	-	-	-	-	-	-	-	-	-	-	-	-	-	61	
37	316-6	-	-	-	-	-	-	-	-	-	-	-	-	-	61	
38	316-7	-	-	-	-	-	-	-	-	-	-	-	-	-	61	
39	316-8	-	-	-	-	-	-	-	-	-	-	-	-	-	61	
40	316-9	-	-	-	-	-	-	-	-	-	-	-	-	-	61	
41	316-10	-	-	-	-	-	-	-	-	-	-	-	-	-	61	
42	316-12T	0.060	0.61	1.69	0.025	0.010	13.06	16.55	2.08	-	234	550	63	81.1	136	
43	316-13T	0.070	0.50	1.50	0.031	0.010	11.10	17.60	2.30	-	264	569	58.5	81.5	136	
44	316-14T	0.060	0.60	1.60	0.026	0.010	13.00	16.50	2.07	-	250	555	50.5	67.6	136	
45	316-15T, 27T	0.040	0.37	1.55	0.025	0.001	12.55	16.50	2.10	-	247	531	54	-	136	
46	316-26T	0.057	0.64	1.64	0.026	0.005	13.02	16.48	2.07	-	250	555	50	68	136	
47	316L-1H	0.040	0.37	1.55	0.025	0.001	12.55	16.50	2.10	-	154	406	43	80	136	
48	316N-1	0.015	0.39	1.66	0.025	0.003	14.90	17.25	2.32	-	259	555	60.7	81.2	136	
49	316N-2	0.010	0.51	1.67	0.027	0.001	13.25	17.50	2.50	0.106	264	574	63.9	82.9	136	
50	316N-3H	0.009	0.65	1.55	0.023	0.002	12.70	17.60	2.74	-	168	454	43.7	77	136	
51	316N-6	0.012	0.45	1.58	0.024	0.004	12.60	17.15	2.46	0.102	310	710	44.2	-	136	
52	316N-7	0.007	0.36	0.51	0.002	0.001	74.95	16.01	-	-	300	588	55	-	136	
53	316N-8	0.008	0.56	1.46	0.028	0.001	12.11	17.73	2.60	0.090	252	558	62	85	136	
54	316N-A	0.011	0.61	0.91	0.017	0.004	11.18	16.26	2.17	-	-	-	-	-	45	
Stainless Steel Welds																
55	304HP-WM-1	0.058	0.68	1.78	0.026	0.005	9.62	19.98	0.06	0.039	-	-	-	-	136	
56a	308-WM-1	0.050	0.56	1.39	0.022	0.004	10.30	19.90	-	-	-	-	-	-	136	

Mat. ID	Heat Designation	Chemical Composition (wt.%)									YS (MPa)	UTS (MPa)	Elong. (%)	RA (%)	Reference
		C	Si	Mn	P	S	Ni	Cr	Mo	N					
56b	308-WM-2	0.034	0.71	1.93	0.022	0.007	9.78	19.60	0.08	-	414	578	38.0	52.0	136
57a	316 WM	0.039	0.39	1.31	0.011	0.005	11.60	19.60	2.20	-	-	-	-	-	136
57b	316TP WM-1	0.020	0.41	1.90	0.013	0.006	12.20	18.80	2.20	-	-	-	-	-	136
57c	316TP WM-2	0.070	0.40	1.82	0.011	0.006	12.50	18.50	2.19	-	-	-	-	-	136
57	316N-WM-1	0.018	0.39	1.70	0.010	0.007	11.47	19.75	2.27	0.075	-	-	-	-	136
59	316N-WM-2	0.017	0.43	1.86	0.011	0.006	12.01	19.49	2.39	-	489	615	30.0	67.0	136
60	316N-WM-3	0.002	0.44	1.46	0.026	0.001	13.14	17.21	2.43	0.078	254	548	57.0	-	136
Cast Austenitic Stainless Steel															
61	CF-8M-1	0.053	0.95	0.80	0.030	0.005	9.52	20.52	2.20	0.045	300	611	45.3	74.6	136
62	CF-8M-2	0.050	1.17	0.86	0.021	0.006	10.03	20.59	2.28	-	308	619	51.0	76.0	136
63	CF-8M-3	0.050	0.79	0.74	0.026	0.009	9.66	18.86	2.23	-	232	561	49.0	62.0	136
64	CF-8M-4	0.050	1.00	0.80	0.030	0.010	9.52	20.50	2.20	-	300	611	45.3	74.6	136
65	CF-8M-5	0.050	1.30	0.80	0.280	0.020	9.32	20.80	2.30	-	352	644	43.3	69.0	136
66	CF-8M-6	0.050	0.60	0.80	0.280	0.010	10.50	20.20	2.16	-	259	521	48.6	77.6	136
67	CF-8M-7	0.050	0.79	0.74	0.026	0.009	9.66	18.86	2.23	-	252	498	50.0	72.0	136
68	CF-8M-8	0.064	0.73	0.54	0.022	0.016	9.03	19.11	2.51	0.048	273	537	63.0	66.8	45
69	CF-8M-9	0.065	0.67	0.53	0.022	0.012	9.12	20.86	2.58	0.0523	322	601	43.6	71.4	45

### B3 Ni-Cr-Fe Alloys and Welds

The various grades, heat treatment, chemical composition, and mechanical properties of the Ni-Cr-Fe Alloys and associated weld metals used in this report are listed in the following table.

Mat. ID	Heat Designation	Chemical Composition (wt.%)								YS (MPa)	UTS (MPa)	Elong. (%)	RA (%)	Reference
		C	Si	Mn	P	S	Ni	Cr	Fe					
1	Alloy 600-1	0.070	0.32	0.51	0.002	0.001	74.86	15.95	8.13	310	710	44.2	-	136
2	Alloy 600-2	0.070	0.29	0.37	0.006	0.001	76.07	15.46	7.12	294	686	42.0	-	136
3	Alloy 600-3	0.010	0.17	0.21	0.007	0	73.33	16.60	6.95	279	677	54.0	63.0	136
4	Alloy 600-4	0.010	0.17	0.21	0.007	0	73.33	16.60	6.95	289	693	63.0	57.0	136
5	Alloy 600-5	0.070	0.34	0.37	0.007	0.001	73.56	15.64	9.46	303	696	39.0	62.0	136
6	Alloy 600-6	0.030	0.05	0.49	0.004	0.001	74.50	16.00	8.37	264	635	55.0	74.0	136
7	Alloy 600-7	0.020	0.17	0.13	0.017	0.010	75.85	15.54	6.81	253	612	50.0	70.0	67
8	Alloy 600-8	0.080	0.19	0.13	-	0.007	77.31	15.70	6.52	567	745	-	51.4	68
9	Alloy 600-9	0.060	0.25	0.20	-	0.007	76.67	15.45	7.24	256	651	-	57.9	68
10	Alloy 600-10	0.080	0.48	0.46	0.010	0.008	73.63	15.72	9.40	267	656	-	49.9	68
11	Alloy 600-11	0.030	1.20	0.99	-	0.012	73.76	15.52	7.58	253	538	-	55.0	68

Mat. ID	Heat Designation	Chemical Composition (wt.%)										YS (MPa)	UTS (MPa)	Elong. (%)	RA (%)	Reference
		C	Si	Mn	P	S	Ni	Cr	Fe	Other						
										0.65 Cb+Ta						
12	Alloy 600-12	0.070	0.73	0.78	-	0.005	74.40	16.00	7.70	0.01 Cu, 0.01 Ti, 0.11 Co, 0.01 Al	170	374	-	45.1	68	
13	Alloy 600-13	0.051	0.31	0.25	0.010	0.0012	73.72	15.80	8.86	0.021 Cu, 0.24 Ti, 0.05 Co, 0.21 Al, 0.0010 B	237	654	45.5	65.8	66	
14	Alloy 600-14	0.050	0.20	0.20	-	0.007	78.04	15.37	6.03	0.08 Cu	312	685	45.5	58.7	70	
15	Alloy 600-15	-	-	0.24	-	0.008	74.21	-	-	0.13 Cu	403	721	43.0	53.0	14	
16	Alloy 600-16	0.050	0.20	0.20	-	0.007	78.04	15.37	6.03	0.08 Cu	312	685	45.5	58.7	61	
16	Alloy 600-16	0.060	0.25	0.20	-	0.007	76.67	15.45	7.24	0.06 Cu, 0.21 Ti, 0.09 Co, 0.13 Al	256	651	-	57.9	61	
17	Alloy 600-17	0.020	0.17	0.13	0.017	0.010	75.85	15.54	6.81	0.06 Cu, 0.11 Ti, 0.01 Co, 0.18 Al, 0.096 Cb	245	595	48.4	67.8	61	
20	Alloy 690-1	0.030	0.11	0.27	0.007	0.001	60.1	29.50	9.44	-	280	691	46.0	60.0	136	
21	Alloy 690-2	-	-	-	-	-	-	-	-	-	-	-	-	-	39	
22	Alloy 690-3	0.020	0.09	0.15	-	<0.001	61.58	29.15	9.00	<0.01 Cu, 0.007 Co	247	643	52.0	64.0	75	
25	Alloy 800-1	0.060	0.38	0.90	-	0.007	32.11	20.35	45.17	0.25 Cu, 0.39 Ti, 0.36 Al	190	546	-	75.0	69	
26	Alloy 800-2	0.060	0.38	0.90	-	0.007	32.11	20.35	45.17	0.25 Cu, 0.39 Ti, 0.36 Al	158	499	-	51.0	69	
26	Alloy 800-2	-	-	-	-	-	-	-	-	-	212	515	-	57.5	71	



Mat. ID	Heat Designation	Chemical Composition (wt.%)									YS (MPa)	UTS (MPa)	Elong. (%)	RA (%)	Reference
		C	Si	Mn	P	S	Ni	Cr	Fe	Other					
30	Inconel 718-1	-	-	-	-	-	-	-	-	-	-	-	-	-	210
31	Inconel 718-2	-	-	-	-	-	-	-	-	-	1200	1515	-	30.5	72
32	Inconel 718-3	-	-	-	-	-	-	-	-	-	-	-	-	-	61
33	Inconel 718-4	-	-	-	-	-	-	-	-	-	-	-	-	-	61
34	Inconel 718-5	-	-	-	-	-	-	-	-	-	-	-	-	-	61
										0.36 Al, 0.03 Cu, 2.96 Mo, 0.91 Ti 4.98 Cb+Ta					
35	Inconel 718-6	0.030	0.35	0.18	-	0.007	52.64	18.59	18.94	-	1110	1304	-	-	61, 73
36	Inconel 718-7	-	-	-	-	-	-	-	-	-	-	-	-	-	61
38	Alloy 690 WM	0.037	0.32	4.47	<0.005	0.001	55.60	29.20	8.71	-	431	656	39.0	49.0	136
39	Alloy 62 *	0.070	0.175	0.325	-	0.006	73.50	17.75	6.90	1.0 Cb, 0.01 Cu, 0.05 Co 0.02 Co, 0.004 Al, 0.01 Cu, 0.044 Mo, 0.08 Ti 1.92 Cb+Ta 0.10 Co, 1.75 Mo, 0.03 Ti 1.46 Cb+Ta 0.02 Co, 0.05 Al, 0.02 Cu, 0.01 Mo, 0.25 Ti 1.77 Cb+Ta 0.01 V, 0.01 W,	-	-	-	-	68
40	Alloy 82-1	0.040	0.10	2.80	-	0.017	63.50	17.28	13.56	-	353	606	-	55.3	68
41	Alloy 82-2	0.040	0.86	2.54	-	0.014	65.05	20.00	8.60	-	322	633	-	53.7	68
42	Alloy 82-3	0.070	0.30	2.48	0.005	0.015	54.70	13.95	25.70	-	355	573	-	47.5	68

Mat. ID	Heat Designation	Chemical Composition (wt.%)									YS (MPa)	UTS (MPa)	Elong. (%)	RA (%)	Reference
		C	Si	Mn	P	S	Ni	Cr	Fe	Other					
										0.002 Mg					
43	NiCrFe WM-1	-	-	-	-	-	-	-	-	-	-	-	-	-	SGFS 1988
44	Arcaloy 8N12	-	-	-	-	-	-	-	-	-	-	-	-	-	68
45	NiCrFe WM-2	-	-	-	-	-	-	-	-	-	-	-	-	-	210
										0.02 Co, 0.004 Al, 0.01 Cu, 0.044 Mo, 0.08 Ti					
46	Alloy 82-4	0.040	0.10	2.80	-	0.017	63.50	17.28	13.56	1.92 Cb+Ta	353	606	-	55.3	68
										0.14 Cu, 0.52 Ti	456	698	35.3	43.5	136
47	Alloy 182-1	0.060	0.61	5.56	0.004	0.006	68.20	15.50	7.25	0.14 Cu, 0.52 Ti	456	698	35.3	43.5	136
48	Alloy 182-2	0.060	0.61	5.56	0.004	0.006	68.20	15.50	7.25	-	405	667	38.1	50.2	136
49	Alloy 182-3	0.038	0.25	2.50	0.004	0.005	73.00	15.10	7.20	-	409	623	34.0	44.0	136
50	Alloy 182-4	0.040	0.21	2.76	<0.005	0.004	72.50	15.00	7.99	0.03 Cu, 0.04 Co, 0.27 Ti	339	565	56.0	72.0	75
51	Alloy 82-5	0.040	0.12	2.92	0.003	0.001	72.85	20.64	0.65	<0.01 Cu	409	623	34.4	43.9	39, 136
52	Alloy 152	-	-	-	-	-	-	-	-	-	-	-	-	-	39
53	Alloy 132	0.040	0.21	2.76	<0.005	0.004	72.50	15.0	7.99	-	409	623	34.4	43.9	39, 136

\* Average composition of first and second layers.

## APPENDIX C    SAMPLE PROBLEM

---

### C1    Background

This Appendix provides the cumulative usage factor (CUF), environmental fatigue multiplier ( $F_{en}$ ), and environmentally assisted fatigue cumulative usage factor ( $CUF_{en}$ ) solution for a sample problem. The sample problem was obtained from Appendix B of Reference [C-1]. The purpose of this sample problem solution is to demonstrate one example of the use of the methodology described in this report to calculate the environmental fatigue multiplier ( $F_{en}$ ) and environmentally assisted fatigue cumulative usage factor ( $CUF_{en}$ ) for a relatively simple problem. The sample problem is not intended to be an exhaustive treatment of more comprehensive component assessments that may be present in operating nuclear power plants.

The sample problem selected for solution in this appendix was the second example problem developed and solved by several industry participants. The purpose of the industry's sample problem efforts was to evaluate the effectiveness of some American Society of Mechanical Engineers (ASME) Code Cases in providing sufficient guidance for environmentally assisted fatigue (EAF) evaluations, and to identify any related guidelines that may be useful for industry applications. The main intentions of the second sample problem were to ensure that transient pairs occurred between peaks and valleys from different transients, to include a complex transient with multiple peaks and valleys, to incorporate a dynamic load event, and to include dissolved oxygen variations between transients and during at least one transient.

During the industry's solution of their first sample problem (documented in Appendix A of Reference [C-1]), considerable time was spent standardizing input parameters and stresses for the fatigue evaluation that preceded the environmental calculations. Those iterations yielded insight into the impact of certain modeling and analysis choices and the resulting differences in the fatigue results, which could be further magnified in the environmental fatigue analysis. Based on that insight, and to minimize differences in the stress and fatigue portions of the analysis, a standard set of stress histories for all transients was provided for all participants to use in the second sample problem. Those stress histories were used as the starting point for the calculations in this appendix. As a result, only minimal portions of the content for the sample problem statement and finite element modeling details used to derive the stresses for the sample problem are included in this appendix. The reader is referred to Appendix B of Reference [C-1] for those details.

### C2    Problem Description

The full problem statement and definitions for the sample problem are provided in Appendix B of Reference [C-1].

The geometry evaluated in the sample problem is shown in Figure C.1. The geometry represents a typical vessel nozzle with attached piping.

The transients evaluated in the sample problem are shown in Table C.1. The transient temperature, pressure, and dissolved oxygen (DO) time histories are plotted in Figure C.2.

The transient stress component histories that were obtained from finite element analysis were provided for the sample problem for both stress cut lines (SCLs) shown in Figure C.1. The

Technical drawing of a nozzle-to-pipe connection. The drawing shows a side view of the assembly with the following dimensions and specifications:

- Overall Dimensions:**
  - Horizontal distance from the pipe face to the nozzle face: 10.5
  - Horizontal distance from the pipe face to the nozzle face (excluding the nozzle thickness): 8.50
  - Vertical height of the nozzle: 4.00
- Internal Dimensions and Features:**
  - Horizontal distance from the pipe face to the start of the nozzle neck: 5.00
  - Horizontal distance from the start of the nozzle neck to the nozzle face: 7.906
  - Radius of the nozzle neck: R 1.9
  - Horizontal distance from the pipe face to the centerline of the nozzle neck: 1.00
- Materials and Welds:**
  - Pipe material: TP316
  - Nozzle material: SA-508
  - Weld type: SS Weld CL (on the pipe side) and DM Weld CL (on the nozzle side)
- Other Labels:**
  - Pipe**: Label for the main pipe.
  - Nozzle**: Label for the nozzle.
  - Safe End**: Label for the end of the pipe.
  - 14.00 D**: Dimension for the pipe diameter.
  - 11.188 D**: Dimension for the nozzle diameter.

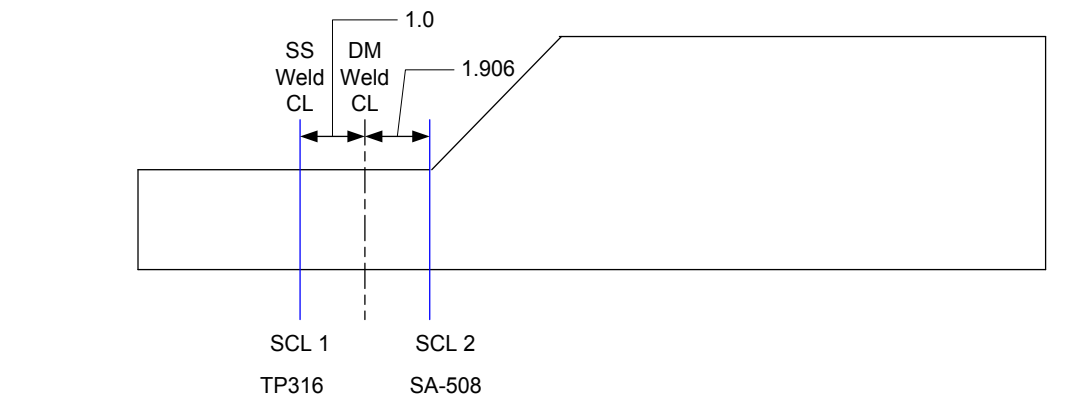


### Figure C.1. Sample Problem Geometry

**Table C.1. Sample Problem Transient Definitions**

Transient No.	Time (sec)	Fluid Temperature (°F)	Heat Transfer Coefficient, h (BTU/s-in <sup>2</sup> -°F)	Pressure (psi)	Resultant Moment (in-kips)	DO (ppm)
1 (20 cycles)	0	450	0.003	2,250	-3,000	0.150
	100	450	0.003	2,250	-3,000	0.150
	450	100	0.003	1,000	1,000	0.150
	1510	100	0.003	1,000	1,000	0.150
	1710	600	0.003	2,250	-3,000	0.150
	3210	600	0.003	2,250	-3,000	0.150
2 (50 cycles)	0	500	0.003	1,500	-2,500	0.550
	100	500	0.003	1,500	-2,500	0.550
	260	100	0.003	2,250	1,000	0.550
	1290	100	0.003	2,250	1,000	0.550
	1540	350	0.003	2,000	-2,500	0.550
	3240	350	0.003	2,000	-2,500	0.550
3 (20 cycles)	0	300	0.003	1,600	0	0.050
	50	650	0.003	1,600	0	0.050
	250	650	0.003	1,600	0	0.050
	275	400	0.003	1,600	0	0.050
	400	400	0.003	1,600	0	0.050
	600	550	0.003	1,600	0	0.050
	700	550	0.003	1,600	0	0.050
	900	350	0.003	1,600	0	0.050
	1000	350	0.003	1,600	0	0.050
	1200	400	0.003	1,600	0	0.050
	1300	400	0.003	1,600	0	0.050
	1500	70	0.003	1,600	0	0.050
	1600	70	0.003	1,600	0	0.050
	2000	300	0.003	1,600	0	0.050
	3800	300	0.003	1,600	0	0.050
4 (100 cycles)	0	70	0.003	400	-3000	0.55
	100	70	0.003	400	-3000	0.55
	3700	170	0.003	400	-2100	0.442
	7300	270	0.003	400	-1200	0.334
	8272	297	0.003	580.32	-957	0.30484
	10072	347	0.003	914.26	-507	0.25084
	13672	447	0.003	1582.13	393	0.14284
	17272	547	0.003	2250	1293	0.3484
	18100	547	0.003	2250	1500	0.01
	26000	547	0.003	2250	1500	0.01
5 (5 events; 10 cycles per event)	<p align="center"><u>Operating Basis Earthquake (OBE) Transient</u>  OBE loading was defined by resultant moment loads. The resultant moment load was specified as +/- 2000 in-kips. Each OBE event was assumed to occur at any time during any of the transients. DO= 0.100 ppm.</p>					

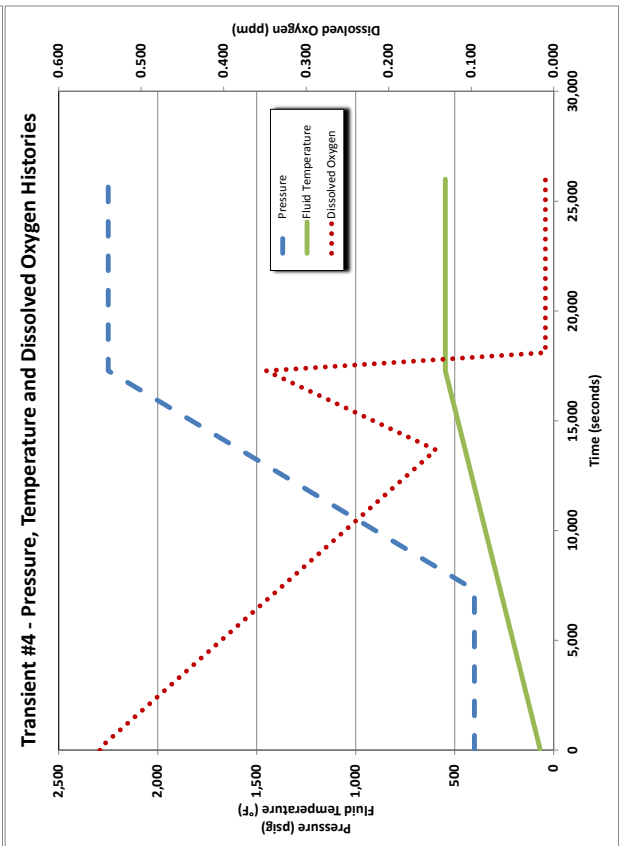
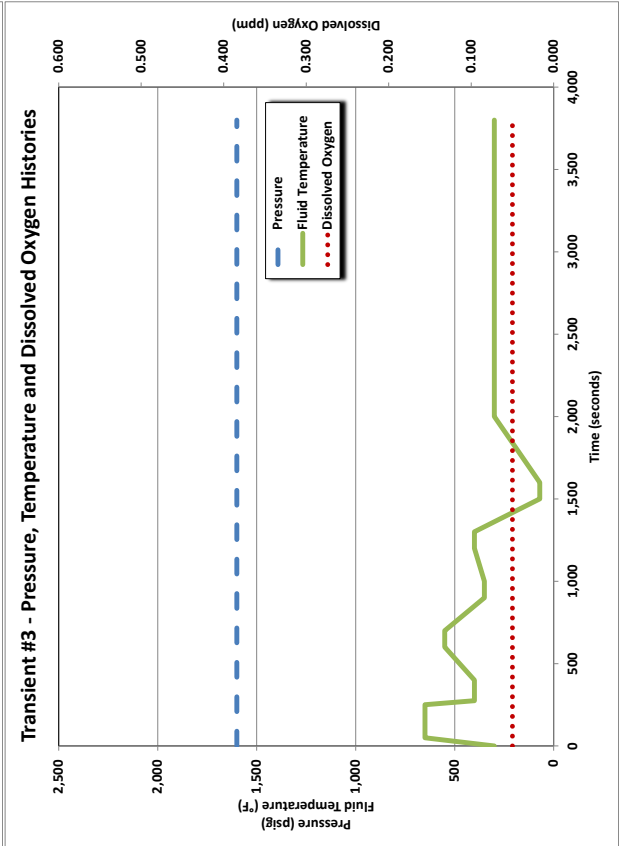
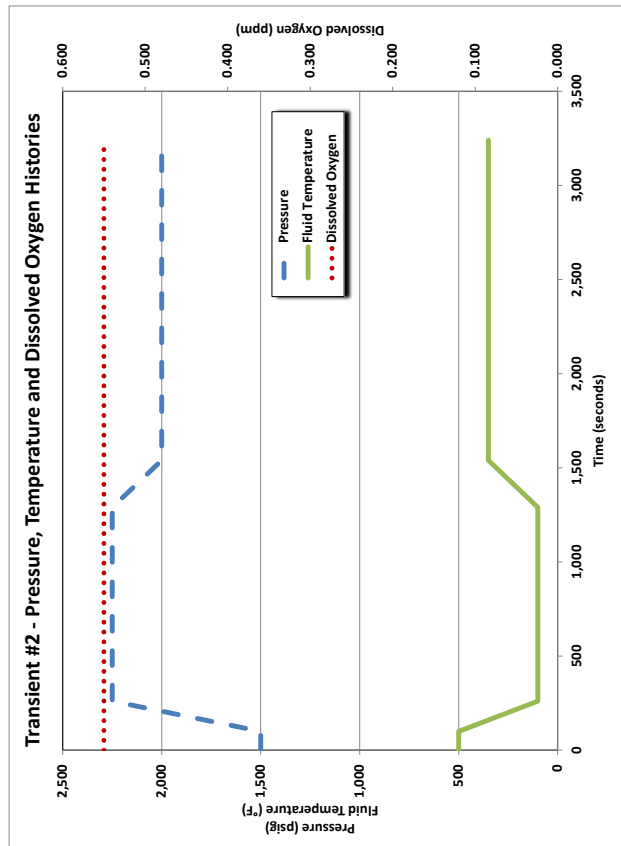
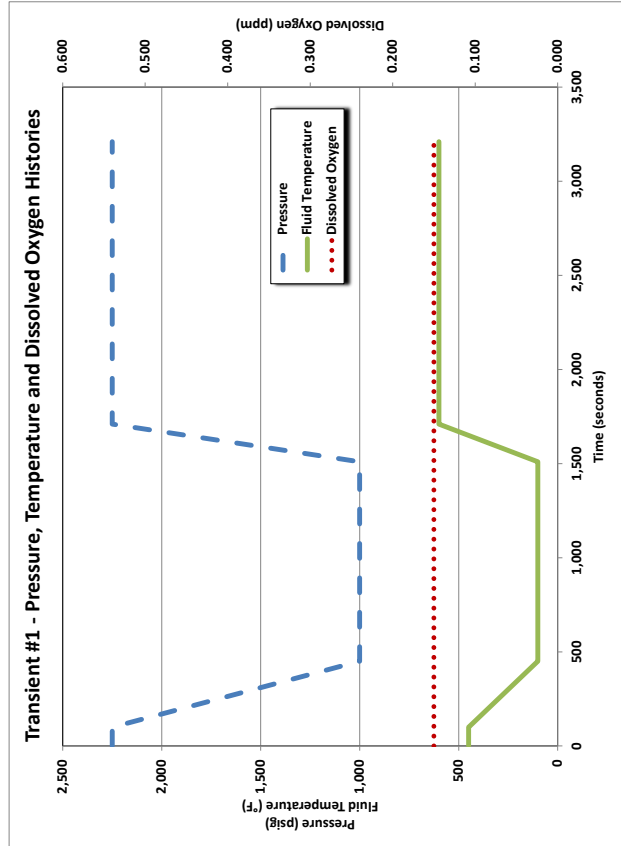


Figure C.2. Sample Problem Transient Time Histories

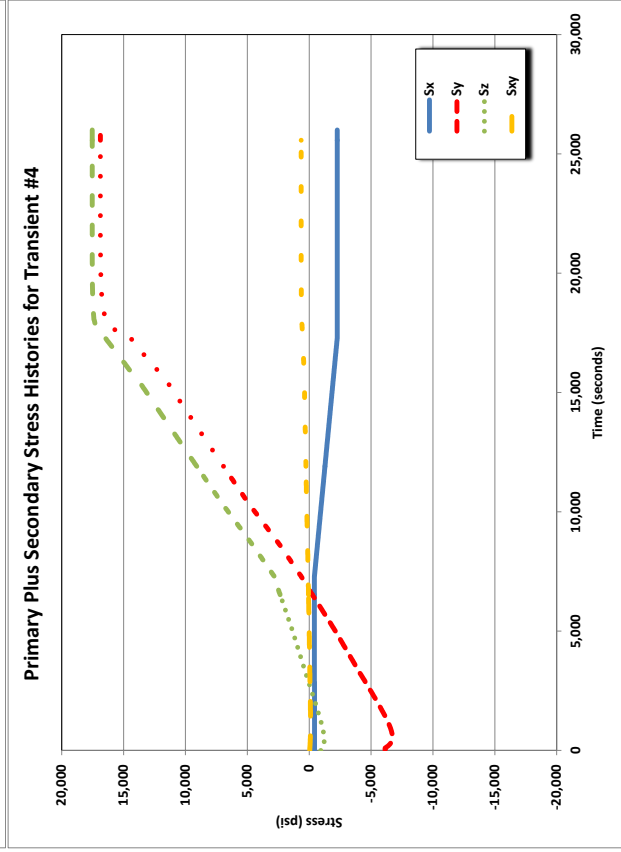
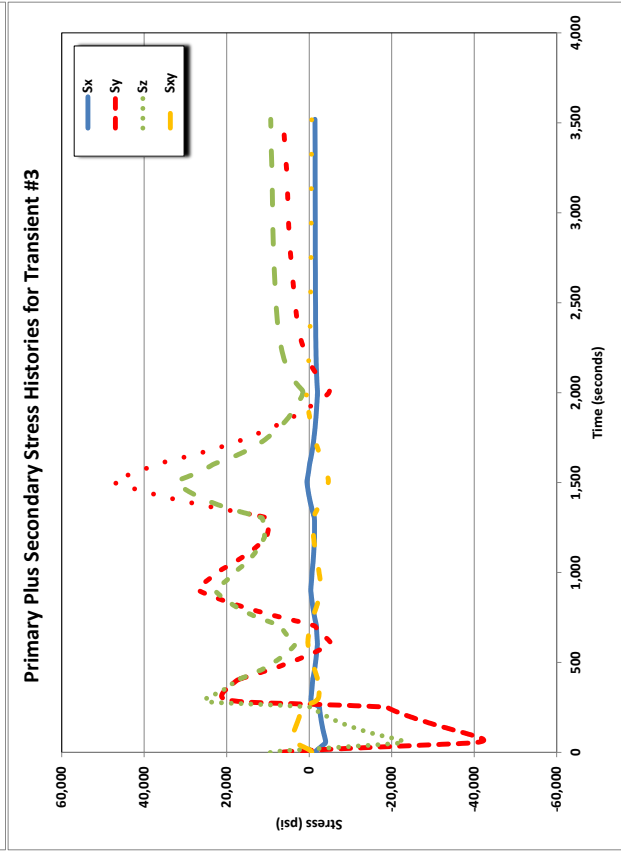
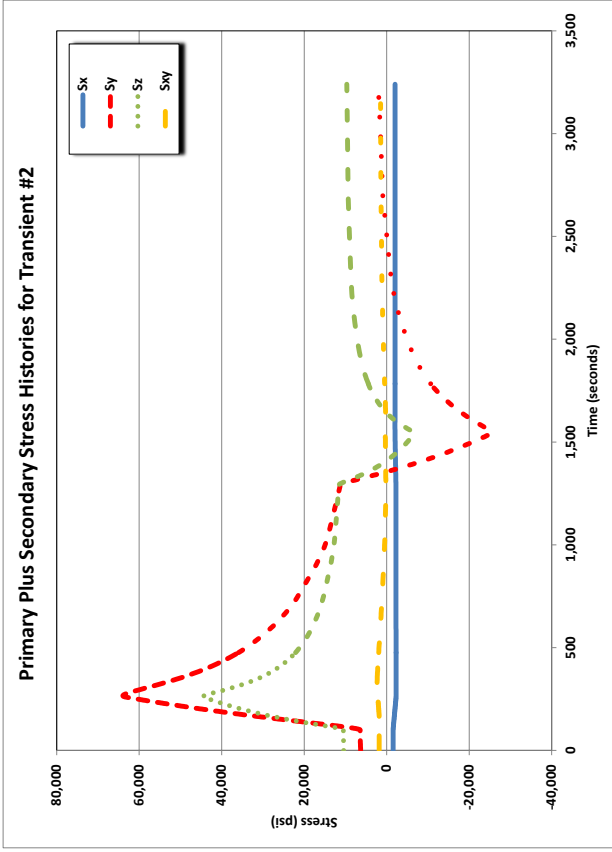
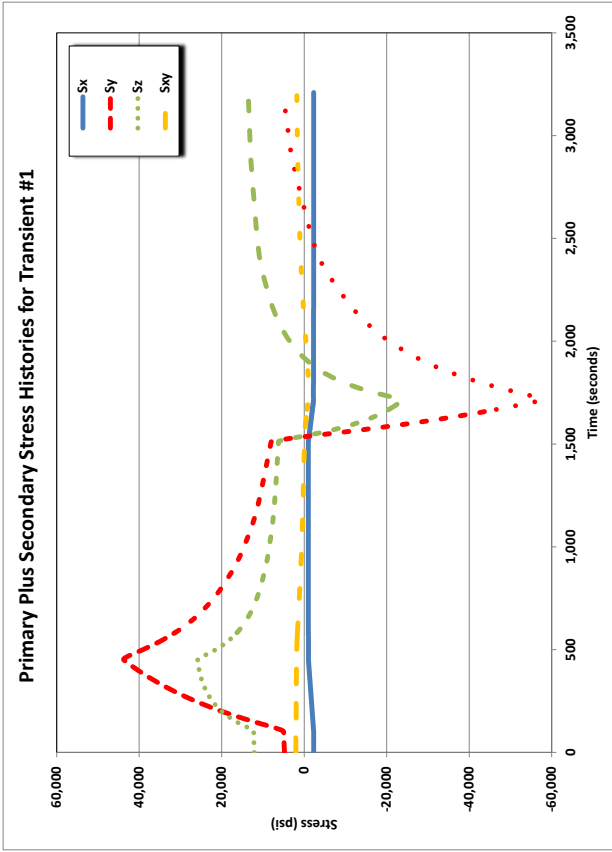


Figure C.3. Sample Problem Transient Membrane Plus Bending Stress Histories for SCL 2

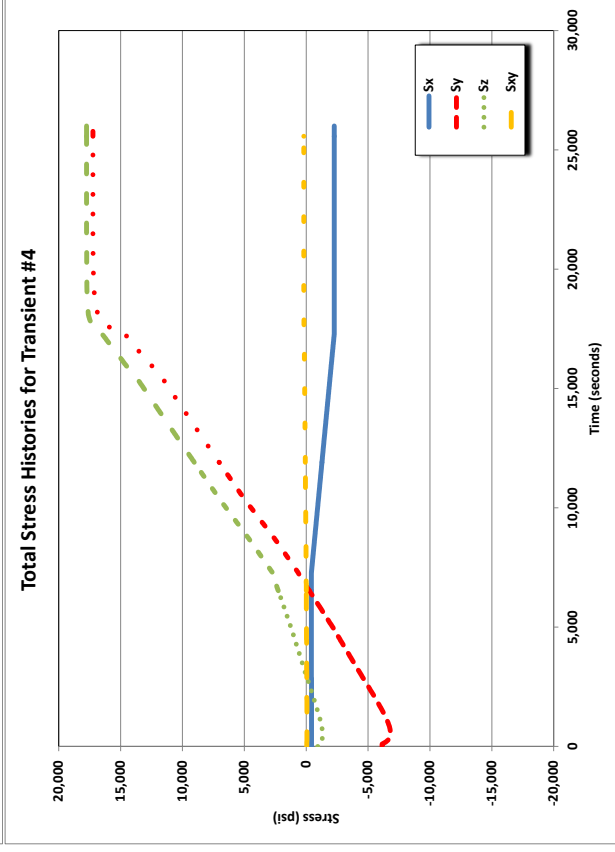
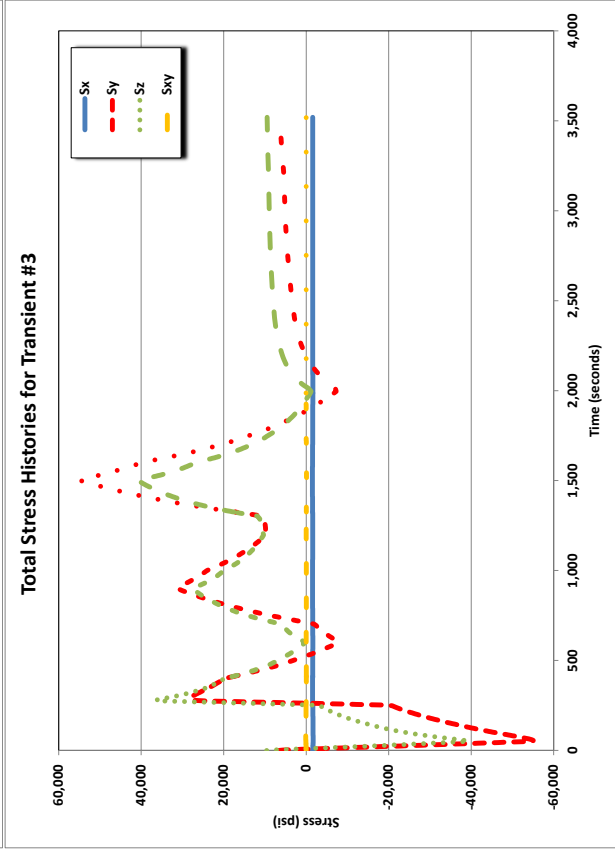
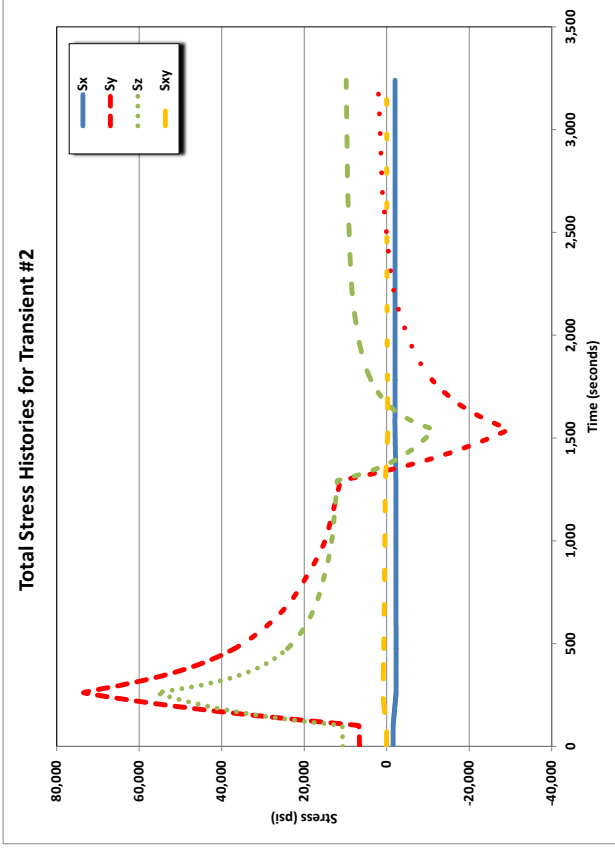
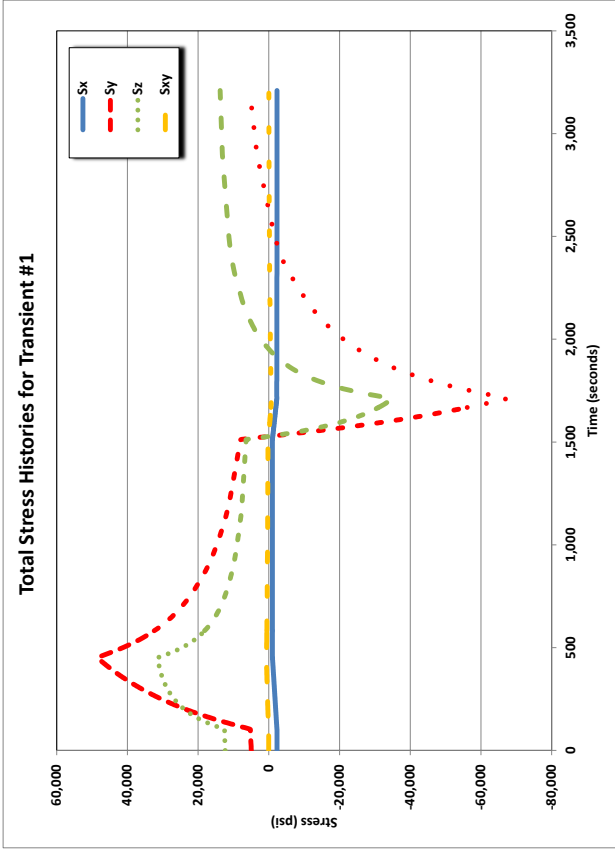


Figure C.4. Sample Problem Transient Total Stress Histories for SCL 2



# Total Stress Histories for All Transients (includes OBE)

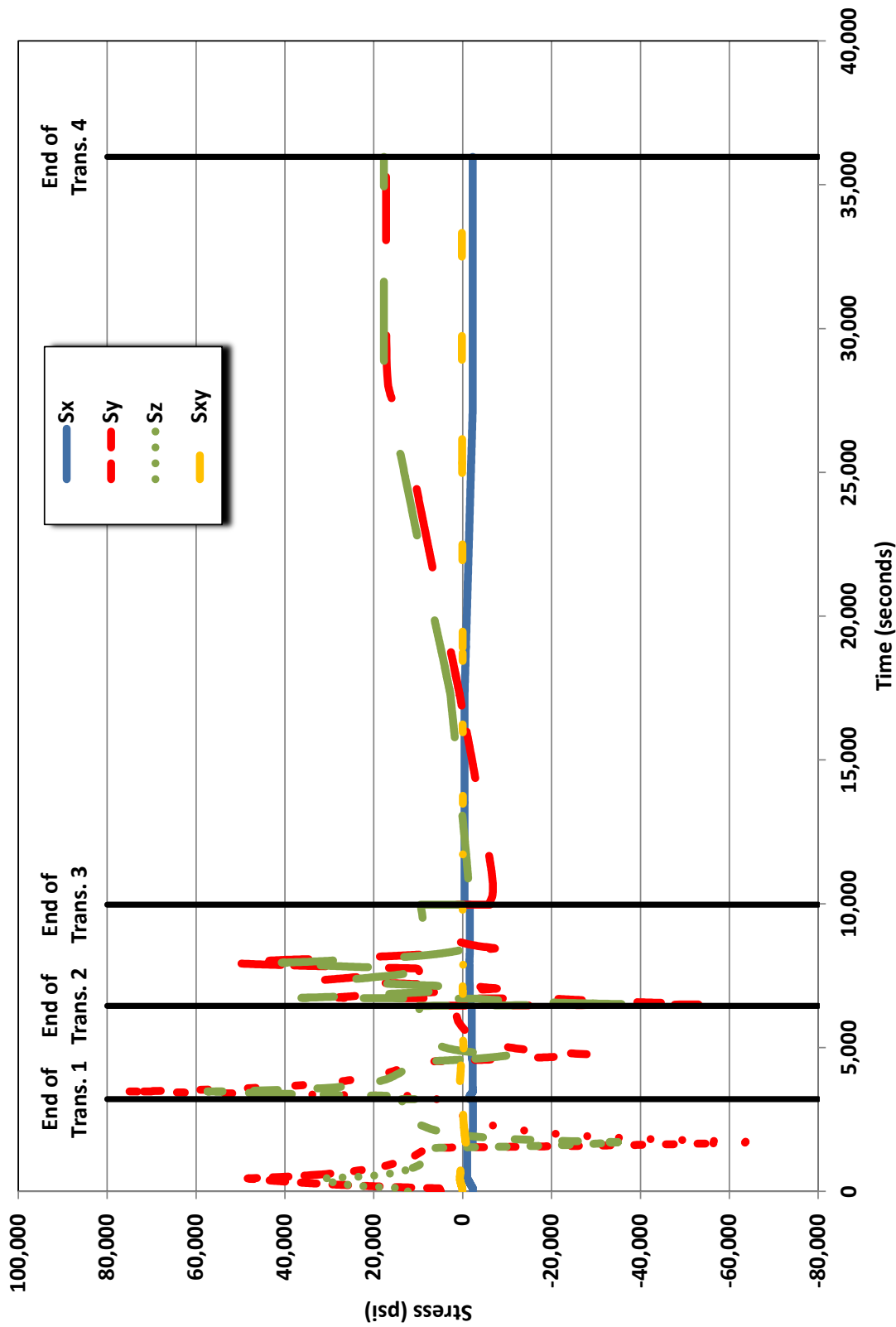


Figure C.5. Sample Problem Combined Transient Stress History for SCL 2

### C3 Evaluation

The CUF for the sample problem was calculated in accordance with the ASME Boiler and Pressure Vessel Code (Code), Subsection NB [C-2] using the provisions of Subarticle NB-3200, “Design by Analysis.” A summary of the steps used to calculate the CUF is as follows:

- A. The alternating stress intensities,  $S_{alt}$ , were calculated for the input stress history (Table C.2) using the following steps (follows ASME Code NB-3216.2 methodology for varying principal stress direction):
  - a. NB-3216.2(a) requires that six components of stress be considered taking into account both gross and local structural discontinuities and the thermal effects which vary during the cycle. The stresses shown in Table C.2 satisfy this requirement and were used as input to the calculation.
  - b. NB-3216.2(b) requires selection of a point in time where conditions are at an extreme (either maximum or minimum algebraically). The maximum total stress values for each of the six stress components were found and identified as  $SX_i$ ,  $SY_i$ ,  $SZ_i$ , etc.
  - c. NB-3216.2(c) requires calculation of the stress differences for the entire stress history for every point in time. These differences were computed as  $S'X = (SX - SX_i)$ ,  $S'Y = (SY - SY_i)$ ,  $S'Z = (SZ - SZ_i)$ , etc.
  - d. NB-3216.2(d) requires calculation of the principal stresses for the entire stress history for every point in time from the stress differences calculated in Step c. These differences were computed as  $S'_1$ ,  $S'_2$ , and  $S'_3$  using the six stress differences (i.e.,  $S'X$ ,  $S'Y$ ,  $S'Z$ , etc.).
  - e. Principal stresses were calculated for the entire stress history by solving a cubic equation for the six component stress differences from Step d.
  - f. NB-3216.2(e) requires calculation of the principal stress differences for the entire stress history for every point in time as  $S'_{12} = (S'_1 - S'_2)$ ,  $S'_{23} = (S'_2 - S'_3)$ , and  $S'_{31} = (S'_3 - S'_1)$  and finding the largest absolute magnitudes of these three differences based on their variations throughout the stress history.  $S_{alt}$  values were calculated as one-half of all of these largest stress amplitudes based on range-pair cycle counting for the entire stress intensity history to identify stress “peaks” (points of local stress maxima) and “valleys” (points of local stress minima).
  - g. The  $S_{alt}$  values were adjusted for the effects of Young’s Modulus (per NB-3222.4(e)(4)) and for the effects of simplified elastic-plastic analysis, i.e.,  $K_e$  (per NB-3228.5).
  - h. Since it was not obvious which case led to the highest  $S_{alt}$  values, all six of the following cases were evaluated<sup>1</sup>:
    - i. Based on maximum total SX stress.
    - ii. Based on maximum total SY stress.

<sup>1</sup> Since the shear stress components (SXY, SYZ, and SZX) have significantly lower values compared to the primary stress components (SX, SY, and SZ), they do not lead to a maximum  $S_{alt}$  situation. As a result, they were not considered in the maximum  $S_{alt}$  selection process.

- iii. Based on maximum total SZ stress.
- iv. Based on maximum membrane plus bending SX stress.
- v. Based on maximum membrane plus bending SY stress.
- vi. Based on maximum membrane plus bending SZ stress.
- i. The  $S_{alt}$  values counted for each case in Step h were designated as  $S_{alt\ 1}$ ,  $S_{alt\ 2}$ ,  $S_{alt\ 3}$ , ...,  $S_{alt\ n}$ . The number of times that each  $S_{alt}$  value occurred during the entire principal stress difference history was determined, and these were designated as  $n_1$ ,  $n_2$ ,  $n_3$ , ...,  $n_n$ , respectively.
- j. From the  $S_{alt\ 1}$ ,  $S_{alt\ 2}$ ,  $S_{alt\ 3}$ , ...,  $S_{alt\ n}$  values calculated for each case in Step h, the applicable design fatigue curve from Appendix A was used to determine the maximum number of allowable cycles,  $N_1$ ,  $N_2$ ,  $N_3$ , ...,  $N_n$ .
- k. Partial usage factors,  $U_1$ ,  $U_2$ ,  $U_3$ , ...,  $U_n$ , were calculated as  $U_1 = n_1/N_1$ ,  $U_2 = n_2/N_2$ ,  $U_3 = n_3/N_3$ , ...,  $U_n = n_n/N_n$ .
- l. The total CUF was calculated as  $U_1 + U_2 + U_3 + \dots + U_n$ .
- m. The highest CUF resulting from all of the six cases identified in Step h was used as the final reported CUF value.

Only CUF and  $F_{en}$  calculations were performed for the sample problem. Therefore, the results of stress limit checks required as a part of ASME Code design calculations are not included in this appendix.

Calculations for  $CUF_{en}$  were performed for the limiting CUF value. Strain rates were calculated based on the total  $S'_{31}$  history which was the limiting CUF case.  $F_{en}$  was computed using the equations in Appendix A of this report using two approaches:

A. Average Strain Rate Approach: In this approach, the  $F_{en}$  for each peak and valley resulting from the  $S_{alt}$  calculation process was computed as follows:

- i. The strain rate was based on the total stress component principal stress difference,  $S'_{31}$ , which was used to compute CUF. For simplicity,  $K_e$  was conservatively not included in the calculation of strain rate.
- ii. The strain rate was calculated between each adjacent valley and peak with increasing stress, as:

$$\dot{\epsilon} = (S'_{31\text{-peak}} - S'_{31\text{-valley}}) / (\Delta t \times E \times 100)$$

where:

- $\dot{\epsilon}$  = strain rate (%/sec)
- $S'_{31\text{-peak}}$  =  $S'_{31}$  stress intensity value at the peak (psi)
- $S'_{31\text{-valley}}$  =  $S'_{31}$  stress intensity value at the valley (psi)
- $\Delta t$  = time increment between the valley and peak (seconds)
- $E$  = the Young's Modulus determined at the maximum metal temperature of the peak and valley (psi)

- iii. To neglect compressive loading in the determination of  $F_{en}$ , the  $F_{en}$  value was set to 1.0 for any valley-to-peak interval where  $\dot{\epsilon}$  was less than zero.
- iv. The  $F_{en}$  was calculated between each valley and peak using the appropriate equation from Appendix A for the material evaluated, and using the maximum metal temperature of the peak and valley.

- v. The  $F_{en}$  was assigned to both the peak and valley for use in the  $CUF_{en}$  calculations.
- vi. The above steps were repeated for all valley-peak intervals for the entire principal stress intensity history.

**B. Modified Strain Rate Approach:** In this approach, the  $F_{en}$  for each peak and valley resulting from the  $S_{alt}$  calculation process was computed using the Modified Rate Approach described in Section 4.1.14, as follows:

- i. The strain rate was based on the total stress component principal stress difference,  $S'_{31}$ , which was used to compute CUF. For simplicity,  $K_e$  was conservatively not included in the calculation of strain rate.
- ii. The  $F_{en}$  integration was set up and performed between each valley and peak with increasing stress, as follows (refer to Figure 80):

$$\dot{\epsilon}_i = \frac{S'_{31\ i+1} - S'_{31\ i}}{100 \Delta t E}$$

where:  $\dot{\epsilon}_i$  = strain rate at any point, i, between the valley and peak (%/sec)  
 $S'_{31\ i+1}$  =  $S'_{31}$  stress intensity value at point i+1 (psi)  
 $S'_{31\ i}$  =  $S'_{31}$  stress intensity value at point i (psi)  
 $\Delta t$  = time increment between points i and i+1 (seconds)  
 $E$  = the Young's Modulus determined at the maximum metal temperature of points i and i+1 (psi)

- iii. To neglect compressive loading in the determination of  $F_{en}$ , the  $F_{en}$  value was set to 1.0 for any point interval where  $\dot{\epsilon}$  was less than zero.
- iv. The  $F_{en,i}$  was calculated between for point i and I=1 using the appropriate equation from Appendix A for the material evaluated, and using the maximum metal temperature of points i and i+1.
- v. The integrated  $F_{en-n}$  for the valley-peak load pair was calculated as:

$$F_{en-n} = \sum_{i=1}^k F_{en,i} \frac{\epsilon_i}{\epsilon_{max} - \epsilon_{min}}$$

where:  $F_{en-n}$  = integrated  $F_{en}$  for valley-peak load pair n  
 $k$  = number of integration points between valley and peak  
 $\epsilon_i$  = strain at any point, i, between the valley and peak computed as  $S'_{31\ i}$  divided by  $E$  evaluated at the metal temperature of point i  
 $\epsilon_{max}$  = maximum strain at the peak computed as  $S'_{31\text{-peak}}$  divided by  $E$  evaluated at the metal temperature of the peak  
 $\epsilon_{min}$  = minimum strain at the valley computed as  $S'_{31\text{-valley}}$  divided by  $E$  evaluated at the metal temperature of the valley  
 $E$  = the Young's Modulus determined at the maximum metal temperature of points i and i+1 (psi)

- vi. The  $F_{en}$  calculated in Step B(v) was assigned to both the peak and valley for use in the  $CUF_{en}$  calculations.

- vii. The above steps were repeated for all valley-peak intervals for the entire principal stress intensity history.
- viii. The total  $CUF_{en}$  was calculated as  $F_{en-1} U_1 + F_{en-2} U_2 + F_{en-3} U_3 + \dots + F_{en-n} U_n$ .

## C4 Results

The highest CUF calculated for the sample problem from Step A(m) in Section C3 is shown in Table C.2. The highest CUF resulted from the using the  $S'_{31}$  membrane plus bending principal stress differences (Case (v) for maximum membrane plus bending SY stress in Step A(h) in Section C3). The entire principal stress difference time history for this case is also plotted in Figure C.6. The peaks and valleys identified in the Table C.2 CUF calculation are also indicated on the plot in Figure C.6.

The  $CUF_{en}$  calculated for the sample problem using the Average Strain Rate Approach is shown in Table C.3.

The  $CUF_{en}$  calculated for the sample problem using the Modified Strain Rate Approach is shown in Table C.4.

The entire principal stress difference time history for this case, as calculated in Step A(f) in Section C3, is provided in Table C.5.

Table C.2. Limiting CUF Results for Sample Problem for SCL 2

Pair A	Pair B	Applied Cycles A	Applied Cycles B	M+B STRESS (psi)	K <sub>e</sub>	Total Stress (psi)	S <sub>alt</sub> (psi)	N <sub>n</sub>	n <sub>n</sub>	U <sub>n</sub>	Max. Metal Temp. (°F)	DO (ppm)
694	447	5	20	125542.9	2.580	144164.4	220490.4	140.005	5	0.0357	566.6	0.150
699	447	50	15	121622.8	2.405	139047.0	198300.6	178.958	15	0.0838	566.6	0.550
699	1021	35	20	104691.5	1.653	126037.5	124507.0	582.468	20	0.0343	600.4	0.550
699	899	15	50	89695.4	1.000	102302.8	57864.5	6339.47	15	0.0024	336.1	0.550
695	899	5	35	84993.9	1.000	98798.6	55882.4	7027.83	5	0.0007	336.1	0.550
185	899	20	30	68222.2	1.000	76465.1	43250.2	15549.1	20	0.0013	336.1	0.550
1432	899	20	10	66665.7	1.000	83098.8	47002.3	11892.7	10	0.0008	336.1	0.550
1432	1653	10	100	49437.0	1.000	61950.9	33687.5	35734.8	10	0.0003	103.0	0.522
1296	1653	20	90	32478.6	1.000	38719.1	22025.4	154852	20	0.0001	366.2	0.522
1136	1653	20	70	27045.6	1.000	33751.1	19388.7	258499	20	0.0001	417.7	0.522
2215	1653	100	50	25255.9	1.000	25668.1	15147.6	1.15E+06	50	0.0000	547.0	0.522
2215	1213	50	20	22343.7	1.000	25298.3	14929.4	1.30E+06	20	0.0000	547.0	0.050
2215	1562	30	20	22047.7	1.000	24970.1	14735.7	1.46E+06	20	0.0000	547.0	0.050
2215	1	10	20	11956.0	1.000	12255.6	7232.5	1.00E+11	10	0.0000	547.0	0.150
1347	1	20	10	3786.5	1.000	4173.0	2412.1	1.00E+11	10	0.0000	450.0	0.150
1347	1595	10	20	3408.0	1.000	3430.2	1963.3	1.00E+11	10	0.0000	398.7	0.050
960	1595	20	10	241.8	1.000	259.9	146.0	1.00E+11	10	0.0000	299.5	0.050
960	960	5	5	0.0	1.000	0.0	0.0	1.00E+11	10	0.0000	299.5	0.050

**TOTAL CUF = 0.1596**

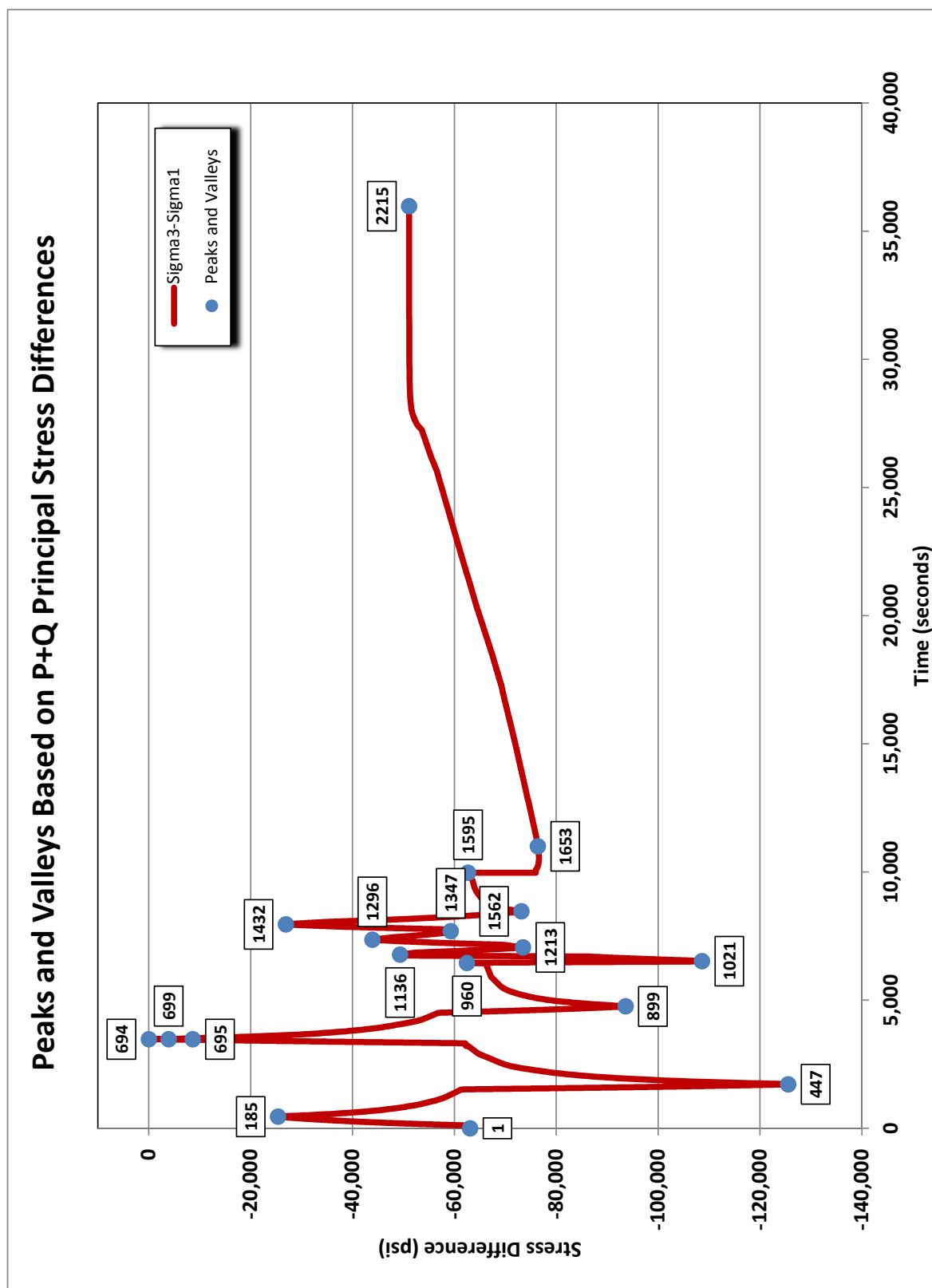


**Table C.3.  $CUF_{en}$  Results Based for Sample Problem for SCL 2  
(Average Strain Rate Approach)**

<b>Pair A</b>	<b>Pair B</b>	<b><math>F_{en-n}</math></b>	<b><math>U_n</math></b>	<b><math>CUF_{en-n}</math></b>
694	447	49.107	0.0357	1.7538
699	447	3.156	0.0838	0.2645
699	1021	3.156	0.0343	0.1084
699	899	3.156	0.0024	0.0075
695	899	1.000	0.0007	0.0007
185	899	15.763	0.0013	0.0203
1432	899	2.802	0.0008	0.0024
1432	1653	2.802	0.0003	0.0008
1296	1653	5.418	0.0001	0.0007
1136	1653	5.865	0.0001	0.0005
2215	1653	198.536	0.0000	0.0086
2215	1213	198.536	0.0000	0.0030
2215	1562	198.536	0.0000	0.0027
2215	1	198.536	0.0000	0.0000
1347	1	1.000	0.0000	0.0000
1347	1595	2.231	0.0000	0.0000
960	1595	10.531	0.0000	0.0000
960	960	10.531	0.0000	0.0000

**TOTAL  $CUF_{en}$  = 2.1738** (Overall  $F_{en}$  = 13.6174)



**Table C.4.  $CUF_{en}$  Results Based for Sample Problem for SCL 2  
(Modified Strain Rate Approach)**

<b>Pair A</b>	<b>Pair B</b>	<b><math>F_{en-nA}</math></b>	<b><math>F_{en-nB}</math></b>	<b><math>U_n</math></b>	<b><math>F_{en-n}</math></b>	<b><math>CUF_{en-n}</math></b>
694	447	45.1590	1.0000	0.0357	45.159	1.6128
699	447	2.2180	1.0000	0.0838	2.218	0.1859
699	1021	2.2180	1.0000	0.0343	2.218	0.0762
699	899	2.2180	1.0000	0.0024	2.218	0.0052
695	899	1.0000	1.0000	0.0007	1.000	0.0007
185	899	7.2220	1.0000	0.0013	7.222	0.0093
1432	899	2.0700	1.0000	0.0008	2.070	0.0017
1432	1653	2.0700	1.0000	0.0003	2.070	0.0006
1296	1653	4.3530	1.0000	0.0001	4.353	0.0006
1136	1653	5.5320	1.0000	0.0001	5.532	0.0004
2215	1653	24.7870	1.0000	0.0000	24.787	0.0011
2215	1213	24.7870	1.0000	0.0000	24.787	0.0004
2215	1562	24.7870	1.0000	0.0000	24.787	0.0003
2215	1	24.7870	1.0000	0.0000	24.787	0.0000
1347	1	1.0000	1.0000	0.0000	1.000	0.0000
1347	1595	1.0000	2.2310	0.0000	2.231	0.0000
960	1595	12.1020	2.2310	0.0000	12.102	0.0000
960	960	12.1020	12.1020	0.0000	12.102	0.0000

**TOTAL  $CUF_{en}$  = 1.8952** (Overall  $F_{en}$  = 11.8726)

**Table C.5. Principal Stress Intensity Histories Used in Limiting CUF Calculation for Sample Problem for SCL 2**

Point No.	Time (sec.)	Membrane + Bending Stresses			Total Stresses			Metal Temp. (°F)	No. of Cycles	DO (ppm)
		S' <sub>12</sub> (psi)	S' <sub>23</sub> (psi)	S' <sub>31</sub> (psi)	S' <sub>12</sub> (psi)	S' <sub>23</sub> (psi)	S' <sub>31</sub> (psi)			
1	0.00	34007.5	29079.5	-63087.0	45032.0	27828.0	-72859.9	450.0	20	0.150
2	10.00	33994.5	29077.5	-63072.0	45002.0	27826.0	-72827.9	449.9	20	0.150
3	20.00	33977.5	29071.5	-63049.0	44976.0	27821.0	-72796.9	449.7	20	0.150
4	30.00	33961.5	29064.5	-63025.9	44954.0	27814.0	-72767.9	449.6	20	0.150
5	40.00	33946.5	29057.5	-63003.9	44934.0	27807.0	-72740.9	449.5	20	0.150
6	60.00	33920.5	29040.5	-62960.9	44899.9	27792.0	-72691.9	449.2	20	0.150
7	80.00	33898.4	29023.4	-62921.9	44873.0	27776.0	-72648.9	448.9	20	0.150
8	100.00	33880.4	29005.4	-62885.9	44850.9	27758.9	-72609.9	448.6	20	0.150
9	103.00	33902.5	28926.5	-62829.1	44871.9	27678.9	-72550.8	448.6	20	0.150
10	105.00	33857.6	28864.6	-62722.2	44605.8	27617.8	-72223.6	447.2	20	0.150
11	107.00	33752.7	28792.7	-62545.3	44275.7	27545.7	-71821.4	445.7	20	0.150
12	109.00	33614.7	28711.7	-62326.4	43940.6	27466.6	-71407.2	444.1	20	0.150
13	111.00	33454.8	28622.8	-62077.5	43606.5	27380.5	-70987.0	442.4	20	0.150
14	113.00	33282.8	28526.8	-61809.6	43276.4	27289.4	-70565.8	440.8	20	0.150
15	115.00	33096.9	28424.9	-61521.7	42952.3	27191.3	-70143.6	439.1	20	0.150
16	117.00	32906.9	28317.9	-61224.8	42634.2	27087.2	-69721.4	437.3	20	0.150
17	119.00	32712.9	28203.9	-60916.9	42321.1	26979.1	-69300.2	435.6	20	0.150
18	121.00	32518.0	28085.0	-60602.9	42015.1	26866.1	-68881.1	433.9	20	0.150
19	123.00	32319.0	27962.0	-60281.0	41715.0	26747.0	-68461.9	432.1	20	0.150
20	125.00	32121.0	27835.0	-59956.1	41421.9	26624.9	-68046.8	430.3	20	0.150
21	127.00	31924.1	27703.1	-59627.1	41132.8	26499.8	-67632.7	428.5	20	0.150
22	129.00	31728.1	27568.1	-59296.2	40850.8	26370.8	-67221.6	426.7	20	0.150
23	131.00	31534.1	27429.1	-58963.2	40576.7	26237.7	-66814.5	424.9	20	0.150
24	133.00	31341.1	27287.1	-58628.3	40306.7	26101.7	-66408.3	423.1	20	0.150
25	135.00	31151.2	27142.1	-58293.3	40042.6	25962.6	-66005.2	421.3	20	0.150
26	137.00	30964.2	26994.2	-57958.3	39783.5	25821.5	-65605.1	419.5	20	0.150
27	139.00	30780.2	26845.2	-57625.4	39531.5	25677.5	-65209.0	417.7	20	0.150
28	141.00	30598.2	26693.2	-57291.4	39283.4	25532.4	-64815.9	415.8	20	0.150
29	143.00	30419.2	26539.2	-56958.5	39041.4	25384.4	-64425.8	414.0	20	0.150
30	145.00	30243.2	26382.2	-56625.5	38804.3	25234.3	-64038.7	412.2	20	0.150
31	147.00	30071.3	26224.3	-56295.5	38573.3	25082.3	-63655.6	410.3	20	0.150
32	149.00	29901.3	26065.3	-55966.5	38346.3	24929.3	-63275.5	408.5	20	0.150
33	151.00	29734.3	25904.3	-55638.6	38123.2	24775.2	-62898.4	406.6	20	0.150
34	153.00	29570.3	25742.3	-55312.6	37904.1	24620.2	-62524.3	404.8	20	0.150
35	155.00	29409.3	25580.3	-54989.6	37691.1	24464.1	-62155.2	402.9	20	0.150
36	157.00	29251.3	25416.3	-54667.6	37481.1	24306.1	-61787.1	401.1	20	0.150

Point No.	Time (sec.)	Membrane + Bending Stresses			Total Stresses			Metal Temp. (°F)	No. of Cycles	DO (ppm)
		S' <sub>12</sub> (psi)	S' <sub>23</sub> (psi)	S' <sub>31</sub> (psi)	S' <sub>12</sub> (psi)	S' <sub>23</sub> (psi)	S' <sub>31</sub> (psi)			
37	159.00	29096.3	25251.3	-54347.7	37276.0	24148.0	-61424.0	399.2	20	0.150
38	161.00	28943.3	25085.3	-54028.7	37075.0	23988.0	-61062.9	397.3	20	0.150
39	163.00	28794.4	24918.4	-53712.7	36877.9	23827.9	-60705.8	395.5	20	0.150
40	165.00	28648.4	24751.4	-53399.7	36685.9	23667.9	-60353.7	393.6	20	0.150
41	167.00	28503.4	24584.4	-53087.7	36495.8	23506.8	-60002.6	391.7	20	0.150
42	169.00	28362.4	24415.4	-52777.8	36309.8	23344.8	-59654.6	389.8	20	0.150
43	171.00	28222.4	24247.4	-52469.8	36127.7	23182.7	-59310.5	388.0	20	0.150
44	173.00	28085.4	24078.4	-52163.8	35948.7	23019.7	-58968.4	386.1	20	0.150
45	175.00	27952.4	23909.4	-51861.8	35773.6	22857.6	-58631.3	384.2	20	0.150
46	177.00	27820.4	23739.4	-51559.8	35601.6	22694.6	-58296.2	382.3	20	0.150
47	179.00	27691.4	23569.4	-51260.8	35433.5	22530.6	-57964.1	380.4	20	0.150
48	181.00	27564.4	23399.4	-50963.8	35267.5	22367.5	-57635.0	378.5	20	0.150
49	183.00	27440.4	23229.4	-50669.9	35106.5	22203.5	-57309.9	376.6	20	0.150
50	185.00	27319.4	23058.4	-50377.9	34948.4	22039.4	-56987.8	374.7	20	0.150
51	187.00	27199.4	22888.4	-50087.9	34792.4	21875.4	-56667.7	372.9	20	0.150
52	189.00	27081.4	22718.5	-49799.9	34639.3	21711.3	-56350.6	371.0	20	0.150
53	191.00	26965.5	22549.4	-49514.9	34489.3	21547.2	-56036.5	369.1	20	0.150
54	193.00	26851.5	22379.5	-49230.9	34341.2	21384.2	-55725.4	367.2	20	0.150
55	195.00	26741.5	22208.5	-48949.9	34198.2	21220.1	-55418.3	365.3	20	0.150
56	197.00	26631.5	22039.5	-48671.0	34056.1	21056.1	-55112.2	363.4	20	0.150
57	199.00	26524.5	21869.5	-48393.9	33917.1	20892.1	-54809.1	361.4	20	0.150
58	201.00	26418.5	21700.5	-48119.0	33780.0	20730.0	-54510.0	359.5	20	0.150
59	203.00	26315.5	21530.5	-47846.0	33647.0	20566.0	-54212.9	357.6	20	0.150
60	205.00	26215.5	21361.5	-47577.0	33515.9	20402.9	-53918.8	355.7	20	0.150
61	207.00	26115.5	21192.5	-47308.0	33386.9	20240.9	-53627.8	353.8	20	0.150
62	209.00	26017.5	21024.5	-47042.0	33260.8	20076.8	-53337.7	351.9	20	0.150
63	211.00	25921.5	20855.5	-46777.0	33135.8	19915.8	-53051.5	350.0	20	0.150
64	213.00	25828.5	20687.5	-46516.0	33014.7	19753.7	-52768.4	348.1	20	0.150
65	215.00	25735.5	20519.5	-46255.0	32895.7	19590.7	-52486.4	346.1	20	0.150
66	217.00	25644.5	20352.5	-45997.1	32778.6	19429.6	-52208.3	344.2	20	0.150
67	219.00	25555.5	20185.5	-45741.1	32663.6	19268.6	-51932.1	342.3	20	0.150
68	221.00	25468.5	20018.5	-45487.1	32551.5	19106.5	-51658.0	340.4	20	0.150
69	223.00	25384.5	19851.5	-45236.1	32441.5	18946.5	-51388.0	338.5	20	0.150
70	225.00	25300.6	19685.5	-44986.1	32333.4	18786.4	-51119.9	336.6	20	0.150
71	227.00	25218.5	19519.5	-44738.1	32227.4	18626.4	-50853.7	334.6	20	0.150
72	229.00	25137.6	19354.6	-44492.1	32122.3	18467.3	-50589.7	332.7	20	0.150
73	231.00	25057.6	19190.6	-44248.1	32019.3	18308.3	-50327.5	330.8	20	0.150
74	233.00	24980.6	19025.6	-44006.1	31919.2	18149.2	-50068.4	328.9	20	0.150
75	235.00	24903.6	18861.6	-43765.2	31819.2	17991.2	-49810.3	326.9	20	0.150

Point No.	Time (sec.)	Membrane + Bending Stresses			Total Stresses			Metal Temp. (°F)	No. of Cycles	DO (ppm)
		S' <sub>12</sub> (psi)	S' <sub>23</sub> (psi)	S' <sub>31</sub> (psi)	S' <sub>12</sub> (psi)	S' <sub>23</sub> (psi)	S' <sub>31</sub> (psi)			
76	237.00	24827.6	18698.6	-43526.2	31722.1	17832.1	-49554.2	325.0	20	0.150
77	239.00	24753.6	18535.6	-43289.2	31626.1	17675.1	-49301.1	323.1	20	0.150
78	241.00	24681.6	18372.6	-43054.2	31532.0	17518.0	-49050.0	321.1	20	0.150
79	243.00	24610.6	18210.6	-42821.2	31439.0	17362.0	-48800.9	319.2	20	0.150
80	245.00	24540.6	18048.6	-42589.2	31347.9	17204.9	-48552.8	317.3	20	0.150
81	247.00	24471.6	17886.6	-42358.2	31258.9	17048.9	-48307.7	315.4	20	0.150
82	249.00	24403.6	17726.6	-42130.3	31170.8	16893.8	-48064.6	313.4	20	0.150
83	251.00	24338.6	17565.6	-41904.3	31085.8	16738.8	-47824.5	311.5	20	0.150
84	253.00	24273.6	17405.7	-41679.3	31000.7	16584.7	-47585.4	309.6	20	0.150
85	255.00	24209.7	17246.7	-41456.3	30917.7	16430.6	-47348.3	307.6	20	0.150
86	257.00	24147.7	17086.7	-41234.3	30836.6	16276.6	-47113.2	305.7	20	0.150
87	259.00	24087.7	16928.7	-41016.3	30758.5	16122.5	-46881.1	303.7	20	0.150
88	261.00	24027.7	16770.7	-40798.4	30680.5	15970.5	-46651.0	301.8	20	0.150
89	263.00	23969.7	16612.7	-40582.4	30604.4	15817.4	-46421.9	299.9	20	0.150
90	265.00	23912.7	16455.7	-40368.4	30529.4	15666.4	-46195.8	297.9	20	0.150
91	267.00	23856.7	16298.7	-40155.4	30456.3	15514.3	-45970.7	296.0	20	0.150
92	269.00	23801.7	16143.7	-39945.5	30384.3	15364.3	-45748.5	294.0	20	0.150
93	271.00	23747.7	15987.7	-39735.5	30313.2	15213.2	-45526.5	292.1	20	0.150
94	273.00	23693.7	15832.8	-39526.5	30243.2	15063.2	-45306.3	290.1	20	0.150
95	275.00	23640.8	15677.8	-39318.5	30173.1	14914.1	-45087.2	288.2	20	0.150
96	277.00	23589.8	15523.8	-39113.6	30106.1	14765.1	-44871.1	286.2	20	0.150
97	279.00	23538.8	15369.8	-38908.6	30039.0	14616.0	-44655.0	284.3	20	0.150
98	281.00	23488.8	15215.8	-38704.6	29971.9	14467.9	-44439.9	282.4	20	0.150
99	283.00	23438.8	15063.8	-38502.6	29906.9	14319.9	-44226.8	280.4	20	0.150
100	285.00	23390.8	14911.8	-38302.7	29842.8	14172.8	-44015.7	278.5	20	0.150
101	287.00	23342.8	14759.8	-38102.7	29779.8	14025.8	-43805.6	276.5	20	0.150
102	289.00	23295.9	14607.9	-37903.7	29716.7	13879.7	-43596.5	274.6	20	0.150
103	291.00	23248.9	14456.9	-37705.8	29655.7	13732.7	-43388.4	272.6	20	0.150
104	293.00	23203.9	14306.9	-37510.8	29595.6	13587.6	-43183.3	270.6	20	0.150
105	295.00	23159.9	14155.9	-37315.8	29535.6	13442.6	-42978.1	268.7	20	0.150
106	297.00	23114.9	14006.9	-37121.9	29477.5	13297.5	-42775.0	266.7	20	0.150
107	299.00	23071.9	13857.9	-36929.9	29419.5	13153.5	-42572.9	264.8	20	0.150
108	301.00	23030.0	13709.0	-36738.9	29363.4	13010.4	-42373.8	262.8	20	0.150
109	303.00	22989.0	13560.0	-36549.0	29307.4	12866.3	-42173.7	260.9	20	0.150
110	305.00	22948.0	13412.0	-36360.0	29252.3	12724.3	-41976.6	258.9	20	0.150
111	307.00	22907.0	13266.0	-36173.1	29198.2	12581.2	-41779.5	257.0	20	0.150
112	309.00	22869.1	13118.1	-35987.1	29146.2	12439.2	-41585.4	255.0	20	0.150
113	311.00	22830.1	12972.1	-35802.1	29094.1	12298.1	-41392.2	253.0	20	0.150
114	313.00	22792.1	12826.1	-35618.2	29043.1	12157.1	-41200.2	251.1	20	0.150

Point No.	Time (sec.)	Membrane + Bending Stresses			Total Stresses			Metal Temp. (°F)	No. of Cycles	DO (ppm)
		S' <sub>12</sub> (psi)	S' <sub>23</sub> (psi)	S' <sub>31</sub> (psi)	S' <sub>12</sub> (psi)	S' <sub>23</sub> (psi)	S' <sub>31</sub> (psi)			
115	315.00	22756.1	12681.1	-35437.2	28994.0	12016.0	-41010.1	249.1	20	0.150
116	317.00	22720.1	12535.1	-35255.3	28945.0	11874.9	-40819.9	247.2	20	0.150
117	319.00	22684.2	12391.2	-35075.3	28895.9	11734.9	-40630.8	245.2	20	0.150
118	321.00	22649.2	12247.2	-34896.4	28846.9	11595.9	-40442.7	243.2	20	0.150
119	323.00	22615.2	12103.2	-34718.4	28800.8	11456.8	-40257.6	241.3	20	0.150
120	325.00	22581.2	11960.2	-34541.5	28753.8	11318.7	-40072.5	239.3	20	0.150
121	327.00	22548.3	11817.3	-34365.5	28708.7	11179.7	-39888.4	237.3	20	0.150
122	329.00	22516.3	11675.3	-34191.6	28663.6	11042.6	-39706.3	235.4	20	0.150
123	331.00	22485.3	11533.3	-34018.6	28621.6	10904.6	-39526.2	233.4	20	0.150
124	333.00	22455.3	11391.3	-33846.7	28578.5	10768.5	-39347.1	231.4	20	0.150
125	335.00	22425.4	11250.4	-33675.8	28536.5	10631.5	-39168.0	229.4	20	0.150
126	337.00	22396.4	11110.4	-33506.8	28497.4	10495.4	-38992.8	227.5	20	0.150
127	339.00	22368.4	10970.4	-33338.9	28457.4	10360.4	-38817.7	225.5	20	0.150
128	341.00	22340.5	10830.5	-33170.9	28418.3	10225.3	-38643.6	223.5	20	0.150
129	343.00	22313.5	10691.5	-33005.0	28380.3	10090.3	-38470.5	221.5	20	0.150
130	345.00	22287.5	10553.5	-32841.1	28343.2	9956.2	-38299.4	219.6	20	0.150
131	347.00	22261.6	10414.6	-32676.1	28306.1	9822.1	-38128.3	217.6	20	0.150
132	349.00	22235.6	10276.6	-32512.2	28269.1	9689.1	-37958.2	215.6	20	0.150
133	351.00	22210.6	10139.6	-32350.3	28234.1	9556.0	-37790.1	213.6	20	0.150
134	353.00	22185.7	10002.7	-32188.3	28199.0	9423.0	-37622.0	211.7	20	0.150
135	355.00	22161.7	9865.7	-32027.4	28163.9	9289.9	-37453.9	209.7	20	0.150
136	357.00	22137.8	9728.7	-31866.5	28128.9	9158.9	-37287.8	207.7	20	0.150
137	359.00	22114.8	9593.8	-31708.6	28096.8	9026.8	-37123.7	205.7	20	0.150
138	361.00	22091.8	9457.8	-31549.7	28062.8	8895.8	-36958.5	203.7	20	0.150
139	363.00	22069.9	9321.9	-31391.7	28030.7	8764.7	-36795.5	201.8	20	0.150
140	365.00	22047.9	9187.9	-31235.8	27999.6	8633.7	-36633.3	199.8	20	0.150
141	367.00	22027.0	9053.0	-31079.9	27968.6	8503.6	-36472.2	197.8	20	0.150
142	369.00	22006.0	8919.0	-30925.0	27938.6	8374.5	-36313.1	195.8	20	0.150
143	371.00	21986.0	8786.0	-30772.1	27909.5	8244.5	-36154.0	193.9	20	0.150
144	373.00	21967.1	8653.1	-30620.2	27881.5	8116.4	-35997.9	191.9	20	0.150
145	375.00	21948.2	8520.2	-30468.3	27853.4	7988.4	-35841.8	189.9	20	0.150
146	377.00	21930.2	8387.2	-30317.4	27826.3	7859.4	-35685.7	187.9	20	0.150
147	379.00	21913.2	8255.2	-30168.5	27800.3	7732.3	-35532.6	185.9	20	0.150
148	381.00	21895.3	8125.3	-30020.6	27774.2	7605.2	-35379.5	184.0	20	0.150
149	383.00	21878.4	7993.4	-29871.7	27749.2	7477.2	-35226.4	182.0	20	0.150
150	385.00	21862.4	7862.4	-29724.8	27724.1	7351.1	-35075.3	180.0	20	0.150
151	387.00	21847.5	7732.5	-29579.9	27700.1	7225.1	-34925.2	178.0	20	0.150
152	389.00	21831.5	7603.5	-29435.0	27676.0	7099.0	-34775.0	176.1	20	0.150
153	391.00	21816.6	7473.6	-29290.2	27653.0	6974.0	-34627.0	174.1	20	0.150

Point No.	Time (sec.)	Membrane + Bending Stresses			Total Stresses			Metal Temp. (°F)	No. of Cycles	DO (ppm)
		S' <sub>12</sub> (psi)	S' <sub>23</sub> (psi)	S' <sub>31</sub> (psi)	S' <sub>12</sub> (psi)	S' <sub>23</sub> (psi)	S' <sub>31</sub> (psi)			
154	393.00	21803.6	7344.6	-29148.3	27630.9	6848.9	-34479.8	172.1	20	0.150
155	395.00	21789.7	7215.7	-29005.4	27608.9	6723.9	-34332.7	170.1	20	0.150
156	397.00	21775.8	7087.8	-28863.5	27586.8	6599.8	-34186.6	168.1	20	0.150
157	399.00	21763.8	6959.8	-28723.7	27566.8	6476.8	-34043.5	166.1	20	0.150
158	401.00	21750.9	6832.9	-28583.8	27546.7	6352.7	-33899.4	164.2	20	0.150
159	403.00	21739.0	6706.0	-28444.9	27526.7	6229.7	-33756.3	162.2	20	0.150
160	405.00	21729.0	6579.0	-28308.1	27507.6	6107.6	-33615.2	160.2	20	0.150
161	407.00	21717.1	6454.1	-28171.2	27488.6	5985.6	-33474.1	158.2	20	0.150
162	409.00	21707.2	6327.2	-28034.4	27470.5	5863.5	-33334.0	156.2	20	0.150
163	411.00	21696.3	6203.3	-27899.5	27452.5	5742.5	-33194.9	154.3	20	0.150
164	413.00	21688.3	6077.3	-27765.7	27436.4	5620.4	-33056.8	152.3	20	0.150
165	415.00	21678.4	5953.4	-27631.8	27419.4	5500.4	-32919.7	150.3	20	0.150
166	417.00	21669.5	5829.5	-27499.0	27403.3	5380.3	-32783.6	148.3	20	0.150
167	419.00	21662.6	5705.6	-27368.2	27388.3	5259.3	-32647.5	146.3	20	0.150
168	421.00	21653.7	5582.7	-27236.3	27372.2	5140.2	-32512.4	144.3	20	0.150
169	423.00	21645.8	5459.8	-27105.5	27356.2	5021.2	-32377.3	142.3	20	0.150
170	425.00	21639.8	5336.8	-26976.7	27342.1	4902.1	-32244.2	140.3	20	0.150
171	427.00	21632.9	5214.9	-26847.9	27327.1	4785.1	-32112.1	138.4	20	0.150
172	429.00	21626.0	5094.0	-26720.0	27313.0	4667.0	-31980.0	136.4	20	0.150
173	431.00	21620.1	4973.1	-26593.2	27300.0	4549.0	-31848.9	134.4	20	0.150
174	433.00	21614.2	4852.2	-26466.4	27286.9	4431.9	-31718.8	132.4	20	0.150
175	435.00	21608.3	4731.3	-26339.6	27273.9	4314.8	-31588.7	130.4	20	0.150
176	437.00	21603.4	4611.4	-26214.8	27261.8	4197.8	-31459.6	128.4	20	0.150
177	439.00	21598.5	4490.5	-26089.0	27248.8	4081.8	-31330.5	126.4	20	0.150
178	441.00	21593.6	4370.6	-25964.2	27236.7	3965.7	-31202.4	124.4	20	0.150
179	443.00	21589.7	4250.7	-25840.5	27226.7	3848.6	-31075.3	122.4	20	0.150
180	445.00	21584.9	4131.9	-25716.7	27214.6	3733.6	-30948.2	120.4	20	0.150
181	447.00	21580.9	4012.9	-25593.9	27203.6	3618.6	-30822.2	118.4	20	0.150
182	449.00	21577.1	3895.1	-25472.1	27193.5	3503.5	-30697.0	116.4	20	0.150
183	450.00	21579.1	3836.1	-25415.3	27212.5	3446.5	-30659.0	115.6	20	0.150
184	451.00	21580.0	3804.0	-25384.0	27243.5	3416.5	-30660.0	114.8	20	0.150
185	454.00	21670.7	3722.7	-25393.3	27615.6	3339.5	-30955.1	113.6	20	0.150
186	459.00	22014.3	3631.3	-25645.6	28424.7	3253.7	-31678.4	112.6	20	0.150
187	467.00	22762.9	3581.9	-26344.8	29713.8	3201.9	-32915.7	111.6	20	0.150
188	477.00	23772.8	3644.8	-27417.6	31199.0	3252.9	-34451.9	110.6	20	0.150
189	478.00	23872.8	3655.8	-27528.5	31335.9	3264.0	-34599.9	110.5	20	0.150
190	488.00	24847.8	3823.8	-28671.7	32661.0	3418.0	-36079.0	109.8	20	0.150
191	492.00	25216.9	3910.9	-29127.8	33146.0	3498.0	-36644.0	109.5	20	0.150
192	502.00	26098.1	4160.1	-30258.2	34294.0	3731.0	-38025.1	108.9	20	0.150

Point No.	Time (sec.)	Membrane + Bending Stresses			Total Stresses			Metal Temp. (°F)	No. of Cycles	DO (ppm)
		S' <sub>12</sub> (psi)	S' <sub>23</sub> (psi)	S' <sub>31</sub> (psi)	S' <sub>12</sub> (psi)	S' <sub>23</sub> (psi)	S' <sub>31</sub> (psi)			
193	509.00	26670.3	4355.3	-31025.5	35023.1	3915.0	-38938.1	108.5	20	0.150
194	519.00	27434.6	4657.6	-32092.2	35994.1	4200.0	-40194.1	108.0	20	0.150
195	529.00	28137.0	4974.0	-33111.0	36871.1	4500.1	-41371.2	107.5	20	0.150
196	539.00	28786.4	5302.4	-34088.8	37681.1	4811.1	-42492.2	107.0	20	0.150
197	549.00	29385.9	5634.9	-35020.8	38419.2	5127.1	-43546.3	106.6	20	0.150
198	553.00	29611.1	5769.1	-35380.2	38694.2	5255.1	-43949.3	106.4	20	0.150
199	563.00	30151.6	6103.6	-36255.3	39358.2	5574.2	-44932.3	106.1	20	0.150
200	573.00	30653.2	6437.2	-37090.4	39966.2	5892.2	-45858.4	105.7	20	0.150
201	582.00	31073.7	6734.7	-37808.5	40473.2	6176.3	-46649.5	105.4	20	0.150
202	592.00	31518.4	7062.4	-38580.7	41012.3	6488.3	-47500.6	105.1	20	0.150
203	602.00	31935.0	7386.0	-39321.1	41510.3	6798.3	-48308.7	104.8	20	0.150
204	612.00	32318.7	7702.7	-40021.4	41965.3	7100.4	-49065.7	104.5	20	0.150
205	617.00	32498.1	7858.1	-40356.1	42178.4	7248.4	-49426.8	104.4	20	0.150
206	627.00	32850.8	8161.8	-41012.6	42600.4	7539.4	-50139.8	104.2	20	0.150
207	637.00	33184.5	8459.5	-41644.0	42995.5	7823.5	-50819.0	103.9	20	0.150
208	647.00	33501.3	8750.3	-42251.6	43367.5	8101.5	-51469.0	103.7	20	0.150
209	657.00	33799.1	9033.1	-42832.1	43716.6	8371.6	-52088.1	103.5	20	0.150
210	661.00	33912.4	9144.4	-43056.8	43849.6	8477.6	-52327.2	103.4	20	0.150
211	671.00	34190.2	9417.2	-43607.3	44180.6	8737.6	-52918.3	103.2	20	0.150
212	681.00	34451.0	9683.0	-44134.0	44485.7	8991.7	-53477.4	103.1	20	0.150
213	691.00	34695.8	9939.8	-44635.7	44768.7	9237.7	-54006.5	102.9	20	0.150
214	701.00	34927.7	10191.7	-45119.4	45037.8	9477.8	-54515.6	102.7	20	0.150
215	721.00	35360.4	10675.4	-46035.8	45536.9	9938.9	-55475.8	102.4	20	0.150
216	731.00	35567.3	10908.3	-46475.6	45782.0	10161.0	-55942.9	102.3	20	0.150
217	741.00	35767.2	11137.2	-46904.4	46013.0	10380.0	-56393.1	102.2	20	0.150
218	751.00	35956.1	11360.1	-47316.3	46231.1	10592.1	-56823.2	102.1	20	0.150
219	761.00	36136.0	11578.0	-47714.1	46437.1	10800.1	-57237.3	102.0	20	0.150
220	781.00	36464.9	11994.9	-48459.8	46812.2	11196.3	-58008.5	101.7	20	0.150
221	801.00	36770.8	12391.8	-49162.6	47159.4	11575.4	-58734.7	101.5	20	0.150
222	815.00	36973.2	12664.2	-49637.3	47388.4	11834.4	-59222.9	101.4	20	0.150
223	825.00	37119.1	12855.1	-49974.2	47561.5	12016.5	-59578.0	101.3	20	0.150
224	835.00	37263.1	13044.1	-50307.2	47726.6	12196.6	-59923.2	101.3	20	0.150
225	845.00	37403.1	13232.1	-50635.2	47886.6	12374.6	-60261.3	101.2	20	0.150
226	855.00	37538.1	13416.1	-50954.1	48040.7	12549.7	-60590.4	101.2	20	0.150
227	875.00	37797.1	13776.1	-51573.1	48333.8	12891.8	-61225.6	101.1	20	0.150
228	895.00	38039.1	14124.1	-52163.2	48605.9	13223.9	-61829.9	101.0	20	0.150
229	915.00	38260.2	14456.2	-52716.3	48855.0	13539.0	-62394.1	100.9	20	0.150
230	955.00	38632.2	15058.2	-53690.3	49270.3	14111.3	-63381.6	100.7	20	0.150
231	995.00	38959.0	15602.0	-54561.0	49634.5	14627.5	-64262.0	100.6	20	0.150

Point No.	Time (sec.)	Membrane + Bending Stresses			Total Stresses			Metal Temp. (°F)	No. of Cycles	DO (ppm)
		S' <sub>12</sub> (psi)	S' <sub>23</sub> (psi)	S' <sub>31</sub> (psi)	S' <sub>12</sub> (psi)	S' <sub>23</sub> (psi)	S' <sub>31</sub> (psi)			
232	1039.00	39281.1	16152.1	-55433.1	49992.7	15149.8	-65142.5	100.4	20	0.150
233	1049.00	39357.0	16272.0	-55628.9	50086.8	15263.8	-65350.6	100.4	20	0.150
234	1059.00	39432.9	16390.9	-55823.8	50174.8	15375.8	-65550.7	100.4	20	0.150
235	1069.00	39505.8	16508.8	-56014.6	50258.9	15487.9	-65746.8	100.5	20	0.150
236	1079.00	39576.7	16624.7	-56201.4	50340.0	15596.9	-65936.9	100.5	20	0.150
237	1099.00	39711.4	16848.4	-56559.9	50492.0	15809.1	-66301.1	100.6	20	0.150
238	1119.00	39835.1	17063.1	-56898.2	50630.1	16014.2	-66644.3	100.7	20	0.150
239	1139.00	39949.8	17268.8	-57218.6	50758.2	16208.2	-66966.5	100.8	20	0.150
240	1179.00	40151.9	17646.9	-57798.9	50983.4	16566.4	-67549.8	100.9	20	0.150
241	1219.00	40318.0	17985.0	-58302.9	51167.6	16887.6	-68055.1	101.1	20	0.150
242	1299.00	40594.3	18570.3	-59164.6	51472.9	17441.9	-68914.7	101.4	20	0.150
243	1379.00	40860.5	19134.5	-59995.0	51767.1	17977.1	-69744.3	101.7	20	0.150
244	1510.00	41284.2	20042.2	-61326.4	52234.6	18835.6	-71070.2	102.2	20	0.150
245	1512.00	41259.6	20143.6	-61403.3	52213.6	18938.6	-71152.3	102.2	20	0.150
246	1513.00	41289.9	20199.9	-61489.7	52432.7	18996.7	-71429.4	103.8	20	0.150
247	1514.00	41380.1	20266.1	-61646.3	52866.9	19063.8	-71930.7	105.5	20	0.150
248	1515.00	41505.4	20338.4	-61843.9	53291.0	19135.0	-72426.0	107.4	20	0.150
249	1516.00	41656.8	20416.8	-62073.6	53724.1	19212.1	-72936.3	109.3	20	0.150
250	1517.00	41830.2	20501.2	-62331.3	54160.3	19294.3	-73454.5	111.3	20	0.150
251	1518.00	42020.5	20590.5	-62611.1	54598.4	19381.4	-73979.8	113.3	20	0.150
252	1519.00	42227.0	20684.0	-62911.0	55036.5	19471.5	-74508.0	115.4	20	0.150
253	1520.00	42441.4	20783.4	-63224.8	55471.6	19566.6	-75038.3	117.4	20	0.150
254	1521.00	42664.9	20886.9	-63551.8	55903.8	19665.8	-75569.5	119.5	20	0.150
255	1522.00	42898.4	20993.4	-63891.8	56333.9	19768.9	-76102.8	121.7	20	0.150
256	1523.00	43137.9	21104.9	-64242.8	56759.0	19875.0	-76634.0	123.8	20	0.150
257	1524.00	43384.5	21221.5	-64606.0	57179.1	19986.1	-77165.2	126.0	20	0.150
258	1525.00	43635.0	21341.1	-64976.1	57596.2	20100.2	-77696.4	128.1	20	0.150
259	1526.00	43885.6	21465.6	-65351.2	58008.3	20218.3	-78226.6	130.3	20	0.150
260	1527.00	44140.2	21591.3	-65731.5	58418.4	20338.4	-78756.8	132.5	20	0.150
261	1528.00	44395.8	21720.8	-66116.6	58822.5	20462.5	-79285.0	134.7	20	0.150
262	1529.00	44653.4	21853.4	-66506.9	59224.6	20587.6	-79812.2	136.9	20	0.150
263	1530.00	44911.1	21990.1	-66901.3	59619.7	20718.7	-80338.4	139.1	20	0.150
264	1531.00	45171.8	22129.8	-67301.6	60011.8	20850.8	-80862.5	141.3	20	0.150
265	1532.00	45431.5	22272.5	-67704.0	60398.8	20985.9	-81384.7	143.5	20	0.150
266	1533.00	45692.2	22418.2	-68110.3	60781.9	21124.9	-81906.9	145.7	20	0.150
267	1534.00	45950.9	22565.9	-68516.8	61160.0	21265.0	-82425.0	147.9	20	0.150
268	1535.00	46209.6	22716.6	-68926.3	61536.1	21408.1	-82944.2	150.2	20	0.150
269	1536.00	46467.3	22868.3	-69335.7	61906.2	21553.2	-83459.4	152.4	20	0.150
270	1537.00	46725.1	23024.1	-69749.2	62273.2	21701.3	-83974.5	154.7	20	0.150



Point No.	Time (sec.)	Membrane + Bending Stresses			Total Stresses			Metal Temp. (°F)	No. of Cycles	DO (ppm)
		S' <sub>12</sub> (psi)	S' <sub>23</sub> (psi)	S' <sub>31</sub> (psi)	S' <sub>12</sub> (psi)	S' <sub>23</sub> (psi)	S' <sub>31</sub> (psi)			
271	1538.00	46981.9	23180.9	-70162.8	62637.3	21850.3	-84487.6	156.9	20	0.150
272	1539.00	47236.7	23340.7	-70577.3	62996.4	22002.4	-84998.8	159.2	20	0.150
273	1540.00	47490.4	23503.4	-70993.9	63352.5	22156.5	-85508.9	161.4	20	0.150
274	1541.00	47744.2	23667.2	-71411.4	63703.5	22313.5	-86017.1	163.7	20	0.150
275	1542.00	47994.1	23834.0	-71828.1	64050.6	22471.6	-86522.2	165.9	20	0.150
276	1543.00	48243.9	24001.9	-72245.8	64395.7	22631.7	-87027.3	168.2	20	0.150
277	1544.00	48492.7	24170.7	-72663.3	64736.8	22792.7	-87529.5	170.5	20	0.150
278	1545.00	48737.5	24342.5	-73080.0	65072.8	22955.8	-88028.6	172.8	20	0.150
279	1546.00	48982.4	24514.4	-73496.7	65406.9	23119.9	-88526.8	175.0	20	0.150
280	1547.00	49225.2	24688.2	-73913.4	65737.9	23285.0	-89022.9	177.3	20	0.150
281	1548.00	49466.1	24863.1	-74329.2	66064.0	23452.0	-89516.0	179.6	20	0.150
282	1549.00	49704.9	25039.9	-74744.9	66387.1	23621.1	-90008.1	181.9	20	0.150
283	1550.00	49942.9	25217.9	-75160.7	66706.1	23791.1	-90497.3	184.2	20	0.150
284	1551.00	50177.7	25397.7	-75575.4	67021.2	23963.2	-90984.4	186.5	20	0.150
285	1552.00	50410.7	25579.6	-75990.3	67334.2	24135.3	-91469.5	188.8	20	0.150
286	1553.00	50642.5	25762.5	-76405.0	67643.3	24309.3	-91952.6	191.1	20	0.150
287	1554.00	50872.4	25946.4	-76818.9	67948.4	24485.4	-92433.7	193.4	20	0.150
288	1555.00	51099.4	26130.4	-77229.8	68249.4	24661.4	-92910.9	195.7	20	0.150
289	1556.00	51324.3	26317.2	-77641.5	68548.5	24838.5	-93387.0	198.0	20	0.150
290	1557.00	51548.2	26503.2	-78051.4	68844.5	25016.5	-93861.1	200.3	20	0.150
291	1558.00	51769.1	26690.1	-78459.2	69137.6	25194.6	-94332.2	202.6	20	0.150
292	1559.00	51989.1	26878.1	-78867.1	69426.7	25374.7	-94801.4	204.9	20	0.150
293	1560.00	52207.0	27066.0	-79273.0	69713.7	25554.7	-95268.5	207.2	20	0.150
294	1561.00	52423.0	27256.0	-79678.9	69996.8	25735.8	-95732.5	209.5	20	0.150
295	1562.00	52634.9	27445.9	-80080.8	70275.8	25916.8	-96192.7	211.8	20	0.150
296	1563.00	52846.9	27636.9	-80483.7	70552.9	26098.9	-96651.8	214.1	20	0.150
297	1564.00	53056.9	27827.9	-80884.8	70827.9	26281.0	-97108.9	216.4	20	0.150
298	1565.00	53264.8	28018.8	-81283.7	71099.0	26464.0	-97563.0	218.7	20	0.150
299	1566.00	53468.8	28211.8	-81680.6	71366.1	26648.1	-98014.2	221.0	20	0.150
300	1567.00	53672.7	28404.8	-82077.5	71632.1	26832.1	-98464.3	223.3	20	0.150
301	1568.00	53874.8	28598.8	-82473.5	71894.2	27018.2	-98912.4	225.6	20	0.150
302	1569.00	54074.7	28792.7	-82867.5	72154.2	27203.2	-99357.5	227.9	20	0.150
303	1570.00	54272.7	28986.7	-83259.4	72411.3	27389.3	-99800.6	230.2	20	0.150
304	1571.00	54467.7	29182.7	-83650.4	72664.4	27576.3	-100240.7	232.5	20	0.150
305	1572.00	54660.7	29379.7	-84040.4	72915.4	27763.4	-100678.8	234.9	20	0.150
306	1573.00	54852.7	29575.7	-84428.4	73163.4	27951.4	-101114.9	237.2	20	0.150
307	1574.00	55043.8	29770.7	-84814.5	73409.5	28139.5	-101549.0	239.5	20	0.150
308	1575.00	55230.7	29968.7	-85199.4	73652.6	28327.5	-101980.1	241.8	20	0.150

Point No.	Time (sec.)	Membrane + Bending Stresses			Total Stresses			Metal Temp. (°F)	No. of Cycles	DO (ppm)
		S' <sub>12</sub> (psi)	S' <sub>23</sub> (psi)	S' <sub>31</sub> (psi)	S' <sub>12</sub> (psi)	S' <sub>23</sub> (psi)	S' <sub>31</sub> (psi)			
309	1576.00	55417.7	30164.8	-85582.5	73894.6	28515.6	-102410.2	244.1	20	0.150
310	1577.00	55602.7	30361.7	-85964.5	74133.7	28704.7	-102838.4	246.4	20	0.150
311	1578.00	55786.8	30558.8	-86345.5	74370.7	28892.8	-103263.5	248.8	20	0.150
312	1579.00	55968.8	30755.8	-86724.6	74604.8	29082.8	-103687.6	251.1	20	0.150
313	1580.00	56147.8	30953.8	-87101.6	74836.9	29270.9	-104107.7	253.4	20	0.150
314	1581.00	56326.8	31151.8	-87478.7	75067.9	29460.9	-104528.8	255.7	20	0.150
315	1582.00	56503.9	31349.9	-87853.8	75298.0	29648.9	-104946.9	258.1	20	0.150
316	1583.00	56679.9	31547.9	-88227.7	75525.0	29839.0	-105364.0	260.4	20	0.150
317	1584.00	56853.9	31745.9	-88599.8	75750.1	30029.1	-105779.1	262.7	20	0.150
318	1585.00	57027.0	31944.0	-88970.9	75973.1	30219.1	-106192.3	265.1	20	0.150
319	1586.00	57198.0	32143.0	-89341.0	76194.2	30409.2	-106603.4	267.4	20	0.150
320	1587.00	57368.1	32341.1	-89709.1	76413.2	30599.2	-107012.5	269.7	20	0.150
321	1588.00	57536.1	32540.0	-90076.1	76630.3	30789.3	-107419.6	272.1	20	0.150
322	1589.00	57702.1	32739.1	-90441.2	76843.4	30980.4	-107823.7	274.4	20	0.150
323	1590.00	57867.2	32938.2	-90805.3	77056.4	31170.4	-108226.8	276.7	20	0.150
324	1591.00	58030.2	33138.2	-91168.4	77266.5	31361.5	-108628.0	279.1	20	0.150
325	1592.00	58192.3	33337.3	-91529.5	77473.5	31553.5	-109027.0	281.4	20	0.150
326	1593.00	58352.3	33536.3	-91888.7	77678.6	31744.6	-109423.2	283.8	20	0.150
327	1594.00	58511.4	33736.4	-92247.8	77883.6	31934.6	-109818.3	286.1	20	0.150
328	1595.00	58669.5	33935.5	-92604.9	78085.7	32125.7	-110211.4	288.4	20	0.150
329	1596.00	58825.5	34134.5	-92960.1	78285.7	32317.8	-110603.5	290.8	20	0.150
330	1597.00	58980.6	34333.6	-93314.2	78484.8	32507.8	-110992.6	293.1	20	0.150
331	1598.00	59133.7	34532.7	-93666.3	78680.9	32698.9	-111379.8	295.5	20	0.150
332	1599.00	59286.7	34731.7	-94018.4	78875.9	32889.9	-111765.8	297.8	20	0.150
333	1600.00	59437.7	34930.7	-94368.5	79070.0	33079.9	-112149.9	300.2	20	0.150
334	1601.00	59587.8	35128.8	-94716.6	79261.0	33271.1	-112532.1	302.5	20	0.150
335	1602.00	59734.9	35328.9	-95063.8	79450.1	33461.1	-112911.2	304.9	20	0.150
336	1603.00	59882.0	35527.0	-95408.9	79638.1	33652.2	-113290.3	307.2	20	0.150
337	1604.00	60027.0	35726.0	-95753.0	79823.2	33842.2	-113665.4	309.5	20	0.150
338	1605.00	60171.1	35923.1	-96094.2	80007.2	34031.3	-114038.5	311.9	20	0.150
339	1606.00	60314.2	36120.2	-96434.4	80189.3	34221.3	-114410.7	314.2	20	0.150
340	1607.00	60454.3	36318.3	-96772.5	80368.4	34410.4	-114778.7	316.6	20	0.150
341	1608.00	60594.3	36515.3	-97109.7	80547.4	34599.4	-115146.9	318.9	20	0.150
342	1609.00	60732.4	36713.4	-97445.7	80723.5	34788.5	-115511.9	321.3	20	0.150
343	1610.00	60869.4	36910.5	-97779.9	80898.5	34977.6	-115876.1	323.7	20	0.150
344	1611.00	61004.5	37106.5	-98111.1	81070.6	35166.6	-116237.2	326.0	20	0.150
345	1612.00	61138.6	37304.6	-98443.2	81241.7	35355.7	-116597.3	328.4	20	0.150
346	1613.00	61272.7	37499.7	-98772.4	81411.7	35543.7	-116955.4	330.7	20	0.150
347	1614.00	61404.7	37696.7	-99101.5	81579.8	35732.8	-117312.5	333.1	20	0.150

Point No.	Time (sec.)	Membrane + Bending Stresses			Total Stresses			Metal Temp. (°F)	No. of Cycles	DO (ppm)
		S' <sub>12</sub> (psi)	S' <sub>23</sub> (psi)	S' <sub>31</sub> (psi)	S' <sub>12</sub> (psi)	S' <sub>23</sub> (psi)	S' <sub>31</sub> (psi)			
348	1615.00	61533.8	37893.8	-99427.7	81744.8	35921.8	-117666.7	335.4	20	0.150
349	1616.00	61663.9	38089.9	-99753.8	81910.9	36108.9	-118019.8	337.8	20	0.150
350	1617.00	61793.0	38285.0	-100078.0	82074.9	36297.0	-118371.9	340.1	20	0.150
351	1618.00	61920.1	38481.1	-100401.2	82237.0	36485.0	-118722.0	342.5	20	0.150
352	1619.00	62047.1	38676.1	-100723.3	82398.0	36672.1	-119070.1	344.8	20	0.150
353	1620.00	62171.2	38871.2	-101042.5	82556.1	36860.1	-119416.2	347.2	20	0.150
354	1621.00	62295.3	39066.3	-101361.7	82714.1	37047.2	-119761.3	349.6	20	0.150
355	1622.00	62419.4	39260.4	-101679.8	82871.2	37234.2	-120105.5	351.9	20	0.150
356	1623.00	62540.5	39456.5	-101996.9	83026.3	37420.3	-120446.6	354.3	20	0.150
357	1624.00	62660.6	39649.6	-102310.1	83177.4	37607.3	-120784.7	356.6	20	0.150
358	1625.00	62779.7	39844.7	-102624.3	83328.4	37793.4	-121121.8	359.0	20	0.150
359	1626.00	62898.8	40036.8	-102935.5	83477.5	37979.5	-121456.9	361.3	20	0.150
360	1627.00	63014.8	40231.8	-103246.6	83624.5	38165.5	-121790.0	363.7	20	0.150
361	1628.00	63129.9	40423.9	-103553.8	83769.6	38350.5	-122120.1	366.0	20	0.150
362	1629.00	63244.0	40618.0	-103862.0	83914.6	38535.6	-122450.3	368.4	20	0.150
363	1630.00	63358.1	40809.1	-104167.1	84057.7	38720.7	-122778.4	370.8	20	0.150
364	1631.00	63470.2	41002.2	-104472.4	84198.7	38905.7	-123104.5	373.1	20	0.150
365	1632.00	63580.2	41194.2	-104774.5	84338.8	39089.8	-123428.6	375.5	20	0.150
366	1633.00	63689.3	41386.3	-105075.7	84476.9	39273.9	-123750.7	377.8	20	0.150
367	1634.00	63798.5	41578.4	-105376.9	84614.9	39457.9	-124072.8	380.2	20	0.150
368	1635.00	63906.5	41769.5	-105676.0	84751.0	39642.0	-124392.9	382.5	20	0.150
369	1636.00	64013.6	41959.6	-105973.2	84886.0	39826.0	-124712.1	384.9	20	0.150
370	1637.00	64118.7	42150.7	-106269.4	85020.1	40008.1	-125028.2	387.2	20	0.150
371	1638.00	64223.8	42340.8	-106564.6	85153.1	40191.1	-125344.3	389.6	20	0.150
372	1639.00	64327.9	42531.8	-106859.7	85285.2	40373.2	-125658.4	391.9	20	0.150
373	1640.00	64432.0	42721.0	-107152.9	85416.3	40555.2	-125971.5	394.3	20	0.150
374	1641.00	64533.0	42910.0	-107443.1	85545.3	40737.3	-126282.7	396.7	20	0.150
375	1642.00	64635.1	43099.1	-107734.3	85673.4	40919.4	-126592.8	399.0	20	0.150
376	1643.00	64736.2	43288.2	-108024.4	85801.4	41100.4	-126901.9	401.4	20	0.150
377	1644.00	64836.3	43476.3	-108312.7	85928.5	41281.5	-127210.0	403.7	20	0.150
378	1645.00	64934.4	43664.4	-108598.8	86054.6	41462.5	-127517.1	406.1	20	0.150
379	1646.00	65033.5	43852.5	-108886.0	86180.6	41643.6	-127824.2	408.5	20	0.150
380	1647.00	65131.6	44039.6	-109171.2	86306.6	41822.7	-128129.3	410.8	20	0.150
381	1648.00	65228.7	44227.7	-109456.4	86430.7	42003.7	-128434.5	413.2	20	0.150
382	1649.00	65324.8	44414.8	-109739.5	86553.8	42183.8	-128737.6	415.6	20	0.150
383	1650.00	65419.8	44601.9	-110021.7	86676.8	42362.8	-129039.7	418.0	20	0.150
384	1651.00	65516.0	44788.0	-110303.9	86798.9	42541.9	-129340.8	420.3	20	0.150
385	1652.00	65610.0	44974.0	-110584.1	86920.0	42719.9	-129639.9	422.7	20	0.150
386	1653.00	65702.1	45161.1	-110863.2	87038.0	42900.0	-129938.0	425.1	20	0.150

Point No.	Time (sec.)	Membrane + Bending Stresses			Total Stresses			Metal Temp. (°F)	No. of Cycles	DO (ppm)
		S' <sub>12</sub> (psi)	S' <sub>23</sub> (psi)	S' <sub>31</sub> (psi)	S' <sub>12</sub> (psi)	S' <sub>23</sub> (psi)	S' <sub>31</sub> (psi)			
387	1654.00	65795.2	45346.2	-111141.5	87157.1	43078.1	-130235.1	427.4	20	0.150
388	1655.00	65887.3	45531.3	-111418.6	87275.1	43255.1	-130530.2	429.8	20	0.150
389	1656.00	65978.4	45716.4	-111694.8	87390.2	43434.2	-130824.4	432.2	20	0.150
390	1657.00	66068.5	45901.5	-111970.0	87506.2	43611.2	-131117.5	434.6	20	0.150
391	1658.00	66158.6	46085.6	-112244.2	87620.3	43789.3	-131409.6	436.9	20	0.150
392	1659.00	66246.7	46270.7	-112517.3	87734.4	43965.4	-131699.7	439.3	20	0.150
393	1660.00	66333.7	46454.8	-112788.5	87845.4	44142.4	-131987.9	441.7	20	0.150
394	1661.00	66421.9	46637.9	-113059.8	87956.5	44319.5	-132276.0	444.1	20	0.150
395	1662.00	66508.0	46820.9	-113328.9	88067.5	44494.5	-132562.1	446.5	20	0.150
396	1663.00	66594.0	47004.0	-113598.1	88176.6	44670.6	-132847.2	448.8	20	0.150
397	1664.00	66677.1	47187.1	-113864.2	88283.7	44846.7	-133130.3	451.2	20	0.150
398	1665.00	66761.2	47369.2	-114130.5	88390.7	45022.8	-133413.5	453.6	20	0.150
399	1666.00	66844.3	47552.3	-114396.7	88497.8	45196.8	-133694.6	456.0	20	0.150
400	1667.00	66927.4	47733.4	-114660.8	88602.9	45371.8	-133974.7	458.4	20	0.150
401	1668.00	67007.5	47915.5	-114923.0	88705.9	45546.9	-134252.8	460.7	20	0.150
402	1669.00	67088.6	48096.6	-115185.1	88809.0	45721.0	-134529.9	463.1	20	0.150
403	1670.00	67168.7	48276.7	-115445.3	88911.0	45895.0	-134806.0	465.5	20	0.150
404	1671.00	67246.7	48457.8	-115704.5	89011.1	46069.1	-135080.2	467.9	20	0.150
405	1672.00	67324.9	48638.9	-115963.8	89111.2	46242.1	-135353.3	470.3	20	0.150
406	1673.00	67402.0	48819.0	-116221.0	89210.2	46414.2	-135624.4	472.7	20	0.150
407	1674.00	67479.1	48998.1	-116477.1	89308.3	46587.2	-135895.5	475.1	20	0.150
408	1675.00	67554.2	49177.2	-116731.3	89405.3	46759.3	-136164.6	477.4	20	0.150
409	1676.00	67630.2	49355.3	-116985.5	89502.4	46930.4	-136432.8	479.8	20	0.150
410	1677.00	67705.3	49534.3	-117239.7	89598.4	47102.4	-136700.9	482.2	20	0.150
411	1678.00	67780.4	49711.4	-117491.9	89693.5	47274.5	-136968.0	484.6	20	0.150
412	1679.00	67853.5	49889.5	-117743.1	89787.6	47444.6	-137232.1	487.0	20	0.150
413	1680.00	67927.6	50066.6	-117994.2	89881.6	47615.6	-137497.3	489.4	20	0.150
414	1681.00	68000.7	50243.7	-118244.4	89975.7	47785.7	-137761.4	491.8	20	0.150
415	1682.00	68071.8	50421.8	-118493.6	90067.7	47955.8	-138023.5	494.2	20	0.150
416	1683.00	68143.8	50597.8	-118741.7	90160.8	48124.8	-138285.6	496.5	20	0.150
417	1684.00	68215.9	50773.9	-118989.9	90251.9	48295.9	-138547.8	498.9	20	0.150
418	1685.00	68287.0	50950.0	-119237.1	90342.9	48464.9	-138807.8	501.3	20	0.150
419	1686.00	68356.1	51126.1	-119482.2	90433.0	48633.0	-139066.0	503.7	20	0.150
420	1687.00	68426.2	51301.2	-119727.4	90521.0	48802.0	-139323.1	506.1	20	0.150
421	1688.00	68495.3	51476.3	-119971.6	90608.1	48970.1	-139578.2	508.5	20	0.150
422	1689.00	68562.4	51651.4	-120213.8	90693.2	49138.2	-139831.3	510.9	20	0.150
423	1690.00	68630.5	51825.5	-120455.9	90778.2	49306.2	-140084.5	513.2	20	0.150
424	1691.00	68697.6	51999.6	-120697.1	90863.3	49473.3	-140336.6	515.6	20	0.150
425	1692.00	68763.6	52173.6	-120937.2	90947.3	49640.3	-140587.7	518.0	20	0.150

Point No.	Time (sec.)	Membrane + Bending Stresses			Total Stresses			Metal Temp. (°F)	No. of Cycles	DO (ppm)
		S' <sub>12</sub> (psi)	S' <sub>23</sub> (psi)	S' <sub>31</sub> (psi)	S' <sub>12</sub> (psi)	S' <sub>23</sub> (psi)	S' <sub>31</sub> (psi)			
426	1693.00	68828.7	52346.7	-121175.4	91029.4	49807.4	-140836.8	520.4	20	0.150
427	1694.00	68893.8	52519.8	-121413.6	91112.5	49973.5	-141085.9	522.8	20	0.150
428	1695.00	68958.9	52691.9	-121650.7	91194.5	50139.5	-141334.1	525.1	20	0.150
429	1696.00	69022.0	52865.0	-121886.9	91274.6	50305.6	-141580.2	527.5	20	0.150
430	1697.00	69085.1	53037.1	-122122.2	91355.6	50471.6	-141827.3	529.9	20	0.150
431	1698.00	69148.1	53209.1	-122357.2	91436.7	50635.7	-142072.4	532.3	20	0.150
432	1699.00	69210.2	53381.2	-122591.5	91515.8	50801.7	-142317.5	534.7	20	0.150
433	1700.00	69271.3	53551.3	-122822.6	91594.8	50964.8	-142559.7	537.0	20	0.150
434	1701.00	69333.4	53721.4	-123054.8	91672.9	51129.9	-142802.8	539.4	20	0.150
435	1702.00	69394.4	53892.5	-123286.9	91751.0	51294.0	-143044.9	541.8	20	0.150
436	1703.00	69453.5	54062.6	-123516.1	91828.0	51457.0	-143285.0	544.2	20	0.150
437	1704.00	69513.6	54232.6	-123746.2	91904.1	51621.1	-143525.2	546.6	20	0.150
438	1705.00	69572.7	54401.7	-123974.3	91981.1	51783.1	-143764.3	549.0	20	0.150
439	1706.00	69631.8	54570.8	-124202.5	92056.2	51946.2	-144002.4	551.3	20	0.150
440	1707.00	69689.8	54739.8	-124429.7	92131.2	52108.2	-144239.5	553.7	20	0.150
441	1708.00	69747.9	54907.9	-124655.8	92207.3	52271.3	-144478.6	556.1	20	0.150
442	1709.00	69806.0	55076.0	-124882.0	92283.4	52433.4	-144716.7	558.5	20	0.150
443	1710.00	69862.0	55245.0	-125107.1	92358.4	52594.4	-144952.8	560.9	20	0.150
444	1711.00	69914.7	55365.7	-125280.4	92335.4	52707.4	-145042.8	562.5	20	0.150
445	1712.00	69926.3	55479.3	-125405.7	92153.4	52815.4	-144968.8	563.7	20	0.150
446	1714.00	69845.4	55689.5	-125534.9	91603.3	53012.3	-144615.6	565.4	20	0.150
447	1716.00	69666.5	55876.5	-125542.9	90974.2	53190.2	-144164.4	566.6	20	0.150
448	1719.00	69272.9	56118.9	-125391.8	89974.0	53422.0	-143396.0	568.0	20	0.150
449	1722.00	68784.2	56320.2	-125104.3	88968.9	53615.9	-142584.8	569.2	20	0.150
450	1726.00	68049.7	56529.7	-124579.4	87653.7	53821.7	-141475.4	570.5	20	0.150
451	1730.00	67269.1	56682.1	-123951.1	86381.6	53973.6	-140355.2	571.6	20	0.150
452	1735.00	66266.5	56801.6	-123068.1	84861.5	54095.5	-138957.1	572.8	20	0.150
453	1740.00	65265.8	56853.8	-122119.7	83417.5	54153.5	-137571.0	573.9	20	0.150
454	1746.00	64091.2	56845.2	-120936.4	81779.5	54154.5	-135933.9	575.0	20	0.150
455	1752.00	62958.4	56770.4	-119728.7	80241.5	54091.5	-134333.0	576.1	20	0.150
456	1759.00	61707.4	56618.5	-118325.9	78575.6	53954.5	-132530.1	577.2	20	0.150
457	1766.00	60527.3	56418.3	-116945.6	77026.6	53770.6	-130797.2	578.3	20	0.150
458	1774.00	59270.1	56136.1	-115406.3	75397.7	53507.7	-128905.4	579.4	20	0.150
459	1782.00	58098.7	55819.7	-113918.5	73893.8	53210.8	-127104.6	580.4	20	0.150
460	1791.00	56877.2	55428.2	-112305.3	72340.9	52841.9	-125182.8	581.5	20	0.150
461	1800.00	55746.4	55011.5	-110757.9	70915.0	52447.0	-123361.9	582.5	20	0.150
462	1810.00	54585.5	54528.5	-109114.1	69462.1	51990.1	-121452.2	583.6	20	0.150
463	1820.00	53516.4	54030.4	-107546.7	68133.2	51516.2	-119649.3	584.6	20	0.150
464	1830.00	52524.1	53524.1	-106048.2	66907.2	51034.2	-117941.5	585.6	20	0.150

Point No.	Time (sec.)	Membrane + Bending Stresses			Total Stresses			Metal Temp. (°F)	No. of Cycles	DO (ppm)
		S' <sub>12</sub> (psi)	S' <sub>23</sub> (psi)	S' <sub>31</sub> (psi)	S' <sub>12</sub> (psi)	S' <sub>23</sub> (psi)	S' <sub>31</sub> (psi)			
465	1831.00	52429.1	53474.1	-105903.1	66791.2	50985.3	-117776.5	585.6	20	0.150
466	1841.00	51509.6	52960.5	-104470.1	65663.3	50496.3	-116159.7	586.5	20	0.150
467	1843.00	51334.4	52858.4	-104192.9	65449.3	50399.3	-115848.7	586.7	20	0.150
468	1853.00	50493.8	52350.8	-102844.6	64423.4	49914.4	-114337.8	587.5	20	0.150
469	1856.00	50254.6	52199.6	-102454.2	64132.4	49770.4	-113902.8	587.8	20	0.150
470	1866.00	49496.8	51702.8	-101199.5	63213.5	49295.5	-112508.9	588.5	20	0.150
471	1870.00	49213.4	51505.4	-100718.8	62872.5	49107.5	-111980.0	588.8	20	0.150
472	1880.00	48536.4	51023.4	-99559.8	62055.5	48646.5	-110702.0	589.5	20	0.150
473	1885.00	48212.9	50785.9	-98998.8	61668.5	48419.5	-110088.0	589.8	20	0.150
474	1895.00	47586.8	50317.8	-97904.7	60915.6	47972.6	-108888.1	590.4	20	0.150
475	1902.00	47169.0	49995.0	-97164.0	60418.5	47663.6	-108082.1	590.9	20	0.150
476	1912.00	46596.8	49540.8	-96137.7	59732.5	47230.6	-106963.1	591.4	20	0.150
477	1921.00	46110.6	49140.6	-95251.3	59156.6	46847.6	-106004.1	591.9	20	0.150
478	1931.00	45598.3	48703.3	-94301.7	58545.5	46430.6	-104976.1	592.4	20	0.150
479	1941.00	45118.9	48276.9	-93395.8	57981.5	46022.5	-104004.1	592.9	20	0.150
480	1942.00	45072.8	48234.8	-93307.5	57927.5	45982.5	-103910.0	593.0	20	0.150
481	1952.00	44626.3	47818.3	-92444.6	57399.5	45585.5	-102985.0	593.4	20	0.150
482	1962.00	44200.8	47418.8	-91619.7	56900.5	45204.5	-102104.9	593.8	20	0.150
483	1966.00	44035.3	47261.3	-91296.6	56707.4	45053.4	-101760.9	594.0	20	0.150
484	1976.00	43628.8	46871.8	-90500.6	56227.4	44681.4	-100908.8	594.3	20	0.150
485	1986.00	43236.3	46488.3	-89724.7	55770.4	44315.4	-100085.8	594.7	20	0.150
486	1994.00	42936.1	46186.1	-89122.3	55421.3	44027.4	-99448.7	595.0	20	0.150
487	2004.00	42567.6	45814.6	-88382.2	54988.3	43672.3	-98660.6	595.3	20	0.150
488	2014.00	42215.1	45450.1	-87665.2	54578.2	43324.2	-97902.5	595.6	20	0.150
489	2024.00	41889.5	45096.5	-86986.1	54202.2	42988.2	-97190.4	595.9	20	0.150
490	2028.00	41765.9	44959.9	-86725.8	54061.2	42856.2	-96917.3	596.0	20	0.150
491	2038.00	41467.3	44628.3	-86095.7	53711.1	42541.1	-96252.2	596.2	20	0.150
492	2048.00	41181.8	44305.8	-85487.6	53382.0	42233.0	-95615.0	596.4	20	0.150
493	2058.00	40907.2	43990.2	-84897.4	53066.9	41932.9	-94999.9	596.7	20	0.150
494	2068.00	40645.7	43681.7	-84327.4	52766.9	41638.9	-94405.8	596.9	20	0.150
495	2072.00	40542.1	43561.1	-84103.2	52648.8	41523.8	-94172.7	597.0	20	0.150
496	2082.00	40288.6	43260.6	-83549.3	52351.8	41238.8	-93590.5	597.2	20	0.150
497	2092.00	40041.1	42968.1	-83009.2	52066.7	40959.7	-93026.4	597.3	20	0.150
498	2102.00	39804.7	42679.7	-82484.3	51795.6	40686.6	-92482.2	597.5	20	0.150
499	2112.00	39578.2	42400.2	-81978.4	51537.5	40419.5	-91957.1	597.6	20	0.150
500	2132.00	39153.4	41861.4	-81014.7	51055.4	39906.4	-90961.7	598.0	20	0.150
501	2134.00	39114.0	41808.1	-80922.1	51010.4	39855.4	-90865.7	598.0	20	0.150
502	2144.00	38912.7	41549.7	-80462.4	50774.3	39610.3	-90384.5	598.1	20	0.150
503	2154.00	38717.3	41297.3	-80014.7	50551.2	39369.2	-89920.4	598.2	20	0.150

Point No.	Time (sec.)	Membrane + Bending Stresses			Total Stresses			Metal Temp. (°F)	No. of Cycles	DO (ppm)
		S' <sub>12</sub> (psi)	S' <sub>23</sub> (psi)	S' <sub>31</sub> (psi)	S' <sub>12</sub> (psi)	S' <sub>23</sub> (psi)	S' <sub>31</sub> (psi)			
504	2164.00	38531.0	41051.0	-79581.9	50339.1	39135.1	-89474.1	598.3	20	0.150
505	2174.00	38356.6	40811.6	-79168.2	50141.0	38907.0	-89048.0	598.4	20	0.150
506	2194.00	38033.0	40355.1	-78388.1	49776.8	38472.8	-88249.6	598.6	20	0.150
507	2214.00	37744.5	39925.5	-77670.1	49452.6	38064.6	-87517.2	598.8	20	0.150
508	2234.00	37463.2	39505.2	-76968.3	49135.4	37666.4	-86801.9	599.0	20	0.150
509	2239.00	37393.5	39401.5	-76795.1	49057.4	37567.4	-86624.8	599.0	20	0.150
510	2249.00	37246.4	39192.4	-76438.8	48883.3	37368.3	-86251.6	599.0	20	0.150
511	2259.00	37098.2	38982.2	-76080.5	48713.2	37168.2	-85881.4	599.0	20	0.150
512	2269.00	36951.1	38771.1	-75722.2	48546.1	36967.1	-85513.3	599.0	20	0.150
513	2279.00	36807.0	38559.9	-75366.9	48382.0	36766.0	-85148.1	599.0	20	0.150
514	2299.00	36520.7	38138.7	-74659.4	48058.8	36365.8	-84424.7	599.1	20	0.150
515	2319.00	36247.5	37721.5	-73968.9	47750.7	35970.7	-83721.3	599.1	20	0.150
516	2339.00	36002.4	37330.4	-73332.7	47476.5	35597.5	-83074.0	599.1	20	0.150
517	2379.00	35574.6	36617.6	-72192.2	46997.1	34920.1	-81917.2	599.1	20	0.150
518	2419.00	35224.4	36002.4	-71226.8	46606.8	34334.8	-80941.6	599.2	20	0.150
519	2499.00	34744.6	35060.5	-69805.1	46073.2	33439.2	-79512.4	599.3	20	0.150
520	2579.00	34401.2	34352.2	-68753.4	45689.8	32766.8	-78456.6	599.4	20	0.150
521	2739.00	33740.6	33000.6	-66741.1	44955.0	31477.0	-76432.0	599.5	20	0.150
522	2899.00	33104.1	31683.1	-64787.2	44244.2	30222.2	-74466.5	599.7	20	0.150
523	3210.00	32518.4	30204.4	-62722.8	43589.3	28808.3	-72397.6	600.0	20	0.150
524	3210.00	36431.2	25862.2	-62293.4	47466.4	24528.4	-71994.8	500.0	50	0.550
525	3220.00	36424.2	25861.2	-62285.4	47449.4	24527.4	-71976.8	499.9	50	0.550
526	3230.00	36414.2	25858.2	-62272.4	47435.4	24524.4	-71959.8	499.8	50	0.550
527	3240.00	36405.2	25854.2	-62259.4	47422.4	24520.4	-71942.8	499.8	50	0.550
528	3250.00	36396.2	25850.2	-62246.4	47411.4	24516.4	-71927.8	499.7	50	0.550
529	3270.00	36381.2	25841.2	-62222.3	47392.4	24507.4	-71899.8	499.5	50	0.550
530	3290.00	36369.2	25831.2	-62200.3	47376.4	24498.4	-71874.8	499.4	50	0.550
531	3310.00	36359.2	25821.2	-62180.3	47364.4	24488.4	-71852.8	499.2	50	0.550
532	3311.00	36318.3	25804.3	-62122.6	47322.4	24473.4	-71795.7	499.2	50	0.550
533	3312.00	36245.5	25784.5	-62029.9	47102.3	24452.3	-71554.5	498.0	50	0.550
534	3313.00	36122.6	25754.6	-61877.2	46695.1	24424.1	-71119.2	496.5	50	0.550
535	3314.00	35964.7	25720.7	-61685.4	46267.0	24391.0	-70658.0	494.8	50	0.550
536	3315.00	35780.8	25679.8	-61460.7	45817.8	24352.8	-70170.7	493.0	50	0.550
537	3316.00	35572.9	25634.0	-61206.9	45356.7	24309.7	-69666.4	491.2	50	0.550
538	3317.00	35347.1	25583.0	-60930.1	44888.5	24262.5	-69151.1	489.2	50	0.550
539	3318.00	35104.1	25527.1	-60631.3	44416.4	24210.4	-68626.8	487.3	50	0.550
540	3319.00	34851.3	25465.3	-60316.5	43943.2	24155.2	-68098.5	485.3	50	0.550
541	3320.00	34587.3	25401.3	-59988.7	43471.1	24095.1	-67566.2	483.2	50	0.550
542	3321.00	34315.4	25331.4	-59646.9	43001.0	24030.0	-67031.0	481.2	50	0.550

Point No.	Time (sec.)	Membrane + Bending Stresses			Total Stresses			Metal Temp. (°F)	No. of Cycles	DO (ppm)
		S' <sub>12</sub> (psi)	S' <sub>23</sub> (psi)	S' <sub>31</sub> (psi)	S' <sub>12</sub> (psi)	S' <sub>23</sub> (psi)	S' <sub>31</sub> (psi)			
543	3322.00	34034.5	25258.5	-59293.0	42532.8	23962.8	-66495.7	479.1	50	0.550
544	3323.00	33745.6	25180.6	-58926.2	42067.7	23890.7	-65958.4	477.0	50	0.550
545	3324.00	33452.6	25098.6	-58551.3	41604.6	23815.6	-65420.1	474.9	50	0.550
546	3325.00	33156.7	25013.7	-58170.4	41144.5	23737.5	-64881.9	472.7	50	0.550
547	3326.00	32857.8	24924.8	-57782.5	40688.3	23655.3	-64343.7	470.6	50	0.550
548	3327.00	32556.8	24833.8	-57390.7	40235.2	23571.3	-63806.5	468.4	50	0.550
549	3328.00	32252.9	24737.9	-56990.8	39785.1	23482.1	-63267.3	466.2	50	0.550
550	3329.00	31947.9	24639.9	-56587.9	39339.0	23392.0	-62731.0	464.1	50	0.550
551	3330.00	31641.0	24538.0	-56179.0	38895.9	23297.9	-62193.8	461.9	50	0.550
552	3331.00	31333.0	24434.0	-55767.1	38457.8	23201.8	-61659.6	459.7	50	0.550
553	3332.00	31025.1	24326.1	-55351.2	38023.7	23101.7	-61125.4	457.5	50	0.550
554	3333.00	30717.1	24215.1	-54932.2	37592.6	22998.6	-60591.2	455.3	50	0.550
555	3334.00	30409.2	24103.2	-54512.3	37165.5	22894.5	-60060.0	453.1	50	0.550
556	3335.00	30101.2	23988.2	-54089.4	36741.4	22787.4	-59528.9	450.8	50	0.550
557	3336.00	29795.2	23870.2	-53665.5	36322.3	22678.3	-59000.7	448.6	50	0.550
558	3337.00	29489.3	23750.3	-53239.5	35906.2	22566.2	-58472.5	446.4	50	0.550
559	3338.00	29183.3	23627.3	-52810.6	35493.2	22453.2	-57946.3	444.1	50	0.550
560	3339.00	28879.3	23502.3	-52381.6	35085.1	22337.1	-57422.1	441.9	50	0.550
561	3340.00	28575.3	23375.3	-51950.7	34680.0	22218.0	-56897.9	439.6	50	0.550
562	3341.00	28273.4	23247.4	-51520.7	34278.9	22097.9	-56376.8	437.4	50	0.550
563	3342.00	27972.4	23116.4	-51088.8	33880.8	21975.8	-55856.6	435.1	50	0.550
564	3343.00	27673.4	22984.4	-50657.8	33486.7	21852.7	-55339.5	432.8	50	0.550
565	3344.00	27375.4	22850.4	-50225.8	33094.6	21727.6	-54822.3	430.6	50	0.550
566	3345.00	27079.4	22714.4	-49793.9	32707.6	21600.6	-54308.1	428.3	50	0.550
567	3346.00	26784.5	22577.5	-49361.9	32322.5	21472.5	-53795.0	426.0	50	0.550
568	3347.00	26492.5	22438.5	-48930.9	31941.4	21343.4	-53284.8	423.7	50	0.550
569	3348.00	26200.5	22298.5	-48499.0	31563.3	21212.3	-52775.7	421.4	50	0.550
570	3349.00	25911.5	22156.5	-48068.0	31189.3	21080.3	-52269.5	419.2	50	0.550
571	3350.00	25623.5	22013.5	-47637.0	30818.2	20945.2	-51763.3	416.9	50	0.550
572	3351.00	25336.5	21869.5	-47206.0	30450.1	20810.1	-51260.2	414.6	50	0.550
573	3352.00	25053.5	21722.5	-46776.0	30087.0	20673.0	-50760.1	412.3	50	0.550
574	3353.00	24770.5	21574.5	-46345.0	29726.0	20534.0	-50259.9	410.0	50	0.550
575	3354.00	24490.5	21426.5	-45917.0	29368.9	20394.9	-49763.8	407.7	50	0.550
576	3355.00	24211.5	21277.5	-45489.0	29013.8	20254.8	-49268.6	405.4	50	0.550
577	3356.00	23935.5	21126.5	-45062.0	28662.7	20113.7	-48776.5	403.1	50	0.550
578	3357.00	23660.5	20975.5	-44636.0	28312.7	19971.7	-48284.3	400.7	50	0.550
579	3358.00	23386.5	20823.5	-44210.0	27966.6	19828.6	-47795.2	398.4	50	0.550
580	3359.00	23115.5	20670.5	-43786.0	27623.5	19685.5	-47309.0	396.1	50	0.550
581	3360.00	22845.5	20517.5	-43362.9	27281.4	19541.5	-46822.9	393.8	50	0.550



Point No.	Time (sec.)	Membrane + Bending Stresses			Total Stresses			Metal Temp. (°F)	No. of Cycles	DO (ppm)
		S' <sub>12</sub> (psi)	S' <sub>23</sub> (psi)	S' <sub>31</sub> (psi)	S' <sub>12</sub> (psi)	S' <sub>23</sub> (psi)	S' <sub>31</sub> (psi)			
582	3361.00	22577.5	20363.5	-42940.9	26942.4	19397.4	-46339.8	391.5	50	0.550
583	3362.00	22311.5	20207.4	-42518.9	26606.3	19250.3	-45856.6	389.1	50	0.550
584	3363.00	22045.4	20052.4	-42097.9	26272.2	19104.3	-45376.5	386.8	50	0.550
585	3364.00	21783.4	19895.4	-41678.9	25941.2	18957.2	-44898.4	384.5	50	0.550
586	3365.00	21521.4	19738.4	-41259.8	25612.1	18810.1	-44422.2	382.1	50	0.550
587	3366.00	21263.4	19580.4	-40843.8	25287.0	18661.0	-43948.1	379.8	50	0.550
588	3367.00	21005.4	19421.4	-40426.8	24964.0	18512.0	-43475.9	377.5	50	0.550
589	3368.00	20748.4	19262.4	-40010.7	24643.9	18360.9	-43004.8	375.1	50	0.550
590	3369.00	20495.3	19102.3	-39597.7	24326.8	18210.8	-42537.7	372.8	50	0.550
591	3370.00	20242.3	18942.3	-39184.7	24011.8	18059.8	-42071.5	370.4	50	0.550
592	3371.00	19992.3	18781.3	-38773.6	23700.7	17907.7	-41608.4	368.1	50	0.550
593	3372.00	19743.3	18619.3	-38362.6	23390.6	17755.6	-41146.2	365.7	50	0.550
594	3373.00	19496.3	18457.3	-37953.6	23083.5	17602.6	-40686.1	363.4	50	0.550
595	3374.00	19251.2	18295.2	-37546.5	22779.5	17449.5	-40228.9	361.0	50	0.550
596	3375.00	19007.2	18132.2	-37139.4	22476.4	17296.4	-39772.8	358.6	50	0.550
597	3376.00	18764.2	17969.2	-36733.4	22175.3	17143.3	-39318.7	356.3	50	0.550
598	3377.00	18524.2	17806.2	-36330.4	21877.3	16990.3	-38867.5	353.9	50	0.550
599	3378.00	18285.1	17642.2	-35927.3	21581.2	16835.2	-38416.4	351.6	50	0.550
600	3379.00	18048.1	17479.1	-35527.3	21288.1	16681.1	-37969.2	349.2	50	0.550
601	3380.00	17811.1	17315.1	-35126.2	20996.0	16527.0	-37523.1	346.8	50	0.550
602	3381.00	17577.1	17150.1	-34727.1	20707.0	16372.0	-37079.0	344.5	50	0.550
603	3382.00	17345.1	16986.1	-34331.1	20421.9	16216.9	-36638.8	342.1	50	0.550
604	3383.00	17113.0	16822.0	-33935.1	20137.8	16061.9	-36199.7	339.7	50	0.550
605	3384.00	16885.0	16657.0	-33542.0	19856.8	15906.8	-35763.5	337.4	50	0.550
606	3385.00	16657.0	16492.0	-33149.0	19577.7	15750.7	-35328.4	335.0	50	0.550
607	3386.00	16429.9	16327.9	-32757.9	19300.6	15594.6	-34895.3	332.7	50	0.550
608	3387.00	16206.9	16161.9	-32368.8	19026.5	15438.5	-34465.1	330.3	50	0.550
609	3388.00	15983.9	15996.9	-31980.7	18753.5	15282.5	-34036.0	327.9	50	0.550
610	3389.00	15761.9	15831.9	-31593.7	18483.4	15126.4	-33609.8	325.5	50	0.550
611	3390.00	15542.8	15665.8	-31208.6	18216.3	14969.3	-33185.7	323.2	50	0.550
612	3391.00	15324.8	15499.8	-30824.6	17950.3	14812.3	-32762.5	320.8	50	0.550
613	3392.00	15108.8	15332.8	-30441.5	17686.2	14655.2	-32341.4	318.4	50	0.550
614	3393.00	14893.7	15167.7	-30061.4	17424.1	14499.1	-31923.3	316.0	50	0.550
615	3394.00	14679.7	15001.7	-29681.4	17164.1	14342.1	-31506.1	313.7	50	0.550
616	3395.00	14468.7	14835.6	-29304.3	16906.0	14186.0	-31092.0	311.3	50	0.550
617	3396.00	14257.6	14669.6	-28927.3	16648.9	14028.9	-30677.8	308.9	50	0.550
618	3397.00	14047.6	14503.6	-28551.2	16393.9	13872.9	-30266.7	306.5	50	0.550
619	3398.00	13839.5	14338.5	-28178.1	16141.8	13715.8	-29857.5	304.2	50	0.550
620	3399.00	13632.5	14172.5	-27805.0	15889.7	13558.7	-29448.4	301.8	50	0.550

Point No.	Time (sec.)	Membrane + Bending Stresses			Total Stresses			Metal Temp. (°F)	No. of Cycles	DO (ppm)
		S' <sub>12</sub> (psi)	S' <sub>23</sub> (psi)	S' <sub>31</sub> (psi)	S' <sub>12</sub> (psi)	S' <sub>23</sub> (psi)	S' <sub>31</sub> (psi)			
621	3400.00	13426.5	14006.5	-27433.0	15639.6	13402.6	-29042.3	299.4	50	0.550
622	3401.00	13222.5	13841.5	-27063.9	15392.6	13245.6	-28638.1	297.0	50	0.550
623	3402.00	13019.4	13675.4	-26694.8	15146.5	13088.5	-28235.0	294.6	50	0.550
624	3403.00	12818.4	13510.4	-26328.7	14902.4	12932.4	-27834.8	292.2	50	0.550
625	3404.00	12618.4	13344.4	-25962.7	14660.3	12775.3	-27435.7	289.8	50	0.550
626	3405.00	12419.3	13178.3	-25597.6	14419.3	12619.3	-27038.6	287.5	50	0.550
627	3406.00	12222.3	13013.3	-25235.5	14180.2	12463.2	-26643.4	285.1	50	0.550
628	3407.00	12025.2	12848.2	-24873.5	13943.1	12307.1	-26250.3	282.7	50	0.550
629	3408.00	11830.2	12683.2	-24513.4	13707.1	12151.1	-25858.1	280.3	50	0.550
630	3409.00	11637.2	12518.2	-24155.3	13474.0	11994.0	-25468.0	277.9	50	0.550
631	3410.00	11444.1	12353.1	-23797.2	13241.9	11837.9	-25079.8	275.5	50	0.550
632	3411.00	11254.1	12188.1	-23442.2	13012.8	11681.8	-24694.7	273.1	50	0.550
633	3412.00	11064.0	12023.0	-23087.1	12783.8	11525.8	-24309.6	270.7	50	0.550
634	3413.00	10875.0	11858.0	-22733.0	12555.7	11369.7	-23925.4	268.3	50	0.550
635	3414.00	10688.0	11694.0	-22381.9	12330.6	11214.6	-23545.3	265.9	50	0.550
636	3415.00	10500.9	11529.9	-22030.9	12106.6	11058.6	-23165.1	263.5	50	0.550
637	3416.00	10315.9	11364.9	-21680.8	11883.5	10902.5	-22785.9	261.1	50	0.550
638	3417.00	10131.9	11200.9	-21332.7	11662.4	10747.4	-22409.8	258.7	50	0.550
639	3418.00	9948.8	11036.8	-20985.6	11442.3	10592.3	-22034.7	256.3	50	0.550
640	3419.00	9767.8	10872.8	-20640.5	11224.3	10437.3	-21661.5	253.9	50	0.550
641	3420.00	9585.7	10709.7	-20295.5	11006.2	10283.2	-21289.3	251.5	50	0.550
642	3421.00	9405.7	10546.7	-19952.4	10790.1	10129.1	-20919.2	249.1	50	0.550
643	3422.00	9227.7	10382.7	-19610.3	10577.0	9973.0	-20550.1	246.7	50	0.550
644	3423.00	9049.6	10219.6	-19269.2	10362.0	9820.0	-20181.9	244.3	50	0.550
645	3424.00	8873.6	10056.6	-18930.2	10149.9	9664.9	-19814.7	241.9	50	0.550
646	3425.00	8696.5	9894.5	-18591.1	9936.8	9510.8	-19447.6	239.4	50	0.550
647	3426.00	8521.5	9731.5	-18253.0	9724.7	9357.7	-19082.5	237.0	50	0.550
648	3427.00	8347.5	9569.5	-17916.9	9515.7	9203.7	-18719.3	234.6	50	0.550
649	3428.00	8173.4	9407.4	-17580.8	9306.6	9049.6	-18356.1	232.2	50	0.550
650	3429.00	8000.4	9245.4	-17245.7	9099.5	8895.5	-17995.0	229.7	50	0.550
651	3430.00	7830.3	9082.3	-16912.7	8893.4	8743.4	-17636.9	227.3	50	0.550
652	3431.00	7659.3	8921.3	-16580.6	8688.4	8590.4	-17278.7	224.9	50	0.550
653	3432.00	7490.2	8759.2	-16249.5	8486.3	8437.3	-16923.6	222.5	50	0.550
654	3433.00	7321.2	8598.2	-15919.4	8284.2	8284.2	-16568.4	220.0	50	0.550
655	3434.00	7153.2	8437.2	-15590.3	8083.1	8131.1	-16214.2	217.6	50	0.550
656	3435.00	6987.1	8276.1	-15263.2	7884.1	7979.1	-15863.1	215.2	50	0.550
657	3436.00	6821.1	8115.1	-14936.1	7685.0	7827.0	-15512.0	212.7	50	0.550
658	3437.00	6656.0	7955.0	-14611.1	7487.9	7674.9	-15162.8	210.3	50	0.550
659	3438.00	6492.0	7794.0	-14286.0	7290.8	7523.8	-14814.6	207.9	50	0.550

Point No.	Time (sec.)	Membrane + Bending Stresses			Total Stresses			Metal Temp. (°F)	No. of Cycles	DO (ppm)
		S' <sub>12</sub> (psi)	S' <sub>23</sub> (psi)	S' <sub>31</sub> (psi)	S' <sub>12</sub> (psi)	S' <sub>23</sub> (psi)	S' <sub>31</sub> (psi)			
660	3439.00	6328.0	7634.0	-13961.9	7095.7	7371.7	-14467.5	205.4	50	0.550
661	3440.00	6165.9	7474.9	-13640.8	6901.7	7220.7	-14122.3	203.0	50	0.550
662	3441.00	6003.9	7314.9	-13318.8	6708.6	7069.6	-13778.2	200.6	50	0.550
663	3442.00	5842.8	7155.8	-12998.6	6517.5	6917.5	-13435.0	198.1	50	0.550
664	3443.00	5682.8	6996.8	-12679.6	6326.4	6767.4	-13093.9	195.7	50	0.550
665	3444.00	5523.7	6837.7	-12361.5	6138.3	6617.3	-12755.7	193.3	50	0.550
666	3445.00	5365.7	6679.7	-12045.4	5952.3	6467.3	-12419.5	190.8	50	0.550
667	3446.00	5208.7	6521.7	-11730.3	5766.2	6318.2	-12084.4	188.4	50	0.550
668	3447.00	5053.6	6363.6	-11417.2	5583.1	6168.1	-11751.2	186.0	50	0.550
669	3448.00	4898.6	6205.6	-11104.2	5400.0	6019.1	-11419.1	183.5	50	0.550
670	3449.00	4744.5	6047.5	-10792.1	5219.0	5869.0	-11088.0	181.1	50	0.550
671	3450.00	4592.5	5890.5	-10483.0	5038.9	5719.9	-10758.8	178.7	50	0.550
672	3451.00	4439.5	5734.5	-10173.9	4858.8	5571.8	-10430.7	176.2	50	0.550
673	3452.00	4289.4	5577.4	-9866.9	4681.8	5423.8	-10105.5	173.8	50	0.550
674	3453.00	4138.4	5421.4	-9559.8	4503.7	5275.7	-9779.4	171.4	50	0.550
675	3454.00	3989.4	5265.4	-9254.7	4327.6	5127.6	-9455.2	168.9	50	0.550
676	3455.00	3841.3	5109.3	-8950.6	4153.5	4980.5	-9134.1	166.5	50	0.550
677	3456.00	3693.3	4954.3	-8647.5	3978.4	4833.4	-8811.9	164.1	50	0.550
678	3457.00	3547.2	4799.2	-8346.4	3806.4	4686.4	-8492.7	161.6	50	0.550
679	3458.00	3401.2	4644.2	-8045.4	3634.3	4539.3	-8173.6	159.2	50	0.550
680	3459.00	3256.2	4489.2	-7745.3	3463.2	4393.2	-7856.4	156.8	50	0.550
681	3460.00	3112.1	4335.1	-7447.2	3294.1	4247.1	-7541.3	154.3	50	0.550
682	3461.00	2969.1	4181.1	-7150.2	3125.1	4101.1	-7226.1	151.9	50	0.550
683	3462.00	2827.0	4027.0	-6854.1	2958.0	3956.0	-6914.0	149.5	50	0.550
684	3463.00	2685.0	3874.0	-6559.0	2790.9	3809.9	-6600.8	147.0	50	0.550
685	3464.00	2544.0	3721.0	-6264.9	2623.8	3664.8	-6288.7	144.6	50	0.550
686	3465.00	2403.9	3567.9	-5971.8	2457.8	3519.8	-5977.5	142.1	50	0.550
687	3466.00	2263.9	3414.9	-5678.8	2291.7	3374.7	-5666.4	139.7	50	0.550
688	3467.00	2124.8	3263.8	-5388.7	2126.6	3230.6	-5357.3	137.2	50	0.550
689	3468.00	1986.8	3110.8	-5097.6	1961.6	3087.6	-5049.1	134.7	50	0.550
690	3469.00	1848.8	2958.8	-4807.5	1798.5	2942.5	-4741.0	132.3	50	0.550
691	3470.00	1711.7	2806.7	-4518.4	1636.4	2799.4	-4435.8	129.8	50	0.550
692	3471.00	1636.4	2674.4	-4310.8	1636.4	2674.4	-4310.8	128.2	50	0.550
693	3471.20	1636.4	2674.4	-4310.8	1636.4	2674.4	-4310.8	128.2	5	0.100
694	3471.40	0.0	0.0	0.0	0.0	0.0	0.0	128.2	5	0.100
695	3471.60	3272.8	5348.8	-8621.6	3272.8	5348.8	-8621.6	128.2	5	0.100
696	3471.80	1636.4	2674.4	-4310.8	1636.4	2674.4	-4310.8	128.2	5	0.100
697	3472.00	1605.2	2549.2	-4154.4	1808.4	2555.4	-4363.9	127.0	50	0.550
698	3474.00	1655.0	2318.0	-3973.0	2351.6	2337.6	-4689.1	125.5	50	0.550

Point No.	Time (sec.)	Membrane + Bending Stresses			Total Stresses			Metal Temp. (°F)	No. of Cycles	DO (ppm)
		S' <sub>12</sub> (psi)	S' <sub>23</sub> (psi)	S' <sub>31</sub> (psi)	S' <sub>12</sub> (psi)	S' <sub>23</sub> (psi)	S' <sub>31</sub> (psi)			
699	3476.00	1809.1	2111.1	-3920.2	2976.7	2140.7	-5117.4	124.4	50	0.550
700	3479.00	2175.5	1842.5	-4018.0	3971.9	1881.9	-5853.8	123.2	50	0.550
701	3483.00	2810.2	1552.2	-4362.3	5293.1	1598.1	-6891.2	121.9	50	0.550
702	3487.00	3528.7	1326.7	-4855.5	6575.3	1374.3	-7949.5	120.9	50	0.550
703	3492.00	4479.2	1126.2	-5605.4	8103.4	1172.4	-9275.8	119.8	50	0.550
704	3498.00	5631.4	985.4	-6616.9	9825.5	1024.5	-10850.0	118.8	50	0.550
705	3505.00	6945.4	930.4	-7875.8	11686.6	958.5	-12645.1	117.7	50	0.550
706	3513.00	8371.2	980.2	-9351.4	13634.6	994.6	-14629.2	116.6	50	0.550
707	3522.00	9866.8	1139.8	-11006.7	15627.6	1135.6	-16763.2	115.6	50	0.550
708	3532.00	11393.4	1413.4	-12806.8	17626.6	1384.6	-19011.2	114.5	50	0.550
709	3542.00	12793.0	1754.0	-14547.0	19432.6	1702.6	-21135.2	113.6	50	0.550
710	3543.00	12927.0	1790.0	-14716.9	19602.6	1737.6	-21340.2	113.5	50	0.550
711	3553.00	14199.6	2184.6	-16384.3	21226.6	2106.6	-23333.3	112.7	50	0.550
712	3555.00	14439.6	2266.6	-16706.2	21528.6	2185.6	-23714.3	112.5	50	0.550
713	3565.00	15578.3	2692.3	-18270.7	22966.7	2586.6	-25553.3	111.8	50	0.550
714	3569.00	16004.2	2867.2	-18871.5	23497.7	2753.7	-26251.3	111.5	50	0.550
715	3579.00	17003.1	3313.1	-20316.2	24746.7	3177.7	-27924.4	110.8	50	0.550
716	3584.00	17470.0	3539.1	-21009.1	25324.7	3391.7	-28716.4	110.4	50	0.550
717	3594.00	18349.0	3992.0	-22341.0	26412.7	3823.7	-30236.4	109.8	50	0.550
718	3601.00	18921.0	4310.0	-23231.0	27113.8	4126.7	-31240.5	109.4	50	0.550
719	3611.00	19694.1	4761.1	-24455.1	28063.8	4556.8	-32620.6	108.9	50	0.550
720	3620.00	20340.2	5165.2	-25505.3	28848.8	4943.8	-33792.6	108.4	50	0.550
721	3630.00	21009.4	5610.3	-26619.7	29661.9	5369.9	-35031.7	107.9	50	0.550
722	3640.00	21629.6	6050.6	-27680.2	30407.9	5790.9	-36198.8	107.4	50	0.550
723	3641.00	21689.6	6094.6	-27784.2	30479.9	5832.9	-36312.8	107.4	50	0.550
724	3651.00	22275.9	6522.9	-28798.8	31187.9	6242.9	-37430.9	107.0	50	0.550
725	3661.00	22827.2	6942.2	-29769.5	31847.0	6645.0	-38492.0	106.6	50	0.550
726	3666.00	23088.4	7147.4	-30235.8	32159.0	6841.0	-39000.0	106.4	50	0.550
727	3676.00	23590.8	7549.8	-31140.6	32763.1	7225.0	-39988.1	106.0	50	0.550
728	3686.00	24060.3	7940.3	-32000.5	33320.1	7599.1	-40919.2	105.7	50	0.550
729	3695.00	24451.7	8280.7	-32732.4	33782.1	7925.2	-41707.3	105.3	50	0.550
730	3705.00	24858.2	8647.2	-33505.5	34265.2	8277.2	-42542.4	105.1	50	0.550
731	3715.00	25234.8	9003.8	-34238.6	34708.2	8617.2	-43325.5	104.8	50	0.550
732	3725.00	25596.4	9349.4	-34945.8	35131.3	8948.3	-44079.6	104.5	50	0.550
733	3730.00	25770.7	9519.7	-35290.4	35334.3	9112.3	-44446.6	104.3	50	0.550
734	3740.00	26113.4	9855.4	-35968.8	35740.4	9432.4	-45172.8	104.1	50	0.550
735	3750.00	26442.1	10185.1	-36627.1	36124.4	9747.4	-45871.9	103.9	50	0.550
736	3760.00	26753.8	10506.8	-37260.6	36487.5	10055.5	-46543.0	103.7	50	0.550
737	3770.00	27050.6	10821.6	-37872.1	36831.6	10355.6	-47187.1	103.4	50	0.550

Point No.	Time (sec.)	Membrane + Bending Stresses			Total Stresses			Metal Temp. (°F)	No. of Cycles	DO (ppm)
		S' <sub>12</sub> (psi)	S' <sub>23</sub> (psi)	S' <sub>31</sub> (psi)	S' <sub>12</sub> (psi)	S' <sub>23</sub> (psi)	S' <sub>31</sub> (psi)			
738	3775.00	27193.9	10975.9	-38169.8	36996.6	10503.6	-47500.2	103.3	50	0.550
739	3785.00	27471.7	11279.7	-38751.5	37323.6	10793.6	-48117.3	103.2	50	0.550
740	3795.00	27736.6	11574.6	-39311.2	37630.7	11074.7	-48705.4	103.0	50	0.550
741	3805.00	27992.4	11862.4	-39854.9	37924.8	11350.8	-49275.5	102.8	50	0.550
742	3815.00	28240.3	12150.3	-40390.6	38210.8	11624.8	-49835.6	102.7	50	0.550
743	3835.00	28705.2	12703.2	-41408.4	38741.9	12153.9	-50895.9	102.3	50	0.550
744	3836.00	28727.3	12730.3	-41457.6	38767.0	12180.0	-50946.9	102.3	50	0.550
745	3846.00	28948.3	12998.2	-41946.5	39027.0	12434.0	-51461.0	102.2	50	0.550
746	3856.00	29164.2	13259.2	-42423.5	39275.1	12683.1	-51958.2	102.1	50	0.550
747	3866.00	29370.2	13514.2	-42884.5	39511.1	12926.1	-52437.3	102.0	50	0.550
748	3876.00	29566.2	13762.2	-43328.5	39735.2	13162.2	-52897.4	101.9	50	0.550
749	3896.00	29932.3	14236.3	-44168.6	40150.3	13615.3	-53765.7	101.7	50	0.550
750	3916.00	30260.4	14682.4	-44942.8	40523.4	14039.5	-54562.9	101.5	50	0.550
751	3933.00	30512.2	15039.2	-45551.3	40806.6	14378.6	-55185.1	101.3	50	0.550
752	3943.00	30655.2	15239.2	-45894.4	40973.6	14569.6	-55543.2	101.3	50	0.550
753	3953.00	30789.3	15434.3	-46223.6	41127.7	14754.7	-55882.4	101.2	50	0.550
754	3963.00	30915.4	15621.3	-46536.7	41270.7	14932.8	-56203.5	101.2	50	0.550
755	3973.00	31034.4	15803.4	-46837.8	41404.8	15104.8	-56509.6	101.2	50	0.550
756	3993.00	31273.5	16162.5	-47436.0	41673.9	15446.9	-57120.9	101.1	50	0.550
757	4013.00	31507.7	16520.7	-48028.3	41937.1	15787.1	-57724.1	101.0	50	0.550
758	4033.00	31736.9	16876.9	-48613.8	42194.2	16126.2	-58320.4	100.9	50	0.550
759	4073.00	32189.5	17585.5	-49774.9	42701.4	16798.4	-59499.9	100.7	50	0.550
760	4113.00	32633.2	18288.2	-50921.5	43196.7	17466.7	-60663.4	100.6	50	0.550
761	4178.00	33196.8	19276.8	-52473.6	43822.1	18404.1	-62226.2	100.3	50	0.550
762	4188.00	33272.9	19408.9	-52681.8	43916.1	18529.1	-62445.3	100.4	50	0.550
763	4198.00	33347.9	19535.9	-52883.8	44002.2	18650.2	-62652.4	100.4	50	0.550
764	4208.00	33418.9	19657.9	-53076.9	44082.2	18766.3	-62848.5	100.4	50	0.550
765	4218.00	33483.0	19775.0	-53257.9	44155.3	18876.3	-63031.6	100.5	50	0.550
766	4238.00	33596.8	19989.8	-53586.6	44283.4	19080.4	-63363.8	100.5	50	0.550
767	4258.00	33689.6	20182.6	-53872.2	44387.5	19262.5	-63650.0	100.6	50	0.550
768	4278.00	33769.2	20354.2	-54123.4	44475.6	19424.6	-63900.1	100.7	50	0.550
769	4318.00	33939.1	20692.1	-54631.3	44664.7	19744.7	-64409.4	100.8	50	0.550
770	4358.00	34102.1	21025.1	-55127.2	44845.9	20059.9	-64905.7	101.0	50	0.550
771	4438.00	34414.2	21675.2	-56089.4	45190.2	20677.2	-65867.3	101.3	50	0.550
772	4500.00	34647.9	22171.9	-56819.8	45448.4	21147.4	-66595.8	101.5	50	0.550
773	4503.00	34705.3	22242.3	-56947.5	45510.4	21216.5	-66726.9	101.5	50	0.550
774	4505.00	34807.3	22297.3	-57104.5	45846.5	21273.6	-67120.1	103.0	50	0.550
775	4507.00	34971.2	22364.3	-57335.5	46249.7	21337.7	-67587.4	104.6	50	0.550
776	4509.00	35168.3	22441.3	-57609.7	46653.8	21411.8	-68065.6	106.2	50	0.550

Point No.	Time (sec.)	Membrane + Bending Stresses			Total Stresses			Metal Temp. (°F)	No. of Cycles	DO (ppm)
		S' <sub>12</sub> (psi)	S' <sub>23</sub> (psi)	S' <sub>31</sub> (psi)	S' <sub>12</sub> (psi)	S' <sub>23</sub> (psi)	S' <sub>31</sub> (psi)			
777	4511.00	35388.4	22525.4	-57913.8	47054.9	21491.9	-68546.8	107.9	50	0.550
778	4513.00	35620.6	22616.6	-58237.1	47450.0	21579.0	-69029.1	109.6	50	0.550
779	4515.00	35865.7	22714.7	-58580.5	47839.1	21672.2	-69511.3	111.3	50	0.550
780	4517.00	36116.0	22819.0	-58935.0	48221.2	21771.2	-69992.5	113.1	50	0.550
781	4519.00	36368.2	22928.2	-59296.4	48596.3	21875.4	-70471.7	114.8	50	0.550
782	4521.00	36623.5	23042.5	-59666.0	48965.5	21983.4	-70948.9	116.6	50	0.550
783	4523.00	36879.8	23161.8	-60041.7	49325.6	22097.5	-71423.1	118.4	50	0.550
784	4525.00	37136.1	23286.1	-60422.3	49680.6	22214.6	-71895.3	120.2	50	0.550
785	4527.00	37391.5	23413.5	-60805.1	50028.7	22335.7	-72364.4	122.0	50	0.550
786	4529.00	37644.9	23545.9	-61190.8	50370.8	22460.8	-72831.6	123.8	50	0.550
787	4531.00	37896.3	23680.3	-61576.6	50704.9	22588.9	-73293.8	125.6	50	0.550
788	4533.00	38145.7	23819.7	-61965.4	51033.0	22720.9	-73753.9	127.4	50	0.550
789	4535.00	38392.2	23961.2	-62353.4	51356.1	22855.0	-74211.1	129.2	50	0.550
790	4537.00	38636.7	24104.7	-62741.3	51673.1	22992.1	-74665.2	131.1	50	0.550
791	4539.00	38877.2	24251.2	-63128.3	51985.2	23130.2	-75115.4	132.9	50	0.550
792	4541.00	39114.7	24399.7	-63514.3	52290.3	23271.3	-75561.6	134.7	50	0.550
793	4543.00	39349.2	24550.2	-63899.3	52589.4	23415.4	-76004.7	136.6	50	0.550
794	4545.00	39581.7	24702.7	-64284.4	52883.4	23561.4	-76444.8	138.4	50	0.550
795	4547.00	39810.3	24857.2	-64667.5	53173.5	23707.5	-76881.0	140.3	50	0.550
796	4549.00	40034.8	25013.8	-65048.6	53457.6	23855.6	-77313.1	142.1	50	0.550
797	4551.00	40257.4	25170.4	-65427.7	53737.6	24004.7	-77742.3	144.0	50	0.550
798	4553.00	40476.0	25329.0	-65804.9	54011.7	24155.7	-78167.4	145.8	50	0.550
799	4555.00	40692.5	25487.5	-66180.0	54282.8	24306.8	-78589.6	147.7	50	0.550
800	4557.00	40906.1	25647.1	-66553.2	54548.9	24458.9	-79007.7	149.5	50	0.550
801	4559.00	41115.7	25808.8	-66924.5	54809.9	24612.9	-79422.9	151.4	50	0.550
802	4561.00	41323.4	25970.4	-67293.7	55068.0	24767.0	-79835.0	153.3	50	0.550
803	4563.00	41527.0	26134.0	-67661.0	55320.1	24923.1	-80243.1	155.1	50	0.550
804	4565.00	41728.6	26297.6	-68026.3	55569.1	25079.1	-80648.3	157.0	50	0.550
805	4567.00	41926.3	26461.3	-68387.6	55814.2	25234.2	-81048.4	158.9	50	0.550
806	4569.00	42123.0	26625.0	-68748.0	56055.3	25391.3	-81446.6	160.7	50	0.550
807	4571.00	42316.6	26789.6	-69106.3	56293.3	25548.4	-81841.7	162.6	50	0.550
808	4573.00	42507.3	26954.3	-69461.6	56528.4	25705.4	-82233.9	164.5	50	0.550
809	4575.00	42696.0	27119.9	-69815.9	56759.5	25862.5	-82622.0	166.4	50	0.550
810	4577.00	42882.7	27284.7	-70167.4	56986.6	26021.6	-83008.1	168.3	50	0.550
811	4579.00	43065.4	27450.3	-70515.7	57210.6	26178.7	-83389.3	170.1	50	0.550
812	4581.00	43246.0	27616.0	-70862.1	57430.7	26337.7	-83768.4	172.0	50	0.550
813	4583.00	43423.8	27781.8	-71205.5	57646.8	26495.8	-84142.6	173.9	50	0.550
814	4585.00	43599.5	27948.5	-71547.9	57860.9	26653.9	-84514.7	175.8	50	0.550
815	4587.00	43773.2	28114.2	-71887.4	58071.9	26811.9	-84883.9	177.7	50	0.550

Point No.	Time (sec.)	Membrane + Bending Stresses			Total Stresses			Metal Temp. (°F)	No. of Cycles	DO (ppm)
		S' <sub>12</sub> (psi)	S' <sub>23</sub> (psi)	S' <sub>31</sub> (psi)	S' <sub>12</sub> (psi)	S' <sub>23</sub> (psi)	S' <sub>31</sub> (psi)			
816	4589.00	43944.9	28279.9	-72224.8	58280.0	26971.0	-85251.0	179.6	50	0.550
817	4591.00	44114.6	28445.6	-72560.2	58485.1	27129.1	-85614.2	181.5	50	0.550
818	4593.00	44281.4	28611.4	-72892.7	58687.1	27287.1	-85974.3	183.3	50	0.550
819	4595.00	44447.1	28776.1	-73223.2	58886.2	27446.2	-86332.4	185.2	50	0.550
820	4597.00	44608.8	28941.8	-73550.7	59082.3	27603.3	-86685.6	187.1	50	0.550
821	4599.00	44769.6	29107.6	-73877.1	59275.4	27762.4	-87037.7	189.0	50	0.550
822	4601.00	44928.3	29272.3	-74200.7	59466.4	27919.4	-87385.9	190.9	50	0.550
823	4603.00	45085.1	29437.1	-74522.1	59654.5	28077.5	-87732.0	192.8	50	0.550
824	4605.00	45239.8	29601.8	-74841.6	59840.6	28234.6	-88075.2	194.7	50	0.550
825	4607.00	45392.6	29766.6	-75159.1	60023.7	28391.7	-88415.3	196.6	50	0.550
826	4609.00	45544.3	29930.3	-75474.6	60204.7	28548.7	-88753.5	198.5	50	0.550
827	4611.00	45693.1	30094.1	-75787.2	60383.8	28704.8	-89088.6	200.4	50	0.550
828	4613.00	45839.9	30257.8	-76097.7	60558.9	28860.9	-89419.8	202.3	50	0.550
829	4615.00	45985.6	30420.6	-76406.3	60732.9	29016.0	-89748.9	204.2	50	0.550
830	4617.00	46129.4	30583.4	-76712.8	60904.0	29172.0	-90076.0	206.1	50	0.550
831	4619.00	46272.2	30745.1	-77017.3	61072.1	29328.1	-90400.2	208.0	50	0.550
832	4621.00	46412.0	30907.0	-77318.9	61239.2	29482.2	-90721.3	209.9	50	0.550
833	4623.00	46550.7	31068.7	-77619.4	61403.2	29637.2	-91040.5	211.8	50	0.550
834	4625.00	46687.5	31229.5	-77917.0	61565.3	29791.3	-91356.6	213.7	50	0.550
835	4627.00	46821.3	31391.3	-78212.6	61725.4	29944.4	-91669.8	215.6	50	0.550
836	4629.00	46956.1	31550.1	-78506.1	61883.5	30098.5	-91981.9	217.5	50	0.550
837	4631.00	47087.8	31710.8	-78798.7	62040.5	30250.5	-92291.1	219.4	50	0.550
838	4633.00	47219.7	31869.7	-79089.3	62195.6	30403.6	-92599.2	221.4	50	0.550
839	4635.00	47349.4	32028.4	-79377.9	62348.7	30555.7	-92904.4	223.3	50	0.550
840	4637.00	47477.2	32187.2	-79664.4	62500.8	30706.8	-93207.5	225.2	50	0.550
841	4639.00	47605.0	32345.0	-79950.0	62650.8	30858.8	-93509.7	227.1	50	0.550
842	4641.00	47729.8	32502.8	-80232.6	62798.9	31008.9	-93807.8	229.0	50	0.550
843	4643.00	47853.6	32659.6	-80513.2	62945.0	31159.0	-94104.0	230.9	50	0.550
844	4645.00	47977.4	32815.4	-80792.8	63090.1	31309.1	-94399.1	232.8	50	0.550
845	4647.00	48099.2	32972.2	-81071.4	63233.1	31459.1	-94692.3	234.7	50	0.550
846	4649.00	48219.0	33128.0	-81347.0	63375.2	31607.2	-94982.4	236.6	50	0.550
847	4651.00	48338.8	33282.8	-81621.6	63515.3	31756.3	-95271.6	238.5	50	0.550
848	4653.00	48455.6	33437.6	-81893.2	63652.3	31904.3	-95556.7	240.5	50	0.550
849	4655.00	48571.4	33592.4	-82163.8	63789.4	32051.4	-95840.8	242.4	50	0.550
850	4657.00	48687.2	33745.2	-82432.4	63924.5	32198.5	-96123.0	244.3	50	0.550
851	4659.00	48800.0	33900.0	-82700.0	64057.6	32345.6	-96403.1	246.2	50	0.550
852	4661.00	48912.8	34051.8	-82964.7	64188.6	32492.7	-96681.3	248.1	50	0.550
853	4663.00	49023.6	34204.6	-83228.3	64318.7	32637.7	-96956.5	250.0	50	0.550
854	4665.00	49133.5	34356.5	-83489.9	64447.8	32782.8	-97230.6	252.0	50	0.550

Point No.	Time (sec.)	Membrane + Bending Stresses			Total Stresses			Metal Temp. (°F)	No. of Cycles	DO (ppm)
		S' <sub>12</sub> (psi)	S' <sub>23</sub> (psi)	S' <sub>31</sub> (psi)	S' <sub>12</sub> (psi)	S' <sub>23</sub> (psi)	S' <sub>31</sub> (psi)			
855	4667.00	49242.3	34506.3	-83748.5	64574.9	32926.9	-97501.8	253.9	50	0.550
856	4669.00	49350.1	34658.1	-84008.2	64702.0	33071.0	-97772.9	255.8	50	0.550
857	4671.00	49457.9	34807.9	-84265.8	64828.0	33215.1	-98043.1	257.7	50	0.550
858	4673.00	49565.7	34956.7	-84522.5	64954.1	33358.1	-98312.2	259.7	50	0.550
859	4675.00	49671.5	35106.5	-84778.0	65078.2	33501.2	-98579.4	261.6	50	0.550
860	4677.00	49776.3	35255.3	-85031.7	65200.3	33644.3	-98844.5	263.5	50	0.550
861	4679.00	49881.2	35403.2	-85284.3	65323.3	33785.4	-99108.7	265.4	50	0.550
862	4681.00	49985.0	35552.0	-85537.0	65444.4	33927.4	-99371.8	267.4	50	0.550
863	4683.00	50087.8	35699.8	-85787.5	65565.5	34068.5	-99634.0	269.3	50	0.550
864	4685.00	50190.6	35846.6	-86037.2	65684.6	34209.6	-99894.1	271.2	50	0.550
865	4687.00	50292.4	35992.4	-86284.9	65803.6	34349.6	-100153.3	273.2	50	0.550
866	4689.00	50392.2	36139.2	-86531.5	65919.7	34489.7	-100409.5	275.1	50	0.550
867	4691.00	50492.1	36285.1	-86777.1	66036.8	34628.8	-100665.6	277.0	50	0.550
868	4693.00	50591.9	36429.9	-87021.8	66152.9	34767.9	-100920.8	279.0	50	0.550
869	4695.00	50690.7	36574.7	-87265.4	66267.0	34907.0	-101174.0	280.9	50	0.550
870	4697.00	50788.5	36718.5	-87507.1	66381.0	35045.0	-101426.1	282.8	50	0.550
871	4699.00	50884.3	36862.3	-87746.7	66493.1	35182.1	-101675.2	284.8	50	0.550
872	4701.00	50981.2	37005.2	-87986.4	66605.2	35320.2	-101925.4	286.7	50	0.550
873	4703.00	51076.0	37149.0	-88225.0	66716.3	35456.3	-102172.6	288.6	50	0.550
874	4705.00	51170.8	37291.8	-88462.7	66826.4	35593.3	-102419.7	290.6	50	0.550
875	4707.00	51264.6	37433.6	-88698.3	66935.4	35729.4	-102664.9	292.5	50	0.550
876	4709.00	51358.4	37574.4	-88932.9	67043.5	35864.5	-102908.0	294.4	50	0.550
877	4711.00	51449.3	37716.3	-89165.6	67150.6	35998.6	-103149.2	296.4	50	0.550
878	4713.00	51541.1	37857.1	-89398.2	67256.7	36133.7	-103390.3	298.3	50	0.550
879	4715.00	51631.9	37996.9	-89628.8	67361.8	36268.7	-103630.5	300.3	50	0.550
880	4717.00	51722.8	38136.8	-89859.5	67466.8	36401.8	-103868.7	302.2	50	0.550
881	4719.00	51811.6	38275.6	-90087.2	67569.9	36534.9	-104104.8	304.1	50	0.550
882	4721.00	51899.4	38414.4	-90313.8	67672.0	36667.0	-104338.9	306.1	50	0.550
883	4723.00	51987.2	38552.2	-90539.4	67773.1	36800.1	-104573.1	308.0	50	0.550
884	4725.00	52074.0	38691.0	-90765.1	67874.1	36932.1	-104806.2	310.0	50	0.550
885	4727.00	52160.9	38827.9	-90988.7	67973.2	37064.2	-105037.4	311.9	50	0.550
886	4729.00	52245.7	38964.7	-91210.4	68072.3	37194.3	-105266.6	313.9	50	0.550
887	4731.00	52329.6	39101.5	-91431.1	68169.4	37324.4	-105493.7	315.8	50	0.550
888	4733.00	52413.4	39237.4	-91650.8	68265.5	37455.4	-105720.9	317.7	50	0.550
889	4735.00	52497.2	39372.2	-91869.4	68361.5	37585.5	-105947.1	319.7	50	0.550
890	4737.00	52579.0	39507.0	-92086.1	68456.6	37714.6	-106171.2	321.6	50	0.550
891	4739.00	52660.9	39641.9	-92302.7	68550.7	37842.7	-106393.4	323.6	50	0.550
892	4741.00	52740.7	39775.6	-92516.3	68642.8	37971.8	-106614.6	325.5	50	0.550
893	4743.00	52820.5	39909.5	-92730.0	68734.9	38098.9	-106833.7	327.5	50	0.550



Point No.	Time (sec.)	Membrane + Bending Stresses			Total Stresses			Metal Temp. (°F)	No. of Cycles	DO (ppm)
		S' <sub>12</sub> (psi)	S' <sub>23</sub> (psi)	S' <sub>31</sub> (psi)	S' <sub>12</sub> (psi)	S' <sub>23</sub> (psi)	S' <sub>31</sub> (psi)			
894	4745.00	52900.3	40043.3	-92943.6	68827.9	38225.9	-107053.9	329.4	50	0.550
895	4747.00	52980.1	40175.2	-93155.3	68919.0	38353.0	-107272.0	331.4	50	0.550
896	4749.00	53059.0	40307.0	-93366.0	69009.1	38480.1	-107489.2	333.3	50	0.550
897	4750.00	53093.9	40372.9	-93466.8	69031.1	38542.1	-107573.3	334.1	50	0.550
898	4751.00	53108.1	40421.1	-93529.2	69018.1	38588.1	-107606.2	335.0	50	0.550
899	4754.00	53061.8	40553.8	-93615.5	68708.1	38712.1	-107420.2	336.1	50	0.550
900	4759.00	52798.7	40727.7	-93526.4	68005.0	38878.0	-106883.0	337.1	50	0.550
901	4767.00	52178.8	40912.8	-93091.7	66874.9	39058.9	-105933.8	338.2	50	0.550
902	4777.00	51324.0	41021.0	-92345.0	65574.8	39169.8	-104744.7	339.2	50	0.550
903	4778.00	51239.1	41026.1	-92265.1	65455.8	39173.8	-104629.7	339.2	50	0.550
904	4788.00	50409.9	41026.9	-91436.8	64299.9	39181.9	-103481.7	340.0	50	0.550
905	4792.00	50095.2	41008.2	-91103.5	63880.9	39164.9	-103045.8	340.3	50	0.550
906	4802.00	49349.8	40922.8	-90272.7	62888.9	39090.0	-101978.9	340.9	50	0.550
907	4809.00	48865.2	40842.2	-89707.4	62262.0	39015.0	-101277.0	341.3	50	0.550
908	4819.00	48211.5	40684.5	-88896.1	61418.1	38868.0	-100286.1	341.8	50	0.550
909	4829.00	47604.7	40495.7	-88100.4	60652.1	38689.1	-99341.3	342.4	50	0.550
910	4839.00	47043.8	40291.8	-87335.6	59944.2	38496.2	-98440.4	342.8	50	0.550
911	4849.00	46529.7	40076.8	-86606.5	59305.2	38292.2	-97597.5	343.2	50	0.550
912	4852.00	46384.7	40010.7	-86395.4	59126.3	38230.3	-97356.5	343.4	50	0.550
913	4862.00	45921.6	39789.6	-85711.1	58551.3	38019.3	-96570.6	343.7	50	0.550
914	4872.00	45493.4	39564.4	-85057.8	58027.3	37804.3	-95831.7	344.1	50	0.550
915	4879.00	45214.2	39406.2	-84620.4	57688.3	37653.3	-95341.7	344.4	50	0.550
916	4889.00	44833.9	39178.9	-84012.8	57221.4	37437.4	-94658.8	344.7	50	0.550
917	4899.00	44479.6	38951.6	-83431.1	56793.4	37221.4	-94014.8	345.0	50	0.550
918	4909.00	44151.1	38726.1	-82877.2	56401.4	37004.4	-93405.8	345.3	50	0.550
919	4912.00	44058.0	38659.0	-82717.0	56290.4	36940.4	-93230.8	345.4	50	0.550
920	4922.00	43753.5	38434.5	-82188.1	55922.4	36725.4	-92647.8	345.6	50	0.550
921	4932.00	43462.0	38210.0	-81672.0	55575.4	36511.4	-92086.8	345.9	50	0.550
922	4942.00	43183.5	37986.5	-81169.9	55244.4	36298.4	-91542.8	346.1	50	0.550
923	4952.00	42918.9	37763.9	-80682.7	54933.4	36085.4	-91018.8	346.4	50	0.550
924	4953.00	42892.8	37741.8	-80634.6	54902.4	36065.4	-90967.8	346.4	50	0.550
925	4963.00	42636.2	37519.2	-80155.4	54594.4	35852.4	-90446.8	346.6	50	0.550
926	4973.00	42392.5	37301.5	-79694.1	54307.4	35645.4	-89952.7	346.8	50	0.550
927	4983.00	42176.0	37106.0	-79282.0	54054.3	35457.3	-89511.7	347.0	50	0.550
928	4993.00	41975.4	36917.4	-78892.9	53820.3	35277.3	-89097.7	347.2	50	0.550
929	5007.00	41707.7	36659.7	-78367.4	53509.3	35031.3	-88540.6	347.4	50	0.550
930	5017.00	41524.1	36481.1	-78005.2	53289.3	34861.3	-88150.6	347.6	50	0.550
931	5027.00	41347.5	36308.5	-77656.1	53083.2	34695.2	-87778.5	347.7	50	0.550

Point No.	Time (sec.)	Membrane + Bending Stresses			Total Stresses			Metal Temp. (°F)	No. of Cycles	DO (ppm)
		S' <sub>12</sub> (psi)	S' <sub>23</sub> (psi)	S' <sub>31</sub> (psi)	S' <sub>12</sub> (psi)	S' <sub>23</sub> (psi)	S' <sub>31</sub> (psi)			
932	5037.00	41182.0	36140.0	-77321.9	52891.2	34534.2	-87425.5	347.8	50	0.550
933	5047.00	41025.4	35976.4	-77001.9	52709.2	34379.2	-87088.4	347.9	50	0.550
934	5067.00	40742.3	35668.3	-76410.6	52384.1	34085.1	-86469.3	348.2	50	0.550
935	5087.00	40494.3	35384.2	-75878.5	52100.1	33814.1	-85914.1	348.4	50	0.550
936	5097.00	40372.7	35246.7	-75619.4	51954.1	33683.0	-85637.1	348.5	50	0.550
937	5107.00	40252.2	35110.2	-75362.3	51814.0	33553.0	-85367.0	348.6	50	0.550
938	5117.00	40135.7	34977.6	-75113.3	51681.0	33426.0	-85107.0	348.6	50	0.550
939	5127.00	40025.1	34846.1	-74871.2	51552.9	33300.9	-84853.9	348.7	50	0.550
940	5147.00	39815.1	34591.1	-74406.2	51312.9	33058.9	-84371.7	348.8	50	0.550
941	5167.00	39621.1	34349.1	-73970.2	51091.8	32827.8	-83919.6	348.9	50	0.550
942	5187.00	39443.1	34119.1	-73562.2	50890.7	32608.7	-83499.4	349.0	50	0.550
943	5227.00	39132.3	33692.3	-72824.6	50540.5	32201.5	-82742.1	349.3	50	0.550
944	5251.00	38972.2	33460.2	-72432.5	50361.5	31980.5	-82341.9	349.4	50	0.550
945	5261.00	38902.8	33364.8	-72267.7	50277.4	31890.4	-82167.8	349.4	50	0.550
946	5271.00	38832.4	33269.4	-72101.8	50194.4	31800.4	-81994.8	349.4	50	0.550
947	5281.00	38762.0	33173.0	-71934.9	50114.3	31708.3	-81822.7	349.4	50	0.550
948	5291.00	38691.5	33077.6	-71769.1	50034.3	31616.3	-81650.6	349.5	50	0.550
949	5311.00	38558.7	32886.7	-71445.5	49883.2	31436.2	-81319.4	349.5	50	0.550
950	5331.00	38437.9	32706.9	-71144.8	49748.1	31263.1	-81011.2	349.5	50	0.550
951	5351.00	38326.2	32535.2	-70861.3	49621.0	31101.0	-80722.1	349.5	50	0.550
952	5391.00	38127.8	32222.8	-70350.6	49398.9	30803.9	-80202.9	349.5	50	0.550
953	5431.00	37963.6	31948.6	-69912.2	49214.8	30543.8	-79758.6	349.5	50	0.550
954	5511.00	37723.7	31520.7	-69244.4	48947.6	30135.6	-79083.1	349.6	50	0.550
955	5591.00	37575.4	31224.4	-68799.8	48782.4	29854.4	-78636.8	349.6	50	0.550
956	5751.00	37296.2	30686.2	-67982.4	48471.1	29342.1	-77813.1	349.7	50	0.550
957	5911.00	37029.2	30166.2	-67195.4	48174.8	28845.8	-77020.6	349.7	50	0.550
958	6231.00	36851.6	29750.7	-66602.3	47976.5	28449.5	-76426.1	349.9	50	0.550
959	6450.00	36709.4	29379.4	-66088.8	47818.3	28094.3	-75912.6	350.0	50	0.550
960	6450.00	37709.4	24757.4	-62466.7	48508.8	23348.4	-71857.3	299.5	20	0.050
961	6452.00	37934.9	24819.7	-62754.6	49589.4	23397.6	-72987.0	304.2	20	0.050
962	6453.00	38192.5	24886.6	-63079.0	50514.4	23450.2	-73964.7	308.1	20	0.050
963	6454.00	38522.3	24971.4	-63493.7	51524.1	23517.9	-75042.0	312.4	20	0.050
964	6455.00	38905.6	25071.6	-63977.2	52575.9	23599.1	-76175.1	316.9	20	0.050
965	6456.00	39331.8	25185.6	-64517.3	53651.2	23693.3	-77344.5	321.6	20	0.050
966	6457.00	39797.6	25313.0	-65110.7	54746.4	23799.9	-78546.3	326.5	20	0.050
967	6458.00	40293.4	25452.8	-65746.2	55850.1	23918.3	-79768.4	331.4	20	0.050
968	6459.00	40817.6	25604.6	-66422.2	56960.9	24048.3	-81009.2	336.5	20	0.050
969	6460.00	41359.4	25767.0	-67126.4	58070.8	24188.8	-82259.6	341.7	20	0.050
970	6461.00	41915.6	25939.4	-67855.0	59177.7	24339.3	-83517.0	346.9	20	0.050

Point No.	Time (sec.)	Membrane + Bending Stresses			Total Stresses			Metal Temp. (°F)	No. of Cycles	DO (ppm)
		S' <sub>12</sub> (psi)	S' <sub>23</sub> (psi)	S' <sub>31</sub> (psi)	S' <sub>12</sub> (psi)	S' <sub>23</sub> (psi)	S' <sub>31</sub> (psi)			
971	6462.00	42486.3	26122.0	-68608.3	60281.4	24499.9	-84781.4	352.1	20	0.050
972	6463.00	43071.6	26314.7	-69386.3	61382.1	24670.7	-86052.8	357.5	20	0.050
973	6464.00	43670.7	26517.6	-70188.3	62479.4	24851.2	-87330.7	362.9	20	0.050
974	6465.00	44277.8	26729.3	-71007.0	63570.3	25040.9	-88611.2	368.3	20	0.050
975	6466.00	44891.1	26949.6	-71840.8	64654.3	25239.0	-89893.3	373.8	20	0.050
976	6467.00	45510.8	27178.6	-72689.4	65731.2	25445.9	-91177.1	379.3	20	0.050
977	6468.00	46136.9	27416.2	-73553.1	66801.1	25661.2	-92462.2	384.9	20	0.050
978	6469.00	46768.7	27662.3	-74431.0	67863.8	25885.0	-93748.7	390.5	20	0.050
979	6470.00	47401.2	27915.0	-75316.2	68918.1	26115.3	-95033.4	396.1	20	0.050
980	6471.00	48033.4	28173.7	-76207.1	69964.1	26351.5	-96315.6	401.7	20	0.050
981	6472.00	48665.1	28438.6	-77103.7	71001.3	26593.9	-97595.2	407.4	20	0.050
982	6473.00	49296.4	28709.5	-78006.0	72030.1	26842.3	-98872.4	413.1	20	0.050
983	6474.00	49927.4	28986.6	-78914.0	73050.4	27096.6	-100147.0	418.8	20	0.050
984	6475.00	50557.9	29269.9	-79827.7	74062.1	27357.1	-101419.2	424.5	20	0.050
985	6476.00	51187.9	29559.2	-80747.1	75065.3	27623.6	-102688.9	430.3	20	0.050
986	6477.00	51817.6	29854.7	-81672.3	76059.9	27896.1	-103956.1	436.1	20	0.050
987	6478.00	52446.9	30156.2	-82603.0	77046.1	28174.6	-105220.7	441.9	20	0.050
988	6479.00	53075.7	30463.9	-83539.6	78023.5	28459.3	-106482.9	447.7	20	0.050
989	6480.00	53703.6	30777.3	-84480.9	78992.7	28749.4	-107742.1	453.6	20	0.050
990	6481.00	54328.9	31094.9	-85423.7	79953.5	29043.9	-108997.4	459.4	20	0.050
991	6482.00	54951.2	31416.8	-86368.0	80906.1	29342.3	-110248.4	465.3	20	0.050
992	6483.00	55570.6	31742.8	-87313.4	81850.5	29644.7	-111495.2	471.2	20	0.050
993	6484.00	56187.1	32072.9	-88260.0	82786.6	29951.2	-112737.8	477.1	20	0.050
994	6485.00	56800.7	32407.2	-89207.9	83714.4	30261.9	-113976.3	483.1	20	0.050
995	6486.00	57411.4	32745.6	-90157.0	84634.1	30576.4	-115210.6	489.0	20	0.050
996	6487.00	58019.1	33088.1	-91107.2	85545.4	30895.2	-116440.6	494.9	20	0.050
997	6488.00	58623.9	33434.8	-92058.7	86448.6	31217.9	-117666.6	500.9	20	0.050
998	6489.00	59225.8	33785.7	-93011.4	87343.6	31544.7	-118888.3	506.9	20	0.050
999	6490.00	59824.8	34140.6	-93965.4	88230.3	31875.6	-120105.8	512.9	20	0.050
1000	6491.00	60420.5	34498.7	-94919.3	89109.3	32209.6	-121318.9	518.9	20	0.050
1001	6492.00	61012.8	34858.6	-95871.3	89981.9	32545.1	-122527.0	524.9	20	0.050
1002	6493.00	61601.5	35220.0	-96821.5	90847.9	32882.1	-123730.0	531.0	20	0.050
1003	6494.00	62186.7	35583.2	-97769.8	91707.4	33220.8	-124928.2	537.0	20	0.050
1004	6495.00	62768.2	35947.9	-98716.1	92560.3	33561.0	-126121.4	543.0	20	0.050
1005	6496.00	63346.1	36314.4	-99660.5	93406.9	33902.6	-127309.5	549.1	20	0.050
1006	6497.00	63920.6	36682.2	-100602.9	94246.8	34245.9	-128492.7	555.2	20	0.050
1007	6498.00	64491.4	37051.9	-101543.3	95080.1	34590.9	-129671.0	561.2	20	0.050
1008	6499.00	65058.7	37423.1	-102481.8	95907.1	34937.2	-130844.3	567.3	20	0.050
1009	6500.00	65622.3	37795.9	-103418.2	96727.5	35285.2	-132012.7	573.4	20	0.050

Point No.	Time (sec.)	Membrane + Bending Stresses			Total Stresses			Metal Temp. (°F)	No. of Cycles	DO (ppm)
		S' <sub>12</sub> (psi)	S' <sub>23</sub> (psi)	S' <sub>31</sub> (psi)	S' <sub>12</sub> (psi)	S' <sub>23</sub> (psi)	S' <sub>31</sub> (psi)			
1010	6501.00	66123.3	38152.8	-104276.0	97218.6	35621.3	-132840.0	578.1	20	0.050
1011	6502.00	66510.5	38481.5	-104992.0	97268.0	35936.4	-133204.4	580.9	20	0.050
1012	6503.00	66802.9	38789.3	-105592.2	97143.6	36236.2	-133379.8	583.1	20	0.050
1013	6504.00	67018.5	39079.7	-106098.2	96928.0	36522.4	-133450.4	585.0	20	0.050
1014	6506.00	67286.8	39618.9	-106905.8	96369.6	37059.7	-133429.3	588.0	20	0.050
1015	6508.00	67386.1	40109.1	-107495.2	95713.4	37553.5	-133266.9	590.5	20	0.050
1016	6510.00	67365.0	40556.9	-107921.9	95009.3	38007.8	-133017.1	592.6	20	0.050
1017	6512.00	67267.1	40969.0	-108236.1	94289.1	38428.0	-132717.1	594.5	20	0.050
1018	6514.00	67096.5	41346.0	-108442.4	93555.6	38814.0	-132369.6	596.2	20	0.050
1019	6516.00	66874.8	41692.0	-108566.8	92819.1	39169.9	-131989.0	597.8	20	0.050
1020	6518.00	66614.0	42006.5	-108620.5	92088.4	39494.2	-131582.6	599.2	20	0.050
1021	6520.00	66321.8	42289.9	-108611.7	91367.1	39787.8	-131154.8	600.4	20	0.050
1022	6522.00	66017.6	42549.9	-108567.5	90659.3	40057.9	-130717.2	601.6	20	0.050
1023	6524.00	65702.5	42787.1	-108489.6	89965.4	40305.1	-130270.5	602.8	20	0.050
1024	6526.00	65376.7	43001.2	-108377.9	89285.4	40529.1	-129814.5	603.9	20	0.050
1025	6528.00	65040.0	43192.5	-108232.5	88619.2	40730.2	-129349.4	604.9	20	0.050
1026	6530.00	64693.1	43361.1	-108054.2	87966.9	40908.6	-128875.5	605.8	20	0.050
1027	6532.00	64343.0	43512.9	-107856.0	87327.5	41070.0	-128397.5	606.7	20	0.050
1028	6534.00	63992.2	43649.8	-107642.0	86700.8	41216.4	-127917.1	607.5	20	0.050
1029	6536.00	63640.7	43771.8	-107412.5	86086.7	41347.7	-127434.3	608.4	20	0.050
1030	6538.00	63288.5	43878.7	-107167.2	85485.3	41463.8	-126949.1	609.2	20	0.050
1031	6540.00	62935.6	43970.8	-106906.3	84896.5	41564.9	-126461.4	609.9	20	0.050
1032	6542.00	62583.2	44051.8	-106635.0	84317.9	41655.0	-125972.9	610.6	20	0.050
1033	6544.00	62236.0	44125.3	-106361.3	83751.0	41737.2	-125488.2	611.3	20	0.050
1034	6546.00	61894.9	44190.2	-106085.1	83197.4	41811.0	-125008.4	612.0	20	0.050
1035	6548.00	61559.7	44246.9	-105806.6	82657.1	41876.1	-124533.2	612.7	20	0.050
1036	6550.00	61230.5	44295.3	-105525.9	82130.1	41932.8	-124062.9	613.3	20	0.050
1037	6552.00	60907.4	44335.2	-105242.6	81616.3	41980.9	-123597.2	613.9	20	0.050
1038	6554.00	60590.2	44366.9	-104957.1	81115.8	42020.5	-123136.3	614.5	20	0.050
1039	6556.00	60279.1	44390.2	-104669.3	80628.5	42051.6	-122680.2	615.1	20	0.050
1040	6558.00	59974.0	44405.1	-104379.1	80154.6	42074.2	-122228.8	615.6	20	0.050
1041	6560.00	59674.8	44411.8	-104086.5	79693.9	42088.2	-121782.1	616.2	20	0.050
1042	6562.00	59381.7	44410.0	-103791.7	79246.4	42093.8	-121340.2	616.7	20	0.050
1043	6564.00	59094.7	44399.9	-103494.5	78812.3	42090.7	-120903.0	617.1	20	0.050
1044	6566.00	58813.5	44381.5	-103195.0	78391.3	42079.4	-120470.6	617.6	20	0.050
1045	6568.00	58537.4	44358.0	-102895.4	77979.9	42062.6	-120042.6	618.1	20	0.050
1046	6570.00	58265.4	44331.1	-102596.5	77576.1	42042.4	-119618.5	618.5	20	0.050
1047	6572.00	57997.7	44300.8	-102298.5	77179.8	42018.7	-119198.5	618.9	20	0.050
1048	6574.00	57734.2	44267.4	-102001.6	76790.9	41991.6	-118782.5	619.3	20	0.050

Point No.	Time (sec.)	Membrane + Bending Stresses			Total Stresses			Metal Temp. (°F)	No. of Cycles	DO (ppm)
		S' <sub>12</sub> (psi)	S' <sub>23</sub> (psi)	S' <sub>31</sub> (psi)	S' <sub>12</sub> (psi)	S' <sub>23</sub> (psi)	S' <sub>31</sub> (psi)			
1049	6576.00	57474.9	44230.7	-101705.6	76409.4	41961.3	-118370.7	619.7	20	0.050
1050	6578.00	57219.9	44190.5	-101410.4	76035.6	41927.4	-117963.0	620.1	20	0.050
1051	6580.00	56969.2	44147.0	-101116.2	75669.2	41890.0	-117559.2	620.5	20	0.050
1052	6582.00	56722.6	44100.4	-100823.0	75310.3	41849.3	-117159.5	620.9	20	0.050
1053	6584.00	56480.3	44050.3	-100530.6	74958.8	41805.1	-116763.9	621.3	20	0.050
1054	6586.00	56242.2	43997.0	-100239.2	74614.9	41757.6	-116372.5	621.6	20	0.050
1055	6588.00	56008.4	43940.3	-99948.7	74278.3	41706.6	-115985.0	622.0	20	0.050
1056	6590.00	55778.8	43880.3	-99659.1	73949.4	41652.1	-115601.5	622.3	20	0.050
1057	6593.00	55440.9	43785.4	-99226.2	73467.2	41565.4	-115032.6	622.8	20	0.050
1058	6596.00	55103.8	43689.8	-98793.5	72986.6	41477.9	-114464.5	623.3	20	0.050
1059	6599.00	54766.7	43594.3	-98361.1	72506.0	41390.3	-113896.3	623.8	20	0.050
1060	6602.00	54432.5	43498.1	-97930.6	72029.7	41302.1	-113331.8	624.2	20	0.050
1061	6605.00	54104.7	43400.4	-97505.1	71563.1	41212.1	-112775.2	624.7	20	0.050
1062	6608.00	53783.2	43301.0	-97084.2	71106.3	41120.4	-112226.6	625.2	20	0.050
1063	6611.00	53468.1	43200.2	-96668.3	70659.3	41026.9	-111686.2	625.6	20	0.050
1064	6614.00	53159.4	43097.7	-96257.0	70222.2	40931.6	-111153.7	626.0	20	0.050
1065	6617.00	52857.0	42993.7	-95850.7	69794.7	40834.6	-110629.3	626.5	20	0.050
1066	6620.00	52561.0	42888.0	-95449.1	69377.1	40735.8	-110112.9	626.9	20	0.050
1067	6623.00	52271.4	42780.9	-95052.2	68969.2	40635.4	-109604.6	627.3	20	0.050
1068	6626.00	51988.1	42672.2	-94660.3	68571.1	40533.1	-109104.2	627.7	20	0.050
1069	6629.00	51711.2	42561.8	-94273.0	68182.8	40429.2	-108611.9	628.0	20	0.050
1070	6632.00	51440.6	42449.9	-93890.6	67804.2	40323.4	-108127.6	628.4	20	0.050
1071	6635.00	51176.5	42336.5	-93513.0	67435.5	40215.9	-107651.4	628.8	20	0.050
1072	6638.00	50918.6	42221.5	-93140.1	67076.5	40106.7	-107183.2	629.1	20	0.050
1073	6641.00	50667.2	42104.9	-92772.1	66727.3	39995.7	-106723.0	629.4	20	0.050
1074	6644.00	50422.1	41986.8	-92408.8	66387.9	39883.0	-106270.9	629.7	20	0.050
1075	6647.00	50183.3	41866.9	-92050.2	66058.2	39768.6	-105826.8	630.0	20	0.050
1076	6650.00	49950.7	41745.7	-91696.4	65738.0	39652.4	-105390.4	630.3	20	0.050
1077	6653.00	49719.8	41624.1	-91343.8	65420.3	39535.9	-104956.2	630.6	20	0.050
1078	6656.00	49488.9	41502.4	-90991.3	65102.6	39419.2	-104521.9	630.9	20	0.050
1079	6659.00	49259.3	41381.1	-90640.4	64786.8	39302.9	-104089.7	631.2	20	0.050
1080	6662.00	49035.5	41260.9	-90296.4	64479.3	39187.4	-103666.6	631.5	20	0.050
1081	6665.00	48817.9	41141.7	-89959.6	64180.5	39072.9	-103253.4	631.8	20	0.050
1082	6669.00	48537.4	40984.6	-89522.0	63796.0	38921.7	-102717.7	632.1	20	0.050
1083	6673.00	48267.9	40829.4	-89097.3	63427.1	38772.2	-102199.4	632.5	20	0.050
1084	6677.00	48009.3	40676.3	-88685.6	63074.0	38624.6	-101698.5	632.8	20	0.050
1085	6681.00	47761.7	40525.1	-88286.8	62736.6	38478.5	-101215.1	633.1	20	0.050
1086	6685.00	47525.1	40375.9	-87901.0	62414.9	38334.3	-100749.2	633.4	20	0.050
1087	6689.00	47299.4	40228.7	-87528.1	62108.9	38191.8	-100300.7	633.6	20	0.050

Point No.	Time (sec.)	Membrane + Bending Stresses			Total Stresses			Metal Temp. (°F)	No. of Cycles	DO (ppm)
		S' <sub>12</sub> (psi)	S' <sub>23</sub> (psi)	S' <sub>31</sub> (psi)	S' <sub>12</sub> (psi)	S' <sub>23</sub> (psi)	S' <sub>31</sub> (psi)			
1088	6693.00	47084.7	40083.5	-87168.2	61818.6	38051.0	-99869.5	633.9	20	0.050
1089	6698.00	46831.7	39904.7	-86736.4	61477.8	37877.4	-99355.2	634.2	20	0.050
1090	6701.00	46603.9	39774.0	-86377.9	60824.2	37755.5	-98579.7	632.3	20	0.050
1091	6702.00	46316.5	39672.0	-85988.5	59679.0	37670.2	-97349.2	627.7	20	0.050
1092	6703.00	45899.6	39538.3	-85437.9	58296.1	37560.9	-95857.0	622.2	20	0.050
1093	6704.00	45379.4	39378.4	-84757.7	56793.2	37430.3	-94223.5	616.1	20	0.050
1094	6705.00	44782.7	39196.1	-83978.9	55231.2	37280.3	-92511.5	609.7	20	0.050
1095	6706.00	44125.2	38993.7	-83119.0	53636.6	37112.2	-90748.9	603.0	20	0.050
1096	6707.00	43411.4	38772.0	-82183.4	52014.7	36926.2	-88940.9	596.1	20	0.050
1097	6708.00	42655.0	38532.6	-81187.6	50381.1	36723.5	-87104.6	589.1	20	0.050
1098	6709.00	41858.1	38276.0	-80134.1	48737.4	36504.2	-85241.6	581.9	20	0.050
1099	6710.00	41036.3	38004.5	-79040.8	47094.9	36270.1	-83365.0	574.6	20	0.050
1100	6711.00	40194.2	37718.9	-77913.1	45457.0	36021.5	-81478.5	567.2	20	0.050
1101	6712.00	39331.7	37419.3	-76750.9	43823.4	35758.7	-79582.0	559.7	20	0.050
1102	6713.00	38448.9	37105.6	-75554.5	42194.3	35481.4	-77675.7	552.1	20	0.050
1103	6714.00	37546.9	36778.1	-74325.0	40570.0	35189.9	-75759.9	544.5	20	0.050
1104	6715.00	36634.3	36438.6	-73073.0	38954.8	34885.8	-73840.6	536.8	20	0.050
1105	6716.00	35713.6	36087.7	-71801.3	37349.6	34569.4	-71919.0	529.0	20	0.050
1106	6717.00	34784.7	35725.3	-70510.1	35754.5	34240.7	-69995.3	521.1	20	0.050
1107	6718.00	33847.8	35351.7	-69199.5	34169.6	33899.7	-68069.3	513.3	20	0.050
1108	6719.00	32903.9	34967.0	-67870.9	32594.9	33546.8	-66141.8	505.3	20	0.050
1109	6720.00	31960.1	34574.3	-66534.4	31032.1	33184.8	-64216.9	497.3	20	0.050
1110	6721.00	31018.1	34174.2	-65192.3	29481.5	32814.0	-62295.5	489.3	20	0.050
1111	6722.00	30078.2	33766.8	-63845.0	27943.2	32434.7	-60378.0	481.2	20	0.050
1112	6723.00	29140.5	33352.0	-62492.5	26417.1	32046.9	-58464.0	473.2	20	0.050
1113	6724.00	28204.8	32930.2	-61135.0	24903.3	31650.4	-56553.8	465.0	20	0.050
1114	6725.00	27271.5	32501.4	-59772.9	23401.7	31245.5	-54647.2	456.9	20	0.050
1115	6726.00	26424.0	32089.6	-58513.6	22373.1	30850.9	-53224.1	450.7	20	0.050
1116	6727.00	25733.8	31711.5	-57445.3	21978.7	30479.7	-52458.4	447.2	20	0.050
1117	6728.00	25174.6	31356.3	-56530.9	21835.1	30123.8	-51958.9	444.5	20	0.050
1118	6729.00	24720.2	31019.1	-55739.3	21824.4	29780.9	-51605.4	442.4	20	0.050
1119	6730.00	24344.3	30696.3	-55040.6	21886.1	29449.2	-51335.4	440.6	20	0.050
1120	6731.00	24034.0	30387.8	-54421.8	21993.1	29129.9	-51123.0	438.9	20	0.050
1121	6732.00	23784.9	30092.9	-53877.7	22140.4	28822.5	-50962.9	437.5	20	0.050
1122	6733.00	23583.0	29809.8	-53392.8	22311.4	28526.5	-50837.9	436.2	20	0.050
1123	6734.00	23425.9	29538.2	-52964.1	22504.4	28241.1	-50745.4	435.1	20	0.050
1124	6736.00	23195.2	29021.8	-52217.0	22918.7	27697.1	-50615.9	433.0	20	0.050
1125	6738.00	23063.5	28539.3	-51602.8	23362.5	27187.6	-50550.0	431.2	20	0.050
1126	6740.00	23019.4	28088.2	-51107.5	23830.2	26710.4	-50540.5	429.7	20	0.050

Point No.	Time (sec.)	Membrane + Bending Stresses			Total Stresses			Metal Temp. (°F)	No. of Cycles	DO (ppm)
		S' <sub>12</sub> (psi)	S' <sub>23</sub> (psi)	S' <sub>31</sub> (psi)	S' <sub>12</sub> (psi)	S' <sub>23</sub> (psi)	S' <sub>31</sub> (psi)			
1127	6743.00	23056.6	27472.0	-50528.6	24536.0	26058.7	-50594.6	427.7	20	0.050
1128	6746.00	23188.5	26931.0	-50119.5	25228.8	25486.9	-50715.7	426.0	20	0.050
1129	6749.00	23358.9	26444.5	-49803.4	25896.0	24973.4	-50869.4	424.5	20	0.050
1130	6752.00	23566.0	26011.6	-49577.6	26537.2	24517.4	-51054.6	423.2	20	0.050
1131	6755.00	23808.7	25631.7	-49440.4	27152.4	24118.6	-51271.0	422.1	20	0.050
1132	6758.00	24067.0	25289.0	-49356.1	27744.4	23759.7	-51504.2	421.0	20	0.050
1133	6761.00	24331.4	24976.4	-49307.8	28314.2	23433.0	-51747.2	420.1	20	0.050
1134	6764.00	24602.0	24693.7	-49295.6	28861.9	23138.4	-52000.4	419.2	20	0.050
1135	6767.00	24876.7	24436.6	-49313.3	29390.1	22871.2	-52261.3	418.5	20	0.050
1136	6770.00	25146.7	24194.6	-49341.2	29901.1	22620.2	-52521.3	417.7	20	0.050
1137	6773.00	25410.3	23968.2	-49378.4	30393.4	22385.6	-52779.0	417.0	20	0.050
1138	6776.00	25667.5	23757.4	-49424.9	30867.2	22167.3	-53034.5	416.3	20	0.050
1139	6779.00	25919.3	23562.7	-49482.1	31324.0	21965.8	-53289.8	415.7	20	0.050
1140	6782.00	26167.8	23384.8	-49552.5	31766.3	21782.3	-53548.6	415.1	20	0.050
1141	6785.00	26412.8	23223.6	-49636.4	32194.3	21616.5	-53810.8	414.5	20	0.050
1142	6789.00	26734.1	23035.1	-49769.2	32742.7	21423.1	-54165.8	413.8	20	0.050
1143	6793.00	27048.9	22873.9	-49922.8	33267.0	21258.5	-54525.4	413.1	20	0.050
1144	6797.00	27347.7	22733.4	-50081.1	33759.9	21115.4	-54875.3	412.5	20	0.050
1145	6801.00	27627.6	22614.2	-50241.8	34217.7	20994.4	-55212.1	411.9	20	0.050
1146	6805.00	27888.5	22516.3	-50404.8	34640.2	20895.4	-55535.6	411.4	20	0.050
1147	6810.00	28188.1	22423.9	-50612.0	35118.8	20802.8	-55921.6	410.8	20	0.050
1148	6815.00	28458.0	22364.8	-50822.7	35542.2	20744.8	-56286.9	410.4	20	0.050
1149	6820.00	28708.7	22331.0	-51039.7	35929.0	20712.7	-56641.7	409.9	20	0.050
1150	6825.00	28966.5	22301.9	-51268.4	36325.4	20685.5	-57010.9	409.5	20	0.050
1151	6830.00	29230.5	22275.5	-51506.0	36730.5	20661.5	-57391.9	409.0	20	0.050
1152	6835.00	29494.9	22249.5	-51744.4	37136.2	20637.4	-57773.6	408.6	20	0.050
1153	6840.00	29759.4	22223.6	-51983.0	37541.8	20613.3	-58155.1	408.2	20	0.050
1154	6845.00	30024.0	22197.8	-52221.8	37947.4	20589.3	-58536.8	407.7	20	0.050
1155	6850.00	30288.4	22172.2	-52460.6	38352.6	20565.4	-58918.0	407.3	20	0.050
1156	6853.00	30491.5	22172.0	-52663.5	38800.0	20563.9	-59363.9	407.9	20	0.050
1157	6855.00	30663.5	22183.2	-52846.7	39168.1	20572.9	-59741.0	408.7	20	0.050
1158	6857.00	30850.3	22201.5	-53051.8	39541.7	20588.6	-60130.3	409.6	20	0.050
1159	6859.00	31046.7	22225.8	-53272.6	39913.8	20610.4	-60524.3	410.5	20	0.050
1160	6861.00	31247.3	22255.7	-53502.9	40280.0	20638.0	-60918.0	411.5	20	0.050
1161	6863.00	31449.9	22290.8	-53740.7	40638.6	20670.9	-61309.6	412.5	20	0.050
1162	6865.00	31653.8	22331.0	-53984.8	40989.3	20709.1	-61698.4	413.5	20	0.050
1163	6867.00	31856.4	22376.0	-54232.3	41330.8	20752.3	-62083.1	414.6	20	0.050
1164	6869.00	32057.6	22425.4	-54483.0	41663.1	20800.0	-62463.2	415.7	20	0.050
1165	6872.00	32352.7	22506.8	-54859.5	42143.4	20879.2	-63022.7	417.3	20	0.050

Point No.	Time (sec.)	Membrane + Bending Stresses			Total Stresses			Metal Temp. (°F)	No. of Cycles	DO (ppm)
		S' <sub>12</sub> (psi)	S' <sub>23</sub> (psi)	S' <sub>31</sub> (psi)	S' <sub>12</sub> (psi)	S' <sub>23</sub> (psi)	S' <sub>31</sub> (psi)			
1166	6875.00	32638.6	22596.3	-55234.8	42601.9	20966.8	-63568.7	419.0	20	0.050
1167	6878.00	32921.6	22692.0	-55613.5	43048.6	21060.7	-64109.3	420.8	20	0.050
1168	6881.00	33203.6	22793.1	-55996.7	43487.1	21160.2	-64647.2	422.5	20	0.050
1169	6884.00	33482.9	22898.3	-56381.2	43917.5	21263.8	-65181.3	424.3	20	0.050
1170	6887.00	33759.2	23007.4	-56766.6	44340.1	21371.3	-65711.4	426.1	20	0.050
1171	6890.00	34032.6	23120.4	-57153.0	44754.7	21482.6	-66237.3	427.9	20	0.050
1172	6893.00	34303.0	23236.1	-57539.1	45162.1	21596.7	-66758.8	429.7	20	0.050
1173	6896.00	34569.9	23353.6	-57923.5	45563.2	21712.5	-67275.7	431.5	20	0.050
1174	6899.00	34834.6	23473.5	-58308.0	45959.7	21830.6	-67790.3	433.3	20	0.050
1175	6902.00	35097.9	23596.5	-58694.4	46352.8	21951.8	-68304.6	435.1	20	0.050
1176	6905.00	35360.0	23722.8	-59082.8	46742.6	22076.1	-68818.7	437.0	20	0.050
1177	6908.00	35620.4	23852.1	-59472.5	47128.3	22203.5	-69331.8	438.8	20	0.050
1178	6911.00	35872.9	23983.7	-59856.5	47501.1	22333.0	-69834.1	440.6	20	0.050
1179	6914.00	36115.5	24116.9	-60232.5	47857.9	22464.2	-70322.1	442.5	20	0.050
1180	6917.00	36348.3	24252.0	-60600.2	48198.9	22596.9	-70795.9	444.4	20	0.050
1181	6920.00	36571.5	24387.7	-60959.2	48525.1	22730.4	-71255.5	446.3	20	0.050
1182	6923.00	36785.3	24524.0	-61309.3	48836.6	22864.5	-71701.1	448.2	20	0.050
1183	6926.00	36989.6	24661.0	-61650.5	49133.6	22999.0	-72132.6	450.2	20	0.050
1184	6929.00	37184.4	24798.4	-61982.8	49416.0	23134.0	-72550.0	452.1	20	0.050
1185	6933.00	37429.7	24982.6	-62412.3	49770.4	23314.9	-73085.3	454.8	20	0.050
1186	6937.00	37669.0	25169.5	-62838.5	50114.7	23498.4	-73613.2	457.4	20	0.050
1187	6941.00	37906.6	25359.9	-63266.5	50455.5	23685.3	-74140.9	460.1	20	0.050
1188	6945.00	38143.5	25553.0	-63696.5	50794.2	23875.0	-74669.2	462.7	20	0.050
1189	6949.00	38379.3	25747.3	-64126.7	51131.0	24065.6	-75196.6	465.4	20	0.050
1190	6953.00	38611.6	25940.8	-64552.5	51462.4	24255.2	-75717.6	468.0	20	0.050
1191	6957.00	38840.3	26133.5	-64973.8	51788.3	24443.9	-76232.2	470.7	20	0.050
1192	6961.00	39065.4	26325.2	-65390.6	52108.7	24631.6	-76740.3	473.4	20	0.050
1193	6965.00	39286.7	26516.1	-65802.8	52423.6	24818.3	-77241.9	476.1	20	0.050
1194	6969.00	39504.5	26706.0	-66210.5	52733.0	25003.9	-77737.0	478.8	20	0.050
1195	6973.00	39718.6	26895.1	-66613.7	53037.0	25188.6	-78225.6	481.4	20	0.050
1196	6977.00	39929.0	27083.2	-67012.3	53335.4	25372.3	-78707.7	484.1	20	0.050
1197	6981.00	40135.8	27270.5	-67406.3	53628.4	25555.0	-79183.3	486.8	20	0.050
1198	6985.00	40338.9	27456.9	-67795.7	53915.8	25736.7	-79652.5	489.6	20	0.050
1199	6989.00	40538.2	27642.3	-68180.5	54197.8	25917.4	-80115.2	492.3	20	0.050
1200	6993.00	40734.0	27826.8	-68560.7	54474.3	26097.0	-80571.3	495.0	20	0.050
1201	6997.00	40926.0	28010.3	-68936.3	54745.2	26275.8	-81021.0	497.7	20	0.050
1202	7001.00	41114.4	28192.9	-69307.3	55010.9	26453.5	-81464.4	500.4	20	0.050
1203	7005.00	41300.1	28374.3	-69674.4	55272.7	26629.8	-81902.5	503.2	20	0.050
1204	7009.00	41483.4	28554.4	-70037.8	55530.9	26804.8	-82335.7	505.9	20	0.050



Point No.	Time (sec.)	Membrane + Bending Stresses			Total Stresses			Metal Temp. (°F)	No. of Cycles	DO (ppm)
		S' <sub>12</sub> (psi)	S' <sub>23</sub> (psi)	S' <sub>31</sub> (psi)	S' <sub>12</sub> (psi)	S' <sub>23</sub> (psi)	S' <sub>31</sub> (psi)			
1205	7014.00	41708.9	28777.7	-70486.6	55848.5	27021.8	-82870.3	509.3	20	0.050
1206	7019.00	41930.4	28999.1	-70929.5	56160.4	27236.6	-83397.0	512.8	20	0.050
1207	7024.00	42148.1	29218.4	-71366.5	56466.7	27449.4	-83916.1	516.2	20	0.050
1208	7029.00	42360.1	29435.0	-71795.2	56765.1	27659.4	-84424.4	519.6	20	0.050
1209	7034.00	42557.7	29644.6	-72202.3	57043.0	27862.3	-84905.3	523.1	20	0.050
1210	7039.00	42739.1	29846.5	-72585.6	57298.5	28057.6	-85356.1	526.6	20	0.050
1211	7045.00	42935.7	30078.6	-73014.3	57575.4	28281.8	-85857.2	530.8	20	0.050
1212	7053.00	43110.4	30356.8	-73467.2	57680.2	28552.8	-86233.0	535.5	20	0.050
1213	7059.00	42983.8	30490.9	-73474.7	57209.4	28693.2	-85902.6	536.7	20	0.050
1214	7064.00	42804.1	30567.0	-73371.1	56797.4	28775.5	-85572.9	537.5	20	0.050
1215	7069.00	42596.5	30616.9	-73213.4	56396.7	28831.3	-85228.0	538.1	20	0.050
1216	7074.00	42380.8	30646.6	-73027.4	56014.1	28866.2	-84880.4	538.6	20	0.050
1217	7079.00	42164.8	30658.9	-72823.7	55651.4	28883.3	-84534.7	539.0	20	0.050
1218	7085.00	41909.3	30654.0	-72563.3	55241.8	28883.4	-84125.2	539.5	20	0.050
1219	7091.00	41662.9	30631.6	-72294.4	54859.6	28865.4	-83725.0	540.0	20	0.050
1220	7097.00	41426.8	30597.5	-72024.3	54500.6	28835.3	-83335.9	540.4	20	0.050
1221	7103.00	41201.9	30555.2	-71757.1	54162.3	28796.7	-82959.0	540.7	20	0.050
1222	7110.00	40956.1	30497.9	-71454.0	53797.1	28743.2	-82540.3	541.1	20	0.050
1223	7117.00	40731.1	30434.8	-71165.9	53467.3	28683.5	-82150.8	541.5	20	0.050
1224	7125.00	40497.3	30361.2	-70858.5	53127.5	28613.2	-81740.7	541.8	20	0.050
1225	7134.00	40262.9	30279.5	-70542.4	52788.7	28534.9	-81323.6	542.2	20	0.050
1226	7144.00	40037.5	30190.3	-70227.9	52465.7	28448.8	-80914.5	542.5	20	0.050
1227	7152.00	39839.5	30110.6	-69950.1	52074.9	28373.4	-80448.2	542.0	20	0.050
1228	7154.00	39713.2	30069.5	-69782.7	51738.6	28337.6	-80076.1	540.9	20	0.050
1229	7156.00	39554.4	30018.5	-69572.9	51374.0	28293.0	-79666.9	539.7	20	0.050
1230	7158.00	39373.1	29958.9	-69331.9	50998.2	28240.1	-79238.3	538.3	20	0.050
1231	7160.00	39176.2	29891.5	-69067.7	50618.3	28179.8	-78798.1	536.9	20	0.050
1232	7162.00	38969.9	29817.4	-68787.3	50238.8	28112.6	-78351.4	535.5	20	0.050
1233	7164.00	38754.8	29736.6	-68491.4	49860.3	28038.6	-77898.9	534.0	20	0.050
1234	7166.00	38533.9	29649.8	-68183.7	49484.0	27958.3	-77442.3	532.5	20	0.050
1235	7168.00	38308.9	29557.1	-67866.0	49110.8	27872.0	-76982.8	531.0	20	0.050
1236	7170.00	38080.7	29459.1	-67539.7	48740.9	27780.1	-76521.0	529.5	20	0.050
1237	7172.00	37852.2	29356.8	-67209.0	48375.2	27683.9	-76059.0	527.9	20	0.050
1238	7174.00	37624.6	29251.2	-66875.8	48015.0	27584.0	-75599.0	526.3	20	0.050
1239	7176.00	37398.2	29142.3	-66540.5	47660.7	27480.6	-75141.3	524.8	20	0.050
1240	7178.00	37172.9	29030.2	-66203.0	47312.2	27373.8	-74686.0	523.2	20	0.050
1241	7180.00	36948.8	28914.9	-65863.7	46969.6	27263.6	-74233.2	521.6	20	0.050
1242	7182.00	36727.2	28797.2	-65524.3	46632.8	27151.0	-73783.8	519.9	20	0.050
1243	7184.00	36508.0	28677.5	-65185.5	46302.0	27035.9	-73337.9	518.3	20	0.050

Point No.	Time (sec.)	Membrane + Bending Stresses			Total Stresses			Metal Temp. (°F)	No. of Cycles	DO (ppm)
		S' <sub>12</sub> (psi)	S' <sub>23</sub> (psi)	S' <sub>31</sub> (psi)	S' <sub>12</sub> (psi)	S' <sub>23</sub> (psi)	S' <sub>31</sub> (psi)			
1244	7186.00	36291.5	28555.6	-64847.2	45976.8	26918.7	-72895.5	516.7	20	0.050
1245	7188.00	36077.7	28431.7	-64509.4	45657.5	26799.1	-72456.6	515.0	20	0.050
1246	7190.00	35866.4	28305.7	-64172.1	45343.9	26677.3	-72021.3	513.4	20	0.050
1247	7192.00	35657.9	28178.1	-63836.1	45035.8	26553.8	-71589.6	511.7	20	0.050
1248	7194.00	35452.5	28049.8	-63502.3	44732.4	26429.5	-71161.9	510.0	20	0.050
1249	7196.00	35249.9	27920.8	-63170.7	44433.9	26304.2	-70738.1	508.3	20	0.050
1250	7198.00	35050.3	27791.1	-62841.4	44140.2	26178.2	-70318.4	506.7	20	0.050
1251	7200.00	34853.6	27660.7	-62514.3	43851.2	26051.3	-69902.5	505.0	20	0.050
1252	7202.00	34659.6	27529.6	-62189.2	43566.7	25923.6	-69490.3	503.3	20	0.050
1253	7205.00	34373.5	27331.8	-61705.4	43148.1	25730.6	-68878.7	500.7	20	0.050
1254	7208.00	34093.4	27132.6	-61226.0	42739.3	25535.9	-68275.2	498.1	20	0.050
1255	7211.00	33819.3	26931.9	-60751.2	42340.3	25339.5	-67679.8	495.6	20	0.050
1256	7214.00	33551.2	26729.7	-60280.9	41951.1	25141.3	-67092.3	493.0	20	0.050
1257	7217.00	33288.9	26526.3	-59815.2	41571.4	24941.4	-66512.9	490.4	20	0.050
1258	7220.00	33032.1	26322.8	-59354.9	41200.0	24741.4	-65941.4	487.8	20	0.050
1259	7223.00	32780.7	26119.3	-58900.0	40836.5	24541.2	-65377.7	485.1	20	0.050
1260	7226.00	32534.6	25916.0	-58450.6	40481.0	24340.9	-64821.9	482.5	20	0.050
1261	7229.00	32293.9	25712.8	-58006.7	40133.4	24140.5	-64273.9	479.9	20	0.050
1262	7232.00	32058.4	25509.9	-57568.3	39793.7	23939.9	-63733.7	477.2	20	0.050
1263	7235.00	31828.4	25306.9	-57135.3	39461.9	23739.4	-63201.3	474.5	20	0.050
1264	7238.00	31603.6	25104.2	-56707.8	39138.1	23538.7	-62676.8	471.9	20	0.050
1265	7241.00	31384.2	24901.6	-56285.7	38822.2	23338.0	-62160.1	469.2	20	0.050
1266	7244.00	31169.6	24699.4	-55869.0	38513.2	23137.4	-61650.7	466.5	20	0.050
1267	7247.00	30958.8	24498.6	-55457.5	38209.8	22938.1	-61147.9	463.8	20	0.050
1268	7250.00	30752.2	24298.9	-55051.1	37911.8	22739.7	-60651.5	461.1	20	0.050
1269	7253.00	30549.4	24100.3	-54649.8	37619.5	22542.3	-60161.8	458.4	20	0.050
1270	7256.00	30350.7	23902.9	-54253.6	37332.6	22346.0	-59678.5	455.7	20	0.050
1271	7259.00	30155.7	23706.8	-53862.5	37051.1	22150.4	-59201.5	453.0	20	0.050
1272	7262.00	29964.0	23511.7	-53475.7	36774.2	21955.9	-58730.1	450.3	20	0.050
1273	7265.00	29775.8	23317.5	-53093.3	36501.9	21762.3	-58264.2	447.6	20	0.050
1274	7268.00	29590.8	23124.5	-52715.3	36234.1	21569.7	-57803.8	444.8	20	0.050
1275	7271.00	29409.1	22932.6	-52341.7	35971.0	21377.9	-57348.8	442.1	20	0.050
1276	7274.00	29230.7	22741.7	-51972.4	35712.3	21187.0	-56899.3	439.4	20	0.050
1277	7277.00	29055.7	22551.9	-51607.6	35458.3	20997.1	-56455.3	436.6	20	0.050
1278	7280.00	28883.9	22363.1	-51246.9	35208.8	20807.9	-56016.8	433.9	20	0.050
1279	7284.00	28659.9	22113.1	-50773.0	34883.4	20557.2	-55440.5	430.2	20	0.050
1280	7288.00	28441.8	21864.9	-50306.7	34566.0	20308.1	-54874.1	426.6	20	0.050
1281	7292.00	28229.6	21618.6	-49848.1	34256.8	20060.6	-54317.3	422.9	20	0.050
1282	7296.00	28023.2	21374.0	-49397.2	33955.6	19814.7	-53770.4	419.2	20	0.050

Point No.	Time (sec.)	Membrane + Bending Stresses			Total Stresses			Metal Temp. (°F)	No. of Cycles	DO (ppm)
		S' <sub>12</sub> (psi)	S' <sub>23</sub> (psi)	S' <sub>31</sub> (psi)	S' <sub>12</sub> (psi)	S' <sub>23</sub> (psi)	S' <sub>31</sub> (psi)			
1283	7300.00	27822.8	21131.5	-48954.3	33662.9	19570.6	-53233.5	415.5	20	0.050
1284	7304.00	27627.6	20891.5	-48519.1	33377.1	19328.8	-52705.9	411.8	20	0.050
1285	7308.00	27436.9	20653.9	-48090.9	33097.7	19089.1	-52186.8	408.1	20	0.050
1286	7312.00	27250.9	20419.1	-47670.0	32824.4	18852.0	-51676.3	404.4	20	0.050
1287	7316.00	27070.2	20187.5	-47257.7	32558.1	18618.1	-51176.2	400.6	20	0.050
1288	7320.00	26895.0	19959.6	-46854.5	32299.4	18387.4	-50686.8	396.9	20	0.050
1289	7324.00	26725.3	19735.0	-46460.3	32048.0	18160.4	-50208.3	393.2	20	0.050
1290	7328.00	26561.0	19514.1	-46075.1	31804.0	17936.6	-49740.6	389.4	20	0.050
1291	7332.00	26402.2	19296.8	-45699.0	31567.4	17716.5	-49283.9	385.7	20	0.050
1292	7336.00	26248.8	19083.0	-45331.8	31338.3	17499.7	-48838.0	381.9	20	0.050
1293	7341.00	26064.6	18820.6	-44885.2	31062.2	17233.6	-48295.8	377.2	20	0.050
1294	7346.00	25889.0	18563.7	-44452.7	30797.8	16972.9	-47770.7	372.5	20	0.050
1295	7351.00	25729.8	18314.4	-44044.2	30590.9	16719.5	-47310.5	368.0	20	0.050
1296	7356.00	25787.7	18120.5	-43908.2	31037.2	16516.1	-47553.2	366.2	20	0.050
1297	7360.00	25944.0	17998.7	-43942.8	31479.1	16387.6	-47866.8	365.3	20	0.050
1298	7364.00	26139.4	17899.0	-44038.3	31921.0	16283.4	-48204.4	364.5	20	0.050
1299	7368.00	26355.0	17817.9	-44172.9	32351.0	16199.9	-48550.8	363.9	20	0.050
1300	7372.00	26578.0	17752.3	-44330.4	32764.3	16133.4	-48897.7	363.3	20	0.050
1301	7376.00	26799.5	17699.1	-44498.6	33158.7	16080.4	-49239.1	362.8	20	0.050
1302	7380.00	27019.0	17658.2	-44677.2	33534.1	16040.9	-49575.0	362.3	20	0.050
1303	7385.00	27287.8	17623.3	-44911.1	33980.2	16008.5	-49988.7	361.8	20	0.050
1304	7390.00	27548.6	17604.7	-45153.3	34401.9	15993.5	-50395.4	361.3	20	0.050
1305	7395.00	27800.7	17598.6	-45399.3	34801.9	15991.5	-50793.4	360.8	20	0.050
1306	7400.00	28043.1	17600.8	-45643.8	35183.6	15998.0	-51181.6	360.4	20	0.050
1307	7405.00	28276.0	17611.1	-45887.0	35546.9	16012.9	-51559.8	360.0	20	0.050
1308	7410.00	28499.2	17629.7	-46128.9	35891.9	16036.2	-51928.2	359.6	20	0.050
1309	7416.00	28754.5	17662.9	-46417.4	36281.7	16075.2	-52356.9	359.2	20	0.050
1310	7422.00	28997.4	17704.5	-46701.9	36649.0	16122.8	-52771.8	358.8	20	0.050
1311	7428.00	29229.0	17751.8	-46980.7	36997.4	16176.0	-53173.4	358.5	20	0.050
1312	7434.00	29449.3	17804.7	-47254.0	37326.8	16234.6	-53561.4	358.2	20	0.050
1313	7441.00	29692.1	17873.6	-47565.7	37687.1	16310.1	-53997.1	357.8	20	0.050
1314	7448.00	29922.9	17947.5	-47870.4	38027.5	16390.3	-54417.8	357.5	20	0.050
1315	7454.00	30143.1	18019.2	-48162.2	38416.7	16466.4	-54883.1	357.7	20	0.050
1316	7458.00	30329.6	18079.1	-48408.6	38753.7	16528.0	-55281.7	358.2	20	0.050
1317	7462.00	30528.0	18145.9	-48673.9	39090.4	16596.5	-55686.9	358.8	20	0.050
1318	7466.00	30731.1	18218.5	-48949.6	39420.6	16671.4	-56092.0	359.4	20	0.050
1319	7470.00	30935.0	18296.2	-49231.2	39742.9	16751.5	-56494.4	360.0	20	0.050
1320	7474.00	31136.8	18378.1	-49514.9	40056.3	16835.7	-56892.1	360.7	20	0.050
1321	7479.00	31384.3	18485.9	-49870.3	40435.0	16946.7	-57381.8	361.5	20	0.050

Point No.	Time (sec.)	Membrane + Bending Stresses			Total Stresses			Metal Temp. (°F)	No. of Cycles	DO (ppm)
		S' <sub>12</sub> (psi)	S' <sub>23</sub> (psi)	S' <sub>31</sub> (psi)	S' <sub>12</sub> (psi)	S' <sub>23</sub> (psi)	S' <sub>31</sub> (psi)			
1322	7484.00	31625.3	18598.7	-50224.0	40798.4	17062.6	-57861.0	362.4	20	0.050
1323	7489.00	31858.3	18715.3	-50573.6	41146.2	17182.4	-58328.5	363.3	20	0.050
1324	7494.00	32083.0	18835.3	-50918.3	41478.8	17305.2	-58784.0	364.2	20	0.050
1325	7499.00	32299.3	18956.9	-51256.2	41797.2	17429.8	-59227.0	365.1	20	0.050
1326	7504.00	32507.5	19079.6	-51587.2	42102.7	17555.1	-59657.8	366.1	20	0.050
1327	7509.00	32709.4	19203.1	-51912.5	42397.4	17681.1	-60078.4	367.0	20	0.050
1328	7514.00	32904.8	19327.6	-52232.4	42681.4	17807.8	-60489.2	368.0	20	0.050
1329	7520.00	33131.1	19477.6	-52608.7	43008.8	17960.3	-60969.1	369.2	20	0.050
1330	7526.00	33349.5	19628.7	-52978.2	43323.7	18113.6	-61437.3	370.4	20	0.050
1331	7532.00	33560.5	19781.0	-53341.4	43626.7	18268.0	-61894.7	371.6	20	0.050
1332	7538.00	33764.0	19934.5	-53698.5	43917.9	18423.3	-62341.2	372.8	20	0.050
1333	7544.00	33960.1	20089.2	-54049.3	44197.5	18579.4	-62776.9	374.0	20	0.050
1334	7550.00	34149.9	20244.2	-54394.0	44467.1	18735.8	-63202.9	375.3	20	0.050
1335	7557.00	34363.6	20425.1	-54788.7	44769.7	18918.2	-63687.9	376.7	20	0.050
1336	7564.00	34570.6	20606.3	-55176.9	45062.2	19100.3	-64162.5	378.2	20	0.050
1337	7571.00	34770.6	20784.2	-55554.8	45344.1	19279.0	-64623.1	379.7	20	0.050
1338	7578.00	34961.5	20956.5	-55918.0	45613.1	19451.8	-65064.9	381.2	20	0.050
1339	7586.00	35168.1	21146.1	-56314.2	45904.3	19641.6	-65545.8	382.9	20	0.050
1340	7594.00	35365.1	21330.7	-56695.8	46181.2	19826.2	-66007.4	384.7	20	0.050
1341	7602.00	35554.4	21513.0	-57067.5	46446.9	20008.2	-66455.1	386.4	20	0.050
1342	7610.00	35735.8	21691.6	-57427.4	46701.0	20186.4	-66887.5	388.2	20	0.050
1343	7619.00	35930.5	21888.0	-57818.5	46973.7	20381.9	-67355.6	390.2	20	0.050
1344	7628.00	36115.5	22079.3	-58194.8	47232.3	20572.1	-67804.4	392.2	20	0.050
1345	7638.00	36309.6	22286.0	-58595.6	47503.1	20777.5	-68280.6	394.4	20	0.050
1346	7648.00	36491.5	22486.6	-58978.1	47756.6	20976.4	-68733.0	396.7	20	0.050
1347	7689.00	36366.2	22934.3	-59300.5	47251.0	21436.0	-68687.0	398.7	20	0.050
1348	7738.00	36108.9	23096.6	-59205.5	46820.0	21602.6	-68422.7	399.2	20	0.050
1349	7753.00	35949.2	23097.3	-59046.5	46272.3	21609.9	-67882.1	397.3	20	0.050
1350	7755.00	35776.3	23058.5	-58834.7	45777.5	21579.1	-67356.5	395.2	20	0.050
1351	7757.00	35561.6	23006.8	-58568.4	45257.2	21536.2	-66793.4	393.0	20	0.050
1352	7759.00	35317.3	22943.6	-58260.9	44726.8	21482.1	-66208.9	390.7	20	0.050
1353	7761.00	35055.1	22870.7	-57925.8	44196.2	21417.9	-65614.0	388.2	20	0.050
1354	7763.00	34780.0	22788.8	-57568.8	43668.7	21344.4	-65013.0	385.7	20	0.050
1355	7765.00	34493.7	22698.2	-57191.9	43145.2	21261.6	-64406.9	383.2	20	0.050
1356	7767.00	34201.7	22599.9	-56801.6	42628.5	21170.8	-63799.3	380.6	20	0.050
1357	7769.00	33904.7	22494.2	-56398.9	42118.8	21071.9	-63190.6	378.0	20	0.050
1358	7771.00	33606.6	22382.3	-55989.0	41616.6	20966.6	-62583.2	375.3	20	0.050
1359	7773.00	33309.4	22265.0	-55574.5	41122.6	20855.1	-61977.7	372.7	20	0.050
1360	7775.00	33013.1	22142.4	-55155.4	40636.6	20737.9	-61374.5	370.0	20	0.050

Point No.	Time (sec.)	Membrane + Bending Stresses			Total Stresses			Metal Temp. (°F)	No. of Cycles	DO (ppm)
		S' <sub>12</sub> (psi)	S' <sub>23</sub> (psi)	S' <sub>31</sub> (psi)	S' <sub>12</sub> (psi)	S' <sub>23</sub> (psi)	S' <sub>31</sub> (psi)			
1361	7777.00	32717.7	22014.2	-54731.9	40158.7	20614.7	-60773.4	367.3	20	0.050
1362	7779.00	32423.3	21880.4	-54303.7	39688.8	20485.5	-60174.3	364.5	20	0.050
1363	7781.00	32130.4	21741.9	-53872.3	39226.8	20351.0	-59577.8	361.8	20	0.050
1364	7783.00	31840.8	21599.6	-53440.4	38772.6	20212.4	-58984.9	359.0	20	0.050
1365	7785.00	31554.4	21453.3	-53007.7	38326.1	20069.4	-58395.6	356.2	20	0.050
1366	7787.00	31271.1	21303.7	-52574.8	37887.4	19922.5	-57809.9	353.4	20	0.050
1367	7789.00	30991.1	21150.1	-52141.2	37456.4	19771.5	-57227.9	350.6	20	0.050
1368	7791.00	30714.3	20993.1	-51707.4	37033.0	19616.5	-56649.5	347.8	20	0.050
1369	7793.00	30441.2	20834.3	-51275.5	36616.0	19459.3	-56075.3	345.0	20	0.050
1370	7795.00	30171.7	20674.1	-50845.8	36205.1	19300.4	-55505.5	342.1	20	0.050
1371	7797.00	29906.3	20512.7	-50419.0	35800.6	19140.1	-54940.7	339.3	20	0.050
1372	7799.00	29644.7	20350.2	-49995.0	35402.8	18978.2	-54381.0	336.4	20	0.050
1373	7801.00	29387.3	20186.6	-49573.9	35011.3	18815.0	-53826.2	333.6	20	0.050
1374	7803.00	29133.7	20022.0	-49155.7	34626.3	18650.3	-53276.6	330.7	20	0.050
1375	7805.00	28884.1	19856.2	-48740.4	34247.6	18484.4	-52732.0	327.8	20	0.050
1376	7807.00	28638.4	19689.3	-48327.7	33875.2	18316.9	-52192.1	324.9	20	0.050
1377	7809.00	28396.6	19521.3	-47917.9	33509.2	18147.9	-51657.1	322.0	20	0.050
1378	7811.00	28158.7	19352.2	-47510.9	33149.4	17977.6	-51126.9	319.1	20	0.050
1379	7813.00	27924.6	19182.0	-47106.6	32795.9	17805.7	-50601.7	316.2	20	0.050
1380	7815.00	27694.5	19010.7	-46705.2	32448.8	17632.5	-50081.3	313.3	20	0.050
1381	7817.00	27468.1	18838.7	-46306.7	32107.7	17458.0	-49565.7	310.3	20	0.050
1382	7819.00	27245.3	18666.4	-45911.6	31771.6	17283.1	-49054.8	307.4	20	0.050
1383	7821.00	27025.8	18494.3	-45520.0	31440.5	17108.1	-48548.6	304.4	20	0.050
1384	7823.00	26809.8	18322.2	-45132.0	31114.2	16932.9	-48047.2	301.5	20	0.050
1385	7825.00	26597.3	18150.1	-44747.4	30793.0	16757.3	-47550.3	298.5	20	0.050
1386	7827.00	26388.1	17978.2	-44366.3	30476.7	16581.5	-47058.2	295.6	20	0.050
1387	7829.00	26182.5	17806.2	-43988.7	30165.4	16405.5	-46570.8	292.6	20	0.050
1388	7831.00	25980.4	17634.3	-43614.6	29858.9	16229.3	-46088.2	289.6	20	0.050
1389	7833.00	25781.5	17462.5	-43244.0	29557.4	16052.7	-45610.1	286.7	20	0.050
1390	7835.00	25586.2	17290.6	-42876.8	29260.9	15875.9	-45136.8	283.7	20	0.050
1391	7837.00	25394.4	17118.9	-42513.3	28969.4	15698.8	-44668.2	280.7	20	0.050
1392	7839.00	25206.0	16947.2	-42153.2	28682.8	15521.5	-44204.3	277.7	20	0.050
1393	7841.00	25021.0	16775.5	-41796.6	28401.1	15344.0	-43745.1	274.7	20	0.050
1394	7843.00	24839.2	16604.2	-41443.5	28123.7	15166.5	-43290.2	271.7	20	0.050
1395	7845.00	24659.8	16433.9	-41093.6	27849.5	14989.6	-42839.0	268.7	20	0.050
1396	7847.00	24482.9	16264.1	-40747.0	27578.5	14813.2	-42391.7	265.7	20	0.050
1397	7849.00	24308.4	16095.4	-40403.8	27310.7	14637.3	-41948.0	262.7	20	0.050
1398	7851.00	24136.4	15927.5	-40063.9	27046.0	14462.2	-41508.1	259.6	20	0.050
1399	7853.00	23966.9	15760.4	-39727.2	26784.6	14287.4	-41072.0	256.6	20	0.050

Point No.	Time (sec.)	Membrane + Bending Stresses			Total Stresses			Metal Temp. (°F)	No. of Cycles	DO (ppm)
		S' <sub>12</sub> (psi)	S' <sub>23</sub> (psi)	S' <sub>31</sub> (psi)	S' <sub>12</sub> (psi)	S' <sub>23</sub> (psi)	S' <sub>31</sub> (psi)			
1400	7855.00	23799.7	15594.2	-39393.9	26526.3	14113.3	-40639.6	253.6	20	0.050
1401	7857.00	23635.1	15428.7	-39063.8	26271.2	13939.8	-40210.9	250.6	20	0.050
1402	7860.00	23392.6	15182.3	-38574.9	25894.3	13680.4	-39574.7	246.0	20	0.050
1403	7863.00	23155.5	14937.6	-38093.1	25524.3	13422.2	-38946.6	241.5	20	0.050
1404	7866.00	22923.7	14694.8	-37618.5	25161.2	13165.4	-38326.6	236.9	20	0.050
1405	7869.00	22697.3	14453.8	-37151.2	24804.9	12909.7	-37714.6	232.3	20	0.050
1406	7872.00	22476.2	14214.9	-36691.0	24455.3	12655.3	-37110.6	227.8	20	0.050
1407	7875.00	22260.5	13977.6	-36238.1	24112.7	12402.1	-36514.8	223.2	20	0.050
1408	7878.00	22050.0	13742.4	-35792.4	23777.0	12150.1	-35927.0	218.6	20	0.050
1409	7881.00	21845.0	13508.9	-35353.9	23448.0	11899.3	-35347.3	214.0	20	0.050
1410	7884.00	21645.2	13277.4	-34922.6	23125.9	11649.8	-34775.7	209.4	20	0.050
1411	7887.00	21450.8	13047.9	-34498.6	22810.6	11401.5	-34212.2	204.8	20	0.050
1412	7890.00	21261.7	12820.1	-34081.8	22502.3	11154.3	-33656.7	200.2	20	0.050
1413	7893.00	21077.9	12594.1	-33672.1	22200.7	10908.6	-33109.3	195.6	20	0.050
1414	7896.00	20899.5	12370.1	-33269.6	21906.0	10663.9	-32569.9	190.9	20	0.050
1415	7899.00	20726.4	12148.0	-32874.4	21618.2	10420.5	-32038.7	186.3	20	0.050
1416	7902.00	20558.1	11927.8	-32485.9	21336.3	10178.6	-31514.9	181.6	20	0.050
1417	7905.00	20393.7	11710.2	-32103.9	21059.1	9938.4	-30997.5	177.0	20	0.050
1418	7908.00	20233.3	11494.9	-31728.3	20786.4	9699.9	-30486.4	172.3	20	0.050
1419	7911.00	20077.0	11281.9	-31358.9	20518.5	9463.0	-29981.5	167.7	20	0.050
1420	7914.00	19924.5	11071.3	-30995.8	20255.2	9227.9	-29483.1	163.0	20	0.050
1421	7917.00	19776.0	10862.9	-30638.9	19996.4	8994.4	-28990.8	158.4	20	0.050
1422	7920.00	19631.4	10656.9	-30288.2	19742.2	8762.5	-28504.8	153.7	20	0.050
1423	7923.00	19490.7	10453.1	-29943.8	19492.6	8532.4	-28025.0	149.0	20	0.050
1424	7926.00	19353.9	10251.8	-29605.7	19247.7	8303.8	-27551.5	144.4	20	0.050
1425	7929.00	19221.1	10052.8	-29273.8	19007.4	8077.0	-27084.4	139.7	20	0.050
1426	7932.00	19092.1	9856.0	-28948.1	18771.6	7851.8	-26623.4	135.0	20	0.050
1427	7935.00	18967.2	9661.5	-28628.7	18540.5	7628.3	-26168.9	130.3	20	0.050
1428	7938.00	18846.1	9469.7	-28315.8	18314.2	7406.7	-25720.9	125.6	20	0.050
1429	7942.00	18691.0	9217.5	-27908.5	18019.8	7114.1	-25133.9	119.3	20	0.050
1430	7946.00	18542.9	8969.6	-27512.5	17733.9	6824.8	-24558.7	113.1	20	0.050
1431	7950.00	18401.8	8726.2	-27128.0	17456.4	6538.9	-23995.3	106.8	20	0.050
1432	7955.00	18482.6	8467.2	-26949.8	18078.2	6243.2	-24321.4	103.0	20	0.050
1433	7958.00	18671.8	8338.2	-27010.0	18653.6	6107.5	-24761.1	101.7	20	0.050
1434	7960.00	18826.6	8261.3	-27087.9	19047.7	6031.7	-25079.4	101.0	20	0.050
1435	7962.00	18993.3	8191.4	-27184.8	19440.8	5966.0	-25406.8	100.3	20	0.050
1436	7964.00	19171.1	8128.7	-27299.9	19832.0	5910.6	-25742.6	99.7	20	0.050
1437	7966.00	19355.9	8072.7	-27428.6	20219.1	5864.4	-26083.5	99.1	20	0.050
1438	7968.00	19545.2	8023.5	-27568.7	20600.6	5827.1	-26427.7	98.6	20	0.050

Point No.	Time (sec.)	Membrane + Bending Stresses			Total Stresses			Metal Temp. (°F)	No. of Cycles	DO (ppm)
		S' <sub>12</sub> (psi)	S' <sub>23</sub> (psi)	S' <sub>31</sub> (psi)	S' <sub>12</sub> (psi)	S' <sub>23</sub> (psi)	S' <sub>31</sub> (psi)			
1439	7970.00	19738.0	7980.7	-27718.7	20976.3	5798.1	-26774.5	98.1	20	0.050
1440	7972.00	19930.5	7943.4	-27873.9	21345.3	5775.5	-27120.8	97.6	20	0.050
1441	7974.00	20122.6	7911.7	-28034.3	21707.4	5759.5	-27466.9	97.1	20	0.050
1442	7977.00	20409.8	7874.5	-28284.2	22237.7	5747.3	-27985.0	96.4	20	0.050
1443	7980.00	20695.8	7849.7	-28545.4	22752.1	5749.2	-28501.4	95.8	20	0.050
1444	7983.00	20978.0	7835.1	-28813.1	23251.2	5762.2	-29013.4	95.2	20	0.050
1445	7986.00	21255.0	7830.0	-29085.0	23734.9	5785.0	-29520.0	94.7	20	0.050
1446	7989.00	21527.0	7834.2	-29361.2	24203.3	5817.4	-30020.7	94.2	20	0.050
1447	7992.00	21793.7	7847.0	-29640.7	24656.9	5858.3	-30515.2	93.7	20	0.050
1448	7995.00	22055.1	7865.1	-29920.1	25098.5	5903.9	-31002.4	93.2	20	0.050
1449	7998.00	22310.8	7888.2	-30199.1	25528.3	5953.8	-31482.1	92.7	20	0.050
1450	8001.00	22561.1	7916.3	-30477.4	25946.4	6008.0	-31954.4	92.3	20	0.050
1451	8004.00	22805.8	7949.5	-30755.3	26352.8	6066.7	-32419.6	91.8	20	0.050
1452	8007.00	23045.2	7988.1	-31033.2	26748.0	6130.2	-32878.1	91.4	20	0.050
1453	8010.00	23279.3	8031.9	-31311.2	27131.8	6198.4	-33330.3	91.0	20	0.050
1454	8013.00	23508.1	8081.1	-31589.1	27504.4	6271.6	-33776.0	90.7	20	0.050
1455	8016.00	23731.4	8135.5	-31866.9	27865.6	6349.5	-34215.1	90.3	20	0.050
1456	8019.00	23950.0	8193.7	-32143.7	28217.3	6430.4	-34647.7	89.9	20	0.050
1457	8022.00	24164.2	8254.8	-32419.1	28560.7	6513.4	-35074.1	89.6	20	0.050
1458	8025.00	24374.2	8318.5	-32692.8	28895.9	6598.3	-35494.2	89.3	20	0.050
1459	8028.00	24579.9	8384.8	-32964.7	29222.7	6685.5	-35908.2	89.0	20	0.050
1460	8031.00	24781.1	8454.0	-33235.1	29541.2	6774.6	-36315.8	88.6	20	0.050
1461	8034.00	24978.0	8525.7	-33503.7	29851.4	6865.7	-36717.1	88.3	20	0.050
1462	8038.00	25233.6	8625.3	-33858.9	30252.2	6990.3	-37242.5	88.0	20	0.050
1463	8042.00	25481.3	8729.5	-34210.9	30638.3	7118.4	-37756.8	87.6	20	0.050
1464	8046.00	25723.7	8836.1	-34559.8	31014.4	7248.1	-38262.5	87.2	20	0.050
1465	8050.00	25961.9	8944.3	-34906.2	31382.7	7378.1	-38760.8	86.9	20	0.050
1466	8053.00	26175.7	9034.5	-35210.2	31818.5	7484.2	-39302.7	87.4	20	0.050
1467	8055.00	26347.3	9101.8	-35449.1	32166.1	7561.6	-39727.7	87.9	20	0.050
1468	8057.00	26531.8	9173.0	-35704.8	32520.8	7643.3	-40164.1	88.5	20	0.050
1469	8059.00	26725.1	9248.2	-35973.3	32877.0	7729.2	-40606.2	89.2	20	0.050
1470	8061.00	26923.5	9326.7	-36250.2	33231.7	7818.5	-41050.2	89.9	20	0.050
1471	8063.00	27125.1	9408.6	-36533.7	33583.4	7911.2	-41494.6	90.6	20	0.050
1472	8065.00	27329.5	9493.8	-36823.3	33931.8	8007.3	-41939.1	91.3	20	0.050
1473	8067.00	27535.0	9581.8	-37116.8	34276.0	8106.2	-42382.3	92.1	20	0.050
1474	8069.00	27741.3	9672.8	-37414.1	34616.0	8208.1	-42824.1	92.9	20	0.050
1475	8071.00	27946.9	9766.4	-37713.3	34951.5	8312.3	-43263.7	93.6	20	0.050
1476	8073.00	28151.4	9862.2	-38013.5	35282.1	8418.6	-43700.8	94.4	20	0.050
1477	8075.00	28354.6	9960.3	-38314.9	35608.1	8527.0	-44135.1	95.2	20	0.050

Point No.	Time (sec.)	Membrane + Bending Stresses			Total Stresses			Metal Temp. (°F)	No. of Cycles	DO (ppm)
		S' <sub>12</sub> (psi)	S' <sub>23</sub> (psi)	S' <sub>31</sub> (psi)	S' <sub>12</sub> (psi)	S' <sub>23</sub> (psi)	S' <sub>31</sub> (psi)			
1478	8077.00	28556.6	10060.6	-38617.2	35929.3	8637.5	-44566.8	96.0	20	0.050
1479	8079.00	28757.2	10163.1	-38920.3	36245.4	8749.9	-44995.3	96.8	20	0.050
1480	8081.00	28956.0	10267.7	-39223.6	36556.5	8864.1	-45420.5	97.7	20	0.050
1481	8083.00	29152.6	10373.7	-39526.2	36862.4	8979.4	-45841.9	98.5	20	0.050
1482	8085.00	29346.8	10481.4	-39828.2	37163.3	9096.2	-46259.5	99.3	20	0.050
1483	8087.00	29538.9	10590.4	-40129.2	37459.1	9214.1	-46673.2	100.2	20	0.050
1484	8089.00	29728.5	10701.2	-40429.7	37749.9	9333.3	-47083.2	101.0	20	0.050
1485	8092.00	30008.7	10869.8	-40878.4	38176.6	9514.2	-47690.9	102.3	20	0.050
1486	8095.00	30283.3	11040.3	-41323.6	38593.2	9696.3	-48289.5	103.6	20	0.050
1487	8098.00	30552.4	11212.4	-41764.8	38999.7	9879.3	-48879.0	105.0	20	0.050
1488	8101.00	30816.0	11386.2	-42202.1	39396.2	10063.3	-49459.6	106.3	20	0.050
1489	8104.00	31075.2	11561.1	-42636.3	39784.7	10247.8	-50032.5	107.6	20	0.050
1490	8107.00	31330.2	11737.0	-43067.3	40165.2	10432.9	-50598.1	109.0	20	0.050
1491	8110.00	31580.9	11914.2	-43495.1	40538.0	10618.5	-51156.5	110.3	20	0.050
1492	8113.00	31827.4	12092.3	-43919.7	40902.6	10804.9	-51707.5	111.7	20	0.050
1493	8116.00	32069.4	12271.7	-44341.1	41259.5	10991.7	-52251.2	113.1	20	0.050
1494	8119.00	32307.3	12451.5	-44758.8	41609.1	11178.6	-52787.6	114.5	20	0.050
1495	8122.00	32541.1	12631.4	-45172.5	41951.8	11365.0	-53316.8	115.9	20	0.050
1496	8125.00	32770.8	12811.4	-45582.2	42287.7	11551.0	-53838.7	117.3	20	0.050
1497	8128.00	32996.6	12991.3	-45987.9	42616.6	11736.8	-54353.4	118.7	20	0.050
1498	8131.00	33218.1	13171.4	-46389.5	42938.8	11922.0	-54860.8	120.1	20	0.050
1499	8134.00	33435.5	13351.5	-46787.0	43254.0	12107.0	-55361.0	121.5	20	0.050
1500	8137.00	33648.7	13531.5	-47180.2	43562.4	12291.4	-55853.8	122.9	20	0.050
1501	8140.00	33857.8	13711.6	-47569.4	43864.1	12475.5	-56339.6	124.4	20	0.050
1502	8143.00	34062.9	13891.4	-47954.3	44159.0	12659.2	-56818.3	125.8	20	0.050
1503	8146.00	34264.4	14070.8	-48335.2	44448.4	12842.1	-57290.4	127.3	20	0.050
1504	8149.00	34462.6	14249.6	-48712.2	44732.4	13023.9	-57756.3	128.7	20	0.050
1505	8152.00	34657.4	14427.7	-49085.1	45011.0	13204.9	-58215.9	130.2	20	0.050
1506	8155.00	34848.6	14605.3	-49453.9	45284.1	13385.0	-58669.1	131.7	20	0.050
1507	8158.00	35036.6	14782.2	-49818.8	45552.0	13564.0	-59116.1	133.1	20	0.050
1508	8161.00	35222.2	14958.6	-50180.8	45816.1	13742.4	-59558.5	134.6	20	0.050
1509	8164.00	35405.6	15134.6	-50540.2	46076.8	13920.1	-59996.8	136.1	20	0.050
1510	8167.00	35587.1	15310.0	-50897.1	46334.1	14097.1	-60431.2	137.6	20	0.050
1511	8170.00	35766.5	15485.0	-51251.5	46588.2	14273.3	-60861.5	139.1	20	0.050
1512	8174.00	36002.3	15717.5	-51719.9	46921.8	14507.2	-61429.0	141.0	20	0.050
1513	8178.00	36234.4	15949.3	-52183.7	47249.4	14739.9	-61989.4	143.0	20	0.050
1514	8182.00	36462.8	16180.0	-52642.8	47571.1	14971.4	-62542.5	145.0	20	0.050
1515	8186.00	36687.4	16409.7	-53097.1	47886.9	15201.4	-63088.3	147.0	20	0.050
1516	8190.00	36907.9	16638.2	-53546.1	48196.4	15429.8	-63626.2	149.1	20	0.050



Point No.	Time (sec.)	Membrane + Bending Stresses			Total Stresses			Metal Temp. (°F)	No. of Cycles	DO (ppm)
		S' <sub>12</sub> (psi)	S' <sub>23</sub> (psi)	S' <sub>31</sub> (psi)	S' <sub>12</sub> (psi)	S' <sub>23</sub> (psi)	S' <sub>31</sub> (psi)			
1517	8196.00	37147.9	16791.1	-53938.9	48540.5	15584.7	-64125.2	152.2	20	0.050
1518	8200.00	37361.6	17024.4	-54386.0	48839.0	15817.4	-64656.4	154.2	20	0.050
1519	8204.00	37570.9	17255.5	-54826.3	49130.8	16047.5	-65178.2	156.2	20	0.050
1520	8208.00	37775.9	17483.8	-55259.7	49416.4	16274.7	-65691.0	158.2	20	0.050
1521	8212.00	37976.9	17709.7	-55686.6	49695.9	16499.2	-66195.1	160.3	20	0.050
1522	8216.00	38173.9	17933.7	-56107.6	49969.8	16721.5	-66691.3	162.3	20	0.050
1523	8220.00	38367.2	18155.8	-56522.9	50237.9	16941.7	-67179.6	164.4	20	0.050
1524	8224.00	38556.5	18375.7	-56932.2	50500.4	17159.5	-67659.9	166.4	20	0.050
1525	8228.00	38741.9	18593.6	-57335.5	50757.1	17375.1	-68132.2	168.5	20	0.050
1526	8232.00	38923.3	18809.4	-57732.7	51008.1	17588.4	-68596.5	170.6	20	0.050
1527	8236.00	39100.8	19023.0	-58123.9	51253.3	17799.5	-69052.7	172.6	20	0.050
1528	8240.00	39274.4	19234.6	-58509.0	51492.8	18008.2	-69500.9	174.7	20	0.050
1529	8245.00	39485.7	19496.0	-58981.6	51784.0	18265.9	-70049.9	177.3	20	0.050
1530	8250.00	39690.8	19754.1	-59444.9	52066.3	18520.1	-70586.3	179.9	20	0.050
1531	8255.00	39889.6	20008.8	-59898.4	52339.6	18770.6	-71110.2	182.5	20	0.050
1532	8260.00	40082.4	20260.2	-60342.5	52604.2	19017.7	-71621.9	185.1	20	0.050
1533	8265.00	40270.2	20508.3	-60778.5	52861.7	19261.4	-72123.1	187.8	20	0.050
1534	8270.00	40453.0	20753.4	-61206.4	53112.2	19501.8	-72614.0	190.4	20	0.050
1535	8275.00	40630.9	20995.1	-61626.1	53355.8	19738.8	-73094.6	193.0	20	0.050
1536	8280.00	40804.4	21234.0	-62038.4	53593.1	19972.7	-73565.8	195.7	20	0.050
1537	8285.00	40974.8	21470.5	-62445.3	53826.1	20204.2	-74030.3	198.3	20	0.050
1538	8290.00	41142.2	21704.6	-62846.9	54054.8	20433.2	-74488.1	201.0	20	0.050
1539	8295.00	41306.7	21936.5	-63243.2	54279.4	20659.9	-74939.3	203.7	20	0.050
1540	8301.00	41500.0	22211.7	-63711.7	54543.4	20928.6	-75472.0	206.9	20	0.050
1541	8307.00	41689.0	22483.5	-64172.5	54801.3	21193.9	-75995.2	210.1	20	0.050
1542	8313.00	41873.5	22751.8	-64625.3	55053.0	21455.5	-76508.5	213.3	20	0.050
1543	8319.00	42053.6	23016.6	-65070.3	55298.5	21713.6	-77012.1	216.5	20	0.050
1544	8325.00	42229.3	23278.0	-65507.3	55537.9	21968.2	-77506.1	219.7	20	0.050
1545	8331.00	42400.5	23536.0	-65936.5	55771.1	22219.2	-77990.2	222.9	20	0.050
1546	8337.00	42567.1	23790.4	-66357.5	55998.1	22466.5	-78464.6	226.1	20	0.050
1547	8343.00	42729.3	24041.2	-66770.5	56218.9	22710.3	-78929.2	229.4	20	0.050
1548	8349.00	42886.9	24288.6	-67175.5	56433.6	22950.4	-79383.9	232.6	20	0.050
1549	8356.00	43065.2	24572.7	-67637.9	56676.1	23226.2	-79902.3	236.4	20	0.050
1550	8363.00	43237.3	24852.1	-68089.3	56910.3	23497.1	-80407.4	240.2	20	0.050
1551	8370.00	43403.2	25126.5	-68529.8	57136.1	23763.1	-80899.2	243.9	20	0.050
1552	8377.00	43563.0	25396.3	-68959.2	57353.5	24024.2	-81377.7	247.7	20	0.050
1553	8384.00	43717.3	25661.5	-69378.8	57563.6	24280.8	-81844.4	251.6	20	0.050
1554	8391.00	43866.9	25922.6	-69789.5	57767.2	24533.2	-82300.4	255.4	20	0.050
1555	8399.00	44031.9	26215.6	-70247.5	57992.0	24816.3	-82808.3	259.7	20	0.050

Point No.	Time (sec.)	Membrane + Bending Stresses			Total Stresses			Metal Temp. (°F)	No. of Cycles	DO (ppm)
		S' <sub>12</sub> (psi)	S' <sub>23</sub> (psi)	S' <sub>31</sub> (psi)	S' <sub>12</sub> (psi)	S' <sub>23</sub> (psi)	S' <sub>31</sub> (psi)			
1556	8407.00	44193.0	26504.2	-70697.2	58211.5	25095.1	-83306.5	264.1	20	0.050
1557	8415.00	44349.5	26787.9	-71137.3	58424.8	25368.8	-83793.6	268.5	20	0.050
1558	8419.00	44498.4	27087.9	-71586.3	58620.7	25659.7	-84280.4	270.6	20	0.050
1559	8428.00	44659.6	27383.5	-72043.0	58841.5	25944.4	-84785.9	275.5	20	0.050
1560	8437.00	44815.4	27673.6	-72489.0	59055.2	26223.8	-85279.1	280.5	20	0.050
1561	8446.00	44965.9	27958.3	-72924.2	59261.8	26497.8	-85759.6	285.4	20	0.050
1562	8461.00	44857.1	28321.6	-73178.7	58713.7	26860.7	-85574.4	289.8	20	0.050
1563	8467.00	44651.9	28399.4	-73051.2	58301.1	26943.3	-85244.4	290.4	20	0.050
1564	8473.00	44429.2	28451.4	-72880.6	57906.2	26999.7	-84906.0	290.9	20	0.050
1565	8479.00	44205.6	28483.4	-72689.0	57533.2	27035.6	-84568.9	291.4	20	0.050
1566	8486.00	43948.5	28499.4	-72448.0	57125.5	27055.4	-84180.9	291.9	20	0.050
1567	8493.00	43701.2	28497.2	-72198.4	56746.0	27056.5	-83802.5	292.3	20	0.050
1568	8500.00	43465.3	28484.2	-71949.5	56389.9	27046.4	-83436.3	292.7	20	0.050
1569	8508.00	43211.3	28459.0	-71670.3	56011.1	27024.0	-83035.1	293.1	20	0.050
1570	8516.00	42973.9	28422.7	-71396.5	55662.7	26990.1	-82652.7	293.4	20	0.050
1571	8525.00	42724.9	28372.8	-71097.8	55301.6	26942.5	-82244.1	293.8	20	0.050
1572	8534.00	42493.9	28317.2	-70811.1	54969.3	26888.7	-81858.0	294.1	20	0.050
1573	8544.00	42257.8	28248.8	-70506.6	54632.9	26822.0	-81454.9	294.5	20	0.050
1574	8555.00	42016.1	28170.9	-70187.0	54290.3	26745.7	-81036.0	294.8	20	0.050
1575	8566.00	41790.5	28092.5	-69882.9	53971.9	26668.6	-80640.4	295.1	20	0.050
1576	8578.00	41562.8	28006.2	-69569.0	53651.9	26583.4	-80235.3	295.4	20	0.050
1577	8591.00	41337.8	27912.0	-69249.8	53337.6	26490.1	-79827.7	295.7	20	0.050
1578	8605.00	41119.7	27809.9	-68929.6	53035.3	26388.6	-79424.0	295.9	20	0.050
1579	8621.00	40894.2	27698.1	-68592.3	52724.0	26277.3	-79001.3	296.2	20	0.050
1580	8638.00	40679.8	27585.5	-68265.3	52429.3	26164.9	-78594.2	296.5	20	0.050
1581	8658.00	40460.9	27461.0	-67921.9	52130.3	26040.4	-78170.7	296.7	20	0.050
1582	8680.00	40247.7	27333.2	-67580.9	51840.6	25912.3	-77752.9	296.9	20	0.050
1583	8704.00	40035.1	27202.8	-67237.9	51552.3	25781.5	-77333.9	297.2	20	0.050
1584	8731.00	39824.2	27070.7	-66894.9	51267.3	25648.8	-76916.1	297.4	20	0.050
1585	8761.00	39618.8	26924.6	-66543.4	50991.7	25502.3	-76494.0	297.6	20	0.050
1586	8803.00	39407.8	26794.4	-66202.3	50709.6	25370.4	-76080.0	297.8	20	0.050
1587	8854.00	39197.5	26660.4	-65857.9	50429.9	25234.4	-75664.3	298.1	20	0.050
1588	8926.00	38986.2	26522.5	-65508.7	50151.5	25094.2	-75245.6	298.3	20	0.050
1589	9012.00	38780.3	26372.3	-65152.6	49882.2	24942.2	-74824.4	298.5	20	0.050
1590	9114.00	38585.3	26191.0	-64776.3	49629.6	24760.5	-74390.1	298.6	20	0.050
1591	9223.00	38406.7	25975.1	-64381.8	49400.1	24546.2	-73946.3	298.8	20	0.050
1592	9377.00	38233.1	25747.8	-63980.9	49178.1	24321.2	-73499.3	299.0	20	0.050
1593	9668.00	38063.5	25510.6	-63574.1	48962.3	24087.0	-73049.2	299.1	20	0.050
1594	9796.00	37922.9	25219.4	-63142.2	48782.4	23801.4	-72583.8	299.3	20	0.050

Point No.	Time (sec.)	Membrane + Bending Stresses			Total Stresses			Metal Temp. (°F)	No. of Cycles	DO (ppm)
		S' <sub>12</sub> (psi)	S' <sub>23</sub> (psi)	S' <sub>31</sub> (psi)	S' <sub>12</sub> (psi)	S' <sub>23</sub> (psi)	S' <sub>31</sub> (psi)			
1595	9969.00	37784.9	24923.6	-62708.5	48605.8	23511.4	-72117.1	299.4	20	0.050
1596	9971.00	48988.8	27018.6	-76007.5	60187.0	25621.8	-85808.9	70.0	100	0.550
1597	9973.00	48988.8	27018.6	-76007.5	60187.0	25621.8	-85808.9	70.0	100	0.550
1598	9974.67	48988.8	27018.6	-76007.5	60187.0	25621.8	-85808.9	70.0	100	0.550
1599	9976.33	48988.8	27018.6	-76007.5	60187.0	25621.8	-85808.9	70.0	100	0.550
1600	9979.67	48988.8	27018.6	-76007.5	60187.0	25621.8	-85808.9	70.0	100	0.550
1601	9983.00	48988.8	27018.6	-76007.5	60187.0	25621.8	-85808.9	70.0	100	0.550
1602	9986.33	48988.8	27018.6	-76007.5	60187.0	25621.8	-85808.9	70.0	100	0.550
1603	9989.67	48988.8	27018.6	-76007.5	60187.0	25621.8	-85808.9	70.0	100	0.550
1604	9993.00	48988.8	27018.6	-76007.5	60187.0	25621.8	-85808.9	70.0	100	0.550
1605	9996.33	48988.8	27018.6	-76007.5	60187.0	25621.8	-85808.9	70.0	100	0.550
1606	9999.67	48988.8	27018.6	-76007.5	60187.0	25621.8	-85808.9	70.0	100	0.550
1607	10003.00	48988.8	27018.6	-76007.5	60187.0	25621.8	-85808.9	70.0	100	0.550
1608	10006.33	48988.8	27018.6	-76007.5	60187.0	25621.8	-85808.9	70.0	100	0.550
1609	10009.67	48988.8	27018.6	-76007.5	60187.0	25621.8	-85808.9	70.0	100	0.550
1610	10013.00	48988.8	27018.6	-76007.5	60187.0	25621.8	-85808.9	70.0	100	0.550
1611	10016.33	48988.8	27018.6	-76007.5	60187.0	25621.8	-85808.9	70.0	100	0.550
1612	10018.67	48988.8	27018.6	-76007.5	60187.0	25621.8	-85808.9	70.0	100	0.550
1613	10021.00	48988.8	27018.6	-76007.5	60187.0	25621.8	-85808.9	70.0	100	0.550
1614	10023.00	48988.8	27018.6	-76007.5	60187.0	25621.8	-85808.9	70.0	100	0.550
1615	10024.67	48988.8	27018.6	-76007.5	60187.0	25621.8	-85808.9	70.0	100	0.550
1616	10026.33	48988.8	27018.6	-76007.5	60187.0	25621.8	-85808.9	70.0	100	0.550
1617	10029.67	48988.8	27018.6	-76007.5	60187.0	25621.8	-85808.9	70.0	100	0.550
1618	10033.00	48988.8	27018.6	-76007.5	60187.0	25621.8	-85808.9	70.0	100	0.550
1619	10036.33	48988.8	27018.6	-76007.5	60187.0	25621.8	-85808.9	70.0	100	0.550
1620	10039.67	48988.8	27018.6	-76007.5	60187.0	25621.8	-85808.9	70.0	100	0.550
1621	10043.00	48988.8	27018.6	-76007.5	60187.0	25621.8	-85808.9	70.0	100	0.550
1622	10046.33	48988.8	27018.6	-76007.5	60187.0	25621.8	-85808.9	70.0	100	0.550
1623	10049.67	48988.8	27018.6	-76007.5	60187.0	25621.8	-85808.9	70.0	100	0.550
1624	10053.00	48988.8	27018.6	-76007.5	60187.0	25621.8	-85808.9	70.0	100	0.550
1625	10056.33	48988.8	27018.6	-76007.5	60187.0	25621.8	-85808.9	70.0	100	0.550
1626	10059.67	48988.8	27018.6	-76007.5	60187.0	25621.8	-85808.9	70.0	100	0.550
1627	10063.00	48988.8	27018.6	-76007.5	60187.0	25621.8	-85808.9	70.0	100	0.550
1628	10066.33	48988.8	27018.6	-76007.5	60187.0	25621.8	-85808.9	70.0	100	0.550
1629	10068.67	48988.8	27018.6	-76007.5	60187.0	25621.8	-85808.9	70.0	100	0.550
1630	10071.00	48988.8	27018.6	-76007.5	60187.0	25621.8	-85808.9	70.0	100	0.550
1631	10119.00	49078.2	27061.5	-76139.7	60322.2	25661.0	-85983.2	71.1	100	0.549
1632	10159.00	49140.3	27107.2	-76247.5	60404.9	25703.4	-86108.3	72.1	100	0.547
1633	10199.00	49186.1	27152.1	-76338.2	60463.9	25745.2	-86209.1	73.1	100	0.546

Point No.	Time (sec.)	Membrane + Bending Stresses			Total Stresses			Metal Temp. (°F)	No. of Cycles	DO (ppm)
		S' <sub>12</sub> (psi)	S' <sub>23</sub> (psi)	S' <sub>31</sub> (psi)	S' <sub>12</sub> (psi)	S' <sub>23</sub> (psi)	S' <sub>31</sub> (psi)			
1634	10239.00	49219.0	27192.5	-76411.5	60506.2	25782.8	-86288.9	74.2	100	0.545
1635	10279.00	49242.0	27227.4	-76469.5	60536.2	25814.9	-86351.0	75.3	100	0.544
1636	10319.00	49257.4	27256.9	-76514.3	60556.9	25841.8	-86398.8	76.3	100	0.543
1637	10359.00	49266.9	27281.2	-76548.1	60570.6	25863.9	-86434.4	77.4	100	0.541
1638	10399.00	49271.5	27301.0	-76572.5	60578.6	25881.6	-86460.2	78.5	100	0.540
1639	10439.00	49272.2	27316.8	-76589.0	60582.2	25895.3	-86477.5	79.6	100	0.539
1640	10479.00	49269.8	27328.9	-76598.7	60582.0	25905.7	-86487.7	80.7	100	0.538
1641	10519.00	49264.6	27337.8	-76602.5	60578.9	25912.9	-86491.8	81.8	100	0.537
1642	10559.00	49257.3	27344.1	-76601.3	60573.3	25917.4	-86490.7	82.9	100	0.535
1643	10599.00	49248.0	27347.7	-76595.7	60565.5	25919.6	-86485.1	84.0	100	0.534
1644	10639.00	49237.2	27349.2	-76586.3	60555.9	25919.7	-86475.5	85.1	100	0.533
1645	10679.00	49224.9	27348.6	-76573.5	60544.6	25917.9	-86462.5	86.2	100	0.532
1646	10719.00	49211.4	27346.4	-76557.8	60532.1	25914.3	-86446.4	87.3	100	0.531
1647	10759.00	49196.9	27342.4	-76539.3	60518.4	25909.2	-86427.6	88.4	100	0.529
1648	10799.00	49181.4	27337.1	-76518.5	60503.7	25902.7	-86406.4	89.5	100	0.528
1649	10839.00	49165.2	27330.4	-76495.6	60488.1	25895.0	-86383.1	90.6	100	0.527
1650	10879.00	49148.2	27322.6	-76470.8	60471.6	25886.2	-86357.8	91.7	100	0.526
1651	10919.00	49130.7	27313.6	-76444.3	60454.5	25876.3	-86330.8	92.8	100	0.525
1652	10959.00	49112.5	27303.8	-76416.3	60436.7	25865.6	-86302.3	93.9	100	0.523
1653	10999.00	49093.9	27293.0	-76386.8	60418.4	25853.9	-86272.4	95.0	100	0.522
1654	11039.00	49074.8	27281.3	-76356.1	60399.6	25841.5	-86241.2	96.1	100	0.521
1655	11079.00	49055.3	27269.0	-76324.3	60380.4	25828.4	-86208.8	97.2	100	0.520
1656	11119.00	49035.5	27256.0	-76291.5	60360.8	25814.6	-86175.4	98.3	100	0.519
1657	11159.00	49015.3	27242.4	-76257.7	60340.8	25800.3	-86141.1	99.4	100	0.517
1658	11199.00	48994.7	27228.2	-76222.9	60319.6	25785.5	-86105.1	100.5	100	0.516
1659	11235.00	48975.3	27215.2	-76190.5	60299.5	25771.9	-86071.4	101.5	100	0.515
1660	11271.00	48955.1	27201.9	-76157.0	60279.2	25758.0	-86037.2	102.5	100	0.514
1661	11319.00	48927.7	27183.6	-76111.2	60252.2	25738.9	-85991.1	103.9	100	0.513
1662	11359.00	48904.9	27167.3	-76072.2	60229.5	25722.2	-85951.6	105.0	100	0.511
1663	11399.00	48882.1	27150.3	-76032.5	60206.7	25704.7	-85911.3	106.1	100	0.510
1664	11439.00	48859.3	27132.8	-75992.1	60183.7	25686.7	-85870.4	107.2	100	0.509
1665	11479.00	48836.3	27114.8	-75951.1	60160.6	25668.2	-85828.8	108.3	100	0.508
1666	11519.00	48813.3	27096.4	-75909.7	60137.5	25649.3	-85786.8	109.4	100	0.507
1667	11559.00	48790.2	27077.6	-75867.8	60114.3	25630.0	-85744.3	110.5	100	0.505
1668	11599.00	48767.0	27058.5	-75825.5	60091.0	25610.4	-85701.3	111.6	100	0.504
1669	11639.00	48743.8	27039.1	-75782.9	60067.5	25590.6	-85658.1	112.7	100	0.503
1670	11679.00	48720.4	27019.6	-75740.0	60044.0	25570.7	-85614.7	113.8	100	0.502
1671	11719.00	48696.9	27000.3	-75697.1	60020.3	25550.9	-85571.2	114.9	100	0.501
1672	11759.00	48673.1	26980.9	-75654.0	59996.3	25531.1	-85527.5	116.1	100	0.499

Point No.	Time (sec.)	Membrane + Bending Stresses			Total Stresses			Metal Temp. (°F)	No. of Cycles	DO (ppm)
		S' <sub>12</sub> (psi)	S' <sub>23</sub> (psi)	S' <sub>31</sub> (psi)	S' <sub>12</sub> (psi)	S' <sub>23</sub> (psi)	S' <sub>31</sub> (psi)			
1673	11799.00	48649.3	26961.3	-75610.6	59972.3	25511.1	-85483.4	117.2	100	0.498
1674	11839.00	48625.4	26941.5	-75567.0	59948.2	25490.9	-85439.1	118.3	100	0.497
1675	11879.00	48601.4	26921.7	-75523.1	59924.0	25470.6	-85394.6	119.4	100	0.496
1676	11919.00	48577.3	26901.6	-75479.0	59899.7	25450.1	-85349.9	120.5	100	0.495
1677	11959.00	48553.2	26881.5	-75434.7	59875.3	25429.6	-85304.9	121.6	100	0.493
1678	11999.00	48529.0	26861.2	-75390.1	59850.9	25408.9	-85259.8	122.7	100	0.492
1679	12039.00	48504.6	26840.8	-75345.5	59826.3	25388.2	-85214.5	123.8	100	0.491
1680	12079.00	48480.3	26820.3	-75300.6	59801.7	25367.2	-85169.0	124.9	100	0.490
1681	12119.00	48455.9	26799.8	-75255.6	59777.1	25346.3	-85123.4	126.0	100	0.489
1682	12159.00	48431.4	26779.0	-75210.4	59752.3	25325.2	-85077.6	127.2	100	0.487
1683	12199.00	48406.8	26758.3	-75165.1	59727.5	25304.1	-85031.6	128.3	100	0.486
1684	12239.00	48382.2	26737.5	-75119.7	59702.7	25282.8	-84985.5	129.4	100	0.485
1685	12279.00	48357.6	26716.5	-75074.1	59677.8	25261.6	-84939.3	130.5	100	0.484
1686	12319.00	48332.9	26695.5	-75028.4	59652.8	25240.2	-84893.0	131.6	100	0.483
1687	12359.00	48308.2	26674.5	-74982.7	59627.8	25218.8	-84846.6	132.7	100	0.481
1688	12399.00	48283.3	26653.4	-74936.8	59602.7	25197.4	-84800.1	133.8	100	0.480
1689	12435.00	48261.0	26634.4	-74895.4	59580.1	25178.0	-84758.1	134.8	100	0.479
1690	12471.00	48238.6	26615.3	-74854.0	59557.5	25158.6	-84716.1	135.8	100	0.478
1691	12519.00	48208.7	26589.8	-74798.5	59527.3	25132.6	-84659.9	137.2	100	0.477
1692	12559.00	48183.8	26568.5	-74752.3	59502.0	25111.0	-84613.0	138.3	100	0.475
1693	12599.00	48158.8	26547.1	-74705.9	59476.8	25089.3	-84566.1	139.4	100	0.474
1694	12639.00	48133.7	26525.7	-74659.5	59451.5	25067.5	-84518.9	140.5	100	0.473
1695	12679.00	48108.7	26504.3	-74613.0	59426.1	25045.8	-84471.8	141.6	100	0.472
1696	12719.00	48083.6	26482.9	-74566.4	59400.7	25023.9	-84424.6	142.7	100	0.471
1697	12759.00	48058.4	26461.4	-74519.8	59375.3	25002.1	-84377.3	143.8	100	0.469
1698	12799.00	48033.2	26439.8	-74473.1	59349.8	24980.1	-84329.9	144.9	100	0.468
1699	12839.00	48008.0	26418.3	-74426.3	59324.3	24958.2	-84282.5	146.0	100	0.467
1700	12879.00	47982.8	26396.7	-74379.4	59298.8	24936.3	-84235.0	147.1	100	0.466
1701	12919.00	47957.5	26375.0	-74332.5	59273.2	24914.3	-84187.5	148.3	100	0.465
1702	12959.00	47932.2	26353.4	-74285.6	59247.6	24892.3	-84139.9	149.4	100	0.463
1703	12999.00	47906.9	26331.6	-74238.5	59222.0	24870.1	-84092.1	150.5	100	0.462
1704	13039.00	47881.8	26309.5	-74191.3	59196.5	24847.7	-84044.2	151.6	100	0.461
1705	13079.00	47856.8	26287.1	-74144.0	59171.3	24824.9	-83996.2	152.7	100	0.460
1706	13119.00	47832.3	26264.8	-74097.1	59146.4	24802.2	-83948.6	153.8	100	0.459
1707	13159.00	47808.1	26243.2	-74051.3	59121.9	24780.3	-83902.2	154.9	100	0.457
1708	13199.00	47783.9	26222.1	-74006.0	59097.5	24758.8	-83856.3	156.0	100	0.456
1709	13239.00	47759.7	26200.9	-73960.6	59073.0	24737.3	-83810.3	157.1	100	0.455
1710	13279.00	47735.5	26179.7	-73915.2	59048.5	24715.8	-83764.3	158.3	100	0.454
1711	13319.00	47711.3	26158.5	-73869.8	59024.1	24694.2	-83718.3	159.4	100	0.453

Point No.	Time (sec.)	Membrane + Bending Stresses			Total Stresses			Metal Temp. (°F)	No. of Cycles	DO (ppm)
		S' <sub>12</sub> (psi)	S' <sub>23</sub> (psi)	S' <sub>31</sub> (psi)	S' <sub>12</sub> (psi)	S' <sub>23</sub> (psi)	S' <sub>31</sub> (psi)			
1712	13359.00	47687.1	26137.2	-73824.4	58999.6	24672.7	-83672.3	160.5	100	0.451
1713	13399.00	47662.9	26116.0	-73778.9	58975.1	24651.1	-83626.2	161.6	100	0.450
1714	13439.00	47638.7	26094.8	-73733.5	58950.7	24629.5	-83580.2	162.7	100	0.449
1715	13479.00	47614.6	26073.5	-73688.1	58926.3	24607.9	-83534.1	163.8	100	0.448
1716	13519.00	47590.4	26052.2	-73642.6	58901.8	24586.3	-83488.1	164.9	100	0.447
1717	13559.00	47566.3	26030.9	-73597.2	58877.4	24564.7	-83442.1	166.0	100	0.445
1718	13599.00	47542.1	26009.6	-73551.8	58853.0	24543.1	-83396.1	167.1	100	0.444
1719	13635.00	47520.4	25990.5	-73510.9	58831.0	24523.6	-83354.7	168.1	100	0.443
1720	13671.00	47498.7	25971.4	-73470.0	58809.1	24504.2	-83313.3	169.1	100	0.442
1721	13707.00	47477.0	25952.2	-73429.2	58787.1	24484.8	-83271.9	170.1	100	0.441
1722	13737.00	47458.9	25936.3	-73395.2	58768.9	24468.5	-83237.4	171.0	100	0.440
1723	13767.00	47440.8	25920.3	-73361.2	58750.6	24452.4	-83203.0	171.8	100	0.439
1724	13797.00	47422.8	25904.4	-73327.2	58732.3	24436.1	-83168.5	172.6	100	0.438
1725	13827.00	47404.7	25888.5	-73293.2	58714.1	24420.0	-83134.0	173.5	100	0.437
1726	13857.00	47386.6	25872.5	-73259.2	58695.8	24403.8	-83099.6	174.3	100	0.436
1727	13887.00	47368.6	25856.6	-73225.2	58677.5	24387.7	-83065.2	175.1	100	0.436
1728	13917.00	47350.5	25840.7	-73191.2	58659.3	24371.5	-83030.8	176.0	100	0.435
1729	13947.00	47332.5	25824.8	-73157.3	58641.1	24355.3	-82996.3	176.8	100	0.434
1730	13977.00	47314.5	25808.8	-73123.3	58622.8	24339.2	-82962.0	177.6	100	0.433
1731	14007.00	47296.4	25792.9	-73089.3	58604.6	24322.9	-82927.5	178.5	100	0.432
1732	14037.00	47278.4	25777.0	-73055.4	58586.3	24306.8	-82893.1	179.3	100	0.431
1733	14067.00	47260.4	25761.1	-73021.5	58568.1	24290.6	-82858.7	180.1	100	0.430
1734	14097.00	47242.3	25745.2	-72987.5	58549.8	24274.6	-82824.4	181.0	100	0.429
1735	14127.00	47224.3	25729.3	-72953.6	58531.6	24258.4	-82790.0	181.8	100	0.428
1736	14157.00	47206.3	25713.4	-72919.7	58513.4	24242.2	-82755.6	182.6	100	0.427
1737	14187.00	47188.3	25697.5	-72885.8	58495.2	24226.0	-82721.3	183.5	100	0.427
1738	14217.00	47170.3	25681.6	-72851.9	58477.0	24209.9	-82686.9	184.3	100	0.426
1739	14247.00	47152.3	25665.7	-72818.0	58458.8	24193.7	-82652.6	185.1	100	0.425
1740	14277.00	47134.3	25649.8	-72784.1	58440.6	24177.6	-82618.2	186.0	100	0.424
1741	14307.00	47116.3	25633.9	-72750.2	58422.5	24161.5	-82583.9	186.8	100	0.423
1742	14337.00	47098.3	25618.0	-72716.3	58404.2	24145.3	-82549.6	187.6	100	0.422
1743	14367.00	47080.3	25602.2	-72682.5	58386.1	24129.2	-82515.3	188.5	100	0.421
1744	14397.00	47062.4	25586.2	-72648.6	58367.9	24113.1	-82481.0	189.3	100	0.420
1745	14427.00	47044.3	25570.4	-72614.7	58349.7	24097.0	-82446.7	190.1	100	0.419
1746	14457.00	47026.3	25554.5	-72580.9	58331.6	24080.8	-82412.3	191.0	100	0.418
1747	14487.00	47008.4	25538.6	-72547.0	58313.4	24064.7	-82378.1	191.8	100	0.418
1748	14517.00	46990.5	25522.7	-72513.2	58295.2	24048.6	-82343.8	192.6	100	0.417
1749	14544.00	46974.3	25508.5	-72482.8	58278.9	24034.0	-82313.0	193.4	100	0.416
1750	14571.00	46958.1	25494.2	-72452.3	58262.5	24019.6	-82282.1	194.1	100	0.415

Point No.	Time (sec.)	Membrane + Bending Stresses			Total Stresses			Metal Temp. (°F)	No. of Cycles	DO (ppm)
		S' <sub>12</sub> (psi)	S' <sub>23</sub> (psi)	S' <sub>31</sub> (psi)	S' <sub>12</sub> (psi)	S' <sub>23</sub> (psi)	S' <sub>31</sub> (psi)			
1751	14607.00	46936.5	25475.2	-72411.7	58240.8	24000.3	-82241.0	195.1	100	0.414
1752	14637.00	46918.6	25459.3	-72377.9	58222.7	23984.0	-82206.7	196.0	100	0.413
1753	14667.00	46900.7	25443.3	-72344.1	58204.5	23968.0	-82172.5	196.8	100	0.412
1754	14697.00	46882.8	25427.5	-72310.3	58186.4	23951.9	-82138.2	197.6	100	0.411
1755	14727.00	46864.9	25411.7	-72276.5	58168.3	23935.8	-82104.0	198.5	100	0.410
1756	14757.00	46846.9	25395.9	-72242.8	58150.1	23919.7	-82069.8	199.3	100	0.409
1757	14787.00	46828.9	25380.0	-72209.0	58132.0	23903.6	-82035.6	200.1	100	0.409
1758	14817.00	46810.8	25364.6	-72175.4	58113.6	23888.0	-82001.6	201.0	100	0.408
1759	14847.00	46792.6	25349.2	-72141.8	58095.2	23872.4	-81967.6	201.8	100	0.407
1760	14877.00	46774.1	25334.2	-72108.3	58076.5	23857.1	-81933.6	202.6	100	0.406
1761	14907.00	46755.1	25319.2	-72074.3	58057.4	23841.9	-81899.3	203.5	100	0.405
1762	14937.00	46735.8	25303.5	-72039.3	58037.8	23826.0	-81863.8	204.3	100	0.404
1763	14967.00	46716.3	25287.0	-72003.3	58018.1	23809.2	-81827.3	205.1	100	0.403
1764	14997.00	46696.7	25270.5	-71967.2	57998.4	23792.3	-81790.7	206.0	100	0.402
1765	15027.00	46677.3	25253.9	-71931.1	57978.7	23775.4	-81754.1	206.8	100	0.401
1766	15057.00	46657.8	25237.2	-71895.0	57958.9	23758.6	-81717.5	207.6	100	0.400
1767	15087.00	46638.2	25220.6	-71858.9	57939.2	23741.6	-81680.8	208.4	100	0.400
1768	15117.00	46618.7	25204.0	-71822.7	57919.4	23724.7	-81644.2	209.3	100	0.399
1769	15147.00	46599.2	25187.3	-71786.5	57899.6	23707.9	-81607.5	210.1	100	0.398
1770	15177.00	46579.5	25170.8	-71750.3	57879.8	23691.0	-81570.8	210.9	100	0.397
1771	15207.00	46560.0	25154.1	-71714.1	57860.0	23674.1	-81534.1	211.8	100	0.396
1772	15237.00	46540.4	25137.5	-71677.9	57840.2	23657.1	-81497.3	212.6	100	0.395
1773	15267.00	46520.9	25120.8	-71641.6	57820.4	23640.2	-81460.6	213.4	100	0.394
1774	15297.00	46501.2	25104.2	-71605.5	57800.5	23623.3	-81423.8	214.3	100	0.393
1775	15327.00	46481.5	25087.7	-71569.2	57780.6	23606.5	-81387.1	215.1	100	0.392
1776	15357.00	46461.9	25070.9	-71532.8	57760.8	23589.4	-81350.2	215.9	100	0.391
1777	15387.00	46442.2	25054.3	-71496.5	57740.8	23572.6	-81313.4	216.8	100	0.391
1778	15417.00	46422.5	25037.6	-71460.1	57720.9	23555.5	-81276.4	217.6	100	0.390
1779	15444.00	46404.8	25022.6	-71427.4	57702.9	23540.3	-81243.2	218.4	100	0.389
1780	15471.00	46387.0	25007.7	-71394.7	57685.0	23525.1	-81210.1	219.1	100	0.388
1781	15507.00	46363.3	24987.6	-71350.9	57661.0	23504.8	-81165.8	220.1	100	0.387
1782	15537.00	46343.6	24970.9	-71314.4	57641.0	23487.8	-81128.8	220.9	100	0.386
1783	15567.00	46323.8	24954.2	-71278.0	57621.0	23470.7	-81091.7	221.8	100	0.385
1784	15597.00	46304.0	24937.5	-71241.5	57601.0	23453.7	-81054.7	222.6	100	0.384
1785	15627.00	46284.2	24920.7	-71204.9	57581.0	23436.7	-81017.6	223.4	100	0.383
1786	15657.00	46264.4	24903.9	-71168.3	57560.9	23419.7	-80980.6	224.3	100	0.382
1787	15687.00	46244.5	24887.2	-71131.7	57540.8	23402.7	-80943.5	225.1	100	0.382
1788	15717.00	46224.7	24870.4	-71095.1	57520.7	23385.7	-80906.3	225.9	100	0.381
1789	15747.00	46204.9	24853.6	-71058.5	57500.6	23368.6	-80869.1	226.8	100	0.380

Point No.	Time (sec.)	Membrane + Bending Stresses			Total Stresses			Metal Temp. (°F)	No. of Cycles	DO (ppm)
		S' <sub>12</sub> (psi)	S' <sub>23</sub> (psi)	S' <sub>31</sub> (psi)	S' <sub>12</sub> (psi)	S' <sub>23</sub> (psi)	S' <sub>31</sub> (psi)			
1790	15777.00	46184.9	24836.9	-71021.8	57480.4	23351.5	-80832.0	227.6	100	0.379
1791	15807.00	46165.0	24820.1	-70985.1	57460.3	23334.4	-80794.8	228.4	100	0.378
1792	15837.00	46145.2	24803.2	-70948.4	57440.1	23317.4	-80757.5	229.3	100	0.377
1793	15867.00	46125.2	24786.4	-70911.7	57419.9	23300.4	-80720.3	230.1	100	0.376
1794	15897.00	46105.2	24769.7	-70874.9	57399.7	23283.2	-80683.0	230.9	100	0.375
1795	15927.00	46085.3	24752.8	-70838.0	57379.5	23266.1	-80645.6	231.8	100	0.374
1796	15957.00	46065.3	24735.9	-70801.3	57359.3	23249.0	-80608.3	232.6	100	0.373
1797	15987.00	46045.3	24719.2	-70764.5	57339.1	23231.8	-80571.0	233.4	100	0.373
1798	16017.00	46025.3	24702.3	-70727.6	57318.8	23214.7	-80533.5	234.3	100	0.372
1799	16047.00	46005.2	24685.5	-70690.7	57298.6	23197.5	-80496.1	235.1	100	0.371
1800	16077.00	45985.2	24668.6	-70653.8	57278.3	23180.3	-80458.6	235.9	100	0.370
1801	16107.00	45965.2	24651.6	-70616.8	57258.0	23163.2	-80421.2	236.8	100	0.369
1802	16137.00	45945.1	24634.8	-70579.9	57237.7	23145.9	-80383.7	237.6	100	0.368
1803	16167.00	45925.0	24617.9	-70542.9	57217.4	23128.8	-80346.3	238.4	100	0.367
1804	16197.00	45905.0	24601.0	-70505.9	57197.0	23111.7	-80308.7	239.3	100	0.366
1805	16227.00	45884.8	24584.0	-70468.9	57176.7	23094.3	-80271.1	240.1	100	0.365
1806	16257.00	45864.7	24567.1	-70431.9	57156.3	23077.2	-80233.5	240.9	100	0.364
1807	16287.00	45844.6	24550.2	-70394.8	57135.9	23060.0	-80195.9	241.8	100	0.364
1808	16317.00	45824.3	24533.3	-70357.7	57115.5	23042.8	-80158.3	242.6	100	0.363
1809	16344.00	45806.2	24518.0	-70324.2	57097.1	23027.2	-80124.4	243.4	100	0.362
1810	16371.00	45788.0	24502.8	-70290.8	57078.7	23011.8	-80090.5	244.1	100	0.361
1811	16407.00	45763.8	24482.4	-70246.2	57054.2	22991.1	-80045.3	245.1	100	0.360
1812	16437.00	45743.6	24465.4	-70209.0	57033.7	22973.8	-80007.5	245.9	100	0.359
1813	16467.00	45723.4	24448.4	-70171.8	57013.2	22956.5	-79969.7	246.8	100	0.358
1814	16497.00	45703.1	24431.4	-70134.5	56992.7	22939.3	-79932.0	247.6	100	0.357
1815	16527.00	45682.8	24414.5	-70097.3	56972.2	22922.0	-79894.2	248.4	100	0.356
1816	16557.00	45662.6	24397.4	-70060.0	56951.7	22904.7	-79856.3	249.3	100	0.355
1817	16587.00	45642.3	24380.3	-70022.6	56931.1	22887.3	-79818.5	250.1	100	0.355
1818	16617.00	45622.2	24362.8	-69985.0	56910.9	22869.5	-79780.3	250.9	100	0.354
1819	16647.00	45602.4	24345.0	-69947.4	56890.6	22851.4	-79742.0	251.8	100	0.353
1820	16677.00	45582.9	24326.9	-69909.7	56870.9	22832.9	-79703.8	252.6	100	0.352
1821	16707.00	45563.8	24308.8	-69872.6	56851.6	22814.5	-79666.1	253.4	100	0.351
1822	16737.00	45545.4	24291.5	-69836.9	56832.9	22797.0	-79629.9	254.3	100	0.350
1823	16767.00	45527.1	24275.4	-69802.5	56814.4	22780.6	-79594.9	255.1	100	0.349
1824	16797.00	45508.8	24259.5	-69768.3	56795.9	22764.3	-79560.2	255.9	100	0.348
1825	16827.00	45490.5	24243.4	-69733.9	56777.4	22748.0	-79525.4	256.8	100	0.347
1826	16857.00	45472.2	24227.5	-69699.6	56758.8	22731.8	-79490.6	257.6	100	0.346
1827	16887.00	45453.8	24211.5	-69665.4	56740.3	22715.7	-79455.9	258.4	100	0.346
1828	16917.00	45435.5	24195.5	-69631.0	56721.8	22699.3	-79421.1	259.3	100	0.345



Point No.	Time (sec.)	Membrane + Bending Stresses			Total Stresses			Metal Temp. (°F)	No. of Cycles	DO (ppm)
		S' <sub>12</sub> (psi)	S' <sub>23</sub> (psi)	S' <sub>31</sub> (psi)	S' <sub>12</sub> (psi)	S' <sub>23</sub> (psi)	S' <sub>31</sub> (psi)			
1829	16947.00	45417.2	24179.5	-69596.7	56703.3	22683.1	-79386.4	260.1	100	0.344
1830	16977.00	45399.0	24163.4	-69562.4	56684.8	22666.8	-79351.6	260.9	100	0.343
1831	17007.00	45380.7	24147.4	-69528.1	56666.3	22650.5	-79316.8	261.8	100	0.342
1832	17037.00	45362.4	24131.4	-69493.8	56647.8	22634.2	-79282.0	262.6	100	0.341
1833	17067.00	45344.0	24115.4	-69459.4	56629.3	22617.9	-79247.3	263.4	100	0.340
1834	17097.00	45325.8	24099.3	-69425.2	56610.8	22601.6	-79212.5	264.3	100	0.339
1835	17127.00	45307.5	24083.4	-69390.9	56592.3	22585.4	-79177.7	265.1	100	0.338
1836	17157.00	45289.3	24067.2	-69356.5	56573.8	22569.1	-79142.9	265.9	100	0.337
1837	17187.00	45271.0	24051.3	-69322.2	56555.3	22552.9	-79108.2	266.8	100	0.337
1838	17217.00	45252.8	24035.2	-69288.0	56536.8	22536.5	-79073.4	267.6	100	0.336
1839	17244.00	45236.2	24020.8	-69257.0	56520.3	22521.9	-79042.2	268.3	100	0.335
1840	17271.00	45219.8	24006.3	-69226.2	56503.6	22507.3	-79010.9	269.1	100	0.334
1841	17283.96	45200.3	24006.5	-69206.8	56484.0	22507.2	-78991.3	269.5	100	0.334
1842	17296.92	45180.7	24006.6	-69187.3	56464.4	22507.3	-78971.6	269.8	100	0.333
1843	17316.58	45151.0	24006.9	-69157.9	56434.5	22507.4	-78941.9	270.4	100	0.333
1844	17336.25	45121.3	24007.1	-69128.5	56404.7	22507.4	-78912.1	270.9	100	0.332
1845	17355.93	45091.6	24007.4	-69099.0	56374.9	22507.5	-78882.4	271.4	100	0.331
1846	17375.61	45062.0	24007.6	-69069.6	56345.0	22507.6	-78852.6	272.0	100	0.331
1847	17395.30	45032.3	24007.9	-69040.1	56315.2	22507.7	-78822.9	272.5	100	0.330
1848	17414.99	45002.5	24008.2	-69010.7	56285.3	22507.9	-78793.2	273.1	100	0.330
1849	17434.69	44972.8	24008.4	-68981.2	56255.5	22507.9	-78763.3	273.6	100	0.329
1850	17454.39	44943.1	24008.7	-68951.8	56225.6	22508.0	-78733.6	274.2	100	0.328
1851	17474.09	44913.3	24009.0	-68922.3	56195.7	22508.1	-78703.8	274.7	100	0.328
1852	17493.80	44883.6	24009.2	-68892.8	56165.9	22508.2	-78674.0	275.3	100	0.327
1853	17513.52	44853.8	24009.5	-68863.3	56135.9	22508.2	-78644.2	275.8	100	0.327
1854	17533.24	44824.0	24009.7	-68833.8	56106.1	22508.3	-78614.4	276.4	100	0.326
1855	17552.96	44794.3	24010.0	-68804.3	56076.1	22508.5	-78584.7	276.9	100	0.326
1856	17572.70	44764.5	24010.2	-68774.8	56046.3	22508.5	-78554.8	277.5	100	0.325
1857	17583.85	44747.7	24010.3	-68758.1	56029.3	22508.6	-78537.9	277.8	100	0.325
1858	17595.00	44730.9	24010.6	-68741.5	56012.5	22508.7	-78521.1	278.1	100	0.324
1859	17607.96	44711.3	24010.7	-68722.0	55992.8	22508.7	-78501.5	278.4	100	0.324
1860	17620.92	44691.8	24010.9	-68702.7	55973.1	22508.8	-78481.9	278.8	100	0.324
1861	17640.67	44662.1	24011.1	-68673.1	55943.3	22508.9	-78452.2	279.4	100	0.323
1862	17660.42	44632.3	24011.4	-68643.6	55913.4	22508.9	-78422.3	279.9	100	0.322
1863	17680.18	44602.5	24011.6	-68614.1	55883.4	22509.1	-78392.5	280.5	100	0.322
1864	17699.94	44572.6	24011.9	-68584.6	55853.5	22509.1	-78362.6	281.0	100	0.321
1865	17719.71	44542.8	24012.2	-68555.0	55823.5	22509.3	-78332.8	281.5	100	0.321
1866	17739.48	44513.0	24012.4	-68525.4	55793.6	22509.3	-78302.9	282.1	100	0.320
1867	17759.26	44483.2	24012.7	-68495.9	55763.6	22509.5	-78273.1	282.6	100	0.319

Point No.	Time (sec.)	Membrane + Bending Stresses			Total Stresses			Metal Temp. (°F)	No. of Cycles	DO (ppm)
		S' <sub>12</sub> (psi)	S' <sub>23</sub> (psi)	S' <sub>31</sub> (psi)	S' <sub>12</sub> (psi)	S' <sub>23</sub> (psi)	S' <sub>31</sub> (psi)			
1868	17779.04	44453.4	24013.0	-68466.4	55733.7	22509.6	-78243.2	283.2	100	0.319
1869	17798.82	44423.5	24013.3	-68436.8	55703.7	22509.6	-78213.3	283.7	100	0.318
1870	17818.62	44393.7	24013.5	-68407.2	55673.7	22509.7	-78183.5	284.3	100	0.318
1871	17838.41	44363.8	24013.8	-68377.6	55643.7	22509.8	-78153.5	284.8	100	0.317
1872	17858.21	44334.0	24014.1	-68348.1	55613.8	22509.9	-78123.7	285.4	100	0.316
1873	17878.02	44304.1	24014.4	-68318.5	55583.7	22510.1	-78093.8	285.9	100	0.316
1874	17897.83	44274.3	24014.6	-68288.9	55553.7	22510.2	-78063.8	286.5	100	0.315
1875	17908.42	44258.3	24014.7	-68273.1	55537.8	22510.2	-78048.0	286.8	100	0.315
1876	17919.00	44242.3	24015.0	-68257.3	55521.7	22510.3	-78032.0	287.1	100	0.315
1877	17931.96	44222.8	24015.1	-68237.9	55502.1	22510.3	-78012.4	287.4	100	0.314
1878	17944.92	44203.3	24015.3	-68218.5	55482.4	22510.5	-77992.9	287.8	100	0.314
1879	17964.75	44173.4	24015.6	-68189.0	55452.4	22510.5	-77963.0	288.4	100	0.313
1880	17984.58	44143.5	24015.9	-68159.4	55422.4	22510.7	-77933.0	288.9	100	0.313
1881	18004.42	44113.6	24016.1	-68129.7	55392.4	22510.8	-77903.1	289.5	100	0.312
1882	18024.26	44083.7	24016.4	-68100.1	55362.3	22510.9	-77873.2	290.0	100	0.311
1883	18044.11	44053.8	24016.7	-68070.5	55332.3	22510.9	-77843.2	290.6	100	0.311
1884	18063.96	44023.9	24016.9	-68040.8	55302.2	22511.1	-77813.4	291.1	100	0.310
1885	18083.82	43994.0	24017.2	-68011.2	55272.1	22511.3	-77783.4	291.7	100	0.310
1886	18103.68	43964.1	24017.5	-67981.6	55242.1	22511.3	-77753.4	292.2	100	0.309
1887	18123.55	43934.1	24017.7	-67951.9	55212.0	22511.5	-77723.5	292.8	100	0.308
1888	18143.42	43904.2	24018.1	-67922.3	55182.0	22511.5	-77693.5	293.3	100	0.308
1889	18163.30	43874.2	24018.5	-67892.6	55151.9	22511.6	-77663.5	293.9	100	0.307
1890	18183.18	43844.2	24018.7	-67862.9	55121.8	22511.8	-77633.5	294.4	100	0.307
1891	18203.07	43814.3	24019.0	-67833.3	55091.7	22511.9	-77603.6	295.0	100	0.306
1892	18222.96	43784.3	24019.2	-67803.5	55061.6	22512.1	-77573.6	295.5	100	0.305
1893	18243.00	43754.2	24019.4	-67773.7	55031.3	22512.1	-77543.4	296.1	100	0.305
1894	18279.00	43699.9	24020.1	-67720.0	54976.8	22512.4	-77489.2	297.1	100	0.304
1895	18309.00	43654.8	24020.5	-67675.2	54931.5	22512.6	-77444.0	297.9	100	0.303
1896	18339.00	43609.6	24020.9	-67630.5	54886.0	22512.7	-77398.8	298.7	100	0.302
1897	18369.00	43564.4	24021.4	-67585.8	54840.7	22512.9	-77353.6	299.6	100	0.301
1898	18399.00	43519.2	24022.0	-67541.2	54795.3	22513.3	-77308.5	300.4	100	0.300
1899	18429.00	43473.6	24023.3	-67496.9	54749.5	22514.4	-77263.9	301.2	100	0.299
1900	18459.00	43427.7	24024.8	-67452.5	54703.5	22515.8	-77219.3	302.1	100	0.298
1901	18489.00	43381.5	24026.6	-67408.1	54657.2	22517.4	-77174.6	302.9	100	0.297
1902	18519.00	43334.4	24028.0	-67362.4	54609.9	22518.6	-77128.5	303.7	100	0.297
1903	18549.00	43286.7	24028.0	-67314.7	54561.9	22518.3	-77080.2	304.6	100	0.296
1904	18579.00	43239.0	24027.1	-67266.0	54514.0	22517.2	-77031.2	305.4	100	0.295
1905	18609.00	43191.3	24026.1	-67217.4	54466.0	22516.0	-76982.0	306.2	100	0.294
1906	18639.00	43143.6	24025.2	-67168.8	54418.1	22514.7	-76932.8	307.1	100	0.293

Point No.	Time (sec.)	Membrane + Bending Stresses			Total Stresses			Metal Temp. (°F)	No. of Cycles	DO (ppm)
		S' <sub>12</sub> (psi)	S' <sub>23</sub> (psi)	S' <sub>31</sub> (psi)	S' <sub>12</sub> (psi)	S' <sub>23</sub> (psi)	S' <sub>31</sub> (psi)			
1907	18669.00	43096.0	24024.2	-67120.2	54370.2	22513.5	-76883.7	307.9	100	0.292
1908	18699.00	43048.2	24023.4	-67071.5	54322.1	22512.3	-76834.4	308.7	100	0.291
1909	18729.00	43000.5	24022.4	-67022.9	54274.2	22511.1	-76785.2	309.6	100	0.290
1910	18759.00	42952.7	24021.5	-66974.2	54226.2	22509.9	-76736.1	310.4	100	0.289
1911	18789.00	42905.1	24020.5	-66925.6	54178.2	22508.6	-76686.8	311.2	100	0.288
1912	18819.00	42857.3	24019.6	-66876.8	54130.1	22507.4	-76637.5	312.1	100	0.288
1913	18849.00	42809.5	24018.7	-66828.2	54082.1	22506.2	-76588.3	312.9	100	0.287
1914	18879.00	42761.7	24017.8	-66779.5	54034.0	22505.0	-76539.0	313.7	100	0.286
1915	18909.00	42713.9	24016.9	-66730.8	53986.0	22503.7	-76489.7	314.6	100	0.285
1916	18939.00	42666.1	24016.0	-66682.0	53937.8	22502.6	-76440.5	315.4	100	0.284
1917	18969.00	42618.2	24015.0	-66633.2	53889.8	22501.3	-76391.1	316.2	100	0.283
1918	18999.00	42570.3	24014.2	-66584.5	53841.6	22500.2	-76341.8	317.1	100	0.282
1919	19029.00	42522.5	24013.1	-66535.6	53793.5	22499.0	-76292.5	317.9	100	0.281
1920	19059.00	42474.7	24012.2	-66486.8	53745.4	22497.8	-76243.1	318.7	100	0.280
1921	19089.00	42426.7	24011.3	-66438.0	53697.2	22496.5	-76193.6	319.6	100	0.279
1922	19116.00	42383.6	24010.4	-66394.1	53653.9	22495.3	-76149.2	320.3	100	0.279
1923	19143.00	42340.5	24009.6	-66350.1	53610.6	22494.1	-76104.7	321.1	100	0.278
1924	19179.00	42282.9	24008.5	-66291.4	53552.7	22492.7	-76045.3	322.1	100	0.277
1925	19209.00	42235.0	24007.5	-66242.5	53504.4	22491.5	-75995.9	322.9	100	0.276
1926	19239.00	42187.1	24006.5	-66193.6	53456.3	22490.1	-75946.4	323.7	100	0.275
1927	19269.00	42139.1	24005.5	-66144.6	53408.0	22488.9	-75896.9	324.6	100	0.274
1928	19299.00	42091.1	24004.6	-66095.7	53359.8	22487.6	-75847.4	325.4	100	0.273
1929	19329.00	42043.1	24003.6	-66046.7	53311.5	22486.3	-75797.8	326.2	100	0.272
1930	19359.00	41995.1	24002.6	-65997.6	53263.2	22485.1	-75748.2	327.1	100	0.271
1931	19389.00	41947.1	24001.5	-65948.6	53214.9	22483.7	-75698.7	327.9	100	0.270
1932	19419.00	41899.0	24000.6	-65899.6	53166.6	22482.4	-75649.0	328.7	100	0.270
1933	19449.00	41850.9	23999.6	-65850.5	53118.2	22481.2	-75599.4	329.6	100	0.269
1934	19479.00	41803.0	23998.5	-65801.4	53070.0	22479.8	-75549.8	330.4	100	0.268
1935	19509.00	41754.9	23997.4	-65752.3	53021.6	22478.5	-75500.1	331.2	100	0.267
1936	19539.00	41706.7	23996.6	-65703.3	52973.3	22477.0	-75450.3	332.1	100	0.266
1937	19569.00	41658.6	23995.4	-65654.0	52924.8	22475.8	-75400.7	332.9	100	0.265
1938	19599.00	41610.5	23994.4	-65604.9	52876.5	22474.4	-75350.9	333.7	100	0.264
1939	19629.00	41562.4	23993.4	-65555.8	52828.0	22473.2	-75301.2	334.6	100	0.263
1940	19659.00	41514.3	23992.2	-65506.5	52779.7	22471.7	-75251.3	335.4	100	0.262
1941	19689.00	41466.1	23991.2	-65457.3	52731.2	22470.3	-75201.6	336.2	100	0.261
1942	19719.00	41417.9	23990.2	-65408.1	52682.8	22469.0	-75151.8	337.1	100	0.261
1943	19749.00	41369.8	23989.0	-65358.8	52634.3	22467.6	-75101.9	337.9	100	0.260
1944	19779.00	41321.6	23988.0	-65309.5	52585.9	22466.2	-75052.1	338.7	100	0.259
1945	19809.00	41273.4	23986.8	-65260.2	52537.4	22464.8	-75002.2	339.6	100	0.258

Point No.	Time (sec.)	Membrane + Bending Stresses			Total Stresses			Metal Temp. (°F)	No. of Cycles	DO (ppm)
		S' <sub>12</sub> (psi)	S' <sub>23</sub> (psi)	S' <sub>31</sub> (psi)	S' <sub>12</sub> (psi)	S' <sub>23</sub> (psi)	S' <sub>31</sub> (psi)			
1946	19839.00	41225.1	23985.8	-65210.9	52488.9	22463.5	-74952.3	340.4	100	0.257
1947	19869.00	41176.9	23984.6	-65161.5	52440.4	22461.9	-74902.4	341.2	100	0.256
1948	19899.00	41128.6	23983.6	-65112.2	52391.9	22460.6	-74852.5	342.1	100	0.255
1949	19929.00	41080.4	23982.4	-65062.8	52343.3	22459.2	-74802.5	342.9	100	0.254
1950	19959.00	41032.2	23981.3	-65013.5	52294.8	22457.8	-74752.6	343.7	100	0.253
1951	19989.00	40983.9	23980.1	-64964.0	52246.2	22456.3	-74702.5	344.6	100	0.252
1952	20016.00	40940.4	23979.1	-64919.5	52202.5	22455.0	-74657.5	345.3	100	0.252
1953	20043.00	40896.9	23978.1	-64875.0	52158.8	22453.8	-74612.5	346.1	100	0.251
1954	20079.00	40839.0	23976.7	-64815.6	52100.5	22451.9	-74552.4	347.1	100	0.250
1955	20109.00	40790.6	23975.5	-64766.1	52051.8	22450.5	-74502.3	347.9	100	0.249
1956	20139.00	40742.2	23974.4	-64716.6	52003.3	22449.0	-74452.3	348.7	100	0.248
1957	20169.00	40693.9	23973.1	-64667.0	51954.6	22447.4	-74402.1	349.6	100	0.247
1958	20199.00	40645.6	23971.7	-64617.3	51906.1	22445.7	-74351.8	350.4	100	0.246
1959	20229.00	40597.8	23969.5	-64567.3	51857.9	22443.2	-74301.2	351.2	100	0.245
1960	20259.00	40550.3	23966.9	-64517.2	51810.1	22440.3	-74250.4	352.1	100	0.244
1961	20289.00	40503.3	23964.1	-64467.4	51762.9	22437.0	-74199.8	352.9	100	0.243
1962	20319.00	40457.3	23961.7	-64418.9	51716.5	22434.2	-74150.8	353.7	100	0.243
1963	20349.00	40412.0	23961.3	-64373.3	51671.1	22433.4	-74104.5	354.6	100	0.242
1964	20379.00	40366.7	23961.6	-64328.3	51625.6	22433.6	-74059.2	355.4	100	0.241
1965	20409.00	40321.5	23962.0	-64283.5	51580.1	22433.7	-74013.8	356.2	100	0.240
1966	20439.00	40276.2	23962.3	-64238.6	51534.7	22433.8	-73968.5	357.1	100	0.239
1967	20469.00	40231.0	23962.7	-64193.7	51489.2	22433.9	-73923.1	357.9	100	0.238
1968	20499.00	40185.7	23963.0	-64148.8	51443.8	22433.9	-73877.8	358.7	100	0.237
1969	20529.00	40140.6	23963.3	-64103.9	51398.4	22434.1	-73832.5	359.6	100	0.236
1970	20559.00	40095.3	23963.8	-64059.1	51352.9	22434.2	-73787.2	360.4	100	0.235
1971	20589.00	40050.1	23964.1	-64014.2	51307.5	22434.3	-73741.8	361.2	100	0.234
1972	20619.00	40004.8	23964.6	-63969.4	51262.1	22434.5	-73696.5	362.1	100	0.234
1973	20649.00	39959.6	23964.8	-63924.5	51216.6	22434.7	-73651.3	362.9	100	0.233
1974	20679.00	39914.4	23965.3	-63879.7	51171.2	22434.7	-73605.9	363.7	100	0.232
1975	20709.00	39869.2	23965.7	-63834.9	51125.8	22434.9	-73560.7	364.6	100	0.231
1976	20739.00	39824.0	23966.1	-63790.1	51080.3	22435.1	-73515.4	365.4	100	0.230
1977	20769.00	39778.7	23966.6	-63745.3	51035.0	22435.2	-73470.2	366.2	100	0.229
1978	20799.00	39733.6	23967.0	-63700.5	50989.6	22435.4	-73424.9	367.1	100	0.228
1979	20829.00	39688.3	23967.4	-63655.7	50944.1	22435.5	-73379.7	367.9	100	0.227
1980	20859.00	39643.1	23967.8	-63610.9	50898.8	22435.6	-73334.4	368.7	100	0.226
1981	20889.00	39598.0	23968.1	-63566.1	50853.4	22435.8	-73289.2	369.5	100	0.225
1982	20916.00	39557.3	23968.5	-63525.8	50812.6	22435.9	-73248.5	370.3	100	0.225
1983	20943.00	39516.6	23969.0	-63485.6	50771.8	22436.1	-73207.8	371.0	100	0.224
1984	20979.00	39462.4	23969.4	-63431.8	50717.3	22436.2	-73153.5	372.0	100	0.223

Point No.	Time (sec.)	Membrane + Bending Stresses			Total Stresses			Metal Temp. (°F)	No. of Cycles	DO (ppm)
		S' <sub>12</sub> (psi)	S' <sub>23</sub> (psi)	S' <sub>31</sub> (psi)	S' <sub>12</sub> (psi)	S' <sub>23</sub> (psi)	S' <sub>31</sub> (psi)			
1985	21009.00	39417.3	23969.9	-63387.1	50671.8	22436.5	-73108.3	372.9	100	0.222
1986	21039.00	39372.0	23970.3	-63342.3	50626.5	22436.7	-73063.2	373.7	100	0.221
1987	21069.00	39326.9	23970.8	-63297.6	50581.2	22436.8	-73017.9	374.5	100	0.220
1988	21099.00	39281.7	23971.1	-63252.8	50535.7	22437.1	-72972.8	375.4	100	0.219
1989	21129.00	39236.6	23971.6	-63208.2	50490.4	22437.2	-72927.6	376.2	100	0.218
1990	21159.00	39191.4	23972.0	-63163.4	50445.1	22437.3	-72882.4	377.0	100	0.217
1991	21189.00	39146.2	23972.5	-63118.8	50399.7	22437.5	-72837.2	377.9	100	0.216
1992	21219.00	39101.2	23972.9	-63074.1	50354.4	22437.7	-72792.1	378.7	100	0.216
1993	21249.00	39056.0	23973.4	-63029.4	50309.1	22437.9	-72746.9	379.5	100	0.215
1994	21279.00	39010.9	23973.8	-62984.7	50263.7	22438.0	-72701.8	380.4	100	0.214
1995	21309.00	38965.7	23974.3	-62940.0	50218.4	22438.3	-72656.6	381.2	100	0.213
1996	21339.00	38920.6	23974.7	-62895.3	50173.0	22438.5	-72611.6	382.0	100	0.212
1997	21369.00	38875.5	23975.1	-62850.6	50127.7	22438.7	-72566.4	382.9	100	0.211
1998	21399.00	38830.4	23975.6	-62805.9	50082.4	22438.9	-72521.3	383.7	100	0.210
1999	21429.00	38785.3	23976.0	-62761.3	50037.0	22439.2	-72476.2	384.5	100	0.209
2000	21459.00	38740.1	23976.5	-62716.6	49991.8	22439.2	-72431.0	385.4	100	0.208
2001	21489.00	38695.1	23976.9	-62672.0	49946.5	22439.5	-72386.0	386.2	100	0.207
2002	21519.00	38649.9	23977.4	-62627.3	49901.1	22439.7	-72340.8	387.0	100	0.207
2003	21549.00	38604.9	23977.8	-62582.7	49855.9	22439.9	-72295.8	387.9	100	0.206
2004	21579.00	38559.7	23978.3	-62538.0	49810.6	22440.2	-72250.7	388.7	100	0.205
2005	21609.00	38514.7	23978.8	-62493.4	49765.3	22440.2	-72205.6	389.5	100	0.204
2006	21639.00	38469.6	23979.2	-62448.8	49720.0	22440.5	-72160.5	390.4	100	0.203
2007	21669.00	38424.6	23979.7	-62404.2	49674.8	22440.7	-72115.5	391.2	100	0.202
2008	21699.00	38379.4	23980.2	-62359.6	49629.5	22440.9	-72070.4	392.0	100	0.201
2009	21729.00	38334.4	23980.7	-62315.1	49584.2	22441.2	-72025.4	392.9	100	0.200
2010	21759.00	38289.3	23981.2	-62270.5	49539.0	22441.4	-71980.4	393.7	100	0.199
2011	21789.00	38244.2	23981.6	-62225.9	49493.7	22441.6	-71935.4	394.5	100	0.198
2012	21816.00	38203.7	23982.0	-62185.8	49453.0	22441.8	-71894.8	395.3	100	0.198
2013	21843.00	38163.2	23982.5	-62145.7	49412.3	22442.0	-71854.3	396.0	100	0.197
2014	21879.00	38109.1	23983.1	-62092.2	49358.0	22442.3	-71800.3	397.0	100	0.196
2015	21909.00	38064.0	23983.6	-62047.6	49312.8	22442.5	-71755.3	397.9	100	0.195
2016	21939.00	38019.1	23984.0	-62003.1	49267.6	22442.8	-71710.3	398.7	100	0.194
2017	21969.00	37974.0	23984.5	-61958.5	49222.3	22443.0	-71665.4	399.5	100	0.193
2018	21999.00	37929.0	23985.1	-61914.0	49177.1	22443.2	-71620.3	400.4	100	0.192
2019	22029.00	37883.9	23985.6	-61869.5	49131.9	22443.5	-71575.4	401.2	100	0.191
2020	22059.00	37839.0	23986.0	-61824.9	49086.6	22443.8	-71530.4	402.0	100	0.190
2021	22089.00	37793.9	23986.5	-61780.4	49041.4	22444.0	-71485.4	402.9	100	0.189
2022	22119.00	37748.8	23987.1	-61735.9	48996.2	22444.2	-71440.4	403.7	100	0.189
2023	22149.00	37703.8	23987.7	-61691.5	48950.9	22444.5	-71395.4	404.5	100	0.188

Point No.	Time (sec.)	Membrane + Bending Stresses			Total Stresses			Metal Temp. (°F)	No. of Cycles	DO (ppm)
		S' <sub>12</sub> (psi)	S' <sub>23</sub> (psi)	S' <sub>31</sub> (psi)	S' <sub>12</sub> (psi)	S' <sub>23</sub> (psi)	S' <sub>31</sub> (psi)			
2024	22179.00	37658.7	23988.2	-61646.9	48905.7	22444.8	-71350.5	405.4	100	0.187
2025	22209.00	37613.7	23988.8	-61602.5	48860.4	22445.3	-71305.6	406.2	100	0.186
2026	22239.00	37568.6	23989.3	-61558.0	48815.1	22445.5	-71260.7	407.0	100	0.185
2027	22269.00	37523.6	23989.9	-61513.5	48769.9	22445.8	-71215.7	407.9	100	0.184
2028	22299.00	37478.5	23990.5	-61469.0	48724.7	22446.2	-71170.9	408.7	100	0.183
2029	22329.00	37433.6	23990.9	-61424.5	48679.5	22446.4	-71125.9	409.5	100	0.182
2030	22359.00	37388.5	23991.6	-61380.1	48634.3	22446.8	-71081.1	410.4	100	0.181
2031	22389.00	37343.5	23992.1	-61335.6	48589.1	22447.0	-71036.1	411.2	100	0.180
2032	22419.00	37298.5	23992.7	-61291.2	48543.8	22447.5	-70991.3	412.0	100	0.180
2033	22449.00	37253.4	23993.2	-61246.7	48498.7	22447.7	-70946.4	412.9	100	0.179
2034	22479.00	37208.4	23993.9	-61202.3	48453.5	22448.0	-70901.5	413.7	100	0.178
2035	22509.00	37163.4	23994.5	-61157.9	48408.2	22448.4	-70856.6	414.5	100	0.177
2036	22539.00	37118.5	23994.9	-61113.4	48363.1	22448.6	-70811.7	415.4	100	0.176
2037	22569.00	37073.4	23995.6	-61069.0	48318.0	22448.9	-70766.9	416.2	100	0.175
2038	22599.00	37028.5	23996.2	-61024.6	48272.7	22449.3	-70722.0	417.0	100	0.174
2039	22629.00	36983.5	23996.7	-60980.2	48227.6	22449.6	-70677.2	417.9	100	0.173
2040	22659.00	36938.6	23997.3	-60935.8	48182.4	22450.0	-70632.4	418.7	100	0.172
2041	22689.00	36893.6	23997.8	-60891.4	48137.3	22450.3	-70587.6	419.5	100	0.171
2042	22716.00	36853.1	23998.5	-60851.5	48096.6	22450.6	-70547.2	420.3	100	0.171
2043	22743.00	36812.6	23999.0	-60811.6	48056.0	22450.9	-70506.9	421.0	100	0.170
2044	22779.00	36758.7	23999.6	-60758.4	48001.8	22451.4	-70453.2	422.0	100	0.169
2045	22809.00	36713.8	24000.3	-60714.1	47956.8	22451.6	-70408.4	422.9	100	0.168
2046	22839.00	36668.8	24000.9	-60669.7	47911.7	22452.0	-70363.6	423.7	100	0.167
2047	22869.00	36623.9	24001.5	-60625.4	47866.5	22452.3	-70318.9	424.5	100	0.166
2048	22899.00	36579.0	24002.1	-60581.1	47821.4	22452.7	-70274.1	425.4	100	0.165
2049	22929.00	36534.1	24002.7	-60536.8	47776.3	22453.1	-70229.4	426.2	100	0.164
2050	22959.00	36489.1	24003.4	-60492.5	47731.2	22453.5	-70184.7	427.0	100	0.163
2051	22989.00	36444.3	24003.9	-60448.2	47686.1	22453.8	-70139.9	427.9	100	0.162
2052	23019.00	36399.3	24004.6	-60403.9	47640.9	22454.3	-70095.2	428.7	100	0.162
2053	23049.00	36354.5	24005.2	-60359.6	47595.9	22454.6	-70050.6	429.5	100	0.161
2054	23079.00	36309.5	24005.8	-60315.3	47550.8	22455.0	-70005.8	430.4	100	0.160
2055	23109.00	36264.6	24006.5	-60271.1	47505.8	22455.4	-69961.1	431.2	100	0.159
2056	23139.00	36219.8	24007.0	-60226.8	47460.7	22455.8	-69916.5	432.0	100	0.158
2057	23169.00	36174.8	24007.8	-60182.6	47415.6	22456.1	-69871.7	432.9	100	0.157
2058	23199.00	36130.0	24008.4	-60138.4	47370.6	22456.5	-69827.1	433.7	100	0.156
2059	23229.00	36085.1	24009.0	-60094.1	47325.5	22456.9	-69782.4	434.5	100	0.155
2060	23259.00	36040.3	24009.7	-60050.0	47280.5	22457.3	-69737.8	435.4	100	0.154
2061	23289.00	35995.4	24010.3	-60005.8	47235.5	22457.7	-69693.1	436.2	100	0.153
2062	23319.00	35950.6	24011.0	-59961.6	47190.4	22458.2	-69648.6	437.0	100	0.153

Point No.	Time (sec.)	Membrane + Bending Stresses			Total Stresses			Metal Temp. (°F)	No. of Cycles	DO (ppm)
		S' <sub>12</sub> (psi)	S' <sub>23</sub> (psi)	S' <sub>31</sub> (psi)	S' <sub>12</sub> (psi)	S' <sub>23</sub> (psi)	S' <sub>31</sub> (psi)			
2063	23349.00	35905.7	24011.7	-59917.4	47145.3	22458.6	-69603.9	437.9	100	0.152
2064	23379.00	35860.9	24012.3	-59873.2	47100.4	22458.9	-69559.3	438.7	100	0.151
2065	23409.00	35816.0	24013.0	-59829.0	47055.3	22459.4	-69514.7	439.5	100	0.150
2066	23439.00	35771.2	24013.6	-59784.8	47010.3	22459.8	-69470.1	440.4	100	0.149
2067	23469.00	35726.3	24014.4	-59740.7	46965.3	22460.3	-69425.5	441.2	100	0.148
2068	23499.00	35681.4	24015.1	-59696.5	46920.2	22460.7	-69381.0	442.0	100	0.147
2069	23529.00	35636.6	24015.7	-59652.3	46875.2	22461.1	-69336.3	442.9	100	0.146
2070	23559.00	35591.8	24016.4	-59608.2	46830.3	22461.5	-69291.8	443.7	100	0.145
2071	23589.00	35547.0	24017.2	-59564.1	46785.2	22462.0	-69247.2	444.5	100	0.144
2072	23616.00	35506.6	24017.7	-59524.3	46744.7	22462.4	-69207.2	445.3	100	0.144
2073	23643.00	35466.3	24018.3	-59484.6	46704.2	22462.8	-69167.0	446.0	100	0.143
2074	23691.00	35394.6	24019.5	-59414.1	46632.2	22463.5	-69095.7	447.4	100	0.146
2075	23731.00	35334.9	24020.4	-59355.2	46572.2	22464.1	-69036.3	448.5	100	0.148
2076	23771.00	35275.1	24021.4	-59296.5	46512.3	22464.7	-68977.0	449.6	100	0.150
2077	23811.00	35215.4	24022.2	-59237.6	46452.3	22465.3	-68917.6	450.7	100	0.152
2078	23851.00	35155.7	24023.2	-59178.9	46392.4	22465.9	-68858.3	451.8	100	0.155
2079	23891.00	35096.0	24024.1	-59120.1	46332.5	22466.5	-68799.0	452.9	100	0.157
2080	23931.00	35036.3	24025.1	-59061.4	46272.6	22467.2	-68739.7	454.0	100	0.159
2081	23971.00	34976.7	24025.9	-59002.6	46212.7	22467.7	-68680.4	455.1	100	0.162
2082	24011.00	34917.0	24026.8	-58943.9	46152.8	22468.2	-68621.1	456.2	100	0.164
2083	24051.00	34857.4	24027.7	-58885.1	46092.9	22468.9	-68561.8	457.3	100	0.166
2084	24091.00	34797.7	24028.6	-58826.3	46033.1	22469.4	-68502.5	458.5	100	0.168
2085	24131.00	34738.1	24029.6	-58767.7	45973.3	22469.9	-68443.2	459.6	100	0.171
2086	24171.00	34678.6	24030.4	-58708.9	45913.5	22470.4	-68383.9	460.7	100	0.173
2087	24211.00	34618.9	24031.3	-58650.3	45853.7	22471.0	-68324.7	461.8	100	0.175
2088	24251.00	34559.4	24032.2	-58591.6	45793.9	22471.6	-68265.5	462.9	100	0.178
2089	24291.00	34499.8	24033.2	-58533.0	45734.1	22472.2	-68206.3	464.0	100	0.180
2090	24331.00	34440.2	24034.2	-58474.4	45674.3	22472.8	-68147.1	465.1	100	0.182
2091	24371.00	34380.7	24035.1	-58415.8	45614.4	22473.5	-68088.0	466.2	100	0.184
2092	24411.00	34321.1	24036.1	-58357.2	45554.6	22474.2	-68028.9	467.3	100	0.187
2093	24451.00	34261.5	24037.1	-58298.7	45494.8	22474.9	-67969.7	468.5	100	0.189
2094	24491.00	34202.0	24038.1	-58240.1	45435.0	22475.6	-67910.6	469.6	100	0.191
2095	24531.00	34142.4	24039.3	-58181.7	45375.2	22476.3	-67851.6	470.7	100	0.194
2096	24571.00	34082.8	24040.3	-58123.1	45315.5	22477.0	-67792.5	471.8	100	0.196
2097	24611.00	34023.3	24041.4	-58064.6	45255.7	22477.7	-67733.4	472.9	100	0.198
2098	24651.00	33963.8	24042.3	-58006.1	45195.9	22478.5	-67674.4	474.0	100	0.200
2099	24691.00	33904.2	24043.4	-57947.7	45136.2	22479.1	-67615.3	475.1	100	0.203
2100	24731.00	33844.7	24044.5	-57889.2	45076.4	22479.9	-67556.3	476.2	100	0.205
2101	24771.00	33785.1	24045.6	-57830.7	45016.7	22480.6	-67497.3	477.3	100	0.207

Point No.	Time (sec.)	Membrane + Bending Stresses			Total Stresses			Metal Temp. (°F)	No. of Cycles	DO (ppm)
		S' <sub>12</sub> (psi)	S' <sub>23</sub> (psi)	S' <sub>31</sub> (psi)	S' <sub>12</sub> (psi)	S' <sub>23</sub> (psi)	S' <sub>31</sub> (psi)			
2102	24807.00	33731.6	24046.4	-57778.1	44962.9	22481.3	-67444.2	478.3	100	0.209
2103	24843.00	33678.0	24047.5	-57725.5	44909.1	22481.9	-67391.0	479.3	100	0.211
2104	24891.00	33606.6	24048.7	-57655.4	44837.4	22482.8	-67320.2	480.7	100	0.214
2105	24931.00	33547.1	24049.8	-57596.9	44777.7	22483.5	-67261.3	481.8	100	0.216
2106	24971.00	33487.7	24050.9	-57538.6	44718.0	22484.3	-67202.4	482.9	100	0.219
2107	25011.00	33428.2	24052.0	-57480.2	44658.3	22485.1	-67143.4	484.0	100	0.221
2108	25051.00	33368.7	24053.1	-57421.8	44598.6	22485.9	-67084.5	485.1	100	0.223
2109	25091.00	33309.3	24054.2	-57363.4	44539.0	22486.5	-67025.4	486.2	100	0.226
2110	25131.00	33249.8	24055.2	-57305.1	44479.3	22487.3	-66966.6	487.3	100	0.228
2111	25171.00	33190.4	24056.3	-57246.7	44419.6	22488.1	-66907.7	488.5	100	0.230
2112	25211.00	33131.0	24057.4	-57188.4	44360.0	22488.8	-66848.8	489.6	100	0.232
2113	25251.00	33071.5	24058.6	-57130.1	44300.2	22489.6	-66789.9	490.7	100	0.235
2114	25291.00	33012.1	24059.7	-57071.8	44240.6	22490.4	-66731.1	491.8	100	0.237
2115	25331.00	32952.7	24060.7	-57013.4	44181.0	22491.1	-66672.1	492.9	100	0.239
2116	25371.00	32893.2	24061.9	-56955.2	44121.3	22492.0	-66613.4	494.0	100	0.242
2117	25411.00	32833.9	24063.0	-56896.9	44061.7	22492.8	-66554.5	495.1	100	0.244
2118	25451.00	32774.5	24064.2	-56838.7	44002.1	22493.5	-66495.6	496.2	100	0.246
2119	25491.00	32715.0	24065.4	-56780.4	43942.5	22494.4	-66436.9	497.3	100	0.248
2120	25531.00	32655.7	24066.5	-56722.2	43882.9	22495.2	-66378.0	498.4	100	0.251
2121	25571.00	32596.4	24067.6	-56663.9	43823.3	22496.0	-66319.2	499.6	100	0.253
2122	25611.00	32534.2	24069.3	-56603.5	43742.9	22497.4	-66240.3	500.7	100	0.255
2123	25651.00	32459.3	24073.8	-56533.2	43650.2	22501.8	-66151.9	501.8	100	0.257
2124	25691.00	32374.4	24079.5	-56454.0	43560.9	22507.6	-66068.6	502.9	100	0.260
2125	25731.00	32286.5	24087.6	-56374.2	43478.9	22514.7	-65993.6	504.0	100	0.262
2126	25771.00	32200.7	24093.8	-56294.5	43401.1	22518.0	-65919.1	505.1	100	0.264
2127	25811.00	32124.2	24089.1	-56213.4	43325.5	22515.9	-65841.5	506.2	100	0.267
2128	25851.00	32050.2	24081.4	-56131.6	43251.9	22509.5	-65761.4	507.3	100	0.269
2129	25891.00	31978.4	24070.7	-56049.1	43180.0	22499.7	-65679.7	508.4	100	0.271
2130	25931.00	31908.4	24058.1	-55966.5	43109.7	22487.3	-65597.0	509.6	100	0.273
2131	25971.00	31840.0	24043.6	-55883.6	43041.0	22472.9	-65513.9	510.7	100	0.276
2132	26007.00	31779.7	24029.3	-55809.0	42980.3	22458.7	-65439.0	511.7	100	0.278
2133	26043.00	31720.5	24014.0	-55734.6	42920.8	22443.4	-65364.2	512.7	100	0.280
2134	26091.00	31643.0	23992.8	-55635.8	42842.7	22422.2	-65264.9	514.0	100	0.283
2135	26131.00	31579.5	23974.8	-55554.3	42778.8	22404.2	-65183.1	515.1	100	0.285
2136	26171.00	31516.6	23957.4	-55474.0	42715.7	22386.8	-65102.5	516.2	100	0.287
2137	26211.00	31454.2	23941.7	-55395.9	42652.9	22371.2	-65024.1	517.3	100	0.289
2138	26251.00	31390.8	23931.2	-55322.1	42589.3	22360.5	-64949.8	518.4	100	0.292
2139	26291.00	31325.2	23927.1	-55252.4	42523.1	22356.2	-64879.3	519.5	100	0.294
2140	26331.00	31259.1	23924.4	-55183.5	42456.5	22353.0	-64809.5	520.7	100	0.296



Point No.	Time (sec.)	Membrane + Bending Stresses			Total Stresses			Metal Temp. (°F)	No. of Cycles	DO (ppm)
		S' <sub>12</sub> (psi)	S' <sub>23</sub> (psi)	S' <sub>31</sub> (psi)	S' <sub>12</sub> (psi)	S' <sub>23</sub> (psi)	S' <sub>31</sub> (psi)			
2141	26371.00	31192.9	23921.7	-55114.5	42389.7	22349.8	-64739.6	521.8	100	0.299
2142	26411.00	31126.6	23918.9	-55045.5	42323.0	22346.6	-64669.6	522.9	100	0.301
2143	26451.00	31060.4	23916.0	-54976.4	42256.3	22343.5	-64599.7	524.0	100	0.303
2144	26491.00	30994.1	23913.3	-54907.3	42189.4	22340.4	-64529.8	525.1	100	0.305
2145	26531.00	30927.8	23910.4	-54838.2	42122.7	22337.1	-64459.8	526.2	100	0.308
2146	26571.00	30861.5	23907.6	-54769.1	42055.8	22333.9	-64389.7	527.3	100	0.310
2147	26611.00	30795.1	23904.8	-54699.9	41989.0	22330.7	-64319.7	528.4	100	0.312
2148	26651.00	30728.8	23901.9	-54630.7	41922.2	22327.4	-64249.6	529.5	100	0.315
2149	26691.00	30662.4	23899.0	-54561.5	41855.2	22324.2	-64179.4	530.7	100	0.317
2150	26731.00	30596.1	23896.1	-54492.1	41788.4	22320.8	-64109.2	531.8	100	0.319
2151	26771.00	30529.7	23893.3	-54422.9	41721.4	22317.6	-64039.0	532.9	100	0.321
2152	26811.00	30463.3	23890.3	-54353.6	41654.5	22314.3	-63968.8	534.0	100	0.324
2153	26851.00	30396.8	23887.4	-54284.2	41587.6	22311.0	-63898.6	535.1	100	0.326
2154	26891.00	30330.3	23884.5	-54214.8	41520.6	22307.6	-63828.3	536.2	100	0.328
2155	26931.00	30263.8	23881.6	-54145.4	41453.6	22304.4	-63757.9	537.3	100	0.331
2156	26971.00	30197.3	23878.6	-54075.9	41386.5	22301.1	-63687.6	538.4	100	0.333
2157	27011.00	30130.8	23875.6	-54006.4	41319.5	22297.7	-63617.2	539.5	100	0.335
2158	27051.00	30064.2	23872.7	-53936.9	41252.4	22294.3	-63546.7	540.7	100	0.337
2159	27091.00	29997.7	23869.7	-53867.4	41185.4	22290.9	-63476.3	541.8	100	0.340
2160	27131.00	29931.1	23866.7	-53797.8	41118.3	22287.6	-63405.9	542.9	100	0.342
2161	27171.00	29864.5	23863.7	-53728.2	41051.1	22284.2	-63335.3	544.0	100	0.344
2162	27207.00	29804.6	23860.9	-53665.5	40990.7	22281.2	-63271.9	545.0	100	0.346
2163	27243.00	29744.6	23858.2	-53602.9	40930.3	22278.0	-63208.3	546.0	100	0.348
2164	27259.56	29696.7	23835.0	-53531.7	40853.4	22255.3	-63108.7	546.1	100	0.342
2165	27276.12	29643.4	23805.1	-53448.5	40779.9	22226.4	-63006.4	546.2	100	0.335
2166	27303.72	29561.3	23748.7	-53309.9	40676.1	22171.9	-62848.0	546.3	100	0.324
2167	27331.32	29489.0	23690.2	-53179.2	40588.0	22115.0	-62703.0	546.4	100	0.312
2168	27358.92	29425.7	23632.0	-53057.8	40512.5	22059.4	-62572.0	546.4	100	0.301
2169	27386.52	29370.0	23576.4	-52946.4	40447.1	22005.9	-62452.9	546.5	100	0.290
2170	27414.12	29320.4	23523.5	-52844.0	40389.6	21954.3	-62343.9	546.5	100	0.278
2171	27441.72	29276.1	23472.5	-52748.6	40338.7	21905.3	-62244.0	546.6	100	0.267
2172	27469.32	29236.0	23424.2	-52660.2	40293.0	21859.0	-62152.0	546.6	100	0.256
2173	27496.92	29199.6	23378.3	-52577.8	40251.9	21814.1	-62066.0	546.6	100	0.245
2174	27524.52	29166.2	23334.2	-52500.4	40214.4	21772.6	-61987.0	546.6	100	0.233
2175	27552.12	29135.5	23292.6	-52428.1	40180.2	21731.9	-61912.0	546.7	100	0.222
2176	27579.72	29107.1	23252.7	-52359.8	40148.5	21693.5	-61842.1	546.7	100	0.211
2177	27607.32	29080.6	23214.8	-52295.5	40119.3	21656.8	-61776.1	546.7	100	0.200
2178	27634.92	29055.8	23178.3	-52234.2	40092.1	21622.0	-61714.1	546.7	100	0.188
2179	27657.00	29037.0	23149.9	-52186.9	40071.4	21594.8	-61666.2	546.7	100	0.179

Point No.	Time (sec.)	Membrane + Bending Stresses			Total Stresses			Metal Temp. (°F)	No. of Cycles	DO (ppm)
		S' <sub>12</sub> (psi)	S' <sub>23</sub> (psi)	S' <sub>31</sub> (psi)	S' <sub>12</sub> (psi)	S' <sub>23</sub> (psi)	S' <sub>31</sub> (psi)			
2180	27673.56	29023.4	23129.4	-52152.8	40056.5	21574.7	-61631.2	546.7	100	0.172
2181	27690.12	29010.3	23109.3	-52119.6	40042.2	21555.1	-61597.2	546.7	100	0.166
2182	27717.72	28989.6	23076.8	-52066.3	40019.7	21524.6	-61544.3	546.8	100	0.154
2183	27745.32	28969.9	23046.2	-52016.1	39998.4	21494.0	-61492.3	546.8	100	0.143
2184	27772.92	28951.3	23015.6	-51966.9	39978.2	21465.2	-61443.4	546.8	100	0.132
2185	27800.52	28933.5	22987.1	-51920.7	39959.0	21437.5	-61396.5	546.8	100	0.121
2186	27828.12	28916.5	22958.9	-51875.5	39940.5	21410.0	-61350.5	546.8	100	0.109
2187	27855.72	28900.2	22931.1	-51831.3	39923.1	21383.6	-61306.6	546.8	100	0.098
2188	27883.32	28884.6	22904.5	-51789.1	39906.3	21358.4	-61264.7	546.8	100	0.087
2189	27910.92	28869.6	22879.4	-51748.9	39890.2	21333.6	-61223.8	546.8	100	0.075
2190	27938.52	28855.1	22854.7	-51709.8	39874.7	21309.1	-61183.8	546.8	100	0.064
2191	27966.12	28841.1	22830.6	-51671.6	39859.7	21285.2	-61144.9	546.8	100	0.053
2192	27993.72	28827.6	22806.9	-51634.5	39845.3	21262.7	-61108.0	546.9	100	0.042
2193	28021.32	28814.6	22783.8	-51598.4	39831.4	21240.7	-61072.1	546.9	100	0.030
2194	28048.92	28801.9	22761.4	-51563.3	39818.0	21219.1	-61037.2	546.9	100	0.019
2195	28071.00	28792.1	22744.1	-51536.2	39807.6	21201.6	-61009.2	546.9	100	0.010
2196	28387.00	28745.0	22648.4	-51393.4	39755.2	21111.7	-60866.9	546.9	100	0.010
2197	28681.03	28716.7	22589.5	-51306.3	39724.0	21054.7	-60778.7	546.9	100	0.010
2198	28975.06	28698.5	22549.0	-51247.5	39703.7	21016.9	-60720.6	547.0	100	0.010
2199	29269.59	28686.5	22522.4	-51209.0	39690.4	20991.1	-60681.5	547.0	100	0.010
2200	29564.22	28678.7	22504.0	-51182.6	39681.6	20973.8	-60655.4	547.0	100	0.010
2201	29858.93	28673.4	22492.0	-51165.4	39675.9	20962.5	-60638.4	547.0	100	0.010
2202	30153.68	28670.0	22484.2	-51154.2	39672.1	20955.3	-60627.4	547.0	100	0.010
2203	30448.45	28667.8	22478.3	-51146.1	39669.6	20949.8	-60619.3	547.0	100	0.010
2204	30743.24	28666.2	22474.8	-51141.1	39667.9	20946.4	-60614.3	547.0	100	0.010
2205	31038.05	28665.2	22472.8	-51138.0	39666.8	20944.6	-60611.3	547.0	100	0.010
2206	31332.86	28664.6	22471.4	-51136.0	39666.1	20942.2	-60608.3	547.0	100	0.010
2207	31859.52	28664.0	22470.0	-51134.0	39665.4	20941.0	-60606.3	547.0	100	0.010
2208	32386.19	28663.6	22468.4	-51132.0	39664.9	20940.4	-60605.3	547.0	100	0.010
2209	32912.86	28663.5	22468.5	-51131.9	39664.8	20939.5	-60604.3	547.0	100	0.010
2210	33439.52	28663.4	22468.6	-51131.9	39664.6	20939.7	-60604.3	547.0	100	0.010
2211	33966.19	28663.3	22467.7	-51130.9	39664.5	20939.8	-60604.3	547.0	100	0.010
2212	34492.86	28663.3	22467.7	-51130.9	39664.5	20939.8	-60604.3	547.0	100	0.010
2213	35019.52	28663.3	22467.7	-51130.9	39664.5	20939.8	-60604.3	547.0	100	0.010
2214	35546.19	28663.3	22467.7	-51130.9	39664.5	20939.8	-60604.3	547.0	100	0.010
2215	35971.00	28663.3	22467.7	-51130.9	39664.5	20939.8	-60604.3	547.0	100	0.010

## C5 References

- C-1. EPRI Report No. 1025823, "Guidelines for Addressing Environmental Effects in Fatigue Usage Calculations," Electric Power Research Institute, Palo Alto, CA, December 2012.
- C-2. ASME Boiler and Pressure Vessel Code, Section III, Rules for Construction of Nuclear Facility Components, "Division 1 - Subsection NB, Class 1 Components," American Society of Mechanical Engineers, New York, NY, July 1, 2013 (2013 Edition).



**BIBLIOGRAPHIC DATA SHEET**

(See instructions on the reverse)

1. REPORT NUMBER  
(Assigned by NRC, Add Vol., Supp., Rev.,  
and Addendum Numbers, if any.)  
NUREG/CR-6909 Rev. 1  
ANL-12/60  
(DRAFT)

2. TITLE AND SUBTITLE

Effect of LWR Coolant Environments on the Fatigue Life of Reactor Materials  
Draft Report

3. DATE REPORT PUBLISHED

MONTH

YEAR

March

2014

4. FIN OR GRANT NUMBER

V6069

5. AUTHOR(S)

O. K. Chopra and G. L. Stevens

6. TYPE OF REPORT

Technical

7. PERIOD COVERED (Inclusive Dates)

8. PERFORMING ORGANIZATION - NAME AND ADDRESS (If NRC, provide Division, Office or Region, U. S. Nuclear Regulatory Commission, and mailing address; if contractor, provide name and mailing address.)

Argonne National Laboratory  
9700 South Cass Avenue  
Argonne, IL 60439

9. SPONSORING ORGANIZATION - NAME AND ADDRESS (If NRC, type "Same as above", if contractor, provide NRC Division, Office or Region, U. S. Nuclear Regulatory Commission, and mailing address.)

Division of Engineering  
Office of Nuclear Regulatory Research  
U.S. Nuclear Regulatory Commission  
Washington, DC 20555-0001

10. SUPPLEMENTARY NOTES

G. L. Stevens, NRC Project Manager

11. ABSTRACT (200 words or less)

The existing fatigue strain-vs.-life ( $\epsilon$ -N) data illustrate potentially significant effects of LWR coolant environments on the fatigue resistance of pressure vessel and piping steels. Under certain environmental and loading conditions, fatigue lives in water relative to those in air can be a factor of  $\approx 12$  lower for austenitic stainless steels,  $\approx 3$  lower for Ni-Cr-Fe alloys, and  $\approx 17$  lower for carbon and low-alloy steels. In 2007, the original revision to this report was published, which summarized the work performed at Argonne National Laboratory on the fatigue of piping and pressure vessel steels in LWR environments. In that document, the existing fatigue  $\epsilon$ -N data were evaluated to identify the various material, environmental, and loading parameters that influence fatigue crack initiation, and to establish the effects of key parameters on the fatigue life of these steels. The environmental fatigue correction factor ( $F_{en}$ ) for incorporating the effects of LWR environments into ASME Section III fatigue evaluations was described. The current revision of this report provides updates and improvements to the environmental fatigue correction factor approach based on an extensive update to the  $\epsilon$ -N data from testing and results available since this report was first published. The updated  $F_{en}$  expressions also address concerns from interested stakeholders related to: (a) the constants in the expressions that result in  $F_{en}$  values of approximately 2 even when the strain rate is very high or the temperature is very low, (b) the temperature dependence of  $F_{en}$  for carbon and low-alloy steels, and (c) the dependence of  $F_{en}$  on water chemistry for austenitic stainless steels. The  $F_{en}$  methodology was validated by comparing the results of five different experimental data sets obtained from fatigue tests that simulate actual plant conditions with estimates of fatigue usage adjusted for environmental effects using the updated  $F_{en}$  expressions.

12. KEY WORDS/DESCRIPTORS (List words or phrases that will assist researchers in locating the report.)

Fatigue crack initiation  
Fatigue life  
Environmental effects  
Carbon and low-alloy steels  
Austenitic stainless steels  
Ni-Cr-Fe alloys  
BWR environment  
PWR environment

13. AVAILABILITY STATEMENT

unlimited

14. SECURITY CLASSIFICATION

(This Page)

unclassified

(This Report)

unclassified

15. NUMBER OF PAGES

16. PRICE



Federal Recycling Program





**UNITED STATES  
NUCLEAR REGULATORY COMMISSION**  
WASHINGTON, DC 20555-0001

OFFICIAL BUSINESS

**OFFICIAL BUSINESS**





**NUREG/CR-6909**  
**Revision 1, Draft**

**Effect of LWR Coolant Environments on the Fatigue Life of Reactor Materials**

**March 2014**